REPORT NO. FRA/ORD-77/10 PB

FLAW DETECTION IN RAILS

DECEMBER 1978

Prepared for

U.S. DEPARTMENT OF TRANSPORTATION
FEDERAL RAILROAD ADMINISTRATION
Office of Research and Development
Washington, D.C. 20590

NOTICE

This document, which is being distributed by the Federal Railroad Administration, was received under the provisions of the bilateral arrangement; US/USSR Agreement for Cooperation in the Field of Transportation, in the hope that it might be of assistance in railway research and operation.

The translation and publication of this document does not constitute approval by the U.S. Department of Transportation of the inferences, findings, or conclusions contained therein. Publication is solely for the exchange and stimulation of ideas.

Technical Report Documentation Page

1. Report No.	2. Government Accession No.	3. Recipient's Catalog No.
FRA/ORD-77/10		

4. Title and Subtitle	5. Report Date
Flaw Detection in Rails	December 1978
	6. Performing Organization Code
	8. Performing Organization Report No.
7. Author(s) Gurvich, A. K. et al	
9. Performing Organization Name and Address University of Oklahoma School of Aerospace, Mechanical & Nuclear Eng. 865 Asp Street, Room 200 Norman, Oklahoma 73069	10. Work Unit No. (TRAIS) 11. Contract or Grant No. DOT-OS-40091
12. Sponsoring Agency Name and Address Department of Transportation Federal Railroad Administration Washington, D.C. 20590	13. Type of Report and Period Covered Translation 14. Sponsoring Agency Code

15. Supplementary Notes
3rd ed., (1971), revised and expanded, translated from the Russian by Robert J. Karriker

16. Abstract

The Physical principles and techniques of magnetic and ultrasonic flaw detection in rails are given. The intended use, working principles and layout of various rail flaw detector systems and the procedure for working with them are described. The methodology of rail inspection, both in the field and at railwelding facilities is also described. The repair of flaw detection equipment on the railroads is examined.

The book has been approved by the Chief Administration of Educational Institutions of the MPS (Ministry of Railroads) as a textbook for rail transportation technical schools and by the Academic Council of the State Committee of the USSR Council of Ministers responsible for professional-technological education as a manual for individual-team instruction production workers. It will be helpful to track facility workers involved in the inspection of rails.

246 figures, 19 tables, 16 entry bibliography

17. Key Words	18. Distribution Statement
Rail Nondestructive Inspection, Rail Flaws, Ultrasonics, Electro-magnetic flaw detection	This Report is available from the sponsoring agency, through the Office of Rail Safety Research, RRD-32, Limited to Quantity Available.

19. Security Classif. (of this report)	20. Security Classif. (of this page)	21. No. of Pages	22. Price
Unclassified	Unclassified		

Form DOT F 1700.7 (8-72)

FLAW DETECTION IN RAILS
3rd ed., revised and expanded
(Translated from Russian)

ABSTRACT

The physical principles and techniques of magnetic and ultrasonic flaw detection in rails are given. The intended use, working principles and layout of various rail flaw detector systems and the procedure for working with them are described. The methodology of rail inspection, both in the field and at railwelding facilities is also described. The repair of flaw detection equipment on the railroads is examined.

The book has been approved by the Chief Administration of Educational Institutions of the MPS (Ministry of Railroads) as a textbook for rail transportation technical schools and by the Academic Council of the State Committee of the USSR Council of Ministers responsible for professional-technological education as a manual for individual-team instruction production workers. It will be helpful to track facility workers involved in the inspection of rails.

246 figures, 19 tables, 16 entry bibliography

Book written by

A. K. Gurvich	Ch. 5; Ch. 9, Sect. 1, 2; Ch. 10, Sect. 1, 4.
V. B. Kozlov	Ch. 6, 7 and 8.
G. A. Krug	Ch. 9, Sect. 3, 5, 7, 8; Ch. 10, Sect. 2, 3, and 5.
L. I. Kuz'mina	Ch. 9, Sect. 6; Ch. 11.
I. M. Lysenko	Ch. 1; Ch. 3, Sect. 2, 5; Ch. 12 and 13.
A. N. Matveev	Ch. 2; Ch. 3, Sect. 1, 2.
E. I. Uspensky	Ch. 4.

TRANSLATION EDITOR'S PREFACE

This book was furnished by Soviet Railway to a group from the United States of America which was sent to the Soviet Union to investigate the state of rail flaw detection in that country. A separate report of that trip is available (Becker, F. L., "Trip Report, U.S. - U.S.S.R. Rail Inspection Information Exchange, August 24, - September 1, 1975", Department of Transportation, Transportation Systems Center, Cambridge, Massachusetts, 02142, DOT-T5C-949, BNW 2311102378, Battelle/Pacific Northwest Laboratories, Richland, Washington 99352, December 1975).

In using this book, the reader must be aware that it was written to be a complete textbook for all persons engaged in ultrasonic rail flaw detection in the Soviet Union. Because of this, much of the information, such as the complete descriptions of the electronic circuits, full maintainance instructions, etc. may be of little interest to American readers. And, some of the specific ultrasonic inspection techniques have been previously translated and reported in the literature.

In spite of this, there will be much information that will be of interest to the American reader. One must be impressed with the depth and breadth of the utilization of ultrasound for rail flaw detection on Soviet Railways.

The editor's intent has been to assist the translator in choosing words and phrases which correspond to terminology used in the United States. Hopefully, this will assist the reader in understanding the original meanings of the Soviet authors.

Don E. Bray

TABLE OF CONTENTS

INTRODUCTION

The rapid rate at which the national economy of the Soviet Union is developing is bringing about significant increases in the volume of loads transported by rail, the further growth of the speed and density of freight traffic on the railroad trunk lines.

The continued development of rail transportation being brought about in compliance with the directives of the XXIV session of the CPSU (Communist Party of the Soviet Union) in accordance with the five-year plan for developing the USSR's national economy for the period 1971-75, based on technological progress, anticipates, among other things, the introduction of the most progressive designs for the upper track structure, particularly jointless track, and of heat processed rails.

Rails are the most important element of a line of track. To a great degree, insuring the necessary speeds and safety of train movement depends on their condition.

One of the effective means for monitoring the condition of rails is the flaw detector, the use of which permits the timely detection of rail flaws when they are welded at rail welding facilities and when they are in use on the line.

Flaw detectors, the operating principles of which are based on the use of magnetic and ultrasonic monitoring methods, are used for detecting flaws in rails.

The development of domestic rail flaw detection proceeded by creating specialized instruments. Each instrument solves a part of the overall problem, i.e. not detecting all posible flaws, but only definite types. The creation of the universal, high-speed flaw detector is a current problem still awaiting solution.

As a result of the large amount of work accomplished by the All-union Scientific Research Institute for Rail Transport (TsNII MPS)*, the Scientific Research Institute for Bridges of the Leningrad Institute for Engineers for Railroad Transportation (NII mostov LIIZhT), the Institute of Metal Physics of the USSR Academy of Sciences and the Siberian Institute for Applied Physics (SFTI) in constructive cooperation with the All-union Scientific Research Institute for Non-destructive Testing Proceedures (VNIINK) and by production workers and railroad workers, traveling removable flaw detectors, portable flaw detectors for rail monitoring in rail welding facilities, and high-speed flaw detector cars were created and introduced.

The quality of rail monitoring, in the case of multiple usage of the indicated flaw detector types, depends to a great degree on the correct organization of this work on the rail sectors and over the line as a whole. This is impossible without studying the existing rail flaw detection procedures and the equipment used from all sides and depth.

This collective work reveals the contemporary state of the technology of flaw detection in rails as related to rail transportation.

Significant additions and changes in connection with the development of the theory and practice of rail flaw detection over the last few years have been included in the third edition. The sections illuminating the physical bases of flaw detection procedures have been significantly broadened and sections on the standardization of ultrasonic monitoring practices, and the description of the equipment and procedures for using the new types of flaw detectors which have found wide-spread application in rail transport have been introduced. In preparing the third edition, the authors took into consideration

---

*Central Scientific Research Institute, Ministry of Railroads.

the experience gained from the use and repair of rail flaw detectors on the line and in rail welding facilities.

Material in the book has been set out taking into consideration the knowledge of the basics of physics, electrotechnology and radio technology possessed by the students within the curricula of the Railroad Transportation Ministry's technical schools.

The authors wish to express thanks to A. I. Vorob'ev, candidate of technological sciences and lecturer at the Novosibirsk Institute for Rail Transportation Engineers, and to the teachers of the "Dortekh" School No. 1 of the Sverdlovsk railroad, B. P. Dovnar, L. P. Ol'shanskaya, and V. A. Shcherbinina, whose recomendations and comments were taken into consideration when preparing the manuscript of the text for publication.

I. Servicing the Rails in the Field.

1. Rail types and markings.

A rail is one of the most significant elements of the upper structure of the railroad track. Train safety is determined first of all by the reliable functioning of the rails. Rail rolling began in the period 1839-43 in Russia. Puddled iron was used for rolling. As a result of the softness of this metal and the presence of a large quantity of slag in it, the rails were very quickly knocked out of commission because of crushing and fracturing.

The first steel rails were laid in Russia in 1866.

As railroad transportation developed, with the increase in the load on the rolling stock axles, in train speeds and in the freight traffic density on the railroads, the weight of the rails increased, the quality improved and the rail profiles were being perfected.

It is necessary to note that the metal industry developed in all parts of the world in close connection with the construction of railroads, particularly with the manufacture of rails.

Over the past twenty years, radical changes have taken place in the railroad economy of our country. Up to 1940, the I-a rail, with a weight of 43.6 kg/m was the heaviest rail on the main lines. In 1948, mass-production of the R50 rail began. In 1953, the R65 rails were being rolled and in 1958, an experimental lot of R75 rails was already prepared.

One of the important undertakings to improve the reliability and longivity of rails was the introduction of oil quenching of the rail over its entire volume, the surface hardening of the rail head and other new heat processing means at the rail mills.

Each rail produced by a rail-rolling mill is marked, which facilitates

the monitoring of rail quality while in production and during their further service on the line.

The following order for rail marking has been established:

1. The following signs (Fig. 1) are stamped on the web of each rail in raised letters not less than 20 mm high during the rolling process:

a) the mark of the manufacturer, e.g. KMK (Kuznetsk Metalurgical Combine);

b) designation for the type of steel, e.g. M (Siemens-Martin steel);

c) the year and month the rail was manufactured, e.g. 1960 g., V (May, 1960);

d) the rail type, e.g. R50; and

e) a mark for the type of heat processing, e.g. Z-0 (Delayed cooling).

The notations mentioned in points a) through e) are rolled at four or five places along the length of the rail.

2. At a distance of one meter from the end of the rail, and at two to five places along its length, the melt number and the ordinal number of the rail are stamped, the number 1 being stamped on the web of the first (lead) rail.

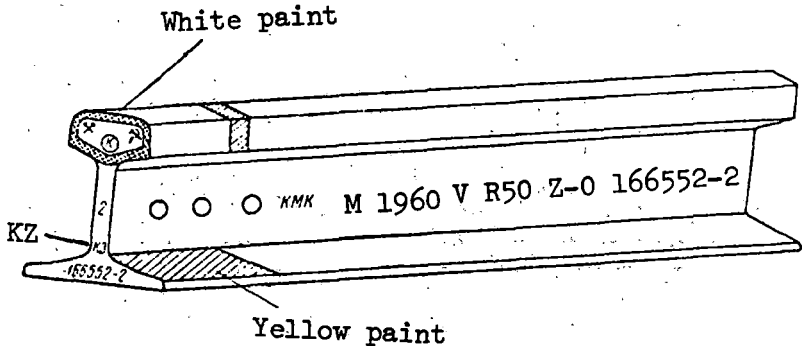

Fig. 1 Rail Marking

As the rail is finished, the melt number and the ordinal rail number are stamped on the butt-end of the base and web respectively after it is cool.

3. Rails with hardened ends are marked on the butt-end of the base with the letters KZ.

In addition to the markings indicated, conventional symbols are made with white, red, dark blue, green, and yellow oil paints. This supplementary marking indicates the following: first quality rails are marked by painting the outline of the butt-end of the head with white paint; second quality rails are marked by painting the butt-end of the web and base with red paint; rejected rails intended for industrial usage are marked by painting the entire butt-end of the rail with dark-blue paint. A white stripe 20-40 mm wide on the surface and on the sides of the rail head 150-200 mm from the butt-end denotes a rail with hardened ends. Hard rails are denoted by painting the top surface of the base for a length of not less than 200 mm with yellow paint.

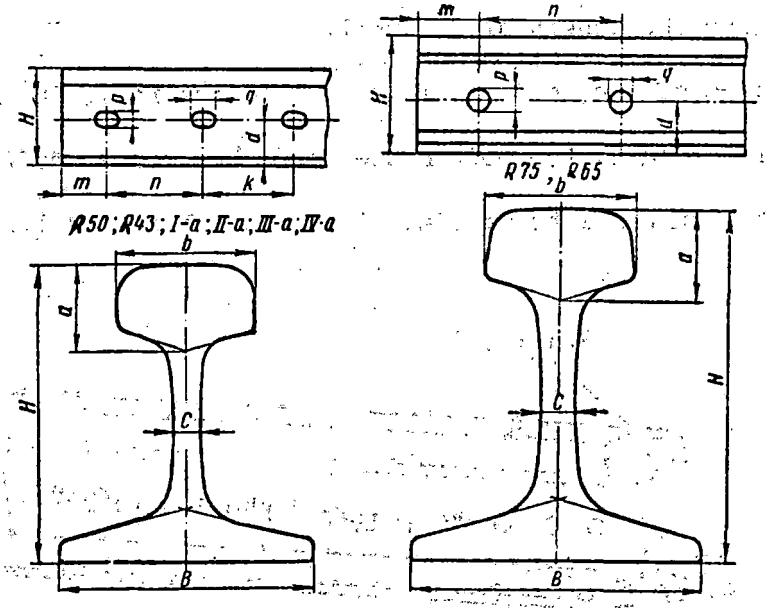

Fig. 2 Outlines of domestic rails

First class rails which are completely hardened have the outline of the butt-end of the head painted green and a green stripe is painted along the

head and web at a distance of 1 m. from the end. The outline of the butt-end of second quality fully hardened rails is painted yellow, with the same green stripe which designates second quality rails.

On the web and the head of surface-hardened rails, two stripes, red and green, are painted 1 m. from the butt-end.

A wrench and hammer and a hammer and sickle stamped near one of the ends of the rail are the marks of the factory inspector of the Main Administration for Material and Technical Supply (GUMTO) of the Ministry of Railroads, signifying technical acceptability of the rails at the rail plants. Cross-sections of domestically produced rails are presented in Fig. 2, and the marking elements and basic rail dimensions in Tables 1-3.

Rail Markings — Table 1

Rail-rolling Mills	Plant Rail Markings		
	Pre-revolutionary	Post-revolutionary	Currently
Kuznetsk Metallurgical Combine	-	KMK	K
"Azovstal'"	-	Kerch. GMZ	A
Novo-Tagil'skiy	-	NTMZ	T
Enakievskiy	RBMO	RGZ EGZ OGZ	EGZ
Im. Petrovskiy	AYuRZBO	GZ and TP	P
Im. Dzerzhinskiy	YuRDMO	Yugostal' DGZ Stal' DGZ	D
Nadezhdinskiy	Nadezhd. BGO	Nadezhd. NKMRT	-
The Metallurgical Plant (Don Basin)	Yuzovsk	YuGZ USSR Yugostal'	-

Table 2

Rail type	Basic rail dimensions in mm (cf. Fig. 2)										
	H	*B*	*a*	*b*	*c*	*d*	*m*	*n*	*k*	*p*	*q*
R75	192	160	48,5	75	20	88,5	96	220	—	30	38
R65	180	150	45	75	18	78,5	95	220	—	36	36
R50	152	132	42	70	15,5	68,5	66	150	140	27	35
R43	140	114	42	70	14,5	62,5	56	110	160	25	33
I-a	140	125	44	70	14	60,5	56	110	160	25	33
II-a	135	114	40	68	13	59,5	56	110	160	25	33
III-a	128	110	37	60	12	57	56	110	160	25	33
IV-a	120,5	100	40	58,5	12	51	56	110	160	23	31

Continuation

Rail type	Weight of one running m, kg.	Cross-sectional area, cm^2	Distribution of metal based on rail profile, cm^2		
			head	web	base
R75	75,10	95,80	31,00	27,30	37,50
R65	65,08	83,12	28,36	23,96	30,80
R50	51,514	65,80	25,45	15,64	24,71
R43	44,653	57,00	24,40	12,20	20,40
I-a	43,567	55,64	25,55	10,73	19,36
II-a	38,416	49,06	22,27	9,72	17,07
III-a	33,48	42,77	18,39	8,51	15,87
IV-a	30,89	39,45	17,71	9,35	12,39

Rail Length

Table 3

Rail type	Length of rail, m.	
	Normal	Shortened for curves
R75, R65, R50, R43	25,0	24,96; 24,92; 24,84;
R50, R43, I-a, II-a, III-a, IV-a	12,50	12,46; 12,42; 12,38

NOTE: The numerical indicator in the rail type designations, e.g. R50, indicates the rounded-off weight of one running meter of rail in kg.

2. Normal working conditions of rails in track.

When trains are in motion, diverse forces act on the rails, causing significant stress and deformation in them. The magnitude of these stresses may vary sharply, depending on the condition of the track, the tread area of the rolling stock wheels, the action of leaf springs, etc. The most common

cause of all possible types of rail damage is unsatisfactory routine maintainance of the line (spikes poorly driven, poor quality joint maintainance, the presence of impacts, places where the track is out of alignment, and poorly anchored track), sharp deviations of the track position in plan and profile, and other track deficiencies.

Timely prevention of disorders and defects in the track is the primary condition for normal rail operation.

Care of the rail begins from the moment they are loaded and unloaded from the platforms. When rails are carelessly unloaded and when they are tossed from the platform, the rails are frequently subjected to blows and bending, as a result of which dents and scratches in the metal, subsequently developing into dangerous cracks, appear on their surface. It is also necessary to protect the rails from blows from spike hammers and other track maintainance equipment in the process of servicing, inasmuch as sharp dents on the edge of the base or the rail are often the origin of transverse cracks in these places.

Normal rail operation may be guaranteed by observing all of the technical rules for laying track and maintaining them while in use.

Rails are removed from the track either due to excessive wear occuring over a period of several years, or when cracks which are dangerous for railroad traffic are detected in the rails.

The rail head is subject to the greatest wear since the wheels of the rolling stock move directly over it. Rail head wear takes place as a result of simultaneous wear and compression of the metal. The rail head wears due to friction of the tread of the wheels when passing over the running surface.

The high effectiveness of rail lubricants has been demonstrated by observations conducted over several years as well as the experiences of domestic

and foreign rail lines. Lubricating the rails on curves decreases the intensity of rail wear by 3-4 times and significantly increases the mileage between the times when the wheels must be reprofiled.

Compression is observed in rails prepared from soft steel, the deformation of the metal extending to great depth. The layers of metal on the surface and inside the rail are displaced, i.e. the rail steel flows. As a result of this, the rail is crushed and loses its original form.

On track sections where there are tight curves or steep descents or grades, the rails wear away significantly more quickly than on the straightaways.

Under the influence of the compression forces from the tread of the rolling stock wheels, the metal on the running surface of the rail head undergoes significant changes: the grains of metal are flattened and become very hard. Such an increase in the hardness of a metal is called 'work hardening'. Due to this work hardening, as the length of time the rails have been in service increases, the intensity of their wear gradually decreases.

Work hardening of the running surface along a length of rail may be uniform or non-uniform. The utilization of flaw detectors is significantly more complicated on rails having non-uniform work hardening.

Rail resistance to wear may be increased by hardening. The hardness of the metal on the surface of the rail head is significantly increased with the hardening process. The depth of the hardening may reach 5-10 mm.

New rails are immediately hardened at the mill, the rails being hardened along the entire length or just at the ends. Rails which are hardened along the entire length at the mill are subjected to reheating. Their ends are hardened after a high frequency current pre-heating. Bulk rail quenching along the entire length is carried out by submerging the entire rail in a

special oil bath. Surface hardening along the entire length is carried out by submerging the upper portion of the rail head in water, by spraying water over the head surface, or by blowing moist, compressed air over the rail head.

3. Classification of rail fractures and flaws.

The causes of fracture and flaw formation in rails. The most important railroad parameters upon which rail failure from fractures and other flaws depends to the greatest degree are the gross tonnage transported along the rails, axle load of the rolling stock, and the speed of the trains.

Rail failure due to flaws and fractures also depends on the time of the year: it is minimal in the summer, increasing in the autumn, and reaching a maximum in the winter (associated with an increase in the brittleness of the metal as the temperature decreases). The greatest number of rail failures occurs in the months of lowest temperatures. A second maximum for rail failures comes in March in the European USSR and in April for the lines in Siberia and the East. This maximum corresponds to the time at which the ballast thaws, and is conditioned by the spring-time period when the tracks are in the greatest need of repair.

Depending on the plan and profile of the track, the greatest rail failure from flaws is observed on grades or descents and on the curved sections of the track. The greatest quantity of flaws in rails arises in anchored rail on small radius curves.

The reasons for fractures and flaws arising in rails on the line are extremely diverse. Lengthy observations and study of the conditions for rail operation have permitted several generalized causes to be established. They may be divided into two groups: operational, e.g. the unsatisfactory condition of the track or the rolling stock, and manufacture, e.g. the presence of flaws originating when the rails are being manufactured. The unsatisfactory condi-

tion of the line or the rolling stock promotes an accelerated rate of failure due to manufacturing causes.

The most commonly encountered types of flaws and rail damage and the reasons for their appearance and development are presented below.

1. Flaking and pitting of the metal on the running surface of the rail head (Fig. 3) appears primarily because of inadequacies in rail manufacturing technology. As the rolled rail cools, cavities from gasses which did not escape are formed throughout. Such gas cavities are both inside the ingot and near its surface. When the rails are rolled, the cavities situated right at the surface of the ingot in many cases emerge onto the rail surface in the form of so-called hair-line cracks, overlaps and scabs. These flaws, unnoticed when the rails are accepted at the mill, lead to the formation of flaking and pitting of the metal on the running surface after the rolling stock has begun to move over the rails. This type of rail damage is easily detected using the usual (visual) inspection methods.

2. Pitting of the metal on the gage-side of the rail head (Fig. 4) arises basically because of inadequate contact strength in the rail owing to contamination of the metal by non-metallic inclusions extending in the direction of rolling in the form of mechanical fibering situated at a depth of 3 - 8.5 mm below the running surface. The microscopic cracks which originate in these places propagate slowly (fatigue related) in the form of oval spots which become longitudinal slanting cracks. While the rails are in service, the upper metal layer over this crack undergoes a second period of work hardening, and it pits. This type of flaw is most frequently observed on the gage side of the rails on the outside line of the track on curves. In the initial stage of development, these flaws may be detected using an ultrasonic flaw detector, and at later stages of development, by external observation.

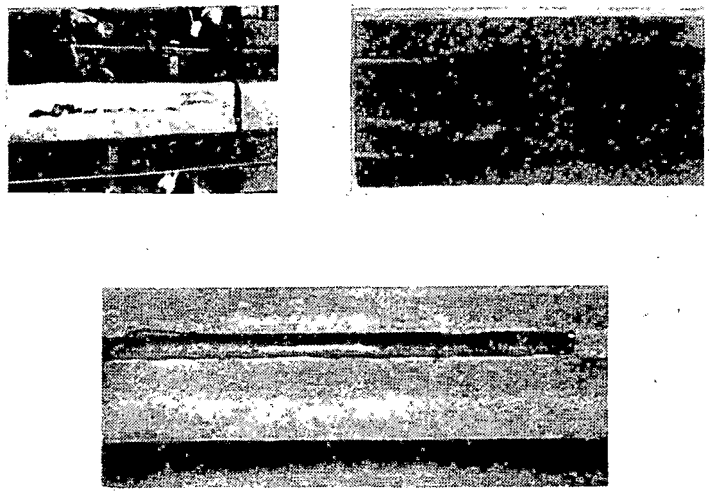

Fig. 3 Samples of flaking and pitting of the metal on the running surface of the rail head.

Fig. 4 Metal pitting on the gage-side of the rail head.

3. Engine burns and thermal cracks in places of wheel slippage (fig. 5) are observed primarily on rails lying in front of entry signals on tracks by a station, especially near the tanks where water is taken on, and on sections of the track where braking is required, etc.

When starting off or braking sharply, the wheels of the engine and cars rub against the metal with great force and, as a result, an intense heating of the surface layer of the rail metal takes place. Because of the high thermal conductivity, the heated surface layer of the rail head cools very quickly and hardens. Thermal cracks form on the running surface of the rail head because of the sudden hardening. As the rails remain in service, these cracks gradually spread to the interior of the rail. Being very fine, they serve as a source for sharp concentrations of stress. Given the impact effect of the wheels, especially at low temperatures, rails with this type of damage fracture easily. Such rail flaws are easily detected by external examination.

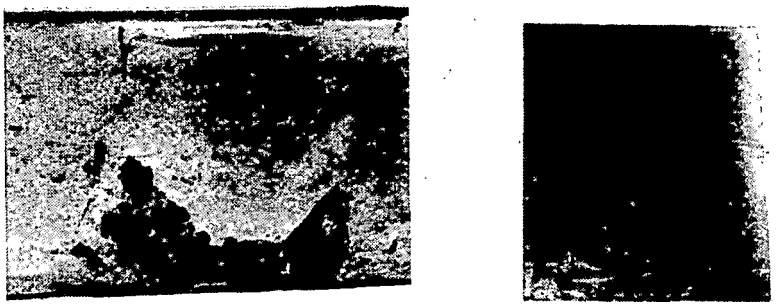

Fig. 5 Engine burns and thermal cracks in places of wheel slippage.

4. Pitting and flaking of the metal on the running surface in the worked layer of the rail head (fig. 6) arise in the metal because of unsatisfactory hardening. Here, sections with a metal structure having great hardness and brittleness, or local, non-uniform changes in hardness from hardened to non-hardened metal, are formed in the worked layer. The effects of the wheels of the rolling stock on the rails forms pitting and flaking in these places. A similar type of damage may take place near the rail ends because of poor face hardening. A weld joint of unequal strength between the weld and the parent metal leads to pitting or to the separation of the welded layer.

This type of damage is detected by external examination and by ultrasonic flaw detectors.

5. Transverse fatigue spots in the head (in the form of light or dark spots) and fractures because of them. The internal transverse fatigue crack in the form of a light or dark spot must be considered the most dangerous type of rail flaw. The particular danger of this flaw is conditioned by the fact that it originates and propagates inside the rail head, without any external signs. Even when this crack emerges onto the surface, it is almost impossible to notice it. The danger of this flaw is heightened even more by the fact that such cracks may originate simultaneously in several places in a rail, as a result of which the rail fractures suddenly into many pieces under the weight of the train.

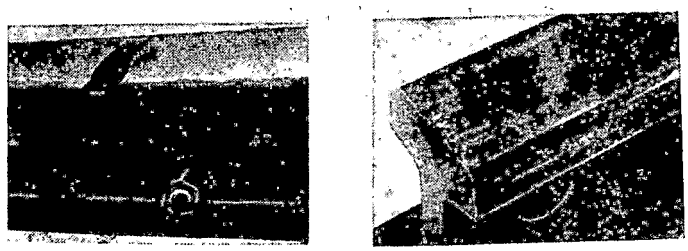

Fig. 6 Pitting and flaking of the metal of the running surface in the worked layer of the rail head.

There are two primary reasons for the formation and propagation of transverse fatigue cracks. The first is the presence of microscopic shatter cracks (flakes) inside the head which are usually situated at a depth of not more than 10 mm from the running surface of the rail.

The flakes are grainy shatter cracks from which fatigue cracks propagate radially under the influence of the load from the rolling stock (fig. 7).

There is a particularly large number of such shatter cracks in rails which were not subjected to delayed cooling or holding in special furnaces after rolling, or which were subjected to such processing, but with violations of the technical conditions. To avert the formation of flakes, all rails undergo delayed cooling in special boxes at the rail manufacturing plants. For this, the rails are cooled to 528-540° C. on racks after rolling and cutting. At the indicated temperature, the steel takes on magnetic properties, which permits the rails to be placed in specially insulated thermal boxes with the aid of magnetic cranes. The boxes are closed with thermally insulated covers and remain covered no less than ten hours. During this time, the gases which had not previously escaped, primarily hydrogen, succeed in evaporating (diffusing), since at this temperature the rail metal still retains its plastic properties. Loading and unloading of the boxes is necessarily done with care to reduce the bending and the cold truing to a minimum.

As a result of operations associated with delayed cooling, flaking is very seldom encountered in rails manufactured in the USSR since 1949.

Fig. 7 Transverse cracks in the rail head caused by flakes and gas bubbles.

Fig. 8 Transverse cracks in the rail head originating from inadequate contact fatigue strength of the metal.

The second cause for the origination and propagation of transverse cracks is not associated with the presence of flakes in the rail head. The beginning of these transverse cracks (fig. 8) originates from undeveloped, internal, longitudinally oblique cracks arising from the large contact stresses experienced by the running surface of the rail head as a result of the effect of the wheels of the rolling stock.

Transverse shatter cracks develop from those longitudinally oblique cracks which are in the zone of residual tensile stresses at a depth of from 2-8 mm. Transverse fatigue cracks originating due to high contact stress develop primarily on the gage side of the rail head. The overwhelming majority of cracks originating from the presence of flakes propagate from the field side of the rail head.

Transverse fatigue cracks have an elliptical form at the start of their propagation, then they take on their own configuration, which approaches the outline of the rail head in profile.

In the fracture, the surface of these spots is light and silvery, which distinguishes it from the remaining grainy fracture of the rail. If a similar

crack emerges onto the surface in the course of development, air comes in contact with it, and, upon oxidizing, the surfaces of the crack grow dark. In the fracture, the surfaces of such a crack have the shape of dark spots.

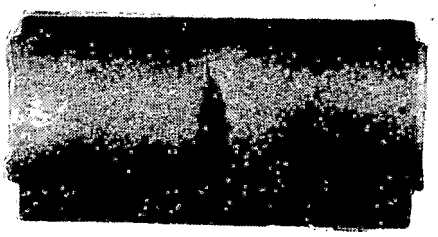

Fig. 9 Transverse cracks in the head as a result of mechanical damage by wheels with flat spots.

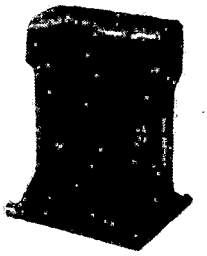

Fig. 10 Transverse cracks in the head from blows with a track maintainance implement or one rail against another.

When examining the rail fractures from the indicated flaws, it is easy to determine the cause from which one or another fatigue spot develops. On the surface of spots developing from flakes, flakes in the form of round, grainy shatter cracks will be easily visible. On the surface of fractures from cracks which developed because of high contact stress, the line of the longitudinally oblique crack will be visible in the rail head. On the surface of the transverse fatigue crack which resulted from contact fatigue stress,

the initial shatter cracks (flakes) in the metal will not have visible centers.

6. Transverse cracks in the head as a result of blows from wheels with large flat spots, track maintainance implements, and one rail against another (fig. 9, 10) develop because of various types of mechanical damage arising as wheels with large flat spots pass over the track, from blows to the track head from track maintainance implements, or blows from knocking rail against rail, etc. Nicks which are stress concentration points appear on the running surface of the rail, and these may serve as places for the formation of cracks even under normal loads. The crack develops rapidly and leads to rail fracture.

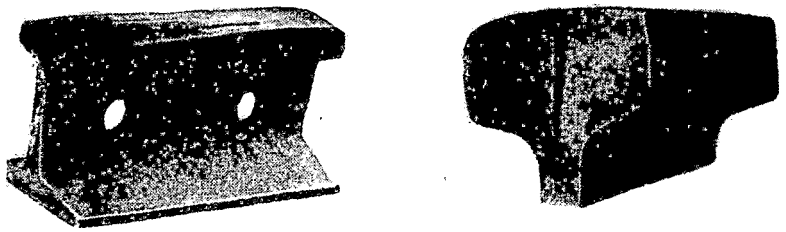

Fig. 11 Vertical splitting of the rail head.

7. Vertical splitting of the rail head and web (fig. 11, 12) represents one of the groups of dangerous flaws. The vertical cracks most often arise in the inner part of the head and may be found both on the ends of the rail as well as at any place along the length. Similar cracks are frequently detected in the rail web.

The presence of residue from a shrinkage cavity, contamination of the metal by non-metallic inclusions, and the build-up of harmful mixtures of phosphorus and sulphur in the metal are the basic causes of splitting in the rail head and web. These factory defects are primarily characteristic of lead rails, i.e. rails cut from the top end of the rail stock, corresponding to the upper part of the ingot.

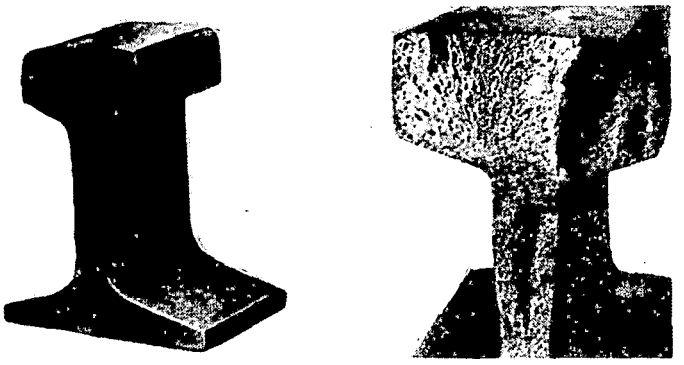

Fig. 12 Vertical splitting of the rail web.

Vertical splitting of the head frequently arises during the first years of service on the line. This flaw is relatively easily detected by a dark band on the running surface. As a result of the effect of the rolling stock wheels, a shiny longitudinal band forms on the surface of the rail head. If the rail is sound and has no internal vertical crack in the head, the running band will be the same color over the entire length and width of the rail. With the rails maintained at the proper cant, this band passes down the center of the head. If, on the other hand, there is an internal vertical crack in the rail head, a dark stripe, which is sharply distinct on the silver running band, will appear above this crack. It may be easily detected by the naked eye.

Formation of the dark stripe over the vertical crack is explained by the fact that when the wheels roll along the rail, a thin layer of metal is compressed over the crack, under the pressure of the wheel tread, and a long groove in the form of a dark band appears on the surface of the head. In addition, the rail head will be broadened in this place when a vertical split is present since the surfaces of the crack separate and the crack becomes

wedge shaped from pressures from the rolling stock wheels.

Films of crushed metal under which longitudinal cracks are detected are sometimes observed on the dark band where the head expands. The development of such flaws is accelerated when the line is not maintained satisfactorily (the presence of places where the track is out of alignment, as well as improper elevation of the outside rail on curves).

In the initial development stage, such flaws are detected by flaw detectors, and when they emerge onto the surface, they may be detected by external examination.

7a. Horizontal splitting of the rail head arises and develops principally in the center portion of the head (Fig. 13). This type of flaw is observed both at the joint and along the entire rail length.

Along with contamination of the metal with non-metallic inclusions, the presence of gas bubbles and flakes extending along the direction of rolling is the primary cause of horizontal splitting of the rail head.

Such defects are primarily detected by flaw detectors. Well-developed horizontal cracks may also be detected upon external inspection.

8. Longitudinal or oblique cracks in the web from the bolt or other holes (Fig. 14). As is known, the joint section is the least durable part of the rail. At the same time, this portion of the rail is subjected to the greatest effect from impacts from the rolling stock wheels when they pass across the joint clearances. On rail sections where the rail joints are poorly maintained, where there are impacts, spillage, sagging of the rail ends, abnormal joint clearances, broken cover plates, or the nuts of the joint bolts not being snuggly tightened, etc., the stress in the joint sections of the rails is several times greater than at well-maintained joints. Exceptionally high stress arises around the edges of the bolt holes.

Fig. 13 Horizontal splitting of the rail head.

Shatter cracks caused by the boring process and corrosion accelerate the crack formation process.

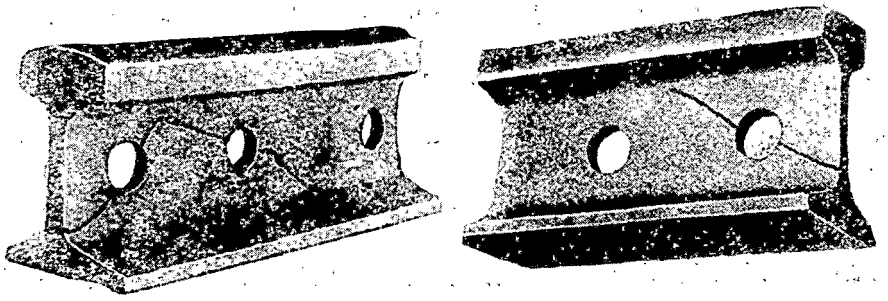

Fig. 14 Oblique or longitudinal cracks in the web from the bolt and other holes.

Experience shows that in all instances where the joint portion of the rail fractures, an old crack serves as the beginning of the fracture. By 'old crack' we have in mind the area of gradual propagation of a fatigue crack which was subjected to corrosion. A crack in the butt-end of the rail under the head grows first along the web in the fillet, and then, at a distance of 50-60 mm from the butt-end it turns upward at an angle to the rolling surface of the rail head. This leads to a piece of the head splitting off.

Cracks passing through the bolt holes always begin in definite places near the surface of the hole and run along the web at an angle of approximately 45° to the longitudinal axis of the rail.

The number of rail fractures at the joints depends significantly upon the length of service of the rails. In the first years of rail service, fractures at the joints are very rarely encountered. With an increase in the period of service, this type of flaw becomes more wide-spread; for old rails it is the most typical.

A sharp increse in rail failure due to joint fractures is observed in the spring when the ballast is thawing out, as well as in the fall when the ballast freezes. On curves, flaws in the joint section of the rails develop more often in the inside rail. On sections with two tracks, flaws arise primarily on the receiving rail end. Cracks and splitting are most frequently encountered up through the first bolt hole. Splitting off of the rail head along a crack beyond the bolt hole is the next most frequent flaw type.

Timely detection of cracks in the joint area of the rails within the boundaries of the cover plates has great significance since rail fractures along these cracks cause accidents or train wrecks.

Fig. 15 Slanted or longitudinal cracks in the web beyond the joint area.

Cracks developed through the bolt holes and emerging onto the butt-end of the rail, and cracks from the butt-end of the rail under the rail head may be detected by striking the rail ends with a hammer. The most highly perfected and reliable method, however, is that of monitoring the rail joints with the aid of an ultrasonic flaw detector.

9. Oblique or longitudinal cracks in the web beyond the joint area of the rail (fig. 15) arise and develop in the web in those places where the markings are stamped, or in places receiving damage from blows from track maintainance equipment, where a concentration of stress, leading to the formation of shatter cracks and other cracks, takes place. It is possible to detect developed flaws of this type during careful external examination. In the early developmental stage, such cracks are detected only by ultrasonic flaw detectors

10. Hair line cracks in the base, cracks, and broken places in the base (fig. 16). One of the widespread and dangerous flaws is a longitudinal crack in the base of the rail. The presence of such a crack often leads to a broken base or to its unexpected brittle fracture under a moving train.

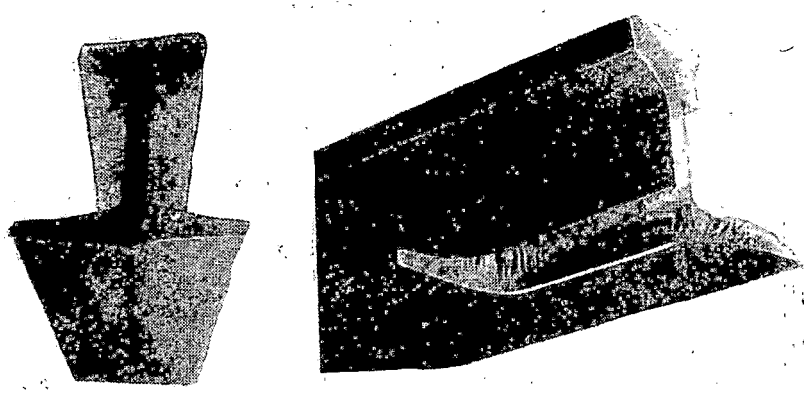

Fig. 16 Hair line cracks in the base, cracks and broken places in the base.

Brittle rail fractures take place, as a rule, close to the cross-tie, near the edge of the base plate, and places where the base is broken are on the cross-tie in an overwhelming majority of cases. This is explained by the fact that the crack along the base develops primarily where the base is supported by the base plate.

Hairline cracks and surface overlaps arising during rolling, primarily in the center third of the width of the rail base, provide the beginning for the formation of cracks along the base. The hairline cracks appear primarily as a result of flattening the gas bubbles which lie under the surface in the ingot. Overlaps along the center of the base are formed as a result of improper adjustment of the rollers used to roll out the ingot. In their external appearance and the extent to which they are dangerous, overlaps resemble hairline cracks. Hairline cracks are usually rolled out so much that it is impossible to notice them from external examination of the rails at the mills. It is for this reason that such rails come to be used in track. Under usage conditions, hairline cracks or overlaps rapidly pass from longitudinal to transverse cracks, under the effect of the loads from the moving trains. They weaken the cross-section of the rail, and, as a result, lead to fracture.

These cracks develop rapidly when the base of the rail is not laid firmly on the base plate since under these conditions the rail is subject to transverse bending.

A loose or improper fitting of the rail base to the base plate may be due to concavity of the upper supporting surface of the base or of the base of the rail itself, because of twisted rail or because of the base plate being positioned askew, because of improper rough-hewing of individual cross-ties when the rail is supported by one edge of the base, because of hidden impacts, etc. Similar destruction of the base may arise as a result of inadequacies

in the rail profile, inadequate thickness of the base, and inadequately small radius of the lower fillet.

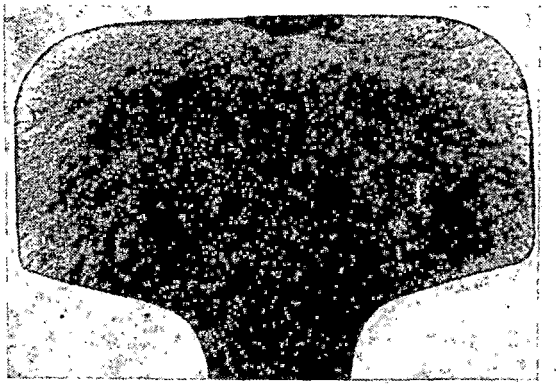

Fig. 17 Thermal cracks in the heads of hardened rails.

The greatest failure due to cracks in the base is observed in the first years of service, especially in the winter and spring periods.

Well-developed cracks may sometimes be detected in the lower fillet near the base plates during careful rail examination. If a light brown stripe is detected in this place, the rail is taken from the track and the bottom surface of the base is carefully examined. Cracks with a depth of 3 mm and more originating in the central part of the base within the thickness of the web may be detected by ultrasonic flaw detectors.

11. Thermal cracks (fig. 17) arise primarily in the rail head because of breaches of tempering technology at the rail manufacturing plants. Such cracks may be formed as a result of unequal heating and cooling of the rails during the tempering process. It is possible to detect such flaws only by using magnetic flaw detectors. Rail failure due to thermal cracks is observed in the first years of service, especially in the winter and spring periods. New tempered rails which are laid in a track should be tested using flaw detectors

before trains are permitted to pass over them in order to prevent rail fracturing due to thermal cracks.

12. Cracks in the head due to welding or rail connectors (fig. 18) originate and propagate because of improper welding procedures. Small weld cracks which subsequently develop into transverse and, sometimes into longitudinal cracks, leading to fracture or splitting off of a piece of the rail head, originate in weld spots.

Such cracks are detected by ultrasonic flaw detectors and by external inspection of the rail joints.

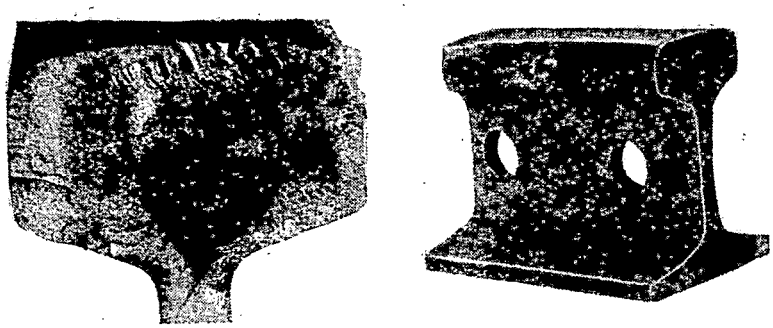

Fig. 18 Cracks in the head due to welding of rail connectors.

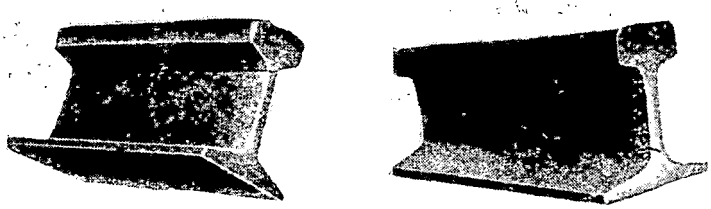

Fig. 19 Longitudinal cracks in the upper and lower fillet areas.

13. Longitudinal cracks in the upper and lower fillet areas (Fig. 19) are most often encountered in old rail types. These cracks are very fine, and, in the initial stage of development, appear as a series of small, serrated shatter cracks. As the flaw develops, the fine shatter cracks join and form a very long, thin crack under the head. In certain instances, this crack passes inside the head and appears because of the presence of an internal vertical separation (piping) in the head. Such cracks appear in the first years of rail service.

The majority of these cracks in the upper fillet are not associated with the presence of piping in the rail head. These cracks spread from the surface into the interior of the rail web in the horizontal plane. Such cracks usually develop in rails after many years of service. They represent cracks from corrosion fatigue arising as a result of a concentration of stress in the upper fillet.

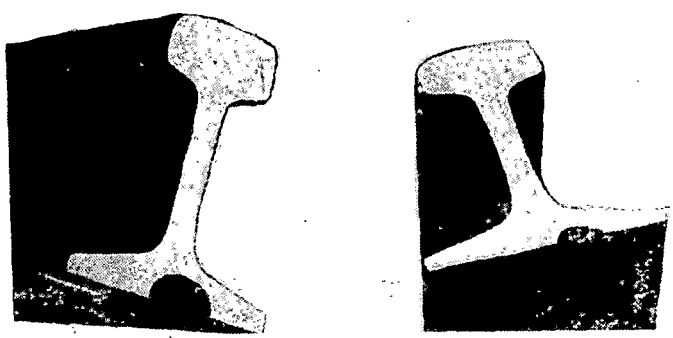

Fig. 20 Transverse corrosion fatigue cracks in the base of the rail.

It is known that stresses in the rail are unequally distributed. In those places where there is any kind of nick, hole, or sharp change from one cross section to another, an increase, or, as is said, a concentration,

of stress always takes place. The sharper the nick and the smaller the fillet conjunction areas, the greater will be these stress concentrations.

Stresses concentrated in the upper fillet are significantly increased when the cant at which the rails are laid is incorrect, i.e. when the transfer of the pressure under the wheels is not central, when the track is improperly maintained (level and gage), when the track has been improperly straightened, upon heavy lateral blows from the wheel tread, etc. The local over-stresses arising under these conditions and metal corrosion lead to gradual development of corrosion fatigue cracks.

Cracks in the lower fillet are encountered significantly less frequently. They appear to be corrosion fatigue cracks arising because of the concentration of stresses caused by the small conjunction radius.

The indicated type of crack is relatively easily detected upon examination of the rails: usually near the place where there is such a crack, a dark brown band, easily visible by the eye with the aid of a mirror, forms along the entire crack. Reliable detection of these cracks is assured using ultrasonic flaw detectors.

14. Transverse corrosion fatigue cracks in the base of the rail (fig. 20) are a new and extremely dangerous type of flaw. This type of rail damage originates and propagates on portions of the tracks with separate fastenings in places where a padding, e.g. a piece of wood, with a high moisture capacity is inserted between the base plate and base of the rail. Moisture which has penetrated into the padding causes intensive corrosion of the rail base. As a result, pockets, which are stress concentrators, form in the base, leading to the formation and propagation of transverse fatigue cracks.

The danger from transverse corrosion fatigue cracks located in the base is particularly great since these cracks are located in an extended zone,

which leads to rail fracture, even with cracks having a small area.

15. Cracks in welded joints (fig. 21) arise primarily due to the presence of silicate inclusions, bubbles, areas of porosity, poor fusion, crater shrinkages, and unsatisfactory working of the weld seam in the welded joints.

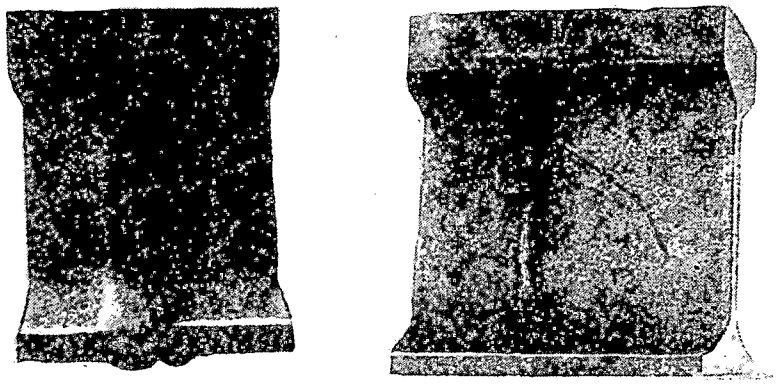

Fig. 21 Cracks in welded joints.

When using welded joints, transverse cracks in the head, oblique and longitudinal cracks in the web, and cracks in the base most frequently develop under the effect of the alternating loads.

Welded joint monitoring is accomplished with ultrasonic flaw detectors in rail welding plants as well as on the line.

16. Transverse cracks in the rail base from impacts and other mechanical damage (fig. 22). Gashes appear on the rail surface as a result of impacts to the rail from an implement, rail hitting against rail, and other mechanical damages.

Places of mechanical damage are stress concentrators, and may serve as places for the formation of cracks, even under normal load. Cracks of this type develop quickly and often lead to rail fracture, especially at low temperatures.

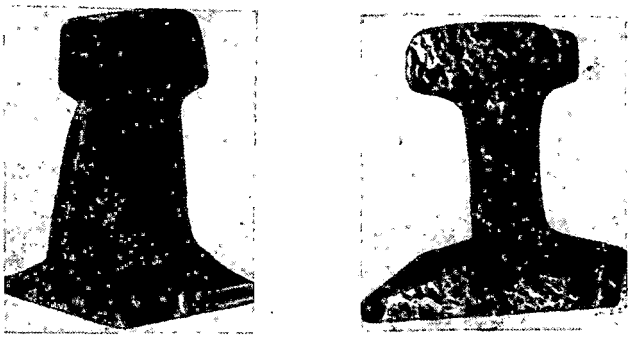

Fig. 22 Transverse cracks in the rail head and base from impacts and other mechanical damage.

17. Transverse rail fractures without visible flaws in the fracture (fig. 23). Brittle rail fractures without visible rail flaws are seldom encountered. Such fractures usually take place suddenly under the trains. It is not possible to prevent this type of fracture by a timely removal of dangerous rail from the line. Brittle fractures are observed primarily in the first years of rail service. The primary cause of brittle fractures without visible flaws is the violation of the normal rail production process, as a result of which rail quality is lowered and sections of brittle rail find their way into the track. These rails fracture in the first years of use and continue to fail until the most unsatisfactory ones are rejected for scrap. The highest quantity of brittle rail fracture is observed in winter at temperatures of -15° C. and lower, especially after passage of a train including cars with dents and flat spots on the wheel treads.

Brittle rail fractures are distinguished from other fractures by the new, shiny, grainy surface without smooth light or dark incipient fatigue cracks. From the point of origin of a brittle rail fracture, convex corrugations

spread out on the surface in a fan-shaped pattern, creating the wavy structure of the fracture. This structure of the brittle fracture permits its point of origin to be unerringly determined. Experience shows that, for the majority of brittle fractures, the presence of fine hair-line cracks along the center of the base of the rail is typical. These cracks, as exceptionally acute stress concentrators, serve as the beginning of the brittle fracture.

Classification of flaws.

In 1934, a system for classifying defects and damage to rails was introduced to allow accurate records to be kept concerning the removal of defective rails from the lines, for the organization of operative rail statistics and for improving the supervision of defective rail reporting. All of the varieties of flaws in rails were grouped into nine basic types. The common characteristics of the forms of destruction and their basic cause was taken as the basis for such a grouping (classification) of defective rails. Here, each typical rail flaw is numbered with a two-digit number. The first digit indicated the common characteristics of one group of flaws and determined the type of flaw. The second digit was unique for each flaw and determined the varieties or the sequential stages of its development.

A record of defective rails on our railroads was kept until January, 1967, according to this system.

Beginning January 1, 1967, a new, standard classification of flaws and rail damage, according to which all rails which are removed from track and which are unsuitable for further use are taken into consideration, was introduced on the railroads of the USSR, Czechoslovakia, the German Democratic Republic, and other Socialist countries.

In the new classification, all flaws, rail damage and fractures are numbered with a three-digit number (flaw number), e.g. 17.1; 21.2; 26.3; etc.

Fig. 23 Transverse rail fractures without visible flaws in the fracture.

The first digit of the number defines the type of flaw or rail damage, as well as the location of the flaw in the rail cross-section (head, web, base).

Types of flaws or rail damage (designated by the first digit) are subdivided in the following matter:

The digits 1, 2, 3, 4 indicate that the flaw is situated in the rail head; 1 - flaking or pitting of the metal on the running surface of the rail head; 2 - transverse cracks in the head and fractures along them; 3 - longitudinal, vertical, and horizontal cracks in the head; 4 - crushing and unequal wear of the rail head.

The number 5 indicates that the flaw or damage is located in the web.

The number 6 indicates that the flaw is located in the base.

The number 7 indicates that a fracture took place throughout the entire cross-section of the rail profile.

The number 8 indicates a bend in the rail in the vertical or horizontal plane.

The number 9 indicates other types of flaws and damage.

The second digit indicates the variation of the flaw or damage, taking into account the basic cause for that defect variety.

The flaw variations designated by the second digit are classified as follows:

0 - flaws and damage associated with inadequacies in rail manufacture technology;

1 - associated with inadequate contact-fatigue strength of the metal;

2 - those determined by inadequacies in the rail profile or by construction of the joint fastening;

3 - arising in connection with inadequacies in routine track maintainance;

4 - resulting from the abnormal effect of the rolling stock on the rails (wheel slippage, flat spots, and others);

5 - caused by impacts from an implement, and other mechanical effects;

6 - associated with inadequacies in welding technology;

7 - connected with defects in tempering technology;

8 - depending on inadequacies in the face hardening of the rails or of the welding of rail connectors;

9 - flaws and damage associated with other causes not enumerated above.

Frequently, a flaw or rail damage arises for several reasons. Thus, inadequacies of track maintainance accelerate the development of flaws. The variations in flaws and damage are classified, based on their primary cause. Thus, for example, a crack in the base of the rail which developed because of hair-line cracks is classified with the digit 0. The 0 indicates an inadequacy in the manufacturing technology.

The first two digits are seperated by a period (.), after which follows the third digit, indicating the location of the flaw along the rail length.

The numerical designations for the location of a flaw or damaged spot along the rail length, as well as the type of joint welding, are established as follows:

1 - a flaw in the joint (at a distance of up to 75 cm from the butt-end);

2 - a flaw beyond the joint;

3 - a flaw at the point of electric contact welding of the rails;

4 - a flaw at the point of high-speed thermal welding;

5 - a flaw at the point of standard thermal welding;

6 - a flaw at the point of oxy-acetylene welding;

7 - a flaw at the point of gas fusion welding;

8 - a flaw at the point of electric arc welding.

Flaws arising in the rail at a distance of up to 10 cm on either side of a welded seam are considered to be weld joint flaws.

In all, there are thirty-eight types of flaws in the classification, and, taking into consideration their division according to the location along the length of the rail and according to the type of rail weld, one hundred varieties are numbered. The flaw classification system is presented in systematic form in Fig. 24. According to this classification, for example, a rail flaw with the number 10.2 may be interpreted thus: a flaking or pitting on the rolling surface of the rail head (indicated by the number 1); associated with inadequacies of rail manufacturing technology (indicated by the second number, 0); the flaw is located beyond the joint (indicated by the third number, 2). Other numbers for flaws in rails are interpreted in the same manner.

After a defective rail is removed from the line, the flawed place is carefully examined, and a number is established for the defect, based on the

classification. The flaw number (figure) is recorded in a PU-4 accounting form.

Fig. 24 Classification of flaw and rail damage types

1st Group--Flaking and pitting of the metal on the surface of the rail head

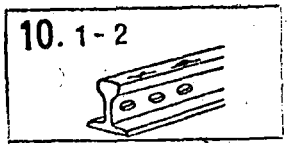

Flaking and pitting because of hair-line cracks, overlaps, scabs, etc.

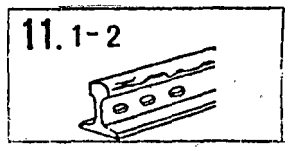

Pitting on the gage side of the head due to inadequate contact-fatigue strength of the metal

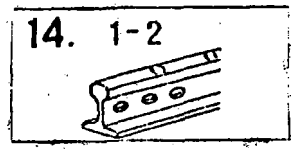

Engine burns and transverse cracks as a result of wheel slippage and sliding

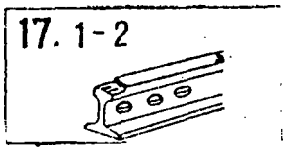

Pitting of the hardened layer

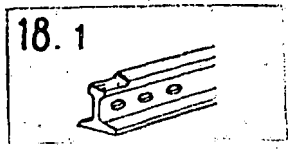

Pitting of the welded layer

2nd Group--Transverse cracks in the rail head and fractures due to them

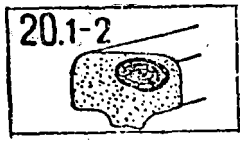

Because of internal shatter cracks (flakes, gas cavities, etc.)

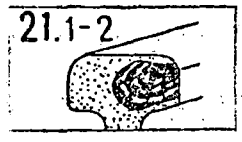

Due to inadequate contact-fatigue strength of the metal

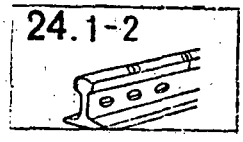

Transverse cracks caused by the passage of wheels with flat spots

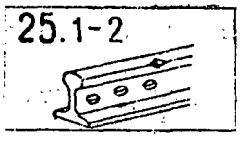

Caused by impacts along the rail, or other types of damage

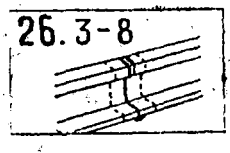

In a welded joint

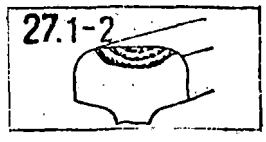

Thermal cracks in the hardened layer of metal

3rd Group--Longitudinal cracks in the head

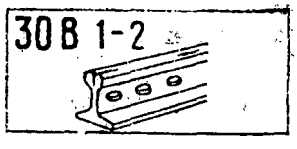

Vertical separation of the head

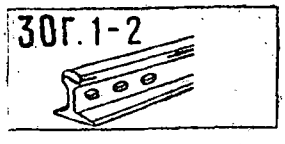

Horizontal separation of the head

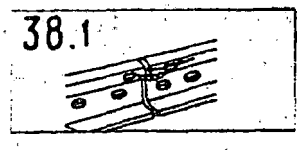

Caused by welding of the joint connections

4th Group--Crushing and uneven wear of the head

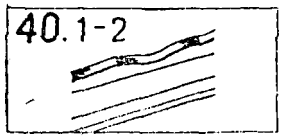

Corrugated deformation of the head (broadly separated)

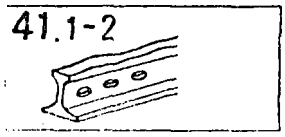

Crushing due to inadequate metal strength

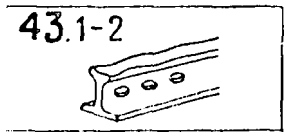

Crushing on the head of the inside rail on a curve due to overloading

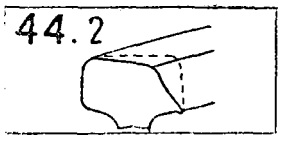

Lateral wear exceeding acceptable standards

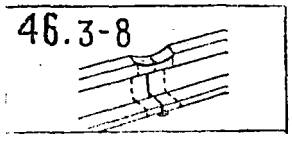

Crushing in the shape of a "trough" at the point of a welded joint

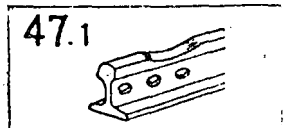

Crushing in the form of a "trough" beyond a hardened end

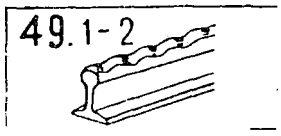

Corrugated deformation of the head (narrowly separated)

5th Group--Flaws and damage to the web

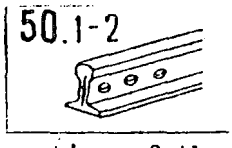

Separation of the web

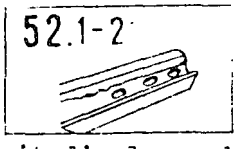

Longitudinal crack in the web under the head and near the base

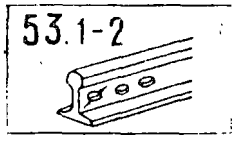

Cracks from bolt holes

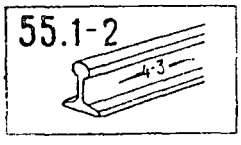

Longitudinal crack in the center of the web

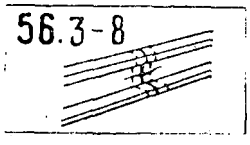

Cracks in the web in a welded joint

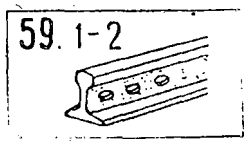

Corrosion of the web

6th Group--Flaws and damage to the base

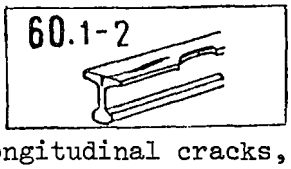

Longitudinal cracks, broken places in the base, and rail fracture due to hair-line cracks in the base

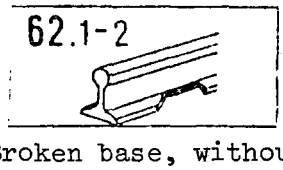

Broken base, without visible flaws in the metal

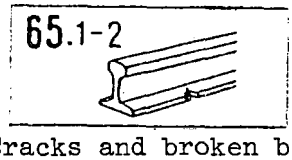

Cracks and broken base due to damage from blows

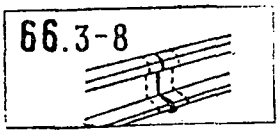

Cracks in the base of a welded joint

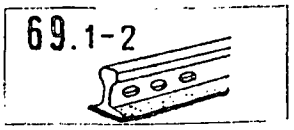

Corrosion of the base

7th Group--Rail fracture throughout the entire cross-section (other than fractures in the 2nd Group)

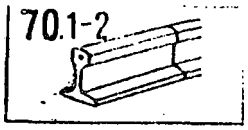

Because of slag inclusions and other flaws in the metal

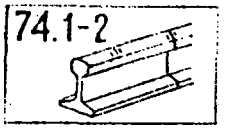

Caused by the passage of wheels with flat spots

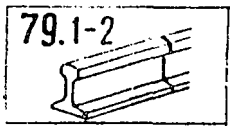

Without visible flaws in the fracture

8th Group--Bending of the rails

Bending of the rails in any plane

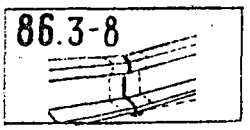

Bending at a welded joint

9th Group

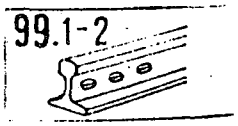

Other flaws

CHAPTER II -- ELECTROMAGNETIC FLAW DETECTION METHODS

1. A Brief Summary of Ferromagnetism

The detection of hidden defects in steel railroad rails using electromagnetic methods is accomplished by magnetization of the rails in the force field of an electromagnet or a permanent magnet. Based on its properties, rail steel should be related to the group of ferromagnetic materials because it magnetizes strongly in a relatively weak magnetic field and preserves a significant portion of the magnetization which was transmitted to it. In all, only four of the chemical elements known today possess ferromagnetic properties, iron, nickle, cobalt, and gadolinium. However, the number of different ferromagnetic materials which are alloys of ferromagnetic elements both with each other and with non-ferromagnetic elements is extremely large.

Electromagnetic properties arise due to the presence of elementary magnetism carriers (electrons moving inside the atom) in the steel atom, and due to the special interaction among several electrons of neighboring atoms. The latter is closely associated with the crystal structure of ferromagnetic materials.

According to contemporary concepts, an atom of any substance has a complex structure consisting of a positively charged nucleus, and negatively charged electrons revolving around it. Any movement of an electron, i.e. movement of an electrically charged particle along a closed path of extremely small dimensions, is similar in every respect to the electrical current $\underline{i}$ in this path.

This elementary electrical current $\underline{i}$ creates its own magnetic field, and, if there is an internal magnetic field, it exerts an orienting effect on it.

The magnetic moment $\underline{m}$ arises as an electron revolves about an orbit of radius $\underline{r}$.

The magnetic moment is a vector, the numerical value of which is equal to the value of current $\underline{i}$ and the area $\underline{s}$ bounded by the path of this current,

$$\mathbf{m} = \mathbf{i} \cdot \mathbf{s}$$

The direction of the magnetic moment vector corresponds to the perpendicular to the area $\underline{s}$ and is associated with the direction of the current $\underline{i}$ in the path according to the right-hand screw rule. The electron, revolving around the atom nucleus, possesses an orbital magnetic moment. In addition, the orbital moment around the nucleus, the electron rotates on its own axis, which also leads to the formation of a magnetic moment, called the spin moment.

Not all electrons take part in creating the magnetic moment of an individual atom, in fact only a small part of them do. This is explained by the fact that the magnetic moments of the majority of electrons have an opposing direction, and mutually offset each other. As a result, these electrons become neutral with regard to magnetism.

Essentially, the magnetic properties of a substance are determined by a small number of electrons, the magnetic moments of which remained uncompensated. The properties of the atoms of a ferromagnetic substance are completely determined by the presence of electrons with uncompensated spin moments. For a ferromagnetic substance, the presence of uncompensated spin moments is a necessary, but insufficient condition.

The second condition concerns the macrovolume of the substance and is determined by the size of the electrical reaction between the electrons of neighboring atoms and the uncompensated spin moments. The spin moments in the macrovolume of a substance form microscopic regions called domains, or regions of voluntary (spontaneous) magnetization under the influence of these forces. The linear dimensions of the microscopic regions of spontaneous magnetization fluctuates within the range 10^{-6} — 10^{-1} cm^3.

In a demagnetized specimen made from a ferromagnetic material such as iron, the magnetic moments of the individual regions of spontaneous magnetization have a different direction and mutually compensate each other. For this reason, the resultant magnetic moment in such a specimen will be zero. Between the boundaries of the regions there are formed transitional layers, inside of which a constant turning of the magnetic moment vector takes place.

The direction of the magnetic moments of the individual spontaneous magnetization regions is primarily determined by the structural characteristics of the ferromagnetic materials.

In order to note these characteristics, it is necessary to polish the surface of the ferromagnetic material, e.g. iron, to a high degree and to etch it with acid. After that, the metal grains, differing in size and shape, will be visible under a microscope. These grains are crystals with irregular surface boundaries. They originate as a result of the simultaneous growth of a large number of crystals, leading to the destruction of their regular boundary outlines. Crystals having boundary surfaces not in the regular form are called crystallites. Thus, the usual piece of iron, as well as steel, is a conglomerate of a large number of separate crystallites. In the absence of an external magnetic field, each crystallite of a ferromagnetic material is divided up into a large number of regions of spontaneous magnetization, about which we spoke earlier.

Inside of each region, the material is magnetized to saturation along one of the crystallographic lines. On these lines, which are lines of easy magnetization, the magnetic properties of the individual crystallites are considerable greater than in the remainder. This nonhomogeniety of magnetic properties along the various crystallographic lines is called magnetic anisotropy.

Magnetic anisotropy determines, to a significant extent, the nature of

the magnetization in the macrovolume of a ferromagnetic material. The reality of the existence of areas of spontaneous magnetization is confirmed experimentally. The experiment consists of covering the carefully polished surface of a demagnetized ferromagnetic specimen with a liquid containing fine iron particles suspended in it. Then, the appearance of the characteristic figures is observed under a microscope. The outlines of these figures are treated by particles of the powder as they settle into the magnetic dispersion fields above the boundary layers which separate the regions of spontaneous magnetization.

And so, a well-demagnetized specimen made of a ferromagnetic material is broken up into a large number of regions magnetized to saturation, separated by boundary layers, and situated in relation to each other so that the resultant magnetic moment of the specimen is equal to zero.

Let us now turn to a brief examination of the separate stages of the magnetization process of such a specimen.

A certain definite number of regions in the specimen will be spontaneously magnetized so that their magnetic moments, each according to its own direction, will be close to the direction of the external field or will form a small angle with it. In the first stage of magnetization, when the external field remains relatively weak, the regions with the indicated magnetic moments will grow at the expense of a decrease in the dimensions of other regions with their magnetic moments at different directions. In other words, the magnetization process in weak fields will consist of displacing the boundaries of the regions of spontaneous magnetization.

As the boundary displacement process is terminating, each crystallite becomes a region of spontaneous magnetization, the magnetic moment of which is directed along the axis of easy magnetization forming the least angle with the external field.

As the external field grows further, the magnetic moments of all the regions begin to rotate in the direction of the field. For this reason, the second stage in the process of the magnetization of a ferromagnetic material is called the rotation process. This stage of the magnetization process is terminated when the magnetic moments of all the regions correspond to the direction of the external field, the sum of the magnetic moments of the regions of spontaneous magnetism providing an additional field which combines with the external field and strengthens it. Due to the additional (intrinsic) field, ferromagnetic materials acquire the property of magnetizing strongly in a relatively weak magnetic field.

As the rotation process is being completed, a ferromagnetic material is magnetized to the state of technical saturation, and a graph of the magnetization corresponding to the two processes (boundary displacement and rotation) is called the technical magnetization curve.

If we begin to decrease the external field after saturation of the electromagnetic material, the magnetic moment vector of each region will gradually diverge from the position coinciding with the external field towards the position corresponding to the beginning of the rotation process. As was indicated above, at the beginning of the rotation process, the magnetic moment of a region of spontaneous magnetization is directed along the axis of easy magnetization, forming the least angle with the external field. Thus, at a value of zero for the external field, the magnetic moments for the regions retain a definite orientation in which the total magnetic moment of the ferromagnetic body (the specimen) is not equal to zero. Consequently, the ferromagnetic body (the specimen) preserves a residual magnetism. In order to reduce this residual magnetism, it is necessary to apply a field in the opposite direction. This will decrease the dimensions of certain regions and increase the volume of others.

Thus, the two properties of ferromagnetic materials which were described, i.e. to be strongly magnetized in relatively weak fields and to retain a residual magnetism, are due to the presence of regions of spontaneous magnetism, and to the combination of the magnetization processes, the boundary displacement process and the process of the rotation of magnetic moments. These same physical manifestations condition other, no less important properties of ferromagnetic materials, about which we will speak later.

Turning to an examination of the basic magnetic values, we will note that since 1963, the International System of Units SI has been universally accepted for their measurement.

T e vector of magnetism J, the numerical value of which is equal to the magnetic moment M of a unit of volume of the body being examined, is the measure of magnetization of a ferromagnetic body. It is necessary to distinguish the words "magnetization" and "magnetism". By "magnetization" we mean the process of increasing the magnetic moment of the body or specimen, whereas by "magnetism" we mean the state of the body (the specimen) characterized by the vector J. For a homogeniously magnetized specimen with a volume V, the numerical value of the magnetism vector is determined from the ratio

$$J = \frac{M}{V}.$$

In the system of units which is in use, magnetism is measured in amperes/meter (amp/m).

Magnetism J depends on the intensity of the magnetic field, H. The intensity vector of a magnetic field characterizes the magnetizing field in the ferromagnetic material or in the core which is created by an electric current from an external energy source. To obtain a homogeneous magnetic field, a ring-shaped coil having w turns, and through which passes a current i of the required value, is used.

The numerical value of the field intensity vector in such a coil under the condition that its diameter substantially exceeds the mean diameter of the turn, may be obtained from the expression

$$H = \frac{wi}{2\pi R_m},$$

where i is the current in amps;

R_m is the mean radius of the coil in m.

The magnetic field intensity is measured in the same units as is magnetism, i.e. in amp/m.

Between the magnetism of a field H and the magnetism of a substance J there is a direct proportionality:

$$J = 4\pi\varkappa H = kH,$$

where $\varkappa$ is the magnetic susceptibility, a physical characteristic of the materials.

For ferromagnetic materials, $\varkappa$ is much greater than zero, and depends on the intensity of the field and on the temperature.

Magnetism J may be examined as an additional (inherent) field, originating as a result of the total effect of the magnetic moments of regions of spontaneous magnetization. Combining with the external field H, which is created by an electrical current from an external energy source, it produces a total field B acting on the substance. The total field, called the magnetic induction, is a vector quantity.

The numerical value of the vector B may be found from the following formula:

$$B = \mu_0 (H + J).$$

The magnetic induction is measured in webers/m^2 or in teslas.

In the last formula, μ_0 indicates the magnetic constant or the permeability of a vacuum, and, in practice, of air.

In the SI system, $\mu_0 = 4\pi \cdot 10^{-7}$ henries/m.

If one were to substitute the value of J indicated above into the formula determining induction, the following relationship would be obtained:

$$B = \mu_0 (H + 4\pi\varkappa H) = \mu_0 (1 + k) H = \mu_a H,$$

where $\mu_a = (1+k)\mu_o$ -- the absolute magnetic permeability measured in tesla m/amp.

It is convenient to employ the concept of relative permeability μ by which we mean the relationship of the absolute permeability to the permeability of a vacuum. Relative permeability is an abstract quantity.

Using the concept of relative permeability, the equation for B may be represented in the following form:

$$B = \mu_a H = \mu_0 \mu H.$$

When examining a magnetic field, the concepts of magnetic flux Φ and of a magnetizing (magnetomotive) force F are used.

The magnetic flux is determined only by a numerical value, i.e. it is a scalar. In a homogeneous field, for a cross-section S, perpendicular to the direction of induction vector B, the flux is determined from the formula

$$\Phi = B \cdot S.$$

The magnetic flux is measured in volt-seconds (v·sec) or in webers.

The magnitude of the magnetic flux Φ may be determined by analogy with Ohm's Law as the ratio of the magnetomotive force (mmf) F to the magnetic resistance R_m:

$$\Phi = \frac{F}{R_м}.$$

For the path l in a uniform field, corresponding in direction with H, we have

$$F = H \cdot l.$$

The magnetizing force is a scalar, and is measured in amperes (amp).

In many handbooks on flaw detection in rails, the dimensionality of magnetic values is indicated in the Absolute Electromagnetic System of Units (cgs), in which the induction B is measured in gauss, the magnetic flux in maxwells (mx), and the intensity of the field in oersteds (oe).

Conversion from the cgs system to the SI System of Units is accomplished using the following relationships:

$$1 \text{ mx} = 10^{-8} \text{ weber};$$

$$1 \text{ gauss} = 10^{-4} \text{ tesla};$$

$$1 \text{ oe} = \frac{10^3}{4\pi} \text{ amp/m} = \frac{10}{4\pi} \text{ amp/cm}.$$

2. Basic Information on the Process of Magnetizing Ferromagnetic Materials in a Stable Magnetic Field.

The stable magnetic field is a field excited by constant or slowly changing electric current. The magnetization process of a ferromagnetic material in such a field is characterized by the so-called original magnetization curve, representing the dependence of the induction B on the intensity of the magnetizing field H. This curve may be obtained experimentally for a ring-shaped ferromagnetic core with an evenly distributed magnetizing winding.

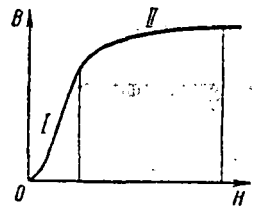

Fig. 25 Original magnetization curve of a ferromagnetic material.

The core is first of all demagnetized, i.e. it is brought to a state in which the total magnetic moment of the regions of spontaneous magnetism is equal to zero.

The original magnetization curve is shown schematically in Fig. 25, where values of the field intensity H are plotted along the horizontal axis (the abscissa), and the values of the magnetic induction are plotted along the vertical axis (the ordinate). The curve which is given is divided into two sections, each of which reflects a specific stage in the magnetization process.

The initial, gently sloping portion of the magnetization curve corresponds to the reversible displacement of the regions of spontaneous magnetization of the material. The process is called reversible if the magnetized material may be returned to its original state, with the induction B, by restoring the initial state with the field intensity H. On the steep (I) section of the curve, magnetization of the material takes place by an irreversible displacement of the boundaries of the indicated regions. When irreversible processes are involved, restoring the original values of the intensity H will not return the material to the original induction value B. Irreversible processes arise as a result of the appearance of factors hindering the displacement of the boundaries of the regions of spontaneous magnetization. These factors appear as a result of mechanical stresses, foreign inclusions, cavities and other flaws in the crystallites of the ferromagnetic material. The upper bend of the curve, together with the transfer to the gently sloping section (II), where the material approaches the state of technical saturation, corresponds to the reversible process of rotation of the magnetic moments of the regions.

Thus, the process of magnetization of a ferromagnetic material is, to a great degree, irreversible. For this reason, reducing the field intensity from the maximum value for a given magnetization curve to $H = \emptyset$ does not result in the original value of the induction B.

On a broader scale, this means that the nature of the induction change for a gradual increase in the field intensity does not coincide with the nature

of the induction change for a gradual decrease of this field to the initial value. The closed curve for magnetization of a ring-shaped ferromagnetic core with an evenly distributed magnetizing winding through a full cycle of the changes of H may serve for experimental confirmation of the indicated dependency. Gradual increase in the current in the magnetizing winding produces a gradual increase in the intensity of the field from initial value $H = \emptyset$ to a maximum value $H = H_s$ (Fig. 26). The branch OA, which is obtained as a result of this, corresponds to the initial magnetization curve.

Turning to a gradual decrease in the field intensity down to the initial value $H = \emptyset$, one may be readily convinced that the newly obtained curve does not correspond with the former; it is higher and, instead of $\emptyset$, it arrives at point B_r.

Thus, at point $\emptyset$, corresponding to the zero value of the field intensity, the magnitude of the magnetic induction does not return to zero, but a certain positive value B_r is retained. Consequently, the change in induction which is taking place in the core will lag behind changes in the field intensity.

In order to reduce the positive induction B_r to zero, it is necessary to apply a field in the opposite direction, i.e. a field with a negative value of H. To do this, it is adequate to reverse the direction of the current in the magnetizing winding. When the field in the opposite direction reaches an intensity H_c, induction in the core will be reduced to zero, i.e. the core will be demagnetized.

In the case in which the field is further increased, to a intensity $-H_s$, the magnetization curve will reach the point A_1, corresponding to the saturation of the core in a field with negative values of H. As the values of this field are decreased, the curve will pass along the line A_1, $-B_r$. At the point corresponding to the zero value of the field intensity, the magnetic induction,

as before, does not return to zero, but takes on the negative value $-B_r$.

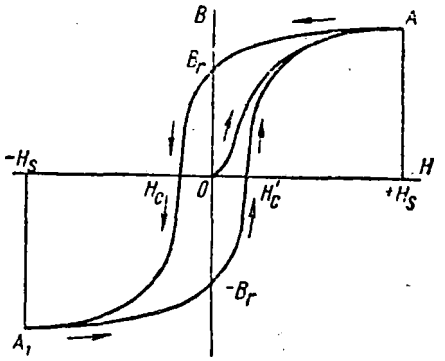

Fig. 26 Symmetrical hysteresis loop of a ferromagnetic material.

In order to reduce this induction to zero, it is necessary to apply a field with a positive value H'_c. As this field is increased, the magnetization curve arrives at point A, where the full magnetization cycle is terminated. Thus, when changing a field from a maximum positive value $+H_s$ to a maximum negative value $-H_s$ and back, the magnetization curve forms a loop, called the symmetrical hysteresis loop.

The hysteresis loop graphically represents the lag of the induction behind the field intensity for a full cycle of changes. The area of the hysteresis loop determines the size of the energy losses on hysteresis for a unit of volume of a ferromagnetic material on magnetic reversal. The energy lost to hysteresis turns into heat which serves to heat up the core.

The hysteresis cycle which is established may be obtained only after multiple changes of the field within the range of acceptable values H_s. For values of H_s at which saturation of the material is attained each time, the established hysteresis cycle is called the maximum hysteresis loop. The section B_rH_c of the maximum hysteresis loop which characterizes the process of demagnetization of the material has great significance in technology. The B_rH_c section of a maximum hysteresis loop is called the demagnetization curve.

The points at which the maximum hysteresis loop intersects with the coordiante axes determine the magnetic values, which are the most important characteristics of a ferromagnetic material.

If one takes the symmetrical hysteresis loop shown in Fig. 26 as a maximum hysteresis loop, its intersection with the axis of the ordinates at point B_r determines the value of the residual induction in the ferromagnetic material. The intersection of the maximum hysteresis loop with the axis of the abscissa at point H_c determines the coercive force, with which the residual induction B_r will be reduced to zero. This coercive force is equal to the intensity of the field.

The initial magnetic permeability μ_{in} and the maximum magnetic permeability μ_{max} also pertain to the number of primary parameters which characterize the properties of ferromagnetic materials during stable magnetization, in addition to the residual induction and the coercive force. It is customary to determine both of these characteristics from the magnetization curve. The indicated curve corresponds with the geometrical location of the peaks of the established hysteresis loops (Fig. 27), which constitute a family of symmetrical hysteresis loops.

The initial permeability μ_{in} characterizes the properties of the materials in very weak fields.

The maximum permeability characterizes the properties of the materials in fields with an intensity close to the magnitude of the coercive force.

One characteristic feature of ferromagnetic materials is the non-linear dependency of the magnetic permeability on the intensity of the magnetic field created for it. Values for B and H of the basic magnetization curve are taken for constructing this dependence. The relative permeability for each point

on the basic magnetization curve is determined by the formula $\mu = \frac{B}{\mu_0 H}$, where μ_0 is the magnetic constant.

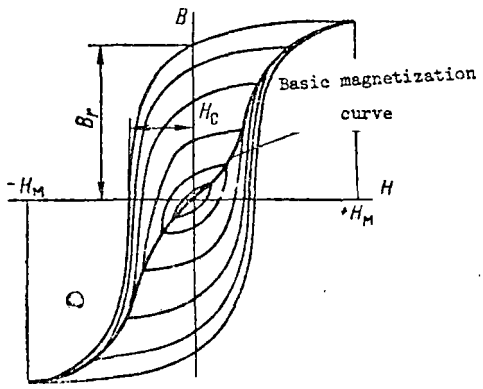

Fig. 27 A family of hysteresis loops and the basic magnetization curve.

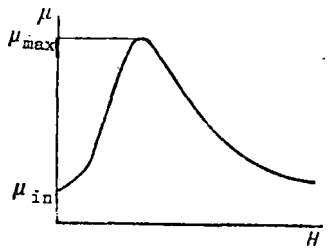

Fig. 28 The dependence of the magnetic permeability on the field intensity.

The nature of the dependence of μ on H is shown in Fig. 28.

Everything which was said above about the magnetic properties of materials is also pertinent to a closed magnetic circuit, e.g. to closed ring-shaped cores.

However, a broken magnetic circuit, i.e. a circuit containing an air gap, which represents a large magnetic resistance in comparison with the remainder of the circuit, is often used in practice. The air gap may change the path of

the magnetization curves and the permeability values substantially. Free poles which create a demagnetizing field H_o, directed toward the internal magnetizing field H_e, arise in a magnetic circuit or in a core with an air gap.

The magnetic properties of such a core are determined by the resultant (true) field:

$$H_i = H_e - H_o$$

The demagnetizing field H_o may be considered to be approximately proportional to the magnetization J. The coefficient of proportionality between them is called the demagnetization coefficient. Using this coefficient, it is possible to state that

$$H_i = H_e - N \cdot J.$$

In most cases, several mean values for N, determined from approximated formulas or from tables for bodies of the given shape and dimensions, are used in practice. Comparing the demagnetization curves of the substance and the specimen (the body), one may make the following comments. As the demagnetization coefficient becomes greater, i.e. the shorter and thicker the specimen, its magnetization curve will take on a more gently sloping form. From this it follows that when large air gaps are present, the path of the magnetization curve is basically determined by the form of the magnetic circuit or core and not by the magnetic properties of the material.

It is customary to divide ferromagnetic materials into two general groups: magnetically soft and magnetically hard.

The ability to be magnetized to saturation, even in weak fields, and small losses to magnetic reversal are distinctive properties of magnetically soft materials.

Magnetically hard materials (materials for permanent magnets) are distinguished by large values for residual induction B_r and coercive force H_c.

Comparing the hysteresis loops which characterize the two groups of materials, one may note that they are most substantially distinct with regard to

the size of the coercive force. The smallest value of H_c for the magnetically soft industrial materials presently in use is 0.004 amp/cm., whereas for magnetically hard materials, the greatest coercive force H_c is approximately 3200 amp/cm.

In other words, magnetically soft materials have a narrow hysteresis loop with a small coercive force, while the magnetically hard materials have a broad loop with a large coercive force.

Comparing the basic magnetization curves, one may note that a steep rise of the curve in the interval for weak fields is characteristic for magnetically soft materials. This is an indicator of the high permeability of magnetically soft materials in weak fields.

The most important magnetically soft materials are commercially pure grade iron, electrical steel, Permalloy, and magnetically soft ferrites.

Among the magnetically hard materials used to prepare cast permanent magnets, alloys of iron-nickel-aluminum or iron-nickel-aluminum-cobalt, as well as steels hardened with martensite (chrome, tungsten, and cobalt steels) have received the most wide-spread application.

3. Basic Characteristics of Ferromagnetic Materials in a Variable Magnetic Field.

In a variable magnetic field, periodically changing from positive to negative maximum value with the same amplitude, the magnetic state of the material and the core is characterized by a symmetrical, dynamic hysteresis loop. As distinct from a stable hysteresis loop, the nature of a dynamic loop is determined not only by hysteresis features (the influence of preceeding states), but also by the influence of other factors, among which eddy currents play a substantial role. Therefore, a dynamic loop may only conditionally be called a hysteresis loop.

As has already been indicated, the area of a hysteresis loop is always determined by the dispersion of energy for a full cycle of magnetic reversal. In the case of a dynamic loop, its area is determined by the dispersion of energy (the transformation of magnetic energy to heat energy) not only as the result of hysteresis, but also as a result of losses to eddy currents. Therefore, for the same core, with identical values for magnetic induction, a dynamic loop is always broader than a stable one.

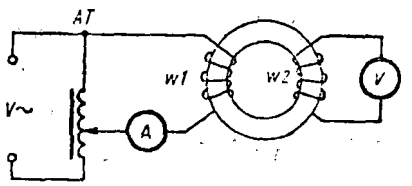

Fig. 29 Schematic for determining the dynamic induction curve of a ring-shaped core.

The shape of a dynamic loop depends on many factors, among which the following are basic: The magnetic properties of the material and the core, the frequency of the magnetizing current, the maximum induction value, the dimensions of the core, and the thickness of the sheets from which the core is assembled. Therefore, in a variable magnetic field, a dynamic loop is valid only for the core being examined and under the conditions given for its operation.

The nonsinusoidal nature of a magnetizing current (the nonsinusoidal nature of the field intensity) or the nonsinusoidal nature of the magnetic flux (induction) also influence the form of the dynamic loop.

The dynamic loop has a form close to an ellipse only in weak fields, i.e.

at small induction values. In this case, a sinusoidal change in the induction corresponds to a sinusoidal change in the field intensity.

The so-called dynamic induction curve is an important characteristic of the behavior of a coil in a variable magnetic field. If the behavior of a ferromagnetic core is characterized by an elliptical loop, the dynamic induction curve expresses the dependence of amplitude values of the sinusoidal induction B_M on the amplitude values of the sinusoidal field intensity H_M. However, this dependence will also represent the dynamic characteristic of the core only for average values of B_M and H_M for the whole period of their variance. To construct a dynamic induction curve, the values of B_M and H_M are found indirectly, based on the existing association between the magnetic and the electrical magnitudes in alternating current circuits with cores and magnetizing windings.

Let us examine this association using the alternating current circuit given in Fig. 29 as an example.

The electrical circuit contains a ring-shaped core with a magnetizing winding w_1 and a measuring winding w_2. Both windings are evenly distributed along the entire length of the ring-shaped core. An autotransformer AT serves to regulate the current in the magnetizing winding w_1. The autotransformer is connected to a sinusoidal voltage source

$$V = V_M \sin \frac{2\pi}{T} t = V_M \sin \omega t,$$

where T is the alternating current period,

ω is the angular frequency, and

V_M is the amplitude value of the feed voltage.

An ammeter serves for measuring the alternating current in the magnetizing winding w_1. The electromotive force in the measuring winding is determined by the voltmeter V.

Two electrical magnitudes are measured with the aim of determining the magnitudes characterizing the magnetic state of the core in a variable field: the alternating current i in the magnetizing winding w_1 and the variable electromotive force e in the measuring winding w_2. Inasmuch as we are speaking of weak magnetization of the core, given a sinusoidal feed voltage V, the current I and the electromotive force e will also change according to the sinusoidal law.

Using the data which have been presented, we will now take up examination of the corresponding association between the indicated electrical magnitudes and those magnetic magnitudes which permit construction of the dynamic induction curve when the core is weakly magnetized.

The amplitude of the sinusoidal magnetic field intensity H_M is directly associated with the true value of I of the magnetizing current in the winding w_1:

$$H_M = \sqrt{2}\frac{w_1 I}{l},$$

where l is the average length of the magnetic line in the ring-shaped core, and w_1 is the number of turns in the magnetizing winding.

There are also other formulas showing the connection between H_M and the amplitude values of the current I_M or the mean value I_{av}. However, the formula indicated above has the most practical value since in most systems (electromagnetic, electrodynamic, heat, and thermoelectric), ammeters show the value I of a sinusoidal current.

The amplitude B_M of a sinusoidal induction is directly associated with the true value of E, the sinusoidal electromotive force, which is induced in winding w_2:

$$B_M = \frac{E}{4.44 f w_2 s}$$

where f is the feed voltage frequency,

w_2 is the number of turns in the measuring winding, and

s is the cross-section of the ring-shaped coil.

The connection between the induction B_M and the average value of the sinusoidal electromotive force E_{av} in winding w_2 is given by the formula

$$B_M = \frac{E_{av}}{4fw_2s}.$$

Using the latter formula, it is possible to obtain more accurate data for B_M. This accuracy is possible because rectifier-type voltmeters, having a greater internal resistance in comparison with other types of volt-meters (excluding cathode-types), may serve to measure the average value of the sinusoidal electromotive force.

The amplitude permeability, determined as the ratio of the maximum induction to the maximum value of the field intensity on the dynamic induction curve, is an important characteristic for the behavior of a ferromagnetic core in a variable magnetic field. The amplitude permeability is calculated from the following formula when the intensity of the field and the induction vary sinusoidally:

$$\mu_M = \frac{B_M}{\mu_0 H_M},$$

where μ_0 is the magnetic constant.

It is necessary to emphasize that μ_M represents the mean value of the magnetic permeability for one period of the feed voltage. In reality, the magnetic permeability of the core changes constantly throughout the entire period of the feed voltage.

In strong magnetic fields, the nonsinusoidal nature of the magnetizing current (the nonsinusoidal nature of the field intensity) or the nonsinusoidal nature of the flux (induction) influences the form of the dynamic loop. Therefore, other conditions being equal, a dynamic loop in the case of nonsinusoidal field intensity is different from the dynamic loop obtained in the case of nonsinusoidal induction.

Let us examine causes precipitating the appearance of nonsinusoidal induction or nonsinusoidal field intensity when magnetizing a core in an electric circuit with a sinusoidal feed voltage, i.e. causes not related to the feed voltage source. With this in mind, we will return to Fig. 29 and introduce the following symbols:

R -- the resistance of the magnetizing winding w_1; and

$x_L = \omega L$ -- the inductance of that winding when the circuit of the measuring winding w_2 is open.

The feed voltage $V = V_M \sin \omega t$ may be reduced to two components, one of which, V_R, overcomes the active voltage drop at resistance R, and the other, V_L, balances the counter-electromotive force of inductance, which is equal to

$$e_L = -w_1 \frac{d\Phi}{dt} = -w_1 S \frac{dB}{dt}$$

Let us assume that all turns of the magnetizing winding are permeated by the same magnetic flux $\Phi = B \cdot S$, i.e. there is no magnetic dispersion, and the active resistance R is much smaller than the inductance x_L, i.e. $R \ll x_L$. These conditions permit us to ignore the drop in voltage V_R in comparison with the feed voltage and accept that:

$$V = V_M \sin \omega t = V_L = w_1 S \frac{dB}{dt},$$

where w_1 is the number of turns of the magnetizing winding,

ω is the angular frequency, and

s is the cross-section of the ring-shaped core.

From this relationship, it follows that

$$B = \frac{V_M}{2\pi f w_1 S} \sin\left(\omega t - \frac{\pi}{2}\right) = B_M \sin\left(\omega t - \frac{\pi}{2}\right).$$

This relationship shows that, given a sinusoidal change in the feed voltage, and $R \ll x_L$, the induction B in the core will also change in accordance with the law of sines.

It is necessary to draw attention to the situation when the amplitude value of the sinusoidal induction

$$B_M = \frac{V_M}{2\pi f w_1 s}$$

does not depend on the magnitudes characterizing the magnetic properties or on the geometric dimensions of the core.

Having proved the sinusoidal nature of the induction B, we turn to an examination of the law of changes in field intensity H, or, of the law of changes in the magnetizing current in the winding w_1, which is the same thing. We will be solving this portion of the problem under examination by graphically constructing a simplified diagram of the magnetization process, according to which a dynamic loop is replaced by the magnetization curve. The sequence of the graphic construction of the field intensity change curve H (curve 1), given a sinusoidal change in induction B, (curve 2) is shown in Fig. 30.

In the center part of this figure, the magnetization curve is presented for values of induction B at which the ring-shaped core reaches saturation. In the right-hand portion of the figure, the sinusoidal induction curve is shown for a full period T. The horizontal straight line ωt serves as the time line for the sinusoid. The magnetization curve permits us to determine each instantaneous value of the field intensity H for a corresponding instantaneous value of the sinusoidal induction B. For example, for a moment of time t, the instantaneous value of the variable field intensity H_t corresponds to the instantaneous value of the induction B_t. The value of H_t which is found is plotted on the ordinate passing through point t on the vertical straight line ωt, which serves as the time line for the variable field intensity. The points t on the two lines ωt (horizontal and vertical) represents the same moment in time. In the same way, ordinates corresponding to other

instantaneous values of sinusoidal induction may be found and plotted. Connecting the ends of these ordinates, we obtain the periodic curve for field intensity H for a time of one period T (at curve 1).

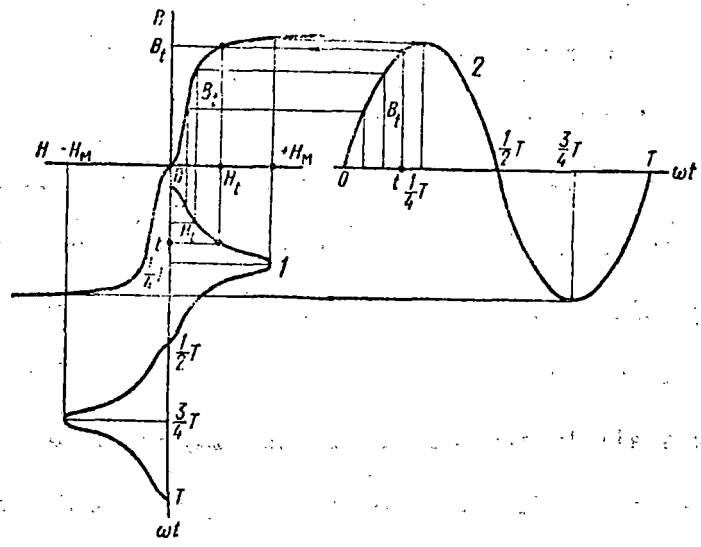

Fig. 30 Nonsinusoidal change of intensity H given a sinusoidal change in induction B.

It may be seen from Fig. 30 that at large values of induction B corresponding to saturation of the core, the periodic graph of H takes on a nonsinusoidal (peaked) form. The means for graphic construction which we have introduced show that the non-linearity of the magnetization curve in areas for large values of B is one cause of the nonsinusoidal nature of H. The same manifestations are observed in reality when the process of magnetization and demagnetization of the core takes place along non-linear branches of the loop.

Using the graphic means which we introduced, it is easy to demonstrate that, if the amplitude of a sinusoid B does not go beyond the bounds of the linear portion of the magnetization curve, there will be no deviations from the sinusoid in the graph of H.

It is known that it is possible to separate any periodic nonsinusoidal curve representing any type of electrical or magnetic value into sinusoidal components of varying frequency, amplitude and initial phase. In individual cases, it is also possible to obtain a constant component along with the sinusoids when this separation is made.

The sinusoidal components of a nonsinusoidal curve are commonly called harmonic components, or, more simply, harmonics. The harmonic having a frequency identical to the frequency of the nonsinusoidal curve is called the first or primary harmonic. The remaining harmonics have frequencies two, three, four, five, six..., times greater than the frequency of the primary harmonic. Therefore, the frequency of the individual harmonics may be greater than the frequency of the primary harmonic by either an even or an odd number of times.

There are several graphic and analytical methods for finding the amplitude and phase of harmonic components of periodic, nonsinusoidal curves. Using one of these methods, it is possible, first of all, to demonstrate that the nonsinusoidal curve H does not contain the ωt time line. Secondly, in addition to the primary harmonic, the curve contains a clearly expressed third harmonic, as well as an amplitude-significant fifth harmonic. Uneven harmonics of the field intensity will exert an influence on the form of a dynamic loop reflecting the process of magnetization of the core in an electrical circuit with a sinusoidal feed voltage and $R \ll x_L$.

Another relationship is possible between the parameters R and x_L in the same electrical circuit. Unlike the previous situation, we will propose that the resistance R is much greater than the inductance x_L, i.e. $R \gg x_L$. This permits us to ignore the drop in voltage V_L in comparison with the feed voltage V and assume $i = V/R$. Inasmuch as $V = V_M \sin \omega t$, the magnetizing

current $\underline{i}$ and the field intensity $\underline{H}$ will also change according to the sinusoidal law. Figure 31 relates to this case. Here a graphic means of constructing the periodic induction curve $\underline{B}$ (curve 1) in the presence of a sinusoidal change in the field intensity $\underline{H}$ (curve 2) is shown.

With no biasing of the core by a constant magnetic field ($H_o = 0$), the time line $\underline{\omega t}$ of the sinusoidal curve $\underline{H}$ passes through the beginning of the magnetization curve coordinates.

For a moment $\underline{t}$, the instantaneous value of the induction $\underline{B_t}$ corresponds to the instantaneous value of the sinusoidal field intensity $\underline{H_t}$ along the magnetization curve.

The values which are found for $\underline{B_t}$ are plotted on the ordinate passing through the point $\underline{t}$ on the horizontal line $\underline{\omega t}$ serving as the time line for the variable magnetic induction $\underline{B}$. The ordinates of $\underline{B}$ for other instantaneous values of $\underline{H}$ are found in the same manner. This permits us to obtain a graph of the changes in the magnetic induction for the time of the full period $\underline{T}$ (curve 1). According to Figure 31, this curve has a nonsinusoidal form which is chopped at the peaks.

The symmetrical nature of the induction curve relative to the line $\underline{\omega t}$ shows that it does not contain even numbered harmonics. Among the odd numbered harmonics, the primary harmonic induction component, the amplitude value of which is greater than the maximum value of the nonsinusoidal curve, plays a fundamental role here. The odd numbered induction harmonics will influence the form of the dynamic loop. This influence is distinct from the influence of the odd numbered harmonics of the field intensity.

It is obvious that the nonsinusoidal nature of one of the values will be reflected to some degree on the form of the dynamic induction curve as well.

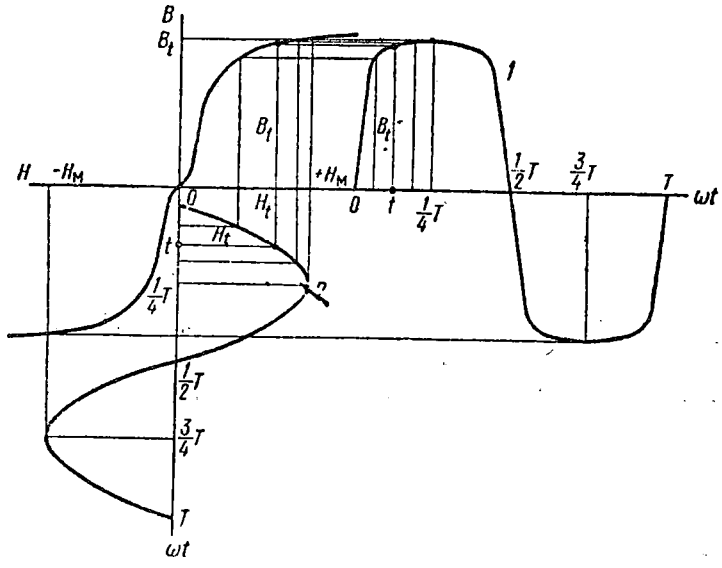

Fig. 31 The sinusoidal change of the field intensity H given a nonsinusoidal change of induction B.

Under practical conditions, it is more often necessary to contend with the presence of harmonics in the field intensity curve. Here, the alternating current in the magnetizing winding, i.e. the magnetizing current, will have harmonics of the same order. In such an instance true values of I, the nonsinusoidal magnetizing current, are used, permitting the determination of the effective value H_e of the field intensity of a certain sinusoid. This value is equivalent to the effective current of the field intensity containing the harmonic components. Then the peak permeability μ_M is determined by the following formula:

$$\mu_M = \frac{B_M}{\mu_0 H_e \sqrt{2}},$$

where B_M is the amplitude value of the sinusoidal induction,

μ_0 is the magnetic constant, and

H_e is the effective value of the equivalent field intensity sinusoid.

The peak permeability μ_M is the average magnetic characteristic for one period of the feed voltage.

An examination of the workings of cores under the conditions of simultaneous magnetization by variable permanent magnetic fields, the amplitude of the variable component of the field intensity being much larger than the intensity of the constant component of the field, holds great interest for magnetic flaw detection.

The magnetic state of the core operating under the given conditions changes according to an asymmetrical dynamic loop.

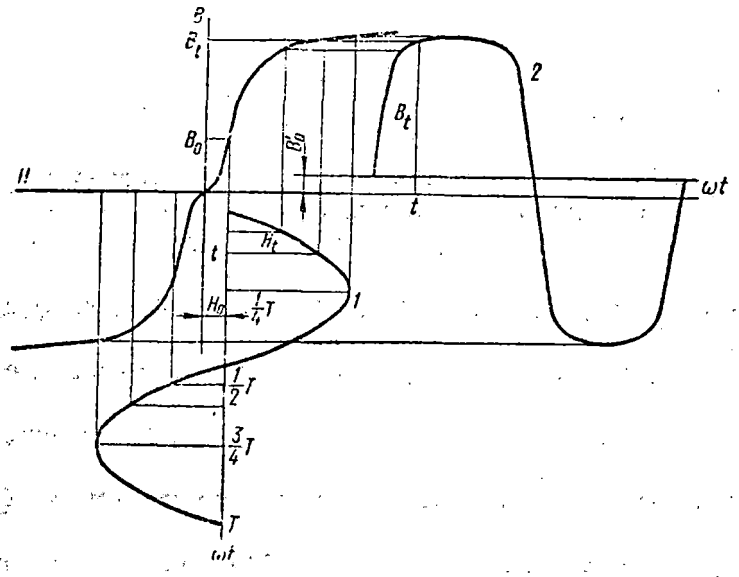

Fig. 32 Nonsinusoidal change of the induction B with a simultaneous magnetization by a constant field with intensity H_o and by a sinusoidal field with intensity H.

The pecularities of this type of magnetization will be elucidated using a simpler example in which the dynamic loop is replaced by the basic magnetization curve (Fig. 32). Here, the condition of simultaneous magnetization is brought about by a constant field with intensity H_o and a variable field with a sinusoidal change in intensity H (curve 1), the amplitude of which is five times greater than the amplitude of H_o.

The vertical straight line passing through the point H_o on the axis of the abscissa of the magnetization curve serves as the time line for the sinusoidal field. Therefore, each point of the variable field sinusoid relative to the beginning of the magnetization curve gives an instantaneous value for the resultant field. For a moment of time t, the resultant magnetic field has an intensity $H_o + H_t$. The instantaneous value of the induction B_t, which is plotted on the ordinate passing through point t, corresponds to the indicated value of the field intensity along the magnetization curve. As a result of analogeous constructions for other instantaneous values of the induction, a series of points is determined which permits the periodic induction curve B in a ring-shaped core (curve 2) to be obtained.

It is not difficult to demonstrate that for one period, the average ordinate of this curve is not equal to zero. Consequently, the nonsinusoidal curve under examination has a constant component. The size of the constant component B'_o of the induction is determined by the distance between the axis of the abscissa and the line ωt, drawn so that relative to it, the average ordinate of the curve being examined is equal to zero for the period.

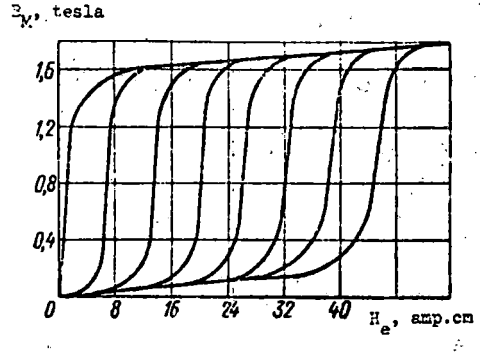

Fig. 33 A family of characteristics for a ferromagnetic material during simultaneous magnetization by a field with a variable and a constant component.

In the absence of a variable field, the constant induction B_o corresponds to the constant field with intensity H_o. When the constant and the variable

fields act jointly, the constant induction B_o decreases to the indicated value of B'_o although the intensity H_o remains unchanged.

The horizontal straight line ωt is the time line for the variable component of the magnetic induction. Since the periodic curve of the variable induction component is asymmetrical relative to the line ωt, it consequently contains both even and odd order harmonics. Of the even numbered harmonics, the second has the greatest amplitude. Under certain conditions, the amplitude of the second harmonic of the variable induction component changes in proportion to the intensity of the constant field H_o.

Working under the condition of simultaneous magnetization by a field with both a variable and a constant component, a primary characteristic of a ferromagnetic material, or of a ring-shaped core prepared from this material, is the dependence of the maximum value of the induction B_M on the effective value of the variable field intensity H_e, obtained at an intensity H_o of the constant component of the field.

A family of these characteristics for a ring-shaped core made of E320 electrical steel for several increasing values of H_o is shown in Fig. 33.

As may be seen from this figure, the greater the value for H_o, the more gently the slope of the initial part of the characteristic becomes. Therefore, during simultaneous magnetization with large values of H_o, a very lengthy period of slow growth for the values of the induction B_M arises.

In addition to ferromagnetic cores, large non-ferromagnetic and ferromagnetic objects, e.g. rails, may also turn out to be in a variable magnetic field.

In a rail which is conducting electricity, the variable magnetic field excites an electromagnetic induction emf, under the influence of which closed eddy currents arise.

In their physical properties, the small eddy currents are analogeous to currents passing through the conductors of electrical circuits. The eddy currents, as is the case with any induced current, attempt to oppose the force which created them. Therefore, the magnetic field of the eddy currents (the secondary field) is in opposition to the primary magnetizing field at every moment. As a result of the skin-effect, the density of the eddy currents is irregular through the cross-section, and has the greatest value near the surface of the object being magnetized. More detailed information about these currents is given in the paragraph describing the flaw detection method based on the use of eddy currents.

4. Magnetization features in the constant magnetic field of a moving electromagnet.

The method of magnetizing rails in the magnetic field of a moving electromagnet has gained practical application. In this case, a U-shaped electromagnet with its poles turned to the running surface of the rail head is used.

The magnetizing windings of the electromagnet are connected to a direct current source. As a rule, magnetizing a rail in the field of a moving electromagnet takes place with constant air gaps between poles and the surface of the head.

The magnetic pole currents (Fig. 34) are partially dispersed, whereas in the rail itself, they branch out into two parts, those between the poles and those beyond the poles.

The magnetic flux between the poles, which comprises no more than 60% of the overall flux stimulated by the magnetizing current in the electromagnet windings, is used during rail flaw detection. Magnetization in a moving field (dynamic magnetization) is usually compared with stable magneti-

zation, whereby the electromagnet is immoble with respect to the rail.

We will examine magnetization in a moving field when both poles of an electromagnet pass over each portion of the rail one after the other. Consequently, each portion of the rail will turn out to be under the influence of a magnetic field, the size of which varies from the maximum positive value under the N-pole to the maximum negative value under the S-pole. With an electromagnet speed of 70 km/h, this entire process of magnetic reversal in the rail takes place during a time of approximately 0.005 sec.

The process of magnetic reversal in a rail within the field of the magnet has a pulse nature. Magnetic reversal of each section of the rail under the poles of a moving electromagnet will take place according to a certain open hysteresis cycle. The nature of this cycle is determined by the properties of the rail material, the relationship between the sizes of the flux between the poles and beyond the poles, as well as by the air gaps between the rail and the poles.

A change in the magnetic flux in the rail accompanies movement of the magnetic field source. Therefore, the section of the rail over which the electromagnet is located at any given moment is divided into two regions. In one of them, the magnetic flux is decreasing and in the other it is growing; it is for this reason that eddy currents arise in the rail.

The closed contours of the eddy currents, being inseparably associated with magnetic fluxes above the poles of the electromagnet, are displaced in unison along the length of the rail. As is known, the eddy currents create their own magnetic field which, according to Lentz's law, opposes any change in the magnetic flux of the rail, i.e. the field of the eddy currents hinders an increase in flux in the rail, and, conversely, reinforces the decaying flux.

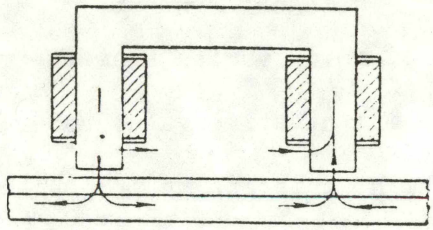

Fig. 34 Diagram of the division of the magnetic flux in the rail into two parts, that between the poles and that beyond the poles.

Obviously, hysteresis and eddy currents affect the process of magnetic flux formation in the section of the rail between the poles in a definite manner. The degree of influence for the indicated factors may be established by comparing the distribution curves of the flux between the poles for various speeds of the electromagnet. One of these curves should correspond to the static case of magnetization, i.e. magnetization when the magnet is stationary.

The influence of hysteresis is established according to the curve of the magnetic flux distribution in the rail when the electromagnet is moved extremely slowly, i.e. when the eddy currents are so weak that the phenomena associated with them are negligible and the hysteresis phenomena associated with magnetic reversal of the rail under the poles are manifested in full measure.

A comparison of this curve with the stationary magnetization curve shows that hysteresis weakly affects the distribution of the magnetic flux in the space between the poles when the electromagnet is moving slowly. Consequently, those significant features which are observed when a rail is magnetized by a

moving constant field source are caused primarily by eddy currents.

Distribution of the longitudinal component of the magnetic flux in the rail head in relation to the shaded poles of an electromagnet, similar in performance to that used in the magnetic flaw detection cars, is shown in Fig. 35. These curves are constructed from average values of magnetic flux in the head of R50 type rail. Curve 1 corresponds to the instance of stationary magnetization. The other two curves characterize the change of the magnetic flux with regard to the electromagnetic poles moving at a speed of 10 km/h (curve 2) and 40 km/h (curve 3). The direction of motion, indicated by the arrow to be along axis X, at the same time determines the front (first) and the rear (second) poles of an electromagnet.

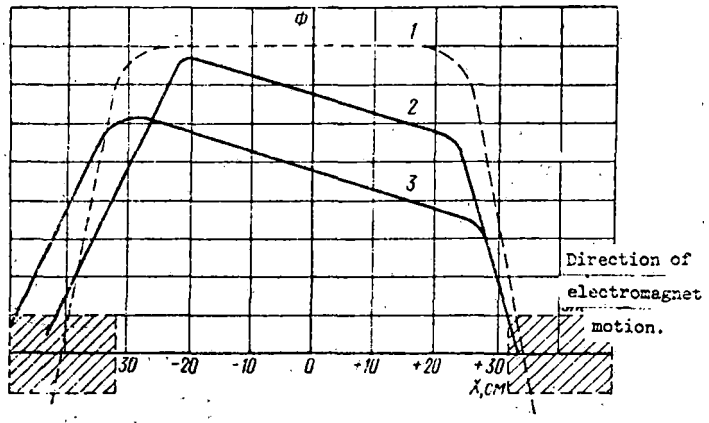

Fig. 35 The average value of the longitudinal component of magnetic flux in a rail head between the poles of an electromagnet.

The average value of the flux in the rail head does not give a full representation of the features of rail magnetization in a moving field. Data which characterize the magnetic state of the metal in the individual layers of the rail head hold great practical interest for the purposes of flaw detection.

These data are presented in experimental investigations carried out by the Novosibirsk Institute of Rail Transport Engineers and by the Uralsk division of the TsNII MPS*, using model testing.

The results of the investigations indicated are presented in Fig. 36 in the form of curves for the distribution of the longitudinal component of the induction vector along a length of rail in a surface layer having a lower boundary at a depth of 5 mm, and in a surface layer with the upper boundary at a depth of 15 mm and the lower boundary at 18 mm. On the same figure, curve 1 is also presented, showing the average induction values in the (rail) head during stationary magnetization. Curve 2 shows the distribution of the induction in the surface layer when the electromagnet is moving at a speed of 41 km/h.

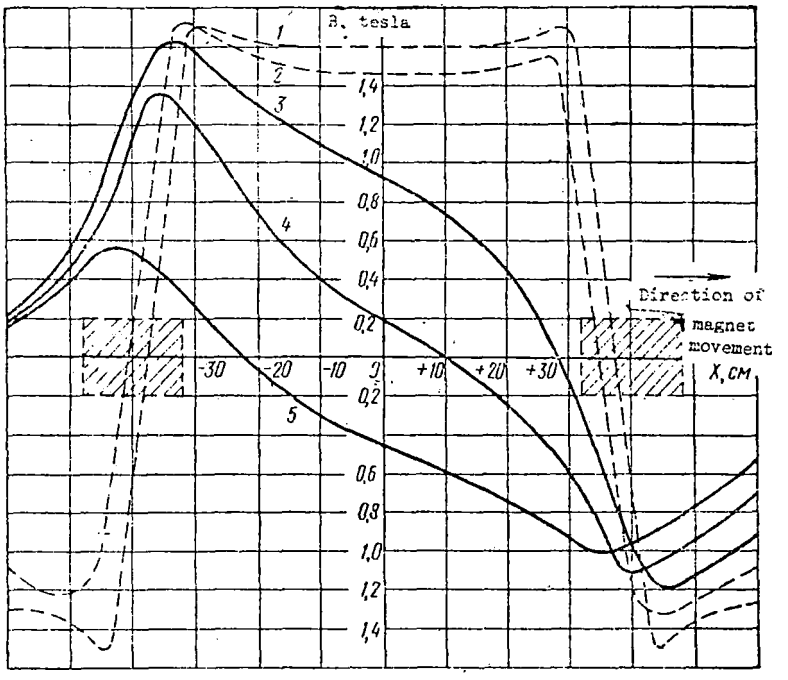

Fig. 36 Distribution curves for the longitudinal component of the magnetic induction in the rail head in the surface layer and in its central section.

*Central Scientific Research Institute, Ministry of Railroads.

A comparison of curves 1 and 2 shows that the longitudinal component of the induction in the surface layer at a speed of 41 km/h preserves values close to those for stationary magnetization and has the same direction (positive) between the poles. Thus, an increase in the speed of the magnetic field source to 41 km/h has little effect on the distribution of the longitudinal component of induction in the surface layer of the rail head.

The remaining curves in Fig. 36 relate to the center part of the rail head, as determined above, and correspond to the following electromagnet speeds: curve 3 - 14 km/h; curve 4 - 27 km/h; curve 5 - 57 km/h.

It is not difficult to notice that between the poles, this series of curves is distinct from the previous ones not only with regard to the values of the induction vector, but also with regard to its direction in various sections of the rail head.

Thus, for example, even at relatively small electromagnet speeds (14 km/h, curve 3), the magnetic induction vector in the zone of the first pole has a negative direction, i.e. opposite to the direction taken as positive for curves 1 and 2. All curves of this series pass through the zero induction value, the point of the zero induction value being displaced to the side of the second pole as the speed of the magnetic field source increases.

In the center layer of the head, the zero induction value exists simultaneously with high values of induction in the surface layer of the head which are independent of the speed for practical purposes. This indicates that magnetization of the rail by a moving constant field is accompanied by a strongly pronounced surface effect (i.e. the magnetic skin-effect).

The values of magnetic induction in various layers of the rail head depend not only on the speed of the magnetizing field source of the electromagnet, but also on the value of the intensity of this field. A higher field intensity

leads to an increase in the values of magnetic induction at all speeds examined above.

The given features of rail magnetization in a moving constant electromagnetic field show that for the detection of internal flaws, the best conditions are those in the zone of the second pole of the electromagnet where the inductance in the head preserves a direction which is identical to that in the surface layer, and has an adequate value.

5. The Magnetic Method

The possibility of detecting flaws by the magnetic method is directly associated with the formation of a clearly expressed non-homogeniety of the magnetic field in the zone of the flaw. In order to clarify this phenomenon, we will imagine the object to be tested to be made in the shape of a long cylindrical rod with the external, homogeneous magnetic field H_e directed along the rod, i.e. it is the same as is the field inside a long coil, through which an electrical current passes.

We will assume that the material of which the rod is made is homogeneous with regard to this magnetic properties and that it has a magnetic permeability equal to μ_1. In a homogeneous external magnetic field, the material of which the rod is made takes on a magnetism J_1. The magnetism vectors in the rod will be parallel everywhere to those which generated it.

Further, we will assume that a certain short section of this rod includes a small internal area made of a material, the magnetic permeability of which, μ_2, is significantly less than μ_1. Then the magnetism J_2 of the material contained in this region will be less than the magnetism J_1 of the remaining sections of the rod. Therefore, a part of the magnetism vectors will break off near the boundary where they encounter the internal area with magnetic permeability μ_2 and begin again at the other boundary of that region. It is

known that each end of a line of magnetism acts as a certain positive magnetic charge, whereas each of its starting points acts as a negative magnetic charge.

As a result, the boundaries or the walls of the areas under examination will be polarized by positive and negative magnetic charges, as is shown in Fig. 37.

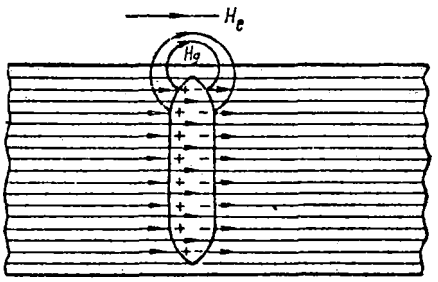

Fig. 37 Diagram of the polarization of the walls of an internal area in a magnetized rod.

Each magnetic charge creates a magnetic field which is directed from it as if from a center. It is not difficult to see that above the section within which the area simulating an internal defect is located, the total field of the magnetic charges is directed in the same direction as is the external field H_e, i.e. its effect is intensified. The total field of the magnetic charges H_g is called the flaw field. By nature, it is concentrated, with a maximum value of intensity directly over the flaw. Detection of this field is the basic principle of the magnetic method of flaw detection in magnetized items.

The forms for practical use of the magnetic method are very diverse, on the part of the methods for magnetizing the items being tested as well as the means for indicating the flaw fields. In practice, two basic types of magnetization are used, pole magnetization and circular magnetization.

Pole magnetization of rails is accomplished using either an electromagnet or a permanent magnet.

In Fig. 38, rail magnetization by an electromagnet with a yoke (1) on which there are magnetizing coils (2) connected with a direct or an alternating current source, are shown schematically. The fact that the closed force lines of the magnetic field intersect the rail surface in two places (where they enter the rail and where they emerge from it) is characteristic of the type of magnetization under consideration. In these places, magnetic fields are formed: a north and a south. Therefore, magnetization in the field of an electromagnet is called pole magnetization.

On the section located between the ends of the electromagnet yoke, the rail is longitudinally magnetized. In this section, transverse cracks obstructing the path of the magnetic field lines will be detected best of all. It is necessary to magnetize transversely to detect cracks which extend along the length of the rail.

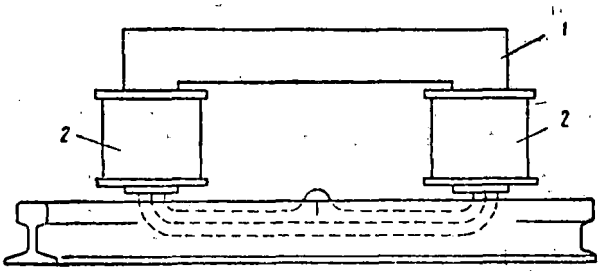

Fig. 38 Diagram of rail magnetization.
1. Yoke; 2. magnetizing coil

The shape of the electromagnet and its dimensions are set based on practical demands.

Circular magnetization is accomplished in the simplest instance by including the section being monitored in a direct or alternating current circuit.

Current-conducting brushes sliding along the running surface of the rail head may serve this purpose.

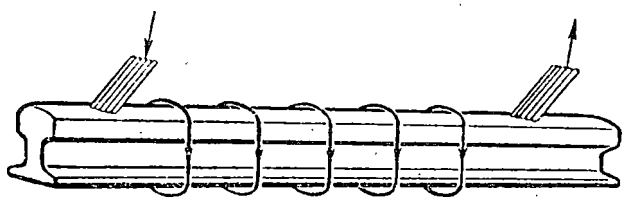

Fig. 39 Distribution of the magnetic force lines around the rail during circular magnetization.

It is known that when current flows, a magnetic field with closed force lines is formed inside and around a conductor. The approximate distribution of the magnetic force lines during circular magnetization is shown in Fig. 39. The force lines of this field do not intersect the surface of the rail, but seemingly surround it, encircling the rail; therefore, circular magnetization is called magnetization without poles. The magnetic force lines of a circular field are perpendicular to flaws oriented in the direction of the current. As a result, when testing a circularly magnetized rail by the magnetic method, longitudinal flaws (splittings, hairline cracks, cracks) will be detected best of all.

A rail may be magnetized in a constant or a variable field. When a constant field is used, the force lines of the magnetic flux are distributed along the entire section of the rail. Therefore, a constant field is, as a rule, used to detect internal flaws. When a variable field is used, only the surface layer of the metal is magnetized, indicating the expedience of using this method to detect flaws emerging onto the rail surface.

As a result of the magnetic field effect, the rails remain magnetized.

Their residual magnetism permits rails to be monitored using the magnetic method without supplemental magnetization. On our rail lines, examination of rails installed on the line usually takes place in the external field of electromagnets (with direct or alternating current) or in the external field of permanent magnets.

The flaw field intensity depends on the type of flaw, the depth at which it lies in the metal, the properties of the surrounding metal, and its magnetism. This complex dependency has no exact mathematical expression even for objects and flaws which are simple in shape. However, in practice, it is important to know at least the nature of this dependency and the order of magnitudes determining the flaw field intensity.

With this aim, investigation of the flaw fields when the objects being monitored were statically magnetized were conducted by the Siberian Institute of Applied Physics.

The indicated dependency was studied based on a model having the form of a pipe with an external diameter of 50 mm and an axial opening 15 mm in diameter. Two closely fitting cylindrical rods went into the openings. The clearance d between the smooth ends of these rods simulated an internal transverse flaw situated under a layer of metal 17.5 mm thick. The size of the gap d could be varied by non-magnetic gaskets. The thinest gasket was 0.01 mm thick, and the thickest was 5.6 mm. The model was magnetized by a constant field in the longitudinal direction. A gap d = 0.01 mm corresponded to a flaw having certain similarities with an internal transverse crack in the rail head.

As the thickness of the gasket was increased, i.e. as the clearance d was increased, the artificial flaw gradually took on the form of an internal cavity with fairly substantial volume and dimensions in the direction of magnetization.

Measurement of the flaw field intensity was conducted by the ballistic method. The measuring coil reacted only to that component of the flaw field which corresponded to the direction of magnetization. Consequently, the longitudinal component of the flaw field defect was measured by the ballistic method.

The curves of the longitudinal component of the flaw field intensity which were constructed as a result of the measurements are presented in Fig. 40. Each of these curves characterize the dependency of the flaw field intensity H_g on the intensity H of the magnetizing field for various values of the gap width d.

The area of the sharp rise in the magnetization curve of the material from which the described model was made corresponds to the interval of the values of H (from approximately 12 - 40 amp/cm). Technical saturation of the material for the model is reached for values of H exceeding 40 amp/cm.

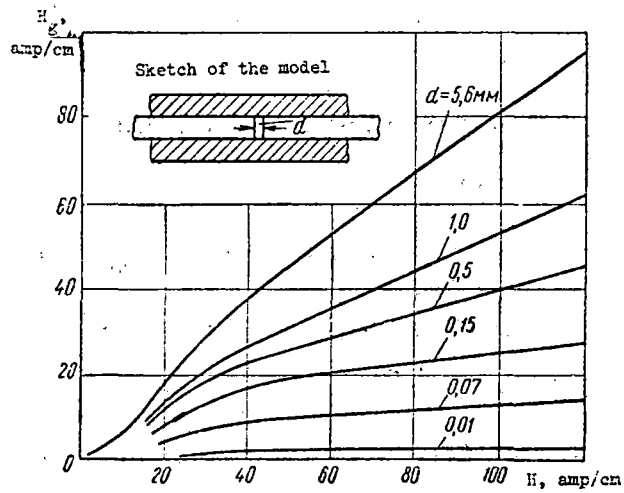

Fig. 40 Graph of changes in the field intensity H_g over an artificial flaw at various values of gap width d.

The three lower curves show that over defects having the shape of transverse cracks, the size of H_g reaches a certain limit value with an increase in the field intensity. Growth in the field intensity H_g ceased when the material from which the model is made reached saturation. When the gap d was increased, the nature of the changes of the field H_g approached a linear dependency on the size of H.

These curves show that fields H_g corresponding to flaws having the shape of a narrow internal crack have the least intensity. Therefore, in comparison to the detection of flaws with great volume, detection of such cracks by the magnetic method will always cause great difficulty.

The clearance between the walls of an internal transverse crack in the rail head is only a few thousandths of a millimeter in thickness. The MRD flaw detector serves to detect such flaws using the magnetic method. The permanent magnets of this flaw detector magnetize the rails along their length, i.e. in the longitudinal direction.

A magnetic induction on the order of $B \cong 0.35$ tesla, which is several times less than the saturation induction of rail steel, is created in the heads of heavy type rails between the poles of a magnet. Data characterizing the distribution of the magnetic fields above the transverse cracks at the indicated values of magnetic induction are presented below.

Above the running surface of the magnetized rail, in addition to the fields caused by flaws, there is always the dispersion field H_o of the permanent magnet. Therefore, when monitoring rails in the external field of a permanent magnet (or of an electromagnet), flaw detection using the magnetic method is reduced to searching out concentrated flaw fields on the background of the dispersion field of a permanent magnet.

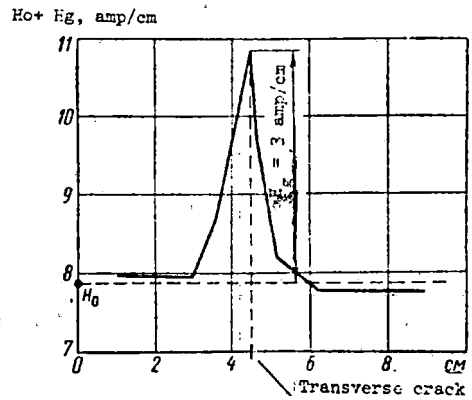

Fig. 41 Graph of the change in intensity of a magnetic field over a rail head with a transverse fatigue crack.

In most cases the field creating the background is much stronger than the local flaw field. As an example, Fig. 41 shows a graph of the change in the intensity of the longitudinal component of a magnetic field over a section of a rail, in the head of which was found the transverse fatigue crack illustrated in Fig. 42.

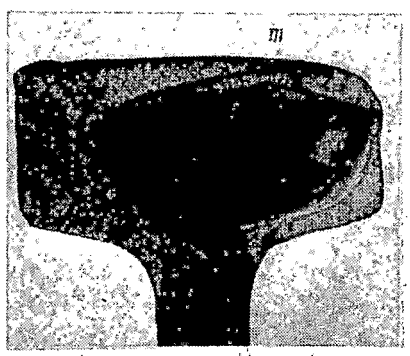

Fig. 42 Rail fracture with a transverse fatigue crack.

The measurements were conducted along a line passing through point m, under which the transverse crack was situated at a depth of 2 - 3 mm. The average value of the dispersion field intensity of the magnet H_o is 7.8 amp/cm (the horizontal dash line) for the section of the rail being examined. The local flaw field, H_g, with a maximum intensity H_g equal to 10.8 minus 7.8 or 3 amp/cm, is isolated distinctly enough on the background of this field. The intensity H_g decays rapidly with distance from the crack (to either side along the length of the rail). On the section of the rail with the transverse crack, the local field H_g is detected not only over the running surface of the rail head, but on the lateral surface and under the head as well.

A graph of the change in the intensity of the longitudinal component of the field H_g near the lateral edge of the head with the same transverse crack is given in Fig. 43. This graph is constructed from measurement data taken at points distributed in the lower section of the lateral edge where the crack was situated at a distance of 3 - 3.5 mm from the surface.

According to this graph, H_o is 7.2 amp/cm and H_g is 2.8 amp/cm. A graph of the change in the field H_g under the head of the defective portion of the rail will have approximately the same characteristics.

Values of H_g measured at a distance of 2.5 mm from the rail head are indicated on all of the graphs. The data which are presented show that over a crack having fairly significant dimensions, and one which is situated inside the head at a relatively great distance from the running surface and from the lateral edge, the field H_g is isolated distinctly enough over the level of the dispersion field of the permanent magnet H_o. However, as the dimensions of the crack decrease and as the depth at which it is situated increases, the field H_g weakens noticably. Thus, for example, for transverse cracks with an area equal to 25% of the cross section of the rail head and situated in the

head at a depth of 5 mm, the field H_g has a maximum intensity equal to 0.8 - 1.0 amp/cm, the dispersion field of the permanent magnet maintaining its former level.

In addition to what was said about the changes in the field H_g along the length of the rail, we will examine the dependencies of this field as the distance from the surface of the rail head increases. With this in mind, three graphs, each of which was constructed from the results of measurements of the field H_g at a definite distance from the surface of the head are given in Fig. 44.

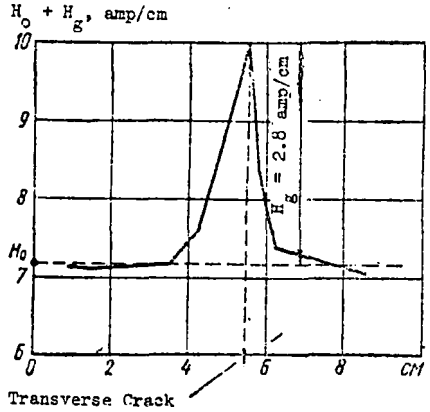

Fig. 43 Graph of the changes in the intensity of the magnetic field near the lateral edge of a rail with a transverse crack.

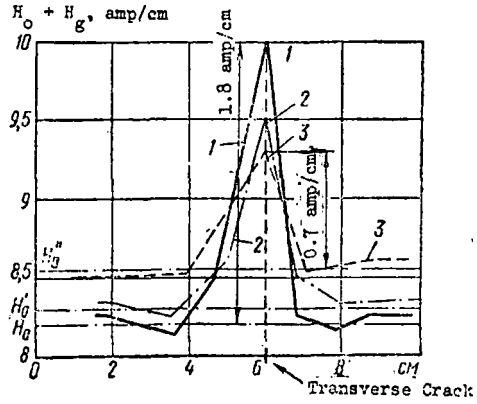

Fig. 44 Graph of changes in the field intensity along a length of rail at various distances from its surface.

Point one (1) on the graph corresponds to values of H_g measured at a distance of 2.5 mm from the surface of the head. Values of H_g are given for distances of 4 and 6 mm from the same surface on the other graphs (points 2 and 3).

The graphs in Fig. 44 show that as distances from the surface of the head increase, the level of intensity of the dispersion field of the magnet (H_o, H_o', and H_o'') increases.

Along with this, values of the field intensity H_g diminish noticably, e.g. along curve 1 at a distance of 2.5 mm from the surface of the rail head, the maximum value of H_g = 1.8 amp/cm (the transverse crack had smaller dimensions than in the previous rail). As this distance is increased to 6 mm (curve 3), the maximum value of H_g equals 0.7 amp/cm. All of this shows that when monitoring rails using the magnetic method, the flaw detector probe should be situated as close to the surface of the rail as is possible.

When analyzing the graphs, the flaw field was evaluated quantitatively by the magnitude of the intensity of the field's longitudinal component at individual points in the defective section of the rail. The graphs which are presented were constructed from measurements of the field intensity magnitudes made by means of a magnetometric circuit with miniture ferroprobes.

The difference between the sizes of the field intensity in two neighboring points along a length of the rail may also serve as a second parameter characterizing the change in the flaw field.

Magnetometric ferroprobe circuits, serving for the experimental determination of the difference in the sizes of the field intensity at two neighboring points along the rail length, are called gradienters. In essence, it is not the field gradient, but the difference in the size of the field intensities $H_g - H'_g = \Delta H_g$ in two neighboring points which is determined by the ferroprobe measuring circuits.

The ferroprobe sensor systems of magnetic rail flaw detectors also react to the magnitude of ΔH_g.

Thus, the flaw field at its various points may be characterized quantitatively by the size of H_g or by the size of $H_g - H'_g = \Delta H_g$.

We will see which of these quantities is more advantageous from the point of view of flaw detection using the magnetic method. In addition, we will point out that flaw detection in rails must meet with such changes in metal structure as are not accompanied by any kind of external signs, and therefore remain unnoticable to the eye. These changes in structure are detected by the magnetic method. Therefore, instances in which the field H_g above a dangerous transverse crack which does not emerge onto the surface of the rail head are erroneously evaluated as the manifestation of a non-homogeniety in the metallic structure are not excluded.

Graphs of the changes of the longitudinal component of the field intensity over a portion with a transverse crack and over a portion with a non-homogeneous metallic structure are given in Fig. 45 for comparison. The section occupied by the field of a flaw having the shape of a transverse crack is usually from 2 - 2.4 cm. As opposed to this, a local non-homogeniety in the metallic structure occupies a relatively larger section along the length of the rail.

In spite of the fact that these fields are distinct in form, they may have an identical magnitude of intensity. Then the maximum size of H_g, in both instances equal to 5.2 amp/cm, would not permit us to determine which of the two fields is caused by the crack. Let us see what another quantitative indicator, which characterizes a non-homogeneous magnetic field, may give for searching out a crack in such a case.

Thus, for a field caused by a crack, the size of ΔH_g for two points at a distance of l = 1 cm is equal to 3.9 amp/cm. In comparison, on the section with the structural non-homogeniety, ΔH_g for the same value of l is 1.7 amp/cm.

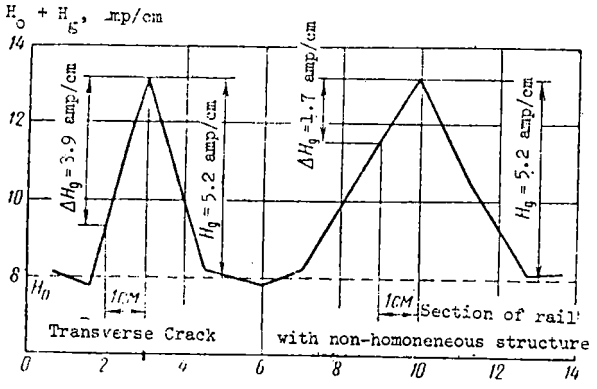

Fig. 45 Graph of changes in the field intensity on a section of the rail with a transverse crack and with a local non-homogeniety in the metallic structure.

As must be expected, the concentrated flaw field is distinct from the other field because of the higher value of ΔH_g. This may also serve as a feature aiding us to detect the internal defect in a rail with a non-homogeneous metallic structure. The field over the transverse crack may have a concentrated nature not only along the length of the rail but also across the width of the head.

Thus, for example, a curve of the change of H_g over a small crack situated to the side of the cross section of the rail head is shown in Fig. 46. This curve was obtained for points situated at a distance of 2.5 mm from the surface of the rail head. The field caused by the crack is concentrated over the flawed portion of the head cross section, and, in points in close proximity along the width of the head, the influence of the crack is not felt for practical purposes. Therefore, the detection of cracks situated to the side of the rail head by the magnetic method causes great difficulty.

So-called probes serve to detect the local fields H_g. A multiturn coil, with or without an iron core, is the simplest type of probe. If this type of coil is moved over the surface of a rail along with the magnetizing apparatus of a flaw detector, an emf impulse will be excited across its contacts on the section where there is a field H_g.

In the case when the magnetizing apparatus, which is creating a permanent magnetic field, is immobile, it is necessary to convey an oscillatory or a rotational motion to the probe coil to excite the electromotive force. When magnetizing parts with a variable magnetic field, the necessity for displacement, rotation, or oscillatory motion of the probe coil decreases inasmuch as the electromotive force will be excited even when the probe coil is not in motion.

In the practice of flaw detection using the magnetic method, probe assemblies using ferroprobes similar to those which are examined below in the section relating to the MRD flaw detector to perform as magnetosensitive elements have found broad application.

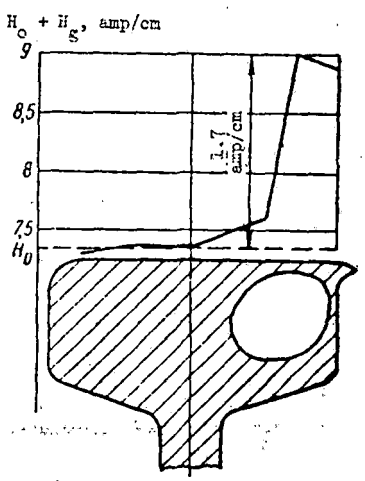

Fig. 46 Graph of the changes of the field intensity across the width of a rail head with a transverse crack.

The ferroprobe type sensor, either in motion or at rest, has a high sensitivity to a permanent magnetic field. Ferroprobe type sensors monitoring changes in the difference of the magnetic field at two points distributed along the length of the rail are used to detect transverse fatigue cracks.

6. The Eddy Current Method.

The detection of flaws in metal components using eddy currents is based on the law of electromagnetic induction, according to which a variable magnetic field excites eddy currents in them.

As is known, eddy currents are locked inside the thickness of metal and therefore cannot be used directly for the detection of flaws. Therefore, observation of those processes which always accompany eddy currents and which may be observed outside of the component being monitored is taken as the basis of the eddy current method. The variable magnetic field in the component being monitored is created by means of a magnetizing coil which is fed from an alternating current source.

When examining the eddy current method, it is necessary to keep in mind that a variable field, even at a relatively small frequency, penetrates only into the surface layer of the component.

The eddy current method envisages two distinct means for magnetization of the component: in the field of a "pass-through" coil, and in the field of a "superimposed" coil. The first type of coil serves to magnetize components which are placed into its opening or which are passed through it. A coil of the second type is placed with its butt-end to the surface of the part during the monitoring process.

Corresponding to the type of coil which is used, variations of the eddy current method have developed: the method of the pass-through coil and the method of the superimposed coil. For obvious reasons, only the superimposed

coil method may be used for monitoring rails which are in place on the line.

To clarify the main point of the eddy current method, let us imagine a flat superimposed coil situated at a distance from all metalic objects. The resistance R_o and the reactance $X_o = \omega L_o$ are the basic parameters of this coil.

A magnetizing coil is fed by an alternating current and excites a variable magnetic field of definite size and phase. This field is the primary, and it depends only on the number of turns, the dimensions of the coil, and the size of the alternating current passing through it. Further, we will assume that the flat superimposed coil is placed with its butt-end to the surface of a metalic part, the dimensions of which are much greater than those of the coil. According to the law of electromagnetic induction, eddy currents, the closed contours of which enclose the lines of the variable magnetic field, will arise in the layer of metal adjacent to the part. The eddy currents, as do any type of electrical currents, create their own magnetic field, which is the secondary, in distinction to the field of the coil. According to Lentz's law, the variable secondary field is opposed at every moment to the primary, i.e. it acts against it. The interaction of the eddy current field (the secondary field) with the field of the coil (the primary field) causes a change in the electrical parameters.

Actually, energy losses due to heating-up of the component by the eddy currents increase, i.e. the resistance of the coil, the value of which becomes equal to R_1, increases. Depending on the material (magnetic or non-magnetic) in which the eddy currents are excited, the inductance, the size of which becomes equal to $X_1 = \omega L_1$, grows or diminishes.

In this manner, the presence of eddy currents in the component being monitored may be established indirectly by measuring the electrical parameters

of the magnetizing coil. One must note that a change in the inductance of the coil when monitoring a non-magnetic material (a light metal) takes place in a manner different from when monitoring a magnetic material.

In a light metal, the opposing field of the eddy currents decreases the primary field of the magnetizing coil. In a magnetic material, in spite of the demagnetizing effect of the eddy currents, the resultant flux in the magnetizing coil is, for practical purposes, greater than the primary flux due to the magnetic properties of the substance. Consequently, in the first case the inductance of the coil decreases, while in the second it increases.

Change of the electrical parameters of the magnetizing coil depends on the electrical conductivity δ and the magnetic permeability μ of the metal on which the coil is mounted and on the frequency of the magnetizing current, as well as the thickness of the metal layer under the coil. The greater the electrical conductivity of the metal and the higher the current frequency, the greater will be the degree to which the coil parameters change. Along with this, the higher the current frequency and the greater the electrical conductivity of the metal, the smaller will be the depth to which the eddy currents penetrate. A crack or other flaw disrupting the continuity of the surface layer of metal is an obstacle for eddy currents. Such an obstacle exerts an effect similar to the effect of a sharp decrease in the electrical conductivity of the metal, which is correspondingly reflected in the electrical parameters of the magnetizing coil. The influence of metal thickness is felt only in those cases in which it is less than the depth to which the eddy currents penetrate in the given metal.

The selection of an optimal frequency for the magnetizing field for flaw detection in metals with definite electrical conductivity and magnetic properties is determined primarily by the depth at which the cracks which are to be detected

are situated. Inasmuch as only that layer of metal adjacent to the surface of the part is subjected to monitoring, to detect cracks at a minimum depth, a sufficiently high frequency is selected so that the depth to which the eddy currents penetrate should not exceed a fraction of a millimeter.

The high sensitivity to changes in the distance between the coil and the surface of the component is one limitation of the method when using the superimposed magnetizing coil. As a result, the presence of intermediate layers (oxide films, protective coverings, etc.) as well as roughness of the surface of the component being checked, result in substantial changes in electrical parameters of the magnetizing coil.

Various types of circuitry which are assumed to be basic for flaw detector construction have been proposed for observation of the change in the electrical parameters of the superimposed coil in the process of using flaw detectors on metallic parts. In one of these circuits, the superimposed coil is connected to the arm of an alternating current bridge in series with a variable capacitance. The remaining arms of the bridge contain resistances, one of which is variable. The alternating current voltage is fed to the bridge diagonal. The magnetizing coil, at the same time playing the part of the sensor coil, is placed with its butt-end on the surface of the part in a place where there are no flaws in the part. Then, with the aid of the variable capacitance, the arm of the bridge with the magnetizing coil is brought into a state of resonance, as a result of which the impedance of the arm becomes purely active, and the current in the arm is in phase with the voltage. After this, the alternating current bridge is balanced in the usual manner.

If the part was made from a ferromagnetic material, displacement of the coil to a defect site leads to an increase in its inductance. Resonance in the arm of the bridge with the magnetizing coil and the capacitance will be destroyed

as a result. The impedance of the arm will have an inductive nature, whereby the current will lag in phase behind the voltage at a certain angle φ. In the bridge circuit, a sharp increase in the voltage of the bridge imbalance and of the phase shift angle between this voltage and the voltage of the generator is observed when the inductance of the magnetizing coil changes insignificantly.

In this manner, an effect consisting of a change in the electrical parameters of the superimposed coil, under the influence of the eddy currents, permits us to accomplish flaw detection using two electrical parameters, the size and the phase of the imbalance voltage in the diagonal of the bridge circuit.

Among the other familiar circuits, the circuit with two coils, a magnetizing coil and a measuring coil, is of practical value for flaw detection using the eddy current method. The coils are fastened together rigidly, and, as a whole, comprise a device similar to the common superimposed type of coil. When such a device is mounted on the surface of a metallic part, eddy currents arise within it, the turns of the magnetizing coil encompasing the resultant flux caused by the interaction of the magnetizing field and the eddy current field. The system consisting of two coils, as well as the bridge circuit, permits flaw detection to be accomplished on the basis of two parameters, namely the size and the phase of the electromotive force in the measuring coil.

The latter variety of the eddy current method is taken as a basic principle for the operation of rail flaw detection based on alternating current. The magnetizing apparatus with a flat core (1) and a coil (2) are contained in the circuit of this flaw detector (Fig. 47). Turns of the measuring coil (3) are placed over the magnetizing coil and the core. As may be seen from Fig. 47, the turns of these coils are situated in two mutually perpendicular planes.

The alternating current in the coil (2) excites a variable magnetic field in the core (1) and the surrounding space.

On the strength of the chosen arrangement of the coils, the primary magnetic flux in the core will not excite an electromotive force in the measuring coil(3). In other words, in the magnetizing apparatus, the coil (3) does not register the variable magnetic flux in the core. All of this will be observed while the magnetic symmetry of the system being examined is preserved relative to the neutral axis passing through the center of the core and the magnetizing coil. Magnetic symmetry presupposes an identical distribution of the lines of the magnetic field in the core and in the space surrounding it to either side of the neutral axis.

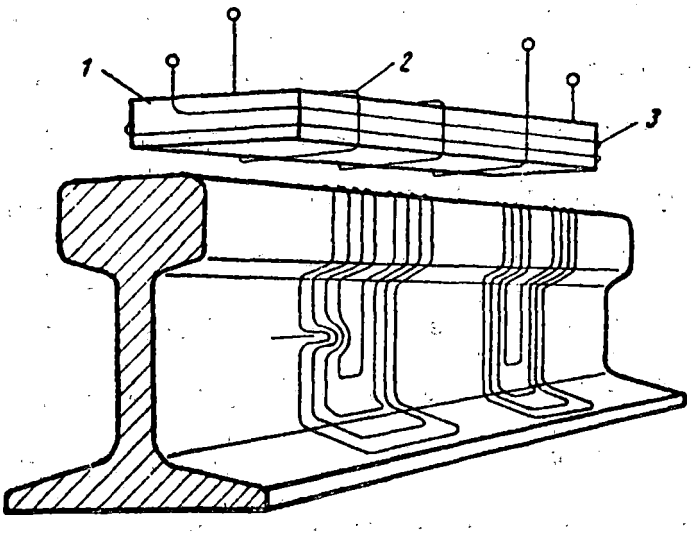

Fig. 47 Diagram showing rail monitoring using the eddy current method.

The magnetizing device is mounted over the rail head so that the longitudinal axis of the core is directed along the rail. The variable magnetic flux passing through the coil (2) excites a primary magnetic field which makes a

flux closure through the core and the section of rail being monitored. Closed eddy currents which vary in time with the frequency of the primary field arise in the surface layer of the rail under the influence of the variable magnetic field.

We will assume that the magnetizing device is situated over a section where the rail contains no flaws and is entirely homogeneous in electrical and magnetic properties. Eddy currents, the identical contours of which will be symmetrically distributed relative to the poles of the core (1), will arise in the surface layer of the rail under the influence of the primary field. As a result, the inherent field of the eddy currents, which opposes the primary field, will not disturb the magnetic symmetry of the magnetizing apparatus, and the electromotive force in the coil will remain close to zero, as was the case earlier. However, this does not mean that there are no components of the field capable of inducting electromotive forces in the coil (3) in a system with magnetic symmetry. The presence of these components may not be excluded, but the electromotive forces caused by them in the coil (3) will be identical in size and in the opposite direction. Movement of the magnetizing device leads to a displacement of the eddy current contours in the rail.

A crack on the rail surface disturbs the normal picture of the distribution of the eddy currents, the closed paths of which take on a form schematically represented in the left part of Fig. 47. The eddy current field causes a redistribution of the primary field under one of the poles of the magnetizing device, destroying the symmetry of the magnetizing system which existed earlier, and an electromotive force will appear in the measuring coil (3). In this case, changes in the phase of the electromotive force in the measuring coil are not taken into consideration.

In practice, the eddy current method for rail flaw detection is accomplished

by means of a variable magnetic field with a frequency of 500 Hz. The eddy currents caused by this field have a maximum density on the rail surface, and they penetrate the metal only to a depth of tenths of a millimeter. It is because of this that only cracks which emerge onto the rail surface may be practically detected using the eddy current method. However, this inadequacy is compensated for in part by certain merits inherent in the eddy current method. The possibility of detecting adequately developed cracks not only on the surface of the rail head, but in the web must be included among these merits. In practice, instances in which cracks have also been detected in the lower fillet have also been noted.

Eddy currents in rails may be simulated not only by a variable, but also by a constant magnetic field. In this case, it is necessary that the constant field be displaced relative to the rail. The eddy current method of flaw detection, with the use of the constant field of an electromagnet moving over the head of the rail being monitored, is described in the fourth chapter.

CHAPTER III -- MAGNETIC RAIL DETECTION (MRD) TYPE FLAW DETECTORS

1. Intended Use and Working Principles of the Flaw Detectors.

Removable, two-channel MRD type rail flaw detectors are designated for monitoring rails in place on the line. A permanent magnet is placed above each rail between the wheels of the flaw detector carriage and the rail is magnetized longitudinally by this magnet.

The magnetic field above the surface of the magnetized rail head is received by the probe apparatus. The voltage which arises at its output passes to the flaw detector amplifier situated in the center part of the carriage frame, where the power supply sources for the plate circuit and the filament circuit are also located. The presence of flaws in the rail is noted by a sound signal in the headphones and by the deflection of a milliammeter needle. The flaw detector reacts to flaws both when in motion and at rest.

The following transverse flaws in the rail head may be revealed by the MRD type flaw detectors: breaks with no visible flaw in the fractures*(flaw type 79.1-2); cracks from wheel slippage (flaw type 27.1-2); and fatigue cracks in the form of light or dark spots (flaw types 20.1-2; 21.1-2; 24.1-2; and 25.1-2) located under the surface of the rail head at a depth of 4 mm or less.

Work with the flaw detector is conducted at the average speed of a pedestrian (3-4 km/hr).

2. The magnetic rail flaw detector MRD-52.

Block diagram of the flaw detector (Fig. 48). The master oscillator (1) is a typical vacuum tube type oscillator having stable vibrations with a frequency range of 5500-6250 Hz. The oscillator is common to both rails, and it feeds the windings of the devices on the right and the left side with alternating current through a power amplifier.

*i.e. brittle fractures -- ed.

The oscillator power amplifier (2) is a tube-type amplifier which permits the power of the master oscillator to be amplified to the desired value.

A step-down transformer is mounted at the output of the oscillator power amplifier. The center tap of the secondary transformer winding is grounded.

The probe assembly (3) consists of two probes mounted on metal collector shoes and balancing screens (not shown in Fig. 48). Each of the probes in the probe assembly has two magnetosensitive elements in the form of the ferroprobes. Alternating currents passing through the ferroprobe windings stimulate a variable, auxillary magnetic field in their cores.

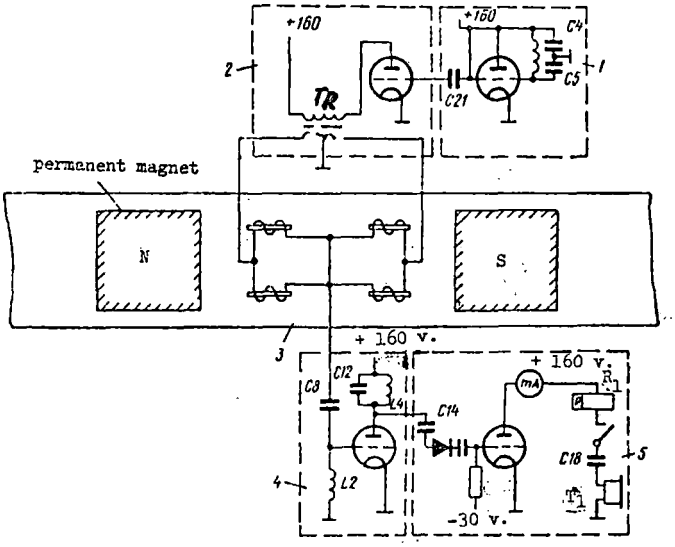

Fig. 48 Block diagram of the MRD-52 type flaw detector.

At their center taps, the electrical circuits of the probes are connected to the input resonance circuit of the following unit. The probe assembly is intended, on the whole, for searching out supplimentary magnetic fields arising above the head of defective sections of the rail.

The resonance amplifier (4) consists of the amplifier tube and two oscillation circuits; the input C8-L2, and the anode C12-L4 (cf. Fig. 48). Both circuits are tuned to a frequency twice that of the oscillator frequency.

The oscillation circuits and the amplifier tube comprise the resonance amplifier, which is intended for amplification of the voltage of the doubled

frequency. This voltage arises on the terminals of the ferroprobe windings when a constant flaw field is superimposed on the constant auxillary field in the coils. This instance corresponds to the condition of the core magnetization represented on the graph in Fig. 32.

A low-frequency amplifier (5), with a signaling device, is intended for final amplification and rectification of the doubled voltage. The amplifier has one tube, in the anode circuit of which a milliammeter and the winding of a polarized relay are connected. The headset is connected through the contacts of this relay.

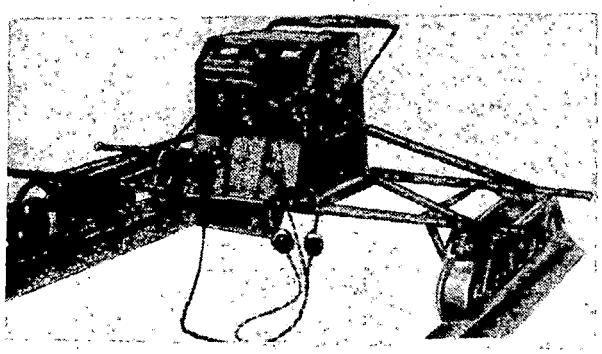

Fig. 49 General view of the MRD-52-TsNII type flaw detector.

The units which have been described are mounted in one apparatus box, where the power supply units for the plate circuit and the fillament circuits of the oscillator and the amplifiers are also located.

A general view of the MRD-52 type flaw detector with the described block circuit is shown in Fig. 49.

The flaw detector's magnetizing device and rail magnetization. Two assembled permanent magnets, situated above the left and the right rail of the track, serve for rail magnetization in the MRD-52 flaw detector. Each magnet consists of two bars (1) (Fig. 50) made of a Magnico alloy, and a yoke (2) of soft

annealed iron completing the circuit between them. The magnets of the left and right rail of the track are turned so that the same poles point in the same direction (it makes no difference which direction).

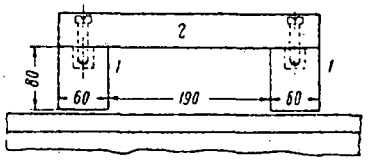

Fig. 50 Sketch of the assembled permanent magnet.

Each Magnico bar has a cross-sectional dimensions of 6 X 6 cm and a height of 8 cm. The Magnico bars are enclosed in aluminum casings with walls 2-millimeters thick.

Under the poles of the magnet, between the surface of the case and the running surface of the rail head, there are clearances of 4.5 - 5 mm. Relatively large clearances are necessary for the flaw detector to pass along a track with joint connections having a substantial elevation of one rail end relative to the next.

The air gap between each of the poles, taking into consideration the thickness of the casing walls, is 6 - 6.5 mm.

The Magnico alloy is related to the category of cobalt steels. Iron, nickel, cobalt, alluminum and copper go into this alloy.

This alloy acquires the necessary magnetic properties only after thermomagnetic processing, which consists of cooling the bars in a strong permanent magnetic field. The field of the thermomagnetic processing should correspond in direction to the field in which the bars will subsequently be magnetized. A prefered direction, in which the residual induction and the coercive force have higher values than in the other directions, is created during thermomagnetic processing.

After thermomagnetic processing, the Magnico bars are demagnetized and then subjected to mechanical processing, which consists of polishing the end-surfaces. Then the magnet is assembled, the bars being fastened to the soft iron yoke. The assembled magnet which is thus obtained should again be magnetized in a closed magnetic circuit.

This type of circuit is created by connecting the free ends of the assembled magnet with the massive auxillary yoke.

The constant magnetic field necessary for saturation may be obtained by putting current-carrying coils on the bars. Let us assume that in the closed circuit of the assembled magnet, a magnetic field is created, the intensity of which gradually increases from zero to a positive value H_m. Under the influence of the strengthening field H, magnetic induction in the magnet material will change according to curve a (Fig. 51). After the intensity of the magnetic field has reached a known value H_m, corresponding to the induction of magnetic saturation B_s, further growth in the induction ceases for practical purposes.

As the intensity of the field is decreased from H_m to zero, the value of the magnetic induction will be determined by the ordinates of curve b, located everywhere above curve a. As the magnitude of the field intensity is decreased to zero, the magnetic induction decreases to a residual induction value B_r. The process of magnetization for the assembled magnet terminates with this step.

If, as the saturation induction B_s is being attained, the magnetic field intensity is decreased to zero and then the magnetizing field source is switched off, the residual induction will have a value of B_r while the magnetic circuit of the assembled magnet remains closed. Then the permanent magnet is removed from the auxillary yoke, making the circuit with its ends. As the magnetic circuit is broken, the assembled magnet automatically comes to another magnetic state determined by the values H_d and B_d, relating to one of the points on the demagnetization curve.

The shift to the region of negative values for H is explained by the fact that when the circuit of the assembled magnet is broken, magnetic poles arise on the free ends. Under the influence of the poles which are formed, an internal magnetic field which is negative, i.e. demagnetizing in direction, will appear in the magnet body. Thus, demagnetization may take place solely under the influence of the magnetic fields which are formed, and may exclude the influence of an external negative field.

We will assume that the intensity of the internal demagnetizing field is equal to H_d. Then the induction B_d (point P) will correspond to this value of field intensity on the demagnetization curve. Consequently, as a result of the break in the magnetic circuit, the residual induction B_r will decrease to a value B_d.

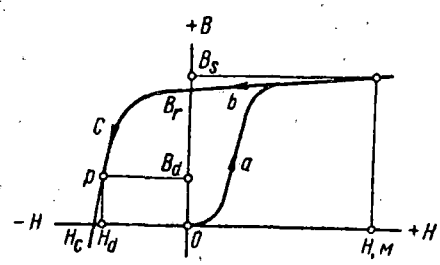

Fig. 51 A part of a hysteresis loop corresponding to the process for the formation of a permanent magnet.

And so, the process for forming a permanent magnet includes the following stages:

1. Magnetization of the material of the magnet to a saturation induction B_s by an external field in a closed circuit
2. Reduction of the external field to zero and formation of the residual induction B_r in the magnet material

3. Breaking the magnetic circuit and forming the internal demagnetizing field H_d and the working induction B_d.

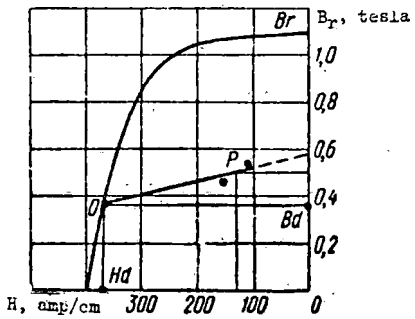

Fig. 52 Demagnetization curve for an assembled magnet when its magnetic circuit is broken.

In a magnet composed of different metals, only the Magnico alloy possesses high values for the residual induction and the coercive force H_c. These properties of a Magnico alloy will also determine the quality of the assembled magnet. A demagnetization curve for a Magnico alloy with average values of 400 amp/cm for H_c and 1.1 tesla for B_r are shown in Fig. 52.

It has been experimentally established that after the magnetic circuit of an assembled magnet has been broken, the field intensity H_d is equal to 375 amp/cm, while the induction B_d in the elements of a magnet made from Magnico is equal to 0.38 tesla. Consequently, point O will correspond to the state of the assembled magnet along the demagnetization curve.

As the poles of the magnet are brought near the rail head, and with an air gap of 6 - 6.5 mm, induction in the Magnico bars increases to a value of B equal to 0.5 tesla, whereas the negative field intensity falls to a value H equal to 130 amp/cm. The point lying to the left of P corresponds to the clearance of 8 mm between the poles and the surface of the head. The point lying to the right of P corresponds to a clearance of 4 mm. The three indicated

points and point O lie on one line, called the line of regression.

As the magnet approaches the rail, the increase in induction does not take place according to the demagnetization curve B_r, H_c, but along the line of regression. As the magnet is removed from the rail, induction and field intensity acquire their former values, corresponding to point O. For the given construction and form of the assembled magnet, it is impossible to rise above point O along the demagnetization curve.

With the normal working clearance under the poles of the permanent magnet, the magnetic induction will have the values given in Table 4.

Table 4

Rail Type	Cross-section of worn head, cm^2	Average value of the magnetic induction, tesla
R65K	28.0	0.30
R50K	25.1	0.35
R43K	24.1	0.40

The values of the magnetic induction indicated in Table 4 constitute only 20 - 25% of the saturation of rail steel.

A permanent magnet has dispersion, i.e. part of the magnetic force lines between its poles passes through the air immediately above the running surface of the rail head.

The intensity H_o of the longitudinal component of the dispersion field of a permanent magnet in the zone in which the flaw detectors are situated reaches 8 - 11 amp/cm for rails from different plants (experimental data).

The ferroprobe and its working principles. The flaw field arising on the background of a stronger dispersion field between the poles of a magnet is

received and isolated by means of probes. The magnetosensitive elements in the flaw detector probe assemblies are called ferroprobes.

A ferroprobe (Fig. 53) has a coil (1) with a multi-turn winding, inside of which is a core made of a nickel-iron alloy. The ferroprobe winding is connected to an oscillator (2), producing a current of frequency f. An alternating current which stimulates a magnetic field changing with the same frequency f (the auxilary field) in the core, passes through the ferroprobe winding. A resonance circuit (3), tuned to a frequency 2f is connected to the ferrobrobe winding. A resonance amplifier (4), at the output of which is a measuring device, follows the resonance circuit.

The resonance circuit and resonance amplifier serve to isolate the second harmonic component of the electromotive force which arises in the ferroprobe winding under certain conditions. As was indicated in Chapter 2, the second harmonic component of the electromotive force, or simply, the second harmonic of the electromotive force, has a frequency which is twice that of the frequency of the alternating generator current.

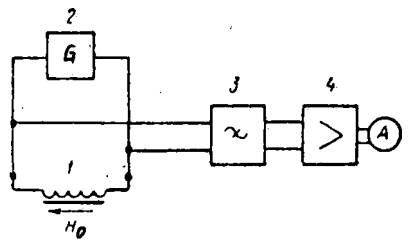

Fig. 53 Principle diagram of a ferroprobe with isolation of the doubled frequency e.m.f.

A second harmonic of the emf arises only in those cases when the core of the ferroprobe works under the condition of simultaneous magnetization by two magnetic fields (a variable and a constant field). The variable field is stimulated by the alternating current of the generator, whereas the constant

field may be, for example, the field of a flaw situated in the magnetized rail.

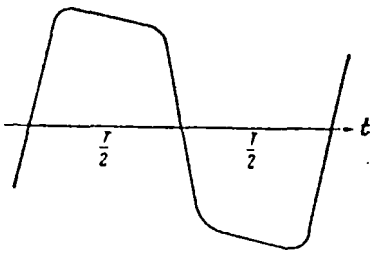

Fig. 54 The change in the variable component of the magnetic field in the core of a ferroprobe in the absence of an external constant field.

Under certain known conditions, which we will mention below, the second harmonic of the electromotive force in the ferroprobe winding is proportional to the intensity of the constant biasing field, which will henceforth be called the external constant field. Therefore, the circuit shown in Fig. 53 may serve to measure the intensity of the external constant field acting simultaneously with the variable field in the ferroprobe core.

It is obvious that the second harmonic of the emf in the ferroprobe winding is induced by the second harmonic of the magnetic flux in the core. Experience shows that in the absence of an external constant field, the periodic curve of the magnetic flux in the core has the form shown in Fig. 54.

Due to the periodic saturation of the core, this curve is clipped on the peaks, and is close in form to the magnetic flux curve found by construction, as shown in Fig. 31. Both curves show that, in the absence of an external constant field, i.e. when the intensity of this field H_o is equal to zero, and, given a periodic saturation of the core, the variable magnetic flux has a non-sinusoidal form. But, in this case, the curve which characterizes its change

in time remains symmetrical relative to the line t.

As has already been indicated, periodic non-sinusoidal curves which are symmetrical relative to the time line do not contain even-numbered harmonics, including the second-order harmonic.

Thus, at H_o equal to zero, the variable magnetic flux in the ferroprobe core does not contain a second-order harmonic, as a result of which, the curve of the electromotive force in the ferroprobe winding will not contain a second-order harmonic either. As a result, the needle of an instrument connected to the output of the resonance amplifier will be in the zero position.

Let us turn to an examination of another case, when the ferroprobe with a variable field in the core is introduced into an external constant field with an intensity H_o. We will assume that the effective value of the variable magnetic field intensity is several times greater than the intensity H_o. A similar instance has already been examined (a graphic construction of the variable magnetic flux curve in a core working under the condition of simultaneous magnetization by two fields, variable and constant, was shown in Fig. 32). Under this condition, the curve of the variable component of the magnetic flux in the core has a form which is asymmetrical with regard to the line and, consequently, contains even-order harmonics.

For the very same reasons, the curve of the variable component of the magnetic flux in a ferroprobe core (Fig. 55) takes on noticable traits which destroy its symmetry relative to the line t. Actually, in the first part of the period, the magnetic flux curve is more sharply clipped than in the second. The time during which the ferroprobe core is saturated also increases in the first part of the period.

The same traits are also present on the curve in Fig. 32, where they are expressed somewhat more weakly, because the graphic construction was carried

out according to the magnetization curve and not according to the dynamic hysteresis loop, and the influence of eddy currents was neglected. Thus, the curve of the variable component of the magnetic flux becomes asymmetrical relative to the time line under the influence of the external constant field, indicating the presence of even harmonics in this curve, among which, the second-order harmonic, i.e. the harmonic with a frequency of 2f, has the greatest amplitude. This harmonic will excite an electromotive force of the same frequency in the ferroprobe winding.

The amplitude of the electromotive force E_M of the doubled frequency may serve as a measure of the intensity of the constant biasing field H_o. To determine values of H_o based on value of E_M, it is necessary to know the dependency between them. The dependency which was indicated (Fig. 56) was obtained for a ferroprobe with a core 7 mm long and 0.25 mm in diameter made from 80-NKhS iron-nickel alloy. The values of H_o, the intensity of the external constant field, are plotted on the x-axis in Fig. 56, while E_M, the amplitude values of the electromotive force of the doubled frequency in one turn of the ferroprobe winding, is presented on the y-axis in millivolts. The dependency of E_M on H_o is linear if the variable magnetic field in the core causes its periodic saturation. When H_o, the intensity of the external field, is equal to zero, the value of E_M will also approach zero. The electromotive force of the doubled frequency changes phase by 180 degrees when the direction of the external constant field is reversed.

Thus, under the condition of simultaneous magnetization of the core by two fields (one variable and one constant), the voltage of the doubled frequency is stimulated in its winding. A resonance circuit consisting of self-induction coils and a capacitor connected in series serves for separation of this voltage. The drop in the voltage at one of the elements of this circuit is amplified,

and may be measured by a voltmeter after amplification.

The single ferroprobe which is described here is the basic element of a flaw detector probe circuit.

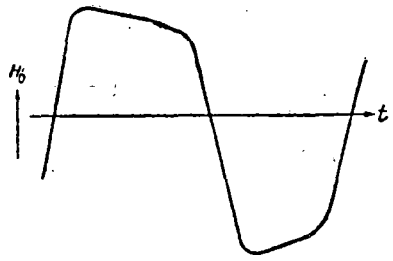

Fig. 55 A curve of the variable component of the magnetic flux during simultaneous magnetization of the core of a ferroprobe by two fields, a variable, and an external constant field.

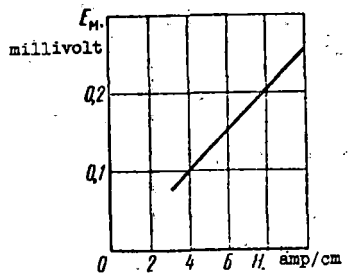

Fig. 56 Dependency of the amplitude of the second harmonic of the emf in one turn of the ferroprobe winding on the intensity of the external constant field.

Connection diagram for the flaw detector probe assemblies. The MRD-52 probe assemblies should locate transverse fatigue cracks regardless of their disposition in the cross-section of the rail head. This demand may be met by checking the rail not with one, but with two identical probes set above the rail head as shown in Fig. 57.

Each probe assembly has two ferroprobes which are mounted on a special backing. The distance between the center-points of the ferroprobes is 1.2 cm.

It was indicated above that a distance $\underline{l}$ equal to 1.2 cm is approximately half of the extent of the field of a transverse crack in the rail head.

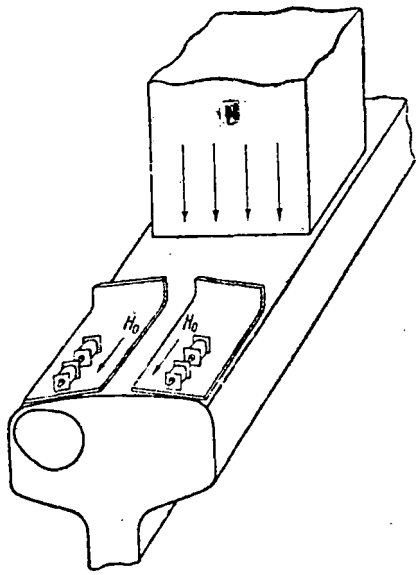

Fig. 57 Disposition of the probe assemblies above the rail head.

The ferroprobe cores are set along the axis of the rail parallel to the running surface of the head. The backing with the ferroprobes is mounted on a separate collector shoe which slides along the surface of the rail head. The cores of all four ferroprobes are at the same distance from the running surface of the rail head, approximately 2.5 mm.

The two probe assemblies are connected according to the differential network shown in Fig. 58. A step-down transformer with a lead-out from the centerpoint of the secondary winding is included in the anode circuit of the generator power amplifier (1) feeding power to the ferroprobe windings. Transformer symmetry with regard to the grounded housing is obtained by a special execution of the secondary windings, which are wound simultaneously with the two wires from the two coils.

The input resonance circuit of the amplifier is connected between the

centerpoints of the probe assemblies and the centerpoint of the secondary transformer winding. The circuit consists of a capacitor and an inductance coil connected in series. It may be seen from Fig. 58 that the input resonance circuit of the amplifier also forms a load circuit for the differentiational network of the probes. The circuit has sharp tuning to a frequency 2f, i.e. to a frequency which is twice the generator frequency.

The dispersion field of the magnet may be taken to be uniform when the small volume which each probe assembly occupies above the rail is at a distance away from the flaws. This means that at all points in the space in which the ferroprobes are located, the dispersion field of the magnet will have an intensity H_o which is identical both in magnitude and in direction. As a result, electromotive forces from the doubled frequency which are identical in magnitude and direction will also arise in the ferroprobe windings. Consequently, just as was the case in the single ferroprobe which we examined earlier, the ferroprobes, and not the generator, are the source for the electromotive force for the doubled frequency in the electrical circuits of the probe assemblies.

The electromotive forces e of the doubled frequency arising in the ferroprobe windings lead to the appearance of currents of the same frequency. If the resistance of the ferroprobe windings and the resistance of the transformer windings are identical, the current i passing through the closed circuits of the probes' differential network will be identical. Here, in the resonance circuit which comprises the load circuit for the probe assembly, the currents i, which are equal in size, have an opposite direction, i.e. they compensate each other.

Therefore, there will be no doubled-frequency current regardless of the size of the magnet's dispersion field intensity H_o in the load circuit of the probe assembly circuit. Consequently, the differential network of the probes permits the influence of the strong but homogeneous dispersion field of the

magnet to be excluded, i.e. the influence of a field which is not associated with flaws in the rails is excluded.

Application of the means described for connecting the probes facilitates the task of observing the flaw field arising on the background of the magnet's strong, interfering dispersion field.

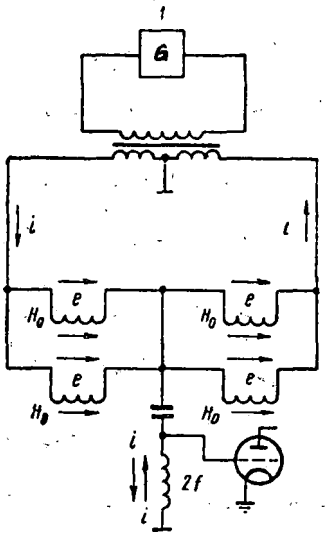

Fig. 58 A differential network for connecting two probes with emf and currents in its circuits in the absence of a field H_g.

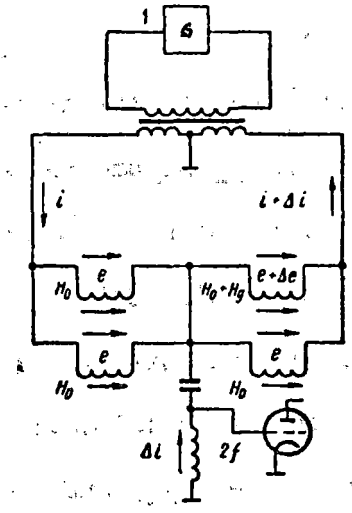

Fig. 59 A differential network for connecting two probes with emf and currents in its circuits in the presence of a field H_g.

Let us examine the work of probes which are connected differentially on sections of rail which contain flaws. We will assume that there is an internal transverse crack in the lateral part of the rail head section, as was shown in Fig. 57. It was noted above that the field of such a "lateral" transverse crack may be noted only above the defective portion of the section of the rail head, i.e. this field will act on the ferroprobe of only one sensor. Let us suppose that one of the ferroprobes of the sensor situated on the side with the "lateral" crack entered the zone in which the magnetic field H_g of the crack is active. At that time, the second ferroprobe of the same sensor, being at a distance of 1.2 cm from the first is beyond the boundaries of this field.

In view of what has been said, the cores of three of the ferroprobes will be magnetized by the dispersion field of the permanent magnet H_o, while the fourth will be magnetized by a total field, $H_o + H_g$ (Fig. 59), where H_g is the intensity of the longitudinal component of the flaw field (of the crack field). In accordance with this, identical electromotive forces e of the doubled frequency equal to $e + \Delta e$. Therefore, the doubled-frequency current passing through a circuit with electromotive force will be increased by Δi and will be equal to $i + \Delta i$.

Consequently, a current Δi, equal to the difference of the opposing currents, one of which is equal to $i + \Delta i$ and the second equal to Δi, will pass through the load circuit on the differential network of the sensors (the circuit which contains the self-induction coil). The current i will cause a voltage drop ΔV on the self-induction coil of the resonance circuit, which will be the voltage on the output of the differential network of the probe. The voltage ΔV, as well as the current Δi, will have a doubled frequency in comparison with the frequency of the alternating current generator.

If the alternating current from the generator periodically saturates the

ferroprobe cores, the voltage ΔV is proportional not only to the difference in currents $(i + \Delta i) - i$, but also to the difference in the magnetic fields, $(H_o + H_g) - H_o = H_g$.

In this manner, when a "lateral" transverse crack in the rail head is detected, the described circuit with four ferroprobes reacts to the difference in the magnetic fields acting where the ferroprobes of one of the probe assemblies are distributed.

It follows from what has been said that checking each rail using two probe assemblies permits, first of all, the exclusion of the interfering influence of the dispersion field of the magnet above the rail head, and, secondly, the direction of transverse cracks located in the lateral part of the rail head cross-section. It is not difficult to demonstrate that two probe assemblies connected according to a differential network permit the detection not only of "lateral" cracks, but also of cracks situated in the center portion of the rail head.

The magnitude of the current Δi and the magnitude of the voltage ΔV associated with this current permit the sensitivity of the probe circuitry to a constant magnetic field to be determined.

By "sensitivity of the probe circuitry", we mean the ratio $\Delta V/H$, showing which voltage ΔV arises on the output of this circuit when one of the ferroprobes is situated under the influence of a constant field with an intensity H equal to 1 amp/cm. When the cores of the ferroprobes are periodically saturated with a frequency of 5000 Hz, the sensitivity of the probe circuitry is 250-270 millivolt·cm/amp.

Besides the differential network with two probes, probes with a single differential network having two ferroprobes (Fig. 60) are finding practical application.

Both ferroprobes of this type probe assembly are situated on one collector shoe, which is shifted to the gage side of the rail head, where transverse cracks most often appear, when the rails are tested. The shoe with two ferroprobes is frequently called a single probe.

Use of the single probe is justified by the fact that its sensitivity to the field of a "lateral" crack is 1.5 - 1.6 times greater than the sensitivity of the previously discribed probe.

When the differential network of the probes was being described, it was assumed that all ferroprobes have totally identical windings and cores. Therefore, in the homogeneous field above the head of a non-defective rail, the voltage at the output of the differential network for the probe is equal to zero; consequently the network is balanced. However, it is difficult to attain the situation in which all four ferroprobe cores have exactly identical magnetic properties, form and dimensions. Therefore, even in a homogeneous magnetic field, there is usually a certain voltage, the "imbalance voltage", at the output of the probe's differential network. This voltage is not associated with flaws in the rail, and it may therefore cause interference during monitoring. The imbalance voltage is reduced to a minimum by balancing the probe circuits.

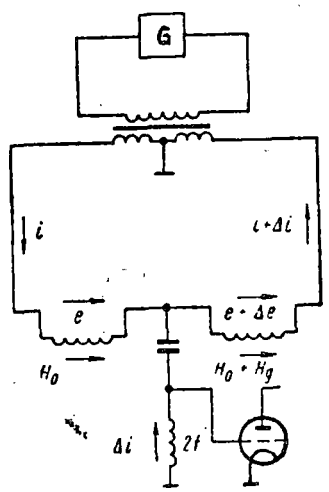

Fig. 60 Circuit of a probe assembly with two ferroprobes.

Probe assembly lay-out.

There are two probe assembly units in the MRD-52 and MRD-66 flaw detectors: one to monitor the right rail and one to monitor the left.

Each probe assembly unit consists of three ferroprobe sensors, two of which are mounted on the running surface of the rail between the poles of the magnet, with the third affixed to the frame of the flaw detector carriage on the side of the gage edge of the rail being monitored. The probes which are mounted on the running surface of the rail are called the "upper" or "primary" probes.

The ferroprobes of upper probe assemblies for the MRD-52 flaw detector are in the form of a coil with a core 7 mm long and 5 mm in diameter. The coil winding has 2500 turns of PEL-0.03 mm wire. A section of 80-NKhS wire made from an iron-nickel alloy (Permalloy), with a diameter of 0.25 mm and a lenght of 7 mm is the coil core.

A sketch of the upper ferroprobe sensor is given in Fig. 61. It consists of the ferroprobes (1), a plastic block (2), and the contact lobes (3). The ferroprobes in the block are set out on the center line. Each upper probe is mounted on the lower base of the metallic collector shoe (1) shown in Fig. 62. In the upper part of the shoe, there is a screw device (2) by means of which the magnetic screen (3) is moved relative to the probe assembly's ferroprobes (4), thus accomplishing its balancing.

Above the lower base of the collector shoe, a metallic covering (6), which slides along the surface of the rail head, is attached by screws (5). The covering is a replacable part of the shoe, and it is replaced with a new one as it wears out.

At the ends of the collector shoes, there are pins (7), freely fitting into the vertical grooves of the holder (8). In the upper part of the holder,

there are grooves at each end, into which the horizontal guide straps which are fixed to the magnet yoke fit. Due to this arrangement, each shoe and its holder may be displaced across the width of the rail head, and affixed in the desired position with the set screws (9). The holder has a spacer rod (10) on which the terminal box (11) is mounted. The three flexible wires leading from the ferroprobe sensor assembly lead into this box where they are connected with the three-pronged plug (13) by a section of flexible three-lead wire (12).

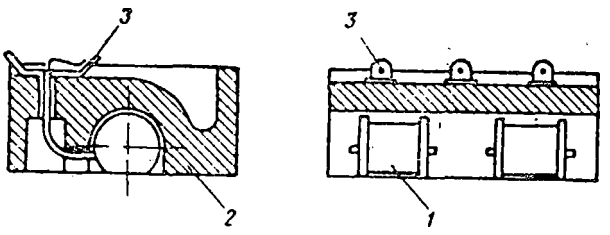

Fig. 61 Sketch of the upper ferroprobe sensor.

All parts of the collector shoe and the sensor are prepared from a non-magnetic material.

As has already been indicated, a screen (3) made of soft iron may be moved over the ferroprobes of the sensor in one direction or another to balance the probe assembly.

Since the screen is situated in the dispersion field of the permanent magnet, it is magnetized. Displacement of the magnetized screen above the probe results in one of its poles approaching the core of one of the ferroprobes, the opposite pole of the screen being moved away from the core of the other ferroprobe. In the same way, the magnetism of the ferroprobe cores is changed, influencing the size of the doubled-frequency emf induced in the ferroprobe windings. It is possible to find a position for the screens at which the voltage on the network output is minimum, i.e. the probes will be balanced.

The probes mounted on the frame of the flaw detector carriage on the gage edge of the rail being inspected are called the "lateral" or "fillet" probes. In the MRD-52 and MRD-66 flaw detectors, the lateral probes are used for secondary verification of the upper probe readings. The flaw detectors' upper probes may react to dangerous sites of damage to the running surface of the rail head, in addition to dangerous internal transverse cracks. From the indications of the upper probes alone, it is difficult, and sometimes impossible, for a flaw detector maintainance engineer to distinguish the readings of flaw detectors above dangerous cracks from the readings above non-dangerous points of damage or non-homogeneous metallic structure.

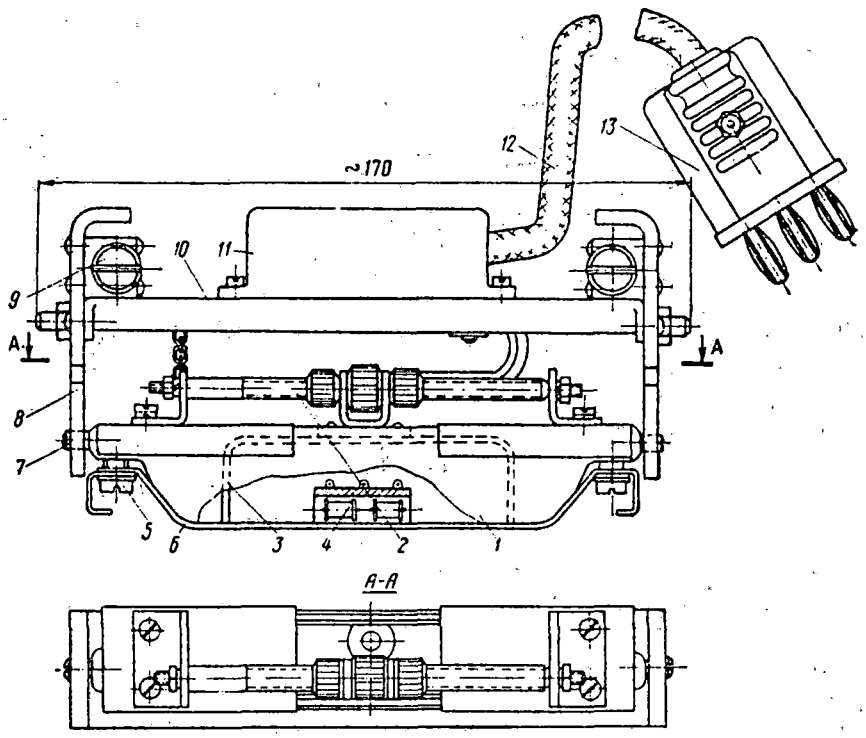

Fig. 62 Sensor assembly for the MRD-52 flaw detector.

Using a probe mounted on the lateral or fillet part of the rail, it is possible to distinguish the readings of a flaw detector situated above the

described transverse fatigue crack from those readings obtained above a non-dangerous point of damage or structural non-homogeniety of the metal during secondary inspection of that place on the rail noted by the upper probes. This is facilitated by the fact that the magnetic flaw field arises not only on the running surface, but also on the gage side of the head and above the head when the rail is magnetized by the U-shaped magnet of the MRD-52 and MRD-66 flaw detector above transverse fatigue cracks. The intensity of this field depends on the proximity of the crack to the surface of those indicated places and the area occupied by the crack. The metal in the lateral surfaces and below the head is not subjected to work hardening and damage from the wheels of the rolling stock. This excludes the possibility of interference occurring, as happens on the running surface, and the probe mounted on the lateral or fillet part of the rail will react only to the field over the dangerous flaw.

The working principles of the lateral probe are the same as for the primary probes. The coils of the probe assembly's ferroprobes are connected according to a differential network. Therefore, they do not react to a homogeneous magnetic field, but, at the same time, they possess a high sensitivity to the concentrated fields of flaws.

The absence of interfering magnetic dispersion fields on the lateral and fillet surfaces of the rail head permit the detected places on the rail to be inspected with a significantly higher flaw detector sensitivity (at greater amplification). As a result, it is possible to reveal fatigue and transverse cracks from the lateral or fillet side of the rail head which are smaller and lie deeper in the rail than is the case from the running surface.

The lateral probe assembly in both the MRD-52 and the MRD-66 flaw detectors are identically constructed.

The lateral probe assembly (Fig. 63) consists of a ferroprobe sensor (1),

a slotted link (2), a brace, (3), a locking assembly (4), a fastening assembly (5), a reflector (6), a mechanism for lowering and raising (7), and the connecting wire with the three-pronged plug (8).

The lateral probe may be mounted on either the lateral or the fillet side of the rail head with the aid of the slotted link nut (2). The locking assembly serves to secure the lateral probe in an off-position. The reflector (6) serves to protect the ferroprobe sensor from damage when the probe assembly moves across the joint plates and at grade crossings.

Each lateral probe may be switched on with one of the primary probes or as a single probe, inspecting rails only from the fillet side. The dispersion field of the magnet has almost no effect on the ferroprobes of the lateral probe assembly. The ferroprobes are shielded, as it were, from the influence of the dispersion field of the magnet by the metal of the rail head. As a result, the sensitivity and selectivity increase. Additionally, the absence of work hardening, dents, engine burns and other damage from the lower edge of the rail head permits the amplification from the amplifier to be increased without fear of increasing the interference.

In this manner, turning on the fillet probe as a single probe permits inspection of the state of the rails to be carried out with significantly greater sensitivity than by switching on two probes in parallel, one of which is situated on the running surface of the rail head.

In practice, it is impossible to increase the sensitivity of the flaw detector when two probes are used since under these conditions, the level of interference from the probe mounted on the running surface increases sharply. Therefore, some MRD flaw detector maintainance engineers make two passes with the flaw detector when checking sections of the line where the greatest rail failure from 20.1 - 2 and 21.1 - 2 type defects is observed. On the first pass,

they use the normal probes mounted on the running surface of the head of the rails being checked, whereas on the second pass, they use only the fillet probes. When the lateral probes are so used, the half of the rail head on the gage side is checked from two sides, providing a high quality check of the rails with regard to detection of transverse fatigue cracks.

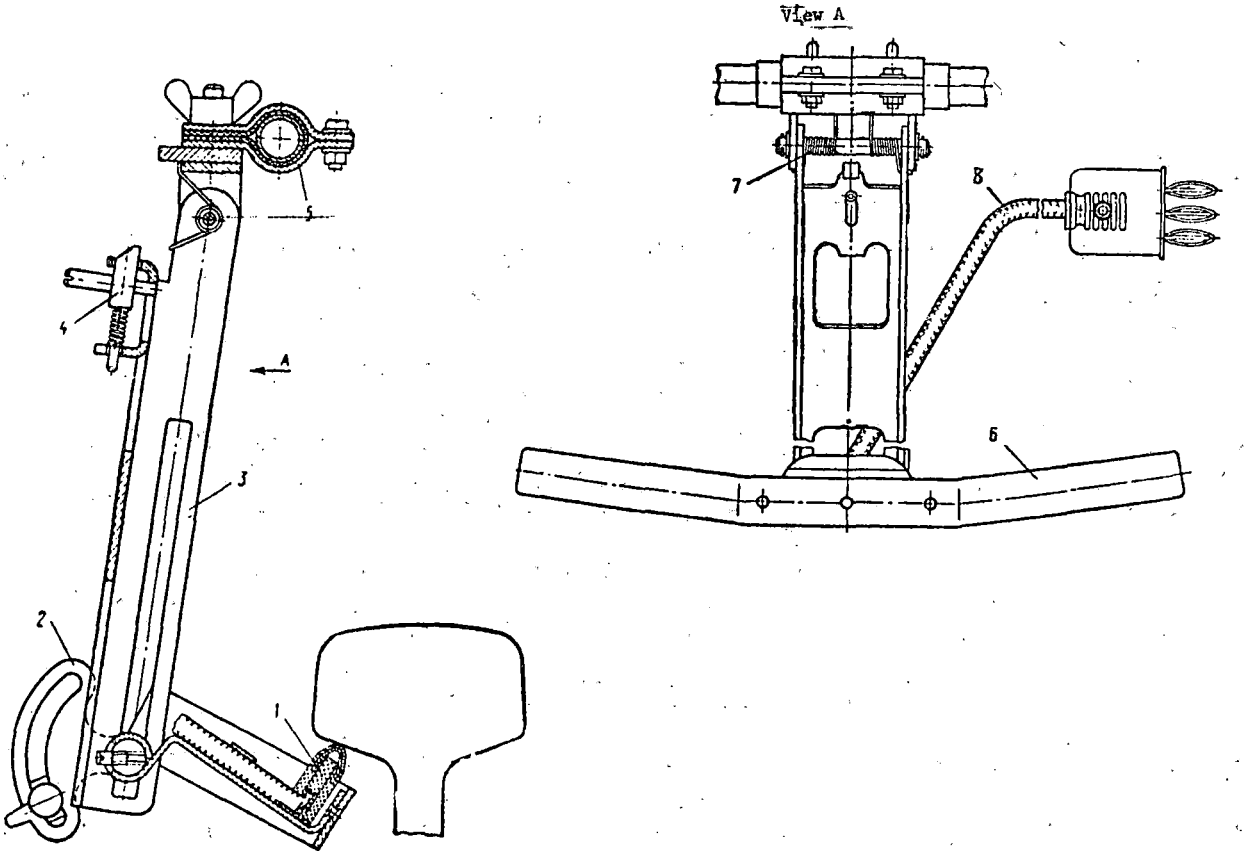

Fig. 63 Sketch of the MRD flaw detector's lateral probe assembly.

The electrical system diagram of the MRD-52 flaw detector (Fig. 64).

The master oscillator is assembled on tube Tul, a 2P1P type. The generator oscillation circuit consists of a self-induction coil wound on a torroid

core of Alsifer (Al-Si-Fe alloy) and two capacitors C4 and C5 connected in series. The self-induction coil L1 is shielded by a metallic casing, and has seven taps. Taps 1 and 2 form the beginning and end of the primary coil winding, while taps 3, 4, 5, 6, and 7 lead out from tuning sections wound onto the primary winding of coil L1. The tuning sections are used to increase or decrease the induction of coil L1 when tuning the generator to the corresponding frequency. The oscillation circuit is connected between the anode of tube Tu1 and its control grid.

The size of the total capacitance of the circuit capacitors C4 and C5 and the inductance of L1 determines the frequency of the generator, which should be constant and be within the range 5500-6250 Hz.

The capacitance C3 and the resistance of R5 connecting the oscillatory circuit with the control grid of Tu1 are selected so that the voltage of the master oscillator has a sinusoidal form.

A high resistance R10 is included in the anode circuit of the generator tube so that the B battery does not shunt the alternating generator voltage.

With the aid of the master oscillator, a stable sinusoidal voltage is obtained. However, the power of this oscillator is inadequate to feed the probes on both sides of the flaw detector. Power amplifiers Tu2 and Tu3, assembled on 2P1P tubes, are installed for the right and left rail in order to increase the power of the master oscillator to the necessary magnitude.

The voltage of the master oscillator is passed through a blocking capacitor C21 and the resistance R1 and R2 to the grid of tubes Tu2 and Tu3 of the power amplifier. With the aid of the blocking capacitor C21 and the resistors R1 and (R2)* - R3(R4)*, stepped down the voltage of the master oscillator to a magnitude at which the power amplifier can amplify it without distortion.

---

*Elements of the symmetrical branch of the diagram are indicated in parenthesis.

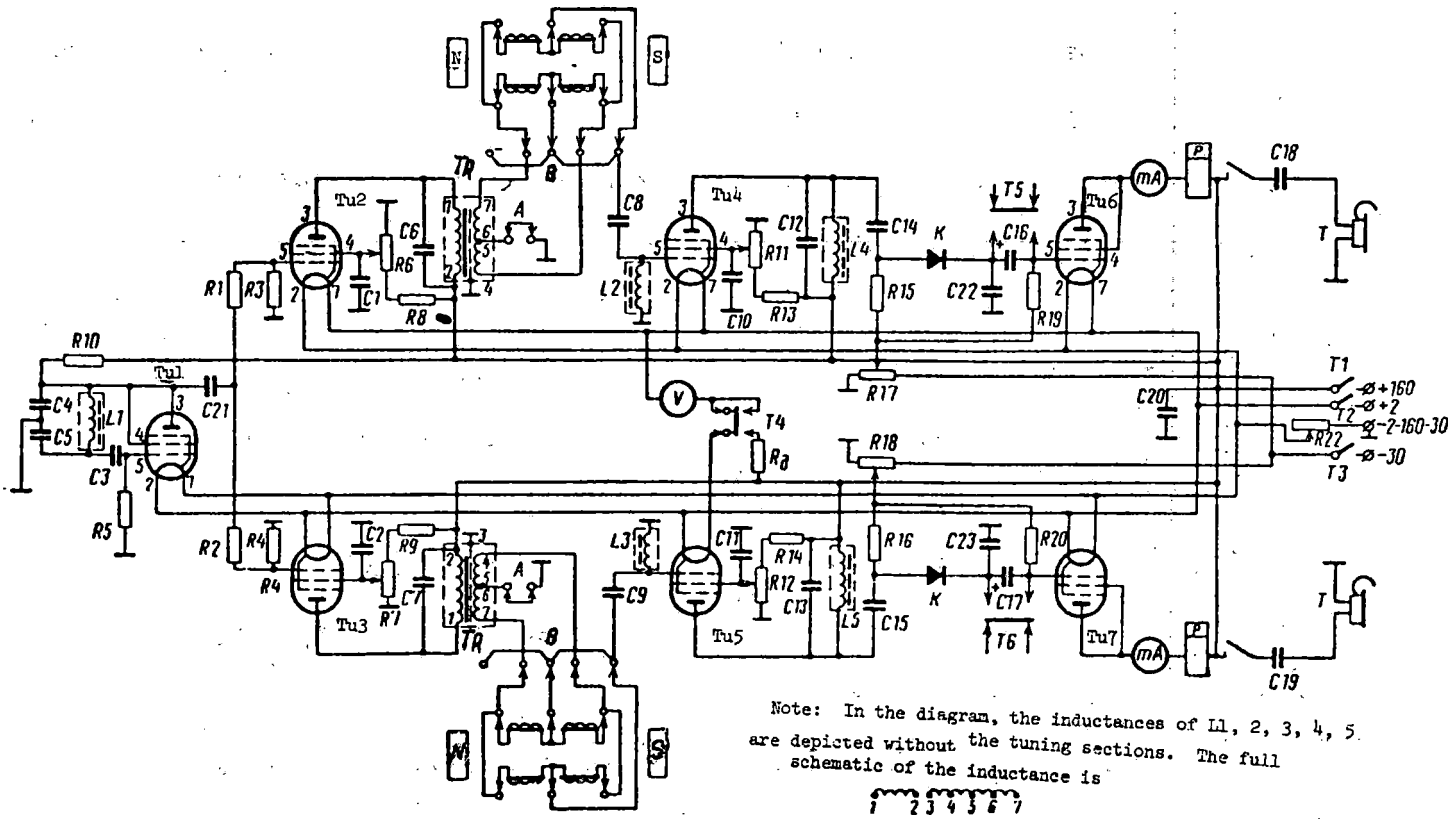

Fig. 64 Principle schematic of the MRD-52 flaw detector.

An output step-down transformer Tr is included in the anode circuit of the power amplifier. There are two identical windings on the low-voltage side of the transformer. The primary transformer winding has two leads 1 and 2. The ends of the secondary windings are denoted by 4-5 and 6-7 respectively. The series connection of the secondary transformer windings is accomplished by connecting leads 5 and 6. This centerpoint of the secondary transformer windings is connected to the corresponding socket on the face panel of the apparatus. When necessary, it may be connected to the body of the apparatus with the aid of a plug.

A capacitor C6(C7) is included in parallel with this winding so that the current flowing through the primary transformer winding is sinusoidal. The capacitance of this capacitor is chosen when the apparatus is tuned. During tuning, the probes should supply the transformer load.

The output voltage of the power amplifier is regulated with the aid of a potentiometer R6(R7) by a knob designated on the face-panel "Power".

A fixed resistance R8(R9) is connected in series with the potentiometer. Resistance R8(R9) is calculated so that when the potentiometer knob is turned to the far right, the power amplifier has maximum amplification. This resistance also limits the size of the anode current.

Experience in using the MRD-52 flaw detectors has shown that there is no need to regulate the generator voltage. Therefore, the potentiometer R6(R7) has been taken out in the most recent versions of the flaw detectors and a fixed resistance has been installed in its place. In this state, the voltage on the secondary transformer windings will be equal to 7-8 volts when the probes are switched on, and 9-10 volts when the probes are off.

Capacitor C1(C2) serves to block the variable component of the screen grid current. This assures the variability of the voltage on it in the presence of the variable voltage on the control grid which enters from the master oscillator.

Normal flaw detector operation depends to a significant extent on the stability of the master oscillator and its power amplifier. The frequency of the master oscillator should be strictly constant, and there should be no even-order harmonic components in the voltage of the oscillator. Being able to meet these demands depends primarily on the value and the stability of the parts of the oscillatory circuit L1, C4(C5), the ratio between resistances R1(R2) and R3(R4) at the tube input Tu2(Tu3), the winding resistance, the transformer load, and the capacitance of the blocking capacitor C6(C7). Therefore,

it is necessary to pay particular attention to the correct selection of these parts of the circuit when repairing the generator and power amplifier. Certain deviations from the rated values may be allowed for the remaining parts included in the circuit of the generator and power amplifier.

The receiver serves to amplify and transform (to rectify and differentiate) the doubled-frequency voltage arising in the probes as the flaw detector passes over the flaw. There is a tuned amplifier which amplifies the doubled-frequency emf pulses which are induced in the probe, a detector K, and a final amplifier in the receiver. In addition, there are signaling devices in the differentiating network.

The basic elements of the tuned amplifier (see Fig. 64) are as follows: a tuned input circuit, consisting of capacitances C8(C9) and a self-induction coil L2(L3) connected in series; an amplifier tube Tu4(Tu5); a tuned oscillatory plate circuit, consisting of capacitances C12(C13) and a self-induction coil L4(L5) connected in series; and a gain control, consisting of a variable resistance R11(R12), a limiting resistance R13(R14), and a capacitance C10(C11).

When there is a differential network of probes, the tuned oscillatory input circuit L2(L3) - C8(C9) is included between the centertaps of the probe windings and the centertaps of the secondary winding of the transformer Tr, and is connected with the control grid of tube Tu4(Tu5). This circuit is tuned to a frequency $2 \cdot f$, equal to 11,000-12,500 Hz. The circuit tuning is accomplished by the selection of capacitance C8(C9) and the inductance L2(L3). The resistance of this circuit is the lowest for the doubled-frequency current.

The control grid of tube Tu4(Tu5), connected to the self-induction coil L2(L3), is energized when the doubled-frequency voltage is split between the centertaps of the probe and the secondary transformer winding. The doubled-frequency voltage on the grid of tube Tu4(Tu5) causes an alternating current

of the same (doubled) frequency in the anode circuit of this tube, where the tuned oscillatory plate circuit is connected.

The tuned plate circuit C12(C13)-L4(L5) has the same values of self-inductance and capacitance as the input circuit, but they are connected in parallel. When capacitance C12(C13) and inductance L4(L5) are connected in parallel, the tuned plate circuit, which is tuned to the same frequency as the input circuit, offers an extremely large resistance for the doubled-frequency currents. Therefore, a current with a frequency $2 \cdot f$ in the tuned plate circuit creates a large voltage drop, which passes to the grid of the following amplifier tube Tu6(Tu7) through the blocking capacitor C14(C15), rectifier K, and the differentiating circuit C16(C17)-R19(R20).

The doubled-frequency voltage is split and amplified in the section of the circuit which has just been examined.

Gain control takes place using the potentiometer R11(R12), designated on the face-panel by "Amplification" (Fig. 65). The capacitor C10(C11), in the same manner as C1(C2) in the circuit of tube Tu2(Tu3), serves to shunt the variable component of the grid screen current. The amplified voltage passes to the rectifier K through a blocking capacitor C14(C15).

Two circuits consisting of resistance R15(R16) and a copper-oxide rectifier K, with a capacitor C22(C23) grounded through its second plate, are connected in parallel to the anode oscillatory circuit through a blocking capacitor C14(C15). With these components and the leakage resistance of the rectifier K itself, half-wave rectification of the amplified doubled-frequency voltage is accomplished. As a result, the capacitor C22(C23) builds up a positive charge. The voltage on the capacitor C22(C23) varies insignificantly from the magnitude of the doubled-frequency voltage on the anode of the amplifier tube Tu4(Tu5) and follows its changes.

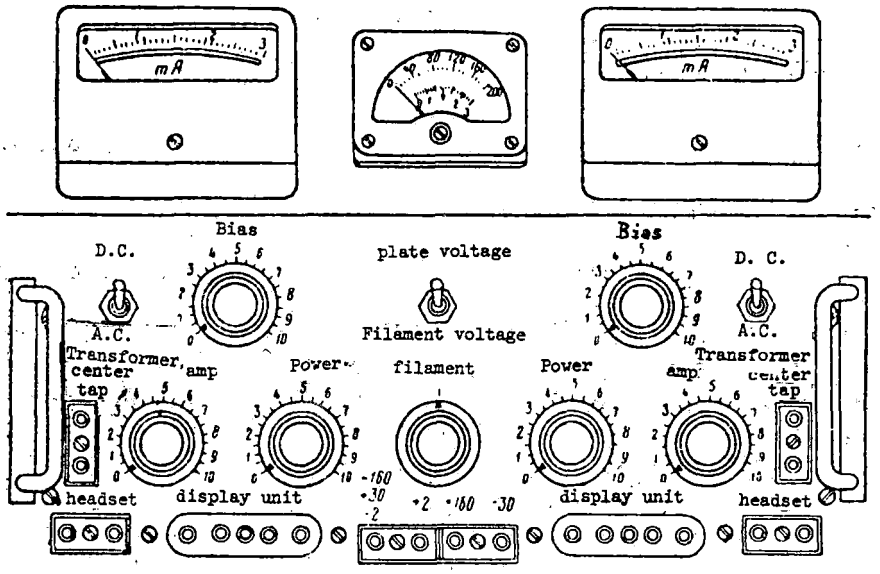

Fig. 65 Face-panel of the generator-amplifier assembly of the MRD-52 flaw detector.

The KVPM-2-10 copper-oxide rectifier K is a column made up of ten rings 2 mm in diameter, which are connected in series. Each ring is covered on one side with a layer of copper-oxide which possesses the property of unilateral conductivity. When tested on a TT-1 testing device, this rectifier afforded a resistance of 20 kohm for the direct current and more than 2 Mohm for the reverse current.

The resistance R19(R20) forms a circuit for the grid current of tube Tu6(Tu7).

The differentiating network C16(C17)-R19(R20) is intended to separate pulses caused by flaws from the other pulses.

It is necessary to keep in mind that the metal on the running surface of the rail head is different because of structural non-homogeniety caused basically by work hardening from blows from the wheels of the rolling stock. When a rail is magnetized, a non-homogeniety in the structure of the metal leads

to the formation of local dispersion fields on the rail surface, not only a above the flaw, but also in places where one structural metallic state leads into another. Above the structural non-homogenities, changes in the local flaw field usually take place on relatively long sections of the rail, with a smooth change from minimum to maximum value.

The change in the dispersion field above a flaw in the form of a light spot takes place over a very short length of rail, with an abrupt increase from minimum to maximum value. Therefore, when the flaw detector is in motion, dispersion fields brought about by flaws cause a sharp increase in the imbalance current in the probe circuit. This feature is used to improve the detectability of light spots on the background of interference caused by non-homogeniety of the structure.

All emf impulses which build up quickly, i.e. impulses caused by flaws, pass through the differentiating circuit almost without weakening. Conversely, impulses which build up slowly pass through the circuit weakened substantially. The differentiating circuit acts as if it were a filter which permits the impulses from flaws to pass through, but not other impulses. This circuit may act only when the flaw detector is in motion since there will be no emf impulse variations when at rest.

When the flaw detector is stopped, i.e. when the probes are stationary above the flaw, a constant, not a pulsing, voltage will be fed to the capacitor C16(C17), for which this capacitor represents an infinitely large resistance (a break in the circuit). When in operation, the differentiating circuit is normally switched into the circuit.

When it is necessary to specify more accurately the location of a flaw, the differentiating circuit is switched off, i.e. the capacitor C16(C17) is shorted by switching the toggle switch T5(T6) to the upper position.

In this mode, the flaw detector may work both at slow speeds and at full stop. In this case, the control grid of tube Tu6(Tu7) will be under a voltage which consists of the imbalance voltage and the voltage arising at the flaw.

The power of the first receiver tube is inadequate to activate the signal relay. Therefore, there is a terminal amplifier on tube Tu6(Tu7) in the circuit. This tube is normally kept in the cut-off state. For this reason, a negative voltage is fed to its control grid by means of a potentiometer R17(R18), denoted on the face-panel by the knob "Bias." In this state, the tube permits current to pass through only when a positive voltage is fed to its control grid. This takes place when the flaw detector passes over a flaw. There is a relay in the plate circuit of this tube which activates, should the plate current exceed 0.9-1.1 milliamp. When the relay is activated, a circuit consisting of capacitors C18(C19) connected in series, and a headset is connected with the pole of plate battery. The charge and discharge current of the capacitor will cause clicks when passing through the headphones. This serves as an audible signal.

The place in the rail above which the local dispersion field causes activation of the relay is determined by the magnitude of the maximum deflection of a milliammeter needle. For this, the differentiating capacitor C16(C17) is shorted out by moving the toggle switch to the upper position. The grid of the receiver's second tube Tu6(Tu7) is directly connected to the rectifier in this instance.

Power supply for the filament of the flaw detector's amplifier and oscillator tubes is provided from a storage battery made up of two NKN-45 elements connected in series. The voltage of the storage battery is 2.5v. The rating of the battery is 45 amp·hr, and the filament current is 0.65 amp.

The plate circuits of the oscillator-amplifier assembly take their power

from two BAS-80 dry cells. The voltage of the two BAS-80 batteries connected in series is 160-180 v. under a load. The rating of the plate batteries is 2.1 amp·hr. The size of the current required by the plate circuits is 6 milliamps. Any type of 40-volt battery is used for biasing.

The power sources are arranged in the equipment box, and are connected to the oscillator-amplifier box according to the wiring diagram presented in Fig. 66. The voltage for the power supply sources is regulated by a voltmeter mounted on the face-panel of the oscillator-amplifier block.

Recently, semiconductor diodes and transistors have been widely used in the rectifiers and voltage converters of various technical radio assemblies.

The primary advantages of transistorized converters are their small dimensions and their efficiency (on the order of 60-80%). The high efficiency of the converters is determined by the small losses in transistors.

Power supply for the plate circuits of the oscillator-amplifier assemblies of MRD-52 flaw detectors is provided from bulky dry cells which have a relatively low rating and a short shelf-life, complicating the working conditions with flaw detectors on the line, and causing significant expense.

This short-coming is eliminated by using a converter which takes its power from a filament battery and produces plate voltage and a voltage for the bias circuits.

Transistorized converters to provide power for the MRD-52 flaw detector were used for the first time by flaw detection workers of the track maintainance service of the Moscow (Moskovskaya) and the Northern (Severnaya) lines. The schematic of one of the converter versions used by the flaw detector specialists of the Moscow line is shown in Fig. 67.

The operating principles are as follows for the converter with a push-pull circuit with self-induction which is being examined.

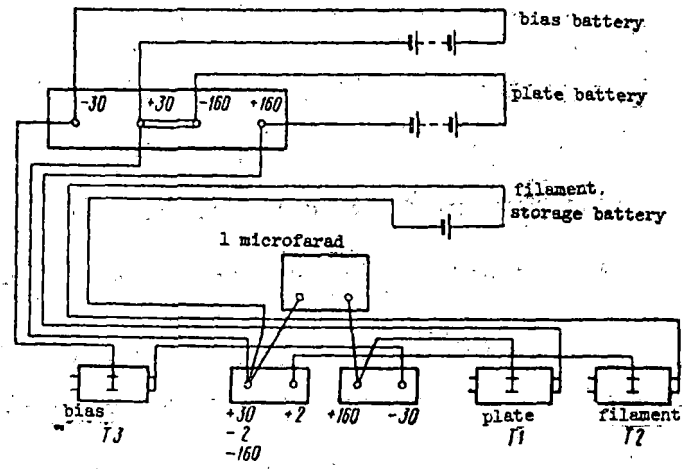

Fig. 66 Connection diagram for the power supply sources for the MRD-52 flaw detector.

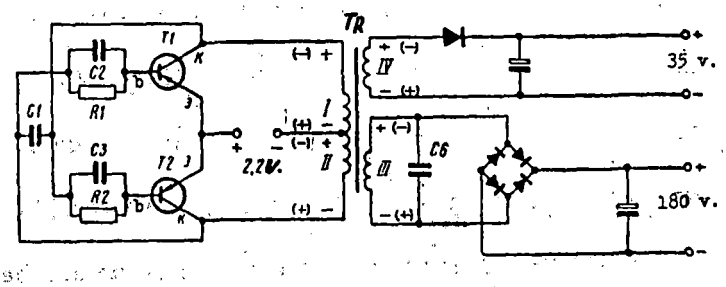

Fig. 67 Schematic of a transistorized converter.

Let us assume that at a certain moment, transistor T1 is open. Then, the voltage of the storage battery (2.2-2.5 v, including a small voltage drop in the transistor on the emitter-collector section) is applied to the half-winding I of the transformer TR. Current in half-winding I is increased from zero to a maximum value. As a result, an emf of the polarity indicated on the schematic by the signs outside the parenthesis will appear in the half-winding and in all other windings of the transformer. Here, the emf of half-winding II creates a voltage at the base of transistor T1, through resistor R1 and capacitor C1 which is negative with regard to the emitter while the emf in the half-winding I at that moment creates a voltage at the base of

transistor T2 through resistance R2 and capacitance C3 which is positive with regard to the emitter.

Since a negative voltage is supplied at the base of transistor T1, the latter will be open until the magnetic flux in the transformer core reaches its saturation value. At the moment of transformer coil saturation, the speed at which the magnetic field changes becomes equal to zero (or very small). Consequently, the emf in all of the transformer windings will become equal to zero (or will be decreased significantly). The decrease in emf which takes place under this condition causes a sharp decrease in the current in the transformer windings. This, in turn, causes the appearance of an emf of the opposite polarity (cf. the signs in parenthesis in Fig. 67) in all of the transformer windings.

Half-winding II creates a positive voltage at the base of transistor T1 in connection with the change in the emf polarity, whereas the emf of half-winding I creates a negative voltage in relation to the emitter at the base of transistor T2, which leads to the closing of transistor T1 and opening of transistor T2. In this manner, transistors T1 and T2 work in sequence. While one transistor is open, a positive closing voltage impulse is fed to the base of the second transistor.

The speed at which the closing and unclosing of the transistors takes place, and, consequently, the steepness of the alternating voltage fronts which are generated, depends to a great degree on the self-capacitance of the transistors and the transformer windings, on the capacitance of the capacitors C1 and C6, and on the transformer induction.

The alternating voltage which is obtained is rectified by diodes on secondary windings III and IV. The voltage of winding III is fed to the plate circuits, while the voltage of winding IV is fed to the oscillator bias circuit and the flaw detector amplifier circuit.

3. The Magnetic Rail Flaw Detector MRD-66.

Block diagram of the flaw detector. The MRD-66 flaw detector (Fig. 68) is an improved model of the removable magnetic flaw detector. The primary units of the flaw detector for monitoring one line of rail are shown in Fig. 68. There are devices of the same type which work in parallel and simultaneously for the other line of rail.

The master oscillator 1, a common tube-type generator of sinusoidal oscillations with a stable frequency of 7000-7500 Hz, is common to both of the rail lines.

The nomenclature and the designation of the remaining units of the MRD-66 flaw detector are the same as for the MRD-52 flaw detector. Therefore, there is no need to describe their designation and the way in which they interact.

Nevertheless, the circuit diagram of the MRD-66 flaw detector probe assemblies is different from the circuit diagram of the MRD-52 flaw detector probe assemblies. In the MRD-66 flaw detector, the two upper probes are connected according to a bridge circuit, the ferroprobes of one probe assembly being connected in series-aiding, while the ferroprobes of the other probe assembly are connected in series-opposed. Such a wiring diagram for the probe assembly's ferroprobes permits the flaw detector's sensitivity to transverse fatigue cracks situated closer to the lateral edge of the rail head to be increased, and excludes the possibility of omitting symmetrical transverse fatigue cracks. (The cracks, above which the flaw field influences identically and simultaneously the adjacent ferroprobes of both probe assemblies are called symmetrical transverse fatigue cracks.)

In this schematic, a switch T1, providing for the operation of the flaw detector in a state with one or with two probes without switching off the probes themselves, has been introduced.

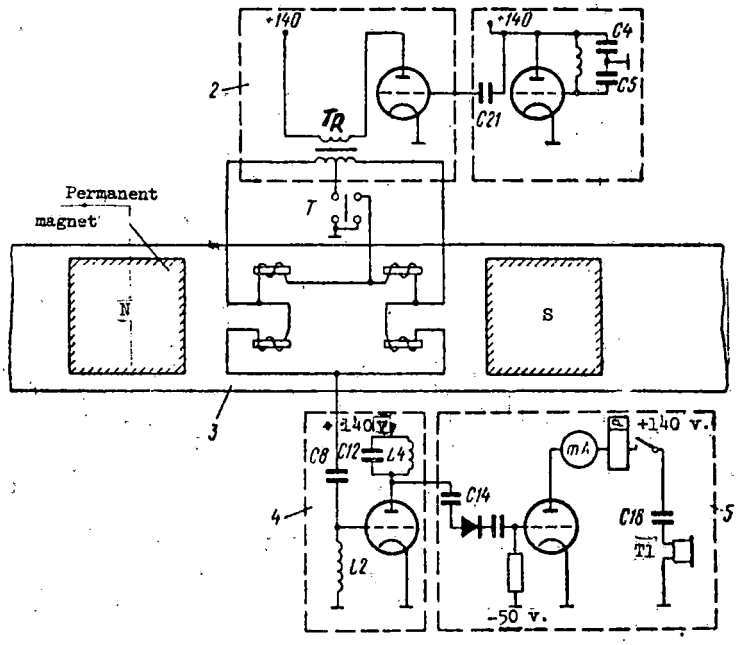

Fig. 68 Block diagram of the MRD-66 flaw detector.

The magnetizing device. Permanent magnets situated above the right and left lines of rail on the track are used to magnetize the rails in the flaw detector. A sketch of the magnet is presented in Fig. 69. Each magnet consists of two bars made of a magnico alloy, and the yoke connecting them is made from soft, annealed iron ("Armco" iron). The bar has cross-sectional dimensions of 50 x 55 mm, and it is 80 mm high. The bars are enclosed in aluminum casings with walls 1.5 mm thick. The magnetization curves (part of the hysteresis loop) and demagnetization curves of the assembled magnet are presented in Figs. 51 and 52. The intensity of the longitudinal component of the magnet field in the zone in which the upper flaw detector probes are situated is from 10-12 amp/cm in rails from different plants.

Probe assemblies. The parameters and the construction of the ferroprobes for the MRD-66 flaw detector probe assemblies are the same as for the MRD-52 flaw detectors. The two upper probes are connected according to a bridge cir-

cuit (Fig. 70). Here the ferroprobes of the probe assembly, the centertap of which is grounded, are connected in series, while the ferroprobes of the probe assembly, the centertap of which is fed to the resonance circuit CL, are connected in series-opposed.

We will examine the work of such a circuit for connecting the probes when they are placed on the running surface of a "sound" rail between the poles of a magnet, and the flaw detector passes over a defect in the shape of a transverse fatigue crack in the rail head. The ferroprobes of the probe assemblies, which are placed in the "neutral" zone between the poles of the magnet on the running surface of the "sound" rail are subjected to the influence of the homogeneous field of the magnet.

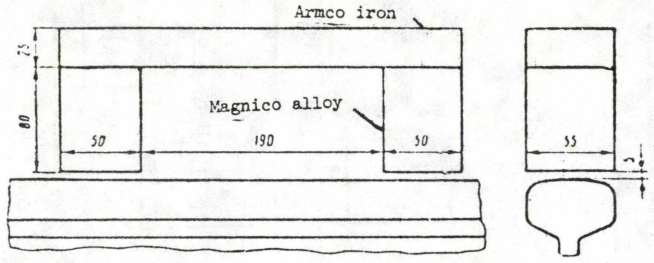

Fig. 69 Sketch of the MRD-66 flaw detector magnet.

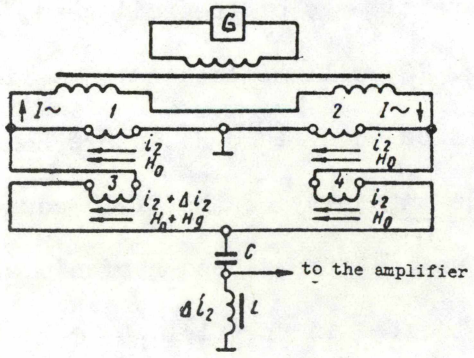

Fig. 70 Schematic for connecting the ferroprobes of the upper assemblies in the MRD-66 flaw detector.

The intensity H_o of this field will be identical in size and direction for each ferroprobe. Under the influence of field H_o, second harmonics of current $i2$, identical in size and phase, will arise in the alternating current i in the winding of each ferroprobe. As a result, in the bridge diagonal, where the resonance circuit is connected, the instantaneous values of $i2$ are normally opposite in phase, i.e. they compensate each other. The absence of the second harmonic $i2$ in the resonance circuit (at the amplifier input) is equivalent to the probe's not reacting to the homogeneous magnet field, no matter how great the intensity of H_o.

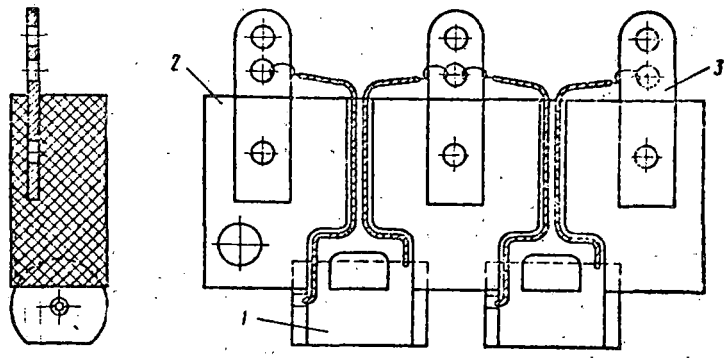

Fig. 71 Sketch of the ferroprobe probe assemblies of the MRD-66 flaw detector.

As the flaw detector rolls over a flaw, e.g. a transverse fatigue crack situated closer to the lateral edge of the rail head, one of the ferroprobes, (e.g. ferroprobe 3 in Fig. 70) will be located in a field $H_o + H_g$, and the remaining ferroprobes will be in a field H_o, where H_o is the intensity of the magnet field and H_g is the intensity of the field caused by the flaw.

In Fig. 70 it is shown that the second harmonic of the current in the winding of ferroprobe 3, located in the field $H_o + H_g$, increases by $\Delta i2$. The current $\Delta i2$ passes through a resonance circuit while the voltage drop of the second harmonic which arose in it is fed to the control grid of the amplifier.

When such probes pass over highly developed transverse fatigue cracks, ferroprobes 1 and 3 will simultaneously be under the influence of the field H_g, and the second harmonic of the current i2 will increase by Δi2 in ferroprobes 1 and 3. An approximate total auxiliary current of the second harmonic $2 \cdot \Delta i2$ will pass through the resonance circuit, causing an increase in the voltage drop of the second harmonic in the amplifier input resonance circuit.

In this manner, the bridge schematic for connecting the ferroprobes of the MRD-66 flaw detector probe assemblies, where the ferroprobes of one probe assembly are connected in series-opposed, promotes the detection of transverse fatigue cracks situated close to the lateral edge of the rail head (lateral cracks) and developed transverse fatigue cracks situated symmetrically within the cross-section of the rail head (symmetrical cracks).

In the 1968 and later-year models of the MRD-66 flaw detectors, ferroprobe sensors with the same construction are used both for the upper probe system and for the lateral probes. A sketch of such a probe assembly is presented in Fig. 71. It consists of the ferroprobes 1, a plastic plate 2, and contact lobes 3. The ferroprobes on the plate are situated along the center-line. Each upper ferroprobe sensor is mounted on the lower base of a plastic collector shoe (shown in Fig. 72), and clamped by a cover plate 2. In its upper section, the shoe has a lock nut 3, with which the magnet screen 4 is moved in relation to the ferroprobes of the probe assembly 5, in order to balance it.

Above the lower base of the collector shoe is fastened a metallic cover plate 6, which slides along the surface of the rail head. The cover plate is a replacable part of the shoe, and it is replaced when it wears out.

On the ends of the shoe, there are projections 7 which fit freely into the vertical grooves of the holder between the magnet poles. Three flexible wires lead from the probe 5, through a flexible cable 8 to a three-pronged plug.

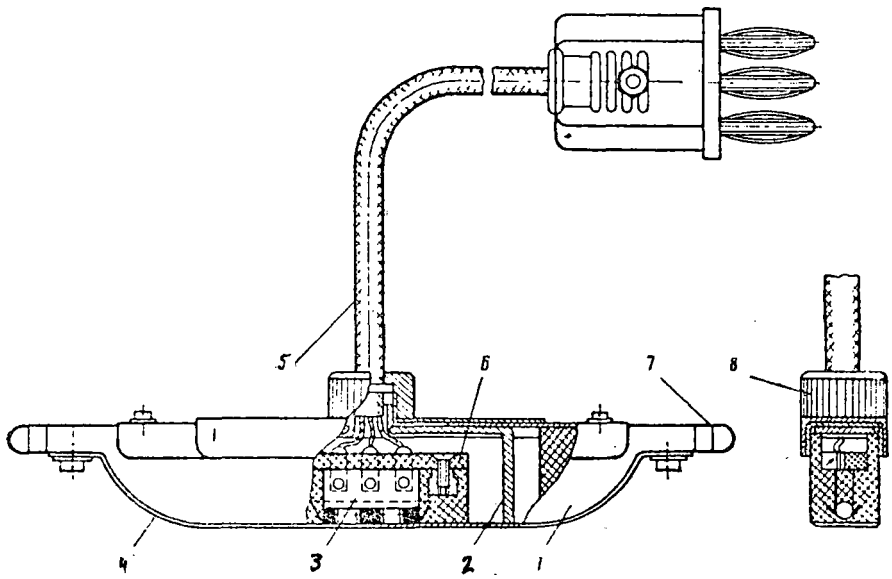

Fig. 72 Sensor assembly of the MRD-66 flaw detector.

Electrical system diagram of the flaw detector (Fig. 73). The intended use and interaction of all the branches and elements of the electrical system of the MRD-66 flaw detector are the same as in the MRD-52 flaw detector. Therefore, there is no need to introduce a detailed description of the intended use and interaction of all the elements of the MRD-66 circuits, as was done for the MRD-52 flaw detector. We will limit ourselves to describing only those branches and parts which are different from the MRD-52.

A different system is used for connecting the ferroprobes in the MRD-66 probe assemblies, and for connecting them to the secondary transformer winding and the input resonance circuit of the amplifier.

The necessity of using the circuit diagram for the probe assembly ferroprobes shown in Fig. 70 arose due to the following factor: the bridge probe system, where the ferroprobes of each probe assembly are connected in series-aiding, does not promote reliable detection of symmetrically transverse fatigue cracks, i.e. those cracks, the dispersion field of which acts on contiguous

ferroprobes of both probe assemblies simultaneously and with the same intensity.

The system used currently in the MRD-52, in which the probe assembly ferroprobes are connected in parallel, has adequately high sensitivity to symmetrical cracks, but, at the same time, its sensitivity to lateral cracks is lower than that of the probe system whose ferroprobes are connected according to a bridge system.

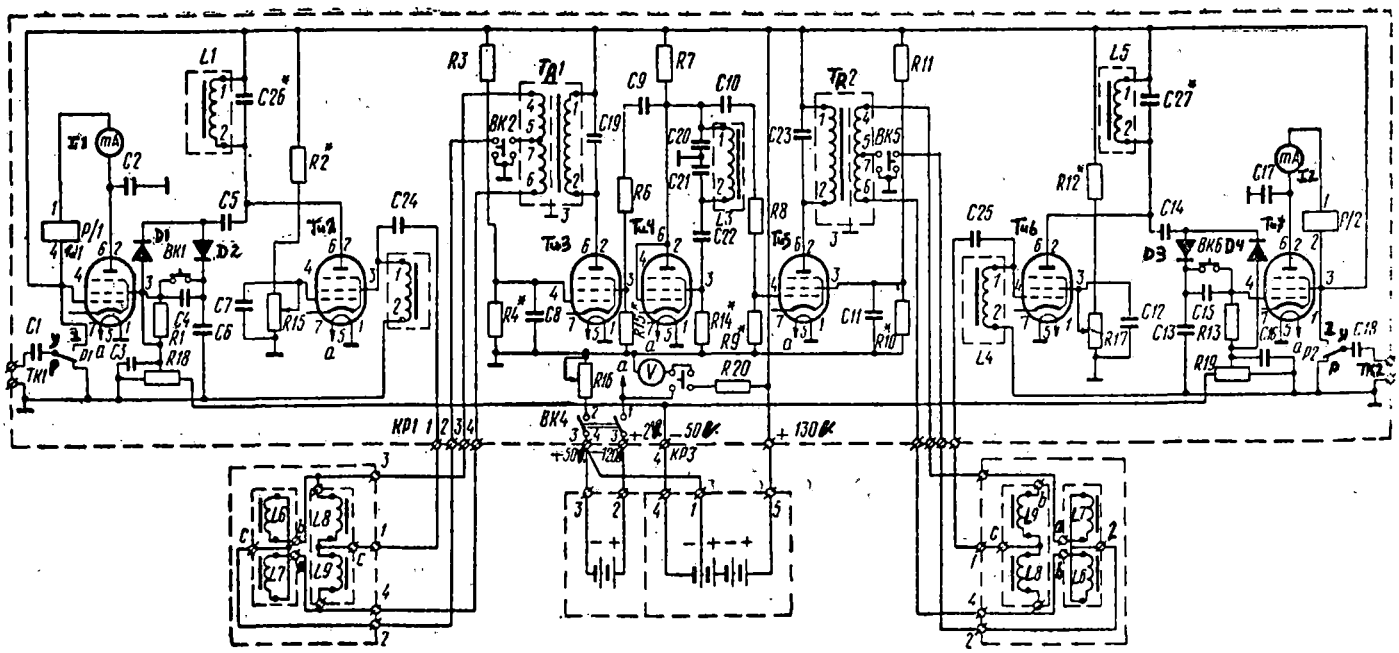

Fig. 73 Principle electrical system diagram of the MRD-66 flaw detector.

The bridge probe system presented in Fig. 70, where the ferroprobes of one probe assembly are connected in series-aiding and the other in series-opposed, has high sensitivity to symmetrical as well as lateral fatigue cracks.

Toggle switches BK2 and BK5 have been introduced into the circuit of the

MRD-66 flaw detector. With these toggle switches, the centertap circuit of one of the probes is broken, and the centertap of the transformer is simultaneously grounded. This is necessary when the flaw detector works with one probe. Switching the BK2 and BK5 toggle switches to the other position, the transformer centertap circuit is broken, and the centertap of one of the probes is simultaneously grounded. This is necessary when the flaw detector works with two probes.

The first detector (rectifier) is composed of two diodes D1-D2 and D3-D4 in the MRD-66 flaw detector's electrical system. Rectification and doubling of the amplified second-harmonic voltage is realized with these diodes and with capacitors C6 and C13.

The self-induction coils L1-L5 of the oscillatory circuits are wound onto SB-5 type armored, carbonyl cores.

Filament power supply of the amplifier and oscillator tubes is provided by a storage battery assembled from two ZhN-45 type elements. The filament voltage is 2 v. The plate circuits of the oscillator-fatigue mechanism are fed from two BAS-80 dry cells. The voltage of the plate batteries should be 130-150 v. The bias voltage of 50 v. is taken from the plate battery. Voltage from the power supply sources is regulated by a voltmeter mounted on the face panel of the oscillator-amplifier block.

4. Preparation of the MRD-52 and MRD-66 and their used in the field.

Preparation of flaw detectors includes testing the operational fitness of all of the electrical systems and power supply sources, and tuning all of the equipment to rail samples having transverse fatigue cracks in the head.

Balancing the probes. The sensitivity and selectivity of the MRD-52 and MRD-66 flaw detectors to flaws in the rails depends to a great degree on the size of the probe assembly imbalance voltage. The second harmonic voltage which

arises in the ferroprobe sensors when they are mounted between the poles of a magnet on a portion of rail surface where there are neither flaws nor surface damage to the rail metal is called the imbalance voltage.

As the imbalance voltage of the probes decrease, the sensitivity and selectivity of the flaw detector to flaws increases. When the level of the probe imbalance increases, sensitivity and selectivity of flaw detectors to flaws decrease. The imbalance voltage causes interference in the flaw detector's operation and hinders its use at the highest sensitivity. This voltage is measured between the centertap of the secondary transformer winding and the centertaps of the probes when the ferroprobes of the probe assemblies are connected in parallel, and between the centertaps of the probes when a bridge connection is used for the ferroprobes.

Let us examine the basic causes of change in the size of the imbalance voltage. Low-level quality control of the probes at the plants (discrepancy in the ohmic and inductive resistances of the coils and in the dimensions and magnetic properties of the Permalloy cores) may be one of the causes. Additionally, there may be a significant imbalance in the probe circuit because of inaccurate positioning of the cores in the probe coils, even when the probe coils have been properly matched and the coils are identical.

The influence of the magnet's field on the ferroprobes of the probe assembly, which occurs when the probes are mounted on the running surface of the rail head between the poles of the magnet, is another cause of the imbalance voltage. In this case, in spite of the fact that the probe is mounted between the magnet poles, and in spite of the partial screening of the ferroprobes, the field where the probes are located nevertheless does not remain adequately uniform. The core of one ferroprobe is situated in a field with an intensity which is different from the intensity of the field in which the core of the

second ferroprobe is located. This causes a doubled-frequency voltage on the probe output, even if the latter is situated on a sound segment of rail.

The size of the voltage imbalance also depends on the shape of the voltage curve from the power amplifier of the oscillator providing current to the ferroprobe coils in the probe assemblies. This curve is not strictly sinusoidal and contains even-order harmonic components including the doubled-frequency. These are insignificant.

Thus, the ferroprobe windings will be, first, under a second-harmonic voltage passing from the oscillator, and, second, under a second-harmonic voltage excited in the ferroprobes themselves. These voltages might be either in or out of phase, depending on the phase of the feed-voltage and the position of the probes relative to the magnet poles.

When the phases coincide, these voltages are added; consequently, the imbalance voltages will grow. When they do not coincide, they subtract from each other, and the imbalance voltage decreases.

It is possible to change the phase of the second harmonic voltage of the oscillator's power amplifier by switching the ends connecting the secondary transformer winding to the ferroprobes (by turning the probe's three-pronged plug around), whereas it is possible to change the phase of the second-harmonic voltage of the ferroprobes by turning the ferroprobe probe assembly (the sensor collecting shoe) 180° with respect to the poles of the magnet, and thereby change the size of the imbalance voltage.

Balancing the probes amounts to selecting the position of the collector shoes relative to the magnet poles, rotating the three-pronged plugs, and moving the brackets (the screens) relative to the ferroprobes in order to reduce the imbalance voltage to a minimum.

For balancing, at first only one probe shoe is mounted between the magnet

poles, with the screen in symmetrical position. Then, by rotating the three-pronged plug and varying the position of the probe in regard to the magnet poles, the minimum imbalance voltage value is obtained. The size of the imbalance voltage may be judged from the readings of a milliammeter. The readings are directly related to the size of the doubled-frequency voltage.

It is recommended that a small amplification be used when balancing the probes. This significantly facilitates observation of the changes in the imbalance voltage. The amplification is reduced to the lowest possible value and a reading of the milliammeter equal to approximately 0.6-0.7 milliamp is set with the "Bias" knob.

A uniform imbalance voltage level in the probe circuit when the flaw detector is moved back and forth at the same speed is one characteristic which shows that the probe is correctly balanced. Therefore, when moving the flaw detector along the rails of a reference siding, the readings of the milliammeter are observed. Identical readings of the milliammeter when the flaw detector is moved back and forth show that the probe is correctly balanced. If the readings of the milliammeter are different, they are equalized by moving the brackets (the screens) slightly relative to the ferroprobes in the probe assembly. It is not difficult to determine which direction to move the brackets by watching the milliammeter.

Having balanced one probe in this manner, the position of the three-pronged plug in the socket and of the sensor shoe with regard to the poles of the magnet are observed. After this, the sensitivity of the individual probe is checked, for which a value for the biasing voltage is selected so that when the probe approaches a flaw, the milliammeter needle will be located in the approximate center of the scale.

The second probe is balanced independent of the first, after which its

sensitivity is tested. If the imbalance level and the sensitivity of both probes are uniform, the probes may be switched on for joint operation. Paired probes having identical sensitivity and imbalance levels are matched for each line of rail.

Test for sensitivity on rail samples with transverse fatigue cracks.

The sensitivity of the flaw detector to flaws is tested at the same time as the flaw detector is being balanced. For this, a siding with rail samples having flaws in the shape of transverse fatigue cracks in the head are used.

By flaw detector sensitivity, we mean the ratio $\Delta i/H$, showing what current Δi arises in the milliammeter circuit and in the relay winding when one of the ferroprobes of the probe assembly is exposed to a constant field H with an intensity of 1 amp/cm.

That sensitivity at which a current of 3 milliamps (i.e. Δi = 3 milliamps) arises in the milliammeter circuit and in the relay winding at the moment at which the flaw detector probes pass above a flaw field with an intensity of 1 amp/cm, is considered to be satisfactory flaw detector sensitivity.

It has been experimentally established that when the rail is magnetized by the U-shaped magnet of the MRD flaw detector over an internal transverse fatigue crack located under a layer of metal 4-5 mm thick and occupying 25% of the cross-sectional area of the rail head, the intensity of the horizontal component of the field H_g equals approximately 0.8 amp/cm.

Consequently, any rail with a transverse fatigue crack which does not emerge onto the running surface and above which the intensity of the horizontal component of the flaw field when the rail is magnetized is equal to 0.8 amp/cm may serve as a standard for tuning the flaw detector.

The intensity of the horizontal component of the flaw field above the crack will be different across the width of the rail head, depending on the

dimensions of the fatigue cracks and the extent to which they approach the running surface of the rail head. Therefore, standardizing the flaw in a rail will consist of determining a point on the running surface above the flaw where the intensity of the horizontal component of the flaw field equals 0.8 amp/cm. It is necessary to have a dispersion field with a known intensity value in order to determine such a point over a flaw.

By comparing the readings of the flaw detector above a field with a known intensity value with the readings at various points above the flaw, the value of the flaw field intensity at these points is determined. In practice, the known field intensity value may be obtained with the aid of a d.c.-carrying conductor. A circular magnetic field, the intensity of which depends on the size of the current flowing through the conductor, other conditions being equal, is formed around the current-carrying conductor.

By varying the size of the current in the conductor, it is possible to obtain the necessary value for the magnetic field. To do this, a turn of well-insulated wire (not more than 0.2 mm in diameter) is wrapped around a rail sample in the cross-sectional plane at a distance 0.4-0.5 m from the site of the flaw (on a "clean" place) so that the part of the turn on the running surface of the rail head is strictly perpendicular to the longitudinal axis of the rail, and pressed snugly to it. To protect the turn from damage from the flaw detector wheels, all of that part on the running surface of the rail head is glued in place with a sheet of thin, dense paper (tracing paper, parchment, etc.). A storage battery is connected to the turn, and a current of 1 amp as measured by an ammeter is extablished using a rheostat (Fig. 74).

At a current of 1 amp, the intensity of the horizontal component of the field above the turn will equal approximately 0.8 amp/cm, which corresponds to the intensity of a flaw field above a transverse fatigue crack situated

at a depth of 4 mm and having an area equal to 25% of the cross-sectional area of the rail head.

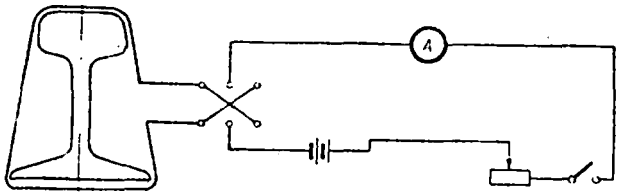

Fig. 74 The current carrying turn.

An MRD flaw detector with one sensor shoe and with the differentiating cell switched off is set on the rail being calibrated to determine the point on the running surface of the rail above the transverse fatigue crack where the intensity of the horizontal component of the flaw field equals 0.8 amp/cm. Then the flaw detector is pushed over to the turn until the maximum reading is obtained on the milliammeter, after which the milliammeter reading is reduced to approximately 1.5 milliamp with the "Bias" knob.

Next, without varying the position of the "Bias" and "Amplification" knobs, the flaw detector is moved over the fatigue crack.

If the reading of the milliammeter is the same as it is above the turn, i.e. equal to 1.5 milliamp when the probe shoe is in the given position above the crack, the intensity of the horizontal component of the flaw field at that point above the running surface of the rail is equal to 0.8 amp/cm and, consequently, the rail sample being examined may be used to tune the flaw detector when the probe shoe is at the indicated point on the rail.

If the readings of the milliammeter at the point being examined are greater than 1.5 milliamp, the sensor shoe is moved toward the center of the running surface of the rail head until the milliammeter reading is equal to 1.5 milliamp.

After this, the position of the sensor shoe across the width of the running surface of the selected rail sample is marked with oil paint. The rail is installed in the test siding; the sensitivity of the MRD flaw detectors is checked with the sensor shoes at the place marked on the rail.

It is possible to obtain a field intensity of 0.8 amp/cm above a turn with a current of 1 amp when the voltage of the turn field and the flaw detector's magnet field are matched.

To match the direction of the magnetic field in the turn with the basic field in the magnet, a flaw detector with a single sensor shoe (with two probes) is set above a flaw according to the maximum ammeter reading, after which the milliammeter reading is reduced to 1.5 milliamp using the "Bias" knob. Observing the readings of the milliammeter, the direction of the current in the turn is changed. When the direction of the field in the turn and in the magnet are matched, the milliammeter will remain equal to 1.5 milliamp or will increase. When the direction of the fields is not matched, the milliammeter readings will decrease somewhat.

If there are no rails with the transverse fatigue cracks on any section of the track, the MRD flaw detector sensitivity is tested using the current-carrying turn.

Testing the flaw detector sensitivity on a rail sample with a transverse fatigue crack in the head or on a current-carrying turn presupposes a test of the fitness of the flaw detector operation and the selection of the necessary working conditions for its basic elements. Here, that operating condition at which the flaw detector indicators do not activate from interference signals but at the same time give distinct readings over a flaw in the rail or over a current-carrying turn is established.

In practice this is done in the following manner: the flaw detector is

set in the working mode on d.c. (the differentiating network is switched off), amplification is set at the maximum, and the flaw detector sensitivity at which there are no indications on sound places in the rail is selected using the "Bias" knob. At this sensitivity, the flaw detector is moved back and forth so that its probe passes over the current-carrying turn or over the flaw, and the readings of the milliammeter are observed. If the milliammeter needle deflects to the stop at the moment the probe passes above the flaw, this indicates that the sensitivity of the probe is adequate.

Having terminated the sensitivity tests in the d.c. working mode, we turn to testing the sensitivity in the a.c. mode (with the differentiating network switched on). For this, the maximum sensitivity at which the flaw detector still does not give a reading on "clean" parts of the rail is selected with the "Bias" knob. With this sensitivity, the flaw detector is again moved along the rail with a speed of 3-4 km/hr so that its probes pass over the flaw. When the probes are correctly balanced, the flaw detector will activate distinctly in both directions. A click will be audible in the headphones, and the milliammeter needle will make small jumps of approximately 0.6-0.7 milliamp.

Occasionally when a flaw detector is tried out with the differentiating network switched on, the sensitivity may be different when the detector is moved in one direction or the other. Since the flaw detector is moved forward under usual operating conditions, a somewhat higher probe sensitivity in this direction is considered normal. If the sensitivity of the probes is less when moving forward than when moving backward, it is equalized by moving both screens slightly.

A flaw detector having the correct balance and possessing adequate sensitivity usually satisfies the following conditions:

1. When the "Bias" knob is set between the first and fifth division, a flaw

in the a.c. working mode does not produce sharp deflection of the milliammeter needle when it starts off, i.e. it does not produce current jumps. The flaw detector activates distinctly from a flaw while moving in either direction

2. A flaw detector in the d.c. working mode gives an indication greater than 3 milliamps on that same flaw when the "Bias" knob is set on zero

3. In both the a.c. and d.c. modes, the flaw detector does not activate on sound sections of the rail.

Small deviations from these conditions may be observed because of changes in the resistances of the amplifier and power regulators.

All of the conditions indicated above are maintained when the "Amplification" control is in the position for maximum amplification.

When testing the sensitivity in the d.c. working mode, large imbalance voltages arise in the flaw detector probes when the flaw detector starts off (the milliammeter needle moves over to the stop).

As the flaw detector continues in motion, the imbalance voltage decreases to the initial value, and the milliammeter needle returns to zero.

This phenomenon is explained as follows: when the flaw detector was stationary, the rail head directly under the poles of the magnet was magnetized more than the portion of the rail head which was between the poles. A sharp drop in the field is observed at the transfer boundary between the less-strongly magnetized and the more-strongly magnetized portion of the rail.

At the start of the flaw detector's motion, the ferroprobes of the probe assemblies, moving from the less-strongly magnetized part of the rail to the more-strongly magnetized part, enter the zone of the sharp field drop, which causes an increase in the imbalance voltage. As the flaw detector is moved further, the sensor probes pass from the magnetized part of the rail head, the imbalance voltage reduced to the original value, and the milliammeter needle moves to the initial position.

These imbalance voltage jumps when the flaw detector starts off do not effect the normal operation of the flaw detector in practice, but it is necessary to keep this condition in mind when determining more precisely the position of a flaw in the rail.

Working on the line with the MRD-52 and MRD-66 flaw detectors.

Working between stations with flaw detectors takes place with the differentiating network switched on and at maximum amplification of the resonance amplifier. When the controls are in this position, the flaw detector is moved along the track and the necessary sensitivity is established using the "Bias" knob.

To establish the necessary flaw detector sensitivity means to select a blocking voltage on the grid of the output tube at which the flaw detector will not activate on "clean" places on the rail or in the presence of insignificant surface defects. Flaw detector operations between stations is tested when the probes pass across a joint clearance.

Sometimes the imbalance voltage level increases sharply on certain rails. This may be explained by the fact that the metal in such rails has different metallic properties than the metal in other rails. On these "peculiar" rails, the sensitivity which was previously established becomes superfluous.

As experience has shown, these "peculiar" rails must be checked in two passes. On the first pass, the rail is magnetized and the field becomes more equal along the length of the rail. On the second pass, the imbalance voltage level usually decreases, consequently, the rail is inspected at the normal sensitivity. If on the second pass, the imbalance voltage remains high, the flaw detector sensitivity is decreased to a normal value. Decreasing the sensitivity does not exclude the possibility of detecting internal flaws in the form of light spots in these peculiar rails.

When the flaw detector is moved along the track, the probe shoes should be situated on the running surface of the rail head symmetrical to the longitudinal axis of the rail. This is particularly important when inspecting rails having a large amount of metal flow near the gage side (Fig. 75) as well as on the curved portions of the track.

When the flaw detector passes over switch frogs, cases have been known in which the shoes wedge between the wing rail and the center of the frog. This may cause damage to the shoes and the holders. To avoid this, the shoes are usually raised a bit and the flaw detector is moved slowly when approaching a frog.

On the bottom of the shoes, dirt and residual oil frequently build up. The ferroprobes are lifted slightly from the running surface because of this, making the balance of the probes and their sensitivity to flaws worse. Therefore, the shoe bottom is inspected periodically, and the dirt and residual oil are cleaned off.

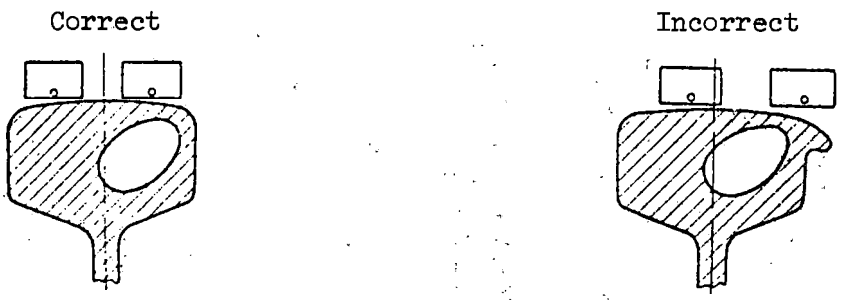

Fig. 75 Position of the sensor shoes on the running surface of the rails.

Two shoes are not accommodated on the running surface of either light or heavy rails showing great lateral wear of the head since in this case the balance of the probes is disturbed and it is impossible for the probes to pass over flaws developing in the central part of the rail head. Such rails are

best tested using a single probe. The single probe is mounted in the center part of the running surface of the rail head, and the flaw detector is used in the normal manner.

Evaluation of the flaw detector readings. Experience using MRD flaw detectors has shown that transverse fatigue cracks are necessarily sought out from among the numerous flaws on the running surface of the rail head (dents from impacts, pitting, flaking, scabs, etc.). In addition, the metal of the running surface may have a distinctly expressed, local structural non-homogeniety caused by work hardening or by the thermal effects from wheel slippage of the rolling stock.

The enumerated non-dangerous points of damage to the rail metal and local non-homogeniety of its structure cause dispersion currents and affect the flaw detector probe in the same way as dangerous fatigue cracks. Additionally, there are occasionally, both a concealed, dangerous flaw and surface damage or a structural metallic non-homogeniety in the same place in the rail. On these portions of the track, it is necessary to search for, as it were, a "flaw within a flaw". Therefore, the correct evaluation of the flaw detector readings has a decisive significance for providing high quality rail monitoring on the line.

With the appearance of an audio signal, the flaw detector is stopped and two to three repetitive passes are made along the noted section at the normal working speed. In making the repeated passes, one must be careful that the magnet's poles pass above the noted place and continue for a distance of not less than 0.5 m. If the flaw detector is activated consistently in the same place during repeated passes, that place should be carefully examined.

The location may be determined by flaw detector with an accuracy of from 3-5 mm. Before the rail is inspected, the probe which is being activated in

the given place is determined, and by this process, the section of the width of the rail head where the flaw lies is revealed.

Having switched off one probe, several repeated passes are made across the noted place. If the flaw is situated under the disconnected probe sensor shoe, the flaw detector will not activate. If the flaw is situated under the sensor shoe which is on, the flaw detector will consistantly note its location.

The flaw site is then established accurately. For this, it is necessary to switch off the differentiating network. It is impossible to establish the flaw site accurately with the differentiating network switched on since, when this is the case, the flaw detector will not react to flaws when moving at slow speeds or at rest.

With the differentiating network switched off, the flaw detector sensitivity is somewhat increased. Therefore, before turning to pin-pointing the position of the flaw, the sensitivity is decreased somewhat using the "Bias" knob. The flaw detector is moved slowly at this sensitivity; the exact position of the flaw is fixed according to the maximum deflection of the milliammeter.

The site of the flaw coincides with the geometrical center of the sensor shoe. The place which is located is examined carefully.

If a clearly distinct place where the crack emerges is not visible in the spot being inspected, the corresponding lateral edge of the rail is cleaned of residual oil and fused flakes of torn metal for a distance of 300-400 mm so that the noted site is in the center of the cleaned portion of the lateral edge. It is necessary to clean the lateral edge of mud and residual oil because they are usually mixed with metallic dust from the brake shoes which, upon becoming magnetized, creates supplimentary fields interfering with the normal operation of the probe.

The lateral probe is set on the cleaned portion of the lateral rail edge. The normal probes are disconnected at this time, and the lateral probe plug is connected to the vacated three-pronged socket. The flaw detector is switched to the "direct current" mode. The flaw detector sensitivity is set at the high maximum, i.e. at the level at which there are still no readings on the sound portion of the lateral edge surface. Then, while moving the flaw detector back and forth, the milliammeter readings are observed. If there is a transverse fatigue crack in the previously noted place, at the moment the lateral probe passes this place, the milliammeter needle will deflect.

Instances are possible in which the probe will activate over a transverse crack only when the flaw detector is moved in one specific direction due to the lack of a balancing device on the lateral probe. This one-way operation of the probe is reliable.

When working with the lateral probe, as with the normal probes, the milliammeter needle will deflect when the flaw detector starts up, and then return to the zero position. It is therefore impossible to make a secondary inspection with a reverse movement of the flaw detector directly over the noted site. It is necessary for the lateral probe to pass above the noted site after the milliammeter needle has already returned to the zero position.

If the lateral probe on the edge gives no reading, it is set under the rail head with the aid of the clamping and hinged devices, and secondary inspection of the noted site is accomplished in the same manner. If there is no reading from the probe when on the side and in the fillet section of the site noted by the flaw detector, this indicates that there is no dangerous fatigue crack in that place, and that the flaw detector readings were caused either by a structural non-homogeniety or by insignificant point of damage to the metal on the running surface of the rail head.

It is known that it is easy to determine in which section of the rail head cross-section a fatigue crack is located using the MRD flaw detector, and, consequently, it is possible to determine its origin. If the crack is situated close to the field edge of the rail head cross-section, or in its central portion, it is most likely that this crack arose from flaking.

On the other hand, if the crack is situated close to the gage edge, it is possible to say with assurance that this crack arose due to great contact stresses. There may be exceptions when the rail was improperly canted. An improperly canted rail is easily recognized by the nature of the scab and other well-known features.

Having detected a rail with a transverse fatigue crack which developed from flaking, the flaw detector maintainance engineers usually inspect the entire rail and record the melt number, the year in which the rail was rolled, and the manufacturing plant. All rails of a given melt may be damaged by flaking. Therefore, knowing the number of the melts which developed flaking, it is easier for the maintainance engineer to orient himself when evaluating flaw detector readings.

Fatigue cracks (flaw type 21.1-2) originate most frequently and propagate most quickly in rails along the inside rail in curves, in the joint zone, and in other places in the rail where increased dynamic impacts of the rolling stock arise on the line.

Transverse cracks (flaw type 21.1-2) originate at the boundary between the work-hardened, flaked layer and the base metal of the rail head. Horizontal splitting, which forms between a work-hardened layer of metal in the rail head and one which is not so-hardened, limits the possibility of the fatigue crack "growing" upwards toward the surface. Therefore the depth at which contact fatigue cracks lie below the running surface is determined by the thickness of the work-hardened layer.

The experience of a number of railroads shows that the 21.1-2 flaws may originate and propagate on any section of the line. The intensity of propagation and the number of flaws of this type on the less active sections may be less in comparison with the sections with especially high traffic volume, but the danger of such flaws to the movement of trains is not diminished.

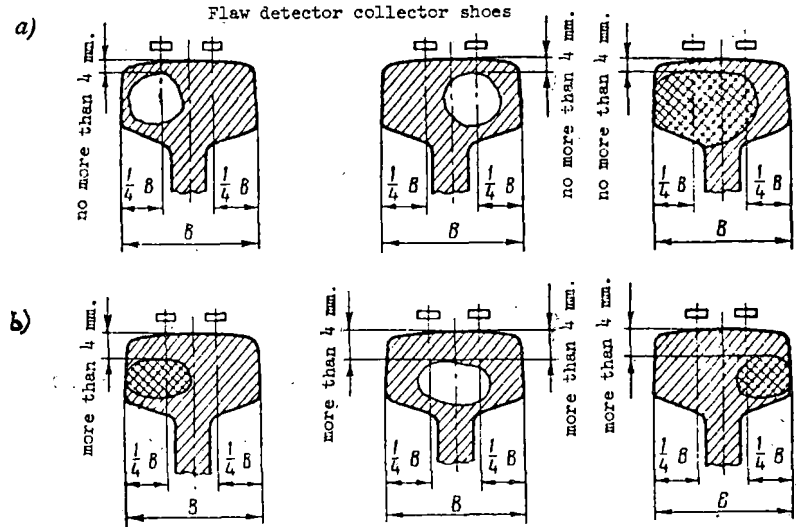

Fig. 76 Dimensions and depth at which transverse fatigue cracks detected by MRD flaw detectors lie: a. "spots" which are detected by the flaw detector b. "spots" which may not be detected by the flaw detector.

Each transverse fatigue crack may grow to dangerous dimensions and cause train wrecks.

The dimensions, and the depth at which transverse fatigue cracks detected by the MRD-52 and MRD-66 flaw detectors lie are shown in Fig. 76.

5. Trouble-shooting the MRD-52 and MRD-66 flaw detectors.

Testing and restoration of the magnets. As is known, each of the MRD

flaw detector magnets consists of two bars made of a Magnico alloy and a yoke made of "Armco" iron.

In the manufacturing process, Magnico rods are heated to a temperature of 1200° C. and cooled in a strong permanent magnetic field. The residual induction of the magnetized Magnico rod reaches 1.2 tesla, and the coercive force, 400 amp/cm. In the MRD flaw detector magnet, the bars are enclosed in an aluminum casing. These casings are intended to avert the possibility of iron and other magnetic elements touching the bars of the magnet. The aluminum casings protect them somewhat from blows and impacts, which, it is known, leads to a reduction of the residual magnetism.

The quality of the permanent magnets for the MRD flaw detectors is evaluated based on the magnitude of the residual magnetic flux in the Magnico bars.

A decrease in the magnet's magnetic flux in the MRD flaw detectors takes place primarily because the bars are not snuggly fitted to the yoke, because of sharp impacts and blows, because of poor-quality bars, and because of the frequent closing and opening of the magnetic circuit when the rail comes in direct contact with the poles of the magnet.

When the bars are not fitted snuggly to the yoke, humidity gets into the gap which is formed, and as a result, the contact surfaces between the bar and yoke rust, and the gap between them increases even more.

Considering the possibility that the indicated types of damage will appear, the magnets of each MRD flaw detector are tested no less than twice a year. When necessary, they are repaired and remagnetized.

Testing the magnet consists of measuring the magnetic flux of each of the bars.

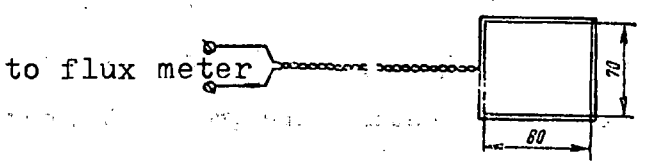

Fig. 77 The measuring frame.

Measurement of the magnetic flux of the bars is accomplished using a flux meter or a milliweber meter, with the aid of a measuring frame consisting of two turns of copper wire 1-1.5 mm in diameter. The equipment box and the probes are removed from the flaw detector before testing. The flaw detector frames are turned over so that the poles of the magnets point upward, and the pole shoes (where they exist) are removed from the magnets. The wire measuring frame (Fig. 77) is connected to a flux meter and is put over one of the magnet bars (until stopped by the yoke). The flux meter needle is set in the approximate center of the scale with an adjusting device and by rotating the measuring frame. The frame is then removed from the bar (the flux meter needle deflecting a specific number of divisions). The value of the magnetic flux in webers is calculated from the number of divisions thus obtained according to the formula

$$\Phi = \frac{N10^{-4}}{2},$$

where N is the number of divisions on the milliweber meter,

10^{-4} is the multiplying factor of a milliweber meter for one turn of a measuring frame, in webers, and

2 is the number of turns in the frame.

For example, before the frame was removed from the bar, the milliweber meter needle was set on 50, and after the frame was removed, the needle deflected

to 82. Then the magnetic flux is $\Phi = \frac{(82-50)10^{-4}}{2} = 1.6 \times 10^{-3}$ weber.

The magnetic flux being created by the other bar of the magnet is tested in the same manner. For normal flaw detector operation, the flux of one bar should be not less than 1.5×10^{-3} weber. The greater the magnetic flux, the better and more consistantly the flaw detector will work when detecting flaws in rails. A magnetic flux in the bar of less than 1.5×10^{-3} weber is not permissible. Therefore, all magnets, the bars of which have a flux of 1.5×10^{-3} webers or less, should be repaired and remagnetized.

The difference between the magnetic fluxes of the bars in the same magnet should not be greater than 5%. Upon detection of either diminished flux levels or of impermissible variation of the flux between bars, the magnet should be repaired and remagnetized.

In the renovation process, the magnet is completely disassembled and the contact surfaces between the yoke, the bars and the pole shoes are examined. Rust and dirt are removed from the contact surfaces. The magnet is carefully assembled so that the ends of the bars touch the yoke and the pole shoes with their whole surfaces. The newly assembled magnet is remagnetized.

The magnets may be remagnetized by various and sundry methods. Under conditions in the railroad flaw detector repair shops, it is recommended that the magnets be remagnetized using alternating current and two magnetizing coils. This method has attained the broadest use.

The principal circuit of the magnetizing device is presented in Fig. 78. This device consists of a yoke 1, two magnetizing coils 2, a fuse 3, and a switch 4.

The magnet is magnetized by a current pulse which is obtained when the magnetizing coils (a low resistance) are switched into an alternating current circuit with a voltage of 380 v. The coil circuit is broken by the fuse when

the alternating current reaches this amplitude value. The yoke 1 is made of iron. Its dimensions are 45 x 80 x 450 mm. There are holes on the edge of the yoke for affixing it to a rigid base (a table, a work bench, etc.).

One of the yoke's surfaces (80 x 450) is polished to assure that the ends of the magnet poles fit snuggly against the yoke. Each of the magnetizing coils 2 contains 50 turns of PBD copper wire 2.5-2.8 mm in diameter. The coil is wound in two layers, with 25 turns in each.

To protect them from damage when they are put on the bars of the magnet, the coils are wound with two or three layers of herringbone tape and impregnaged with insulation compound. The coils are connected in parallel so that the poles of both coils are added together (see Fig. 78).

The fuse element is a piece of copper wire clamped between two rigid contacts affixed to an insulation panel. The wire is 0.34-0.35 mm in diameter (one conductor of a light cord) and is 25-30 mm long.

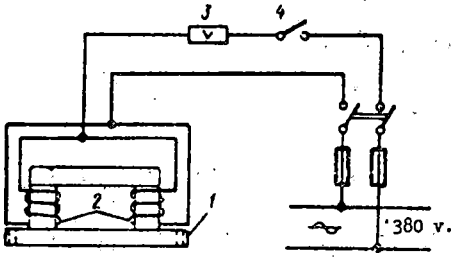

Fig. 78 Diagram of the remagnetizing device.

The insulation panel with the fuse element should be fastened and covered on all sides by a metal box with four sides and a hinged top since, when the fuse element burns, steam and sparks from the melted metal may inflict serious injury to the servicing personnel.

A VPKZ-25 or other equivalent may be used as the switch 4.

The yoke, the magnetizing coils, and the switch are mounted on a place

on the table or workbench specially set aside for that purpose, where the work of remagnetizing the magnet will be conducted. The fuse element is mounted on a special panel.

When remagnetizing the magnets using this circuit, it is necessary to strictly adhere to the following sequence of operations:

1. Place switch 4 in the off position
2. Mount the magnet with the coils already placed over the bars on the yoke 1 with the butt-ends of the poles fitting snuggly against the yoke
3. Insert and tighten the fuse element 3
4. With the knife switch on the panel switched off, connect the magnetizing device to the alternating current circuit with 380 v.
5. Switch on the knife switch on the 380 v. a.c.-circuit panel
6. Switch on the magnetizing coils using switch 4.

When switch 4 is closed, the fuse element will burn out at the moment of maximum current value of the positive or negative halfcycle. After this, it is necessary to switch off the knife switch on the alternating current circuit panel and put switch 4 in the off position. Then it is necessary to take the magnet from yoke 1, take off the magnetizing coils, and measure the flux of each bar with a fluxmeter. If the flux which is measured is less than the acceptable value (less than 1.5×10^{-3} weber), then it is necessary to subject the magnet to secondary magnetization.

One must keep in mind that in recent models of the MRD flaw detectors, the thickness of the magnet's yoke has been decreased to 25mm. It is necessary to increase the cross-section of the yoke by placing a specially-prepared yoke (a plate 25-30 mm thick) on it in order to decrease the resistance to magnetic flux when such magnets are magnetized. The whole surface of the plate should contact the primary yoke snuggly.

If the difference between the magnetic fluxes of the bars exceeds 5% after repeated magnetization, those bars are replaced.

The repaired and remagnetized magnet is painted with oil paint. It is necessary to pay particular attention to how the contact contour between the bar and the yoke is painted. In these places, painting should be carried out especially carefully so that moisture does not penetrate into the crack between the contact surfaces of the bars and the yoke. This excludes the possibility of corrosion arising in the indicated places.

Matching the coils and the ferroprobe cores. The two coils of the ferroprobes of one probe assembly should have the same ohmic and inductive resistance.

The resistance of the coils (2500 turns of PEL-0.03 wire) is measured with a UM-2 bridge; it should not differ by more than $\pm$ 10 % for both coils. From among the coils selected according to the resistance, matching the paired coils for a single probe is accomplished based on the impedance.

The probe coils are selected based on their impedance using the circuit presented in Fig. 79. This circuit is assembled from a balancing transformer Tr; a sound frequency generator, e.g. the ZG-2A; a cathode oscillograph; an LV-9 or VKS-7 cathode voltmeter; and a resonance circuit C8-L2, the characteristics of which are the same as those of the input resonance circuit of the receiver. The spare transformer supplied with each flaw detector by the factory may be used as the balancing transformer.

The coils being tested, connected in series and without their cores, are connected in parallel with the secondary transformer winding.

When the two series-connected coils are switched on, the voltage between the outside points of the secondary transformer winding should equal 6 v. When the voltage is less than 6 v. in the secondary transformer winding and

the generator voltage is at a maximum, the transformer is switched on between the generator and the balancing transformer, permitting the voltage in the secondary winding of the balancing transformer to be raised to 6 v. The generator frequency should be near 6000 Hz.

As may be seen, the circuit forms a bridge, the arms of which are the two coils being tested and two halves of the secondary transformer winding. When the total resistance of the coils is equal, the voltage between points D on the bridge diagonal will almost equal zero, a cathode voltmeter with a 1.5 v. scale will not make a noticable deflection, and a horizontal line will be observed on the oscillograph at its maximum sensitivity.

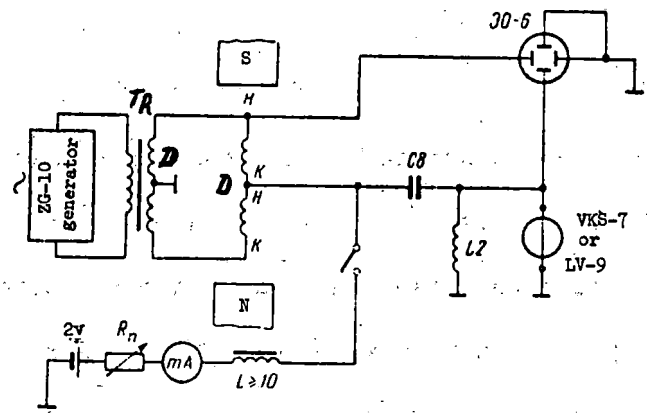

Fig. 79 Circuit for matching coils and ferroprobe cores for the probe assemblies.

If the needle of the cathode voltmeter makes a noticable deflection and a horizontal figure eight is observed on the oscilloscope screen, this means that the resistances of the coils being matched are different, and no voltage compensation is obtained. Changing each of the coils in sequence, a pair having identical impedance is matched. The probes are fitted from among the paired coils which were selected.

Connection of the coils should be accordant, i.e. the end of one coil winding is connected to the beginning of the other. The cores are matched for the probe being made up. The same circuit is used to match the cores. The cores are cut from non-annealed Permalloy wire 0.25 mm in diameter. The length of the cores should be identical, equal to 7 mm. It is practically impossible to balance the probes when the cores are of different lengths.

For matching the cores, it is necessary to have a uniform, constant magnetic field with an intensity of 12 amp/cm, i.e. the same field in which the probes are situated between the poles of a U-shaped flaw detector magnet. In practice, this type of field may be obtained with the two magnetized Magnico bars used in the flaw detector. These bars are fitted in one plane with the opposing poles facing each other at a distance of approximately 500 mm.

The probes are mounted between the poles so that the ferroprobe cores are directed along the field. Moving the probe in the direction of one or the other pole, that place is found where the difference between the doubled-frequency voltages being measured by the cathode voltmeter would not exceed 0.02 v. A straight line will be observed on the oscillograph in this case.

If the cores have identical magnetic properties, the doubled-frequency voltage at inductance L2 of the oscillatory circuit will not exceed 0.02 v. when the probe is turned 180° in the magnetic field and when it is moved 8-10 mm to one side or the other. When the doubled-frequency voltage is higher, it is possible to reduce it by moving the cores inside the coil. If the attempt to lower the voltage by moving the cores is unsuccessful, the cores are changed, and a reduction is attained in the doubled-frequency voltage, down to the selected position using point.

After the cores have been matched, the probe sensitivity is tested by passing a 0.8 milliamp direct current through its coils. The same circuit is used for this, but a circuit consisting of a choke (coil) with L ≥ 10 henry, a milliameter, a variable resistance R_p equal to 1000 ohm, and a 2 v. storage battery are connected to the center-tap of the probe. The choke (coil) L serves to short out the doubled-frequency voltage. A voltage not less than 1.3 v., which is observed from readings of the cathode voltmeter, should be in the C8-L2 circuit tuned to the doubled-frequency of the generator when the coils and cores are correctly matched. After this, the probes are grouped in pairs based on their sensitivity. Probes with identical sensitivity, as determined by the size of the voltage in the circuit, are accepted for paired operation.

Tuning the input and anode circuits of the receiver. In certain cases, the amplification of the resonance amplifier diminishes noticably because of variations in the capacitance and the inductance values of the oscillatory circuits during their service life. This circumstance demands periodic testing and tuning of the oscillatory circuitry.

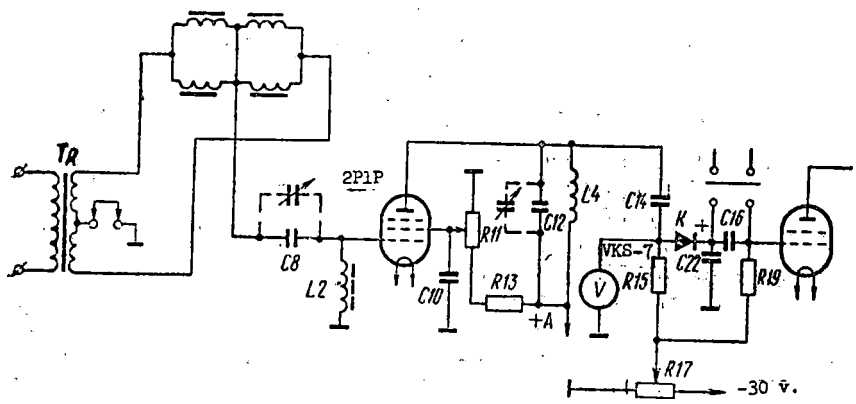

Fig. 80 Circuit for tuning the MRD flaw detector circuits.

By changing the capacitance or inductance going into its elements, it is possible to tune the circuit. According to one means for tuning the circuit, the receiver-oscillator assembly is removed from the box and power is connected to it. The center-tap of the transformer TR (Fig. 80) is grounded with the plug, and one of the probes is connected. A cathode voltmeter is connected after the blocking capacitor C14. An 800-1000 micromicrofarad variable capacitor which is preliminarily graduated, is connected in parallel with capacitor C8(C9). A magnetized object (a knife, screwdriver, etc.) is brought up to the probe causing the cathode voltmeter needle to deflect. Changing the capacitance of the circuit with the variable capacitor and the inductance L2 by resoldering the ends or by rotating the cores, the readings of the voltmeter are observed. At the maximum voltmeter readings, the circuit is considered to be tuned to resonance.

The plate circuit, in which a displaced capacitance is connected in parallel with capacitance C12, is fine-tuned in the same manner. It is sometimes necessary to tune the resonance circuits after replacing the 2P1P tubes or the probes. This is explained by the fact that the 2P1P tubes and the ferroprobe sensors may have a certain spread in characteristics, but since the tubes and probes are situated in resonance circuits, they may affect the tuning of the circuits.

Measuring the sensitivity of the probes. Periodically, but not less than once every quarter, test measurements are made of the probe sensitivity of flaw detectors working on the line. Measurement of the probe sensitivity is also conducted when the flaw detectors are repaired.

The probe sensitivity of each flaw detector is measured on a current-carrying conductor using the circuit presented in Fig. 81. For this, a conductor made of copper wire 0.5-0.6 mm in diameter is laid out on a wooden or

other non-metallic surface. A direct current source is connected to the conductor. The magnitude of the current passing through the conductor should be 1 amp. With an oscillator frequency of 6500-7000 Hz, the voltage on the secondary transformer winding under a load should be 6 v., the circuit LC (corresponding completely to the parameters of the input circuit of the MRD flaw detector) being tuned to a resonance at a frequency 2·f.

When testing the sensitivity, the assembled shoe and probe are moved across the current-carrying conductor. By comparing the magnitudes of the second harmonic voltage measured by the cathode voltmeter at inductance L, a judgement is made concerning the sensitivity of the probes being tested. Before the probe sensitivity test, the screen (the bracket) is put in a position symmetrically centered in relation to the ferroprobes. The probe imbalance voltage should be no more than 35 millivolts.

A probe having inadequate sensitivity will cause an increase in the second harmonic voltage in an inductance L of up to 200 millivolts and more when it is moved along the conductor carrying a current of 1 amp.

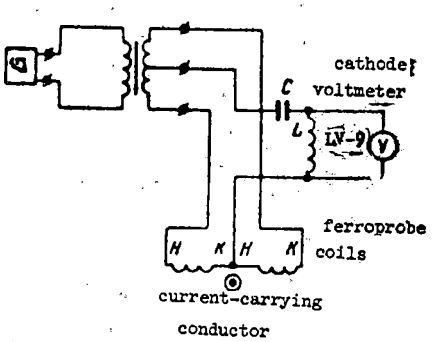

Fig. 81 Circuit of the device for testing the MRD flaw detector probe sensitivity.

The sensitivity of the two sensor shoes on one side of the MRD flaw detector should be identical. If in the flaw detector the two sensor shoes for one rail have differing sensitivity, one half of the width of the rail head will always be inspected with a diminishied sensitivity. It is impossible to increase the monitoring sensitivity of the indicated half of the rail head by increasing the amplification since when the amplification is increased excessively, much interference appears and is picked up by the sensor having the higher sensitivity.

When the sensor shoes are unequally sensitive on one side, it is difficult to balance the entire flaw detector probe system.

The greatest number of instances of decreased probe sensitivity is connected with an increase in the gap between the ferroprobe and the running surface of the rail head. The closer the ferroprobe is situated to the running surface of the rail head, the higher the probe sensitivity.

The gap between the ferroprobe and the running surface of the rail head is composed of the total thickness of the protective sheet, the shoe bottom, and half the diameter of the ferroprobe coil. Any increase in this gap causes a sharp decrease in the probe sensitivity. Therefore it is necessary to take care that residual oil and dirt do not build up on the protective plate, and not to permit any gap between the shoe bottom and the protective plate. Nor is it permissible to allow any sagging of the bottom within the shoe, lack of alignment of the probe blocks, etc.

Possible types of damage to flaw detectors and means for eliminating them.

Good attendance, careful periodic examination of the weak mounting points and moving connections, cleaning the contacts, etc., prevent the breakdown of the apparatus during work time due to a flaw in the circuitry.

The most probable causes of damage to the MRD flaw detectors are as follows:

1. Failure of normal operation on both sides of the flaw detector is possible only when there is trouble in the power supply circuits or in the master oscillator circuit. When trouble-shooting these flaws, the power supply circuits are tested with a test apparatus, the oscillator tube is replaced, the connections of the elements leading into the oscillator circuit are examined, and the status of the power supply sources is checked.

2. A break in one side of the flaw detector when working may be detected by comparing or replacing the individual parts of the apparatus. For example, the probe leads, tubes, etc. may be exchanged (one by one, without fail), permitting the moment when operation is restored to be established after the replacement of each part.

3. A break in the circuit providing alternating current power to the probe windings is detected from the milliameter readings. The milliameter needle will be deflected to the stop even at full cut-off voltage and minimum amplification due to the break in the differntiational wiring circuit of the probes. The same phenomenon is observed when there is a break in the grid bias circuit.

4. A break in the probe center-tap circuit causes total loss of probe sensitivity to flaws. When working between stations with the flaw detector, this type of damage is difficult to notice since one of the probes may be sound and react accurately at the joint gap. Therefore its fitness for work is checked periodically (several times in the course of a working day) by bringing a magnetized object up to each of the probes.

5. Separation of the probe block away from the protective bottom of the shoe causes a loss in the sensitivity of the probe and a large imbalance. This damage is frequently observed in warm weather. To eliminate this defect, the bracket (screen) is removed and the backing of the probe is lightly clamped to the shoe bottom, after which it is covered with an insulating compound.

6. A drop in the receiver amplification may be noted from a drop in the flaw detector sensitivity. The receiver amplification depends primarily on the tuning accuracy of the oscillatory circuits of the resonance amplifier, and, especially on data from the plate circuit.

The circuits are tuned by changing the effective number of turns of the torroid coil or by capacitance matching. It is helpful to have a calibrated capacitor when matching capacitances.

A voltage decrease may also take place because of a loss of emission from the tubes or from changes in the copper exide rectiviers. These defects may be eliminated both during periodic inspection in the repair shop as well as on the line by replacing the indicated elements with new ones which are known to be in good working order.

Chapter IV -- Electromagnetic Flaw Detector Cars

1. Intended Use and Working Principles of Flaw Detector Cars

The flaw detector car is intended for testing rails in position on the line. It is moved about by a separate locomotive, with speeds of up to 70 km/hr, and it detects various flaws in the rails, including hidden flaws (transverse and longitudinal cracks in the head.)

Sufficiently developed transverse cracks (spots) with a size of 20% or more of the rail head are detected by the flaw detector car. Horizontal separation of the metal of the rail head, which frequently turns into extremely dangerous vertical cracks, as well as vertical separation of the metal of the rail head, are also detected. Flaws are not detected within the joint area covered by plates, in welded joints, or in the rail base.

A block diagram of the flaw detector car is presented in Fig. 82. The magnetic field is created by square electromagnets (E1) and (E2) (one electromagnet for each rail of the track).

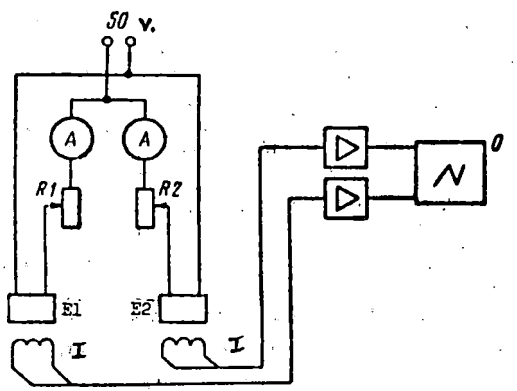

Fig. 82 Block diagram of the flaw detector car.

The two electromagnets (inductors) consist of a core of soft steel with windings. The coils are hooked up in series and connected to a d.c. source.

The electromagnets are suspended from the frame of the inductor carriage so that an 8-12 mm clearance is extablished between the running surface of the rail head and the coils of the electromagnets. The effect of the rail is to short out the poles of the electromagnet, it being a magnetic conductor, i.e. a continuation of the cores. The magnetic flux created by the electromagnets flows almost entirely through the rail. The distribution of the magnetic current in the rail and the electromagnet core is shown schematically in Fig. 83. That part of the magnetic flux which is directed along the rail, i.e. paralled to its longitudinal axis, is called the longitudinal component.

The longitudinal component of magnetic flux Φ_x in a rail between the poles at a given induction, B, will be determined by the cross-section of the rail, F i.e.

$$\Phi_x = BF.$$

The electromagnets create a magnetic flux somewhat larger than this value since a certain part of it passes through the air between the poles of the electromagnets (1) and also through the rail (2), the wheels (3) and the frame of the inductor carriage.

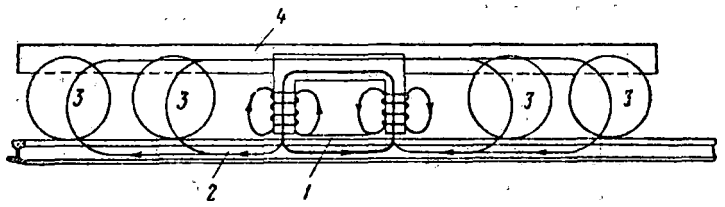

Fig. 83 Schematic for distribution of the magnetic flux.

Flaws are detected due to changes in the magnetic flux over the head of the magnetized rail. An induction probe coil is affixed between the poles of each electromagnet, in the immediate proximity of the running surface of

the rail head, for registering these changes. The plane of the coil windings is perpendicular to the longitudinal axis of the rail. The coil therefore reacts to changes in the longitudinal component of the flux. If this flux, which runs through the coil, changes, then an emf will arise in the coil.

Each rail, in position in the track, has faults or damage of various types in the form of indentations from blows from a spike hammer, cavities, engine burns, cracks, etc., which cause local dispersive flux as the rail is magnetized. Joint gaps cause a large dispersive flux. In addition, the rails are tightly pressed to the base plates on the crossties by spikes or lag bolts. The base plates, along with the spikes, effectively increase the area of the rail (the volume of the metal) and, in the loose plate zone, the magnetic flux over the rail will be diminished since part of it passes through the base plate. Consequently, the magnetic current passing through the probe coil changes when the coil is in motion over the rail: in sections between the ties it increases, and over the base plates it decreases. Above cavities, where disperive flux arises, the coil is penetrated by magnetic flux which is signigicantly greater than over the sound sections of the rails. However, this is observed for the short distance, determined by the dimensions of the cavity. Over a joint gap, the magnetic flux passing through the coil will be still greater.

Thus, the probe coil is penetrated by a magnetic flux of varying values as the flaw detector car is in motion. EMF pulses, the nature and value of which will also be different, are induced into the coil.

EMF pulses from the probe coil pass to the input of an amplifier which amplifies these pulses without substantial distortion. The vibrators of the

oscillograph O are connected to the amplifier output (cf. Fig. 82). In many flaw detector cars, an unamplified circuit is used for registering the pulses; the sensors I are connected directly to high-sensitivity vibrators. With the aid of the vibrators, continuous registration of the emf forces is realized on a movie film, which moves through the oscillograph at constant speed.

After recording, the film is processed, i.e. it is developed, fixed and dried. Processing of the film takes place in the developing machine which is mounted in the car.

The EMF pulses are registered on the film as two lines, corresponding to the two rails, and this is called the oscillogram. The nature of each impulse is seen separately. The joint gaps, face plates, cavities, and engine burns, as well as dangerous flaws which produce impulses of a definite form are identified (a detailed description of the pulse forms is given below).

2. Layout of the flaw detector car.

All of the equipment of the flaw detector car is distributed in a specially adapted 4-axle passenger car with a frame length of 20.2m (Fig. 84). The heating boiler and galley are located in the front part of the car, the end with the covered platform; further on are living compartments. At the other end of the car is the control room, where the switchboards (2, 3), by means of which the work of the flaw detector is controlled and the control panel (1) are located. Between the control room and the living quarters, there is a compartment where the developing machine (4) and a work bench with a device for rewinding the film are mounted. In the same compartment, water tanks (5) with a capacity of 0.5 m^3 are mounted above the ceiling. Water from these tanks is used only for processing the movie film in the developing machine.

The windows in this compartment have opaque shades with which they are covered when film is being rewound.

Several flaw detector cars are equipped with an electric power assembly mounted in an iron box which is fastened to the frame of the car under the equipment compartment (between the buffer beam and the car's rear truck).

Between the car's trucks are a special, so-called inductor carriage (6), boxes with storage batteries (7), and a railroad car-type d.c. generator (8) which is connected with the axle of the front truck by a belt drive system.

The inductor carriage (Fig. 85) has the electromagnets suspended from it. It consists of a smooth, welded frame (1), two outside pairs of wheels (2), and two inside wheels (3). The electromagnets (4), which are suspended from the frame of the carriage, are situated between the wheel sets. The carriage is attached to the frame of the car (7) by connecting rods (5) and (6). Angle brackets (8) and (9) are bolted to the center beam of the car's frame.

Each connecting rod of the carriage is attached to the angle brackets so that when the car is traversing sharp curves, the position of the carriage is correctly maintained over the track. For this purpose, washers with a spherical surface, which permit each connecting rod to deviate to a certain angle in the horizontal and vertical planes, are inserted between each angle bracket and the buffer spring (10). Therefore, the vibrations of the frame (body) on the leaf springs as well as the deflection from the track axis in the curves does not influence the inductor carriage.

The buffer springs (10) serve to soften the jolts encounted during sharp changes in the speed of the car. Tension in these springs is created by tightening the nuts at the end of each connecting rod. In case the tension is wrong, a break-down in the smooth motion of the carriage upon acceleration or deceleration is observed. At this time, the carriage begins to move in

jerks because of so-called "play" in the buffer springs. Such carriage jerking may produce additional emf impulses in the sensor coils. Therefore, the tension in the buffer springs should insure smoothness of movement to the inductor carriage by suppressing jolts arising when the car brakes and by damping the sharp jolt which is possible when the engine starts off.

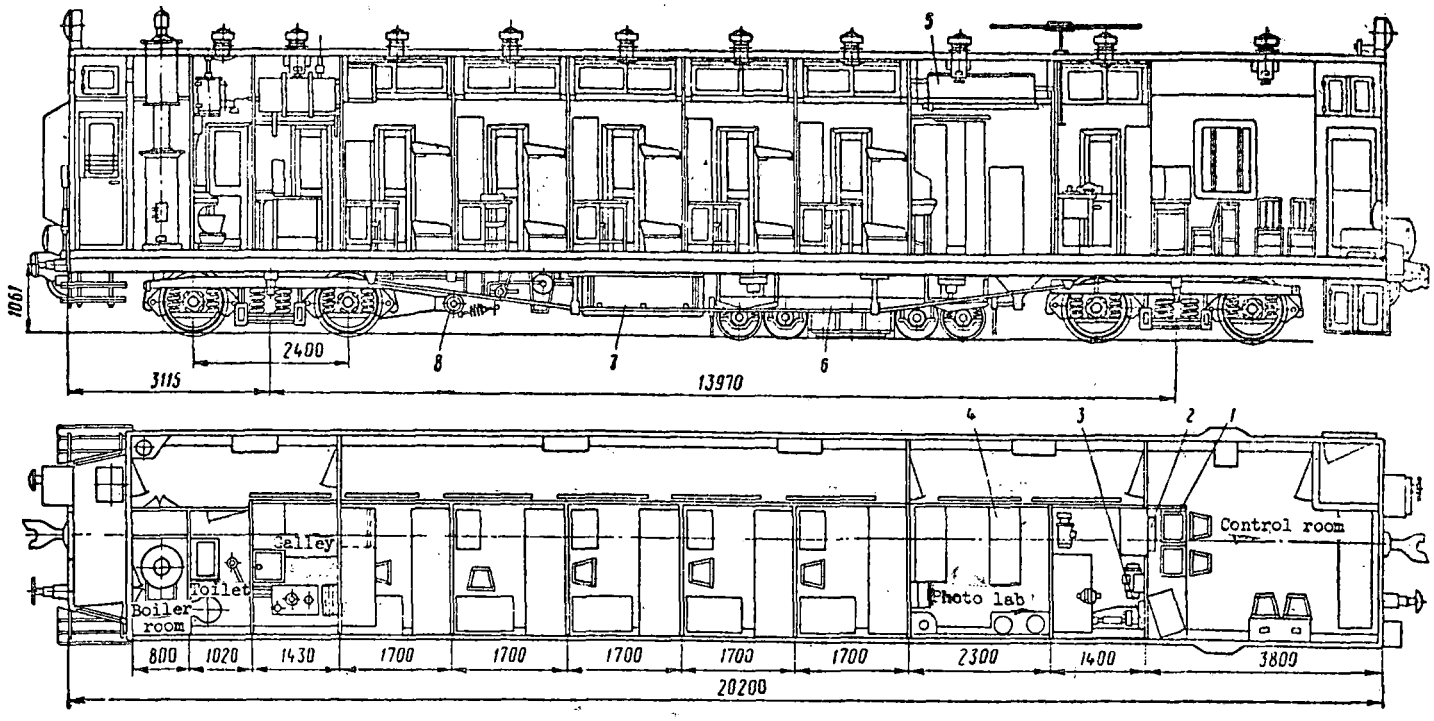

Fig. 84. Flaw detector car.

It is necessary for the clearance between the poles of the electromagnets and the rails to remain constant while in motion along the track for the flaw detector to work normally. Therefore, the frame of the inductor carriage with the electromagnets is suspended on two intermediate wheel pairs without spring support. Here the leaf springs of the outer wheel pairs are adjusted so that approximately 2/3 of the weight of the carriage frame with the electromagnets

is transferred to the external wheel pairs. Such a weight distribution is mandatory. This guarantees that the carriage will be prevented from derailing since the wheels of the unsprung axles are flangeless.

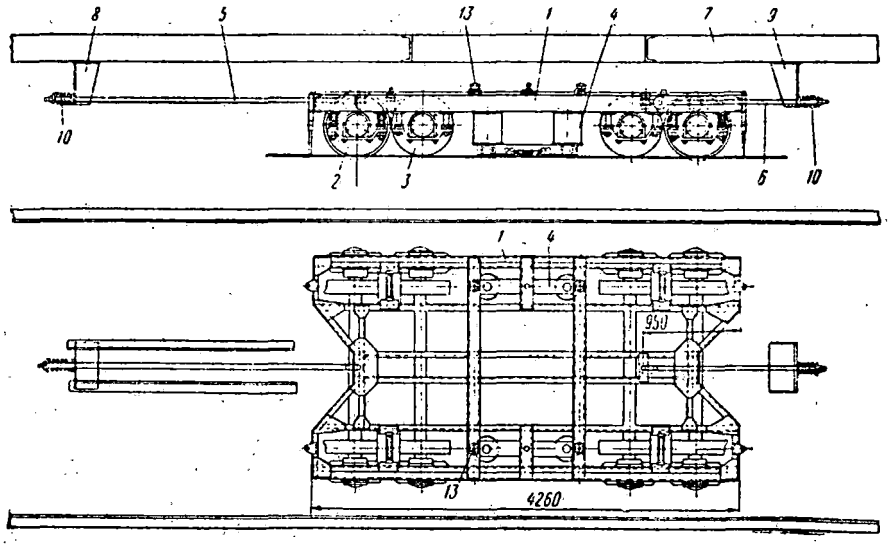

Fig. 85 The inductor carriage.

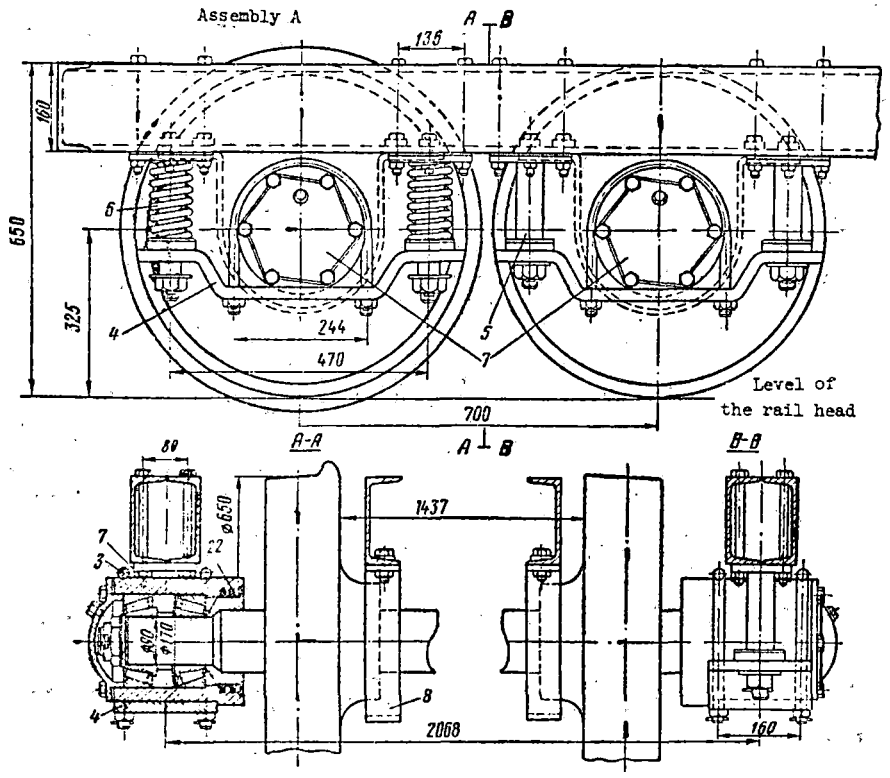

Fig. 86 Mounting of the wheel pairs for the inductor carriage.

The mounting for the wheel pairs on the inductor carriage is shown in Fig. 86. Each axle box (7) is securely fastened to a bracket (4) with the aid of two clamps. The brackets (4) of the unsprung axles are fixed to supports (5) on the carriage frame. The supports (5) pass through an opening in the brackets (4) on the outside axles, and the frame is supported by means of springs (6). Safety brackets (8) are installed from the inside of the carriage for each wheel pair to insure safe movement.

The condition of the wheel pairs and their mountings is carefully observed while they are in use. Such faults as loss of lock washers or cotter pins; dents; cracks in the wheels; broken leaf or buffer springs; faulty axle boxes; etc. are not tolerated. Special attention is paid to checking the fastenings of the clamp nuts (3) which support the greatest load.

According to established rules, wheel pairs on the inductor carriage are subjected to full examination every 100,000 km, or not less than once every 5 years, in addition to the usual inspections. In the complete examinations, the wheel pairs are rolled out from under the carriage, and the axle journals and all open parts of each axle are checked with a flaw detector. The wheels are also carefully checked. Complete examination and repair of the wheel pairs takes place at specially equipped repair points on the line.

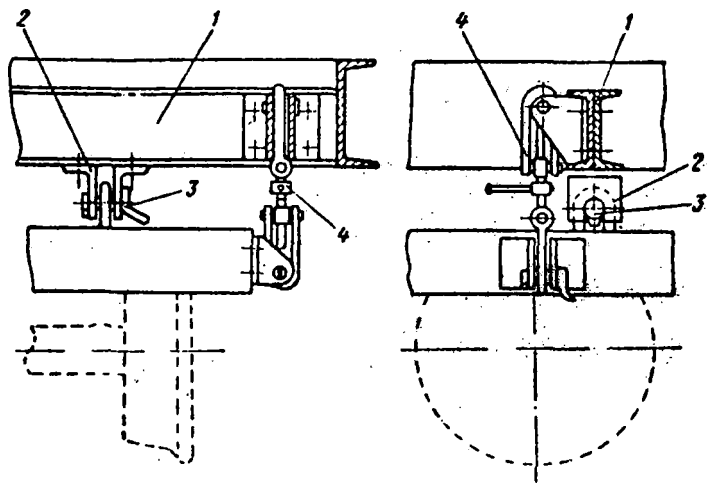

Fig. 87 Suspension of the induction carriage from the car frame.

The wheel pairs are cared for in accordance with the "Instruction on Examination, Sorting, and Repair of Shunting Engine and Hand Car Wheel Pairs", affirmed by the Ministry of Railroads.

The overall weight of the carriage with the electromagnets is about 5 tons. When not in operation, the inductor carriage is raised with the aid of threaded tightening devices and fastened to the car's frame when the car is being moved to the place where it will be used as a component of a passenger train.

Additional stays (1) (Fig. 87) made from channel bars are provided for fastening the carriage to the car's frame. Four special eyes (2) are affixed to the lower edges of these channel bars. Upon termination of the carriage-raising procedure, securing pins (3) are inserted into these eyes. After this, the threaded tightening devices (4) are released slightly so that the weight of the carriage is equally distributed on all four securing pins.

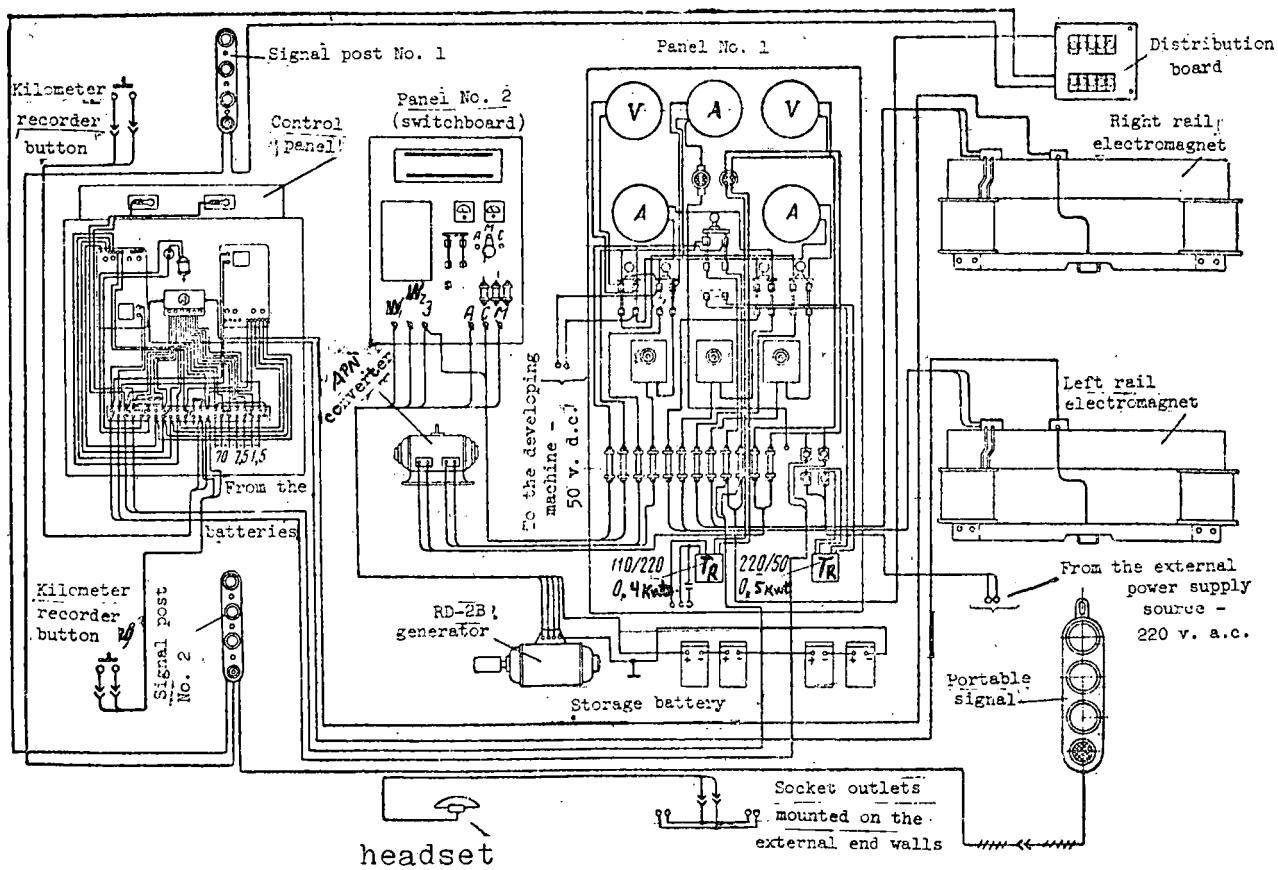

Fig. 88 Electrical wiring diagram of the flaw detector car.

The electromagnets are switched into the d.c. circuits using rheostats, which permit the current in the electromagnet windings to be increased gradually and a definite value for the magnetizing current to be established. In addition, these rheostats are necessary when the electromagnets are turned off. Using them, the magnetizing current is first reduced to a minimum. Without a preliminary lowering of the magnetizing current to approximately 2.5 amp, the electromagnets must not be turned off since the insulation of the electromagnets and the generator might be ruined. This damage can be caused by a cut-off current, originating from the rapidly disappearing magnetic field. As a result, a large self-induction emf arises in the electromagnets.

The rheostats and the electromagnet switches, as well as ammeters showing the value of the magnetizing current, are mounted on a panel which is installed in the equipment section of the car (Fig. 88). Switches for the control panel power supply circuits, for the developing machine and the converter are also mounted on panel #1. The start rheostat for the APN-10 converter is mounted alongside and to the left of the electromagnet rheostats. A voltmeter showing the a.c. voltage is mounted in the upper right-hand portion of the panel, and, next to it, an ammeter showing the current being used by the converter. A d.c. voltmeter showing the voltage of the power supply for all the flaw detector circuits is mounted in the upper left-hand corner of the panel.

Voltage for the flaw detector power supply enters from the car's power plant through panel #2 (the switchboard), which is installed in the car's control room.

3. The electromagnets and probes.

The electromagnets are suspended from the frame of the inductor carriage on threaded connecting rings (1) (Fig. 89), thereby permitting regulation of the clearance between the rail and the poles. For normal operations, the clearances should be the same at both poles.

The clearances are checked and adjusted using feeler gauges in the shape of metalic vanes of determined thicknesses (10, 12, 15 mm). If it is necessary, for example, to establish a 10-mm clearance, a single 10 mm feeler gauge is placed on the rail head under each pole of the electromagnet. Both poles of the electromagnet are lowered down onto these feelers and tightened in this position. Upon tightening, the electromagnet rises up somewhat, and the feeler gauge is easily taken out by hand. The established clearance is from then on checked systematically with full current in the electromagnet windings. For this purpose, feeler gauges are prepared from nonferrous metals (duralumin, brass, bronze, etc.).

The electromagnet windings are made from 3.53 mm PDP wire. Each coil contains 1215 turns of this wire. An iron sleeve (2) and textolite brushes (3) serve as the coil shell. The sleeve is insulated from the winding by a layer of pressboard. On the outside, the winding is covered with a waterproof layer and enclosed by a protective iron covering (4). The coils are freely mounted on the core and compressed by the pole pieces (5) (cf. Fig. 89). To insure the necessary snugness of fit, each coil is heated up after the pole pieces have been mounted. For this purpose, wooden wedges are driven into the clearance between the core and the coil sleeve from the top of the electromagnets.

The snugness of the coil fit has great significance. The fact is that a rapid wearing-away of the insulation is observed in that part of the winding which touches the textolite brushes in coils which are mounted loosely, i.e. without wedging. This takes place due to a displacement of the winding when the car is in motion, during jolting, braking, etc. Insulation wear and baring of the wires leads to shorting out of the coil turns and a malfunctioning of the electromagnets. Shorting out of the turns takes place very frequently

because, under the influence of a magnetic field, metallic dust and isolated small fragments from burrs on the rails get in between the windings and the lower brush of the coil shell. To avoid such damage, it is recommended that rubber gaskets be used in addition to wedging the coils. The gaskets are prepared from sheet sponge rubber and are placed between the winding and the textolite brushes of the coil. Such a gasket well preserves the insulation of the winding from wear and damage.

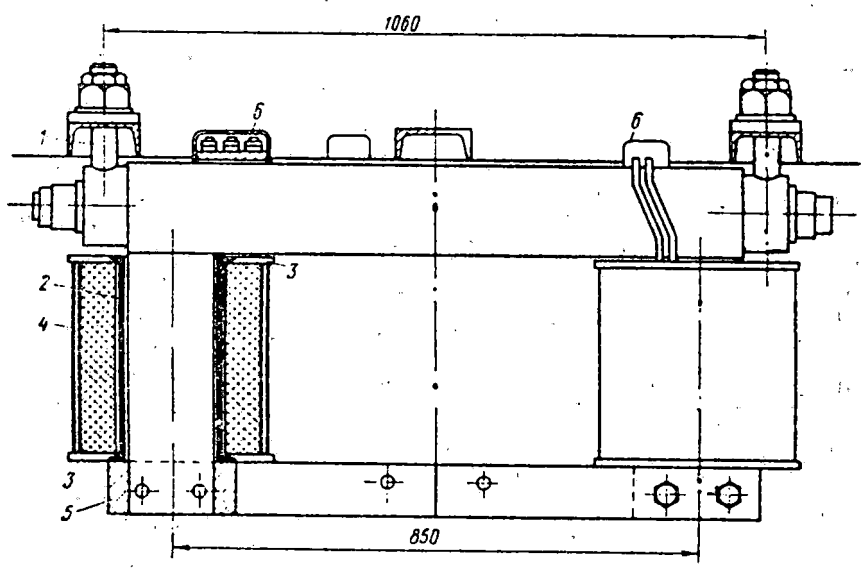

Fig. 89 The Electromagnet.

The pole pieces of the electromagnets are connected by two parallel stays (4) (Fig. 90) which are used for mounting the probe coils. These stays are prepared from textolite or duralumin 8-10 mm thick. The probe collector shoe is mounted between them. With the aid of the collector shoe, the probe coil moves along the rail in the immediate proximity of the running surface of the rail head. For this purpose, each probe coil is placed inside a body (1) which is affixed to the shoe so that the bottom of the shoe (2), which is prepared of bronze, non-magnetic steel, or brass 0.5-1 mm thick, acts as a pad between

the coil and the rail. The collector shoe is held in position by the pin (3), which is attached to the parallel stays (4).

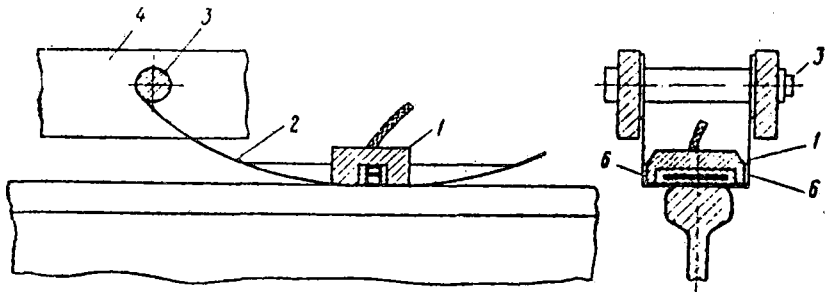

Fig. 90 Collector shoe with the probe coil.

The construction of the collector shoe eliminates the possibility of transverse displacement of the probe coil relative to the stay (4), while permitting its free rotation on the pin (3), i.e. vertical displacement, which is possible when it passes across a joint clearance or on rails with hair-line wear patterns. When the car is in motion, the collector shoe slides along the running surface of the rail head under the influence of its own weight and the weight of the body with the coil. The collector shoes are sometimes supplied with steel wire springs, about 1 mm in diameter, for better contact with the rail. A small supplimentary pressure on the collector shoe is especially necessary when the bushing on pin (3) is dirty.

The method of pressing the collector shoe to the rail using soft sponge rubber is widespread on the line. A piece of such rubber is pressed onto the collector shoe, and supported by a special square bracket passing to the parallel stays (4) from above. The soft sponge rubber presses the collector shoe to the rail and damps undesirable vibration of the sensor. These vibrations occur in cases of inaccuracies when shortened collector shoes are assembled and mounted, and when the weight of the collector shoe is inadequate for the probe to work without additional pressure.

The probe coil itself is made on either a textolite or a plexiglass shell and has dimensions along the length of the rail of 3-4 mm and across the rail of 75 mm (Fig. 91). Coils with 600-800 turns (PE wire, 0.07-0.1 mm in diameter) are used for working with amplifiers. In an unamplified circuit, the number of coil turns should be 160-180 (PEL wire, 0.12-0.14 mm in diameter). If vibrators with a relatively low sensitivity, e.g. MOV2, type V, are used concurrently, the dimensions of the coil are slightly increased to a length of 6 mm along the rail, and instead of 3-4 mm, the height of the coil becomes 6-7 mm.

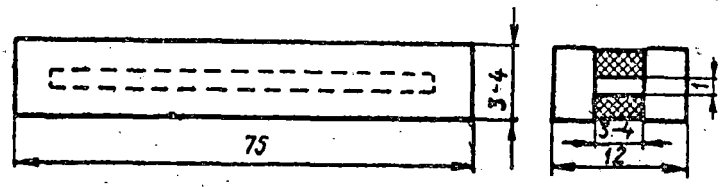

Fig. 91 The probe coil.

The coil is mounted in the shell cavity so that the lower turn of its windings is no farther than 0.5 mm from the bottom of the collector shoe. After the coil has been installed, the cavity in the housing is poured full of an insulating material (a mixture of wax and resin). The housing is affixed to the shoe with screws (6) so that there is no clearance between them and the collector shoe bottom (cf. Fig. 90).

The collector shoe is mounted between the electromagnet poles so that the coil is shifted from the center-point of the interpolar distance some 220-230 mm in the direction opposite the motion of the car, i.e. 220-230 mm closer to the rear pole of the electromagnet. Such a shift of the coil position is necessary because in this position, the greatest detectability of rail flaws is achieved.

4. The car power plant and converters.

The power equipment of the flaw detector car, supplying the flaw detector apparatus with lighting and the signaling mechanisms with electrical energy,

consists of a car power plant and voltage converters. The car's power plant consists of a generator, working from the axle of the car, automatic voltage regulators, a switchboard and a storage battery. Flaw detector cars are equipped with one of two types of power plants, either d.c. generators or a three-phase a.c. generator.

The Car Power Plant with a d.c. Generator.

The power plant consists of an RD-2B type generator with a DShchR-8A switchboard and a 40-TZhN-250 or a 26-VPM-400 storage battery.

The load S of the car power plant which supplies electric lighting to the car (Fig. 92) includes the electromagnets, converters and other components of the flaw detector. When the car is in motion and the voltage of the generator has normal value, the alternating current relay is in the position at which its armature (1) is connected to contact (3). In this position of the armature, the storage battery B and the load S are connected to the generator terminals. Thus, when the car is in motion, the storage battery is charged, and the supply for load S passes through the supply system resistor 8. If the generator produces a voltage higher than that which is acceptable, which occurs at high speeds, the voltage regulator comes into action. This regulator disconnects contacts 5 and 4 and the resistance 6 is switched on in series with the shunt field winding of the generator. The current in the field winding W decreases in connection with this, leading to a lowering of the generator voltage to the normal value.

At low speeds (less than 25 km/hr), when the voltage on the generator contacts becomes less than the voltage on the storage battery contacts, the armature of the alternating current relay falls away from contact 3 and connects contact 7. In this position, the generator armature relay is disconnected from the circuit and power is supplied for the load S from the storage battery.

The supply system resistor 8, switched on in series with load S, serves the purpose of lowering the voltage in the load circuit where the lighting lamps may overheat since the voltage of the generator is greater than the voltage of the storage battery when the car is in motion.

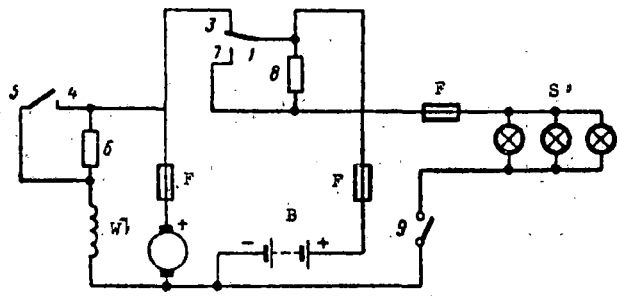

Fig. 92 Principal schematic of the car power plant with d.c. generator.

The alternating current relay, the voltage regulator, the supply system resistor 8, the knife switch, and the fuse F are mounted on a standard switchboard. A voltmeter and an ammeter for monitoring the power plant's operating mode are also mounted on the switchboard.

The standard DShchR-8A switchboard for the car power plant is represented in Fig. 88 (panel #2). The supply system and other auxillary resistances are mounted in the upper part of the panel under wire mesh. In the center part, the alternating current relay and the voltage regulator are mounted on the left-hand side under a protective metal housing. The voltmeter selector switch is mounted to the right of the knife switch. With the aid of this selector switch, the voltmeter is used to check separately the voltage on the generator contacts, the storage battery contacts and on the circuit contacts. Three melting-type fuses are mounted below the selector switch: for the generator circuit, the storage battery, and the load circuit. The first and second shunt field windings of the generator and the ground, which is the car frame,

are connected to terminals W1, W2, and 3 respectively. The positive terminal of the storage battery, the circuit (load), and the positive terminal of the generator are connected to terminals A, S, and M respectively. The overall schematic of the car power plant with DShchR-8A switchboard is represented in Fig. 93. According to this schematic, the shunt field winding W2 gets current from the generator through variable resistor 1. The definite value of the field current in the winding is established by regulating the sliding contact of this resistor. The field current in winding W2 is established for flaw detector cars so that the charging current for the storage battery at full charge and with the knife switch open would be no more than 12 amp.

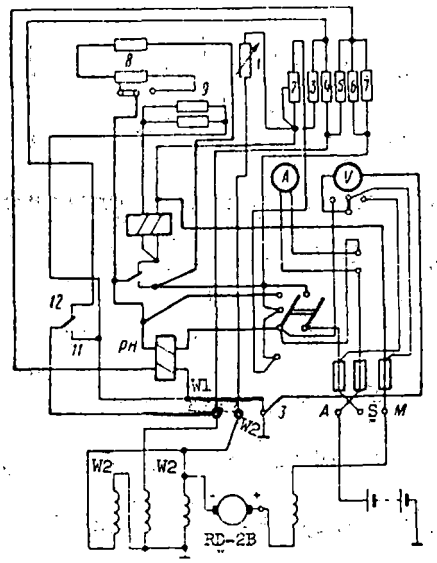

Fig. 93 Schematic of the car power plant with the DShchR-8A switchboard.

The other field winding W1 is connected to the generator terminals in series with resistances 3 and 4, depending on the position of the voltage regulator armature PH. Both of these resistances will be switched into the circuit in series with W1 when the armature is in the center position. With a decrease

in the generator voltage (as the speed of the flaw detector car is reduced), the armature will make contact with the stationary contact 12 and will switch out resistance 4. As a result, the field current in the winding increases and the generator voltage increases. In the case when the generator voltage exceeds the acceptable value, the armature of regulator PH makes contact with stationary contact 11 and will switch out the winding W1, which will cause a lowering of the generator voltage.

A SRN-2B-4 regulator with carbon contacts is mounted on the DShchR-8A switchboards. Given variations in the load and the speed of the car, this regulator maintains a constant generator voltage with an accuracy of ±3% of the established value. The rated voltage of the RD-2B generator is 52 v. While in operation, the armature of the SRN-2B-4 regulator oscillates between the stationary contacts 11 and 12, the sparking which arises between them destroying the contact surfaces. Therefore, it is necessary to clean the carbon contacts of the regulator periodically with fine abrasive paper.

The Car Power Plant with an Alternating Current Generator.

A three-phase GSV-8 generator is used as the alternating current generator. It works with selenium rectifiers, a magnetic amplifier, a ballast resistor bridge and a 40-TZhN-250 storage battery.

The ballast resistor bridge and the magnetic amplifier assure automatic regulation of the generator field current when the speed of the car changes. Because of such regulation, the voltage supplied by the generator into the load (lighting) circuit is maintained at between 47-54 v., and the voltage charging the storage battery, within 65-70 v. The fundamental schematic of the power plant, in which the electromagnetic coils of the flaw detector are hooked up in parallel with the lighting circuit CO, i.e. to the 47-54 v. voltage, is represented in Fig. 94.

When the car is standing or moving at slow speeds, i.e. the generator is not working, the lighting system, as well as the electromagnetic windings are supplied with power from the storage battery. The current from the positive terminal of battery AB passes through fuse 13, the ammeter, the non-linear resistance HC, the load CO and the electromagnets, along winding 5 or the magnetic amplifier and the series field winding 4 of the generator. The voltage drop at the non-linear resistance HC represents about five volts, and because of this, the voltage in the electromagnet windings is less, by this magnitude, than at the storage battery terminals.

Voltage on the battery terminals is measured by the voltmeter V using the selector switch PV. Ammeter A shows the current expended in the load circuit, and the charging and discharging current in the battery is controlled by another ammeter. The readings of these instruments is the same when the generator is not working.

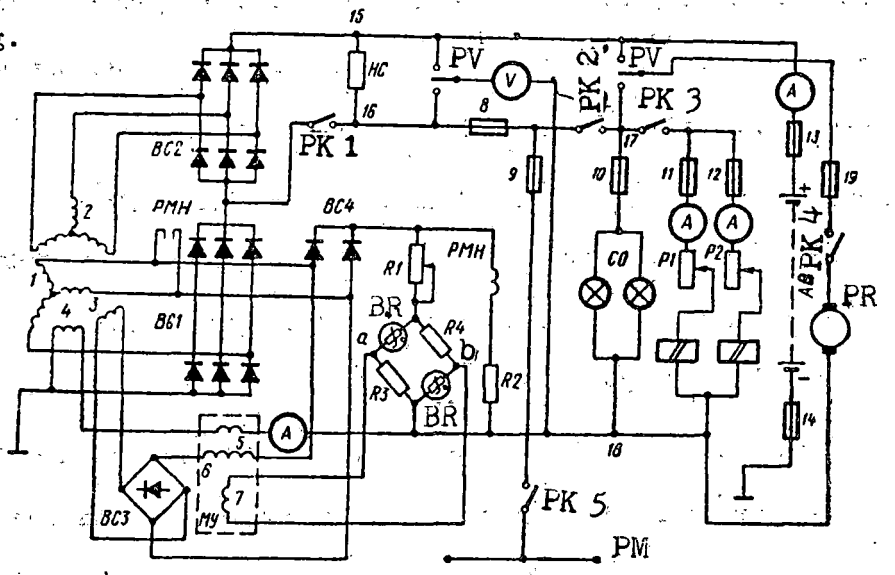

Fig. 94 - Schematic of the flaw detector car power plant with the GSV-8 Alternating Current Generator.

The generator has two three-phase windings. The primary (1), connected in a "star", and the secondary (2), which may be connected in a "star" or in a "delta". The secondary winding serves primarily to charge the storage batteries.

The converter PR, which requires increased voltage and uses a comparatively small current, is connected in parallel with the storage battery in the flaw detector cars. When necessary, the transformer may be switched into the lighting circuit (cf. Fig. 94). Such a switching takes place when the power supply for the converter comes from the locomotive via the undercar bus-bar pm.

The generator also has two field windings in addition to the two three-phase windings. The field windings 4, from which the load current passes, facilitate a voltage increase in the primary 1 and the secondary 2 generator windings. When speeds of 35-40 km/hr are attained, the voltage across windings 1 and 2 becomes higher than the storage battery voltage, and the equipment requiring electricity is supplied with power from the generator. The lighting circuit and the electromagnets take power from the primary, i.e. the power winding 1 through rectifier BC1, whereas the storage battery charging current and power supply for the converter comes from the secondary winding 2 of the generator through the rectifier BC2.

The generator gives off full power at car speeds of about 45 km/hr (at 1,000 rpm of the rotor). Here the useful power at the rectifier outputs is 5.5 kwt. A part of the power is expended on non-linear resistor HC. The generator current may create a voltage drop to 18 v. at this resistor. This voltage, combined with the voltage on the selenium rectifier BC1, (with the voltage between the shell and terminal 16), assures that the storage battery will charge when the load is switched into the system. Fuses 8-14 and 19 are melt-type fuses.

At various car speeds, the generator voltage is maintained within definite limits thanks to automatic regulation. The automatic regulation is realized thus: when the car speed reaches 25-30 km/hr, a current, which has been rectified by selenium rectifier BC3, appears in field winding 3.

The frequency of the current coming to rectifier BC3 depends on the rotor

speed of the generator, i.e. on the speed of the car, and changes from 100-400 Hz. As a result, the inductive resistance of winding 6 of the magnetic amplifier MY increases as the speed increases. Thus, the current in field winding 3 decreases, attaining a minimal value at a frequency of 400 Hz, i.e. at the maximum speed of the car.

The entrance of the current into the field winding 3 also depends on the current in the control winding 7 of the magnetic amplifier. There is no current in this winding if the ballast resistor bridge is in equilibrium. The equilibrium of the bridge is established using resistance R1. Resistance R1 is selected so that there is no voltage between terminals a and b of the bridge and no current in control winding 7 at a voltage of 54 v. in the load CO, i.e. the state of equilibrium is established for the bridge with maximum voltage in the load circuit.

If the generator gives a voltage lower than 54 v., the over-all current across the bridge decreases, while remaining the same across the ballast resistor BR (type 1B5-9). This decrease is proportional to the increase in resistance R4. In this case, the equilibrium of the bridge is destroyed, and current will pass along control winding 7 of the magnetic amplifier. The greater this current is, the smaller will be the resistance of winding 6 in the magnetic amplifier.

A decrease in the resistance of winding 6 leads to an increase in the field current in winding 3, and, consequently, to an increase in the generator voltage. An increase in the load current which passes along winding 5 of the magnetic amplifier leads to the same result as an increase in the current in the control winding 7. If the generator voltage exceeds the acceptable value, which may happen as a result of a defect in one of the elements in the circuit, the maximum voltage relay PMH, the contacts of which will short-circuit two phases of the primary generator winding, will activate.

The R-106 maximum voltage relay, the ballast resistor bridge and rectifier BC4 are mounted on one common panel and they form the PR-208B automatic system block. The selenium rectifiers BC1 and BC2 make up the second block, the BC-201A, and they are mounted in a metal box which is filled with oil to cool the rectifier elements. An MY-20A magnetic amplifier is mounted along with these blocks and the PY-215D control panel.

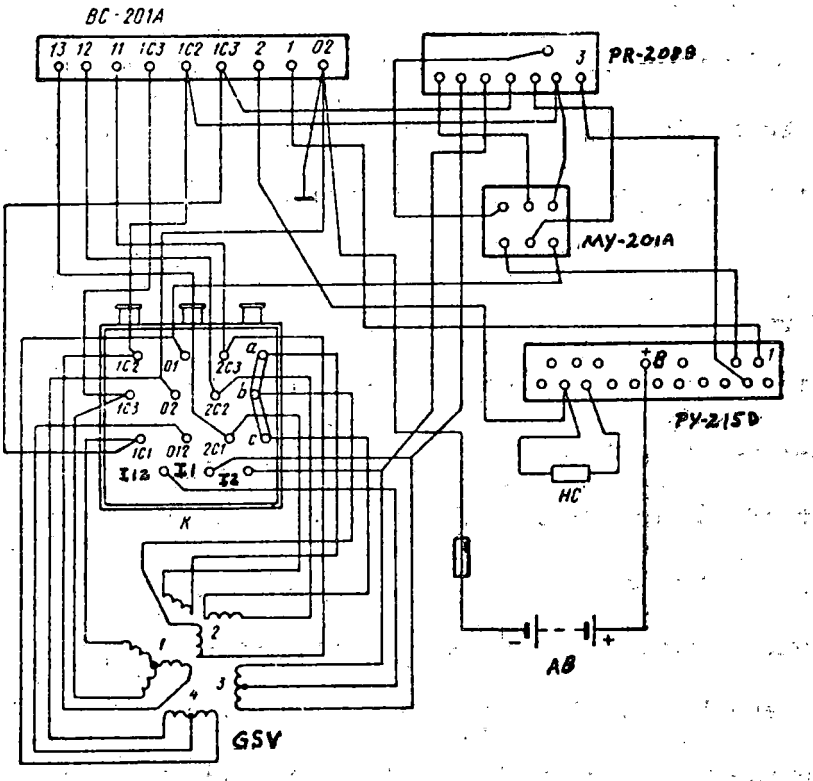

Fig. 95 Mounting diagram of the car electric plant with the GSV-8 a.c. generator.

The BS-203A non-linear resistance HC between terminals 15 and 16 is set according to the requirements for fire safety in the boiler compartment of the car. The terminal box, which is mounted on the generator housing, is represented in the mounting diagram (Fig. 95). According to this diagram, the secondary

winding (2) of the generator is connected in a "star". In order to switch the winding from the "star" to the "delta", it is necessary to disconnect terminals a, b, and c, and to connect together terminals 2C1 and c, 2C2 and b, and 2C3 and a. The "delta" connection is made in the summer, when working with acid as well as with alkaline batteries. The secondary winding 2 in the generator is connected in a "star", as shown in Fig. 95 for work in the wintertime.

Storage Batteries.

The 26-VP-400 battery, consisting of 26 elements connected in series, each with a 400 Amp·hr rating, is used as the acid storage battery. Before they are mounted on the car, the storage batteries are charged in a manner different from the way they are charged when in use. This operation is called "forming".

Before forming, the VPM-400 cells are filled with an electrolyte with a density of 1.19-1.2 g/cm^3 (sulphuric battery acid dissolved in distilled water). Six hours after being filled, the first forming charge is applied to the cells with a current of 36 amp for a period of 20 hr, after which the charge is lowered to 18 amp. The over-all duration of the first forming charge is 72 hr. After a two-hour interval, the batteries are discharged. The second forming charge then is applied, at first with a 60 amp current, then 30 amp. The 60 amp charging current is applied to the battery until the voltage in each cell reaches 2.35-2.4 v. Then the charging current is lowered to 30 amp. Charging is terminated when a constant voltage of 2.6-2.7 v. is established in the cells.

During the time of the forming charges, a constant electrolyte level is maintained in the cells and the density is constantly observed. The electrolyte level, its temperature and its density during the process of applying the forming change, and the subsequent usage are set according to instructions from the supplying plant.

After the two forming cycles, the battery is available for use. Its full capacity is attained after ten full charge-discharge cycles. To maintain the normal service life of the battery, it is not permitted to be discharged below 45 v. (1.75 v. in each cell).

The service life of the VPM-400 cells under normal use conditions, maintaining 100% of their 400 A·hr rating, is 500 charge-discharge cycles, with an additional 100 cycles with a rating of not less than 300 A·hr.

The 40-TZhN-250 battery, consisting of 40 sections connected in series, and each with a rating of 250 A·hr, is used as the alkaline storage battery. It requires three liters of electrolyte to fill one element. The electrolyte is a solution of caustic potassium hydroxide in distilled water, with a density of 1.19-1.21 g/cm^3 for summer conditions and 1.24-1.26 g/cm^3 for winter conditions.

To prepare the electrolyte with a density of 1.19-1.21 g/cm^3, one part, by weight, of solid caustic potassium hydroxide is taken with three parts, by weight, of distilled water, and for the 1.24-1.26 g/cm^3 electrolyte, the percentage weight of the caustic potassium hydrate is increased by about 40%. The solution is allowed to settle for 6-12 hr. and the clear portion is used for filling the cells. Two to six hours after filling, the storage battery is charged. The first forming charge takes place with a 65 amp charge over a period of 12 hours, after which the cell is discharged with a current of 50 amp to a voltage of not lower than 1 v. on each element. The cell, having released not less than 80% of its nominal rating after the first discharge, is charged a second time with a 65 Amp current for a 6 hr. period. After this, the cells are placed on the flaw detector car for use.

While in use on the flaw detector car, the 40-TZhN-250 battery should be charged with a current of not less than 12-15 A. and not more than 60 Amp.

Discharging the battery below 40 v. is not permissable since at this level, its service life is significantly shortened (the voltage on each element should not be lower than 1 v.).

The work of the alkaline or acid storage battery is evaluated by its efficiency based on its capacity η_e, i.e. the relationship of the number of A·hr, Q_d, obtained at discharge to the number of A·hr, Q_c, given when it was charged, i.e.

$$\eta_e = \frac{Q_d}{Q_c} \cdot 100.$$

The magnitude of η_e for acid storage batteries is 85-90%, and for alkaline batteries, it is 65-70%. Therefore, during the use period, it is necessary to pay strict attention that the mode and the time for discharging and charging the battery are correct.

Exchange and forming of storage batteries, as well as repair of the car's power plant equipment is performed by the organization of Rail Car Services according to the flaw detector car's place of registry.

The Converters.

The flaw detector car needs alternating current with voltages of not less than 220 and 110 v. to supply power to the developing machine and the oscillographs, respectively. This current is obtained by using converters. The APN-10 a.c./d.c. generator is used as a converter which gives current with a voltage of 110-115 v. Its armature has two windings: one, with a commutator, for d.c. current, and the other, with rings, for a.c. (Fig. 96). According to the factory schematic, the field coils are connected with the rotor's d.c. winding through a start rheostat, whereas the field coils are interconnected in a mixed circuit. In order to use the APN-10 generator as a converter of d.c. to a.c., it is necessary to feed a constant voltage to the commutator, i.e. to start the d.c. generator as an electric motor. Then, it is possible

to take the a.c. voltage which is created by the second armature winding from the rings.

The factory schematic of the APN-10 generator is altered somewhat (cf. Fig. 96) for working as a converter under flaw detector car conditions. The field windings are connected to each other in series, and are connected in parallel with the armature. In some instances, a 10-20 ohm resistor is switched into the field winding circuit so that the frequency of the alternating current in the converter would be close to 50 Hz.

The APN-10 converters are inadequate in that when the load changes, or when the input voltage changes, their voltage and a.c. current frequency change within broad limits.

The oscillographs and the developing machine may receive power simultaneously from the APN-10 converter. The developing machine requires a converter which raises the voltage to 220-230 v. Switching on the developing machine sharply reduces the voltage and the a.c. frequency. Therefore, the working voltage is established after the converter has been switched on with the aid of the start rheostat. The flux in the field windings is increased by the rheostat, which leads to a higher alternating current voltage. If the load diminishes when the oscillograph is switched off, the voltage in the converter rises by 15-20 v., which has no significance for the developing machine. But, when the developing machine is switched off, the load on the converter is diminished by a factor greater than two, a result of which is that the alternating current voltage rises sharply. This circumstance demands special attention from the attendant when working with the developing machine and the oscillographs. In connection with this, instead of one APN-10 converter, two PND-5 converters are used in some flaw detector cars, one of which is used to supply power to the oscillographs and the other to the developing machine.

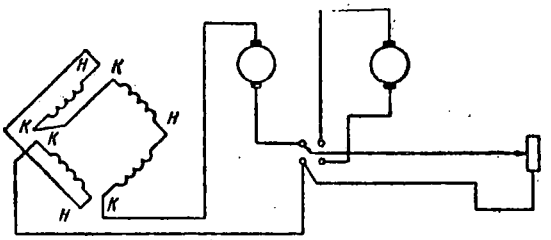

Fig. 96 Circuit diagram of the APN-10 generator windings.

The PND-5 (Fig. 97) converter consists of a d.c. electric motor and an a.c. generator combined on a single shaft. On one side of the shaft is a commutator, and on the other, is the a.c. generator ring. The field windings of the electric motor and the generator are distributed on one stator and are separated.

As may be seen from the schematic, coils 1 and 2, connected in parallel with the electric motor rotor, are the primary field coils of the generator and the electric motor. In addition, there are auxillary field coils 3 and 4 which are connected in series with the rotor of the electric motor. Resistors 5, 6, and 7 of the centrifugal frequency governor 8 are connected to the circuit of the electric motor's parallel coils. If the voltage of the power supply for the electric motor falls below 50 v., the rotor speed decreases and the alternating current frequency from the generator will also decrease.

When the rotor speed diminishes, the regulator contacts open up and resistance 5 or 6 is switched into the electric motor's field coil circuit. Switching in these resistances lowers the current in the field coils, and the magnetic flux will therefore diminish between the poles of the electric motor. Decreasing the magnetic flux, as is known, produces an increase in the motor's rotor speed and consequently, an increase in the alternating current frequency. If, on the other hand, the voltage increases, the speed of the electric motor

will also increase. In this case, the regulator contacts will short-circuit resistance 6, and the current in the field coils will grow. Increasing the field flux causes an increase in the magnetic flux between the poles of the electromagnet and, consequently, a decrease in the speed of the motor. Thus, the presence of the centrifugal governor insures the stability of the voltage and the a.c. frequency.

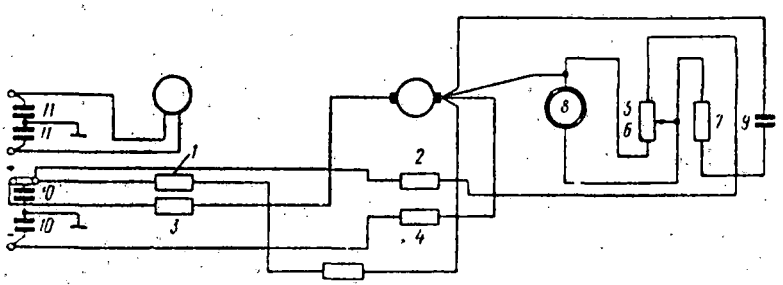

Fig. 97 Schematic of the PND-5 Converter.

The converter works at an input voltage of 43-60 v., giving an a.c. voltage of from 110-130 v. at a frequency of 49.1-51.5 Hz.

The second generator field coil, connected in series with the electric motor rotor, serves to improve the stability of the generator's voltage.

To eliminate the static interference which is created by the contacts of the centrifugal governor, the converter is equipped with a spark discharge circuit consisting of a capacitor 9 and a resistor 7.

To reduce the interference created on the electric motor commutator and on the generator rings, the brushes on the electric motor and the generator are interlocked with protective capacitors 10 and 11.

The TO-300B and the more powerful APO-0.3 converters are also used in flaw detector cars. The converters are mounted in the lower part (in a cabinet) of the switchboard on shock absorbers which absorb the noise created by the

converters when they are in operation. In a series of flaw detector cars, the converters are mounted under the car in special boxes, from where the noise is inaudible in the car.

The basic technical characteristics of the converters are presented in Table 5.

Table 5

Characteristic	Type of converter			
	PND-5	APN-10	APO-0.3	PO-300B
Electric motor input voltage, v	43-60	40-60	43-60	50
Current used, amps	12	13	15	9
Rotor speed, rpm	3000	1000-1800	3000	3000
Alternating current voltage, v.	110-130	90-150	110-132	95-120
Frequency, Hz	49.5-50.5	35-50	48.5-51.5	49-51
Alternating current power, watt	300	207-345	340	200
External dimensions, mm				
Height	250	330	265	300
Length	600	470	587	420
Width	250	250	286	220
Weight, kg	58	65	60	55

When standing at stations, the flaw detector car may be connected to an external a.c. circuit. For this purpose, terminal plugs are mounted on each end of the car. Voltage from an external source is supplied through the plugs to the flaw detector switchboard, and, via the converters, to the primary winding of the step-down transformer (cf. Fig. 88).

A three-phase step-down transformer is used on some flaw detector cars. The secondary windings of the transformer are switched into the circuit of the power plant's selenium rectifiers instead of into the primary and secondary windings of the generator. Thus, the secondary switches (contactors) K2, K3, K4, and K5 (Fig. 98) are mounted between the rectifiers, the generator and the step-down transformer TR. Using these switches, the generator is disconnected from rectifiers BC1 and BC2 and connected to the secondary transformer windings. Such a system is used in refrigerator car trains. It permits

recharging of the storage batteries when standing at the station while simultaneously supplying all the flaw detector components from the external power supply using the standard outfittings of the car in the same manner as when the flaw detector car is in motion and the generator is working.

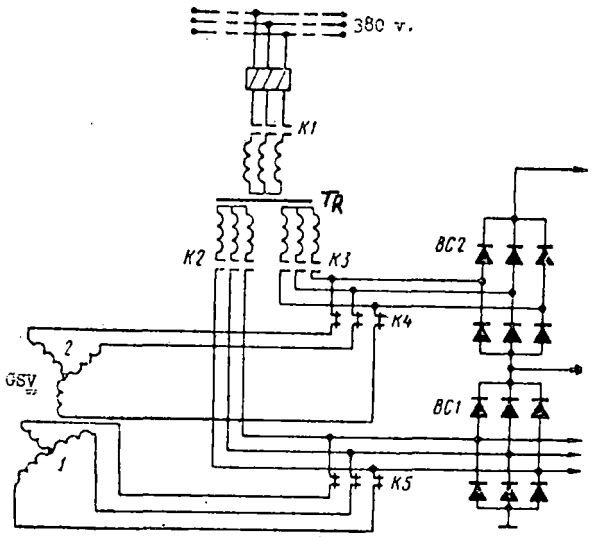

Fig. 98 The step-down transformer circuit diagram.

Power for the developing machine and the car's lighting may also be supplied from the energy generated by the locomotive. For this purpose, the car's lighting circuit is hooked up to the locomotive and the storage batteries are disconnected. To do this, the appropriate fuse is removed from the car's power plant switchboard. The undercar bus-bar PM (cf. Fig. 94), which at each end of the car terminates in a flexible conductor with rubber insulation having female terminal plugs, is used to hook up the car's illumination system to the locomotive. On the locomotive, the latter are to be found in those places where the signal lanterns are mounted.

Usually, energy from the locomotive is used only to heat the air and to supply power to the converters when the developing machine is working. The voltage differences in the current from an electric or a steam loco-

tive is taken into consideration. The excess voltage is reduced by a supplimentary resistor which is hooked up in series with those things which use energy from the locomotive. When working with a steam engine, the heating for the air in the developing machine and the power supply for the converter are taken from a turbine generator. For this, the steam engine is equipped with a stepped-up turbine generator providing 5.5 kwt. of power.

5. The Electric Power Assembly.

The electric power assembly serves to power the developing machine, and it consists of a portable AB-0-2/230 power plant with a power of 2 kw. The assembly gives simple phase a.c. with a voltage of 220-230 v., and works when the temperature of the surrounding air is in the range of -50°--$+50^{\circ}$ C. A flaw detector car with such an assembly may work without taking energy from the locomotive. The presence of the electric power assembly also permits processing of the movie film without being hooked up to an external power supply. This is significant since in several instances, hooking the car up to an electrical circuit is associated with a large time loss due to the complexity of switching at the station, and other reasons.

The assembly consists of a single cylinder air cooled gasoline motor, a single phase generator, and two instrument block units.

The Motor.

A four-cycle, small displacement motor such as the UD-1 with magneto ignition is used in the assembly. The motor is equipped with an automatic speed regulator, and has forced air cooling. For cooling the cylinder and the cylinder head, there are ribs over which air is blown from a centrifugal fan. The fan blades are cast as part of the motor fly wheel, and they are covered with a cowling which directs the air stream onto the cylinder and the head.

A-66 or A-70 gasoline is recommended as fuel for the motor. The gas tank

is not attached to the motor, but is mounted separately in a protective iron housing under the car. Gasoline flows from the tank to the carburetor by gravity feed. As is known, the carburetor serves to form the mixture of gasoline vapor and air.

The ignition of the mixture in the cylinder takes place somewhat before the piston arrives at the uppermost position (at the top dead-center point -- TDC). This ignition advance is established to be within 3-9° before the top dead center point (3-9° BTDC). When the motor is running, i.e. when the speed exceeds 2000 rpm, the ignition advance is automatically increased to 17°. This increment is realized with the aid of a special automatic device with which the magneto is equipped. Ignition advance is necessary for more complete burning of the air-fuel mixture. Otherwise, the motor will overheat, and its efficiency will decrease.

Intake of the air-fuel mixture and exhaust of the expended gasses from the cylinder is regulated by a system of valves.

To assure normal functioning of the valve mechanism, a clearance on the order of 0.2 mm is established between each valve lifter and the valve. The clearance is checked periodically with a feeler gauge after every 50-60 working hours, with the engine cold. When necessary, the clearances are adjusted with the aid of nuts on the top of the valve lifters.

The governor mechanism.

One of the fundamental demands made of a motor when working with a generator is to provide a constant number of revolutions. For this purpose, the motor is equipped with a centrifugal governor which is mounted to the side of the motor on the valve box side.

The governor mechanism consists of a hollow shaft 1 (Fig. 99) which is mounted on two ball bearings and is connected via a pinion 2 with the engine

camshaft. Rockers 3 with springs 4 are mounted on the governor shaft. The clutch 5 for the magneto drive 6 is mounted on the back end of the shaft. The follower 7 is located inside the hollow shaft.

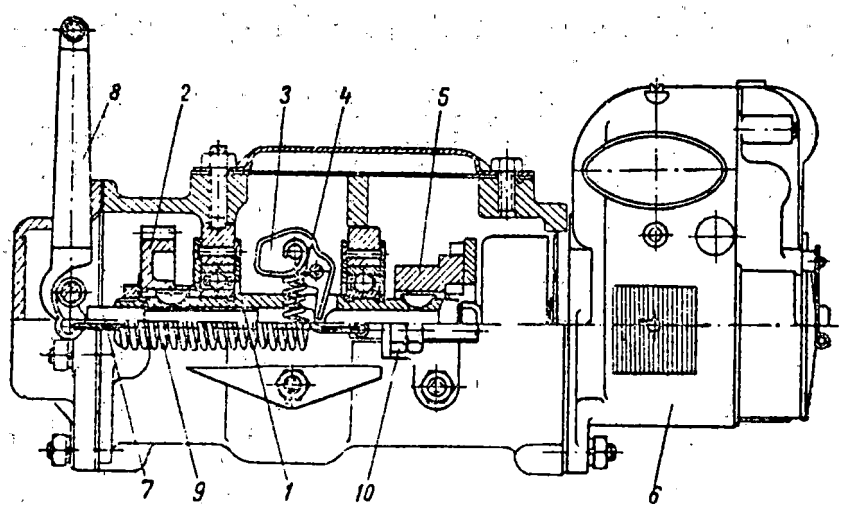

Fig. 99 Centrifugal governor mechanism.

When the speed of the motor is increased, the rockers separate under centrifugal force and displace the follower, which transfers the motion to the lever 8. This lever is connected to the carburetor choke by a solid tie rod, and it partially closes the choke. Partial closing of the choke reduces the quantity of the mixture entering the cylinder, and the speed of the motor falls off. When the speed decreases, the regulator parts are displaced in the opposite direction under the influence of the springs, which leads to an increase in the amount the choke is open, and, consequently, to an increase in the number of revolutions of the motor.

At rated power, the motor makes 300 rpm and consumes about 1.5 kg. of gasoline per hour. In practice, under conditions in the flaw detector car, the assembly does not always work at full power. In this case, the gasoline consumption is significantly reduced. When the power of the assembly is not

fully utilized for a long period of time, for example, in the summer, the speed of the motor diminishes somewhat. This happens due to a change in the tension of the speed regulator spring 9. The tension on the spring is regulated by means of nuts 10.

Under the conditions in which the motor is used in the flaw detector car, the need to wash out the air filter arises fairly frequently. This filter for removing the dust from the air gets dirty, especially when the assembly is used for exposing movie film when the car is in motion. Cleaning is done on an average of every 10-20 hr. of motor running time under such conditions.

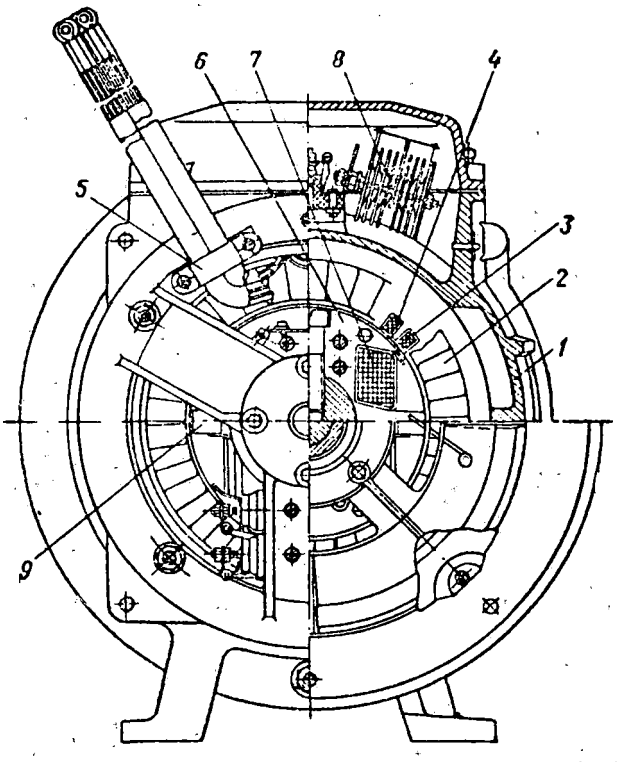

Fig. 100 The generator.

All other parts of the motor (the oil filter, the pump, the ignition system, etc.) are subjected to periodic inspection and preventive maintainance in accordance with the usage instructions which are included with each assembly by the supplying plant.

The instructions also set out rules for starting and stopping the motor and rules for servicing the assembly as a whole.

The generator.

The generator (Fig. 100) consists of a stator, a rotor, and a connecting box, with which the rotor is connected to the motor crank shaft. The stator is a cylindrical body 1 made of an alluminum alloy. Packets of electrical steel 2 are packaged inside the body. The packets have slots into which the generator's power winding 3 and secondary winding 4 are inserted. The beginnings and the ends of these windings are led out of the stator and affixed with bracket 5.

The rotor is fitted with two distinct poles 6 and has a field winding 7. The beginning and the end of the field winding are soldered to contact rings which are mounted on the rotor shaft on the end opposite the connecting box. The field winding gets power from the secondary generator winding via the selenium rectifier 8. Thus the rotor is an inductor. It creates a constant magnetic field which, in rotation, induces the necessary emf in the stator windings. For the initial excitement of the emf (for the generator's self-excitation) two permanent magnets are mounted on the transverse axis of the rotor.

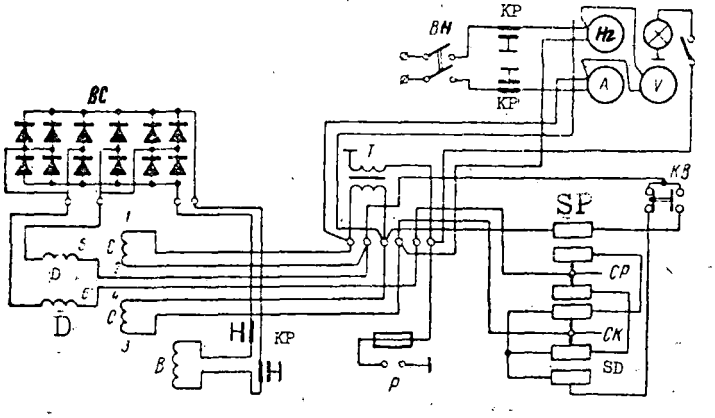

Fig. 101 The AB-02/230 assembly wiring diagram.

The generator is mounted on the same frame as the motor, and together they form a single block which is located in the metal box under the car.

The electrical diagram.

The diagram of the unit (Fig. 101) has three circuits. One of them consists of the generator power winding C, which is fitted in two sections, a regulating resistance CK and a supplimentary resistance SD. These resistances are included between the sections of the winding, between outputs 2 and 3. The voltage of the power winding is fed to the output terminals through ammeter A, a load switch BH and duct capacitors KP, which are installed to suppress static interference. A voltmeter V, which controls the voltage in the power winding, and a frequency meter Hz, connected to one of the sections of the winding (to the terminals of leads 3 and 4), are included in this circuit.

The second circuit is for the lighting. It contains a step-down transformer T, which is connected to the lead terminals of the power winding (leads 1 and 4). From the secondary winding of this transformer, a voltage of 12.5 v. is fed across the switch to the light bulb on the instrument panel and to plug P, where, when necessary, a portable lamp may be plugged in.

The third circuit consists of the generator field windings B, the selenium rectifier BC, the secondary winding D and adjusting resistances. The secondary generator winding is fitted in the same manner as the power winding, as a matched, two-section unit which diminishes static interference. After rectification by the selenium rectifiers, the voltage from this winding is supplied to the contact rings of the rotor for supplying power to the field windings.

Resistance CP, connected in series with the adjusting resistances CK and SD is included with the aim of regulating the field current between the sections of the secondary winding (between output 5 and 6). Such a circuit for

connecting resistances permits the required voltage level to be established on the output terminals of the unit, and assures that this level is automatically maintaining when working with a changing load. This effect is obtained in the following manner.

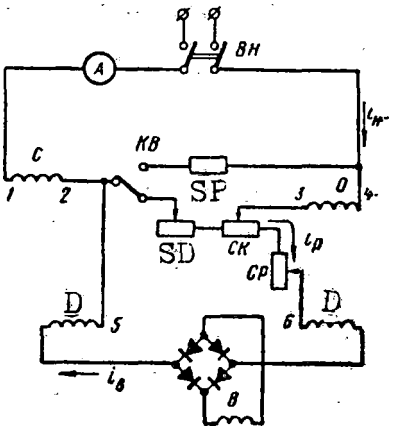

Fig. 102 Circuit diagram of the generator windings.

The voltage on the output terminals of the power winding depends, as is known, on the magnitude of the field current. If the generator is running with no load, this current is determined by the emf of the secondary winding and by the over-all resistance of the entire field circuit. The resistance of this circuit may be changed by moving the contact blade of the adjusting resistance CP, as well as that of CK and SD. However, resistances CK and SD are part of the power winding circuit and fulfill the role of potentiometers (Fig. 102). When the load is switched onto the generator, the part of the working current $\underline{i_w}$ in the power winding will branch off into the field circuit and combine (geometrically) with the initial current $\underline{i_B}$. The greater the load on the generator, the greater the current in the field circuit will be, because of that part of the working current which branches off into this circuit. Increasing the field current leads to an increase in the emf of the power winding. The emf also increases in the secondary winding, which leads to an

increase in the field current at the expense of the i_B component. Thus, the voltage level on the power winding terminals is automatically maintained constant. With the correct adjustment of the resistances, the voltage deviation from the established value will not exceed $\pm 4\%$ when changing from zero to rated load.

While in use, a slow voltage change is sometimes observed as the generator heats up or cools off, especially in the wintertime. In this case, the necessary voltage level is established by moving the contact blade of resistance CP when necessary.

A power winding switching was anticipated to insure reliable generator self-excitation. The switching is accomplished after the motor has started by pressing the excitation button KB. When this button is pressed, one half of the power winding is switched into the field circuit through a limiting resistor SP. After excitation, the button is released and the generator switches onto the load.

All adjusting resistances, the excitation button, the lighting transformer and the plug for the portable lamp are mounted on a separate block which is fastened to the generator housing. The instrument block, together with load switch BH and a lamp are mounted in the car control room, where the work of the assembly is monitored.

The unit is a source of current with dangerous voltage (220-230 v.). Therefore, servicing is conducted with strict observation of rules for safety which have been established for working with electrical equipment.

6. The recording apparatus.

Amplifiers.

Both amplifiers are mounted on the same chassis and form an amplifier unit, which is mounted in the control panel in the car control compartment.

The amplifier should amplify signals (electromotive forces) entering from the probes without distortion. Undistorted amplification should be in the range of 30-1000 Hz.

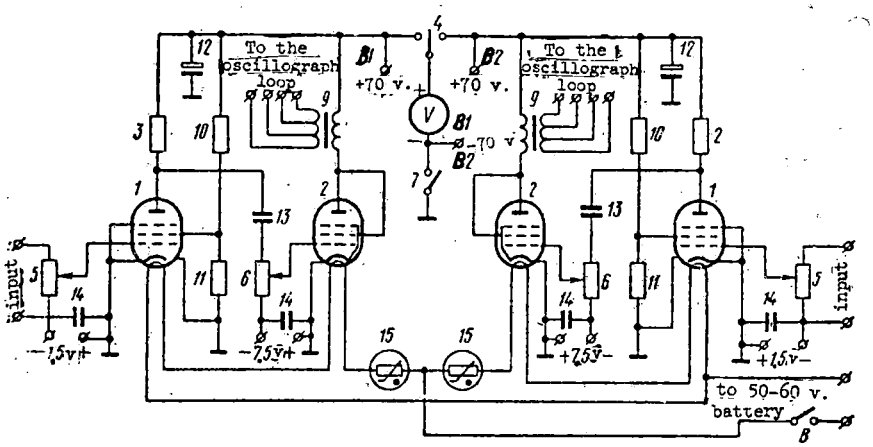

Fig. 103 Block diagram of the flaw detector car amplifiers.

The block diagram for the amplifiers is shown in Fig. 103, and a description of their parts is presented in Table 6. The first stage of each amplifier works on a 6Zh8 tube with resistance 3 as the plate load, and the second stage works on a 30P1S tube. Power supply for the tube filaments comes from the car's 50 v. d.c. circuit. Ballast resistors 15 are included in the filament circuit to stabilize the power supply mode. To assure the stability of the amplifier work mode, the anode power supply is also individually provided to each amplifier from separate BAS-70 batteries. The consumption of these batteries is insignificant, and their service life is from 300-350 hours.

Separate 1.5 and 7.5 v. batteries are also used to supply the bias voltage to the circuits of the first and second tubes of each amplifier. Such separate power supply eliminates the harmful influence of one amplifier on the functioning of another.

To test the voltage of the B batteries in the system, an M4-2 voltmeter with a scale to 150 v. was anticipated. By switching button 4 to the left or

right, the voltage on the anode battery is measured with respect to the right or left amplifier. The voltmeter and the handle of the switch button are mounted on the control panel of the amplifier block.

Table 6

Designation on the schematic in Fig. 103	Nomenclature	Type and description of the part
1	Radio tube	6Zh8
2	Radio tube	30P1S
3	Resistance	VS-0.25; 300 kohm
4	Voltmeter switch	-
5	Variable resistor	SP-0.5; 47,000 ohm
6	Variable resistor	SP-0.5; 1 Mohm
7,8	Tumbler switch	-
9	Transformer	
	I winding	10,000 turns, PEL-0.1
	II winding	240 turns, PEL-0.29
10	Resistance	VS-0.25; 15 Kohm
11	Resistance	VS-0.25; 10 Kohm
12	Electrolytic capacitor	KE; 10 μf; 150 v.
13	Separation capacitor	KBG/ 0.03 μf; 200 v.
14	Capacitor	KBG; 0.5 μf; 200 v.
15	Ballast resistor	0.3B-17-35

Two potentiometers 5 and 6 were fitted to regulate the amplification in the system. The handles of these potentiometers emerge on the control panel of the amplifier block (Fig. 104).

Potentiometer 5 on the amplifier input permits coarse adjustment, and, in practice, is used only in the initial tuning. The more exact adjustment of the working mode is done using potentiometer 6 in the control grid circuit of the second stage. The amplification is regulated depending on the speed of the car and is based on the magnitude of the emf pulse representations on the oscillograph screen.

The output transformer 9 has several leads from the secondary winding which correspond to the characteristics of various vibrators.

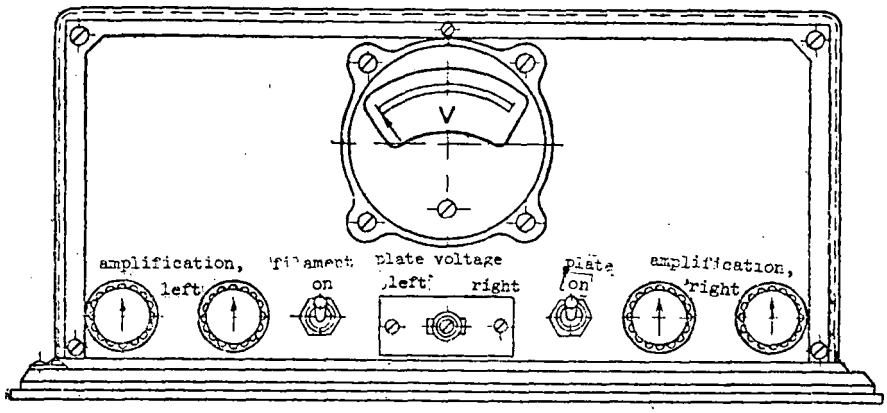

Fig. 104 Control panel of the amplification block

Vibrators.

The oscillographs are equipped with M0V2 or N135 dynamic vibrators. A vibrator of this type (Fig. 105) is a permanent magnet 1 in the shape of a half-cylinder, with a small mirror 4 in the middle of a wire loop 3 which is stretched across prisms 2 and passes through the magnet's field. A ray from a light source situated inside the oscillograph falls on the mirror. If an electric current passes along the loop, the loop will turn through a difinite angle to one or the other side, depending on the direction of the current in the loop, (as a result of the interaction of the current with the magnetic field.) The angle of rotation increases with an increase in the current. Thus, when an electric current passes through the vibrator loop, the mirror rotates at a given angle proportional to the current, and deflects the ray of light falling on it. If alternating current is passed through the loop, its deflection angle will change every half period, and, when the time constant of the loop with the mirror is small, it will oscillate with a frequency equal to the frequency of the alternating current. The vibrator magnet is prepared from a Magnico alloy and placed in a plastic housing together with the loop and mirror. The housing is then filled with a special liquid.

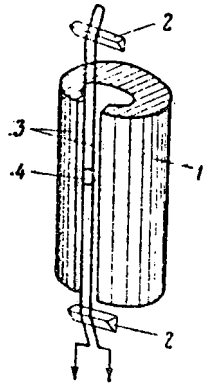

Fig. 105 The dynamic vibrator

The ability of the vibrator to reproduce electrical oscillations is determined by its sensitivity to current and by its own free vibration frequency. By vibrator sensitivity to current we mean the size of the angle of rotation of the mirror as the current in the loop increases by one milliamp. Because the angle of rotation for the mirror is extremely small, a linear magnitude, the deviation of the ray of light reflected from the mirror onto the film or the oscillograph screen, is considered instead (measured in mm). Its free vibration frequency characterizes the ability of the vibrator to reproduce electrical oscillations of a given frequency without distortion.

A graph showing the degree of amplitude distortion for electrical sinusoidal oscillations reproduced by the vibrators, depending on the frequency of these oscillations, is called the vibrator frequency characteristic. The frequency characteristic at a given sensitivity gives a complete idea of the capabilities of the vibrator, i.e. its ability to register one process or another.

Electrical oscillations with a frequency many times smaller than the free

vibration frequency of the vibrator are reproduced without distortion for practical purposes. However, when recording complex non-sinusoidal oscillations, including, for example, the emf in the flaw detector car sensors, certain distortions of the amplitude of higher order components are permitted. That maximum frequency at which the distortions reach the acceptable limit determine the working frequency range of the given vibrator. For MOV2 vibrators, the limit of the working range corresponds to approximately one third of its free vibration frequency range in air.

The basic vibrator characteristics are presented in Table 7.

Table 7

Vibrator	Working frequency band, Hz	Sensitivity, mm/mamp		Resistance, ohm	Maximum permissible current amplitude, mamp
		on the film	on the screen		
MOV2-I	1500	0.25	1.0	1	100
MOV2-II	3000	0.5	0.2	1	150
MOV2-IV	900	1.0	4.0	5.0	25
MOV2-V	500	3.5	14.0	5.0	10
MOV2-VIII	300	13.0	52.0	9	2
N135-0.6	600	11-13	44-52	9	2
M135-0.9	900	6-9	24-36	9	5
N135-1.5	1500	2-6	8-24	9	10
N135-2	2000	0.5	2	4	50
N135-3	3000	0.25	1	4	100

The MOV2 vibrators are the most suitable for working with the flaw detector car's amplifiers. The Type IV and Type V vibrators, for which leads from the secondary winding of each output transformer are provided, are also used.

M135 vibrators, the sensitivity of which should be not less than 4 mm/mamp, or the MOV2 Type V and VIII vibrators (close to them in their characteristics) are used when working without an amplifier.

Oscillographs.

Two universal eight-loop oscillographs, the MPO-2 or the N102, are used

in the flaw detector car. They are mounted on the control panel and work successively. In addition to the replacable vibrators (loops), there is an optical system and a device for photographing and making visual observations of the electrical oscillations in each oscillograph.

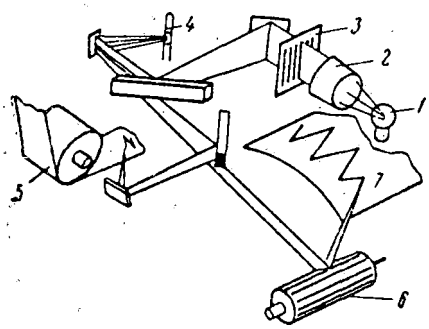

Fig. 106 Optical system of the oscillograph

A 7.5 w. electric bulb 1 (SG-2) with a concentrated (point) filament, situated at the focus of a converging lens 2, which is mounted in the illumination chamber of the oscillograph, serves as a light source in the oscillograph's optical system (Fig. 106). A ray of light from the bulb falls on the vibrator mirror 4 through a diaphragm 3 and the optical system. Reflecting off of the mirror, the ray passes through a series of lenses and falls simultaneously on the movie film 5 passing through the oscillograph and on the drum mirror 6. From here, it falls on the glass screen for visual observation. The image on the screen is magnified to four times that of the image on the movie film for better observation.

The film may pass through the oscillograph with a speed of from 1 to 5000 mm/sec, which is set by switching levers in the film drive mechanism's gear-box. The film drive mechanism's gear box is set in motion by an electric motor with an electromagnetic clutch which is turned on separately from the motor.

Asynchronic a.c. motors with a power of 30 w. and a rating of 2850 rpm are used in the oscillographs.

The speed at which the movie film moves through the oscillograph in the flaw detector car is set at 50 mm/sec. However, while in operation, it may vary within certain limits because of increases or decreases in the current passing from the APN-10 converter. With this in mind, a selector switch, with which the current in the converter's field winding circuits is changed, is mounted on the control panel. In this way, it is possible to preserve approximately the same registering scale on the film at flaw detector car speeds of 40-70 km/hr.

A simplified electrical schematic of the MPO-2 oscillograph is shown in Fig. 107. A voltmeter 2, from the reading of which the power supply voltage is established between 6 and 6.5 v. with the rheostat 3, serves to monitor the power supply voltage of the illuminating bulb 1. The electromagnetic clutch 5 of the film drive mechanism is supplied with direct current from the selenium rectifiers 4. An electric bulb, which is wired in series with the clutch winding, signals that the clutch is switched on and, consequently, that the film is in motion. When the bulb is at full incandescence, the rated current is established in the clutch winding. This bulb is a start rheostat. The resistance in the bulb increases according to the degree of incandescence of the filament, and the current in the clutch winding decreases. Switching the film drive mechanism on and off is accomplished with the aid of switch button 7 or by closing or opening the plug-type jacks 8.

A detailed description of the lay-out of the oscillograph's components and rules for maintaining and repairing them are set out in the manual which is included with each oscillograph by the supplier.

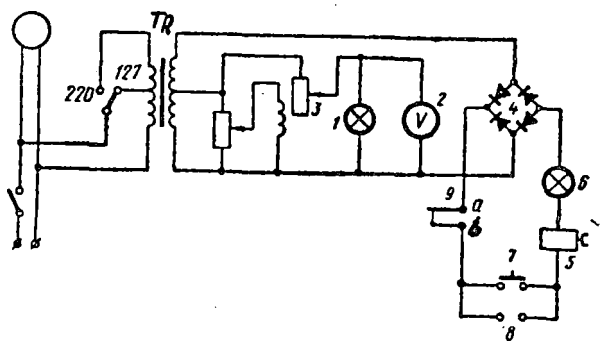

Fig. 107 Electrical diagram of the oscillograph

When they are mounted on the control panel, the oscillographs undergo a reworking, consisting of the removal of the automatic switch 9 which is included in the electromagnetic clutch power supply circuit. This switch, connected with the driving cylinder of the film drive mechanism, disconnects the electromagnetic clutch circuit after five meters of movie film have passed through the oscillograph. For working in the flaw detector car, where an average of 4.5 m. of film is expended for each kilometer of tested track, this switch is not necessary. It is either removed from the oscillograph or is disconnected by shorting out the wires leading to contacts a and b. Additionally, the cassettes which are provided with the oscillograph by the supplier have a small capacity. They contain only about five meters of film in all. Therefore, new cassettes with a capacity of 100-300 m. are prepared for working in the flaw detector car.

The film is fed from the supply cassette to the take-up cassette using

the oscillograph tape drive mechanism, and it is rewound onto the take-up cassette with the aid of an auxiliary electric motor which is mounted on the control panel. Through a reducing gear, this electric motor sets in rotation a wide pulley, from which rotation is transmitted to the reel of the take-up cassette by means of a belt drive system. Instead of a belt, a thin cotton rope is usually used. The rope is tightened just enough to permit it to slip on the pulley when film ceases to be fed into the take-up cassette. Such slippage is necessary since, given a constant film feed-in speed, the rotation of the cassette take-up reel should gradually diminish so that the film does not wind too tightly and so that it does not pile up without being wound onto the reel in the take-up cassette.

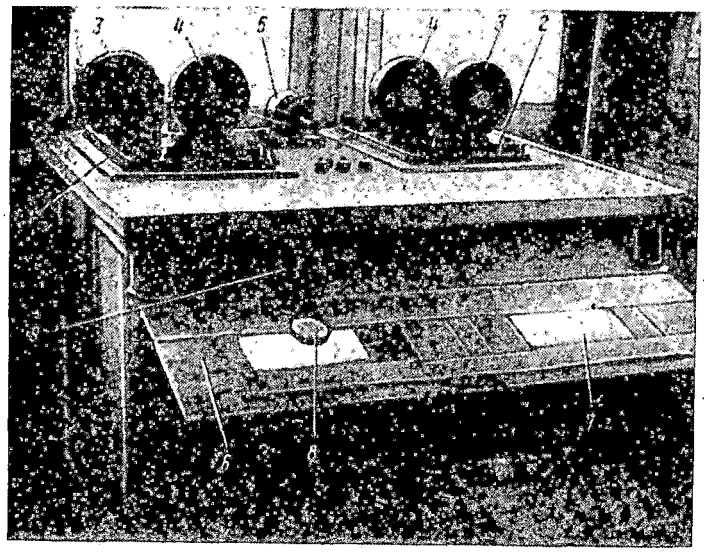

Fig. 108 The control panel (without the amplifier unit).

Since the electric motors in the oscillographs were not designed for lengthy running periods, the two oscillographs in the flaw detector car should work in succession without excessive over-heating. Over-heating may cause flaws in the optical system and damage to the vibrators (cracks may form in

the housing or the air-tight seal may be destroyed at excessive temperatures).

The control panel.

An over-all view of the control panel with the two mounted oscillographs 1 and 2, in which cassettes 3 and 4 have been inserted, is shown in Fig. 108. The electric motor 5 for winding the film on the take-up cassette is mounted between the oscillographs. Inside the control panel table are batteries supplying power to the amplifiers and electrical installation wiring. Spare batteries, portable measuring devices, etc. are also stored there. A collapsible table 6 with two windows 7 serves for interpreting the recordings on the film. The film is viewed above these windows using a magnifying glass 8. Translucent glass panes are installed in the windows 7; while interpreting the film, they are illuminated from below by electric light bulbs.

Magnifying glasses 10-15 cm. in diameter with a focal length of 20-25 cm. are used for interpreting the film. The magnigying glasses are attached to a support 9 at the distance at which the best visability is obtained. Two workers interpret the film at the same time. Good illumination of the film through the viewing windows, adequate magnification, a comfortabe position at the table for the interpreter, the absence of interfering light sources and other distracting factors are all necessary when interpreting the film. Maintaining these conditions has great significance since examination of a large quantity of film may lead to rapid vision fatigue, which shows up negatively in the quality of the interpretation. When examining film in the daytime, the windows in the control section of the car are covered with dark curtains. The windows of this section are also curtained over when working with the oscillographs in the daytime, when daylight hinders observation of the image on the screen of either oscillograph, especially on bright, sunny days.

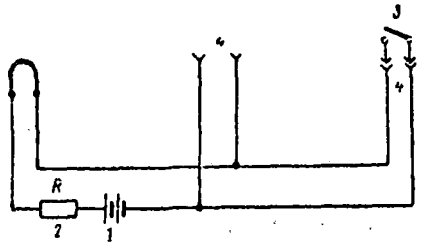

Fig. 109 Kilometer marker circuit

The kilometer marker serves to register the kilometer signpost on the film. A third vibrator of any type, which is connected to a circuit consisting of a battery 1, a limiting resistor 2 and a telegraph key 3 (Fig. 109) is used as a marker. The key is attached to the terminal of the observation window on that side of the car on which the kilometer markings are situated along the track.

The observer, sitting at the observation window, keeps track of the kilometer sign posts and, by closing the marker circuit with the key, makes a notation on the film. Closing the key takes place at the moment when the observation window comes even with the kilometer sign. After this, the kilometer number is registered on the film using Morse code.

The following abbreviated code has been worked out by experience for registering the digits:

1	.-	6	-....
2	..-	7	-...
3	...-	8	-..
4	....-	9	-.
5	.....	0	-

Good results have also been attained from the use of a telephone dial. The telephone dial is hooked up instead of the telegraph key, the kilometer number being dialed out directly. The kilometer sign position is fixed by the

digit 1, i.e. when the car approaches the kilometer sign, a 1 is dialed, and at the moment when the flaw detector comes even with the post, the dial is released. Then the kilometer number is dialed in the usual manner. Here, each digit is shown by the corresponding number of dashes of equal length.

At the start of work on a section, the kilometer number is registered in full, then, for all subsequent kilometer signs, only the last two or three changing digits are recorded.

The marker vibrator for registering the kilometer number on the film is mounted in the oscillograph so that the light spot from it does not strike the film when the key is open and appears close to the edge of the film, by the perforation, when the key is pressed. The accuracy of the kilometer sign position marking on the film is very important for subsequent processing of the film since the count of the individual rail lengths is made from the kilometer sign. In case an error is made in the notation, it would be difficult to orient oneself on the line when searching out the defective rails noted by the car. In order to eliminate errors in the numeration of the rail lengths, metallic checking devices are installed on the first length of each kilometer in all track sections where flaw detector cars are working.

An ordinary base plate, which leans against the rail in the upper fillet, and with the other edge on a cross tie, is used as the checking device. This checking device is then spiked down.

The checking device is noted on the flaw detector oscillogram by a characteristic signal which permits the correct count of the rail lengths for each kilometer.

Dry cells, which are housed inside the control panel with the amplifier batteries, are used in the kilometer marker circuit; the limiting resistances are also mounted there.

The size of the limiting resistor 2 depends on the vibrator type and the battery voltage. Computation of the resistor size is made by the formula

$$R = \frac{U}{0.7\ Y},$$

where U is the battery voltage, in volts, and

Y is the maximum amplitude of the current, in amps, for the selected vibrator.

The 0.7 coefficient is established to limit the current to be 30-35 % less than the maximum acceptable for the given vibrator (the resistance of the vibrator filament is not taken into consideration).

7. The Developing Machines.

Small 60P-1, 60P-3 or 60P-4 developing machines are used in the flaw detector cars.

The 60P-1 machine is intended for processing 35-mm movie film, and consists of the following basic parts: a loading device, a photochemical film processing section, a dryer, and a drive mechanism with signaling devices. All the work of developing, fixing, and washing the film takes place in total darkness within the machine, with full illumination in the car itself.

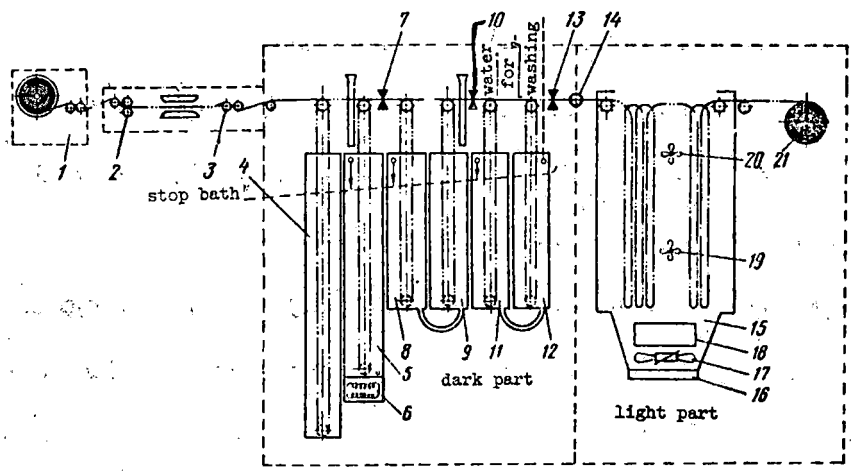

Fig. 110 The developing machine diagram.

The film follows a multi-loop path in the machine. From the supply

cassette 1 (Fig. 110), the film is transported through a blocking mechanism 2 and a light labyrinth at gate 3 into the loading magazine 4, which is situated in the dark section of the machine that is shut off by light-proof doors. From the loading magazine, the film enters into the developing tank 5, under which an electric heater 6 is mounted for heating the developer. From the developing tank, the film passes through a rubber squeege 7, which removes the moisture from its surface, and enters into tanks 8 and 9 with the fixer. The film then passes through squeege 10 into tanks 11 and 12 with water for washing. After the tanks with water, the film passes through squeege 13 and a light labyrinth 14, and passes into the dryer 15, where it also follows a multi-loop path. Air is sent through the dryer from below at a certain pressure by a fan 17. The air first passes through a filter 16 and an electric heater 18. With the aid of small fans 19 and 20, the air is blown about in the dryer and comes out through an opening in the top. The dried film then goes to the take-up cassette 21, from where it is taken off for interpretation as the cassette fills up.

Transport of the film in the machine is achieved by sprockets moving the film over smooth, driven rollers. The sprockets are distributed one to a section on the upper bar of the loading machanism of each tank and of the dryer, and are set in rotation at a specific speed by an electric traction motor through a reducing drive. The reducing drive permits the output of the machine to be regulated by means of a switch to 185, 93 or 47 m/hr. When necessary, a lower output, equal to 23 m/hr, may also be obtained. For this, the possibility of changing the gear ratio of the reducing drive by hand was anticipated in designing the drive system.

Depending on output, the time the film stays in each section of the machine for each operation will also change.

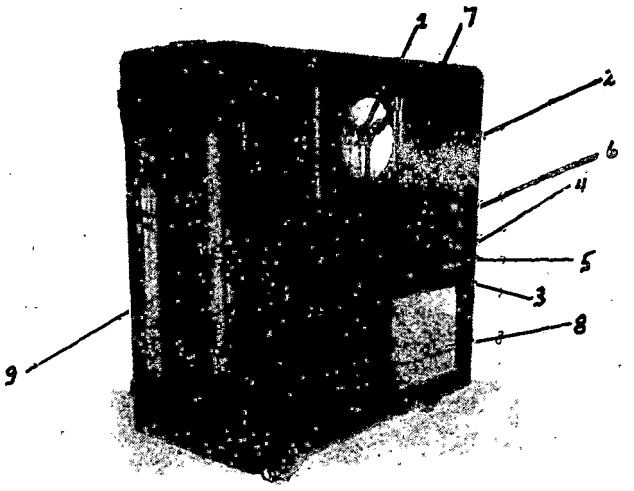

Fig. 111 General view of the developing machine.

1. take-up cassette, where the developed and dried film is wound
2. control panel
3. opening for the hand drying system
4. nozzle for water fed into the washing tanks
5. nozzle for emptying the used solutions (the pipe through which the used solutions are discharged under the car is hooked to this nozzle)
6. jack plug for hooking up the electric power
7. counter showing the amount of film which has passed through the machine
8. air filter
9. dryer

With the full number of loops, the length of stay for the film in each of the sections is shown in Table 8. The amount of film which each section of the machine may contain is indicated in meters. The general view of the 60P-1 is shown in Fig. 111.

The 60P-3 and 60P-4 machines do not differ from the 60P-1 machine in the principles of their mechanisms, outside dimensions, or productivity. They are improved versions intended for processing two types of film, 16- and 35-mm. As distinct from the 60P-1, they are equipped with an auxillary fan to blow the solution residue from the film as it moves from one tank to another.

Table 8

Time the film is ...., min.	Productivity of the machine, m/hr			Quantity of film, m
	185	93	47	
in the loading magazine	2.6	5.2	10.0	8
in the developer	2.3	4.5	9	7
in the fixer	3.4	6.6	13.5	10.6
in the wash	3.4	6.6	13.5	10.6
in the dryer	10.2	20.4	41.0	32

Under the conditions in the flaw detector car, the output of the developing machine is determined primarily by the temperature and the humidity of the air entering the dryer. At high humidity and an air temperature lower than 20° C, the output diminishes since the film will not dry successfully during the time it is in the dryer. Therefore to speed up the drying process, the filter covering the entrance to the ventilation channel is removed when the machine is mounted in the car. Instead of a filter, the channel is closed off with a fine metal screen or with common gauze stretched over a frame. This prevents pieces of film, paper, etc, which may be sucked up by the fan and cause the film in the machine to catch fire, from entering into the air channel.

Removing the filter leads to a higher speed for the air current in the dryer, which significantly shortens the drying time for the film in spite of the fact that in the flaw detector car, the electric air heating is somewhat inadequate.

The electric air heating is accomplished in each machine by a coil of Nichrome wire. The factory schematic for connecting the coils is designed for an a.c. power supply of 220 v. The coils are switched on using packet rotary switches 1, 2, and 3 (Fig. 112) mounted on the developing machine's control

panel. The circuit for connecting the coils is redone for working in the flaw detector car in accordance with the power supplied from the car's power plant. When it is reworked to accommodate a 50 v. power supply (cf. Fig. 112), the first section uses 0.3 kw, the second 0.6 kw, and the third, 0.9 kw, the combined power being 1.8 kw. Usually only one or two sections are redone. The schematic for connecting the coils in the other sections are preserved for 220 v. power supplied from an external circuit or from a gasoline powered electrical unit. The 50 v. voltage for the heater is supplied separately. To avoid burning out the coils, they are switched on only after the fan is switched on. For this purpose, the voltage on the packet rotary switches 1, 2, and 3 passes through packet rotary switch 4, which operates the fan.

The power supply for the fan which feeds air into the dryer of the 60P-1, and for the fans which are located inside the dryer is single phase alternating current. The electric traction motor of the developing machine is supplied with three-phase, 220-volt alternating current. The over-all power requirement is about 300 w. In the 60P-3 developing machine, there are three three-phase motors with an over-all power of 400 w. The three-phase current is created by conversion of the d.c. from the car power plant with the aid of an APN-10 or a PND-5 converter and a transformer which steps up the alternating current voltage to 220 v. A diagram of the mechanism for supplying the developing machine with three-phase current is presented in Fig. 113. In this diagram, the third phase is created by connecting a capacitor bank C with an over-all rating of 10-18 microfarad to the secondary windings of transformer 4. The rating is set for the capacitors by matching it with the voltage which is measured by the voltmeter between terminals 1, 2, and 3 with the load switched on, i.e. when the fans and the traction motor are operating. With a correctly matched rating for C, the voltage between terminals 1-2, 1-3, and 2-3 should be the same.

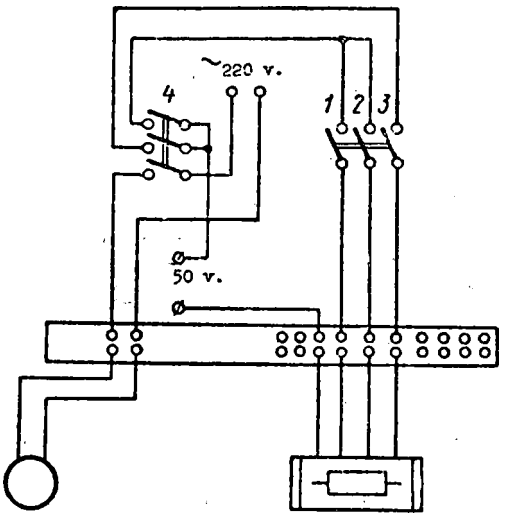

Fig. 112 Diagram of the developing machine's electric heater for 50 v. power supply.

The transformer and the capacitor banks are located below the flaw detector switchboard in the car control compartment. Wires from terminals 1, 2, and 3 are connected to the plug of the developing machine, and the necessary changes are made in the machine so that, aside from the three-phase electric motors, no other load is connected to the third phase (terminal 3).

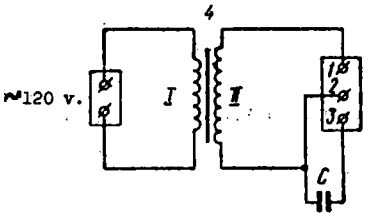

Fig. 113 Diagram of the converter which converts single phase current into three phase.

The voltage from the eternal electrical circuit and the gasoline driven units (through the requisite switches) is also fed to transformer terminals 1

and 2. The primary transformer winding is disconnected from the converter beforehand when working from these sources.

The 60P-1 and the 60P-3 and 60P-4 developing machines are equipped with interlocking devides which give off a sound signal for 1.5-2 min. before the film runs out in the supply cassette and, at the moment when the film in the cassette does run out, the machine stops automatically. The supply cassette holds 300 m. of film.

When the end-of-film signal is received, the machine is usually reloaded, i.e. the supply cassette is usually changed and another one with new film is mounted. Reloading takes place in the light without switching off the machine. During the reloading time, the film passes from the loading magazine into the tanks. The time which the machine can work with the store of film in the loading magazine is determined by the output of the machine. Thus, at highest output (185 m/hr), it may work from the loading magazine for 1.5 min; with lower output, this time is increased correspondingly to 3-6 minutes.

When the film processing is terminated, the machine is loaded with a leader (film without the emulsion), for which old film without the light-sensitive layer is used. The length of the leader is 70-75 m. When the machine started the next time, the film to be processed is joined to the leader, and passes through the entire film channel of the machine.

A detailed description of the machanisms of each developing machine and rules for servicing them are set out in the manual which is provided by the supplier with each machine. In this manual, norms for chemical consumption and the composition of the developer and fixer solutions are given.

For processing film on which the impulses have been recorded, it is necessary to use a rapid contrastive developer. A hyposulfite solution is used as a fixer.

The developer in the machine tank is not heated electrically since this involves a large expenditure of electrical energy. The developer is heated to 25° C. in the flaw detector car before being poured into the machine. Heating to a higher temperature is not recommended since the light-sensitive layer of the film might fuse.

Fresh developer and fixer are added every 200-300 m. of film when the machine is in operation. The solutions are introduced through a loading hopper in full light. Water for washing constantly enters the machine at a rate of 15-20 l/hr from the tanks mounted in the developing section of the car.

Wooden plates which float on the surface of the solutions are placed into the tanks to keep the lequids from splashing out when the car is jolted. The plates are prepared to the dimensions of the tank, with slots cut out to allow passage of the film.

Under the conditions in the flaw detector car, the complete consumption of chemicals in the solutions (without additions) is relatively slow. Up to 1800 m. of film may be processed in one developing solution, whereas the fixer solution requires changing after processing 1300 m. Taking into consideration that in many instances, reducing the time for processing film is important, the consumption of chemicals in the machine increases somewhat.

A movie-type film with a sensitivity of not less than 45 units is used as the film for the flaw detector car. All of the rules for fire safety must be observed when working with film in the car. Smoking, striking matches and any other work with open flame is prohibited in the room in which the film is stored or where people work with it. Storing film in tables, cupboards, stands, etc., is catagorically forbidden. Trimmings, pieces of fogged and other used film should be collected in a metal box and destroyed. The film supply, as well as the exposed film is stored in special metal boxes or in fire-proof

film safes in the compartment of the car where the developing machine is installed. The walls and floor of this section are covered with a layer of iron over asbestos.

Only the working quantity of film calculated for checking the track along a given route should be kept in the flaw detector car. Storage of a greater quantity of film for relatively lengthy periods takes place in specially equipped storage facilities where the flaw detector car is permanently assigned.

8. The work of the flaw detector car on the line.

The work of the flaw detector car, i.e. checking the rails, begins after a careful adjustment of its instruments. Adjustment takes place in a definite sequence. At first, the vibrators are tuned. They are mounted in the oscillograph so that a record of both rail lines is made symmetrical to the perforations. The vibrators are successively mounted, first in one oscillograph and then in the other. The amplifier output should be connected to the sensor coils and the output to the vibrators. The amplifiers are turned on when the vibrators are being mounted.

The illumination and the motor of the oscillograph are turned on to adjust the vibrators. The filament of the illuminating bulb is brought up to normal working voltage of 6 - 6.5 v. according to the oscillograph volt meter, and the diaphragm is set at 2 or 2.5. After this, the vibrators are placed in the position at which the light reflected by them (the "spot") is seen on the screen using regulating knobs on the oscillograph panel.

When the vibrators are correctly installed and with no interference in the amplifier, two straight, bright lines, symmetrically distributed in the middle of the screen, should be visible when the motor is turned on. The upper line, looking at the screen from the side of the gear box, should refer to the vibrator connected to the amplifier for the right rail, based on the direction in which the car is moving (boiler room foreward).

The position of the kilometer marker-vibrator is established with the key closed, so that the bright line which corresponds to it is at the edge of the oscillograph screen above the line for the right rail. When the key is opened, the line on the screen from the marker should disappear upwards, without crossing the screen. If it goes down, crossing the screen, it is necessary to switch the ends of the wires leading to the vibrator terminals.

If wavy curves are seen on the screen instead of straight lines when the vibrators are installed, this signifies the presence of troubles which must be eliminated. Usually troubles of this type arise as a result of the brushes on the PAN-10 converter's commutator sparking from self-excitation of the amplifier or from a voltage pulsation in either the alternating or direct current circuits.

Installation of the vibrators takes place in the same order when working without an amplifier. Here, the sensor coil, which, as in the previous instance, should be mounted in a working position between the poles of the electromagnet, is connected to each vibrator. Whether the sensor coils are correctly connected to vibrators is tested by the deflection of the "spot" on the oscillograph screen when the electromagnet is switched on and off. When the electromagnet is switched on, the "spot" of the corresponding vibrator should be deflected upward, and when it is switched off, it deflects downward. If the opposite picture is observed, the wires from the sensor to the terminals of the given vibrator are switched. The current in the electromagnets is set at a minimum (with full resistance in the rheostats) for such tests.

The over-all resistance of each probe coil circuit is checked after the vibrators have been installed and before going out onto the track. When working without an amplifier, the resistance is checked at the oscillograph terminals with the vibrator turned off.

Further tuning of the equipment takes place when the car is in motion and with the electromagnets turned on. This adjustment consists of regulating the amplification and setting the working value of the magnetizing current in the electromagnet windings.

When the car is in motion, the emf in the probe coils is represented on the oscillograph screen in the form of two "running" curved lines consisting of separate pulses which are formed when the probes pass over base plates, joints coverplates and the clearances between the rails. The emf from the joint cover plates and from the clearances have a large amplitude which cover the entire width of the oscillograph screen. Pulses from the base plates are relatively small. Therefore, adjusting the flaw detector sensitivity to rail defects is conducted based on pulses from the base plates.

When working without an amplifier, the sensitivity is determined by the number of turns and by the resistance of the probe coil, by the vibrator characteristics, and by the speed of the flaw detector car. The relationship of these values is selected to be that at which the necessity of regulating the sensitivity falls off in the interval of working speeds for the car. When working with amplifiers, the sensitivity is established with the aid of amplifier controls. The amplitude of pulses from the base plates is established to be equal to approximate 8-12 mm. on the oscillograph screen.

When changing from one type of rail to another, the amplitude of pulses from the base plates changes. This change is connected with an increase in the distance the probe coil is from the base plate on the heavier type rails and with the change in the magnetic induction in the rails, as well as with the change in the ratio of the volume of the metal in the baseplate to the volume of the metal of the part of the rail lying on it. The pulse amplitud from the base plates decreases when changing to a heavier type rail. The

amplitudes of pulses from flaws may be considered to be independent of the rail type for practical purposes. Therefore, on light rails, the sensitivity is set so that the pulse amplitudes from the base plates are 4-5 mm greater on the screen than those from R-43 and heavier rails.

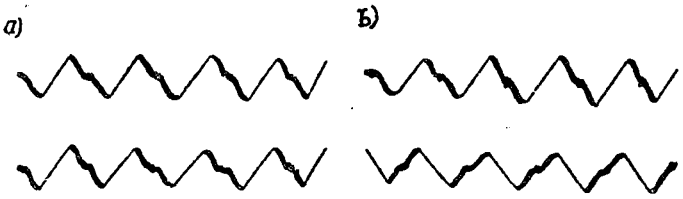

Fig. 114 Oscillograms of pulses from the baseplates.

Additionally, oscillograph adjustment is conducted according to the pulse phase. In this case, by "phase" we mean the sequence of the pulse image on the screen, i.e. the direction in which the light ray tracing the pulse moves. The phase of pulses from the base plates is established to be the same on the screen for both the left and the right rail, which has great significance for subsequent interpretation of the film. The shape of curves on the screen with the pulse phase set correctly and incorrectly is shown in Fig. 114 a and b, from which it may be seen that pulses from the base plates are symmetrical curves. Examining them from left to right, it may seem that each pulse begins to be traced by the light ray with a downward motion. The thinnest line of each pulse proceeds upward at an angle from left to right. To set the necessary impulse phase on the screen, it is necessary to interchange the terminals of the probe coils at the amplifier input. Therefore, each probe coil is connected to the amplifier input with a pronged plug, and the necessary phase is selected by reversing the plug.

Correct installation of the probe coils, which should be fixed in relation to the electromagnets, is important for normal working of the flaw detector. All air gaps from which the collecting shoe may be displaced in the trans-

verse direction are therefore eliminated from the mountings of the sensor collecting shoe. Additionally, the collecting shoe and its mountings are checked periodically at special stopping places. On sections where a rail break-down in accordance with flaw 21.2 is observed, the probe coil is mounted in the collecting shoe with a certain shift to the inside of the track. Usually the coil is shifted 15-20 mm to the inside of the track relative to the rail axis, thereby compensating for the probe displacement when the gauge widens in the sharply curved sections of the track.

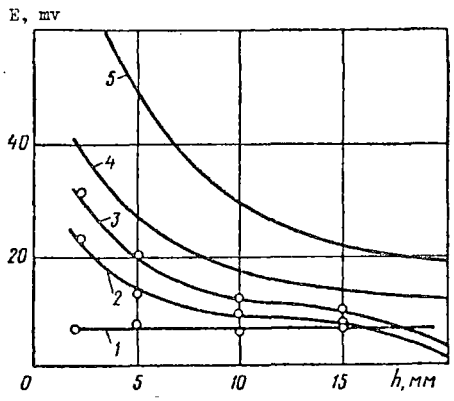

Fig. 115 Influence of the height the sensor is lifted on the magnitude of emf impulses from flaws and baseplates.

During operation, a layer of dirt and residual oil frequently builds up on the bottom of the collecting shoe and the probe coil is separated from the rail head, which leads to a decrease in the sensitivity of the flaw detector. When the axis of the probe is lifted 12-15 mm from the rail running surface (Fig. 115), hidden flaws 20.2 and 21.2 (curves 3, 2) will, for practical purposes, no longer be detected from the oscillogram, since pulses from them are almost equal in magnitude to pulses from the base plates (curve 1), while large flaws which open on to the surface (curves 4, 5) are recorded by pulses, the amplitude of which is 2-3 times less than that with the probe in normal

position. Therefore, it is necessary to clean the bottom of the collecting shoe carefully when it becomes dirty. On sectors where the rails are covered with a great deal of mud or dirt, cleaning takes place at specially designated stops.

A series of operational abnormalities also arises from the contacts on the segments of the probe under the car being dirty (especially when the block covers have not been mounted tightly enough). When the contacts are dirty, the resistance in the probe coil circuit increases, which influences the flaw detector sensitivity negatively when working without an amplifier. Therefore, the leads from the probes are, without fail, equipped with end pieces which are, along with the terminals, carefully cleaned when they are hooked up, and the terminal nuts are tightened snugly.

As is known, when the car is in motion with the electromagnets, significantly large eddy currents are excited in the rail. The penetration depth and the density of the eddy currents depend on the geometric dimensions (the distance between the poles) of the magnet, the magnitude of the magnetic field it creates, and the speed of the flaw detector car. The greater the electromagnet field, the greater will be the density of the eddy currents in the rail, other conditions being equal, and the better the flaws will be revealed.

EMF pulses are excited in the probes as a result of changes in the resultant magnetic field in the flaw zone. The resultant field is formed due to the compounding of the eddy currents' magnetic field and the primary electromagnet field. Shallow surface flaws in the rail metal) e.g. such as cavities on the head, quenching cracks, etc.) have little influence on the over-all picture of the distribution of eddy currents in the rail metal mass. At the same time, local dispersion fields are caused by the flaws being situated in a strongly magnetized layer of metal.

A dispersion field is frequently called a polarization field. The polarization field has a small length along the rail, and the emf pulse in the probe is therefore very short-lived when the flaw detector is in motion. It is depicted on the flaw detector oscillogram as a vertical line with a large positive section.

Over-all, the form of emf pulses caused by surface flaws differs significantly from the form of pulse caused by large, deeply hidden flaws in the rails. Such flaws not only form dispersion fluxes, but also cause significant changes in the eddy current fields. This fact is extremely important since it permits a judgement to be made concerning the nature of the defect in the rail based on the nature of the emf pulses.

The magnetizing current in the electromagnet windings is set to be the maximum possible, i.e. equal to 18-20 Amps (the magnetizing force is approximately 48,000 ampere-turns), with a clearance of no more than 12 mm between the rail and the electromagnet poles to insure the best possible detectability for the flaws.

9. Basic factors determining optimal working conditions of the flaw detector car apparatus.

The speed of the car, the magnetization of the rails, the location of the probe coils and the characteristics of the vibrators and amplifiers are included among the basic factors which determine the working conditions of the flaw detector car.

Speed of the Car.

The flaw detector car apparatus normally works at speeds of 30-70 km/hr. At speeds less than 30 km/hr, the sensitivity to internal hidden flaws in the rails drops off significantly, and the form of the signals from certain flaws changes.

As was shown above, the sensitivity to flaws is characterized, by the

magnitude of the emf in the probe coil, i.e. by the magnitude of the signal which pases from the probe to the input of the registering mechanism. Other conditions being equal, the magnitude of the signal (the amplitude of the pulse) depends on the speed of the flaw detector car. Graphs characterizing this dependence are shown in Fig. 116. When working with an amplifier, the pulse amplitude to be registered on the film may be changed within known limits by regulating the amplification.

However, in the given instance, in addition to sensitivity, the detectability of the flaws has great significance. By detectability we mean those distinguishing features of the signals caused by the defects, and due to which they may be separated from the over-all mass of pulses registered on the film.

The distinguishing features of signals caused by flaws are identifiable on the film only when they exceed in amplitude the pulses from the base plates. Therefore, the detectability of flaws is evaluated by the ratio of the signal amplitude E, to the amplitude of impulses from the base plates E_o, i.e. by the ratio E/E_o. The greater this ratio, the better the detectability.

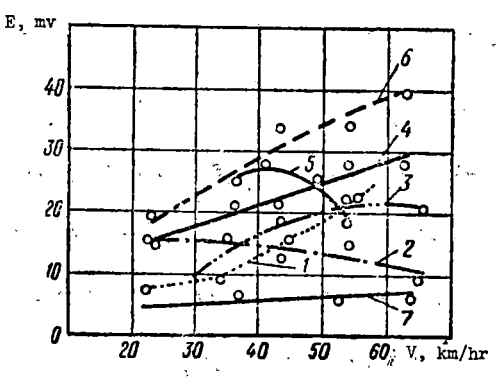

Fig. 116 Typical dependencies of the pulse amplitudes on the speed of the flaw detector car.

When the speed is increased, almost all signals from flaws grow (curves 3, 4, 6), whereas certain surface flaws are registered by pulses, the amplitude

of which increases with an increase in speed (curves 2, 5). Pulses from the baseplates (curve 7) increase much more slowly with an increase in speed than do pulses from the flaws. Therefore, the greater the speed, the better will be the detectability of the flaws. However, certain hidden 21.2 type flaws (curve 3) are registered by pulses, the amplitude of which reaches its greatest value at speeds of 55-65 km/hr. Therefore, within the interval of the flaw detector car's working speed, this speed is considered to be the best.

On the approaches to closed signals, stops, etc., when the speed drops down to 25 km/hr and less, internally hidden flaws in the rails are not detected from the oscillogram as a rule. In addition, at a speed of 25 km/hr the flaw detector apparatus automatically switches over to power supplied from the storage battery, which may be permitted only for a limited period. The length of sections covered at such speeds are reduced to a minimum when the flaw detector car is in operation.

Magnetization of the rail and the position of the sensor coil.

The magnitude of the emf grows with an increase in the magnetization of the rails. Magnetization is determined by the magnitude of the current in the electromagnet windings (by the number of amp-turns) and by the magnitude of the clearance between the rail and the poles. At a given current value of 20-18 amp, which is the maximum possible (with the rheostats fully open), the clearances between the rail and the poles are set at 8-12 mm. At such a current and with this clearance, the magnetization of the rail when the electromagnets are immobile (in a stationary state) reaches the saturation point. It is identical almost the entire length between the poles. The magnetic flux beyond the poles is 50% of the flux passing through the rail in the interpolar area.

When in motion, however, this picture of rail magnetization changes sharply. The pecularities of rail magnetizing by the rapidly moving field of an electromagnet were described in Chapter II. Fundamentally, they consist of the fact that surface layers of the metal magnetize to a greater degree than do the internal layers, and, in addition, that the magnetization of the internal layers lags in time, and the average cross-sectional magnetization (induction) becomes significantly less than that which was attained in a stationary position for the given number of amp-turns (cf. Fig. 35). Such a complex magnetizing process is explained by the action of the eddy currents.

The eddy currents are excited when the car is in motion due to the pulse excitation of the field on the rails being checked. Actually, the magnetizing field acts on each rail section for only a brief period. This may be traced using any one cross-section as an example. This section magnetizes at first in one direction with the approach of the electromagnet (cf. Fig. 83). Then as it passes under the first pole, where the direction of the magnetizing field sharply reverses in a very short time, it is remagnetized. Further, when it passes under the second pole, this section remagnetizes again, and after the electromagnet is removed, it preserves a residual magnetization. This process takes place in hundredths of seconds. At a speed of, for example, 70 km/hr, the time in which the chosen section passes from the first to the second pole is about 0.04 sec. Consequently, on a section passing the interpolar distance of the electromagnet, the magnetizing current excites in one direction for a few hundredths of a second. Inasmuch as the sensors are mounted between the electromagnet poles, it is precisely on this section that it is interesting to trace the magnetization process.

In the first instant, when the section remagnetizes under the first pole, a new, reverse direction of magnetization in the given section is observed

only in the surface layer of rail metal. A large eddy current density is observed in the same layer. As the section is moved toward the second pole of the electromagnet, the magnetization and the eddy currents penetrate into the inner layers of the metal.

The eddy currents create their own magnetic field (the reaction field), which is directed against the electromagnets' magnetizing field. By virtue of this, the eddy currents weaken the magnetization of the rails and hinder the instantaneous magnetizing of the internal layers. Distortion of the static picture of rail head magnetization (cf. Fig. 35) is thus explained.

Distortion of the static picture of rail head magnetization is already beginning at the start of the flaw **detector** car's motion, and at speeds of up to 20 km/hr, is accompanied by a rapid decrease in the mean value of the magnetic induction. Then the induction decrease takes place more slowly, and, at speeds of 40-70 km/hr, no substantial difference in the degree of the rail head magnetization is noticed for practical purposes.

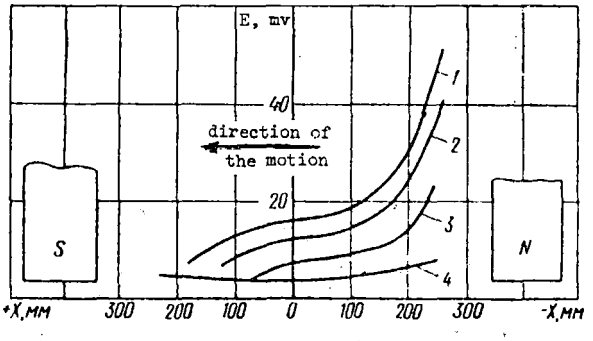

Fig. 117 Dependence of the signal magnitude on the position of the probe between the electromagnet poles.

Due to the unequal magnetizing of the rail head on the section between the electromagnet poles, sensitivity of the flaw detector to flaws is dependent upon the location of the probe coil in the space between the poles. Curves

characterizing this dependence are presented in Fig. 117.

As the sensor is placed nearer to the electromagnet pole to the rear, with regard to the direction of motion, signals from flaws (curves 1, 2, 3) increase, especially in the section with the x-coordinate equal to -200 mm and further toward the pole. At the same time, the magnitude of signals from the base plates grows insignificantly (curve 4). Hidden 21.2 type flaws which have small dimensions (curve 3) are noted by signals, the magnitude of which begins to exceed noticably the signals from the base plates only when the sensor is at a point x = -220 -- -230 mm. When the probe coil is moved nearer the rear coil, there appears a series of interference signals, i.e. signals not connected with the flaws, and which make interpretation of the oscillogram more difficult. Therefore, displacement of the probe in the direction of the rear pole a distance of 220 -- 230 mm from the mid-point of the interpolar distance is optimal. With the probe in this position, all types of flaws in the rail head are most advantageously detected.

This position for the probe corresponds to the position of greatest magnetization of the rail head (cf. Fig. 35). Experimental data show that in this area, which is located near the second electromagnet pole, the field and the eddy currents (Fig. 118) penetrate into the rail head to the maximum depth.

Characteristics of the vibrators and amplifiers.

The basic demand for registering emf pulses on film is to preserve the form of these pulses, i.e. to preserve those distinguishing features by which the pulses are identified when interpreting the oscillograms.

It is known from the theory of harmonic analysis that each single pulse contains an uninterrupted series of simple sinusoidal oscillations. The amplitudes and phases of these oscillations are determined by the shape of

the given impulse. If the frequency of the oscillations is set out on the x-axis, and the amplitude on the y-axis, the graph which is obtained will characterize the amplitude spectrum for the given pulse (Fig. 119).

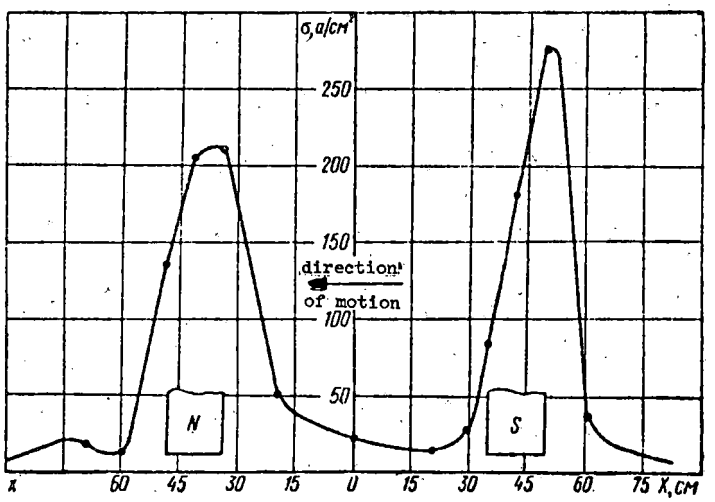

Fig. 118 Distribution of the density of transverse eddy currents at the rail surface at a speed of 40 km/hr.

Pulses from surface faults in the rail head have broader spectra (curves 1, 2) than the spectra of pulses from dangerous flaws (curve 3).

The frequency interval in which the basic energy of the pulse is concentrated is called the spectrum width. The spectrum width is usually limited by a frequency beyond which the oscillation amplitudes do not exceed 10-20 % of the maximum. The vibrator in the amplifier should reproduce the amplitudes of all oscillations composing the spectrum width of the given pulse without significant distortion in order to preserve the shape of the pulse.

The spectrum width of pulses from dangerous flaws does not exceed 400 Hz, i.e. the primary part of these pulses' energy falls on the spectrum components in the frequency range 0-400 Hz. Therefore, such pulses are well-registered by the N135-0.6 vibrators which have a working frequency range of 600 Hz, and

also by the MOV-2, VIII vibrators, with a working frequency range of 300 Hz. The sensitivity of these vibrators is such that preamplification of the pulses is not required. They are usually produced with a sensitivity of 12-17 mm/mamp, and the rated sensitivity is 14 mm/mamp. For vibrators with a sensitivity of 12-15 mm/mamp, a probe coil with 180 coils is usually used in the flaw detector cars, whereas, with greater sensitivity, the number of turns in the coil is decreased to 160. The resistance of each such coil should be about 30 ohm. Therefore, for a coil with 180 turns, PEL-0.14 wire is recommended, whereas for 160 turn coilings, PEL-0.12 wire is recomended.

When working with MOV2 Type V or N135-1.5 vibrators, which have a relatively low sensitivity, the resistance of the coil should be 6-7 ohm. Therefore, the number of turns is reduced somewhat, to 150. Coils with this number of turns and which are used with the above named vibrators are wound with PEL-0.29 or PEL-0.27 wire. To limit the amplitudes of the pulses registered, a 68- or 47-ohm SP-2 adjusting resistor is included in the circuit of each probe coil, either in series or in parallel with the vibrator.

Using an unamplified recording system with the MOV2 or N135 vibrators improves the "clarity" of the oscillograms, inasmuch as the emf pulses from the surface flaws in the metal of the running surface of the rail head, having broad spectra, are registered with a significantly reduced amplitude by these vibrators. The decrease in the amplitude takes place because the primary portion of the high-frequency component of these pulses is not reproduced by the indicated vibrators. In addition, the inductance of the probe coil grows noticeably when recording pulses with a broad spectrum. Therefore, many pulses from small pits, scabs, etc., are practically unnoticable on the oscillograph.

Amplifiers are usually employed when working with the MOV2 Type I vibrators, or with others of similar sensitivity. In this case, the shape not only of the pulses from the flaws, but also of many pulses from surface damage and from a welded joint are preserved on the film while recording due to the broader working frequency band of these vibrators. The distinguishing features of pulses received from welded joints are basically preserved when recording with vibrators having a working band of 1500 Hz and more. Therefore, a recording scheme employing amplifiers is used primarily on sections with a large number of welded rails or when there are no MOV2 Type VIII or Type V, or N-135-0.6; -.05; -1.5 available.

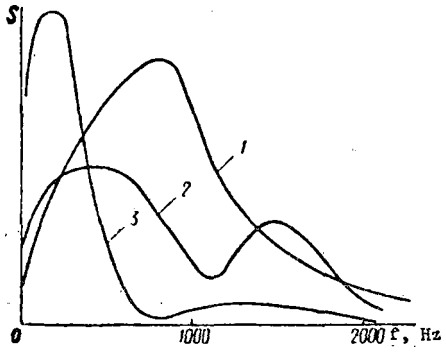

Fig. 119 Typical pulse spectra from flaws and surface rail damage.

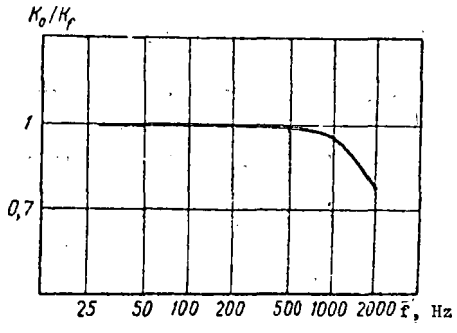

Fig. 120 Frequency response of the amplifier.

The bandwidth of each amplifier (Fig. 120) should be coordinated with the working frequency band of the vibrators to be used. Stability of the voltage from the power supply batteries is the basic requirement when working with an amplifier. It should not deviate from the rated value by more than ±3%.

10. Oscillogram interpretation.

From an examination (interpretation) of the oscillograms, it is possible to establish the location of defective rails on the line and to determine the nature of their damage. A list is compiled as a result of the interpretation. Based on this list, the line workers make on-site inspection and replacement of rails. Oscillogram interpretation is one of the most responsible procedures; it is conducted simultaneously by two workers who constantly check each other.

The following rules for interpreting the oscillograms have been worked out in practice. Their observance is strictly mandatory.

1. The film should always be examined from the emulsion side and in the direction in which the kilometer count increases. The direction the film is to be moved during interpreting is determined by the direction of car movement f the car moved in the direction in which the kilometer count increases, the ilm should be moved from left to right; if, on the other hand, the car was going in the direction in which the kilometer count decreased, the film should be shifted from right to left.

2. The kilometer and the rail length number, as well as the side of the track (left or right) on which the flawed rail lies, is indicated when filling out the list of defective rails. During the interpretation process, the rail count and specification of the proper side of the track is always made in the direction in which the kilometer count increases, without regard to the direction of the car's motion. The first rail length is considered to be that which is situated opposite the kilometer sign post. If the kilometer sign

post is at the end of the rail length of opposite a joint cover plate, the following length, on the next kilometer section, is taken as the first rail length.

In individual districts or track sections, special checking devices are placed along the right rail of the track to indicate the first rail length. A base plate, fastened by one spike to the cross-tie on the outer side of the track, so that the other end of the base plate leans against the upper fillet of the rail, is used as the checking device. This type of checking device is noted by a characteristic pulse which is readily distinguished on the oscillogram. The checking devices are usually placed one at the beginning of each first-rail length on the fifth or sixth cross-tie, counting in the direction in which the kilometer count increases. The rail length numbers on grade crossings, and bridges, as well as the numbers of short rail lengths in those kilometer sections where flawed rails have been noted are also registered in the list for orientation in order to avoid errors when counting the rail lengths. These orientation points are easily visible on the film, and they permit the noted rails to be found easily on the line. Usually the upper curve on the oscillograph screen in the flaw detector car corresponds to the right rail line when the car moves in the normal direction. The kilometer markings should be registered near this curve (above it).

3. The recordings on the film should always be read from left to right when the oscillogram is interpreted, regardless of the direction of car motion or movement of the film.

The shape of the emf in the probe coil is determined by the nature of changes in the magnetic flux above the rail.

It is known that the faster flux changes take place, the greater the emf in the coil: increasing the flux, causes an emf in one direction, and decreasing

it causes the emf to move in the other direction (Fig. 121). Above the base plates, for example, the magnetic flux decreases relatively smoothly, i.e. the reduction takes place over a long distance along the rail, whereas at a joint cover plate the current falls to a minimum much more rapidly. Over the joint clearance, the flux grows with even more rapidity. At the beginning of the joint cover plate, where the flux decreases, an emf arises in the coil in one direction, whereas at the end of the cover plate, where the flux increases, the emf arises in the other direction. The same thing also happens over joint clearances.

From an examination of the emf curve, one may see that it consists of separate pulses. The pulse corresponding to the decrease in the magnetic flux at the base plate at first grows to a maximum in a downward direction, if the curve is examined from left to right, while the pulse corresponding to an increasing flux at the joint clearance at first grows to a maximum in an upward direction. Each such pulse consists of two symmetrical parts, an upper and a lower, between which a zero line may be drawn. It is accepted to call that part of the pulse which is situated below the zero line (when reading from left to right) negative, and that part situated above the zero line, positive. Correspondingly, pulses beginning in the negative part are called 'negative', and those beginning in the positive part are called 'positive'. Thus, a positive pulse corresponds to an increase in the flux above the rail, and a negative pulse, to a decrease.

It is also accepted tc divide pulses depending on the magnitude of the amplitude of the positive and negative parts. If the positive and negative parts have an identical amplitude, i.e. an identical height relative to the zero line, such a pulse is called 'symmetrical'. If, on the other hand, the positive and negative parts have different amplitudes, such a pulse is called

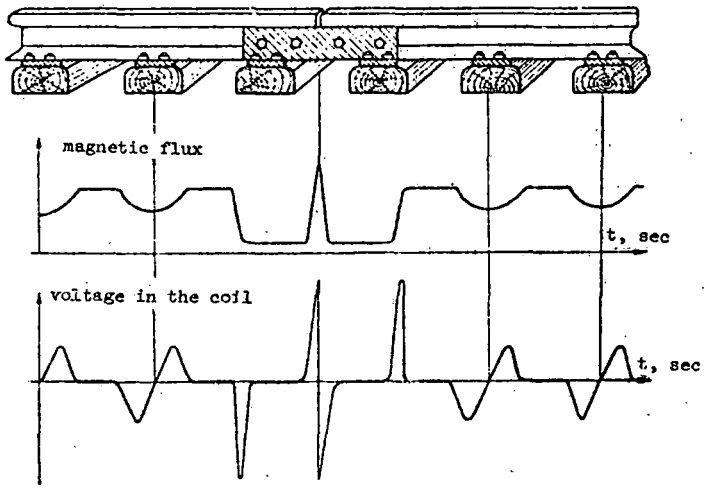

Fig. 121 Flux in the rail and voltage in the probe coil.

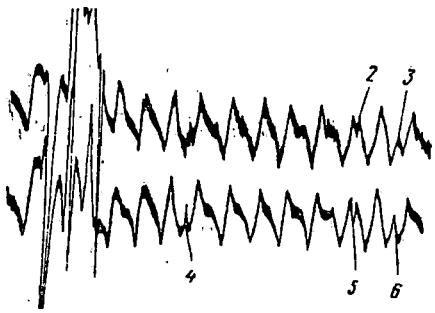

Fig. 122 Film section sample.

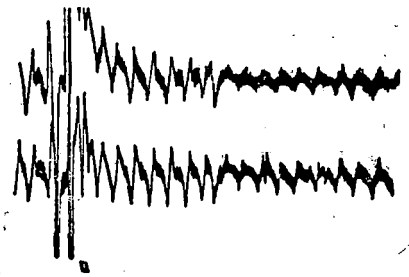

Fig. 123 Film sample with a recording taken at a grade crossing.

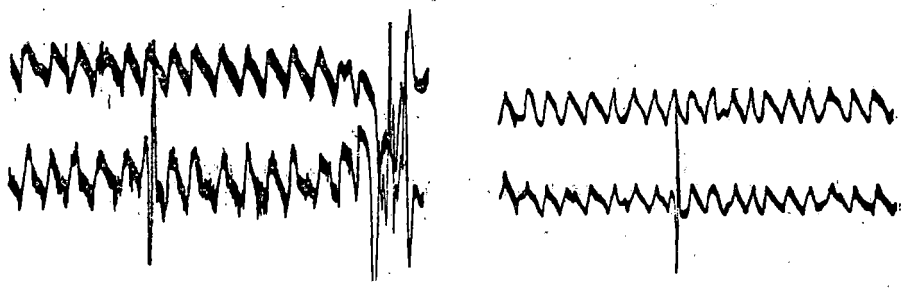

Fig. 125 Examples of records of 30G.2 flaws on film.

asymmetrical. Pulses which have only a positive or negative part are also encountered. Such pulses are called unidirectional. For example, the beginning and end of joint plates are noted by unidirectional pulses, the beginning of the cover plate, where the magnetic flux decreases, being noted by a negative pulse, and the end of the cover plate, where the flux increases, by an analogeous positive pulse.

The width (duration) of the pulse, i.e. the distance from the beginning to the end of the pulse along the zero line, is also taken into consideration in the interpretation. It may be seen from Fig 121 that the width of the pulse from the base plate is greater than the dimension of the base plate itself. This is explained by the fact that a decrease in the magnetic flux begins before the edge of the base plate. The same flux change picture is observed at the ends of the joint cover plates and at the gap.

A length of rails is registered on the film at a scale of 1:200 - 1:250. A photograph of a section of film, magnified approximately three times, is shown in Fig. 122. It may be seen from this photograph how the steeply inclined lines are thinner, while, e.g. at the joint, a part of the line is almost invisible. This is explained by the fact that with a rapid change of the emf in the probe coil, the light-sensitive layer on the film is weakly exposed (a great translational velocity). On other rail sections, e.g. between the cross ties, where the translational velocity is not high, there is the greatest degree of darkening on the film. One may also see from this photograph that the difference between pulses arising from the base plates is extremely insignificant, and may even be noted by one point with strong darkening.

The record left by rail anchors (1,2,3,4,5, and 6) is also depicted in Fig. 122. The record of each rail anchor is characterized by a peculiar distortion of the pulse from the base plate, and depends on the construction

of the rail anchor, the tightness of fit to the rail, etc. The middle of the thin line of the base plate pulse corresponds to the middle of the cross tie. When determining the ordinal number of the cross ties, it is taken into consideration that the pulse from a base plate on a cross tie in the joint zone is not visible on the film.

The record of the rail length on a grade crossing (Fig. 122), as well as on bridges, is characterized by the fact that the amplitude of pulses from the base plates is sharply diminished along the entire length of the wheelguide guard rail. If the ends of the wheelguide rail are not bent back, they are noted by undirectional pulses, as are the joint cover plates, i.e. a negative pulse corresponds to the beginning of the wheelguide guard rail (in the direction in which the car is moving), and positive pulse corresponds to the end. A decrease in the amplitude of pulses from the base plates on grade crossings is explained by an over-all decrease of the magnetic flux over the rail due to the increase in the volume of metal because of the wheelguide guard rails.

Flaws in the rails are recorded on the film by pulses which differ from each other, thereby making it possible to determine the nature of the flaw based on the shape of the pulses. Thus, pulses from surface flaws in the metal of the head are positive as a rule. Their formation is associated with significant dispersion fluxes above flaws of this type.

In the majority of the cases, negative pulses are formed from internal flaws, regardless of whether or not they emerge onto the rail surface.

Pulses from flaws may be distributed on any part of the graph corresponding to the record of a sound rail section.

It is necessary to consider that the pulse is situated on the conditional zero line when evaluating it during interpretation, independent from its position on the curve.

Evaluation of pulses from flaws takes into consideration their distinguishing features, including the following: the pulse phase, by which is meant the initial direction of the pulse from the zero line; the length and symmetry of the pulse; and the pulse amplitude.

The pulse amplitude is evaluated in units equal to the standard amplitude of a pulse from an ordinary base plate. Pulses, the amplitude of which exceeds the amplitude from the base plate, must be given consideration. Usually, pulses with a magnitude of 1.5 units and more are considered. Pulses with smaller amplitude are not examined in practice.

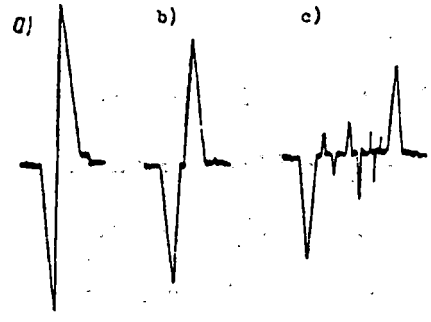

Fig. 124 Diagram of pulses from longitudinal separation of the metal in the head.

Pulses corresponding to horizontal longitudinal separation of the rail head (Fig. 124) are the most widespread. These are negative symmetrical pulses with an amplitude which characterizes to a certain degree the development of the flaw.

If the amplitude of a pulse is equal to 2 units or less, the flaw is, as a rule, hidden and small (cf. Fig. 124a) The span of the flaw along the rail length determines the width of the pulse. When such a flaw is of significant length, a darkening is formed in the center of the pulses (cf. Fig. 124b). The darkening characterizes the brief cessation in the process of changing

emf in the probe above the flaw center. Examples of records of 30G.2 flaws on film are given in Fig. 125.

The pulse from a vertical internal separation of the rail head is similar to this pulse. When the separation in the head has a span of up to 20 cm., the pulse from it is analogeous to the pulse shown in Fig. 124a. However, in most cases, the vertical separation in the head has significantly greater length, and this is noted at the beginning of the separation by a unidirectional negative pulse, and at the end, by a unidirectional positive pulse. Between them, there are usually other smaller, narrow pulses of various shapes (Fig. 124c), caused by irregularities in the separation, by a spread or crushing of the rail head, etc.

Pulses, the characteristic feature of which is a sharply defined asymmetry, are caused by contact-fatigue flaws in the form of light and dark spots in the head; the amplitude of the negative part is signaifcantly greater than the amplitude of the positive part. Typical pulses denoting light or dark spots are shown in Fig. 126.

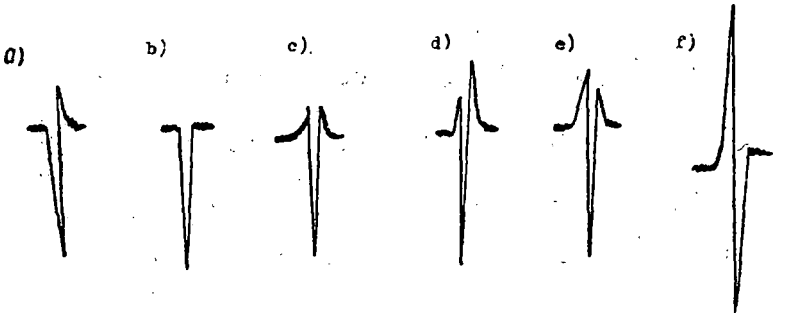

Fig. 126 Typical pulses from light and dark spots in the rail head.

In most cases, a light spot is recorded as a pulse such as a or b. As a rule, the amplitude of such a pulse from a light spot is less than that from

a dark spot, and is usually equal to 1.5-2 times the amplitude of the standard pulses from the base plates. The degree to which the flaw is developed is characterized to some extent by the amplitude of the negative part. Dark spots with a crack emerging on the side or the fillet of the rail are usually recorded by pulses in the shapes of c, d, and, rarely, in the shape of e. The amplitude of the negative part of these pulses usually exceeds the amplitude of pulses from the base plates by three times or more.

Developed light spots situated in the center of the rail head are sometimes noted by symmetrical positive pulses in the shape of f, which are analogeous to a pulse from the joint gap, but with a significantly smaller amplitude. The dark spots, and transverse rail fractures are registered in the same manner, but with a greater amplitude.

As was indicated above, surface flaws in the rail metal are also noted by positive pulses. However, pulses from the surface flaws are as a rule unidirectional or asymmetrical and are narrower. Usually they are narrow enough that they are easily distinguishable from pulses caused by dangerous flaws (Fig. 127). In most cases, the amplitudes of such pulses do not exceed the amplitude of (pulses from--tr.) the base plates, while pulses from internal flaws have a greater amplitude, even crossing the signal from the other rail.

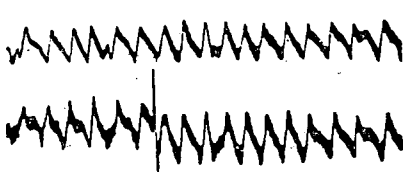

Fig. 127 Sample of a record of surface damage in the metal of the rail head.

Incipient flaws (light spots) are registered in rare instances by a unidirectional negative pulse like b (cf. Fig. 126). The diversity of the pulses

from flaw types 20.2 and 21.2 is explained by the peculiarities of their position in the rail head, by the degree of development, and by other factors, the significance of which is still inadequately studied.

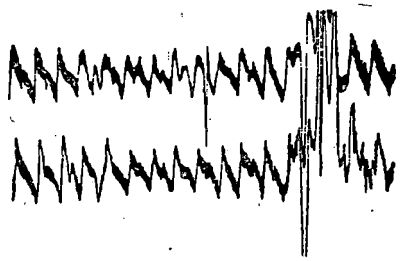

Fig. 128 A record of the 21.2 flaw on film.

The longitudinal horizontal separation which changes to a transverse crack is often encountered. It is registered as a 30G.2 type flaw or as a 20.2 or 21.2 type flaw, depending on which part of the flaw is dominant. A film record of 20.2 and 21.2 type flaws made by a pulse in the shape of a is shown in Fig. 128.

Certain large cavities in the rail surface and scab cracks are noted by pulses similar in form and amplitude to the value of pulses from dangerous flaws. Samples of such pulses (1, 2, and 3), along with samples of pulses (4, 5, 6) from dangerous flaws are given in Fig. 129 for comparison. Pulse 1 is analogeous with pulse f (cf. Fig. 126), however, it is narrow, i.e. it is of significantly less duration than pulse f. The amplitude of such positive symmetrical pulses from surface rail damage does not usually exceed 1.5-2 units, whereas signals from flaws having the shape of f have a greater amplitude and frequently pass beyond the edges of the film. Pulses 2 and 3 from large cavities, gouges or scabs which have split have, as a rule, the first positive part greater than the second positive part, while the build-up (the leading edge of the pulse) is larger than the edge of pulses in the form of e (cf. Fig. 126), by which certain 20.2 and 21.2 type flaws are noted. Additionally,

as distinct from pulses related to 20.2 and 21.2 type flaws, they have a relatively short duration.

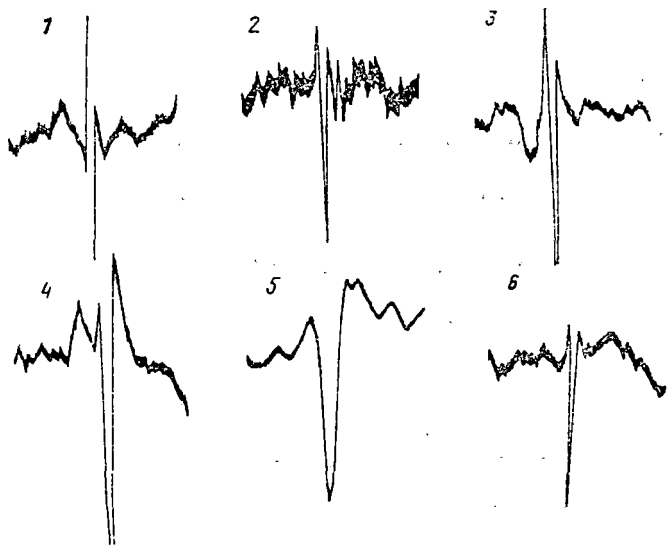

Fig. 129 Samples of pulses from large cavities, scabs which have split, and internal defects in the rail head.

All of these characteristic features are distinct when the film is interpreted only if the film is examined at normal magnification. Should the film be inadequately exposed, or should the record be made using a small longitudinal scale, these pulses are difficult to distinguish from pulses related to the 20.2 and 21.2 type flaws. In this case, rails which have been noted by such pulses are included as "questionable". These are most often checked based on film records from the previous inspection tour. If, on the film from the previous inspection tour, the rail was already noted in the same place by a pulse which was not considered at the time due to small amplitude, and if, on the given inspection tour, this pulse has "grown", it is considered to be defective and is specified for replacement since the growth of the signal corresponds to the development of an internal flaw in the given rail.

In the case when a rail was noted on film from a previous inspection tour

by a pulse which was repeated with the same or with a smaller amplitude, this indicates the presence of surface damage which need not be considered a flaw. If there is no mark on the film from the previous inspection tour, or, if that film is not available, the rail which was noted by the questionable pulse will be subjected to on-site inspection.

On-site inspection is made in all cases when it is necessary to make clear to which flaw type any pulse relates. The rail noted by the pulse is checked on the line using a removable MRD flaw detector equipped with probes for the side and fillet of the rail, or by using an ultrasonic URD-63 or DUK-13 flaw detector. The place on the rail which was marked by the questionable pulse is carefully checked using one of these flaw detectors.

Other flaw detectors may also be used in specific instances to test rails, based on indications by the flaw detector car.

In the absence of removable and portable flaw detectors, when emergency rail examination is being made using the usual on-site inspection techniques, those rails which have no surface damage capable of causing an electromotive force impulse in the probe coil in the places noted by the flaw detector car are included among the defective rails.

In order to find the flawed spot in the rail, its position relative to the cross ties, a count of which is made based on pulses from the base plates, is indicated in the interpretation list. It is usually indicated in the list that the flaw is situated on a given cross tie or between two certain cross ties, and closer to the first of the second. The cross tie number is indicated taking into account the joint cross tie. The accuracy attained using such a system is completely adequate in practice for on-site inspection of rails when it is necessary to determine the nature of a flaw noted on the film more exactly.

In the case when split rails and rails with flaws which threaten the

immediate safe movement of trains are found during the process of film interpretation, the flaw detector car workers should immediately inform the local track workers of this fact so that they may take measures to reduce the speed of rail traffic and replace such rails.

11. Troubleshooting the flaw detector apparatus.

Among the most frequently encountered faults of the flaw detector car with the photographic recording system are those which show up immediately after their development, as well as others which form over a relatively long period and do not immediately make their presence known. Among the latter are included, for example, any change in the characteristics of the amplifiers, the vibrators, or of the probe or magnetizing coils. Periodical inspection of these components in the intervals between planned repair is anticipated by the current regulations for flaw detector car usage.

Flaw detector car repair takes place at a special plant. The car body, the rolling parts, the brake assembly, the storage batteries, the generator, and its drive system are all repaired at a car repair plant, while the flaw detector equipment is repaired at the electrotechnical plant operated by the Ministry of Railroads.

The electromagnet coils go out of order relatively often when in use. The primary reasons for their doing so are an inadequately snug fit on the poles, poor insulation of the winding from the metalic sleeve, and insulation break-down.

Insulation break-down takes place when working on worn rails, when the fine metallic flakes rip away from the rail under the influence of the magnetic forces and are attracted toward the electromagnet with great speed, perforating the winding insulation, and shorting out several layers of the coil. Such instances of break-down take place when the protective metal casing does not cover the lower portion of the coil snugly.

Another reason for insulation break-down comes from switching the electromagnets off without first lowering the current with the rheostat. In this case, an excessively large voltage (the extracurrent) arises between the windings of the coil, causing damage to the windings.

When the coil is not snugly mounted on the poles, it moves when the car is in motion. The insulation wears through and the coil windings either short each other out or they short out on the body of the car through the metallic sleeve.

In all cases of insulation break-down and short circuiting of the coil windings, it is necessary to repair them, the old windings being replaced with new ones.

The vibrator characteristics have a great significance for normal operation of the flaw detector. The characteristics (frequency and amplitude) are recorded before the vibrators are mounted in the oscillograph; these characteristics are periodically checked while the vibrators are in used. Such checks are necessary since the initial parameters change over a period of time. When the temperature conditions for working with the vibrators is violated or when the rules for taking care of them are not observed, this process is accelerated.

The circuit described in Fig. 130 is made to record the frequency characteristic. According to this hook-up, the vibrator being tested is mounted in the oscillograph is that the light reflection (the "spot") is situated in the center of the screen. Then, the sound generator output and a cathode voltmeter are hooked up to the vibrator terminals.

The alternating current voltage from the generator is set according to the cathode voltmeter so that the peak-to-peak amplitude (dimension A on Fig. 130) is 100 mm at a frequency of 50 Hz. Then, keeping the alternating current voltage from the generator constant, the frequency is varied between 50 and 100 Hz

and dimension A is measured with each change. A graph of the dependence of the amplitude on the frequency is constructed from the data obtained. The generator frequency is plotted on an arbitrarily selected scale on the x-axis, and the measured values of A are plotted on the y-axis.

In order to combine the graphs of all tested vibrators, their relative values (i.e. not the absolute values of A) are plotted on the y-axis. To do this, the magnitude of A_1, measured at a frequency of 50 Hz is taken as 100% and the remaining values A_1, A_2, ..., A_n, are plotted in percents of A_1 (each ordinate is determined in percents as $A_2/A_1 \times 100$, $A_3/A_1 \times 100$, etc.). The points which are obtained are connected by a smooth curve which comprises the frequency characteristic.

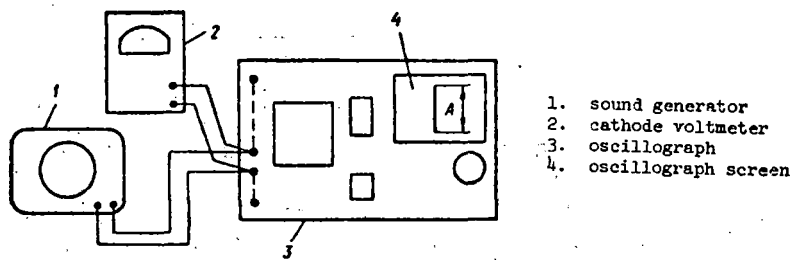

Fig. 130 A circuit for checking the vibrators.

Normally, the frequency characteristics of the vibrators should have the shape shown in Fig. 131. If the characteristic is represented by a broken line with troughs and peaks, the vibrator is considered to be faulty.

Having the frequency characteristic and knowing the magnitude of the alternating current voltage from the generator V (millivolts) at which this characteristic was obtained, it is possible to determine the sensitivity of the vibrator. Usually, the sensitivity is given in mm/mamp for direct current. In our case, it may be determined for a current with a frequency of 50 Hz according to the formula

$$\tau = \frac{A_1 R}{2 \cdot 4V}$$

where R is the resistance of the vibrator in ohms.

It is possible to determine the sensitivity of the vibrator at any frequency by this formula, inasmuch as all values of A are known when the characteristic is taken. Knowing the sensitivity at a frequency of 50 Hz, τ is usually determined for other frequencies according to the frequency characteristic, where the ordinates are given in percents.

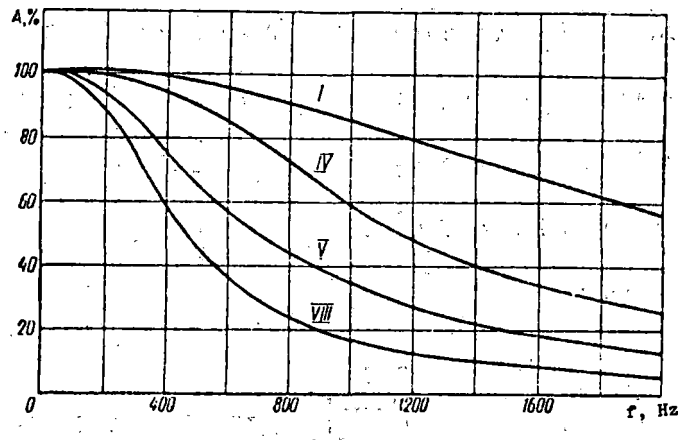

Fig. 131 Vibrator frequency characteristics.

When the frequency characteristic is recorded, one other indicator is tested, the ability of the vibrator to reproduce both a positive and a negative amplitude in the same manner, i.e. the sensitivity of the vibrator should be the same for both a positive and a negative current value. To do this, the zero position of the "spot" when no voltage is supplied to the vibrator is marked on the oscillograph screen when the frequency characteristic is recorded, using either a colored or an ordinary pencil. Then, when measuring the size of A, the deflection of the vibrator to both sides of this point is checked. If the vibrator shows a significant difference in the reflections to either side, it is considered to be unsuited for work.

Vibrator repair is not conducted in the on-line flaw detector laboratories. The MOV2 and N135 vibrators are repaired in factories specially adapted for that purpose because they are measuring devices.

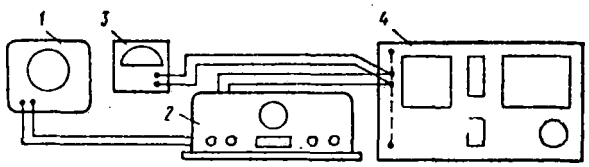

Fig. 132 Circuit for testing the amplifiers.
1. Sound generator; 2. Amplifier; 3. Cathode voltmeter; 4. Oscillograph

Amplifier faults are basically limited to damage to the electrical contacts in the tube sockets and, in the places where the probes are connected, to irregularities in the power supply system for the plate, filament and bias circuits. Checking for and eliminating these faults does not present serious difficulty. Changes in the amplitude and frequency characteristics of the amplifiers, which take place as a result of aging of the tubes and other components of the electrical system, constitute more significant abnormalities.

The frequency characteristic is tested in the same way as with the vibrators. The one difference is that a generator 1 is hooked up to the amplifier input 2 (Fig. 132), instead of the probes, while the output voltage of the amplifier U_{out}, i.e. the voltage which passes to the vibrator, is measured by the cathode voltmeter 3. To check U_{out}, the vibrator is removed from the oscillograph or switched out of the circuit. Having measured the output voltage of the amplifier while feeding in alternating voltage of various frequencies (with the voltage remaining constant), a graph is constructed. This is the frequency characteristic. The frequency characteristic has the form represented in Fig. 120 for a normally functioning amplifier. The amplification coefficient for each amplifier is determined when such a test is made. It will be equal to the ratio of the output voltage U_{out} to the input voltage U_{in} The amplification coefficient for a normally functioning amplifier should be close to unity, within a frequency range of 30-1000 Hz and higher.

The amplitude characteristic is the other important characteristic. It is determined using the same hook-up which is used to record the frequency characteristic (cf. Fig. 132). If the frequency characteristic is recorded with a constant voltage on the amplifier input, the amplitude characteristic is recorded with a constant frequency f for the input voltage; only the magnitude of the voltage is varied. The amplitude characteristic is recorded with an input voltage frequency of 150-200 Hz. It should be a straight line between coordinates U_{in} and U_{out} within an input voltage interval of from several millivolts to 1.0-1.5 v.

In instances when the frequency of the amplitude characteristic does not correspond to the indicated data (with a normal power supply voltage), the amplifier should be repaired. The repairs should include testing and repair of those circuit components which do not correspond to the data indicated in Table 6.

12. Basic Directions for Further Improving Flaw Detector Cars.

The flaw detector car is a high-performance rail flaw detector. It provides for mass inspection of rails on long track sections in relatively short periods of time. However, in connection with the uninterrupted growth in the density and speed of train traffic, new demands will be made of the flaw detector car. It is necessary, for example, that its working speed not be less than the speed of train traffic on a certain section. Increasing the operating speed will stimulate a series of difficulties associated with the passage of the flaw detector car along sections of rail line with high freight traffic density.

Along with this, it is necessary to increase the productivity of the flaw detector car and to equip it with new flaw detecting equipment which will permit the results of rail examinations to be obtained immediately, i.e. while the car is still in motion and not after a film has been processed. Such an

operational level for supplying the results of the tests is extremely important. It is a necessary condition for further increasing the safety of train passage on the railroads.

As a first step in this direction, an attempt was made to replace the photographic recording of the flaw detector indications with a recording on paper tape. A special instrument, the "defectograph", which provides oscillographs on a common paper tape instead of film, and on a larger scale, was developed to replace the oscillographs. When the defectographs are used, the productivity of the flaw detector car increases significantly because the rather lengthy operations connected with processing film in the developing machine are eliminated. Several flaw detector cars experimentally equipped with defectographs are in use.

The defectograph is a device consisting of a receiver-amplifier unit 1 (Fig. 133), a pen recorder 2, an ink supply pump 3, the tape drive mechanism with drive gear 4 and a power supply unit 5. The defectograph works with the same flaw detector car probes which are used when working with oscillographs and amplifiers. Power is supplied at 110-130 v. a.c. from the flaw detector car converter. The probes are connected to the input of the receiver-amplifier unit and, following the usual procedure, their polarity is established according to an oscillograph made by switching the electromagnets on and off either when the car is in motion or at rest.

One peculiarity of the procedure for establishing the polarity of the sensors of a flaw detector car equipped with a defectograph while it is at rest is that under these circumstances, the paper recording tape should be in motion. The tape is made to move using the tape drive mechanism, working from the electric motor, i.e. the movement of the paper tape is not connected with the (speed of the) car axle. The scale for recording the rail lengths

is adjusted by (varying -- tr.) the tape transport speed. When the defectograph is in operation, the speed is usually set at about 100 mm/sec. The oscillogram time scale exceeds the accepted recording scale on film by about two times, which permits interpretation without using a magnifying lens.

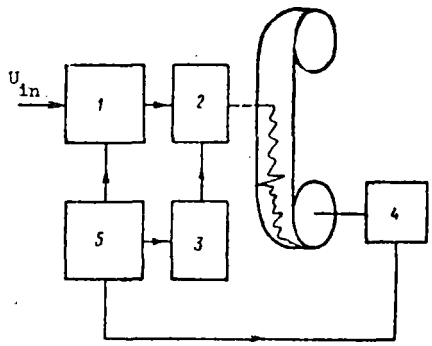

Fig. 133 The defectograph (block diagram).

Certain features of the car recorder have a negative effect on the quality of the oscillogram. In brief, the pulses recorded on the paper tape by the defectograph are often different from those recorded on film. The fact is that the pen recorder is a galvanometer, the lay-out diagram of which is analogeous to a vibrator (cf. Fig. 105). Instead of the reflector (the mirror), a thin glass tube, which is rigidly affixed to two wire threads, is mounted between the threads stretched in the magnetic field.

The opening of the tube (of the capillary) is situated at a certain distance from the paper tape. Ink, under a specific pressure, is ejected through the capillary onto the paper tape. The ink is fed in bit by bit at a definite rate. Such a discrete ink supply is realized using a pump. The discrete supply and the pressure fluctuations at the capillary opening are recorded. Therefore, powerful but brief pulses may sometimes not be "registered" completely due to the capillary's high oscillation rate, i.e. a part of the pulse may not be visible on the tape.

In connection with this, it is extremely important to establish the pressure and the supply rate correctly, as well as the speed at which the tape is driven. At an excessively high pressure or with the tape driven at a slow speed, the ink smudges the oscillograph, and, with inadequate ink ejection pressure, pulses, especially short-lived and small-amplitude pulses (from internal flaws), may not be visible on the oscillogram. It is necessary to take this circumstance into consideration when adjusting a faulty defectograph since it reduces the quality of the flaw detector car's work, causing dangerous flaws to be overlooked, especially internal flaws which do not emerge onto the surface.

The indicated features are also taken into consideration when the oscillogram is interpreted; all pulses records are viewed to be continuous, regardless of the actual magnitude of discontinuities in the inked line.

Due to the presence of discontinuities in the inked line, the shape of pulses, especially the initial phase, (showing the nature of the fronts, etc.), are poorly distinguished upon occasion. In this case, poorly distinguished pulses, as well as other questionable pulses, are checked by on-site inspection of the noted rail. Experience shows that the necessity of on-site inspection grows as a result of the lower quality of the oscillogram on the paper tape in comparison with the oscillogram on the film, i.e. on-site inspection is made more often when the defectograph is used than when working with the oscillograph.

The necessity for on-site inspection is a common short-coming inherent in any means for registering and interpreting oscillograms, either on paper tape or on film. The fact is that in many instances, as was indicated above, it is impossible to give an unambiguous evaluation of the degree to which a noted rail in defective, based on the oscillograph, and only an on-site inspection

permits supplimentary data to be gathered for a more reliable evaluation.

A substantial amount of time is required for such examination, which lowers the productivity of the flaw detector car.

It is necessary to develop new means which are more effective than the visual evaluation of signals according to an oscillogram for evaluating the flaw detector readings in order to raise the productivity of the flaw detector cars and the reliability of effective rail detection.

The evaluation of the flaw detector readings should be automated. The work of the automatic equipment should be to extract and process that information which is fed in as pulse signals from the probes, the sensitive elements of the flaw detector. It is also necessary that the automatic processing of signals take place immediately, while the flaw detector car is in operation, and that the results be provided without significant time lag.

Research shows the possibility of developing this type of equipment. However, there are difficulties, namely that equipment which functions automatically should evaluate the signals which are fed to its input correctly without a substantial number of errors. In this case, we may include among the basic errors the fact that a signal from a dangerous flaw in the rail may be evaluated as being from surface damage which is not dangerous, and, conversely, a signal from surface damage may be taken to be a flaw.

The automatic device may be considered suitable if errors of this type are rarely encountered when it is in operation. For example, it is possible to agree to consider the work of an automatic device satisfactory if, out of 100 signals fed in, 99 or 98 would be correctly evaluated, i.e. the number of erroneous decisions should not exceed 2% on the average. The quality of the automatic device's work is best evaluated based on the number of false marks on the registering flaw detector tape, in percent, in comparison with the

number of fixed (noted) defective rails on the tape. If this constitutes 3-5%, the work of the automatic device may be considered satisfactory for the time being.

Another important characteristic is the sensitivity of the automatic device to flaws. Signals from the probe, carrying information about the condition of the rails, are amplitude limited at the input to the automatic device. Signals below the threshold level should not be received. Experience shows that the lower the signal threshold level, the higher the sensitivity of the flaw detector to defects. The sensitivity may be high enough for flaws in the incipient stage of development to be noted. However, the number of errors in signal evaluation grows sharply here.

The quality of work done by an automatic flaw detection device should be evaluated by percentage of admissable error. One of the basic directions of experimental work towards perfecting the flaw detector car is the development of the means for lowering the percentage of error while at the same time increasing the sensitivity of the flaw detector to flaws.

Stabilizing the position of the probe relative to the rail head has great significance for improving the reliability of detecting flaws in the rails using flaw detector cars. As presently constructed, the probes have a free displacement relative to the rails, especially on the curved parts of the track, where the track gage is substantially increased. The familiar methods of stabilization using clamping rollers or collector shoes may not always give the needed effect due to the unavoidable high speed vibration in such designs.

Vibrations create electrical disturbances which distort the probe signals and lead to a decline in the flaw detector's sensitivity to flaws. It is, therefore, necessary to develop a stabilizing device which would not contact the rails. Simultaneously, it is necessary to replace the magnetizing system

of the flaw detector car. It has been established that the greater the field of the electromagnets, the greater will be the detectability of the flaws. The question of creating the most effective magnetizing system for a high-speed flaw detector is currently of great interest.

Another important measure towards perfecting the flaw detector car is the development of a new system of probes, the sensitive elements, which would permit obtaining more complete information concerning the status of the rails than is presently possible when working with a single induction coil. It is possible, for example, to obtain more information concerning the state of the rails being checked in the following manner.

The square flaw detector car electromagnet creates a field $\underline{H_o}$ which may, in a given instance, be represented as consisting of two vectors, a vector $\underline{H_{ox}}$, directed along the rail, which is called the longitudinal component of the field $\underline{H_o}$, and the vector $\underline{H_{oz}}$, parallel to the z-axis, the so-called vertical component (Fig. 132). Thus, the electromagnet field $\underline{H_o}$ is represented by the vector sum $H_o = H_{ox} + H_{oz}$. It is known that eddy currents are induced in the rails when the flaw detector car moves. The greater the speed, the greater the density of the eddy currents.

The eddy currents are distributed in the rail head in a manner such that the magnetic field created by them (the reaction field $\underline{H_r}$) is directed against the field of the primary, i.e. against the field of the electromagnet. Consequently, the eddy current field $\underline{H_r}$ may also be represented as consisting of two components, the longitudinal, $\underline{H_{rx}}$, and the vertical $\underline{H_{rz}}$, which combine with the primary electromagnet field $\underline{H_{ox}} + \underline{H_{oz}}$ to create the net resultant field. Consequently, given a movement, both the longitudinal and the vertical component of the field will be expressed by the sum:

$$H_x = H_{ox} + H_{rx};$$

$$H_z = H_{oz} + H_{rz}$$

When the continuity of the rail metal is broken due to the presence of a crack, the distribution of the eddy currents in the zone where the crack is located will be different from the distribution on a sound rail section. This local redistribution of the eddy currents will cause a change in the reaction field, and, consequently, in the net field.

The longitudinal component of the reaction field H_{rx} is formed by currents flowing in closed circular paths in the vertical plane n - n, i.e. across the rail, while the vertical component is formed by currents flowing along the rail, in the horizontal plane m - m (cf. Fig. 134). It is obvious that longitudinal cracks in the head will be well detected due to changes in the longitudinal component H_x since such cracks intersect the eddy currents in the n - n plane.

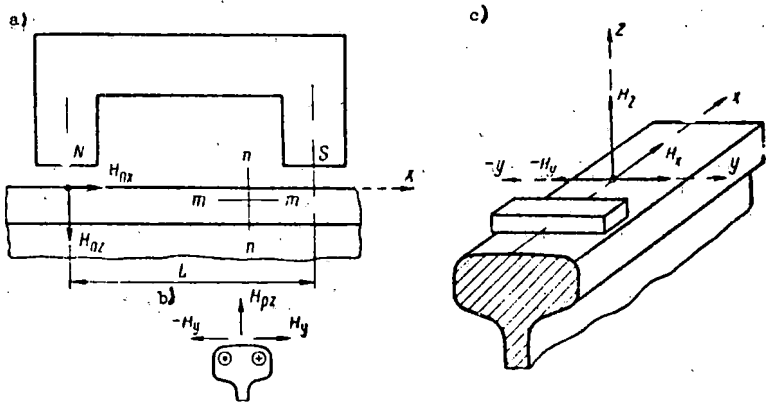

Fig. 134 Diagram of the rail magnetization by the constant field of a moving electromagnet.
a. magnetization of the rail b. the transverse and vertical components of the field c. position of the probe

Flaws in the form of transverse fatigue cracks forming a definite angle (the angle of incidence) with surface n-n will also cause distortion of the

eddy current paths in this plane. The fact is that each crack represents a large resistance for currents, and the currents skirt the crack, as a result of which, the reaction field, and consequently, the net field $\underline{H_x}$ or $\underline{H_z}$ changes in the zone where the crack is situated.

Thus, a change in the field $\underline{H_x}$ or $\underline{H_z}$ signals the presence of a flaw in the rail. It is possible to detect a change in the field with the aid of various sensing elements, including induction probes.

A multiwind coil without an iron core is used as the induction probe in the flaw detector cars using oscillograph recording. The plane of the coil windings is perpendicular to the direction of the x-axis (cf. Fig. 134). This type of probe reacts to changes in only one longitudinal component of the field, $\underline{H_x}$. An emf pulse which is fixed on the oscillogram is formed in the probe when $\underline{H_x}$ changes. However, this pulse does not contain complete information concerning the condition of the rail. An emf pulse at the flaw may also be obtained because of changes in $\underline{H_z}$ and because of changes of the magnetic field in the direction of the y-axis, i.e. from using the third, the transverse component. This component is formed by the eddy currents which flow along the rail head (in the horizontal plane m - m) when (the car) is in motion. The direction of the longitudinal currents from a head-on view, and the formation of the field along the y-axis is shown in Fig. 134b. When a flaw is present, especially in the form of a vertical crack, the paths of the eddy currents flowing around the rail will intersect to a greater degree than in the n - n plane, and the fields from these currents (the vertical $\underline{H_{rz}}$ and the transverse $\underline{H_y}$ components) will undergo large changes in the flaw zone. If, on a sound section of the rail, $-H_y \approx +H_y$ in the presence of a flaw, a difference $\underline{\Delta H_y}$, which may be recorded using an induction probe oriented to this component, is formed.

Thus, the presence of a flaw may be recorded using induction transducer-probes which react to changes of the three components of the field when searching for flaws in the rails using a moving U-shaped electromagnet. Each component will cause an emf pulse in the probe of a magnitude and form which will be determined by the nature of the flaw, its degree of development, and its position within the head. This condition is used to evaluate the extent of the rail flaw detected by a flaw detector, based on the characteristic features of the pulses (on their amplitude and their form in the experimental sample of the automatic apparatus which is undergoing on-site testing on certain lines).

An automatic apparatus, the use of which should solve the problem of perfecting the flaw detector cars, as presented above, is presently being developed along two directions. Each approach uses different methods to solve the problems posed. Selection of the best method and completion of the design of the apparatus are only possible based on the generalization of the results of on-site testing under various conditions.

Chapter V -- Ultrasonic Flaw Detection Methods.

1. The physical bases of ultrasonic flaw detection.

Ultrasonic, as well as sonic, vibrations are the mechanical, elastic vibrations of the particles of any medium. Elastic vibrations, at frequencies above 20 KHz, i.e. above the sound frequency perceptable to the human ear, are called ultrasonic vibrations. Elastic vibrations at ultrasonic frequencies may be excited in gaseous, liquid, and solid media. The vibrational motion of the excited particles causes the propagation of an ultrasonic wave, which is accompanied by a transfer of energy, due to the presence of the elastic bonds between the particles.

Wave propagation takes place at a definite speed, called the ultrasonic wave speed, which is measured in m/sec. It is necessary to distinguish the wave speed from the particle vibration speed when these waves are propagated.

The direction of particle vibration may be different from the direction in which the wave is propagated, and this determines the type of wave. In the longitudinal wave (a compression wave), the particles vibrate along the direction in which the wave is being propagated, and in the transverse (a shear wave), the vibration is perpendicular to this direction.

Longitudinal waves may be excited in any medium, and transverse waves only in solid media. The velocity of the wave is determined by the physical properties of the medium and by the wave type. The velocity of transverse waves C_t is approximately one half the speed at which longitudinal waves C_l are propagated.

The propagation of an elastic wave of any type is accompanied by the formation of zones in which the particles are in an identical vibrational state. The minimum distance between such zones is called the wave length.

The greater the wave length, the greater the velocity and the smaller the

particle vibration frequency. Wave length λ is associated with velocity C and frequency f by the relationship

$$\lambda = \frac{C}{f} \qquad (1)$$

Thus, a change in the length of an ultrasonic wave in any medium may be acheived only by varying the frequency of the excited vibrations. With the frequency remaining the same, the length of the longitudinal wave in any medium will be approximately twice that of the transverse wave.

With the frequency remaining constant, the amplitude of the particle vibrations will be more significant as the intensity of the wave is greater. By ultrasonic wave intensity we mean that quantity of energy transfered by the wave in one second to an area of 1 cm^2 which is perpendicular to the wave's direction of propagation.

As it is propagated, even in a strictly defined direction, with no divergence whatsoever, wave entensity decreases. Weakening of the intensity (wave attenuation) may be associated with absorption during which the mechanical energy of the particle vibrations is converted to heat energy, and with the dispersion of the ultrasonic wave on nonhomogenieties in the medium. Dispersion depends on the relationship of the wave length to the mean diameter of the nonhomogeniety. The attenuation of ultrasonic vibrations used for flaw detection in rails is basically determined by dispersion of the ultrasound at grain boundaries. In practice, the larger the metallic structure, the greater the dispersion.

It is therefore natural that ultrasound attenuation in the welded joint zone will be more substantial than in the parent metal.

Reduction of the ultrasound intensity due to attenuation takes place according to the exponential law

$$I_x = I_0 e^{-2\gamma x}, \qquad (2)$$

where I_x is the ultrasound intensity at a distance x from the place where the intensity is equal to I_0;

γ is the attenuation coefficient, measured in cm^{-1}; and e is the natural logarithmic base (e = 2.718).

The attenuation coefficient grows rapidly as the frequency is increased during flaw detection in metals.

The values for the velocity, wave length, and the attenuation coefficient for an ultrasound frequency of 2.5 MHz, and the medium usually used for flaw detection in rails are presented in Table 9.

Table 9

medium	medium density, g/cm3	wave velocity, m/sec		wave length at f = 2.5 MHz, mm		attenuation coefficient for a longitudinal wave at f = 2.5 MHz, cm^{-1}
		c_l	c_t	λ_l	λ_t	
1	2	3	4	5	6	7
air	0.0012	330	-	0.13	-	1.0
water	1.0	1450	-	0.58	-	0.001
plexiglass	1.18	2670	1121	1.06	0.45	0.5
steel	7.8	5900	3260	2.36	1.3	0.02

An ultrasonic wave in a homogenious medium is propagated in straight lines in the shape of a diverging beam. If a foreign medium, the dimensions of which are much smaller than the wave length, is encountered in its propagation path, the wave undergoes diffraction, i.e. it seemingly skirts the inclusion without any reflection (Fig. 135a). However, if the dimensions of this medium are equal to or exceed the wave length, then in the most common instance, both a partial reflection of the wave from the boundary with this medium, as well as penetration into it may be noted (Fig. 135b).

A foreign medium is any medium, the acoustical impedance of which is different from the acoustical impedance of the medium in which the wave is propagated.

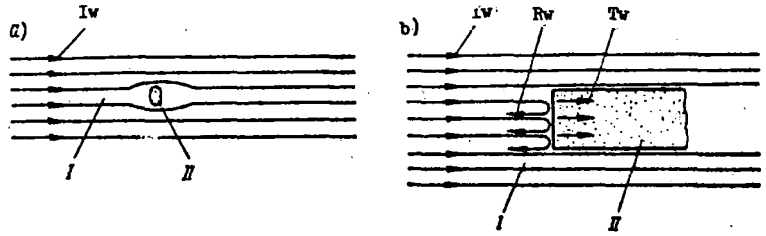

Fig. 135 Propagation of an ultrasonic wave in medium I, in which a foreign medium, II, is situated: a. dimensions of medium II much smaller than the wave length; b. dimensions of medium II equal to or greater than the wave length.

By acoustical impedance z we mean the produce to the wave velocity C times the density of the medium ρ, i.e.

$$z = C\rho. \tag{3}$$

It is obvious that the acoustical impedance of the same medium will be greater for a longitudinal wave than for a transverse wave.

The energy distribution between the reflected and the transmitted waves, when they fall on the boundary between two media, is determined primarily by the relationship of the acoustical impedances of these media.

The reflection coefficient (i.e. the ratio of the intensities of the reflected and the incident waves) when the wave strikes perpendicular to the edge of the boundary between these media is equal to

$$R = \left(\frac{z_1 - z_2}{z_1 + z_2}\right)^2. \tag{4}$$

When the acoustical impedances z_1 and z_2 are equal, the incident wave passes from one medium into the other without any losses from reflection.

The greater the difference in the acoustical resistances, the greater will be the intensity of the reflected wave.

According to formula (4) and the data in Table 9, the reflection coefficient from the boundary between steel and air and steel and water are 1.0 and 0.88 respectively for an ultrasonic wave. For practical purposes, the property for ultrasound to be completely reflected from the boundary between steel and water or air, which usually fill the flaws in rails, is employed in flaw detection in rails. Here, the ultrasound frequency is chosen to be such that the wave length in the rail is not greater than the minimum transverse dimensions of flaws subject to detection. Therefore, when monitoring the rails, ultrasonic vibrations with a frequency of 2 - 4 MHz, i.e. with a wave length of 0.8 - 2.8 mm, is usually used.

Plates made of a material possessing piezoelectric properties are used to excite and record ultrasonic vibrations at such frequencies. If the piezoelectric plate is subjected to compression or extension, electrical charges appear on its surfaces. The charge sign is determined by the nature of the deformation (compression or extension), and the magnitude by the force applied.

The conversion of mechanical deformations into electrical voltage is called the direct piezoelectric effect. The piezoelectric effect is reversible. The reverse piezoelectric effect is manifested in the change of the plate dimensions under the influence of an electrical voltage. The nature of the deformation is determined by the polarity of the voltage applied.

It is thus possible to transform electrical vibrations into ultrasonic, and conversely, ultrasonic into electrical, with the aid of a piezoelectric plate. The greatest transformational effect is achieved when the free vibration rate of the plate corresponds to the frequency of the electrical voltage being applied, or the frequency of the influencing ultrasonic vibrations.

The free vibration of the plate f_0 depends on the thickness of the plate d, and may be computed from the formula

$$f_0 = \frac{k}{d}, \tag{5}$$

where k is the vibration coefficient, depending on the material of which the piezoelectric plate is made.

Piezoelectric plates made of ceramic materials like barium titanate and lead zirconate titanate (PZT) are usually used for flaw detection in rails. For a plate of barium titanate, the vibration coefficient $k \cong 2.5$ MHz·mm, and for PZT, $k \cong 1.8$ kHz·mm. The piezoelectric properties of PZT plates are greater than the piezoelectrical properties of plates made of barium titanate.

One must note that plates made of barium titanate lose their piezoelectric properties at 120° C., and plates made from PZT lose theirs at 300° C. These properties may be restored by polarization of the plates.*

If an acoustical contact is created between a plate which is connected to an alternating voltage generator and the material, a longitudinal ultrasonic wave with a particle vibration frequency for the medium equal to the frequency of the applied electrical voltage will be excited in the material (Fig. 136a). Near the radiator, in the zone called the near field (the Fresnel field), the wave will be propagated without divergence. The center of the near field may be calculated from the formula

$$L_n = \frac{a^2}{\lambda} = \frac{a^2 f}{C}, \tag{6}$$

where a is the radius of the radiator.

In the far field of the zone, at a distance of approximately l_n from the radiator, gradual divergence of the rays begins, and the wave changes from

*The plate is maintained for four hours under the influence of a constant voltage, calculated at 1,000 v/mm thickness of the plate for polarization.

flat to spherical. The waye field takes on the form of truncated cone, half of the included angle being equal to (cf. Fig. 136a)

$$\varphi_{\nu} \approx 0{,}61 \frac{\lambda}{a}. \qquad (7)$$

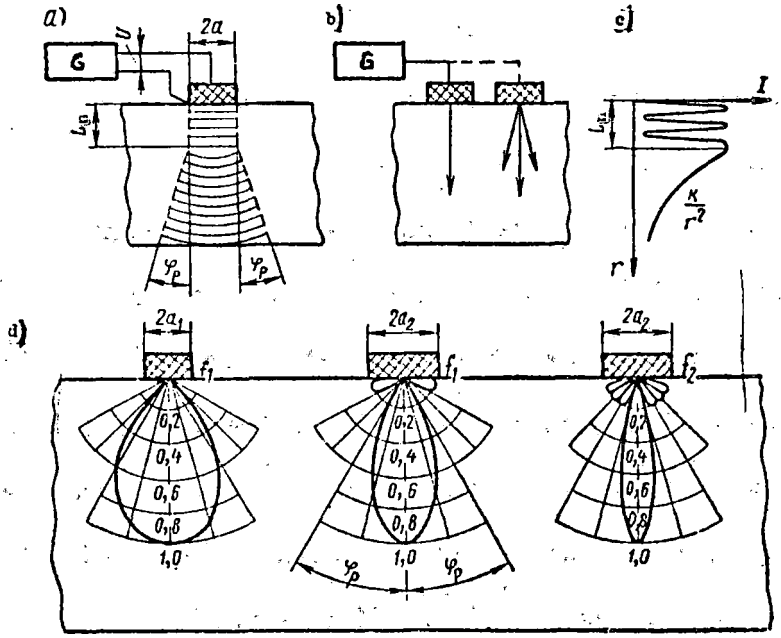

Fig. 136 Ultrasonic wave spreading. a - the field of an ultrasonic wave created by a round radiator, b - conventional representation of the ultrasonic wave c - intensity of the field I on the sensor axis, d - polar diagram of round radiators, under the condition that $a_1 f_1 < a_2 f_1 < a_2 f_2$.

At an ultrasound frequency of 2.5 MHz and with a radiator diameter of 12.5 mm, settings which are widely used in flaw detection in rails, the length of the near field in the steel is about 15 mm, and the divergence angle does not exceed 14°. Thus, ultrasonic vibrations propagate in the form of a slightly diverging, beam, called the ultrasonic ray. By convention, the ultrasonic ray is represented graphically by a straight line with an arrowhead, corresponding to the acoustical axis of the ultrasonic beam and indicating the direction of the wave propagation, or by using three lines, the middle line corresponding to the acoustical axis of the ultrasonic beam (Fig. 136b).

One must note that in the near field, the intensity of the ultrasonic field, both along the beam, as well as across its section, is unequally distributed and changes from point to point; in the far field, as a result of the divergence of

the ultrasound beam, the intensity falls off smoothly in inverse proportion to the square of the distance from the radiator (Fig. 136c).

As may be seen from formulae (6) and (7), the greater the directivity of the ultrasonic field, the higher will be the ultrasound frequency and the greater will be the radius of the radiator. The directivity of the field is conventionally represented as a graph in polar coordinates, which is called the directivity diagram, and which characterizes the angular dependence of the radiation intensity in the far field. The narrower the directivity diagram, the greater the ultrasound frequency and the greater the radiator radius, i.e. the greater the magnitude of the product af (Fig. 136d).

During flaw detection, it is occasionally necessary to introduce an ultrasonic wave at an angle to the surface of the item being inspected. To do this, a wedge with angle β, usually prepared from organic glass (plexiglass), is placed between the piezoelectric plate and the item being inspected.

In most common cases, the transfer of the longitudinal wave from the plexiglass into the steel as it falls on the separation boundary with angle β is accompanied by the appearance of four waves (Fig. 137a): two reflected (the longitudinal C_{l_1} and the transverse C_{t_1}) and two refracted (the longitudinal C_{l_2} and the transverse C_{t_2}). The angles of reflection and refraction, always calculated with regard to the perpendicular to the separation boundary between the two media, is associated with the angle of incidence by Snell's Law:

$$\frac{\sin\beta_l}{C_{l_1}} = \frac{\sin\beta_t}{C_{t_1}} = \frac{\sin\beta}{C_{l_1}}, \quad \frac{\sin\alpha_l}{C_{l_2}} = \frac{\sin\alpha}{C_{t_2}} = \frac{\sin\beta}{C_{l_1}}, \tag{8}$$

where C_{l_1} and C_{t_1} are the velocities of the longitudinal and transverse waves in the wedge;

C_{l_2} and C_{t_2} are the velocities of the longitudinal and transverse waves in the metal being inspected;

β_l and β_t are the angles of reflection of the longitudinal and transverse waves in the wedge; and

α_{l_2} and α are the angles of refraction of the longitudinal and transverse waves in the metal being inspected.

It follows from formula (8), that the angle of reflection for waves of the same type as the incident wave is always equal to the angle of incidence ($\beta_1 = \beta$); the angle of reflection for a wave of a type other than the incident wave, as well as the angles of refraction for these waves is greater, as the propagation velocity of these waves increases.

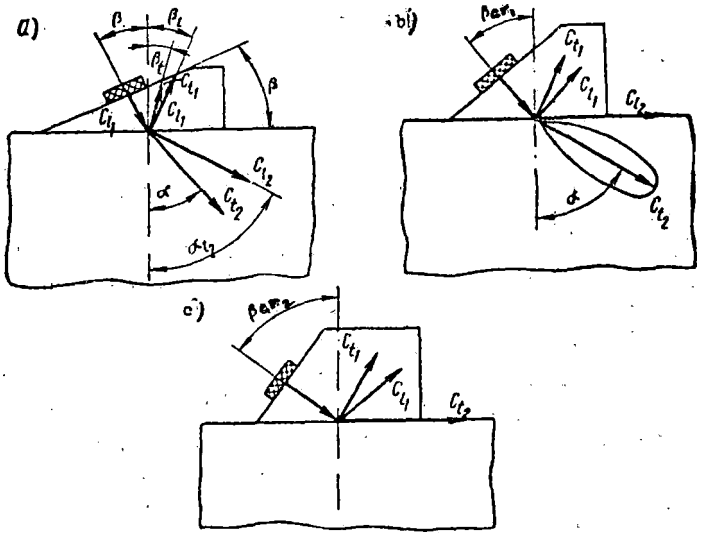

Fig. 137 Reflection and refraction of a longitudinal wave as it strikes the separation boundary between two solid media at an angle:
a - at $\beta < \beta_{cr_1}$; b - at $\beta = \beta_{cr_1}$; c - at $\beta = \beta_{cr_2}$.

As the angle of incidence is increased, beginning from a certain value β_{cr_1} (Fig. 137b), called the first critical angle, the refracted longitudinal wave will not penetrate into the second medium ($\alpha_{l_2} = 90^\circ$).

If the angle of incidence is further increased, there comes a moment (Fig. 137c) when the longitudinal wave begins to move along the interface;

the corresponding angle of incidence is called the second critical angle.

The values of the critical angles satisfy the equalities:

$$\sin \beta_{cr_1} = \frac{C_{l_1}}{C_{l_2}}; \quad \sin \beta_{cr_2} = \frac{C_{l_1}}{C_{t_2}}. \tag{9}$$

In the case when the incident wave passes from plexiglas into steel, these values are $\beta_{cr_1} = 29^\circ$ and $\beta_{cr_2} = 55^\circ$. At angles of incidence less than the second critical angle and greater than the first, only the transverse wave will arise in the second medium.

The fields of both the transverse and the longitudinal waves have a near and a far field. The polar diagram of the transverse wave field is narrower as the oscillation frequency and the diameter of the radiator are increased, and as the angle of incidence β is reduced.

The angle between the perpendicular to the surface of the item and the axis of the field directivity diagram for the transverse wave is called the beam transmission angle, and is designated by α. Approximate values of the transmission angle α for various values of the wedge angle may be calculated from formula (8), and more exact values may be measured experimentally.

Depending on the operating conditions of the electrical alternating voltage generator, both transverse and longitudinal waves may be introduced into the item being inspected either in a continous manner (Fig. 138a) or in the form of high-frequency pulses of a given duration τ (Fig. 138b,c). Ultrasonic vibration pulses emitted into the item being inspected are normally called transmitted pulses.

The piezoelectric plate is damped so that the duration of the transmitted ultrasonic pulse does not substanitally exceed the duration of the electrical voltage which is applied. The damper, the primary task of which is to increase attenuation of the free vibrations of the plate after the action of the electric exciter impulse on it, consists of a layer of textolite, asbestos, rubber,

or epoxy resin with a filler which contacts the opposite side of the plate. It is necessary to note that damping the plate is accompanied by a reduction in the effectiveness with which electrical energy is transformed into ultrasonic, or ultrasonic energy into electrical.

For convenience during inspection, and in order to avoid mechanically damaging or wearing out the piezoelectric plate, the latter, along with the damper, is put into special devices called probes. Probes intended to introduce a wave perpendicular to the surface of the item being monitored are normally called direct (or normal) probes, and those which introduce the wave at an angle are called angle, or prismatic, probes (cf. Fig. 139).

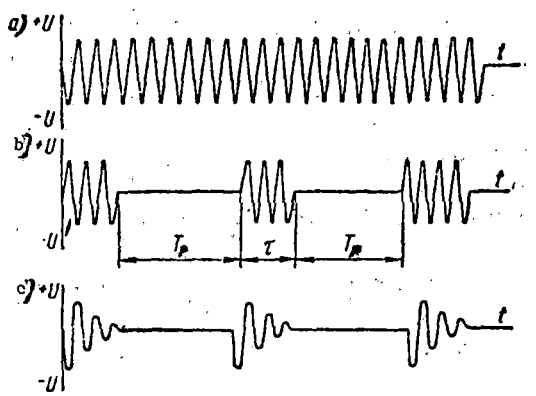

Fig. 138 Radiation.
a. continuous b. in the form of square pulses c. exponential form

The wedge angle of the angle probe is equal to the angle of incidence of the wave; it is always greater than the first, but less than the second, critical angle, and usually equal to 30, 40, 47, or 50 degrees.

The dimensions and the wedge configuration are chosen so that the ultrasonic longitudinal and transverse waves which are reflected into the prism are for practical purposes, completely damped inside of it.

It is necessary to note that the actual values of the transmission angles

for a longitudinal wave into steel is somewhat different from the values obtained when making calculations based on Snell's Law.

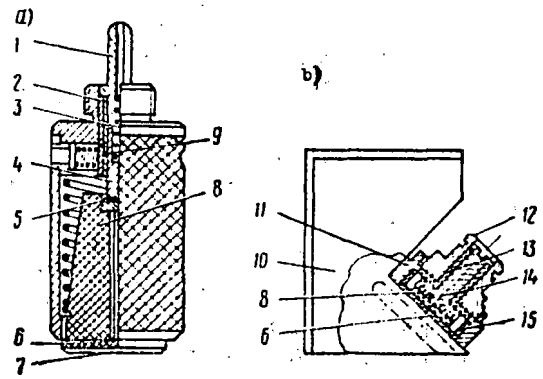

Fig. 139 Probes.
a. Normal b. Angle
1. connector; 2. bushing; 3. spring; 4. contact; 5. plate; 6. piezoelectric; 7. base; 8. damper; 9. braiding; 10. wedge made of transparent plastic; 11. housing; 12. conector; 13. insulation bushing; 14. contact cover piece; 15. insulation ring.

A graph from which the magnitude of the transmission angle may be determined for a transverse wave in steel, depending on the prism angle, is presented in Fig. 140.

An ultrasonic wave may not be introduced into any specimen being inspected if there is a thin layer of air between it and the probe, i.e. if there is no acoustical contact. An acoustical contact is usually obtained by occupying the space between the radiating surface of the probe and the specimen with a couplant. When acoustical contact is provided between the probe and the specimen, a wave, which is introduced into the specimen in the form of an ultrasonic vibration pulse, will reflect from the latter at an angle equal to the wave's angle of incidence on the reflecting surface (Fig. 141), upon reaching an internal discontinuity or a surface.

Propagation of the ultrasonic wave, or its multiple reflection between two surfaces in the item, will continue until the vibrations are completely damped. A part of the ultrasonic energy may return to the probe after reflection in the form of a pulse echo. The time interval T between the transmitted pulse and the pulse echo, also called the echo signal, is determined by the length of the path of the ultrasonic pulse in the item, and is equal to:

(for a normal probe) $$T = \frac{2l}{C_l}; \tag{10}$$

or, (for an angle probe)

$$T = \frac{2l}{C_t} + 2t_p, \tag{11}$$

where C_l and C_t are the velocity of the longitudinal and transverse waves, respectively;

l is the path traversed by the ultrasonic wave in the metal from the probe to the surface reflecting the wave back in the opposite direction; and

t_p is the time the ultrasonic pulse requires to pass through the probe wedge (in one direction).

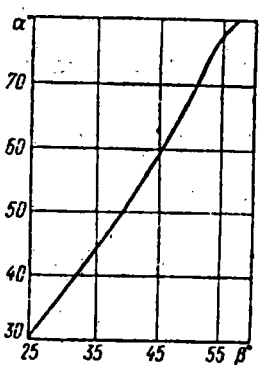

Fig. 140 The dependence of the transmission angle α of a transverse wave into steel on the prism angle β.

The path of an ultrasonic ray in metal being inspected and the corresponding voltage oscillograms are shown in Fig. 141. Instead of the high frequency pulses, their envelopes (i.e. the detected pulses) are represented. As will be shown below, this is what is usually observed on the flaw detector screens.

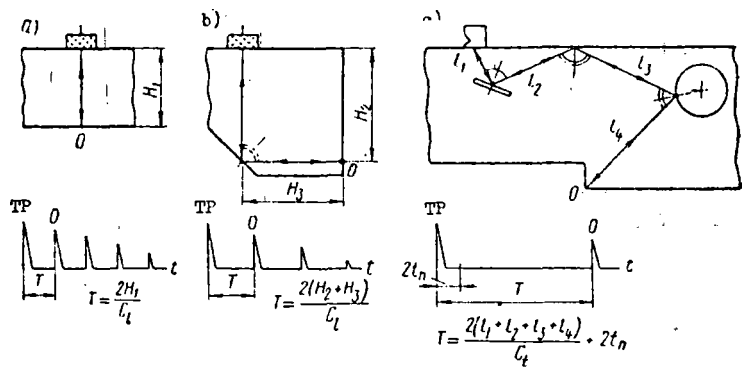

Fig. 141 The reflection of an ultrasonic wave when it is excited in an item being inspected: a, b -- by a normal probe; c -- by an angle probe; TP -- transmitted pulse; 0 -- pulse echo reflected from point 0.

NOTE: Diagrams of the propagation of an ultrasonic beam are presented in the upper part of figs. a, b, and c. In the lower part, the distribution of the ultrasonic pulses on the probe in time t are represented.

One must note that wave reflection will take place only at an angle equal to the angle of incidence. If the irregularities in the reflecting surface are much smaller than the wave length, such a surface is called a mirror surface, and a reflection from it is called a mirror reflection. If the irregularities in the surface are equal to the wave length, the reflection will be diffuse, the reflecting wave scattering in various directions at various angles. This explains the fact that the amplitude of a pulse echo from an irregular surface

is less than the pulse echo from a mirror surface when an ultrasonic wave strikes it perpendicular to the surface (Fig. 142a). At the same time, when an ultrasonic ray strikes at a certain angle to the separation boundary, the intensity of the ray reflected toward the sensor will be greater as the irregularities of the reflecting surface become more significant (Fig. 142b).

As follows from what has been said, it is possible to detect internal flaws by sending ultrasonic energy into an item and investigating the process of ultrasonic vibration propagation in it.

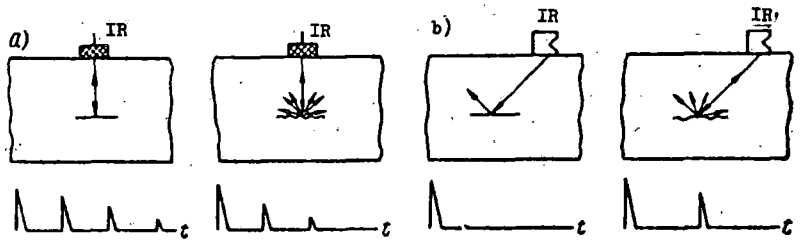

Fig. 142 Mirror and diffuse reflections when the wave strikes the reflecting surface: a. perpendicularly b. at an angle
NOTE: In the upper part of figures a. and b., the propagation pattern of the ultrasonic beam is represented, and in the lower portion is shown the distribution in time t of the ultrasonic pulses on the probe.

Three basic ultrasonic flaw detection methods are distinguished, corresponding to the trait by which the flaw is detected: the shadow method (Fig. 143a); the mirror-shadow method (Fig. 143b); and the pulse-echo method (Fig. 143c).

In the shadow method, the trait by which the flaw is detected is the decrease in intensity (amplitude) of the ultrasonic wave which passed through the specimen from the radiating probe I to the receiving probe R (cf. Fig. 143a). The probes are situated on opposite surfaces of the specimen making it possible to employ this method only if the specimen is accessible from two sides.

In the mirror-shadow method, the trait by which the flaw is detected is the decrease in intensity (amplitude) of the ultrasonic wave radiated by probe I, reflected from the opposite side of the item, and received by probe R (cf. Fig. 143b). An opposing surface which reflects ultrasound like a mirror is called the bottom surface, and the pulse reflected from it is the bottom pulse.

In the pulse-echo method, the trait by which the flaw is detected is the reception of a pulse-echo reflected from any given flaw by the probe R (cf. Fig. 143c).

If the detection of a flaw is determined both by the appearance of a pulse-echo from the defect and by a decrease in the bottom pulse, this means that the monitoring is being conducted simultaneously using two methods: the pulse-echo method and the mirror-shadow method.

When examining the methods, two probes were used in each case, one of which fulfilled the function of the radiator (I) and the other, the receiver function (R). A circuit of this type for hooking up the probes is called a separate circuit. At the same time, for the mirror-shadow and the pulse-echo methods, using only one probe IR, hooked up in a combined circuit, is possible during pulse radiation. Here the same probe fulfills the functions of radiating the transmitted pulse and receiving the pulse-echo (Fig. 144).

Presently, the pulse-echo and mirror-shadow methods are used for the most part.

2. Pulse-echo flaw detection.

The pulse-echo method of flaw detection is based on sending brief transmitted pulses of ultrasonic vibrations into the specimen being inspected and recording the reflections of these pulses (the pulse-echos) from the detected flaws. The amplitude of the pluse-echo depends on the dimensions of the flaw,

its depth in the rail, its form, its orientation, and the roughness of the reflecting surface.

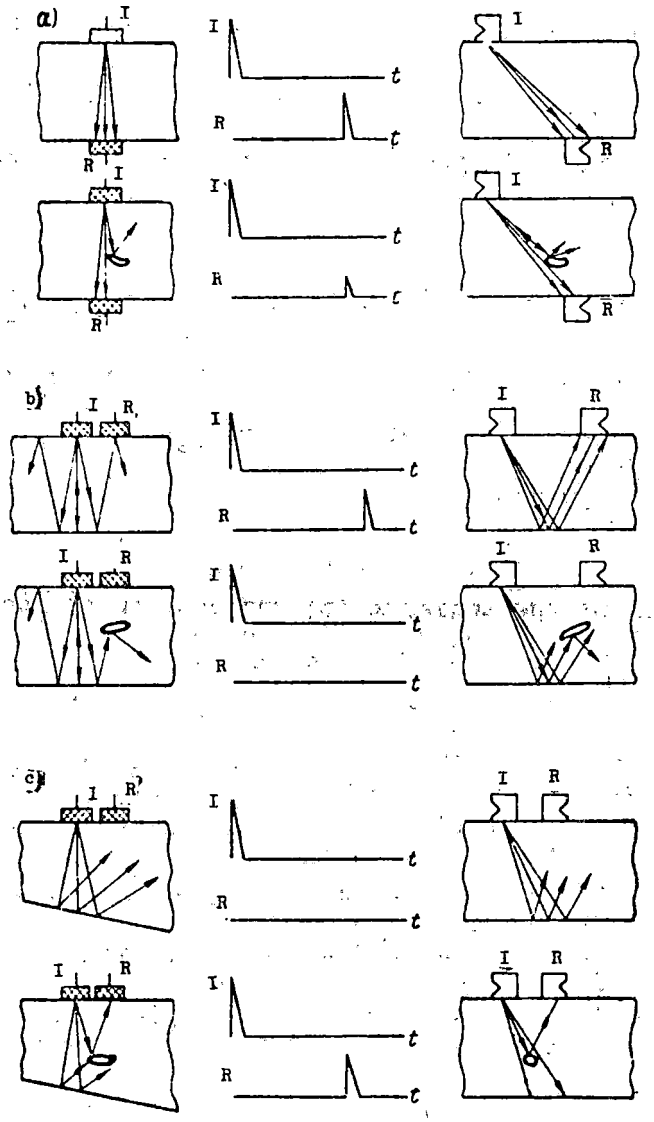

Fig. 143 Diagrams for transmitting a beam and distribution of the pulses in time t on the radiating I and the receiving R probes while inspecting using the a. shadow method; b. mirror-shadow method; c. pulse-echo method. The probes are hooked up in a separate circuit.

The amplitude of the pulse-echo grows as the dimensions of the flaw increase, until the dimensions of the flaw exceed the dimensions of the ultrasonic beam in the cross-section of which the flaw is situated (Fig. 145a).

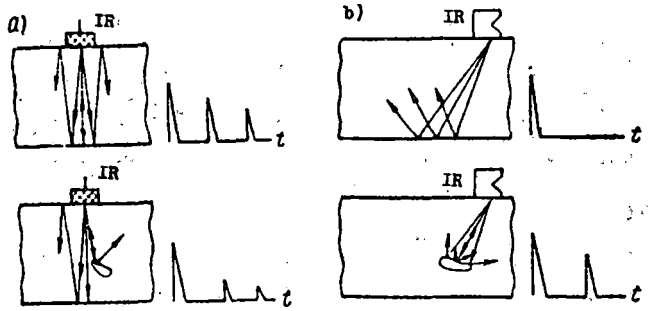

Fig. 144 Beam transmission and pulse distribution diagrams in time t on a probe IR, hooked up in a combined circuit while inspecting using the a. mirror-shadow method; b. the pulse-echo method

The amplitude of pulse-echos from flaws of the same size decreases as the distance o from the sensor to the flaw increases (Fig. 145b). The dependence of the pulse-echo amplitude U on the distance r when the flaw situated in the far zone is determined by the expression

$$U = kU_0 \frac{S_a}{r^n} e^{-2\gamma r} \qquad (12)$$

where k is a coefficient taking into consideration the flaw dimensions, the effectiveness of the transformation of electrical voltage into ultrasonic vibrations and back, and the quality of the acoustical contact;

S_a is the area of the piezoelectric plate;

U is the amplitude of the transmitted pulse: and

n is an exponent, the size of which depends on the configuration of the flaws: for flat flaws perpendicular to the acoustical axis of the probe and not substantially exceeding the dimensions of the piezoelectric converter, n = 1; for cylindrical flaws, the length of which exceed the

width of the ultrasonic beam, n = 1.5; for spherical or disc-shaped flaws, the dimensions of which are less than the diameter of the transducer, n = 2.

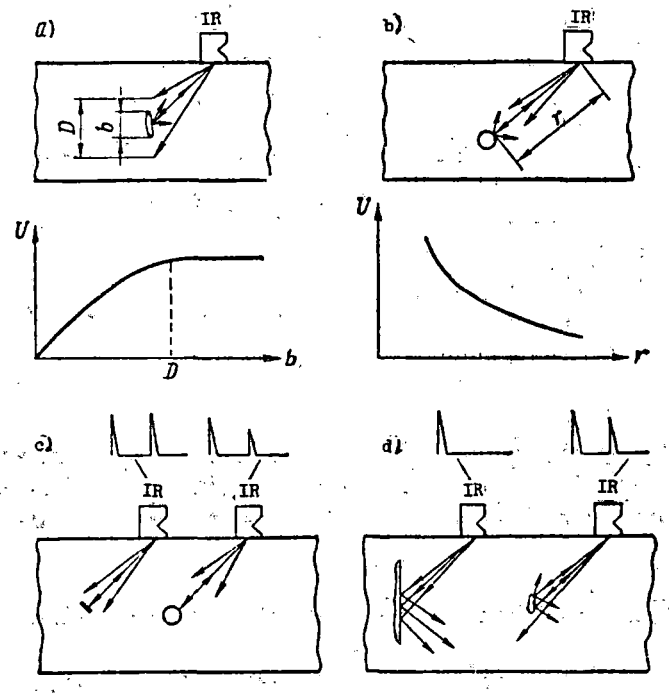

Fig. 145 Dependence of pulse-echo amplitude U;
a. on the dimensions of the flaw b. on the distance between the probe and the flaw c. on the configuration d. on the roughness of the flaw surface

When the flaw is lying at the same depth, the amplitudes of the pulse-echoes are to a large degree determined by the configuration of the reflecting surface of the flaw (Fig. 145c), and by the ratio of the size of the unevenness of the reflecting surface to the wave length (cf. Fig. 142). One must note that during flaw detection in rails, it is possible for the amplitude of the pulse-echo from a large flaw with a mirror reflecting surface to be substantially less than the pulse-echo from a small flaw with a diffusely reflecting surface (Fig. 145d).

In addition to the pulse-echo amplitude, the conditional length of the flaws and their location, i.e. the flaws' coordinates, are measurable characteristics of detected flaws. When inspecting using a normal probe, only the depth at which the reflecting surface (the flaw) is situated is measured. Here the depth H of the reflecting surface (Fig. 146a) is determined by the ratio

$$H = \frac{C_l t}{2}, \tag{13}$$

where t is the time an ultrasonic pulse takes to pass from the surface on which the probe is sitting to the reflecting surface, and back.

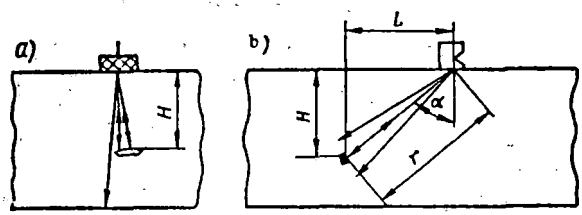

Fig. 146 Measurement of the flaw position coordinates during monitoring with:
a. normal probe b. angle probe

When sound waves are transmitted using an angle probe, the flaw coordinates (the depth H and the distance L from the radiation center of the probe) are determined by measuring the length of the path r which a pulse must traverse in the metal in one direction, and the subsequent conversion of this measurement into coordinates H and L, based on the known beam transmission angle (Fig. 146b). These magnitudes are associated by the relationships

$$H = r\cos\alpha = \frac{C_l t}{2}\cos\alpha = \frac{C_l (T - 2t_n)}{2}\cos\alpha; \tag{14}$$

$$L = r\sin\alpha = \frac{C_l t}{2}\sin\alpha = \frac{C_l (T - 2t_n)}{2}\sin\alpha, \tag{15}$$

where T is the time interval between the moment of transmitted radiation and the pulse-echo reception;

t_p is the propagation time for the ultrasound through the probe wedge;

t is the propagation time for the ultrasound in the metal.

At known values of C_t, t_p and α, determining the coordinates is reduced to measuring the time T, for which depth gages were included in modern flaw detectors. In a specialized apparatus, the depth meter scale is graduated directly in mm of depth H and distance L for determined values of α.

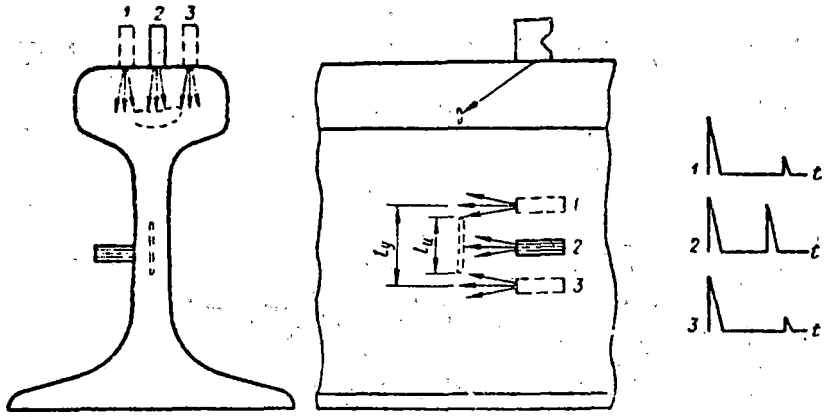

Fig. 147 Diagram of the measurement of the nominal length of a flaw.

The nominal length l_y is determined by the length of the probe displacement zone along the surface of the specimen being inspected, within the boundaries of which pulses from the detected flaw are fixed (Fig. 147). The nominal length l_y may be greater or less than l_u, depending on the nature of the flaw, its distance from the probe, the sensitivity of the flaw detector, and the quality of the acoustical contact.

The basic parameters of the pulse-echo method, which determine the reliability of ultrasonic rail inspection, are: the frequency of the ultrasonic vibrations; the dimensions of the piezoelectric converter; ultrasonic monitoring sensitivity, the accuracy with which the depth meter works, the probe indicator, the beam transmission angle, and the dead zone.

The frequency and the dimensions of the piezoelectric converter are determined by the type of flaw detector used, and, in practice, these remain unchanged while it is in use.

The remaining monitoring parameters are determined by adjustments to the apparatus and by its work capability. Actually, the sensitivity of any given flaw detector may vary greatly, depending on the service life of the tubes, the power supply voltage, etc. The accuracy with which the depth meter works may be reduced as a result of any failure of the electrical parameters of the circuit, and depends on the degree to which the true value of the beam transmission angle corresponds to the value taken when computing the depth meter scale. The beam transmission angle is determined by the wear on the probe wedge, the temperature of the surrounding environment, and other factors. In connection with this, it is necessary to check these basic monitoring parameters systematically on special calibrating devices.

In the Soviet Union, a set of standards, approved as GOST (State Standard Specification) 14782-69 "Welded Joint Seams. Methods for Ultrasonic Flaw Detection" is used for calibrating the basic monitoring parameters.

We will examine each of the parameters which is subjected to calibration and the order of calibration.

Sensitivity. In ultrasonic flaw detection, actual, boundary, and nominal sensitivity are distinguished. Actual sensitivity determines the minimum dimensions of flaws of various types which are reliably detected in items or compounds of certain type. It may be evaluated by statistical processing of the monitoring results and metalographic investigations of a series of objects of this type.

Boundary sensitivity determines the minimum dimensions of an artificial, optimal (from the standpoint of detectability) reflector (a flaw model) which

is still reliably detected in the item at the given instrument setting. The area S (in mm^2) of a hole with a flat bottom oriented perpendicularly to the acoustical axis of the probe is used as a unit for measuring the boundary sensitivity. The hole is bored into a test sample of the given item (Fig. 148a).

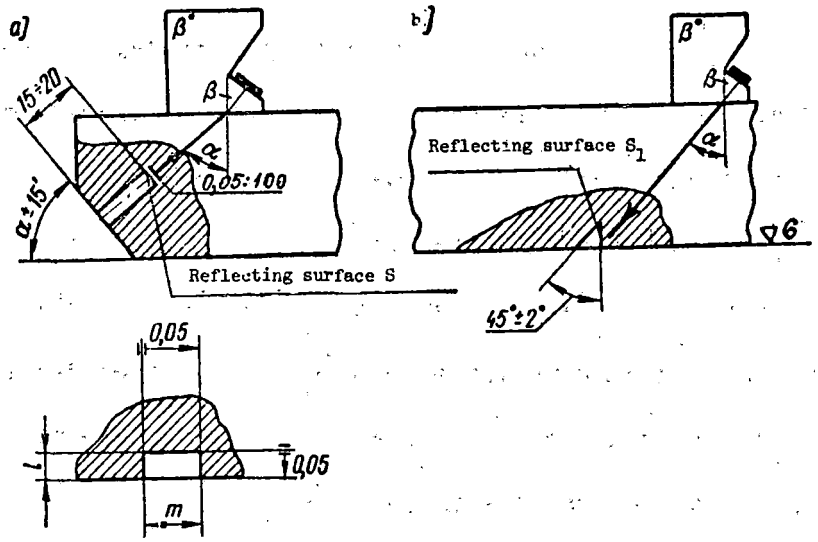

Fig. 148 Artificial reflectors
a. in the shape of a hole with a flat bottom b. an angular reflector

Due to the complexity of preparing a hole with a flat bottom precisely, when using angle probes to evaluate the boundary sensitivity, an angular reflector may be employed (Fig. 148b).

The area S of a flat-bottomed hole is associated with the equivalent area S_1 of an angular reflector by the relationship $S \approx NS_1$, where N is a coefficient equal to 2.5 for a probe with a wedge angle of 30-35°; 1.5 for a probe with a wedge angle of 37-40°; and 0.5 for a probe with a wedge angle of 49-50°.

An angular reflector may be relatively easily prepared with the aid of a chisel fashioned, for example, from a turning tool (R-18 steel).

The nominal sensitivity is characterized by the size and the depth at which previously mounted artificial calibration reflectors made in the calibration sample from a material with definite, strictly specified acoustical properties (which are reliably detected by flaw detectors), are situated.

Calibration Standard No. 1 (Fig. 149) is used for standardizing the nominal sensitivity. The nominal sensitivity of a flaw detector and probe, as measured on Calibration Standard No. 1, is expressed in terms of the maximum depth K (in mm) at which a cylindrical reflector reliably registered by all of the flaw detector indicators is situated (the sensor in position A, Fig. 149).

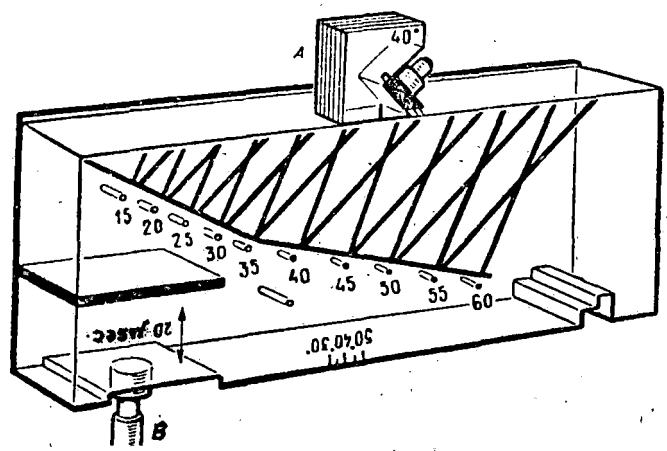

Fig. 149 The No. 1 Calibration Standard

If the actual and the boundary sensitivities determine the sensitivity of the method as a whole when inspecting a specimen of a given type, the nominal sensitivity characterizes only the sensitivity of the flaw detector and probe. It is apparent that the boundary sensitivity may always be converted into nominal sensitivity. To do this, having adjusted the flaw detector to the given boundary sensitivity based on a test sample, it is nesessary to transfer the probe to a No. 1 Calibration Standard and establish which openings are reliably detected at the given instrument setting. The hole with the highest number which is

reliably detected by the flaw detector indicators gives the nominal sensitivity of the device with the given sensor. Thus, a definite value for the boundary sensitivity corresponds to each value of the nominal sensitivity. It is necessary to remember that the boundary sensitivities of two instruments adjusted to the same nominal sensitivity will be identical if the ultrasound frequency, the wedge angle, and the dimensions of the probes of these devices are equal.

In many instances, the flaw detector sensitivity is adjusted based on test samples in which cylindrical holes or saw cuts are made. We will call this type of sensitivity equivalent sensitivity.

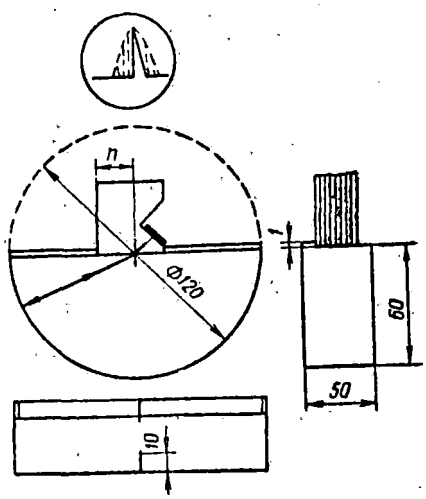

Fig. 150 Calibration Standard No. 3.

The precision of the depth meter is characterized by the relative error in measuring the time interval between the moment at which the transmitted pulse is radiated and the moment its reflection is received with regard to the true value of the measured magnitude, and it is determined on a No. 1 Calibration Standard (Fig. 149, pos. B).

In the absence of a calibration standard, the depth meter accuracy may be checked with any sample where the dimensions and the ultrasound speed in the item are known.

The probe indicator (n) is the distance from the point at which the acoustical axis of the ultrasonic beam (the radiation center) emerges to the front edge of the probe (Fig. 150). A calibration standard made of mild steel is used to determine the beam emergence point.

The beam emergence point is situated on the probe opposite the center of the semi-circle of the No. 3 Calibration Standard when the probe is mounted in the position at which the pulse-echo amplitude from the cylindrical surface is maximum.

The angle between the perpendicular to the surface on which the probe is mounted and the line connecting the center of the cylindrical reflector with the beam insertion point when the probe is mounted in the position at which the pulse-echo amplitude from the reflector has a maximum value is called the ultrasonic beam transmission angle (α).

The beam transmission angle is measured on a No. 2 Calibration Standard (Fig. 151) made from metal with the same acoustical properties as the metal being inspected. The angle α is directly calculated on the calibration standard scale opposite the radiation center mark of the probe[1]. A sample cut from the rail web may be used as a sample of the metal being inspected.

The dead zone is determined by the minimum depth at which a flaw may be situated so that the pulse-echo from it does not correspond in time with the transmitted pulse. The size of the dead zone depends on the duration of the transmitted pulse, and, for angle probes, also on the prism construction.

Actually, it is necessary that the time T which passes between the instant of radiation of the transmitted pulse and the instant at which the pulse-echo returns be greater than the duration of the ultrasonic pulse τ, so that the

[1]A No. 1 Calibration Standard and the scale from a No. 2 Calibration Standard are included in the DUK-11IM, DUK-13IM, and UZD-NIIM-6M devices.

pulse-echo from the flaw can be perceived distinctly from the transmitted pulse.

Time $\underline{T}$ is associated with the depth at which the flaw is situated by the relationships:

for a normal probe

$$T = \frac{2H}{C_{l_2}};$$

for an angle probe

$$T = \frac{2H}{\cos \alpha C_{t_2}} + 2t_p.$$

Setting the value of time $\underline{T}$ equal to the duration of the ultrasonic pulse $\underline{\tau}$, we abtain the value for the size of the dead zone M:

when working with a normal probe

$$M = \frac{C_{l_2}\tau}{2}; \tag{16}$$

when working with an angle probe

$$M = \frac{1}{2} C_{t_2} \cos \alpha (\tau - 2t_p). \tag{17}$$

When $\underline{\tau}$ is $\leq 2t_p$, which occurs in the angle probe designs which are used, there may not be a dead zone if the ultrasonic vibrations which were reflected in the probe wedge are fully damped after multiple reflection and do not return to the piezoelectric plate. The presence of pulse-echos appearing in the probe wedge as a result of multiple reflections of the transmitted pulse makes the registration of pulse-echos from flaws situated close to the surface impossible, thereby creating a dead zone 3 - 10 mm in size. The size of the dead zone depends on the beam transmission angle and the dimensions of the reflector.

When working with an angle probe, the dead zone is normally defined as the minimum depth at which a cylindrical reflector may be situated so that the pulse-echo from it may be distinguished from the transmitted pulse, and from the pulse-echos from noises returning from the wedge. A cylindrical reflector 2 mm in diameter and with a length greater than the width of the ultrasonic beam should be bored into a specimen made from the material being inspected. To test

the size of the dead zone when monitoring the rails, cylindrical reflectors are made in a No. 2 Calibration Device, as shown in Fig. 151. The basic parameters of the pulse-echo method are summarized in Table 10, and the accepted symbols and units of measurement are indicated.

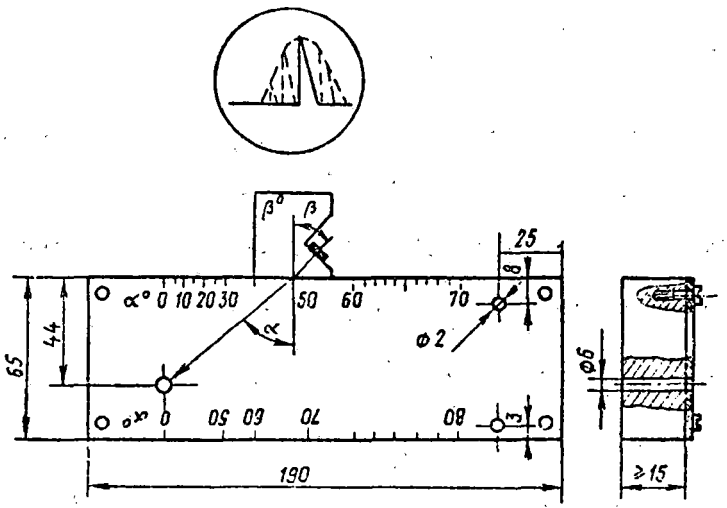

Fig. 151 A No. 2 Calibration Standard

Table 10

Basic inspection parameters							
	pulse-echo method			mirror-shadow method			
parameter	conventional symbol	unit	rough value	parameter	conventional symbol	unit	rough value
ultrasound frequency	f	MHz	2—3	ultrasound frequency	f	MHz	2—3
sensitivity; boundary	S	mm²	5—30	sensitivity; boundary	K_{dm}	—	0,0—0,8
nominal	K	mm	15—50	nominal	K_y	—	0,0—0,8
beam insertion angle	α	deg.	0—65	beam insertion angle	α	deg.	0—40
converter dimensions	a	mm	3—10	converter dimensions	a	mm	3—10
working accuracies of depth meter	A	%	2—5				
dead zone	M	mm	3—8				

The pulse-echo method is widely used when inspecting the rails to detect welding flaws and transverse cracks which develop in the rail head in rails on the line. However, this method does not permit detection of numerous flaws which are reliably detected by the mirror-shadow method.

3. Mirror-shadow flaw detection.

Mirror-shadow flaw detection may be accomplished using the following:

1) a normal probe and the first bottom pulse of the longitudinal wave

2) a normal probe and the second bottom pulse of the longitudinal wave

3) two angle probes and the bottom pulse of the transverse wave

4) two angle probes and the bottom pulse of the longitudinal wave.

With any monitoring method, the bottom pulse-echo amplitude varies somewhat as the probe is being moved, due to the acoustical contact being broken, and it falls off sharply when a flaw is detected (Fig. 152). Therefore, in all cases, a predetermined number of decreases in the bottom pulse, may, and should be considered the sign of a flaw.

The larger the flaw, the more significant is the reduction in magnitude of bottom pulses caused by this defect.

For a bottom pulse, the magnitude of reduction may be evaluated by a reduction coefficient K_c equal to

$$K_c = \frac{U_b}{U_0}, \tag{18}$$

where U_o is the bottom pulse amplitude when no defect is present;

U_b is the minimum amplitude of the same bottom pulse when the flaw is situated in the ultrasonic beam zone.

The reduction magnitude K_c caused by the same flaw will be different using different monitoring methods. The reduction coefficient when monitoring with the first bottom pulse is usually used for qualitative evaluation of the detec-

tability of flaws. This coefficient is called the flaw detectability coefficient, and it is denoted by K_d.

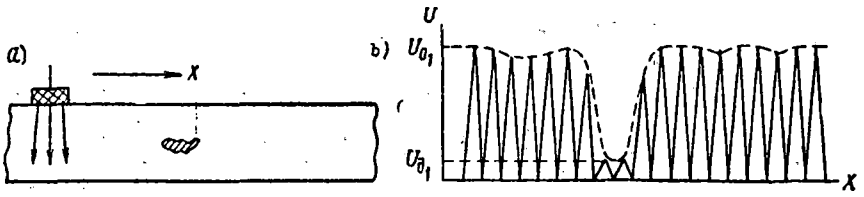

Fig. 152 Monitoring using the mirror-shadow method: a. Probe movement diagram; b. Picture of the amplitude change U of the bottom pulse-echo at various probe positions x.

The size of the coefficient K_d changes between 0 and 1; it is smaller as the flaw is larger. For flaws, the dimensions of which are substantially smaller than the wave length, $K_d = 1$; if the flaw covers the ultrasonic beam completely, $K_d = 0$. Thus, it is possible to evaluate the dimensions of a flaw based on the size of the detectability coefficient in certain instances. For any means of monitoring, the detectability of the flaw is better, i.e. the sensitivity is greater, as the bottom pulse reduction, based on which the monitoring is conducted, is more significant. The dependencies of the bottom pulse attenuation coefficients when detecting flaws at various depths using the methods indicated above are shown in Fig. 153. Analyzing the figure, the following conclusions may be drawn:

1) The sensitivity of the mirror-shadow methods are less than the sensitivity of methods using normal probes, other conditions being equal

2) When using angle probes, the sensitivity is greater as the angle at which the ultrasonic beam is transmitted into the metal is smaller

3) The method based on passing a transverse sound wave through the rail with the aid of angle probes is the least sensitive, other conditions being equal

4) That method of monitoring based on the second bottom pulse is the most sensitive; the sensitivity of this method to flaws situated at shallow depths approaches the sensitivity of the monitoring method using a normal probe and the first bottom pulse

5) The sensitivity of all four methods increases as the depth at which the flaw is situated and the thickness of the item decrease.

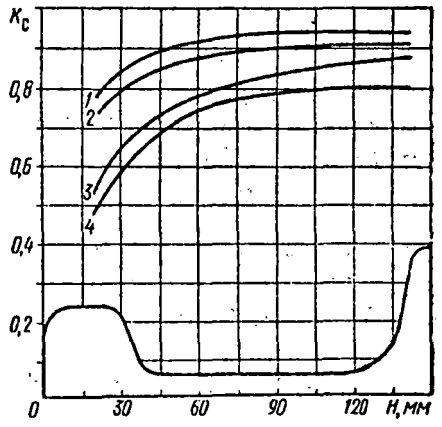

Fig. 153 Dependencies of the reduction coefficient K_c of the bottom pulse amplitude on the depth H at which a flaw is situated when using the mirror-shadow monitoring method: 1. angle probe, $\alpha = 40^\circ$; 2. angle probe, $\alpha = 2^\circ$; 3. normal probe using the first bottom pulse; 4. normal probe using the second bottom pulse.

It is necessary to note that when the flaw is situated on the acoustical axis of the probe, the sensitivity of the mirror-shadow method increases with an increase in the directivity of the probe field, i.e. with an increase in the ultra-sound frequency and the size of the transducer.

In practice, instances when the detected flaws are struck by the side part of the ultrasonic beam are probable. Such flaws are frequently encountered in rails in the form of cracks developing from the surface of the web. Fig. 154 illustrates the detection of these flaws.

In the process of flaw development (or, in the process of the probe approaching the flaw, which is the same thing), the distance X from its edge to the beam axis becomes equal to $|X_o| \simeq l \tan \phi_i$, where ϕ_i is one half of the included angle of the primary lobe of the probe directivity patern, the bottom pulse begins to decrease. If the edge of the flaw reaches the axis of the diagram ($X = 0$), the detectability of this flaw is $K_d \cong 0.5$; finally, when the flaw covers the beam entirely ($X \geq 2|X_o|$), the detectability coefficient will be equal to zero ($K_d = 0$).

Considering that, for the probes used during flaw detection in rails, $\tan \phi_i \approx \phi_i$, since $\phi_i < 9^\circ$, and that

$$\varphi_p \approx 0{,}61 \frac{\lambda}{a} \approx 0{,}61 \frac{C_{l_2}}{af},$$

we obtain

$$|X_0| \approx 0{,}61 C_{l_2} \frac{l}{af}. \qquad (19)$$

It is apparent that the greater the value of X_o, the smaller the dimensions necessary for a crack developing from the lateral surface of the item to be detected. As follows from equation (19), X_o is greater, and consequently, the detectability of the flaws being examined is better as the depth at which they lie is greater, and as the parameter af is less, i.e. as the directivity of the probe field is smaller. The relationships $K_d = F(X)$, which clarify the statement, are shown in Fig. 154. Naturally, the sensitivity of the monitoring method using the second bottom pulse to flaws detected by the side part of the ultrasonic beam, as well as to flaws situated on the axis of the beam, is greater than the sensitivity of the monitoring method based on the first bottom pulse.

Thus, given the same flaw detector parameters, the sensitivity for the monitoring method using the second bottom pulse is, as a rule, higher than the sensitivity of the monitoring method using the first bottom pulse.

In the mirror-shadow method, following the analogy of the pulse-echo method, it is necessary to distinguish three concepts of sensitivity; true sensitivity, boundary sensitivity, and nominal sensitivity. Here the boundary sensitivity is characterized by the maximum value detectability coefficient K_{dm} of flaws which are detected by the instrument at a given setting.

The nominal sensitivity of a mirror-shadow flaw detector is determined by the maximum magnitude of the coefficient K_y, which is analogeous to K_d, and which determines the minimum relative reduction of the bottom pulse registered by the flaw detector indicator, i.e.

$$K_y = \frac{U_m}{U_o}, \tag{20}$$

where U_o is the bottom reflection amplitude (of the first, second, ..., n-th); and

U_m is the amplitude of the same bottom reflection, but reduced until a signal appears in the flaw detector indicator ($U_m < U_o$).

It is apparent that the sensitivity of the flaw detector is greater as the value of K_y is greater.

For measuring and calibrating the nominal sensitivity of a mirror-shadow flaw detector, it is expedient to use a calibrated attenuator connected to the input of the receiving channel of the flaw detector, as is shown in Fig. 155.

Under normal conditions, a bottom pulse, the amplitude of which is U_o, is fed into the receiving channel input without reduction. When the button is pushed, the bottom pulse amplitude on the receiving channel input is diminished to U_n using the attenuator contact blade. If the attenuator contact blade is set so that the flaw detector indicator is activated, the magnitude of the bottom pulse reduction U_n/U_o may be read off on the attenuator scale, i.e. this is the nominal sensitivity of the flaw detector. This type of attenuator, which is essentially a flaw simulator in the mirror-shadow flaw detector,

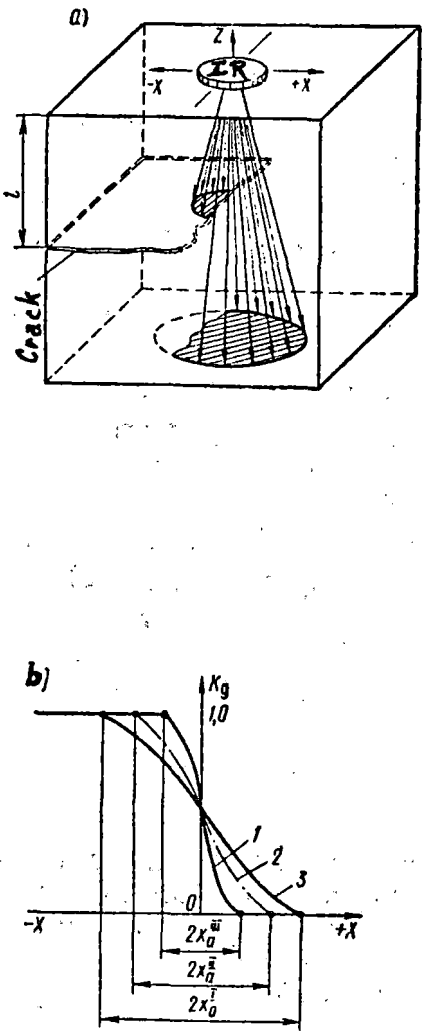

Fig. 154 Detection of flaws developing from the lateral surface of an item:

a. flaw inspection diagram; b. dependence of the detectability coefficient K_d at various depths l at which the flaw is situated, and various parameters af of the sensor; 1 - for $l = l_1$ and $(af)_1$; 2 - for $l = l_1$ and $(af)_2$; 3 - for $l = l_2$ and $(af)_2$; $l_2 > l_1$ and $(af)_2 < (af)_1$.

allows the following operations to be conducted:

1) adjustment of the flaw detector to a given sensitivity without using a calibration device;

2) checking the nominal sensitivity of the flaw detector while in use; and

3) measurement of the detectability coefficient of the noted flaw and evaluation of its dimensions/size at the same time.

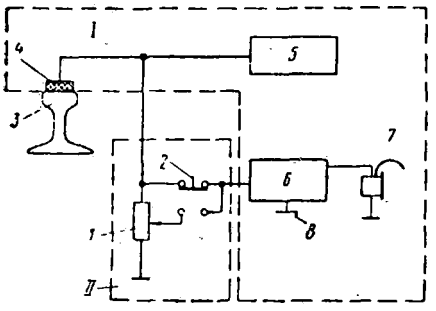

Fig. 155 Circuit diagram of the flaw simulator.
I - ultrasonic mirror-shadow flaw detector II - flaw simulator
1. attenuator; 2. button (switch); 3. monitored item (rail); 4. probe; 5. ultrasonic vibration generator; 6. receiving channel; 7. audio indicator; 8. sensitivity adjustment handle.

One must note that when inspecting using the first bottom pulse, the nominal sensitivity corresponds to the boundary sensitivity ($K_y = K_{dm}$), and that, at this point, the boundary sensitivity may not be higher than the nominal sensitivity.

When monitoring with a normal probe using the second bottom pulse, the boundary sensitivity is substantially higher than the nominal, and it is determined by the relationship $K_{dm} \approx \sqrt{K_y}$.

Thus, for example, when adjusting the flaw detector to the nominal sensitivity at which activation of the indicator takes place with a decrease in any bottom pulse by a factor of two ($K_y = 0.5$), flaws with a detectability coefficient $K_d \approx K_y \approx 0.5$ will be detected when monitoring using the first

bottom pulse whereas, when monitoring using the second bottom pulse, flaws with a detectability coefficient $K_d = \sqrt{K_y} = \sqrt{0.5} \approx 0.7$ will be detected.

The maximum nominal sensitivity to which the instrument may be adjusted is determined by the level of interference arising while monitoring the rails. When monitoring using the mirror-shadow method, all interference may be classified into five basic categories (Fig. 156):

1) Interference caused by breaking the acoustical contact due to mechanical damage or dirty contact surfaces (Fig. 156a)

2) Interference arising as a result of changes in the reflecting properties of the bottom surface (Fig. 156b)

3) Interference associated with the change in the ultrasound damping because of structural nonhomogeneities in the metal being monitored (Fig. 156c)

4) Interference conditioned by localized areas where the contact and bottom surfaces are not parallel (Fig. 156d)

5) Interference appearing when the sensor is transversely displaced when monitoring items, the width of which is equal to the diameter of the ultrasonic beam (Fig. 156e).

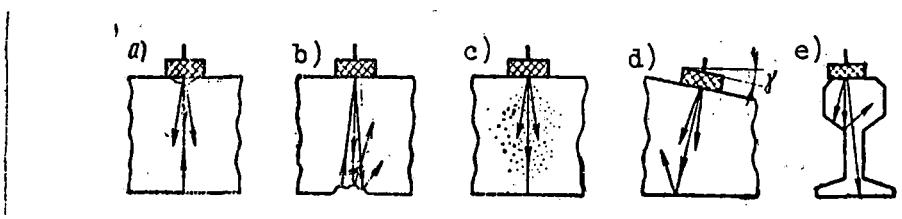

Fig. 156 Illustrations of conditions causing interference when using the mirror-shadow monitoring method: a. Broken acoustical contact b. Change in the reflecting properties of the bottom surface c. Localized structural changes d. Localized areas where the contact and bottom surfaces are not parallel e. Transverse probe displacement

The interference level may be evaluated by an interference coefficient equal to

$$K_i = \frac{U_i}{U_o} \tag{21}$$

where U_o is the amplitude of the bottom reflection (of the first, second,..., n-th) when there is no interference; and U_i is the minimum amplitude of the same reflection in the presence of interference.

The least value of the interference coefficient corresponds to the greatest interference. For each of the enumerated interference types, these coefficients are equal, respectively, to:

$$K_{ia} = \frac{U_{ia}}{U_0} = \frac{U_0 - \Delta U_a}{U_0}; \tag{22}$$

$$K_{is} = \frac{U_{is}}{U_0} = \frac{U_0 - \Delta U_s}{U_0}; \tag{23}$$

$$K_{ib} = \frac{U_{ib}}{U_0} = \frac{U_0 - \Delta U_b}{U_0}; \tag{24}$$

$$K_{in} = \frac{U_{in}}{U_0} = \frac{U_0 - \Delta U_n}{U_0}; \tag{25}$$

$$K_{id} = \frac{U_{id}}{U_0} = \frac{U_0 - \Delta U_d}{U_0}, \tag{26}$$

where U_{ia}, U_{is}, U_{ib}, U_{in}, U_{id}, are, respectively the amplitudes of bottom pulse-echos when the acoustical contact has been broken, when the structure deteriorates, when the status of the bottom surface changes, when the surfaces are not parallel, or when the probe has been displaced; and ΔU_a, ΔU_s, ΔU_b, ΔU_n, ΔU_d are, respectively, decreases in the bottom pulse-echo amplitude when the acoustical contact has been broken, when the structure deteriorates, when the condition of the bottom surface changes, when the surfaces are not parallel, or when the probe is displaced.

Given the simultaneous effect of a number of different types of interference, the total interference is equal to:

$$K_{i\Sigma} = K_{ia} \cdot K_{is} \cdot K_{ib} \cdot K_{in} \cdot K_{id} \tag{27}$$

Other conditions being equal, the interference resistance of any method will be greater as the size of the coefficient $K_{i\Sigma}$ increases.

It is apparent that of all the mirror-shadow methods, that means which assures the maximum interference resistance quality and sensitivity under equal conditions will be optimal.

Taking into account that in rail flaw detection, the means of monitoring using the first, as well as the second bottom pulse has found the greatest applicability, we will examine their non-interference properties.

Interference caused by a break of the acoustical contact (dirtying of the surface, pitted places, engine burns, etc.) is analogeous in its effect to a sub-surface flaw. Inasmuch as the methods under investigation are similarly sensitive to such flaws, the interference coefficients should be the same, i.e. $K^{I}_{ia} = K^{II}_{ia}$, other conditions being equal. The values of the interference coefficients caused by breaking the acoustical contact are presented in Fig. 157 as an example.

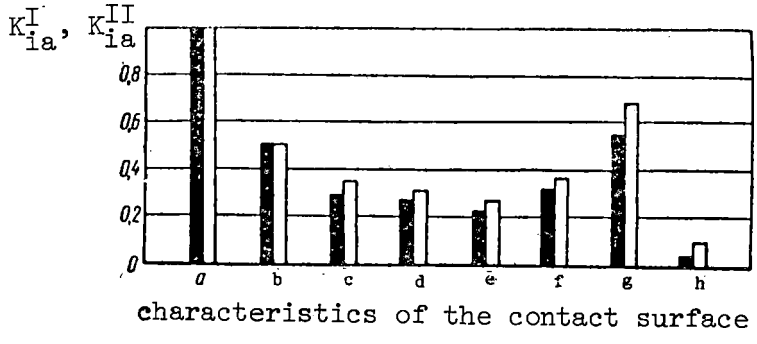

Fig. 157 Dependence of the interference coeffieients K^{I}_{ia} and K^{II}_{ia} on the condition of the surface. a. clean; b, c, d, e -- covered, respectively, with one, two, three, and four layer of oiled tracing paper; f, g, h -- covered with a 0.4 mm layer of oil, corundum, and earth; black column - first bottom pulse; white column - second bottom pulse.

As may be seen from Fig. 157, the interference coefficient when monitoring using the second bottom pulse-echo is not lower than when monitoring using the bottom pulse. In addition, it turns out that the interference resistance qualities when the contact surface is dirty is somewhat higher when using the second bottom pulse than when using the first. This is explained by the fact that the loss of energy in the contacting layer for the first as well as the second bottom pulse are the same; at the same time, dirtying the surface leads to a decrease in the pulse amplitude when the first bottom pulse is reflected from the contact surface.

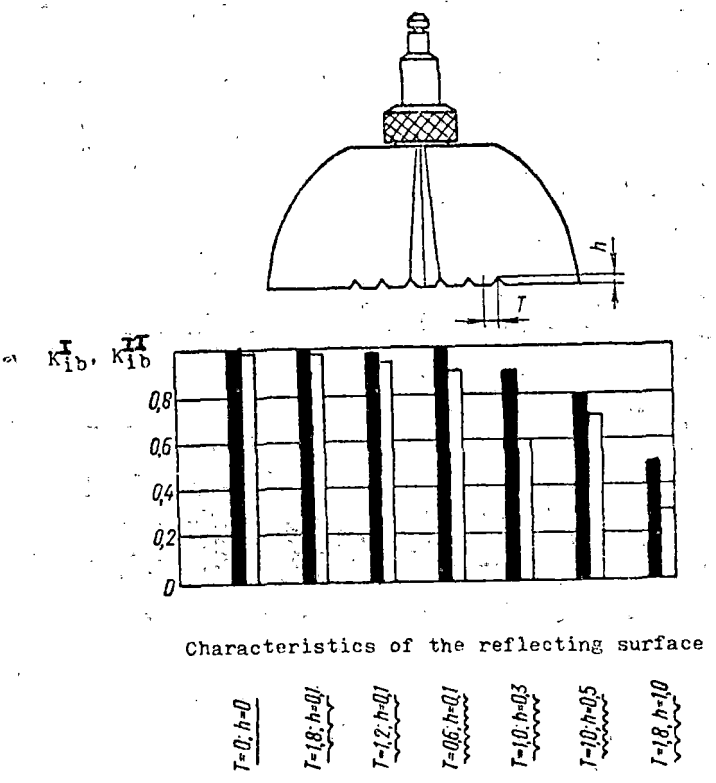

Fig. 158 Dependence of the interference coefficients K_{ib}^{I} and K_{ib}^{II} on the nature and size of the unevenness of the bottom surface of the samples.

Interference caused by a change in the reflecting properties of the reflecting surface (corrosion of the base, a thin layer of water between the cross tie and the rail base, etc.) is equivalent to the effect of a flaw situated near the bottom surface (Fig. 158); in connection with this, $K_{ib}^{II} \approx (K_{ib}^{I})^2$.

The welded joint is the basic cause for the appearance of interference associated with structural nonhomogeniety. Attenuation of the bottom pulse caused by dispersion of the ultrasound on the structure of the welded joint is, as a rule, equal to, and in some cases exceeds, the attenuation caused by an internal flaw.

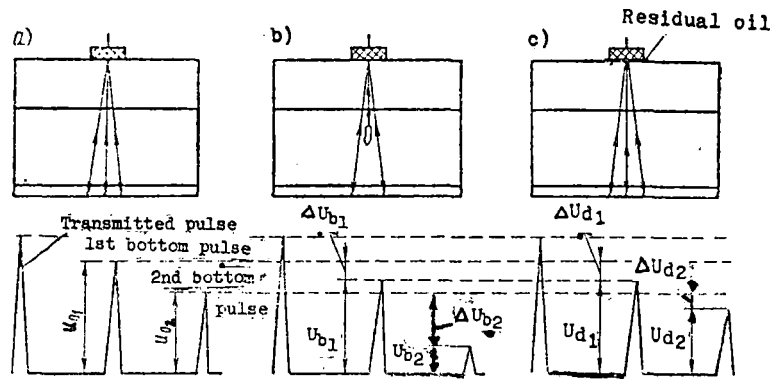

Fig. 159 Illustration of the detection of a flaw when monitoring using the first and second bottom pulses: a. on a section without a flaw; b. when there is a flaw present; c. when the acoustical contact is broken.

It has been established that the interference resistance of the monitoring method which uses the second bottom pulse to interference associated with transverse probe displacement and with localized areas where the running surface of the rail head and the rail base are not parallel, is not lower than the interference resistance when monitoring using the first bottom pulse. At the same time, the interference resistance of the monitoring method using the second bottom pulse to non-parallelism due to corrugation is less than the corresponding interference resistance of the monitoring method using the first bottom pulse.

The facts expounded above permit us to draw the conculsion that, in comparison with the monitoring methods using the first bottom pulse, the monitoring method using the second bottom pulse has not only a greater sensitivity, but, in many cases, has better interference resistance. In connection with this, when monitoring using the second bottom pulse, flaws in rails with a dirty surface, which would not be detected when monitoring with the first bottom pulse, may be discovered (Fig. 159).

The basic parameters of the mirror-shadow method of rail monitoring are presented in Table 10.

The detectability coefficient of the flaw and the nominal length of the flaw at an assigned nominal flaw detector sensitivity are related to the basic measurable characteristics of flaws detected using the mirror-shadow monitoring method.

4. Principles for constructing ultrasonic flaw detectors.

Flaw detectors intended for ultrasonic rail monitoring are based on the mirror-shadow and pulse-echo methods. With any method, the introduction of ultrasonic vibrations from the probe into the metal takes place through the running surface of the rail head.

It is necessary to distinguish three zones in the rails, from the point of view of distinguishing features of ultrasonic monitoring: the welded joint zone, the bolted joint zone, and the remainder of the rail, normally called the parent metal zone.

Defects in the parent metal in the web zone and its continuation into the head and the base are, as a rule, vertical and horizontal cracks and separations (27.2; 30V.2; 30G.2; 50.2; 52.2; 55.2; 60.2 type flaws).

Flaws in the form of vertical, longitudinal cracks and separations substantially dispersing the ultrasonic vibrations being propagated do not, for

practical purposes, reflect the wave in the direction of the probe. Therefore, the mirror-shadow method is used for detecting flaws in the indicated groups. Of the previously examined methods for monitoring with rail flaw detectors, those monitoring methods using the normal probes, plus the first and second bottom pulses have found practical application.

In the bolted joint zone, in addition to the flaws indicated above, flaws in the form of cracks developing in the walls of the bolt holes appear frequently. Therefore, monitoring the bolted joints is presently conducted in the same manner as is monitoring of the parent metal. In this case, however, "false" activations of the indicators take place when the probe passes over the bolt hole. This complicates monitoring when the flaw detector is in constant motion.

The appearance of false indicator actuations may be excluded by introducing into the flaw detector an auxilliary normal probe which is switched on when passing over the bolted joints.

The function diagram of a flaw detector for monitoring the bolted joints and the parent metal in the web zone and its continuation into the head and the base is presented in Fig. 160. The generator G produces electrical vibration pulses; the probe I converts the electrical vibrations into ultrasonic vibrations and radiates them into the rail being monitored. The ultrasonic pulse reflected from the opposite surface of the rail (the base), which is called the bottom surface, is received by the same probe and converted into an electrical vibration pulse. This pulse (the bottom pulse) is amplified and detected in the receiver R.

At the moment of radiation, the pulse transmitted from the generator G is fed into the time delay input stage TD. Here, stage TD produces a pulse which is shifted in time a certain definite amount in regard to the transmitted pulse at its own output. Thus, it is as though the pulse is delayed for a

certain time, called the time delay, in TD. The size of this time period is set using T. The pulse from the output stage TD is fed to the gate pulse generator, or, as it is also known, the gating pulse generator.

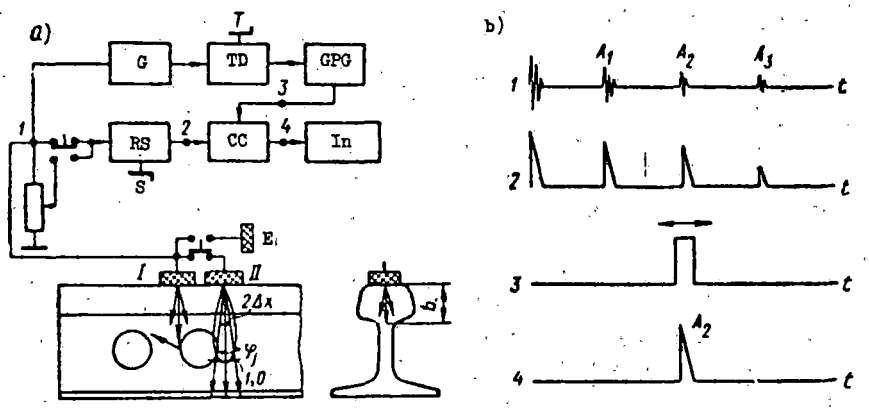

Fig. 160 Function diagram of a mirror-shadow flaw detector for monitoring rails:
G - ultrasonic vibration generator; RS - receiving-switching element; TD - time delay stage; GPG - gate pulse generator; CC - matching stage; I^n - indicator; T - knob to adjust the gate-pulse generator ("Rail type"); S - sensitivity adjustment handle; I - primary stage; II - secondary probe; E - dummy device for balancing out the sensitivity.

At the moment when the delayed pulse is fed, this generator produces a square-shaped pulse used in the following pulse for separation (gating) of the necessary pulse-echo signals, and is therefore called the gating pulse, or the gate-pulse. It is apparent that the gate-pulse may be shifted in time with regard to the transmitted pulse with the aid of the knob T in the time delay stage.

The gate-pulse is fed into the coincidence stage input CC. Pulses from the receiver output are fed to the second input of this stage. The coincidence stage is an amplifier of the type that works only during the process of supplying the gate-pulse. Therefore, from the coincidence cascade, those bottom pulses with which the gate-pulse corresponds in time will be fed to the indicator I (Fig. 160b). The coincidence of the gate-pulse and the corresponding bottom pulse is produced with the aid of knob T in the time delay stage. It is apparent that the time delay of the gate-pulse when tuning to the same bottom pulse will be determined by the height (i.e. the type) of rail.

The indicator IN is activated when the bottom pulse amplitude is decreased to a definite value; the flaw detector sensitivity is adjusted according to a flaw simulator with the aid of the "Sensitivity" knob (S). Adjustment for monitoring a given type of rail using the first or second bottom pulse is accomplished using knob T, usually called "Rail Type".

When a flaw detector has been adjusted to a nominal sensitivity K_y, according to a flaw simulator, and when monitoring using the first bottom pulse, flaws with a detectability coefficient $K_d \leq K_y$, will be discovered in the parent metal. When monitoring, using the second bottom pulse, flaws with a detectability coefficient $K_d \leq \sqrt{K_y}$ will be detected.

As was noted above, the secondary probe II is connected to probe I when passing over the bolted joints.

Probe II is located at a distance somewhat exceeding the diameter of the bolt holes from probe I. Here the bolt hole does not cover both ultrasonic beams, and, above the flawless bolt holes, a bottom pulse will always be received. If, however, there turns out to be a crack near the bolt hole, at a given probe position, both ultrasonic beams will be either completely or partially covered. This leads to a sharp decrease or to the complete disappearance

of the bottom pulse, and, correspondingly, to the actuation of the indicator.

A similar probe circuit diagram exists, as it were, as an ultrasonic gage, passing freely over defect-free holes, and recording those holes with cracks whose projection onto the horizontal surface emerges beyond the bolt hole projection (Fig. 161).

Depending on monitoring speed, a cathod ray tube, an audio signaling device or a recording device which locates a decrease in the bottom pulse to the size being determined by the nominal sensitivity of the flaw detector are used as indicators.

The maximum rail monitoring speed when using the mirror-shadow method is determined by the directivity diagram of the probe, by the ultrasonic pulsing frequency, and by the time lag of the indicator. Given ultrasound pulse radiation, the indicator time lag may be evaluated by the minimum number of bottom pulses N during attenuation of which the indicator actuates. It is apparent that the speed should be such that all desired flaws have sound waves passed through them no less than N times along the axis of the beam or in the area of the beam close to it as the probe moves along. Having denoted the width of this beam area by ΔX, we obtain the relationship for calculating the monitoring speed V:

$$\frac{\Delta X}{V} \geqslant \frac{1}{F} N,$$

from which

$$V \leqslant \frac{F}{N} \Delta X,$$

where F is the pulse repetition rate,

1/F is the transmitted pulse period,

$\Delta X/V$ is the time during which each point in the zone being monitored is located in the area of a beam ΔX wide (cf. Fig. 160), and

$\frac{1}{F}N$ is the time when the zone being monitored is struck by N pulses.

Taking into consideration that all flaws being sought are located at the place at which the rail head merges with the web, and below, at a distance exceeding the near field of the probe, the minimum width of the zone ΔX will be equal to

$$\Delta X_{\min} \approx 2b \tan \varphi_j, \tag{28}$$

where φ_j is the angle being read from the axis of the directivity pattern.

To assure identical conditions for flaw detection in the cross section being monitored, the size of angle φ_j should be such that the intensity of the field at each point in a zone of width ΔX is approximately the same.

If we accept that the field intensity in the extreme points of zone ΔX will not be less than half the intensity on the acoustical axis of the sensor, according to the equation for the directivity pattern of a normal sensor, known from the study of acoustics, the angle φ_j is equal to

$$\varphi_j = 1{,}37 \frac{C_{l_2}}{2\pi a f}. \tag{29}$$

In this case, the monitoring speed is determined by the expression

$$V \leqslant 10\,600 \frac{bF}{afN}. \tag{30}$$

Thus, for example, for reliable rail minitoring (b = 40 mm), using a flaw detector with the following parameters: F = 200 Hz; a = 6 mm; f = 2.5 MHz; N = 5, the speed at which the probes move, according to the given formula, should not exceed 1.2 km/hr.

To increase the monitoring speed, it is necessary to raise the pulsing frequency of the transmitted pulse F, and diminish, where possible, the number of pulses N with which a flaw must be struck for its detection.

The function schematic of the mirror-shadow flaw detector which was given is fully achieved in the UZD-NIIM-6M devices.

URD-58 and URD-63 flaw detectors are distinguished by not having a flaw simulator, or ultrasonic gage, and by not being able to work using the second

bottom pulse. Telephone headsets are used as indicators in the URD-58, URD-63 and UZD-NIIM-6M flaw detectors.

Monitoring of the welded joint zone cannot be accomplished using the mirror-shadow method and a normal probe. It is necessary to note that adequately large welding flaws situated in the web zone and where it merges with the head and the base, as well as transverse cracks in the rail head, may be discovered when monitoring using the mirror-shadow method by using angle probes. In practice, however, the pulse-echo method, which has greater sensitivity than the mirror-shadow method in the given instance, is used to discover these defects during flaw detection in rails.

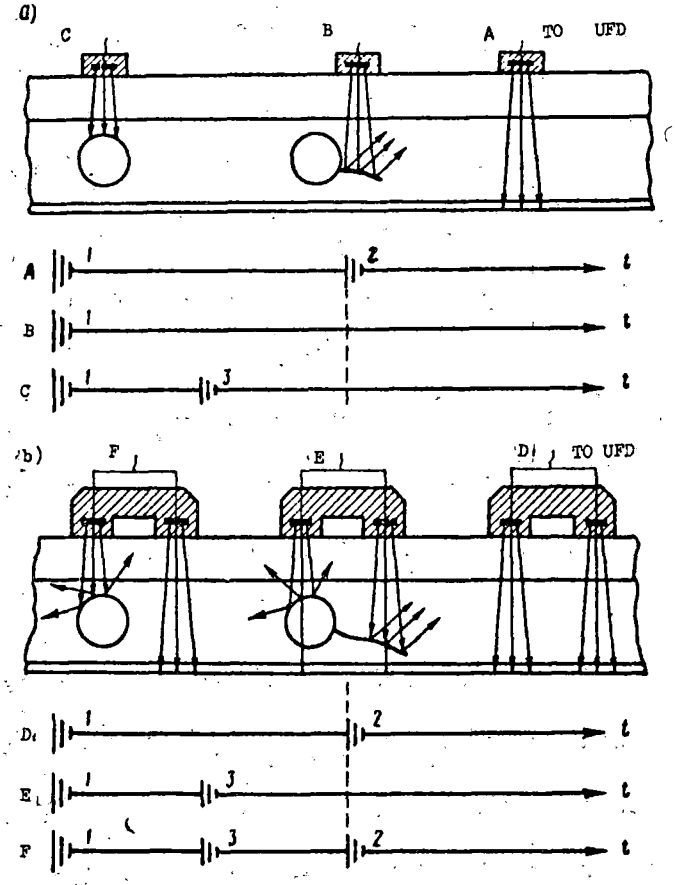

Fig. 161 Position diagram and corresponding oscillograms of pulses on the probe:
a. common; b. special 1. transmitted pulse 2. bottom pulse 3. pulse from bolt hole.

When monitoring the rails using the pulse-echo method, the sound wave is passed through the welded joints or the parent metal of the head using angle probes.

In pulse-echo flaw detectors, an indication that a flaw has been discovered may take place with the appearance of the pulse-echo from the flaw on the screen of a cathode ray or by the sound signal in the telephone headset, based on the firing of a tube, etc. A system for the time selection of pulses fed to the receiver input should be designed in the flaw detector so that the indicator would not be activated from the transmitted pulse.

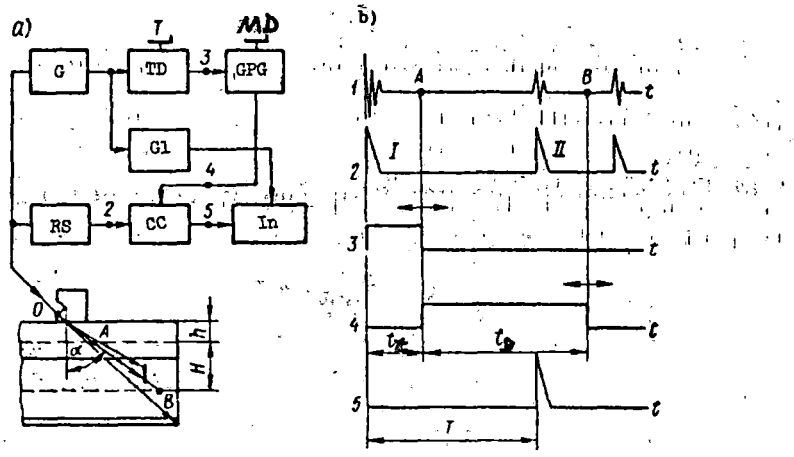

Fig. 162 A pulse-echo flaw detector.
a. function diagram b. voltage shapes/forms at points in the functional diagram.

Pulse-echos may appear not only from the internal flaws, but from roughness on the rail surface. Knowing the coordinates for the location of the reflecting surfaces, it is possible to distinguish the useful pulse-echos from flaws from the false signals. Depth meters were designed for determining the coordinates of the reflecting surfaces in the flaw detectors.

The function diagram of a pulse-echo flaw detector is shown in Fig. 162.

Of the totality of pulses appearing at the receiver output (point 2, Fig. 162), only those pulses which coincide in time with the gate-pulse produced by the gate-pulse generator are fed into the indicator.

The beginning of the gate-pulse, and consequently, the depth h of the beginning of the layer being monitored, are determined by the duration of the pulse t_t on the time delay stage output TD. The depth h is associated with time t_t by the relationship

$$h = \frac{C_{t_2}(t_t - 2t_p)}{2} \cos\alpha. \quad (31)$$

For rail monitoring, beginning from the surface (h = 0), it is necessary that the gate-pulse time delay be equal to the time it takes the ultrasound to pass into the probe wedge, i.e. $t_t = 2t_p$.

The delay-pulse duration determines the size of the layer being monitored H. The size of H is associated with the duration of the gate-pulse t_g by the relationship

$$H = \frac{C_{t_2} t_g}{2} \cos\alpha. \quad (32)$$

Thus, by changing the duration of the gate-pulse, it is possible to change the size of the layer being monitored, and, at $t_t = 2t_p$, the depth which is monitored.

The coordinates of a reflecting surface situated in the layer being monitored are determined with the aid of a depth meter (a device for measuring the time interval T between the transmitted pulse and the pulse-echo). Depth meter scales are, as a rule, graduated in mm for probes with different beam transmission angles.

When monitoring welded joints, angle probes moved by hand along the rail periphery in the weld zone are used.

Monitoring the parent metal of the head along the entire rail length is accomplished using an angle probe with a beam transmission angle $\alpha \approx 60^\circ$. The

probe is moved along the running surface of the rail above the web. For detecting the types of flaws shown in Figs. 20 and 21, the probe is turned relative to the longitudinal axis of the rail at an angle γ equal to 30-37°. In this case, the flaws are discovered by a beam reflected from the lower surface of the rail head (Fig. 163). This configuration for passing sound waves through the rail head is used in the URD-63 and UZD-NIIM-6M flaw detectors.

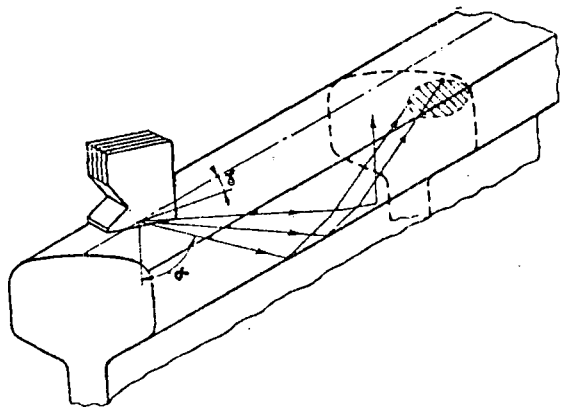

Fig. 163 Diagram for passing sound waves through a rail when detecting type 20 and type 21 flaws.

It may be seen from a comparison of the function diagrams of a mirror-shadow and a pulse-echo flaw detector that they share a series of common features. It is apparent that for simultaneous monitoring of the parent metal in the head and web zones of the rail, in the bolted and welded joints, it is expedient to combine a flaw detector working on the mirror-shadow method with one working on the pulse-echo method into one piece of equipment. The UZD-NIIM-6M is such a device.

The electrical diagrams of contemporary flaw detectors are constructed using the latest achievements of radio electronics. It is, therefore, necessary to know the operating principles of vacuum and semiconductor devices and the basics of pulse radio technology for studying the flaw detector devices.

Chapter VI -- The URD-52 Ultrasonic Rail Flaw Detector Cart.

1. Intended use and working principles of the flaw detector cart.

The TsNii URD-52 ultrasonic flaw detector cart (Fig. 164) permits detection of the following flaws in the joint sections of rails:

a. Cracks in the upper fillet more than 10 mm in length, (flaw type 52.1-2)

b. Horizontal cracks in the rail web more than 10 mm in length (flaw type 55.1-2)

c. Inclined cracks developing from bolt holes (flaw type 53.1-2), whose projection onto the running surface of the rail is more than 10 mm

d. Vertical and horizontal separations in the head and web (flaw types 30V.1-2; 30G.1-2) with a length of 10 mm or more

e. Transverse fatigue-type cracks in the form of light or dark spots situated above the web (flaw types 20.1-2; 21.1-2).

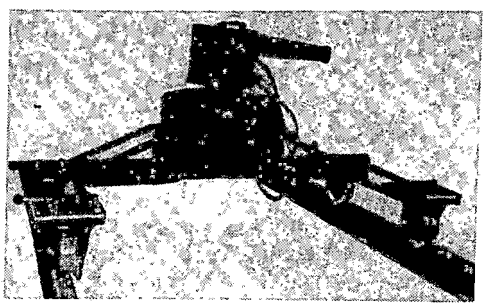

Fig. 164 The URD-52 TsNII flaw detector cart.

The operation of the flaw detector cart is based on the periodic sending of short ultrasonic vibrations into the rail from the running surface and receiving the reflected oscillations from the base of the rail or from a flaw.

The duration of the electrical oscillations of the circuit, which a piezoelectric element, is 5-7 microseconds at an oscillation frequency of 2.7 MH_z (Fig. 165). The disappearance of the bottom pulse or the appearance of another signal situated to the left of the bottom reflection serve as signs of the presence of a defect in the rail being tested.

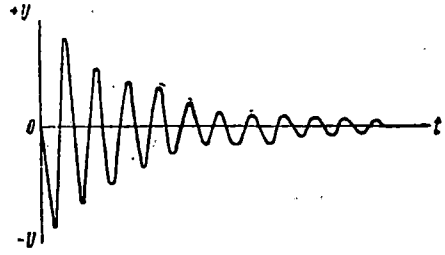

Fig. 165 Damped electrical oscillations.

Principle sections (blocks) of the circuit. The flaw detector diagram (Fig. 166) includes the following five blocks: the generator 1; the probe 2; the receiver 3; the cathode-ray display 4; and the power supply block 5.

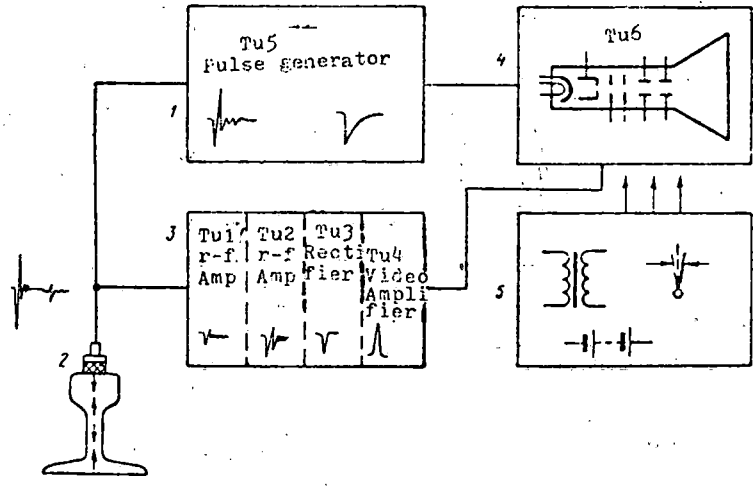

Fig. 166. Block diagram of the URD-52 flaw detector.

The generator creates electrical pulses to excite ultrasonic oscillations in the piezoelectric element and simultaneously to trigger the scan voltage necessary for oscillograms on the display screen.

The probe transforms high-frequency electrical pulses into mechanical ultrasonic oscillations and also carries out the reverse transformation of mechanical ultrasonic oscillations into electrical pulses.

The receiver amplifies the electrical oscillations taken from the piezoelectric element plates and transforms their shape (rectification).

The cathode-ray display is intended for observation of the electrical oscillations arising in the piezoelectric element. The signals from the piezoelectric element enter the receiver, are rectified, sent to the vertical deflecting plates of the cathode-ray display and create sharply peaked upward pips in various places on the fluorescent base line (the time axis). Since the generation of ultrasonic pulses and creation of the scan voltage take place simultaneously and many times per second, the eye of the observer perceives the image on the screen to be stationary (Fig. 167).

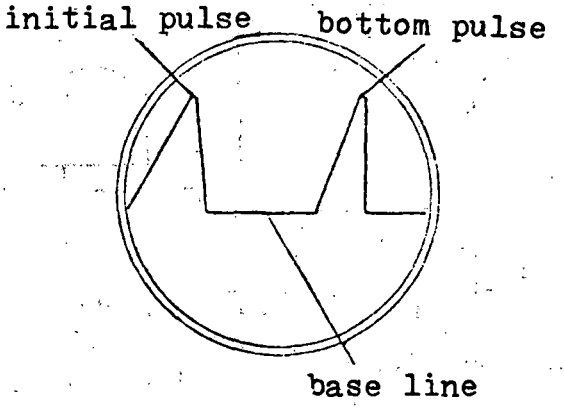

Fig. 167 Oscillogram on the flaw detector display.

The power supply block provides the necessary energy for all sections of the flaw detector. A low-voltage direct current is transformed into a high-voltage pulsing current adequate for powering the cathode-ray tube and the plate circuits of the amplifier tubes in the power supply block.

2. The electrical schematic of the flaw detector.

The high-frequency electrical pulse and scan voltage generator. The generator is built around a TG1-0.1/1.3 thyratron, and it has a relatively simple schematic (Fig. 168). The thyratron is used as a switch connecting

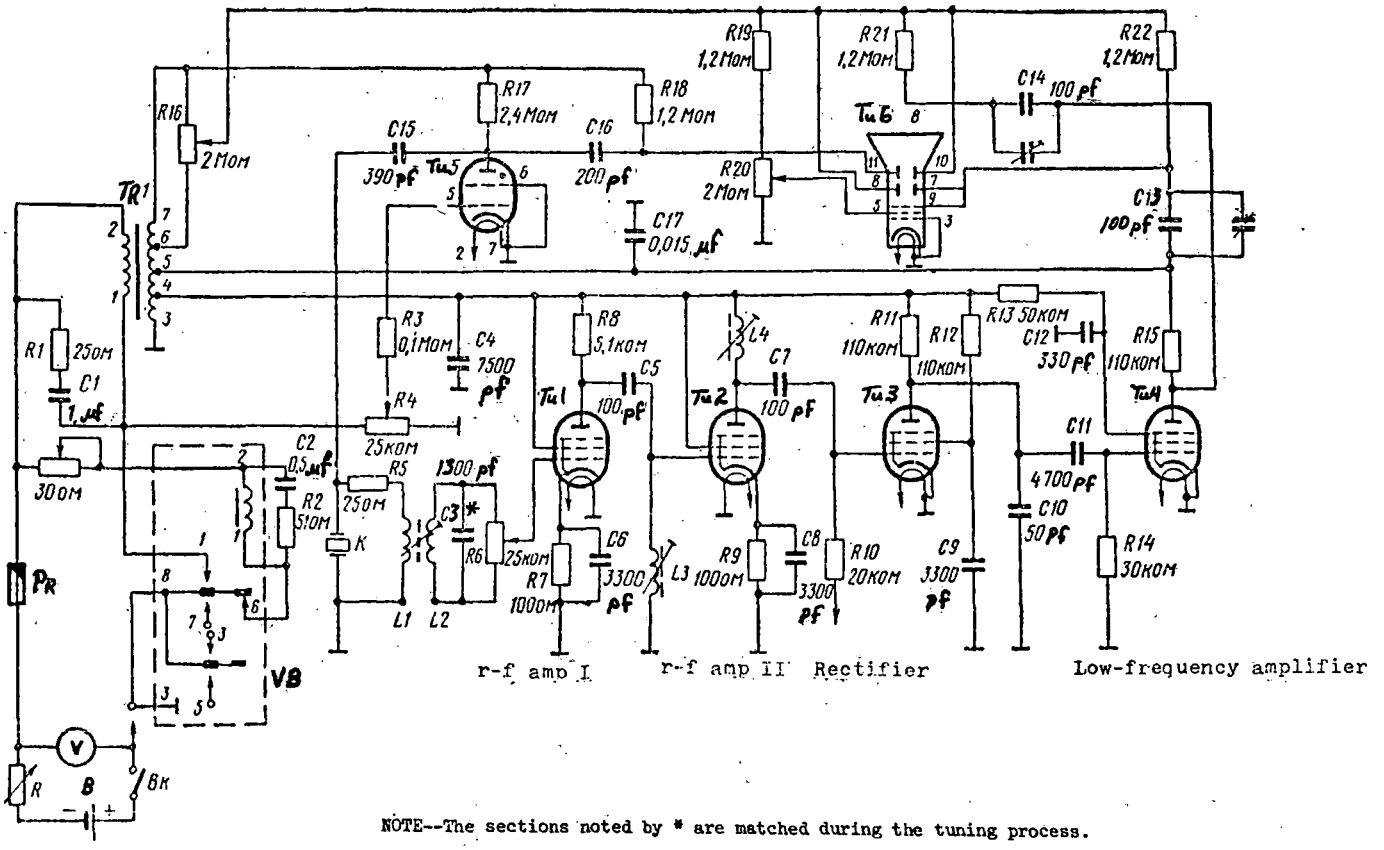

NOTE--The sections noted by * are matched during the tuning process.

Fig. 168 The primary schematic of the URD-52 flaw detector.

the wire running from point a to the ground (cf. the equivalent circuit in Fig. 169). When the switch is open, capacitor C15 is charged through the high-resistance R17 to the maximum voltage which is close to the voltage of the power supply source.

When the thyratron fires (the closing of the switch) the charge on the capacitor instantaneously (in one burst) passes to the electrical circuit consisting of the piezoelectric element K and the inductor L1. Impact excitation of the circuit takes place. The burst of current in the circuit consisting of the capacitor C15, the thyratron, and the piezoelectric element reaches 5-7 amp, with a voltage of 70-100 volt. Thus, the instantaneous power reaches a high magnitude.

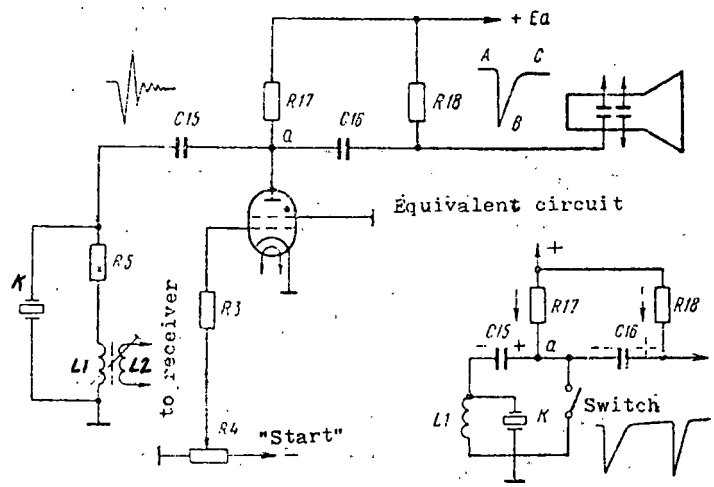

Fig. 169 Schematic of the high-frequency electrical pulse and scan voltage generator.

The frequency of the damped electrical oscillations in the circuit is determined by the capacitance of the piezoelectric element and the inductance of coil L1. This frequency is selected to be a bit higher than the particular mechanical resonance frequency of the piezoelectric element, which is equal to 2.5 MHz when the plate thickness is 1 mm (0.75 mm for the TsTS-19). It is necessary for the oscillations of the piezoelectric element to cease within 5-7 microsec after excitation in order to shorten the duration of the initial pulse. Rapid cessation of the oscillations of the L1K circuit after impact excitation is attained by mechanical damping of the piezoelectric element which is compressed on one side with a leather or cardboard washer. Electrical damping of the piezoelectric element consists of a resistance R5 equal to 25 ohm in the L1K circuit.

When the piezoelectric element is connected, the polarity of the voltage entering from the thyratron is taken into consideration, and therefore the piezoelectric element is always inserted with the side marked "+" to the replacable bottom.

The sawtooth scan voltage (cf. Fig. 169) is obtained when capacitor C16 is charged through resistance R18 at the same moment the thyratron fires, i.e. the voltage at point a is equal to the voltage on the chassis. The electron beam momentarily deflects from right to left on the display screen and then, as capacitor C16 builds up a charge, it will shift from left to right, forming the base line, when the thyratron fires. The speed at which the electron beam shifts across the display screen (line A-B) as the thyratron fires (the return) is so great that the eye does not notice the illumination on the screen at that moment, and begins to see it only as the beam is slowly displaced during the time the capacitor C16 is charging through resistance R18 (line B-C, the straight-line shape).

To simplify the circuit, non-linear scan is used in the flaw detector, i.e. initially the beam moves across the screen rapidly and then slows down.

When passing sound waves through light rail (120 mm high), not only the first, but also the second and third bottom reflections are visible on the cathode ray tube screen. The distance between them on the base line will gradually diminish because of a decrease in the scan speed.

The thyratron fires automatically at definite instantaneous voltage values on the first grid and the plate. The repeated firing of the thyratron is possible only when there is a following power supply pulse, i.e. during the following work cycle of the flaw detector. By changing the magnitude of the negative voltage on the first grid of the thyratron with the variable resistance R4 ("Start"), it is possible to change the moment at which the thyratron fires relative to the increasing voltage of the power supply pulse. With a large negative voltage on the first grid of the thyratron, it is necessary to apply a greater voltage to the plate in order for it to fire. With an increase in the negative value U_{g_1} on the first grid of the thyratron,

firing takes place at a higher voltage on the plate (Fig. 170). In the flaw detector, the thyratron activates at a voltage of about 900 v. The frequency with which the power supply pulses are repeated depends on the operation of the V-5 or V-4,8 vibrating breaker. In practice, this frequency is approximately 100 Hz.

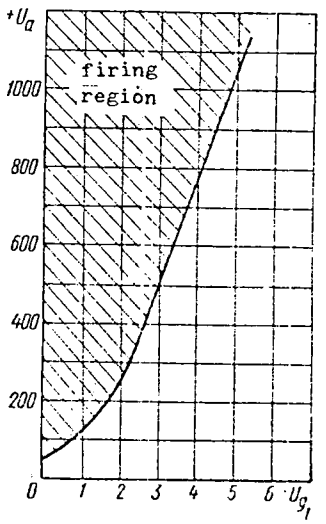

Fig. 170 Characteristic of the TG1-0.1-1.3 thyratron.

The probe. Construction of the probe is shown in Fig. 171. The piezoelectric plate 5 is clamped by a ring 2 and a face 4 to the damping washer 6.

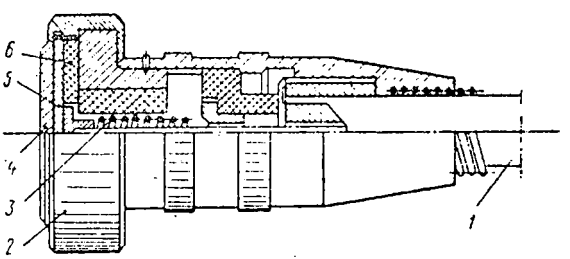

Fig. 171 URD-52 flaw detector probe.

The electrical contact between the co-axial cable's central connector 1 and facing of the piezoelectric plate is made using a spring 3. The co-axial cable braid is connected to the probe jacket covering.

The electrical capacitance of 1.5 m. of co-axial cable has no value due to the relatively high capacitance of the piezoelectric plate itself. The protective wearface shown in Fig. 171 is one-half of the ultrasonic wave length in thickness and it is prepared from U-9 steel.

The thickness of the wearface is selected on the basis of the conditions for resonance. For resonance, the ratio

$$h = \lambda/2,$$

where h is the thickness of the plate in mm and λ is the wave length of the ultrasonic oscillation in mm, exists between the wave length and the thickness of the vibrating plate for resonance at a particular frequency.

The transfer of ultrasonic energy into the rail is at a maximum when the thickness of the wear face is approximately $\lambda/2$.

The wave length of ultrasonic oscillations in steel is determined by the formula

$$\lambda = C/f = \frac{5\ 900\ 000}{2\ 700\ 000} = 2.19.$$

In practice, the thickness of the wear face is selected to be 1.2 mm. Wear down to 0.9 mm is permitted. As the thickness of the wear face decreases further, passage of the ultrasonic waves into the rail is impaired.

When the probe is assembled, the contact surface between the piezoelectric element and the wear face is lubricated with oil (automobile engine oil or transformer oil) to remove the air. The ring fastening the wear face and the probe jacket should draw and compress the piezoelectric element and the damping washer tightly, otherwise, mechanical damping will not take place.

Instead of a steel wear face, it is convenient to use a wear face made of plexiglass, ebonite or another material which transmits ultrasound significantly less freely than steel. Use of such a wear face diminishes the reflection of the ultrasonic energy at the transition layers (the

piezoelectric element, the oil film, the rail steel). Thus, with a steel wear face, a greater amount of ultrasonic energy is transmitted to the rail, in comparison to that reflected within the piezoelectric element. The thickness of a wear face prepared, for example, from plexiglass may be from 2 - 6 mm. The oscillation frequency of the piezoelectric element plate used with a wear face made of plexiglass will be a bit lower than when a steel wear face is used, namely 2.5 MHz. In this case, electrical contact between the piezoelectric plate and the probe jacket is made by inserting a thin piece of foil into the space between the plexiglass bottom and the silver covering of the piezoelectric plate. A thin layer of oil exists between the piezoelectric element and the wear face, and its size depends on the thickness of the foil which is used.

In practice, use of a plexiglass wear face permits sound to be passed into rails even when the running surface is uneven. Small cavities, engine burns and pits on the rails do not hinder the passage of the ultrasound.

The receiver. The flaw detector receiver is built according to a direct amplification circuit, and contains two radio-frequency amplification stages, a detector, and one video amplifier stage (cf. Fig. 168). There is a band-pass filter, consisting of the connected circuits L1L2 at the amplifier input, the number of turns in coil L2 being twice as great as the number of turns in coil L1. This provides the best matching of the receiver input circuit and the circuit of the piezoelectric element K. A potentiometer R6, connected in parallel with coil L2, permits the voltage fed to the grid of the first tube to be changed smoothly.

The first stage is a radio-frequency amplifier. The resistance R8 serves as the plate load for tube Tul. To create automatic biasing on the grid of tube Tul, the cathode of the tube is connected to the chassis through

resistance R7, blocked by capacitance C6. The high-frequency electrical oscillations amplified by tube Tul are fed to the grid of tube Tu2 through a blocking capacitor C5. In the grid circuit of tube Tu2, an oscillating circuit, which is a load for tube Tul, is connected. There is no capacitor built into this circuit. Its part is played by the capacitance of the coil and the wiring between the turns, the input and output capacitances of the tubes. Circuit L3 is tuned to a frequency of 2.9 MHz (coil L3 is wound with 140 turns of 0.07 mm PEL wire). When the piezoelectric element is excited from the thyratron, voltage on the receiver input reaches 100 v. A voltage on the order of fractions of a volt arises due to the effect of the reflected ultrasonic oscillations on the face of the piezoelectric element. The rapid restitution of the amplification capability of the receiver after overloading by the initial excitation pulse is achieved because of the low Q-factor of the oscillatory circuits.

The amplitude characteristic of the receiver, i.e. the dependence of the output voltage on the voltage supplied to the input, is shown in Fig. 172. It may be seen from the graph that the receiver's amplification begins to diminish when the size of the voltage fed to the input is greater than 8 millivolt.

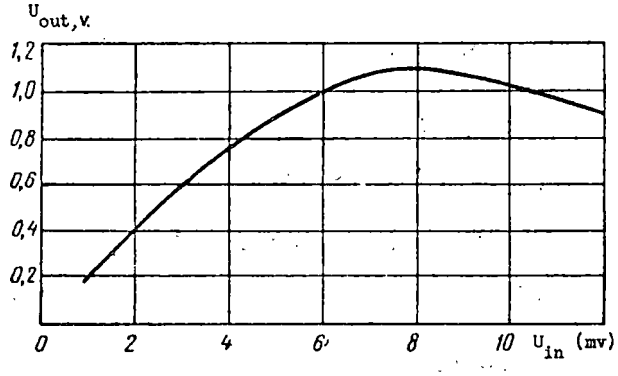

Fig. 172 Amplitude characteristics of the receiver.

The frequency of the receiver, i.e., the dependence of the output voltage on the frequency of the voltage fed to the input at a constant value is shown in Fig. 173. The maximum value of the rectifier U_{out} on load R11 (cf. Fig. 168), as may be seen, is attained at a signal frequency of 3 MHz. It is mainly the input circuit L2 that influences the receiver's tuning, and therefore, its adjustment (using a brass core) was anticipated.

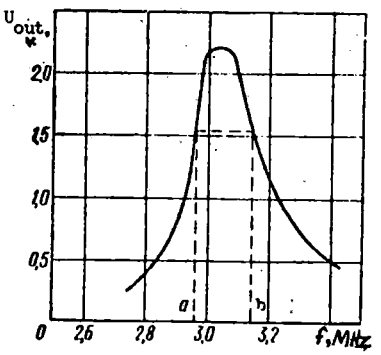

Fig. 173 Frequency characteristics of the receiver.

The band width of the effectively amplified frequencies is about 200 kHz. Such a wide band of amplified frequencies permits rapid restoration of the amplification capability of the receiver after being overloaded by the initial pulse. The total amplification of the two receiver stages at a frequency of 3 MHz should be greater than 1000 when an unmodulated signal of 1 mv is fed to the input.

Plate rectification of the signals is used in the flaw detector receiver. The plate rectifier is assembled around tube Tu3 (6Zh3).

Rectification is realized due to the non-linearity of the tube characteristic when a negative bias (-6v) is fed to the first grid.

Resistance R11 serves as the rectifier plate load. For taping the high-frequency component of the signal, resistance R11 is shunted using capacitor C10.

The electrical impulses, lacking the high-frequency components (the envelope) are transmitted to the grid of the input amplifier tube using capacitor C11.

As has already been indicated, rectification of the signals arising on the wear faces of the piezoelectric element improves the visibility of the pulses on the display screen. After the rectifier, the pulses II lack the high-frequency component I and have a definite polarity (Fig. 174). Here, the brightness of the oscillogram's illumination increases sharply due to a decrease in the translational speed of the beam across the screen.

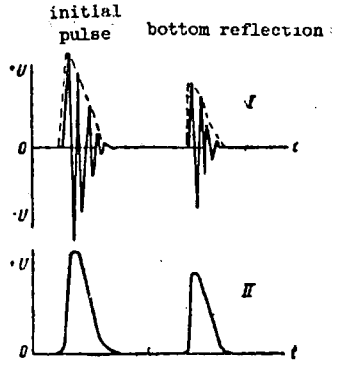

Fig. 174 Electrical impulses before and after rectification.

The amplified signals are fed from the output tube to the vertically deflecting plates. The normal deflection of the cathode-ray tube beam is provided when the voltage of 100 v. is supplied to the deflecting plates. The output tube permits such a voltage to be obtained, but, for this, its plate and shield circuits are supplied with an increased voltage. In view of the negative polarity of the pulses passing from the plate of the rectifier tube (the output tube shuts off completely when there is a signal on its grid), the negative bias is not fed to the grid of the output tube. Due to this, we are able to take full advantage of the amplification capability of the tube; signal distortions which arise have no particular value.

The cathode ray display. An 8-LO-29 cathode ray tube with electrostatic beam deflection serves as the display in the URD-52 ultrasonic flaw detector cart.

A shading tube placed on a protruding flange of the flaw detector case is supplied with the flaw detector to permit observation of the oscillograms on the screen on sunny days.

The electron beam is focused on the screen by supplying the necessary voltage to plate 9 (cf. Fig. 168) using the variable resistance labeled "Focus" (R20). An auxillary voltage is fed to one of the horizontal deflection plates using the variable resistance R16 labeled "Shift" for displacing the entire oscillogram in the horizontal plane.

Vertical displacement of the oscillogram on the screen is obtained by changing the moment at which the thyratron fires relative to the power supply pulse.

Distribution of the voltage between the deflecting plates during pulsed power supply is such that when the power supply voltage is reduced, the horizontal luminescent base line will drop down on the screen. Thus, by turning the "Start" knob, it is possible to shift the entire oscillogram up or down.

In the flaw detector circuit, the cathode of the tube is under the chassis voltage, whereas the plates are under the total voltage of the power supply pulse (1600 v). Therefore, the variable resistances "Focus" and "Shift" are carefully insulated from the flaw detector chassis using insulation washers.

The pulsed power supply for the cathode ray tube requires that a part of the pulsed power supply voltage be fed to the vertically deflecting plates, as well as the amplified signals from the piezoelectric elements. This voltage is fed to the deflecting plates through capacitor C13. In the latest models of the flaw detector, in addition to this capacitor, there are also

semi-variable condensors which are connected in parallel with capacitors C13 and C14. By trimming them, the best focus of the electron beam is achieved on the screen and maximum brilliance is attained.

The flaw detector's power supply block. A 5-ZhN-45 storage battery with a voltage of 6.25 v., a power transformer, and a V-4.8 vibrating breaker are included in the power supply block for the flaw detector. The voltage from the storage battery is fed to the apparatus through a fuse and a rheostat, and is controlled by a volt meter. The bank of storage batteries is situated in a box, and the volt meter, the fuse, the switch, and the rheostat are also mounted there.

The power supply is connected using flexible wire with terminal fittings. The polarity of the supplied voltage is designated by the signs "+" and "-" on the jacket terminal fitting.

The periodicity of the flaw detector operations permitted a pulsed current to be used for providing power for the tubes' plate circuits instead of direct current (Fig. 175).

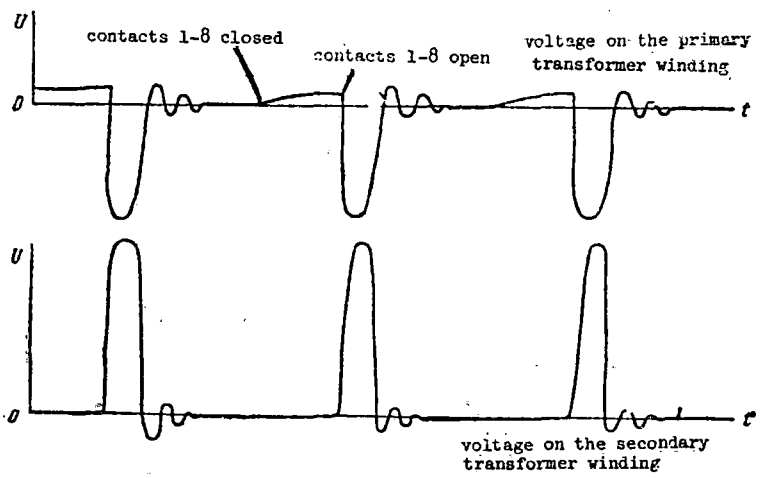

Fig. 175 Shape of the voltage pulses on the windings of the power transformer.

The pulsed current is attained when the vibrating breaker, which breaks the circuit of the primary winding of the power transformer periodically (100 times per second) with its contacts 1-8 (cf. Fig. 168), is normally connected to the storage battery.

The time diagram of the flaw detector operation (Fig. 176) shows that the break between the cycles, i.e. the time during which the vibrating breaker operates, is 0.01 sec. The time that an ultrasonic pulse takes to pass from the contact surface of the rail to its base and back is approximately 56 microsec. This is called the working cycle. It may be seen from the diagram that a continuous power supply for the plate circuits of the tubes is not useful since in this instance the greater part of the energy is lost. Therefore, plate supply for the tubes in the cathode-ray tube is fed only at that moment when the working cycle of the flaw detector is being completed, with a certain time margin, specifically in the course of 200 microsec.

The number of working cycles of the flaw detector depends on the frequency of the power supply pulses when the vibrating breaker is in operation since transmission of the ultrasonic pulse into the rail takes place only once at the moment the vibrator contacts are broken.

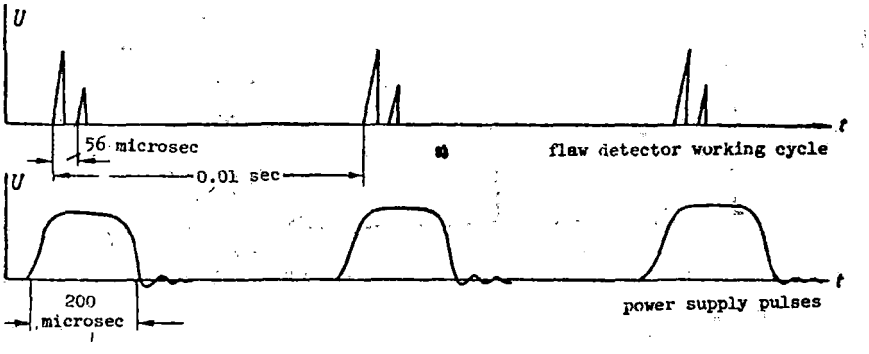

Fig. 176 Time diagram of the flaw detector operation.

To provide for more reliable operation of the vibrating breaker, a rheostat (R = 30 ohm) has been introduced into the breaker's start winding. Using this rheostat, it is possible to establish the necessary voltage. The knob for this rheostat appears on the front panel of the flaw detector, but it is necessary to turn it only when adjusting the flaw detector or when changing the vibrating breaker.

When the flaw detector is connected to a power supply source, direct current passes through the start winding of the vibrating breaker, creating a magnetic field. The reed of the vibrating breaker is attracted by the electromagnet, breaking the start winding circuit. In this manner, the reed oscillates automatically, like the vibrator of an electric bell, opening and closing the electrical circuit. The oscillation frequency of the vibrating breaker reed depends on the elasticity of the spring and on the mass of the reed itself. On the average, it is equal to 100 Hz.

Beside the start contact, there are four additional pairs of contacts on the reed of the vibrating breaker. Only one pair of them is used in this circuit. They serve to connect the winding of the power transformer to the storage battery bank.

Let us examine one oscillation period of the vibrating breaker reed. Contacts 1-8 (cf. Fig. 168) are closed for a short time, and the primary winding of the power transformer is connected to the storage battery. The current through it gradually increases and reaches 80% of the sustained value. Inside the primary winding, a magnetic field arises. It is primarily concentrated in the transformer core. In the following moment, the contacts break the circuit of the power transformer's primary winding. The magnetic field, rapidly diminishing after cessation of the power in the winding, intersects the turns and induces a self-induction emf in them. The speed

with which the magnetic flux changes (increases) after the current has been switched off in the winding is very great; therefore the voltage of the self-induction emf is greater than the voltage which is being supplied by the storage batteries. Even under full load of the power transformer, the emf reaches a magnitude of 30 v. In order to obtain the even greater voltage necessary to supply power to the cathode-ray tube, the transformer has a secondary winding located on the same core as the primary. Consequently, the magnetic field will also intersect these turns after the current has been switched off in the primary winding.

The highest voltage in the secondary winding reaches 1600 v ± 20%. Portions of this voltage (145 v and 220 v) are used to supply power to the plate circuits of the receiver tubes.

A break in the power transformer's primary winding circuit and in the vibrator's start winding is accomplished without sparking. This is achieved by using a spark suppression circuit consisting of a resistance and a capacitor.

The secondary winding of the power transformer is switched on so that at the moment when a negatively polarized pulse appears in the primary winding, positively polarized pulses arise in the secondary winding (leads 4, 5, 6 and 7).

When in operation, the vibrating breaker requires a current of 0.3 amp.

A current of 2.4 amp, including 0.3 amp each to pentodes Tu1-Tu4 (6Zh3), and 0.6 amp each for the TG1-0.1/1.3 thyratron Tu5 and the 8L029 cathode-ray tube Tu6 is used for heating the tubes and the cathode-ray tube. The total current consumption from the storage batteries at a voltage of 6 v is 2.7 amp.

The electrical energy stored in the storage batteries is adequate for 18 hr. of uninterrupted flaw detector operation.

To insure continuity of flaw detector operation on the line, it is necessary to have two storage batteries, one of which should be receiving a booster charge.

3. Construction of the flaw detector cart.

The flaw detector cart is a movable, removable apparatus mounted on a light four-wheeled carriage. The frame of the carriage is welded together from thin-walled steel tubing (cf. Fig. 164). Along the length of the frame, seats are attached for the flaw detector operators. The cross-section of the frame is occupied by the battery storage box, in which there is a 5-ZhN-45 alkaline storage battery, a volt meter, the filament rheostat, and a section for tools and spare parts. There is also a small reserve canister for storing the oil or emulsion necessary for flaw detector operation. The open cross-sections of the carriage frame are covered with wire mesh.

On the upper part, a turning device and a lock nut holding the instrument box are mounted on top of the battery storage box. This device permits the instrument box to be turned toward either flaw detector operator at an angle of up to 120° when working on the line.

The flaw detector's instrument box (Fig. 177) is designed to be a portable suitcase-type device with a removable front cover. All of the control knobs, the cathode-ray screen, and the jack for connecting the power supply and the probe are brought out onto the front panel of the instrument box.

The carriage wheels are insulated from the frame with insulating bushings. The electrical insulation of the wheels permits operation on sections of track equipped with an automatic blocking system and locomotive signaling without shorting out the rail circuit.

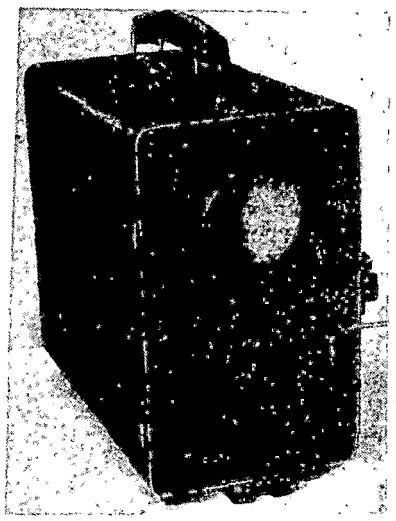

Fig. 177 The instrument box of the URD-52 flaw detector.

In the center part of the frame there is a handle for moving the carriage along the track. The handle is connected to the frame by a hinge.

The carriage wheels are fitted with ball bearings. It is necessary to change the lubrication in the bearings at least once a year.

4. Preparation for operation and inspection in the field.

Switching on the flaw detector. It is necessary to have a charged storage battery in the battery storage box in order to switch on the flaw detector, carefully observing the polarity when it is connected. Whether or not the battery is properly connected is tested by using the monitoring volt meter. When improperly connected, the needle on the instrument will deflect to the left.

The power supply cable leading out from the battery storage box has a plug on the end with a notation of the polarity of the voltage being supplied. The cable plug is inserted into the jack on the instrument box, again carefully observing the polarity. When the cable is improperly connected to the instrument box, the base line will not appear on the cathode-ray tube.

Power supply to the flaw detector is fed using a switch. A rheostat is incorporated so that a full voltage is not immediately supplied, especially when the battery has just been charged. A voltage of 6 v, according to the monitoring volt meter, is set using the rheostat.

After the flaw detector tubes have been permitted to warm up for a minute, the base line is brought onto the screen using the "Shift," "Focus" and "Start" knobs. An upward vertical blip and then a horizontal line passing slightly below the axis of the cathode-ray tube should be visible from the left.

In order to test the flaw detector sensitivity, the probe's terminal piece is inserted into the jack located on the front panel.

Testing for sensitivity. The sensitivity of the flaw detector is tested on a standard piece of rail having a bolt hole and a hole 3.2 mm in diameter which has been bored out at the same height. The running surface of the reference rail should be free from corrosion and covered with a coat of oil. When the probe is placed completely on the running surface of the reference rail, in addition to the initial pulse, the bottom reflection pulse will also be seen on the cathode-ray screen. The flaw detector's gain control is set in the position at which the width of the bottom pulse near the base will be approximately 10-12 mm on the base line.

The probe is moved along the running surface of the rail to the place over the 3.2 mm hole in the web. Here a supplimentary upward vertical signal should appear on the cathode-ray tube screen between the initial pulse and the bottom reflection. It is not recommended to provide full amplification here since the initial pulse increases greatly in duration and will cover the reflection from the 3.2 mm hole on the screen. It is necessary to test the probe and lubricate it with oil.

When the probe is placed on the running surface of the rail above the bolt hole, the bottom reflection disappears from the cathode-ray tube, but another vertical signal, situated closer to the initial pulse, appears. The presence of the markings noted above on the screen indicates that the flaw detector is ready for work, that it has normal sensitivity, and that it is ready to be operated on the line.

Operation on the line. Before beginning to work on the line with the flaw detector, it is necessary to fill the reserve canister with oil or with a soap emulsion, and to place in the tool box a mirror, detonating cartridges, wire feelers and a piece of chalk for marking defective joints directly on the track. Monitoring the joint sections of rails takes place in sequence on the right and left rail. The lock nut is loosened one to two turns to free the turning device of the instrument box. The light-shading tube, which is mounted at eye level for the flaw detector operator sitting on the carriage frame, is placed on the flange on the instrument box. Power is fed to the flaw detector.

In order to monitor the joint sections of rails, the running surface is lubricated with a liquid. Then the probe is moved along the running surface by hand, trying not to move it off of the axis of the rail. Sometimes, a simple device in the form of a U-shaped bracket with an opening in the center is used to center the probe on the axis of the rail.

Normally, when monitoring a rail, the base line on the cathode-ray tube takes on the form shown in Fig. 167. The signal of the bottom reflection, which is in the right-hand part of the screen, indicates that the ultrasonic oscillations transmitted by the probe are propagating from its position to the lower surface of the base of the rail and returning.

When flaws in the form of inclined cracks beginning from the bolt holes and passing through the rail are present, the ultrasonic vibrations cannot return to the probe which transmitted them. Therefore the bottom reflection is not visible on the screen. The bottom reflection is also not seen on the screen when there is a vertical separation of the metal in the head or the web since in this case the longitudinal ultrasonic oscillations are dispersed to the side.

Cracks which are horizontally oriented, e.g. in the upper fillet, may cause the appearance of a signal located to the left of the bottom reflection on the indicator screen. The bottom reflection signal either disappears entirely or is sharply diminished in amplitude. In all cases, supplimental vertical signals from the base line are situated to the left of the bottom signal and decrease its amplitude.

At that place in the rail which corresponds to the disappearance of the bottom reflection on the screen, it is necessary to conduct a repeat test and inspect the rail carefully from the outside. The bottom reflection may disappear not only because of the presence of cracks or separations, but also due to poor acoustical contact of the probe with the running surface of the rail. Poor acoustical contact may be caused by sand getting under the probe, lack of lubrication, or by unevenness in the running surface of the rail (dents, etc.).

An experienced flaw detector operator may determine without error the presence of cracks which develop from bolt holes, whose projection onto the horizontal surface has a linear dimension of not less than 10 mm. Vertical separation of the metal in the head or web are very clearly detected from the disappearance of the bottom reflection. In approximately the same way, fatigue cracks in the form of a bright spot are detected under the condition

that they are situated over the rail web. In this latter instance, disappearance of the bottom reflection is observed over a section with a length approximately equal to the diameter of the piezoelectric element, even when the flaw is in a strictly vertical position.

It is possible to establish the presence of a bright spot more precisely by passing a wave through the rail from the side.

The bottom reflection may disappear over a great length when there is a vertical longitudinal separation of the metal, which, as a rule, gives no secondary pulses on the cathode-ray tube screen. It is necessary to note the boundaries for the disappearance and reappearance of a bottom reflection signal on the rail and then to increase amplification in the receiver and test the rail again within the section where the bottom reflection disappeared.

If a secondary signal situated close to the initial pulse appears on the display screen, more than likely, this will indicate a horizontally situated crack.

Shifting the probe to the gage or the field side of the rail a bit permits the approximate location of the flaw to be established relative to the axis of the rail. When the indications of magnetic flaw detectors operating on a constant magnetic field are dubious, the URD-52 flaw detector may render substantial aid.

A description of the secondary rail monitoring when flaws in the form of a bright spot is presented below. Secondary monitoring takes place in a series of three steps. The first step is to pass a wave through the rail from the running surface (Fig. 178) using an erect probe. The bottom reflection does not appear on the screen when a flaw is present. The section of the rail over which the bottom reflection disappears is of varying length in different instances. In the case of a strictly vertical transverse flaw,

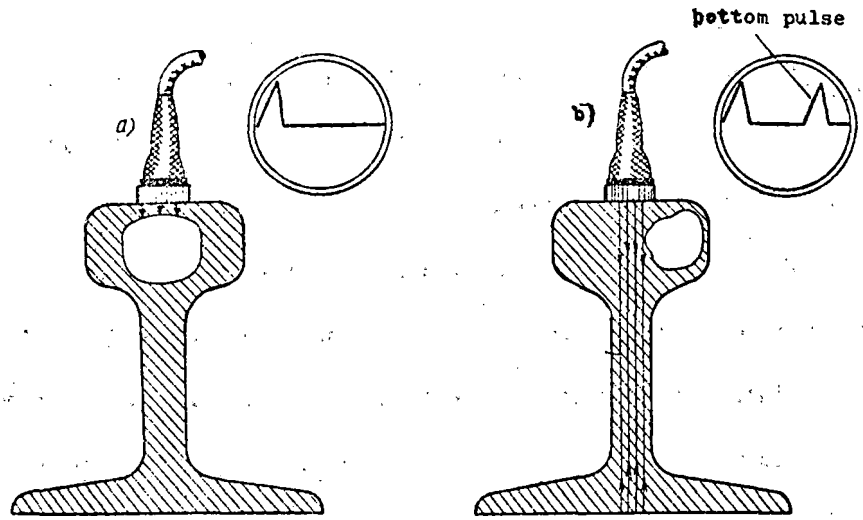

Fig. 178 Secondary monitoring of a rail from the running surface:
a. flaw in the center part of the rail head;
b. a flaw to the side of the rail head section.

the disappearance of the bottom reflection is observed for a length of 15 mm. If the flaw is situated at an angle to the running surface, the length of the section within which the bottom reflection disappears increases.

The second step for monitoring the rail consists of testing it from the side with a normal probe (Fig. 179). Passing a wave in from the side also

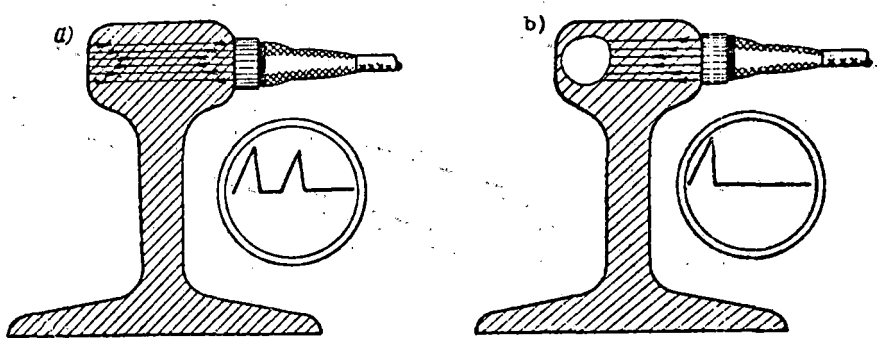

Fig. 179 Secondary monitoring of rails from the side.
a. no flaw present b. Type 21 flaw present

permits transverse flaws in the head to be detected according to the disappearance of the bottom reflection. Flaws which are not situated above the rail web may be revealed during such a test. The lateral surface of the rail is cleaned of mud and lubricated with oil, and, when necessary, the scab and other uneven places are filed down. If the rail is sound (Fig. 179a), one, two, and sometimes even three ultrasound reflections will be visible from the opposite side of the head. The vertical signal on the screen (the first bottom reflection) is situated closer to the initial pulse than when testing the rail from the running surface. If there is a bright spot in the rail head (Fig. 179b), no reflection is observed from the opposite surface.

The third step in monitoring consists of passing a wave through the rail using an angle probe with an angle of 47°.

Rail monitoring using a flaw detector with an angle probe takes place as shown in Fig. 180.

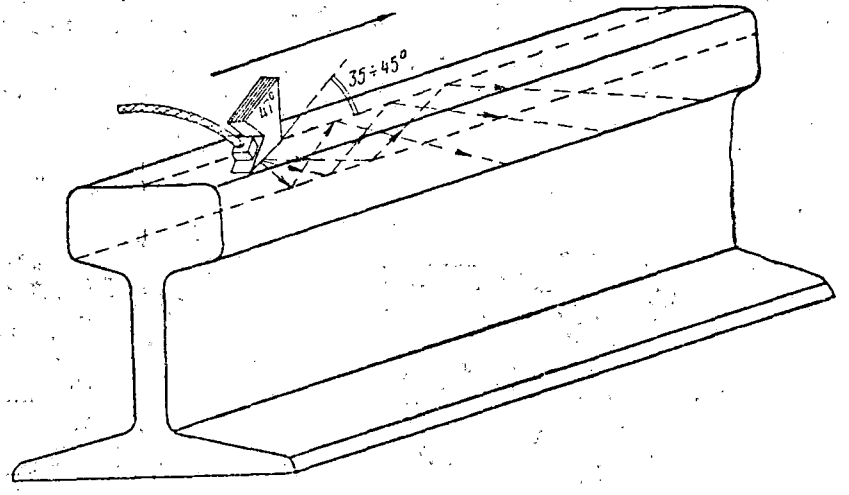

Fig. 180 Monitoring rails for the presence of transverse fatigue cracks using the angle probe.

The probe is turned so that the axis of the ultrasonic beam is at an angle of 35-40° to the longitudinal axis of the rail and the probe is moved slowly back and forth over the dubious site. If there is a fatigue flaw in the form of a spot (a transverse crack) to the side of the rail head, a pulse will appear on the screen and it will shift as the probe is moved about on the rail.

When using the flaw detector for inspection purposes, it is convenient to increase the receiver's amplification. For this, the 6Zh3 tubes are replaced by 6Zh4 tubes. The basing of these tubes is identical, and no adaptations are required. Only the first two receiver tubes are replaced.

It is not expedient to conduct secondary monitoring of the readings of flaw detectors working on a variable magnetic field since these flaw detectors reveal only flaws which emerge onto the rail surace, and these flaws may be detected either visually or with the aid of magnetic powder.

5. Repair and adjustment of the URD-52 flaw detector cart.

Careful and accurate handling of the flaw detector serves to guarantee its uninterrupted use. In the majority of cases, the flaw detector malfunctions due to unsatisfactory operation of the vibrating breaker or breaks in the cable.

The operation of a flaw detector with a vibrating breaker which has been in operation for 600 hr. is not without interruptions. To increase the period of reliable service of the vibrating breaker, it is necessary to use free contacts not connected to the circuit (cf. pos. 3 or 5 in Fig. 168), contacts 8 and 4 being connected to the chassis.

As practice has shown, numerous attempts at repairing the vibrating breaker have not provided good results: it is possible to open the vibrating breaker and clean the contacts only in exceptional cases.

Poor operation of the vibrating breaker (the contact points burning) leads to the self-induction emf pulses which arise when the primary winding of the power transformer is open. These pulses have a smaller magnitude in comparison with normal pulses and much spark-related interference appears. The base line on the flaw detector screen begins to move about randomly or does not appear at all due to inadequate voltage on the cathode-ray tube electrodes.

The voltage arising in the secondary transformer windings is controlled by a VKS-7 cathode voltmeter with a DNE-2 voltage divider or by an A4-M2 cathode voltmeter with an extension probe designed to measure high voltage. The cathode voltmeter should show a voltage of 1600 v ± 20%. When the contacts of the vibrating breaker burn, the voltage diminishes to 1000 v. The power transformer cannot be switched on without a load from the circuit side. In the latter instance, the voltage on the step-up winding may reach 15,000 v and the transformer may break down.

The presence of an initial pulse on the base line indicates that the flaw detector is passing on the high-frequency energy pulses from the thyratron. If it is not possible to receive bottom signals on the scan line when a wave is passed through the rail, it is necessary to search for a defect in the probe.

Probe defects basically can be reduced to short circuits in the central cable and in the cable jacket, and to breaks. The malfunctioning of the probe may also be caused by the breakdown of the piezoelectric element. To restore its operating capability, it is necessary to place a circular layer of foil under the entire surface of the piezoelectric plate on the side of the damping washer. In general, the flaw detector may operate temporarily with a small piezoelectric element one half to one quarter of the size of the whole piezoelectric element. In this case, it is necessary to increase

the receiver gain using the "Amplification" knob. Ultrasonic oscillations may be reflected from the section of the rail under the head and create certain interference on the left side of the flaw detector screen in this case.

Lack of lubrication in the probe and poorly tightened clips result in the initial pulse lengthening, its great width along the base line occasionally reaching half the diameter of the display screen.

This phenomenon is eliminated by dissembling the probe, lubricating the wear face and the damping washer with oil, and also by tightening the probe wear face down tightly with the clip.

It is absolutely essential that the probe wear face have a flat surface. The wear face surface is lapped on a lapping plate or on thick glass using fine emory cloth or lapping paste. When the thickness of the wear face is less than 0.9 mm, transmission of the ultrasonic oscillations is already beginning to cease. When the probe is worn to this extent, it is necessary to replace the wear face.

A break in the probe's cables (two are required for outfitting the cart) is determined by the shape of the initial pulse on the base line when the probe is connected. Connecting a probe which is out of order or a probe without a piezoelectric plate will not cause a change in the initial pulse on the screen.

The flaw detector cables are made from co-axial RK-31 or RK-74 cable. The application of other cables or wires makes working with the flaw detector more difficult under winter conditions because of the loss of flexibility at low temperatures.

If it turns out that the vibrating breaker is working normally, when the flaw detector is turned on, i.e. there is a base line on the screen, and it occupies a stable position but there is no initial pulse on the base line,

it is necessary to test the receiver tubes and to determine whether or not the circuit coils are intact. The coils are tested with a TT-1 tester and the tubes with an IL-12 or IL-14 tester. Occasionally the thyratron does not provide the necessary charging speed, i.e. ionization of the gas takes place slowly. In such a case, there is a base line on the screen, a small initial pulse, but no bottom reflection signals. However, before searching for damage in the receiver, it is necessary to replace the thyratron with one known to be in good condition.

The leakage resistances R21 and R22, mounted on the cathode-ray tube panel, frequently go out of order. The size of these resistances is 1.2 Mohm. The oscillogram on the screen often appears and then grows darker and gradually disappears when damage of this type is present. The TT-1 tester or another device permitting measurement of resistances of 1-2 Mohm is used to measure the leakage resistances.

After major repair or replacement of the power transformer, it is useful to test the polarity of the pulse voltage fed to the thyratron plate and grid (the third and fifth lugs on the socket). The polarity is determined using an SI-1 electron oscillogram. When the polarity of the input pulse voltage on the thyratron plate is correct, the oscillogram on the screen will have the shape represented in Fig. 181 (1 and 2 are positive voltage pulses). The moment at which the thyratron activates (fires) is distinctly noted on the oscillogram in the form of thin lines on the peaks of the power supply voltage pulses (1). In this case, the oscillograph is connected to the third lobe of the thyratron's socket and to the flaw detector chassis. The polarity of the voltage on the thyratron grid is determined by connecting the oscillograph to the fifth lobe of the thyratron socket. The shape of the oscillogram on the screen when the polarity is correct is shown in

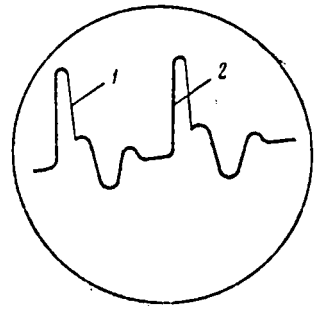

Fig. 181 Proper polarity of pulses on the thyratron plate.

Fig. 182. When the polarity of the pulse is incorrect, the thyratron does not fire.

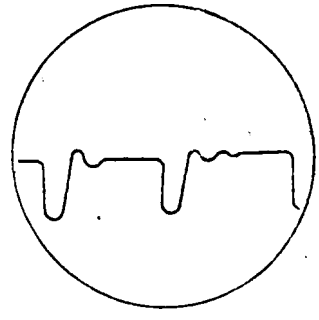

Fig. 182 Polarity of pulses on the thyratron grid.

When the polarity on the grid and plate are correct and the oscillograph is connected to the third lobe of the thyratron socket, the change in the moment at which the thyratron activates is observed by the displacement of the thin lines of the power supply pulses on the oscillogram when the "Start" knob is turned. When the "Start" knob is turned, the base line should move from below to above on the flaw detector screen. A slight angular displacement

of the base line is permissible. This may be considered to be the final step in determining the polarity of the power supply pulses fed to the tubes.

The most frequently encountered defects in the flaw detector's electrical system are the malfunctioning of tubes and other components, and of the vibrating breaker.

One should not test the tube conditions using the TT-1 tester with a pulsed power supply since in this case, the tester will give erroneous readings. The voltages on the tube electrodes may be measured using only S1-20 and SI-1 oscillographs.

Voltage on output 4 of the power transformer should be 145 v ± 15%; on output 5,220 v ± 15%.

It is possible to test the amplification of the receiver only in the shop and with the following equipment on hand: a GSS-6 standard-signal generator, a VKS-7 or A4-M2 cathode voltmeter, a TT-1 tester or an AVO-5-M1 volt/ohm meter (VOM) and an S1-20 or SI-1 electron oscillograph.

With the exception of L1 and L2 (cf. Fig. 168), the circuit coils of the receiver are not tuned. The specified number of turns, the diameter of the wire and the impregnation provide the inductance for the circuit coils without subsequent tuning.

If a break has occurred in the circuit coils when the equipment is in use, it is necessary to rewind them using 0.05-0.07 mm wire. One hundred and thirty turns are wound onto the frame of circuit coil L3, and one hundred and forty turns onto the frame of coil L4; then the coil is impregnated with bakelite varnish. Two to three hours later, the coil may be connected into the flaw detector circuit.

Should the necessity of tuning the circuit coils L3 and L4 arise, it is necessary to provide the plate power from an outside direct current source

with a voltage of 70-90 v. This source may be, for example, a BAS-80 battery. To do this, the wire leading to the fourth lug of the power transformer is disconnected. The vibrating breaker is removed from the socket, and the wire designated "+80 v." is connected to the disconnected wire from the power transformer. The wire from the negative terminal of the BAS-80 battery is connected to the flaw detector chassis. As usual, flaw detector tube heating is provided by the 6 v. storage battery.

The circuit L2 which is being tuned is connected into the plate circuit of tube Tu2 in place of the circuit L4. Circuit L3 and capacitor C5 are disconnected from the grid of tube Tu2 (the fourth lug of the tube socket). A modulated signal of 10,000 microvolts and a frequency of 2.9 MHz with a modulation depth of 100% is fed to the grid of tube Tu2 from the GSS-6 generator using a cable (jack 10). The VKS-7 or A4-M2 voltmeter is connected to the grid of tube Tu4 (the fourth lug in the socket), which has been removed from the socket beforehand.

When the circuit is properly tuned to a frequency of 2.9 MHz, the insertion of a brass rod or a rod of alsifer, ferite or magnetite into it will cause a decrease in the readings of the cathode voltmeter. If, on the other hand, insertion of the brass rod causes an increase in the cathode voltmeter readings, it is necessary to unwind five to ten turns of wire from the circuit coil and repeat the measurement. It is necessary to do this until insertion of the brass rod into the circuit causes no increase in the reading of the cathode voltmeter. If more wire is unwound than is necessary, inserting a brass rod into the circuit will cause a decrease in the readings of the cathode voltmeter, whereas introduction of a magnetodielectric into the circuit will cause an increase in the readings.

After circuit L3 has been tuned, it is disconnected from the system and circuit L4 is connected in its place. This circuit is tuned in the same way, the only difference being that the generator frequency should be reduced to 2.8 MHz.

After tuning, the circuits are replaced in the system and the power supply of the flaw detector is again switched to pulsed, i.e. the BAS-80 battery is disconnected and the wire running from the plus terminal of the battery is resoldered to the fourth lug of the power transformer. The tubes and vibrating breaker are replaced.

Circuits L1 and L2 are directly tuned according to the size of the bottom pulse reflection and the pulse from the standardizing 3.2 mm hole in the web of the rail while the flaw detector is in operation. Circuits L1 and L2 are tuned using a brass core which is screwed into the coil (fine tuning). Coarse tuning is accomplished by the selection of the capacitance C3; its size is between 1000 and 1300 micromicro farads.

When tuning the input circuits it is necessary to take care that the width of the initial pulse near the base, as well as of the bottom reflection pulse, is as small as possible, but at the same time, that the height of the pulse on the standardizing flaw (the 3.2 mm hole) on the scan line be not less than 20 mm. This is usually easily achieved if the piezoelectric element is satisfactory and if the probe wear face is 1.2 mm thick.

Using a wear face made of plexiglass or ebonite causes a decrease in the frequency of the radiated oscillations. In this case, it is necessary to rewind the input circuit L1 for normal flaw detector operation. The old winding is removed from the frame and eleven turns of PEShO-0.35 wire is wound in its place.

The remaining circuits are not tuned since the flaw detector sensitivity is entirely adequate.

In the case of a loss of sensitivity in the flaw detector due to bad tubes, it is useful to polarize the piezoelectric element.

The polarizing set-up is a slow power rectifier capable of providing 1500-2000 v. of direct current. This type of rectifier may easily be prepared in a railroad repair shop specializing in flaw detector repair. The rough circuit of a rectifier for polarization of piezoelectric elements is presented in Fig. 183. The transformer should have an iron cross-section of about 8 cm^2, preferably with a large opening. A 2Ts2, 1Ts1 or 1Ts11P high-voltage k notron may serve as the rectifier. It is also possible to use two AVS-5-1-A high-voltage selenium rectifiers. The capacitor C should be calculated for a working voltage of 2000 v. and have a capacitance of not less than 0.1 microfarad. It is necessary to set the limiting resistance R with a size of 1-1.5 Mohm to the conditions of operational safety.

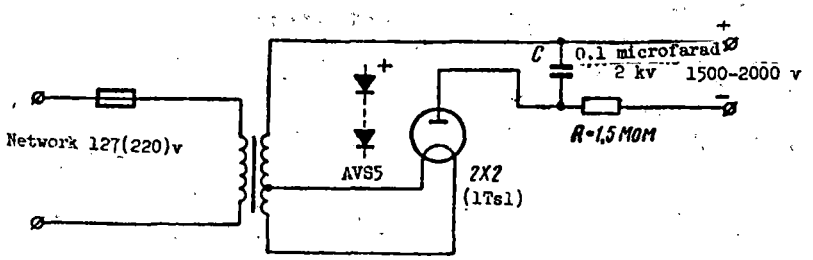

Fig. 183 Diagram of the rectifier for polarization of the piezoelectric elements.

It is absolutely necessary to preserve the polarity of the voltage fed to the piezoelectric element when connecting to the rectifier. The duration of polarization is about one hour. It is possible to connected several piezoelectric plates to the rectifier simultaneously for polarization. The whole apparatus should be covered with a case with the inscription "Danger! High Voltage".

Chapter VII -- The URD-58 Ultrasonic Rail Flaw Detector Cart.

1. Intended Use and Working Principles of the Flaw Detector Cart.

The URD-58 TsNII ultrasonic flaw detector cart (Fig. 184) is intended for continuous testing of rail in place on the line. The following flaw types are revealed in rails with the aid of the flaw detector: vertical separations of the metal running longitudinally in the web or in the rail head above the web which are 10 mm or more in length (flaw types 30V.1-2); horizontal separation of the metal or cracks in any place in the rail web which penetrate not less than 7.5 mm in the metal (flaw types 52.1-2 and 55.1-2); internal horizontal separations in the rail head situated above the web (flaw types 30G.1-2); horzontal separation of the head which develops from the side and penetrates into the head not less than half its width; cracks from hairline cracks in the rail base below the web from a depth of 3 mm and with a length of more than 10 mm; inclined cracks situated at any height in the rail within the bounds of a rectangle limited by the thickness of the web; developed transverse (inclined) vertical cracks in the form of dark and light spots situated above the web; inclined cracks extending not less than 10 mm from the bolt holes (flaw type 53.0) are detected in the joint area using the flaw detector. All of the flaws noted above are also detected in the joint section of the rail with the exception of those which are situated above or below the bolt holes.

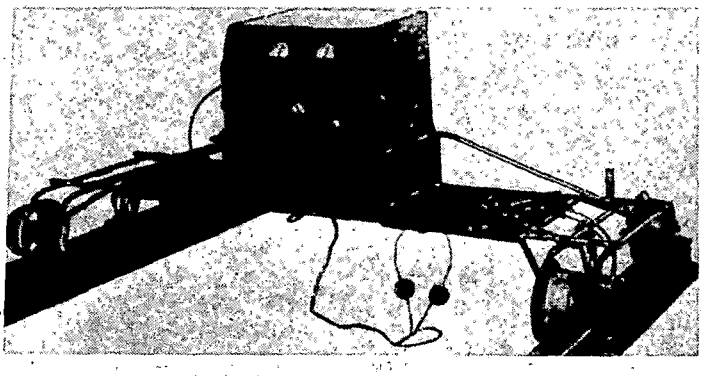

Fig. 184 View of the URD-58 flaw detector cart.

The URD-58 flaw detector, as well as the URD-52 flaw detector, sends short ultrasonic pulses at a repetition frequency of 200 Hz into the rail. At a maximum rail monitoring speed of 2-3 km/hr, and with the pulsing rate of 200 pulses/sec, the rail will have a wave passed through it for each 3-4 mm of the line that is covered. When the diameter of the piezoelectric element is 12 mm, continuous sounding of the rail is effectively obtained.

The flaw detector monitors the magnitude of the ultrasonic energy reflected from the base (the first bottom pulse), noting its diminution with an audio signal and by deflection of a milliammeter needle (the mirror-shadow monitoring method). The ultrasonic energy of the first bottom pulse is transformed in the flaw detector to direct current which controls the contacts of a polarized relay. The audio signal is switched on by the relay contacts only in the absence of the direct current in the windings. The size of the direct current passing through the relay winding is, from a certain value, directly proportional to the energy of the first bottom pulses since all of the remaining signals occurring on the receiver output, including the powerful initial pulse, are dispersed using a time gate and a variable time delay.

The ultrasonic oscillations are generated by piezoelectric elements made from barium titanate or PZT-19, which is the same as in the URD-52 flaw detector, except that their diameter is 12 mm. The piezoelectric elements are stimulated by a thyratron. The ultrasonic oscillations reflected from the rail base are transformed by the piezoelectric elements into an emf which is fed to the receiver, consisting of two stages (Fig. 185).

The high frequency (2.5 MHz) oscillations which make up the pulse are rectified after amplification, and enter the time gate (the coincidence tube).

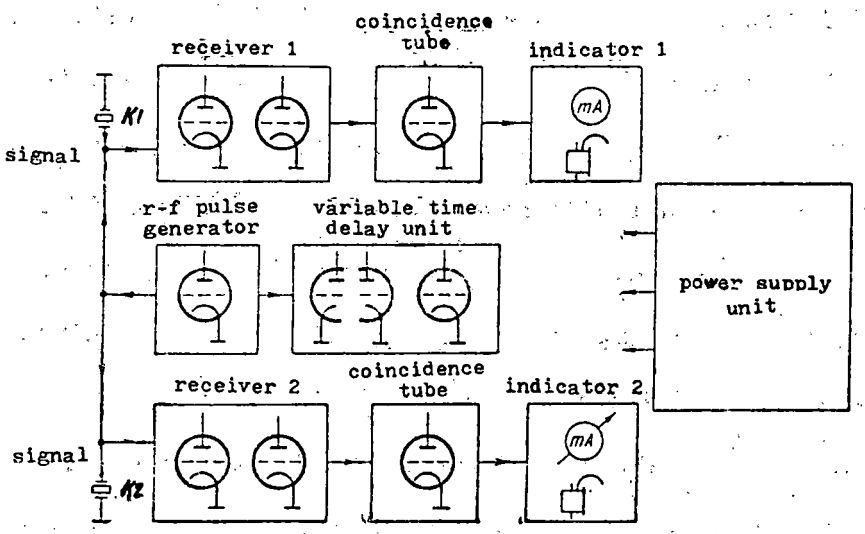

Fig. 185 Block diagram of the URD-58 flaw detector.

The time gate's task is to transmit into the indicator unit only the signal corresponding to the first bottom pulse, and to prevent the transmission of the initial pulse and all other signals.

Short pulses, delayed by the variable time-delay unit, are also fed to the time gate in addition to the signals from the amplifier. By changing the time delay of these pulses relative to the transmitted pulses (from a high-frequency pulse generator designed around the TG1-0.1/1.3 thyratron), it is possible to achieve a position where the artificially delayed pulses and the first bottom pulses will be fed to the time gate simultaneously. Only under this condition will the time gate pass pulse signals into the indicator unit. When pulses pass to the grid of the time gate at the wrong time, this causes it to close, and, consequently, decreases the current holding the relay armature in the up position.

As may be seen from the block diagram, the high-frequency pulse generator, the variable time delay unit and the power supply unit are common elements in the double-rail flaw detector.

The receiver's time gates (the stages) and the indicators (the flaw detector channels) are identical. The thyratron, which connects both channels at the moment of pulsing, is the connecting link in the circuit.

When the reflected signals are received, both flaw detector channels act independently, providing a pick-up of the separate signals from both rails.

In a de-energized state, the armature of the polarized relay should close the audio signaling circuit. This permits self-checking to be accomplished for all elements of the flaw detector circuits. Actually, when any tube malfunctions, or when any wire breaks, there are no bottom pulses. Consequently, the relay loses power and switches the signaling circuit on.

An inadequate quantity or lack of the wetting liquid will also be noted by an audio signal.

The small mechanical inertia of the RP-4 armature of the polarized relay permits distinct sound signals to be obtained when the rails are tested at a speed of 3 km/hr.

The joint sections of rail are monitored as the flaw detector is in motion. Audio signals arising when the bottom pulses disappear at the joint gap and over bolt holes are audible in the headset. Cracks or other flaws will cause an increase in the duration of the individual audio signals. This increase is easily detected by the flaw detector operators.

An interpretation of Fig. 186 will explain the interaction of the separate blocks of the flaw detector. The times 1, 2, 3 and 4 at which triggering signals are transmitted from the high-frequency pulse generator to the variable time delay unit are noted on graph I. These represent separate operating cycles of the flaw detector, 1 and 2 corresponding to the test of a sound rail, whereas 3 and 4 correspond to the test of a rail having a horizontal crack at the level of the bolt holes. The times at which

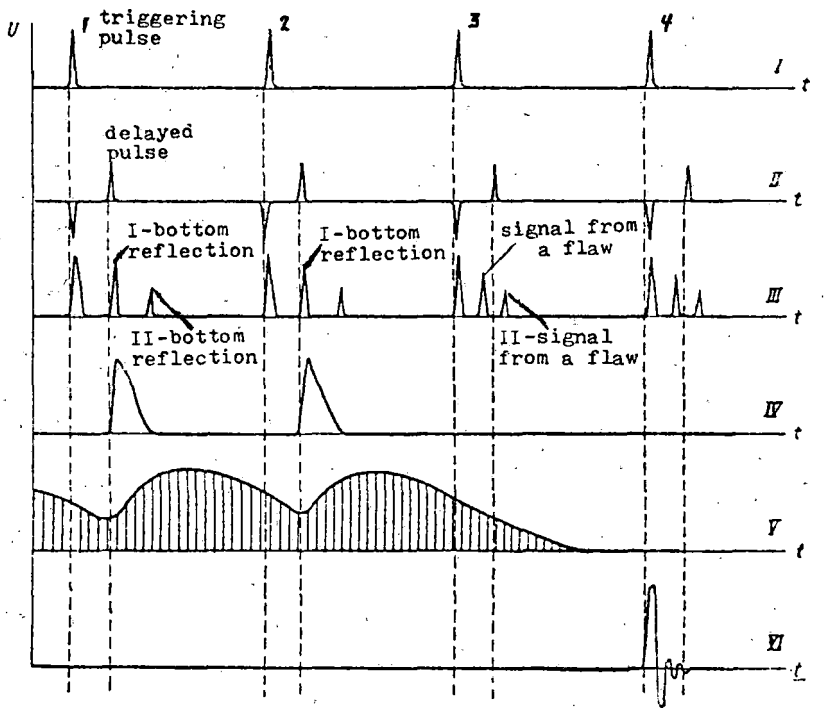

Fig. 186 Time diagram of the individual flaw detector units.

the artificially delayed pulse arrives at the time delay unit are noted in chart II. The signals on the receiver output are found in chart III (similar signals are visible on the URD-52 flaw detector screen, i.e. the initial pulse, the first and second bottom pulses or the signals from a flaw). The voltage at the time selector output (the coincidence tube) when the artificially delayed pulse coincides with the first bottom pulse (operating cycles 1 and 2) is shown in chart IV.

Should the artificially delayed pulse and the signal from the flaw not coincide (cycles 3 and 4), there is no voltage on the time selector output. Chart V shows the presence of a voltage in the relay winding when there is a voltage on the time selector output (cycles 1 and 2), and a decrease in voltage when the bottom reflection signals do not coincide (cycles 3 and 4).

The instant at which an audio frequency current is sent to the headset, when the relay contacts are closed because of a decrease in the voltage on its winding, is shown in chart VI.

2. The Electrical Schematic of the Flaw Detector Cart.

The electrical schematic of the flaw detector manufactured by the "Transsvyaz" plant is represented in Fig. 187. The flaw detector consists of two channels of the same type which are intended for testing the right and left rail on a line of track. The high-frequency pulse generators (Tube Tu5), the variable pulse time delay unit (Tube Tu6), the power supply unit, the transformer and vibrator Vb are elements common to both channels.

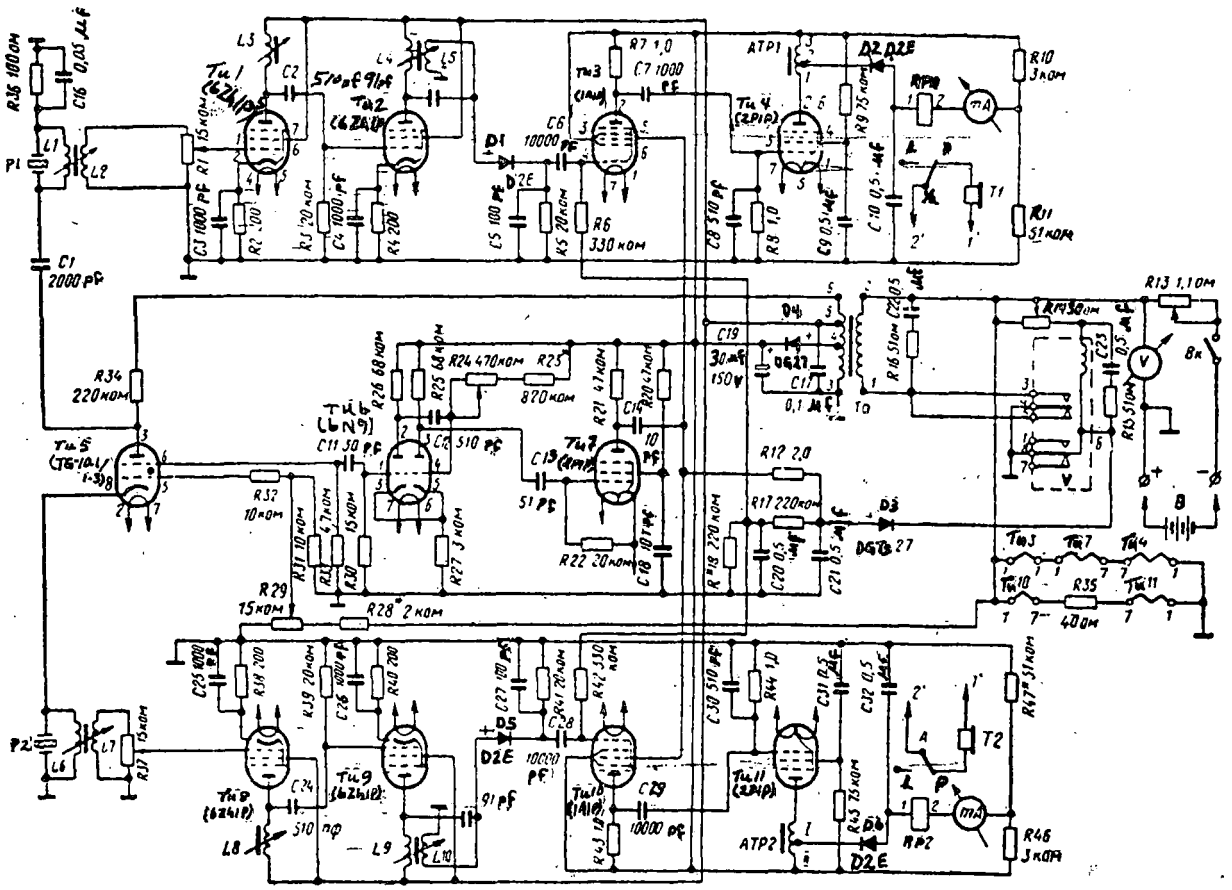

Fig. 187 Principal schematic of the URD-58 flaw detector manufactured by the "Transsvyaz'" plant.

The high-frequency electrical pulse generator. A thyratron, two oscillating circuits, a charging resistor and a reservoir capacitor are included in the generator circuit (Fig. 188).

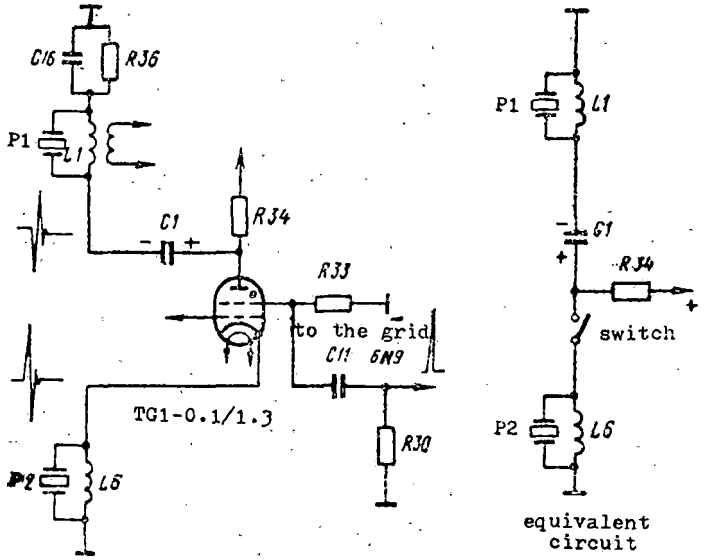

Fig. 188 Schematic of the URD-58 flaw detector's high-frequency pulse generator.

The generator works as follows. As the positive voltage grows on the thyratron plate, capacitor C1 builds up a specified charge. After a certain time, the thyratron fires, i.e. the cathode plate gap becomes conductive. The electrical energy built up by capacitor C1 is fed into the network of oscillating circuits L1P1 and L6P2, consisting of inductances and capacitors (piezoelectric elements), in one burst.

In the circuit, the thyratron acts as a switch, closing the circuit of the charged capacitor C1 with the chassis. The internal resistance of the thyratron is very low at the moment of firing, and, therefore, a large burst of current is obtained in the piezoelectric element's circuit (up to several amps).

Because of the plates' piezoelectric condition, they begin to oscillate mechanically when the burst of current from the charged capacitor is fed to them. Decaying high-frequency oscillations arise in the electrical circuits L1P1 and L6P2; the high frequency depends on the magnitudes of the inductances and capacitances included in the circuit. The piezoelectric plate itself serves as a capacitance. The frequency of the mechanical (ultrasonic) oscillations which arise is close to the natural oscillation frequency of the piezoelectric converter. Thus, the phenomenon of resonance, at which the amplitude of the mechanical vibrations of the piezoelectric elements is the greatest, is utilized.

The high voltage supplied to the thyratron plate from the power supply unit has the form of triangular (sawtooth) pulses. The moment at which the thyratron fires, relative to the maximum value of the voltage, is regulated by supplying a negative bias to the thyratron grid. This voltage is taken from the potentiometer, the knob of which is found on the face panel with the label "Start."

Separate operation of the two piezoelectric elements, excited simultaneously by the same thyratron, is obtained because of the inclusion one piezoelectric element in the thyratron plate circuit while the second is in the cathode circuit.

When the discharge of the energy built up by capacitor C1 terminates, the thyratron becomes non-conductive and disconnects the plate and cathode circuits. The capacitance coupling through the thyratron's plate-cathode gap weakens when the screen grid is connected to the chassis through a resistance.

The pulse time delay unit. The circuit of the pulse time delay is designed around tubes Tu6 (6N9, a double triode) and Tu7 (2P1P, a pentode) (cf. Fig. 187).

The circuit works as follows. When the thyratron fires, the current passing through the resistance into the screen grid circuit (R33) creates a voltage drop on it. Before the thyratron fires, an automatic biasing voltage forms on the grid of the left side of tube Tu6 (6N9), cutting it off. The right triode of the 6N9 tube is open at this time, and its plate current has a maximum value since the grid of this triode is under a significant positive voltage. At the moment the thyratron fires, a positive pulse from the thyratron screen grid, which causes a plate current to pass through the tube, is fed to the grid of the left triode of the 6N9 tube. The left triode conducts for a short time. The voltage gradient on resistance R26 (the plate load) is transmitted to the grid of the right triode through capacitor C12. Since the voltage gradient on the left triode plate will have a negative polarity, the right triode will be non-conductive at that time. The time during which the right triode is in a non-conducting state may be varied by increasing or decreasing resistance R24 ("Rail Type").

A positively polarized rectangular pulse 1 is obtained on the plate load resistance of the 6N9 tube's right triode (Fig. 189). This pulse is transferred from the plate load of the right triode R25 (cf. Fig. 187) to the differentiating circuit (RC) C13, R22 in order to separate the

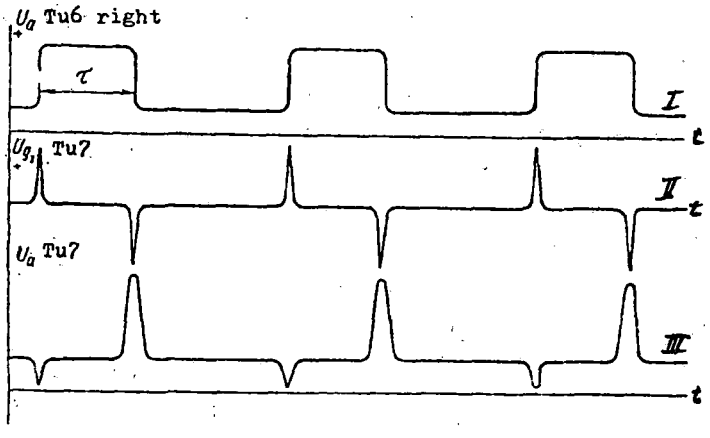

Fig. 189 Time delay.

leading and trailing fronts of the rectangular pulse. The leading front creates a positive pulse after differentiation, whereas the trailing front creates a negative pulse II (cf. Fig. 189). These pulses are fed to the grid of tube Tu7 (cf. Fig. 187), but only the negative pulse is amplified since the tube grid is at a state of zero potential relative to the cathode.

A positively polarized voltage gradient in the form of a short pulse III (cf. Fig. 189) is obtained on the plate load resistance R21 of tube Tu7. This pulse, with a voltage of about 35 v, is used in the circuit to unblock the time selector tubes which all this time are nonconducting due to the large negative bias on the grids.

The time gate (coincidence tube). The time gate is designed around tube Tu3 (Tul0), a 1A1P (cf. Fig. 187) and operates as follows. On the tube's first grid, a negative cut-off voltage of 14 v. is fed to the first grid of the tube, whereas an initial pulse and bottom reflection signals, which are positively polarized, are fed to the same grid from the receiver's diode detector. The negative cut-off voltage of 35 v. and a positively polarized unblocking pulse are fed to the third grid of the tube through capacitor C14, through the time delay unit. Consequently, it is necessary to satisfy two conditions for tube Tu3 (Tul0) to pass a signal from the receiver: a) the signal should appear simultaneously with the unblocking pulse from the time delay unit, and b) the size of the signal should be greater than the cut-off voltage on the first grid of the 1A1P tube (Tu3, Tul0).

The receivers. The receivers of the flaw detector are resonance amplifiers with a sufficiently broad transmission band. The receiver for the flaw detector's first channel consists of two 6Zh1P tubes, Tul and Tu2 (cf. Fig. 187). The receiver's amplification coefficient at a resonance

frequency of 2.5 MHz is not less than 2000 at a transmission band width of 150 kHz. The receiver for the second channel is in no way different from that for the first channel.

There is a diode detector designed around the D2E germanium diode (D1, D5) at the receiver output. In the flaw detector, the (diode) detector is necessary so that there are only pulses of a specified polarity, without the high-frequency component which is routed to the chassis by the capacitor C5 (C27) at the receiver output.

Amplification of the receiver is tested very simply: only the amplitude of the first bottom reflection pulse is measured when the probe is placed on a rail without flaws. The amplitude of the first bottom pulse on the detector load should be no less than 30 v. Measurements are made using SI-1 or S1-20 oscillographs.

Power supply for the plate and screen circuits of the receiver tubes comes only with the transmission and reception of reflected signals.

The indicator unit. A milliammeter and headset serve as the indicator in the flaw detector. Electrical signals entering from the time selector plate have a high pulse duty factor (the ratio of the interval to the pulse base width) and a sufficiently high amplitude. To reduce the pulse duty factor of the pulses in the flaw detector, an integrating circuit, consisting of the resistance R8 (R44 for the second channel of the flaw detector) and a capacitor C8 (C30) is employed. When the electrical signal passes to this circuit, the capacitor charges rapidly and then discharges slowly through the resistor. Thus, the brief electrical signals change their form and become more prolonged.

The signals pass to the first grid of the 2P1P amplification tube Tu4 (Tu11) after integration. A matching autotransformer, which acts as a

"ringing circuit" when there is a sharp decrease in the tube's plate current, is connected to the plate circuit of this tube.

In this case, free oscillations, the frequency of which is determined by the inductance of the winding and the capacitance between the turns of the winding, arises in the windings of the autotransformer. An autotransformer in good working condition, with no short-circuited turns, creates oscillations at a frequency of about 50 kHz with a duration of up to 900 μsec when a negative signal is sent to the grid. These oscillations are sent to the D2E diode detector D2 (D6).

Use of the "ringing circuit" permits a constant current component which controls the contacts of the RP-4 relay RP1 (RP2) to be obtained on capacitor C10 (C32) after rectification.

When negative signals are periodically fed to the tube grid through the use of the "ringing circuit," the direct current level, which keeps the relay contacts open, is maintained in capacitor C10 (C32). As a result, there is no audio signal in the headsets. A break of two or three bottom signals leads to a decrease in the potential on capacitor C10 (C32), the relay loses power, and switches the contacts, giving a signal for the presence of a flaw. A milliammeter, showing the current which is proportional to the energy of the first bottom pulses, is connected in series with the relay winding.

The polarized relay is regulated with a bias so that when there is no current in its winding, its contacts connect the headset to the audio frequency current circuit (to the vibrator circuit). Resistances R10-R11, and R47-R46 form voltage separators which create a reverse current in the circuit of the relay and diodes D2 and D3, fascilitating a more rapid activation of the relay, and diminish the level of the initial current (the hum) through the milliammeters.

The power supply block. The flaw detector takes power from a 6.25 v. storage battery. The energy consumption does not exceed 12 watts. In order to save energy, the power supply for the plate circuits of the flaw detector's receivers and the high frequency electrical pulse generator is supplied by pulses arising on the power transformer winding when the vibrator is in operation. This circuit is analogous to the power supply circuit of the URD-52 flaw detector.

When the storage battery B is connected to the instrument box, the electromagnetic vibrator V begins to work. Contacts 3 and 5 successively connect the power transformer to the current source. The current in the primary transformer winding grows to a specific size then breaks off sharply when the winding is disconnected by the vibrator contacts. At this instant, a self-induction emf of 35 v. arises on the primary windings 1 and 2. On the secondary winding, which is on this same coil, this emf is transformed to a magnitude determined by the relationship of the number of turns in the primary and secondary windings. The secondary winding of the power transformer has two leads 4 and 5 for receiving voltages of 65 v. and 90 v. Capacitor C17 eliminates the high-frequency oscillations arising in the transformer windings when the vibrator is in operation.

Vibrator contacts 1 and 7 are spares and are not used in the circuit.

The high voltage is taken from the secondary transformer winding. Under full load, it is equal to 300 v. ± 20% (the power supply voltage is 6 v.) and has the form of decaying electrical pulses with a duration of 0.002 sec. The entire working cycle of the flaw detector (ultrasonic pulsing and reception of the reflected signal) continues about 0.001 sec.

A rheostat R14 is connected into the circuit of the vibrator's start winding in order to regulate the vibrator's operation. Using the rheostat,

it is possible to change the voltage fed to the vibrator, and thus, to change somewhat the bias voltage which is taken from capacitors C20 and C21 (to change the level of the indicator activation).

The variable time delay unit, the time gates, and the final amplification tubes Tu4 and Tull draw direct current obtained by half-wave rectification of the pulsed voltage. A DG-Ts27 (D7Zh) germanium diode D4 serves as the rectifier. The electrolytic capacitor C19 smooths the pulsation of the pulsed voltage. The direct current requirement is approximately 15 milliamp at 65 v.

The bias voltage in the flaw detector is obtained after rectification of an extra-current arising on the start winding of the vibrator. This voltage (about 35 v.) is fed to capacitor C21 through a D7G germanium diode D3.

The current for the audible frequency (about 200 Hz), which is used for signaling, is taken from the primary winding of the power transformer, and is graphically represented in the form of sharply peaked pulses.

Beginning in 1965, the Dnepropetrovsky Electrotechnical Plant manufactured flaw detectors with P4G or P-217 transistorized converters. The schematic of a flaw detector with this type of converter is shown in Fig. 190.

3. Construction of the Flaw Detector Cart.

The flaw detector is mounted on a light four-wheeled carriage, in the center of which is an instrument box in a case. Between the carriage wheels and above the rails there are shoes (probes) and devices for mounting them along the axis of the rail being tested.

In the center of the carriage, under the instrument box, there are liquid containers. The unoccupied cross sections of the of the cars are

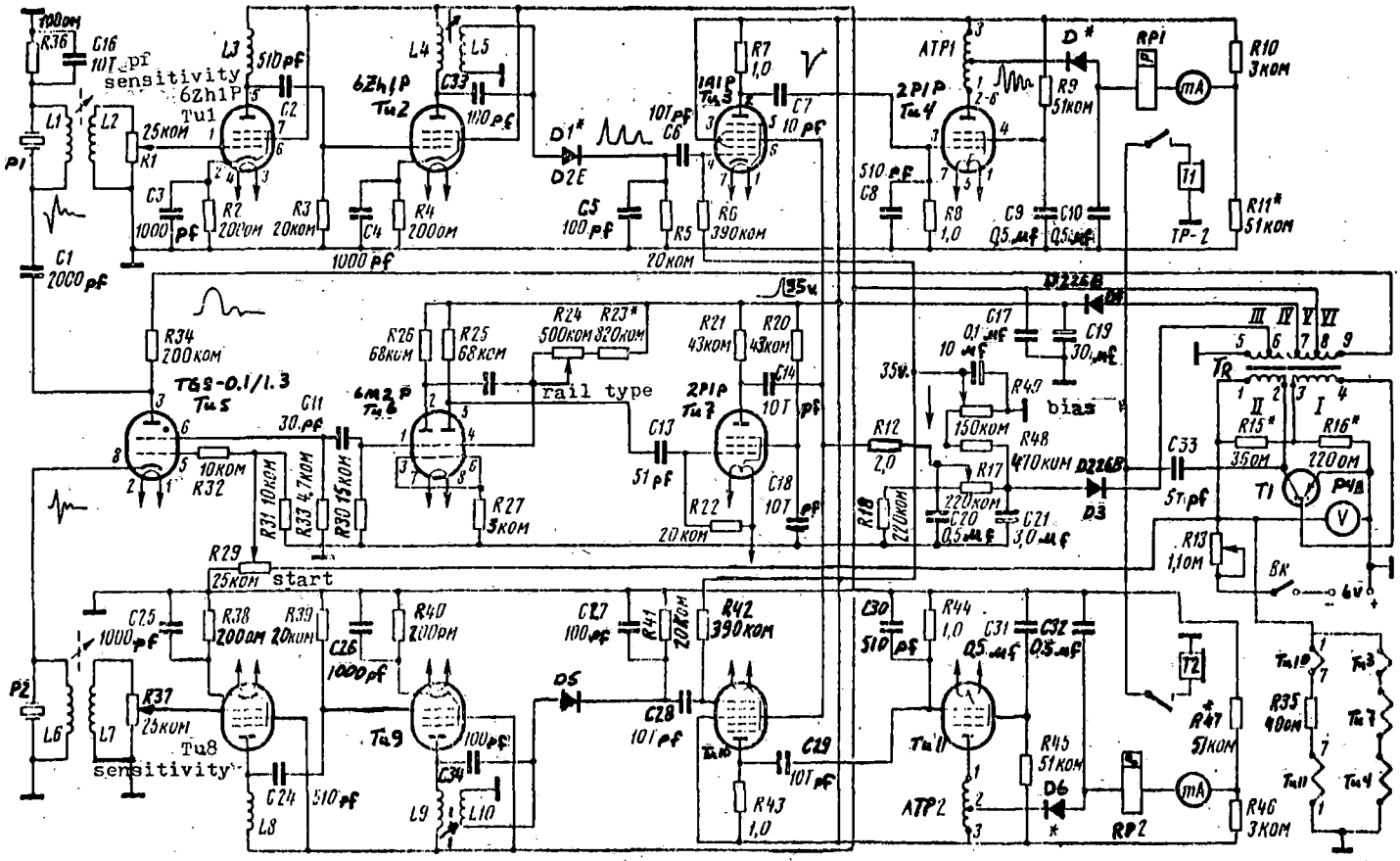

Fig. 190 Basic diagram of the URD-58 flaw detector (manufactured by the Dnepropetrovsky plant of the MPS--Ministry of Railroads).

covered with wire mesh. A removable handle on a hinge is mounted in the center of the frame for controlling the movement of the carriage along the rails.

The mounting and centering device is a system of levers and springs through which a stop plate with a wheel is pressed to the side of the rail, facilitating placing the shoe in the center part of the running surface of the expanded track (on curve sections of the line).

The flaw detector probes consist of the centering devices, shoes with a

protective base plate, and the piezoelectric elements. Each centering device is connected to the flaw detector carriage frame by two bolts and electrically insullated from it.

The centering devices on the left and right side of the flaw detector are the same. The device consists of a system of levers, a support wheel, and spring. The support wheel 1 (Fig. 191), which is pressed to the side of the rail head by a spring 2 in the working position, is situated on one of the levers. On lever 3, connected with the wheel lever by a hinge, there is the carriage 4 for fastening the shoe. The entire system is constructed so that when the flaw detector carriage is removed from the track, the support wheel and the lever pivot and come to rest in a horizontal position, raising the shoe higher than the running surface of the rail. The shoe is a solid steel body 5 having a replaceable plexiglass base plate on the bottom. There is a connector for the cable in the upper part of the shoe. In the

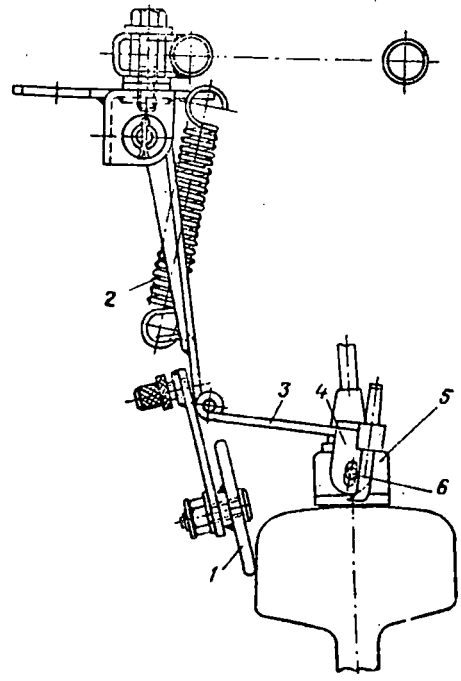

Fig. 191 Mechanical device for centering the shoe on the running surface of the rail head.

sides of the shoe body, studs 6 are provided to make a pivoting connection between the shoe and the carriage. The shoe fastening permits it to shift slightly in two planes. Freedom of movement is necessary for the shoe in order to obtain a snug fit between the base plate and the running surface of the rail on corrugated track and when monitoring joints where one rail is a bit higher than the other.

The construction of the shoe is shown in Fig. 192. The piezoelectric element used in the flaw detector is 12 mm in diameter; it is made from barium titanite or PZT-19 ceramic. In the first case, the thickness of the piezoelectric element is 1 mm, in the second, it is 0.72-0.75 mm. The textolite leg 3 (cf. Fig. 192) is glued to the piezoelectric element 2 using BF-2 glue. Electrical contact with the piezoelectrical facings is realized on the outside through a liner made of thin foil, and on the inside by a contact spring which passes through a hole in the textolite leg.

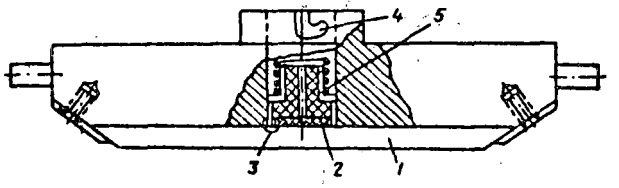

Fig. 192 Construction of the URD-58 flaw detector shoe.

Transmission of the ultrasonic oscillations into the base plate 1 takes place through a layer of oil (automobile engine oil or other mineral oil). The piezoelectric element is tightly fitted to the base plate by a spring 5. The spring is compressed when the connector, which fits into grooves in the shoe body 4 with lugs, and is tightened in place by turning it 30°, is hooked up.

The plexiglass base plate is 4 mm thick, and it is designed to test from 70-100 km of track. After this, the base plate is replaced with a new one or its worn surface is reworked using a file. The thickness of the base plate should not be less than 2.5 mm. The base plates of both flaw detector shoes should have an identical thickness where possible.

Rails are moistened with water, which flows by force of gravity from the tank to small tubes situated in front of each shoe, to provide the best accoustical contact during flaw detector operation. The quantity of water which is used is regulated by taps on each side of the flaw detector.

It has been determined when testing the flaw detector under various climactic conditions and on various rail lines, that brushes and wicks for moistening rails covered with a layer of residual oil do not improve the accoustical contact between the probes and the rail. However, the experience of several railroad lines shows that using brushes and wicks provides significant savings in the water which is used, which is very important when working on lengthy sections of the line.

Wicks made of fabric or porolon, to which the water is supplied, are used to decrease the water consumption; brushes made of felt are mounted in front of the shoe.

4. Preparation for Work and Inspection in the Field.

When working on the line with the flaw detector, it is necessary to pay particular attention to the timely charging of the storage batteries, the status of the shoes (the presence of oil between the plexiglass bottom and the piezoelectric plate) and the cables. It is necessary to have an adequate supply of liquid in the tanks.

Replacing the storage battery takes place in the following manner: the cover is removed, the discharged battery is removed from the circuit and

replaced with a charged battery. After this, the cover is replaced on the instrument box and the battery.

The placement of the shoes is regulated by a screw which is installed on the bar with the support wheel in a manner such that the shoes are located in the middle of the running surface of the rails being tested. The flaw detector is turned on, and a voltage of 6 v. is established using the rheostat.

It is absolutely necessary that the running surface be moistened in order for the ultrasonic oscillations to penetrate into the rail. For air temperatures above freezing, the moistening is with water, and, at temperatures below freezing, with a 50% solution of industrial alcohol. Minimum rate of consumption for the moisturizing liquid is 2 liters for every kilometer of track.

Flaw detector adjustment reduces to selecting the instant the thyratron is triggered using the "Start" regulator. Usually, the knob of this regulator is set according to markings made at the factory. Then, the time of the pulse delay corresponding to the time it takes for ultrasonic oscillations to pass through the body of the rail to the base and back (about 60 microseconds), is selected.

The delay time is regulated by the knob for the resistance labeled "Rail Type." The regulator for sensitivity, e.g. for the left side of the flaw detector, is placed in position 3 (the sensitivity regulators on the front panel have divisions) so that the milliammeter needle indicates 0.5-1.0 ma. Then, rotating the "Rail Type" knob, a maximum milliammeter reading is obtained for the left side and then the sensitivity regulator knob is moved to position 5. This concludes the tuning of the flaw detector. All that remains is to test the sensitivity. To do this, the amplification is reduced

(the sensitivity regulator is moved to position 3) and the headset is switched in. In this case, if there is no sound in the headset, the sensitivity of the flaw detector is considered to be normal.

It is possible to establish the necessary sensitivity level by turning the "Bias" knob until the audio signal disappears when the sensitivity regulator is set in the third position.

Normal sensitivity will be when the sensitivity is set in position 5; moving the knob two divisions assures that the indicator will activate when the first bottom pulse is reduced by about 50% (a nominal sensitivity of 0.5).

After setting the flaw detector sensitivity, it is possible to begin testing the rails. For this, the operator moves the flaw detector carriage foreward, having opened beforehand the taps supplying liquid under the shoes. If the rail is sound, there will be no signal in the headset. When the shoe passes over bolt holes and the joint, the audio signals will be audible in the headset.

At first, it is necessary to reduce the speed when passing through the joint zone of the rails and clearly distinguish each signal in the headset, to explain the cause for its appearance (measure the projection of the bolt holes on the running surface), and to compare the flaw detector readings. Subsequently, as requisite experience is acquired, it is possible to test the joint zone without slowing the speed of the cart. The fact is that the ear of the operator becomes accustomed to the characteristic sequence of sounds occurring as the shoe passes over the joint section of the rail, and all audio signals are perceived as a single audio signal of a specific tone.

If there is a crack or other flaw in the rail joint zone, the duration of the individual audio signal, e.g. from the bolt hole, increases, and the overall tone changes sharply. When such a signal is received, it is

impossible to indicate the flaw site accurately, and therefore, it is necessary to reverse immediately, and, slowly moving the flaw detector, make the reading more clear.

There are instances when sand and mud come under the shoe bottom. Here, too, the audio signal is switched on, but returning and repeating the pass over this place does not cause the signal to be repeated in the headset.

Holes for the joint connectors may also be detected, but when the plugs are firmly seated, the audio signal may not occur. In the case when the shoe comes off of the rail, the audio signal should be audible in the headset at all positions of the sensitivity regulator (1-10).

Under winter conditions, the concentration of the alcohol-water solution is selected according to the temperature of the surrounding air. Pure alcohol has a freezing point of -90° C. Moistening the rail should take place with the taps only partially open, so that the liquid flows in a fine stream. In addition, when working on rails having clean running surfaces and little wear (dents and engine burns), the quantity of liquid necessary for moistening may be reduced, and it may be fed out drop by drop. It is convenient to use a porolon sponge, having surrounded it with a rubber band so that the alcohol falls onto the porolon and does not flow off of the running surface of the rail.

Experience in using flaw detectors has shown that on track sections where the running surface of the rails is very dirty and covered with a layer of residual oil, it is helpful to add to the water surface activators which permit the oil and mud on the rails to be converted into an emulsion; the emulsion is easily washed from the running surface of the rail using water.

A soap solution is widely used as the surface activator, but there are other active emulsifiers, e.g. the universal detergents OP-7 or OP-4.

Adding two tablespoons of the emulsifier to a bucket of water permits the flaw detector to be operated on rails completely covered with residual oil or machine oil. The consumption of liquid depends on the state of the rail surface, and may fluctuate between 1.5-8.0 liter per 1 km of track tested.

When the audio signal is received in the headset, the flaw detector is stopped, and it is moved backwards. On the second pass, the shoe wipes the mud from the surface, and the running surface is again moistened. In the case when the audio signal still appears during the second pass, the boundaries within which the signal appears are noted on the rails, slowly moving the flaw detector back and forth. If the running surface is dirty, it must be cleaned with emery cloth and the test repeated. If the running surface is clean and there are no cavities or residual oil, the site must necessarily be marked with chalk or oil paint. After a careful inspection, an entry in the log book is required, according to the rules in the instructions. It is helpful to test the noted defective site in the rail with both the right and left sides of the flaw detector in order to be sure of their identical operation.

The nature of the flaw is determined in the following manner.

First, the flaw detector's sensitivity is reduced (the sensitivity knob on the front panel of the flaw detector is moved to position 9), and a second test is made, noting the boundaries within which the signal arises. When the length of the sector on the rail where the readings occur is reduced sharply, or when the readings become intermittent, this indicates the uneven development of a flaw, and a 30V.2 flaw with a length of from several centimeters to several meters is usually found. Then, using the regulating screw, the flaw detector shoe is shifted closer to the gage side and then to the field side of the rail, one side after the other. The boundaries of the

section in which the flaw detector gives a reading are marked on the side of the rail head. When the flaw is obviously located closer to the gage or field side of the rail and the mark changes along the length of the rail as the probe is shifted along the rail axis, most frequently a 30G.1-2 flaw is found. Near transverse flaws (type 21.2), the reading along the length does not vary sharply with the change in the sensitivity. The side of the rail head from which the flaw is propagating is established by shifting the shoe 5-6 mm from the axis to one side.

When a transverse flaw is suspected, the flaw detector readings are monitored using a reference probe, with or without a wedge-shaped fitting. This probe should be kept in the flaw detector tool box.

The wedge-shaped fitting permits ultrasonic oscillations to be sent into the rail at an angle to the running surface. The angle of the plexiglass wedge is 47°. Ultrasonic oscillations transmitted into the rail will propagate at a transmission angle equal to approximately 60°.

The presence of a transverse flaw in the rail head is specified more precisely in the following manner. The wedge-shaped fitting is put on the reference probe, which has been lubricated beforehand with oil. The end of the reference probe cable is connected to the jack on the instrument box instead of the shoe. It is not necessary to make any type of adjustments in this case other than to increase the receiver amplification (the sensitivity regulator is placed in position 10, indicated on the sensitivity regulator scale). The running surface of the rail is liberally moistened with the liquid for a distance of 0.5 m to either side of the place where there is a flaw detector reading, and this place is marked with chalk. Gradually moving the probe with the wedge-shaped fitting, to the noted defective section, the audio signal is monitored. If there is a flaw in the rail head,

the audio signal will be switched off at a specific instant. It is necessary to conduct the test when moving the probe to the right and to the left of the chalk mark on the rail head. A vertically situated flaw will cause the audio signal to switch off in the headset at the same distance from the mark when the probe is moved from the right or from the left. Type 21.2 flaws are revealed by mounting the probe with the 47° wedge at an angle of $32\text{-}35^{\circ}$ to the rail axis. To detect the flaws more surely, a standard rail which contains a 21.2 type flaw should be on hand in the repair shops and the practical skills necessary for the detection of these cracks should be worked out.

External inspection will not provide any idea about the nature of the flaw in most cases because, most frequently, the detected flaws are internal and do not emerge onto the surface.

A mirror and a sharp wire probe, which are required for examining the base of the rail, substantially aid the flaw detector operator when making an external inspection of defective sites on the rail. Frequently, slight indentations passing precisely along the axis of the rail are found in the rail base. These indentations (cavities caused by corrosion and rolling defects) give stable flaw detector readings when they are of adequate dimensions, even though they are not dangerous. Such places must be examined carefully, and, if they correspond exactly, for example, with a cavity caused by metal corrosion, a supplimentary test of the object revealing the corrosion fatigue crack using a DUK-13 IM flaw detector with wedge-shaped, 37-degree probes is required. However, if the flaw does not register when the sensitivity regulator of the URD-58 flaw detector is in position 10, this rail may be left in the line without secondary inspection with the DUK-13 IM.

5. Repair and Adjustment of the URD-58 Flaw Detectors.

When repairing the URD-58 flaw detectors the fact that it contains two identical channels for the simultaneous testing of the right and left rail lines must be taken into consideration. The high-frequency pulse generator, the delay unit and the power supply unit are common elements which are used for both flaw detector channels.

The use of direct-heating battery tubes connected in series in groups of two or three in the flaw detector somewhat hinders the diagnosis of troubles. The connection of the filaments of two groups of direct-heating tubes is shown in the basic circuit in Fig. 190.

Tube Tu8, which is used in the delay gating pulse unit, is included in the first group of three tubes. A malfunction of any of these three tubes in the first group (Tu8, Tu7, Tul0) leads to trouble with the entire flaw detector since the delay unit which is disabled is common to both channels. A malfunctioning of one of the tubes in the second group (Tu9, Tul1) or a break in resistance R44 disables only one flaw detector channel.

Thus it is possible to determine the unit or stage in which the trouble appears. A careful examination of the flaw detector wiring diagram is required in order to begin the repair. All obvious troubles which may be noted by examination (e.g. poor soldering or a tube which is broken or has come loose from its socket) is usually not difficult to fix. As experience in the repair of electrical devices has shown, locating the trouble occupies more than 90% of the time necessary to restore the operational capabilities of the instrument. When making repairs in a repair shop, the contacts in the RP-4 polarized relays are cleaned and the current for activating and releasing the armature is tested. The current-conducting cables leading to the probes and the headsets must be replaced.

The TG-1-0.1-1.3 thyratrons with an 8-pronged base must be replaced with TG-3-0.1/1.3 thyratrons with a 7-pronged base. A socket replacement is required for this change. In the later model flaw detectors from the Dnepropetrovsky Electrotechnical Plant, TGZ-0.1/1.3 and 6N2P tubes are used instead of the outdated 6N9S tubes.

The SI-1, S1-8, S1-20 and other electronic oscillographs are widely used for tuning the flaw detector after repair and for locating troubles which are not readily apparent. First, the operation of the high-frequency oscillator is checked with the aid of the oscillograph. Connecting the oscillograph to the thyratron plate, the instant of firing may be observed while turning the "Start" knob. The amplitude of the positive and negative pulses when the probes are connected should not be less than 25 v.

Industry has recently produced new KN-102I diode thyristors. These are semiconductor devices which permit the passage of pulses with a current of up to 10 amp and a voltage of 180-250 v. The instant at which these thyristors pass from non-conducting to conducting state (a resistance of several ohms) is determined by the voltage which is applied.

In the URD-58 flaw detectors, the thyratron may be replaced by similar devices without substantial modification. The "Start" resistance knob may then be removed and resistance R29 is connected in series with the thyristor plate load (Fig. 193). This resistor must be adjusted once when tuning the flaw detector in the shop.

It is necessary to move the start circuit for the pulse delay unit (C11) and to connect it to a circuit coil L6. Flaw detectors with the KN-102I diode thyristors were tested in 1969 on the Northern line at temperatures down to -37° C. and they exhibited full operational capability under these conditions.

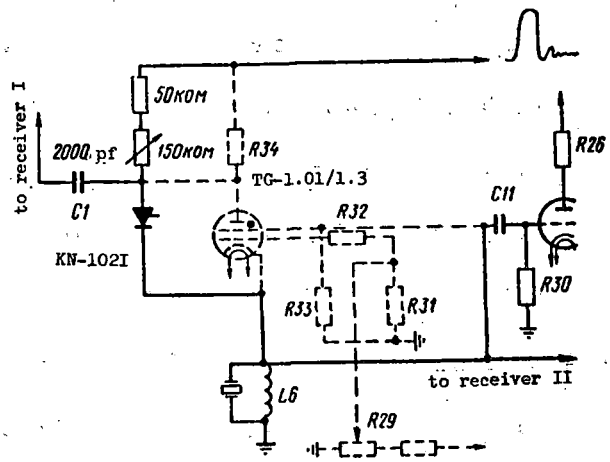

Fig. 193 Schematic of the pulse generator of the URD-58 flaw detector with a KN-102I.

Besides making adjustments more simple, this change brings about a savings of 0.6 amp in the power supply, which is very important since overall, the entire flaw detector requires only 2 amp of current.

The pulse delay unit is tested by connecting the oscillograph to the plate of tube Tu8. There should be a positive pulse with an amplitude of not less than 33 v. at this point. Oscillograph synchronization should be external from the pulse generator (the thyratron cathode or the circuit coil L6). The gating pulse time delay is 30-100 microsec.

The lower limit is tuned by the selection of resistor R21, the upper limit, by the selection of the variable resistor R19 or capacitor C12 (it is possible to install a larger resistor at R19, e.g., 1 Mohm, with some disturbance to the upper limit of the gating pulse delay). Oscillograms of the voltages at various points in the circuit are shown in Fig. 190 (the base circuit). The width of the gating pulse, measured at the base, should be in the range 10-20 microsec. It is determined by the capacitance of

capacitor C15 and the size of resistor R25. The greater the resistance R25, the broader the width of the gating pulse.

In most cases, when the high-frequency oscillator and the pulse delay unit are operating normally and the flaw detector is not working, it follows to search for the cause of the trouble in the bias circuit common to both channels.

When repairing flaw detectors in the repair shop, it is helpful to make a separate adjustment of the bias on both channels (Fig. 194). In order to do this, the variable resistance shaft must be removed to the front panel and designated as "Bias Rt," leaving the handle which is there with the designation "Bias" in order to regulate the left channel.

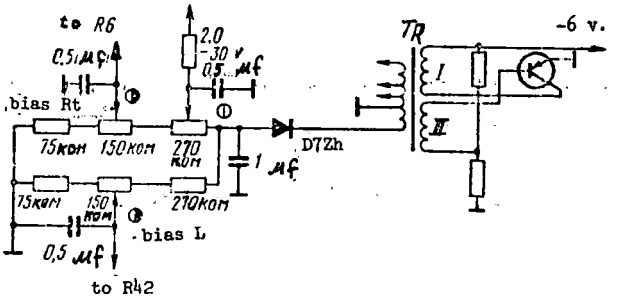

Fig. 194 Circuit for the separate adjustment of the bias in both channels in the URD-58 flaw detector.

The separate adjustment of the bias for the right and left channels permits the same sensitivity to be established in both channels when the probes are different. This is accomplished through the use of the sensitivity regulator on the input according to the divisions on the regulator scale. The need for strict matching of probe pairs is thereby eliminated. It is helpful to mark the number "3" on the scale of the knob labeled "Sensitivity" in red paint. When the knob is set at this position, the audio signal should

occur in the headset when the indicator activation threshold is adjusted with the "Bias" knob.

It is necessary to mark with yellow paint the section between divisions "5" and "6" of the same regulator which corresponds to the working sensitivity of the flaw detector (nominal sensitivity of approximately 0.5).

The working sensitivity of the flaw detector on the line and its tuning is tested by turning the "Sensitivity" knob counter-clockwise until the audio signal appears. The appearance of the audio signal in the headset when the knob is pointing to the number "3" indicates normal sensitivity. If the audio signal appears when the knob is set at "4," the bias must be decreased with the "Bias" knob in order to obtain the appearance of the audio signal only when the "Sensitivity" knob is set in position "3."

Horizontally situated cracks developing under the rail head which do not pass through the rail (flaw type 52.1-3) are most difficult to detect. The URD-58 probes (piezoelectric element diameter-12 mm, USO* frequency-about 2 MHz) have a dead zone of 4 mm for 52.1-3 flaws when monitoring R50 rails.

At a rated flaw detector sensitivity of about 0.5, only a crack which passes into the rail web to a depth of 7.5 mm. may be detected. Total overlap of the bottom signal is observed at a crack depth of 9 mm. (cf. Fig. 154).

The transistorized voltage converter, which is used in the URD-58 flaw detector instead of a vibrator, does not have adequate cooling when used in the summer. It is recommended that a radiator of any type be prepared from aluminum or copper with an active area of not less than 18 cm^2, depending on local conditions. A basic rule must be observed when preparing the

*USO--abbreviation for "ultrasonic oscillations."

radiator--the surfaces of the transistor bottom and the radiator should touch as snuggly as possible.

Changing the P4G in the converter for a P-217 transistor gives good results. The voltage increases by approximately 20%. The frequency at which pulses are repeated when the thyratron is used as a high-frequency pulse generator should not exceed more than 350 Hz, otherwise the phenomenon of interchannel interference is observed.

The basic difficulties of the flaw detector are most often found in the shoes and the connecting cables. When the wire which carries the pulsed voltage to the piezoelectric elements breaks, one half of the flaw detector ceases operation. It is possible to detect the break in the shoe cable by connecting the standard probe without the wedge-shaped fitting. If connecting the probe or shoe from the other half of the flaw detector restores operation, it is necessary to terminate the cable or wire conducting current to this shoe.

Particular care is necessary when disassembling and reassembling the shoes. The sequence of these operations is as follows. The contact head is removed by turning it 30°. The lug post is unscrewed and the shoe is taken out of the bracket. The spring and head of the piezoelectric element are taken out, and the shoe bottom is wiped with a clean rag and lubricated with several drops of oil.

To assemble the shoe, it is necessary to have a strip of thin foil and to lay it on the surface of the piezoelectric plate, which has been previously lubricated with oil. The end of the foil is then affixed to the cylindrical part of the piezoelectric element holder. The contact bushing is placed on this part of the holder and all of this is put into the opening in the shoe. Then, the contact bushing and the piezoelectric element holder are

lightly pressed to the bottom of the shoe using one finger. After the compressing spring has been installed, the contact head with the conducting wires may be inserted.

When changing the shoe bottom, it is necessary to take care that the thickness of the plexiglass is the same on both shoes. This is required because the speed of ultrasound is significantly lower in plexiglass than in steel, and the difference in the heights of the bottom does not permit the pulse delay to be set accurately using the "Rail Type" knob simultaneously for both lines of track. When the plexiglass bottoms are showing signs of wear, it is helpful to smooth the surface which contacts the rail. This is done with a broad file.

When the flaw detector is in operation, the water which is used to moisten the rail unavoidably gets into the shoe. To provide the best insulation of the piezoelectric element from the water, a paper insert is installed between the ski body and the bottom, and the holes drilled in the shoe body are filled with oil. But even this type of protection does not entirely guarantee that the piezoelectric element will be free from water penetration. In view of this, the shoe is dissembled, the droplets of water are removed from below the piezoelectric element and the shoe bottom is wiped dry through the opening. It is lubricated with oil and reassembled every two to three days.

Timely routine maintenance permits work with the flaw detector to proceed uninterrupted.

Testing the flaw detector's amplification channels and matching the piezoelectric elements. The flaw detector's amplification channels are tested using an oscillograph which is connected to the load on the detectors of the first and second amplification channels, one after the other.

Before testing is begun, the flaw detector's receiver device is taken out of the box. The power supply and the probe shoes are connected to it.

One of the flaw detector shoes is mounted on an R43 or R50 rail, the running surface of which has been lubricated with oil. This shoe is used to test both amplification channels. This permits the effect of the quality of the piezoelectric elements or of the plexiglass base plates, etc. to be excluded when evaluating the amplification.

The sensitivity adjustors are set in position "10" (maximum amplification) for both channels before the test.

When one of the oscillograph channels (resistance R5 or R41) is connected to the detector load, a series of vertical pulses appears on the screen (the oscillograph is switched on to operate with slave sweep). The height of the vertical pip (of the first bottom reflection) is set at approximately 20 mm. using the vertical amplification control on the oscillograph. After this, the oscillograph cable is switched to the detector load of the other channel and the shoes change places. Normally, the height of the bottom reflection signal on the second amplification channel output should be the same as on the first channel output. The flaw detector "Start" knob is set so that the height of the bottom reflection signal is at a maximum before the beginning of the measurements.

When there is identical amplification in both flaw detector amplification channels, the piezoelectric elements are matched. A satisfactorily functioning piezoelectric element and an amplifier should supply a voltage of not less than 30 v. (the bottom reflection) to the detector node when the probe is placed on a sound section of rail.

After observing on the oscillograph scale grid the size of the bottom signal received from the first channel with one (the first) shoe, the second ski is connected to this channel instead of the first. If the difference

in the height of the bottom reflection signal is less than 1 mm., in this case, the two piezoelectric elements are considered to be identical, for practical purposes.

In those cases where the difference in the height of the bottom reflection signals is greater than 1 mm., identical piezoelectric elements are matched by first replacing the piezoelectric element which gives the weaker signal.

The quality of the adhesive joint between the piezoelectric elements and the textolite leg is tested according to the lag of the initial pulse on the oscillograph screen. When the shoe is snuggly pressed to the rail, there should be a saddle extending to the sweep trace between the initial pulse and the first bottom reflection on the oscillograph screen. When the shoe is removed from the rail, the width of the initial pulse should not vary significantly.

The quality of the adhesive joint may also be tested without using the oscillograph. To do this, a headset is connected to the flaw detector and the flaw detector is tuned for testing IIIa type rail. Removing the shoe from the rail should cause the audio signal to switch on when the sensitivity knob is set at position "10." BF-2 glue is used to glue the textolite leg to the piezoelectric element. The glue is spread on the textolite leg two or three times, with a drying time of 15-20 minutes in air between each application. After this, the piezoelectric plate is snuggly pressed to the textolite leg. The final drying time takes 12 hr. at room temperature.

Checking the vibrator operation. With a correctly matched spark suppression circuit and accurately adjusted clearances between the contact points, the vibrator operates almost without sparking. The vibrator contacts

burn during sparking, leading to losses and variation of the current in the separate work cycles of the flaw detector.

The correctness and accuracy of the vibrator operation is checked using an oscillograph which is connected to winding 1-2 of the power transformer (cf. Fig. 187). A constant picture of the pulse voltage is visible on the oscillograph screen when the vibrator is working accurately. The oscillograph synchronization should be internal, and the scan should be continuous. A variable resistance R14 (30 ohm) has been furnished for adjusting the operation of the vibrator in the flaw detector. With this resistance, the voltage on the vibrator start winding may be changed while at the same time the amplitude of the armature oscillations are increased or decreased. The variable resistance knob is installed on the front panel.

The bias voltage in the flaw detector is obtained by rectification of the self-induction emf on the vibrator start winding. Therefore, a change in the voltage in this winding using resistance R14 leads to a change in the bias voltage. In this manner, the vibrator adjustment knob permits us simultaneously to change the flaw detector sensitivity (cut-off of the third and first grids of the time gate) and to select the optimum value for the start-up voltage for precise vibrator operation.

Testing the coincidence and indicator units. The coincidence and indicator units are also tested using either the SI-1 or S1-20 oscillograph.

On a normally functioning piece of equipment, a negative pulse, which will disappear completely when the coincidence between the delayed signal and the bottom reflection is disrupted, is observed on the plate of the coincidence tube when monitoring a defect-free rail. Breaking the contact between the shoe and the rail also leads to the disappearance of the negative signal on the coincidence tube plate.

Experience in using flaw detectors on the line shows that the R7 resistor (1 Mohm) and the coupling capacitor C7 (10,000 pf) which are shown in Fig. 187, malfunction most often in this unit.

The 1A1P tubes have a significant performance spread, especially where the third grid is concerned.

When certain tubes function unsatisfactorily in the coincidence circuit, it shows up particularly on the operation of the following indicator unit. The 1A1P tube should cut off completely at the third grid at a voltage of 28 v. Certain specimens require a greater voltage (32-35 v.) for cut-off. Therefore, part of the energy of the initial pulse passes into the indicator unit and causes a deflection of the milliammeter needle from zero, which makes the functioning of the relay worse.

Adjusting the indicator unit can be accomplished by obtaining the maximum current through the milliammeter through matching the D2E diodes D2 and D6, which should be of good quality. The current passing through the milliammeter should be about 2 mamp, but on occasion it may reach 3 mamp. An open-circuit current of about 0.1 mamp (one division on the scale) is permitted through the milliammeter and the relay.

When the current grows above this norm, it is necessary to replace the 1A1P tube. In the extreme case, it is possible to replace resistor R11 (R47), with the aim of increasing the supporting voltage on the diode D2 (D6).

The activation threshold for the RP-4 relay should be within the norms. Deviations from the norm are eliminated by adjusting the contacts in the following manner.

The flaw detector is switched on, the shoe is placed on the rail, and the headset on one side is switched on. By turning the "Sensitivity" knob, the current passing through the relay and the milliammeter is decreased.

Normally, decreasing the current to 0.8 mamp should increase the throw-over in the RP-4 relay ammature, and the sound signal will be switched on in the headset. Changing the instant of throw-over for the relay armature is accomplished by horizontal contact bolts, which are loosened from the terminals beforehand. Both flaw detector relays should be adjusted to the same activation current. The contacts of these relays are usually cleaned approximately once a month using a strip of writing paper.

The flaw detector power supply unit with the semiconductor voltage converter. Experience gained in using the URD-58 ultrasonic flaw detectors shows that the mechanical voltage converter is most often the cause of operational difficulties in the flaw detector. The instability of the converter operation has a particularly negative effect on the indicator unit (the needles of the instruments are always fluctuating, and at certain times, clicking signals not associated with flaws appear in the headsets). In addition, using a mechanical converter does not permit any increase in the ultrasonic pulse repetition frequency, and in practice limits it to 200-220 cycles/sec.

In association with this, a new transistorized voltage converter (using a germanium triode) has been developed for the flaw detector.

The basic diagram of the converter is given in Fig. 195. It consists of a relaxation oscillator with self-excitation (an auto-oscillator) assembled with a half-wave rectifier on diode D7B in a single-cycle circuit. When it is switched on and the transistor's resistance is low, i.e. when it is open, almost all of the voltage from the battery is fed to winding 1-2. As it increases, this voltage creates an emf in the remaining windings, including the feedback winding 8-9. With this voltage, the transistor closes, shutting off the current into winding 1-2. In this period, the energy contained in the transformer core is transferred into the load circuit. The transistor opens again, and the cycle is repeated.

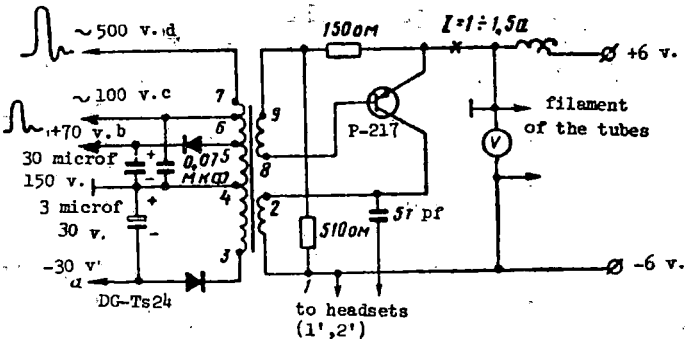

Fig. 195 Circuit diagram for the transistorized converter.

The resistance in the base circuit permits the consumed and, consequently, the output power of the converter to be regulated. The converter is designed according to a blocking oscillator circuit. The voltage which is inducted in winding 3-5 is rectified by the D7V semiconductor diode, and it is fed to a 30 microf electrolytic capacitor which smooths out the pulsation.

For constant converter operation, a certain negative bias, taken from the separator's 510- and 150-ohm resistances, is supplied to the base of the transistor. Winding 8-9 forms the excitation circuit. The commutation frequency within the converter depends primarily on the quantity of iron in the magnetic circuit, the clearance in the core, and the number of turns for the primary and excitation windings. In this case, the commutation frequency is about 350 cycles/sec. The windings are distributed on the transformer coil in the following manner.

The primary winding 1-2 is wound first. Then follow the remaining windings 3-5, 4-5, 5-6, 6-7, from which a useful load is taken off. The excitation winding 8-9 is wound last. The polarity of the pulsed voltage on the secondary winding 3-4, 4-5, 5-6 is indicated on the circuit diagram. In those cases when the voltage polarity on winding 4-5 is reversed, it is

necessary to change the ends of the excitation winding and the primary winding at the same time. Converter efficiency is decreased because of the 0.07 microf blocking capacitor. Increasing this capacitance leads to a decrease in the commutation frequency and decreases somewhat the overall voltage on the rectifier load. The necessary voltage and the commutation frequency are obtained by the selection of the resistance in the transistor base circuit. In the given circuit, transistors having a collector breakdown voltage of not less than 25 v. (the P4G and P-217) work well.

The rated voltage magnitudes in relation to the chassis, with a load from the flaw detector side of the circuit are:

point a -- -30 v. d.c.;

point b -- +70 v. d.c. at a pulsation of not less than 0.5 v.;

point c -- 100 v. pulsing current (measurement conducted using the SI-1 oscillograph);

point d -- 500 v. pulsing current (measurement conducted using SI-1 oscillograph).

The converter transformer is protected from improper accidental connection of the battery by two D7Zh diodes connected in parallel. When the P-217 transistors are used, it is not possible to provide such protection. The converter's current requirement is 1.0-1.2 amp, and depends on the quality of transistor used.

The converter was tested under various conditions. Experience shows that lowering the temperature of the surrounding air does not influence a semiconductor converter, but the electrolytic capacitors used in it should of necessity be freeze-proof. Tests of the flaw detector operation at air temperatures as low as 50° C. have shown the full work capability of the transistor under these conditions without special protection measures being necessary.

This type of semiconductor converter was mounted as a separate unit in flaw detectors manufactured in 1959-60 by on-line repair shops specializing in flaw detector repair. When mounting the converter, resistance R34 in the flaw detector circuit and resistance R18 in the rectifier bias circuit (cf. the basic circuit in Fig. 187) are each decreased to 150 kohm. Capacitor C17, with a 0.1 microf capacitance, is replaced by a 0.07 microf capacitor which is in the converter unit using the semiconductor transistor. The headsets are connected to the primary converter winding (cf. Fig. 190), i.e. to points 2' and 1' in the circuit. All of the parts of the flaw detector which relate to the vibrating power pack circuit are eliminated from the chassis. This includes capacitors C22, C19, and C23, and resistors R16, R15, and R14 (cf. Fig. 187) as well as the transformer with the vibrator and rectifier.

The hole which is left on the front panel of the flaw detector after resistance R14 is removed is occupied by an NM-5 neon signal bulb, connected through resistance R, equal to 91 kohm, to point 7 in the transformer.

Table 11

Possible Difficulties in the URD-58 Flaw Detector and Means for Correcting Them

#	Difficulty	Causes	Procedure for Correction
1	Current not fed to voltmeter when flaw detector is switched on	Power supply rheostat malfunctioning	Replace the rheostat or rewind it
2	Voltmeter indicates voltage when the converter is on, but converter is inoperative	a) D7V diode out of order (2 Ea.)	a) Temporarily short out the diodes using a jumper. If they are out of order, replace them.
		b) P-4G (P-217) transistor out of order	b) Replace the transistor with a good one
		c) Break in the power transformer or in the transistor base circuit	c) Test the transformer and the transistor base circuit
3	The converter is operational, but it supplies inadequate voltage	a) Circuit requirement has been increased (short circuit)	a) Switch off the d.c. and a.c. current circuits one after another
		b) Transistor regime has been disrupted	b) Test the continuity of the separator resistances
		c) There are short-circuited turns in the transformer	c) Replace the transformer
4	There is a bottom pulse on the detector load, but the indicator does not switch in the audio signal	a) There is no strobe pulse from the delay block	a) Test the strobe pulse from the delay block and replace the 2PIP tube in the delay block
		b) There is no +70 v. d.c. voltage	b) Test the D7V (DGTs-24) diode and the electrolytic capacitor
		c) Second detector is faulty	c) Replace the D2E diode
5	Only one channel of the flaw detector operates	a) The probe is inoperative	a) Replace the probe
		b) The receiver and stages are malfunctioning	b) Check for whether or not there are signals on the detector load
		c) The indicator's 2PIP tube is out of order	c) Replace the 1A1P and and 2PIP tubes

Table 11 (Continued)

#	Difficulty	Causes	Procedure for Correction
6	The flaw detector's sensitivity is very high; there are many false activations of the indicator	a) The receiver amplification has been decreased	a) Test for receiver amplification by connecting a good shoe (probe) and measuring the amplitude of the first bottom pulse
		b) The probes are worn	b) Replace or file the probe protectors with a file
		c) The negative bias voltage is higher than normal (the level at which the indicator activates)	c) Test the bias voltage on the first and third grids of the coincidence cascade tube (1A1P) with a tester
		d) The activation current in the relay is increased	d) Test the activation in the RP-4 relay. If it is higher than normal, replace the relay
7	One flaw detector channel influences the other	a) The frequency at which the converter operates is greater than 350 Hz	a) Test the frequency at which the converter operates. If it is more than 350 Hz, connect an auxillary capacitance to the 0.07 microf capacitance in the -100 v. circuit (the tube plates)
		b) The instant at which the thyratron fires has been incorrectly selected	b) Select the proper instant for thyratron firing using the "Start" knob
		c) The thyratron is faulty	c) Replace the thyratron
8	Weak sound in the headsets	a) The headset is out of order	a) Repair or replace the headsets
		b) The audio signalization circuit is incorrectly connected	b) The audio signalization circuit should be connected through a 0.005 microf capacitor to the first transformer winding
9	The voltage converter overheats during extended operation	a) The collector current is increased	a) Test the transistor operating regime and the collector current (It should not be more than 1.5 amp)

Table 11 (Continued)

#	Difficulty	Causes	Procedure for Correction
9	(cont)	b) There is no cooling radiator	b) Put the transistor radiator on
10	The flaw detector is unsuccessful at providing consistent operation on light rails (type IVa)	The pulse-delay adjustment band width is inadequate	Test the minimum time delay (40 microsec); if it is not maintained, decrease resistance in the "Rail Type" adjustor circuit
11	Unstable operation on rails covered with a layer of residual oil	Poor acoustical contact between the probes and the rail	Resort to pre-moistening using the surface activants 285 (OP-7; OP-4, or denatured alcohol). Increase the amplification (Set the attenuator on the 8th or 9th position) Pour 2-3 drops of oil into the probe
12	The flaw detector notes nearly every rail spike with an audio signal	a) The ultrasonic oscillations are dispersing due to corrosion of the base	a) Increase the amplification; put the sensitivity knob on the 9th or 10th position. If the signal does not disappear, test the doubtful site using a DUK-13 IM flaw detector with a wedge-shaped 37-degree probe
		b) The metallic base plate is seated snuggly against the base of the rail, or the wooden padding is missing; there is water between the rail and the base plate	b) Increase the gate pulse delay slightly. If this leads to the audio signal being switched off, pay no further attention to similar signals

Chapter VIII -- The URD-63 Ultrasonic Single-Rail Flaw Detector.

1. Intended Use and Working Principles of the Flaw Detector.

The ultrasonic single-rail flaw detector (Fig. 196) is primarily intended for selective rail monitoring, largely based on data from flaw detector cars. Pulse-echo and mirror-shadow flaw detection methods are used in the URD-63 flaw detector. When working with the flaw detector using the mirror-shadow method, the same flaws which are located by the URD-58 flaw detector may be detected: vertically situated separations of the metal in the head, web and base of the rail (flaw types 30V.1-2 and 60.1-2); horizontally situated metal separations and cracks in the rail head and the web (flaw types 30G.1-2 and 52.1-2); cracks in the joints from the bolt holes (flaw type 53.1-2); developed transverse fatigue cracks (flaw type 21.1-2); etc. One normal probe is used when working using the mirror-shadow method.

If the flaw detector is operating using the pulse-echo method, a wedge-shaped "zig-zag" probe is used (Fig. 197), permitting detection of transverse flaws developing in the side of the rail head. Two wedge-shaped probes, which are switched on one after another, depending on the angle of

Fig. 196 The URD-63 Ultrasonic Single-Rail Flaw Detector.

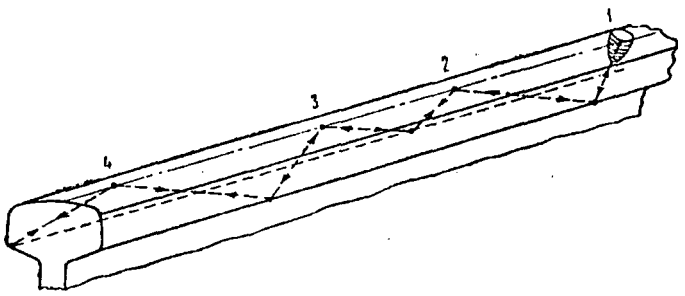

Fig. 197 The wedge-shaped probe for detecting transverse fatigue flaws in the side of the rail ("zig-zag").

inclination of the possible flaws, are used for testing for the presence of transverse 21.2 fatigue cracks which are only slightly developed in the right and left rail of the track.

Using a normal and a wedge-shaped probe in the URD-63 flaw detector permits detection of all of the types of flaws which develop in rails when they are in use; the only exception to this are those types of flaws which arise at the edge of the rail base.

The URD-63 flaw detector is transistorized and simple in construction, and it contains a minimum number of elements.

The repetition rate of the ultrasonic oscillation (USO) pulses sent into the rail is from 300 to 1000 Hz at a radio pulse oscillation frequency of 2.5 MHz in the URD-63 flaw detector. All piezoelectric elements are the same (TsTS-19, 12 mm in diameter and from 0.72-0.75 mm thick).

The use of a second detector (rectifier) and a reservoir capacitor (an integrator) permitted the creation of an inertial flaw notation system which activates only upon a decrease in the bottom pulse energy during two to three operational cycles of the USO oscillator. This increases the anti-static properties of the flaw detector.

Generation of USO pulses in the probe is accomplished using a blocking oscillator built around P-601 transistors. The piezoelectric element of the probe and the induction coil which is connected in parallel with it are connected to the transistor emitter circuit.

Excitation of the oscillation circuit, which consists of the probe's piezoelectric element and the induction coil, is accomplished by the sharp trailing front of the current pulse from the blocking oscillator. When there is an abrupt break in the current supply into the inductance coil connected to the transistor emitter circuit, an oscillatory process arises in the electrical circuit. The amplitude of the pulse fed to the piezoelectric element reaches 25 v. at a power supply source voltage of 9-10 v. overall. The oscillatory process lasts 5-7 microsec. in the probe's piezoelectric element circuit, and it permits a USO pulse of adequate strength to be sent into the rail with little power drain on the battery.

The ultrasonic energy which is reflected from the base of the rail is converted to d.c., which controls the key circuit playing the part of the electromechanical relay in the removable URD-58 flaw detector. An adjustable time-delay and a coincidence stage are used for isolating signals corresponding to the bottom reflections.

The high-frequency (2.5 MHz) oscillations which make up the pulse pass from the piezoelectric element of the probe to the receiver, which has a maximum amplification of about 500, after which it is fed to the rectifier.

An audio indication of a flaw is achieved using a headset, the audio frequency current being supplied to the headset from the blocking oscillator when working with the normal probe and from the resonance circuit when working using the pulse-echo method. The frequency of the current pulses fed to the headset is determined by the frequency of the blocking oscillator.

The tone of the sound in the headset is different when pulses are fed from the blocking oscillator through the switching circuit, when a flat probe is operating, and when only the echo signals are supplied after their conversion in the resonance circuit.

The block diagram for the URD-63 flaw detector is shown in Fig. 198. The basic element of the flaw detector is the pulse generator PG. This unit determines the USO pulsing rate and triggers all remaining units. When the generator activates, a current pulse with a steep front excites electrical oscillations, which quickly decay in the probe's piezoelectric element.

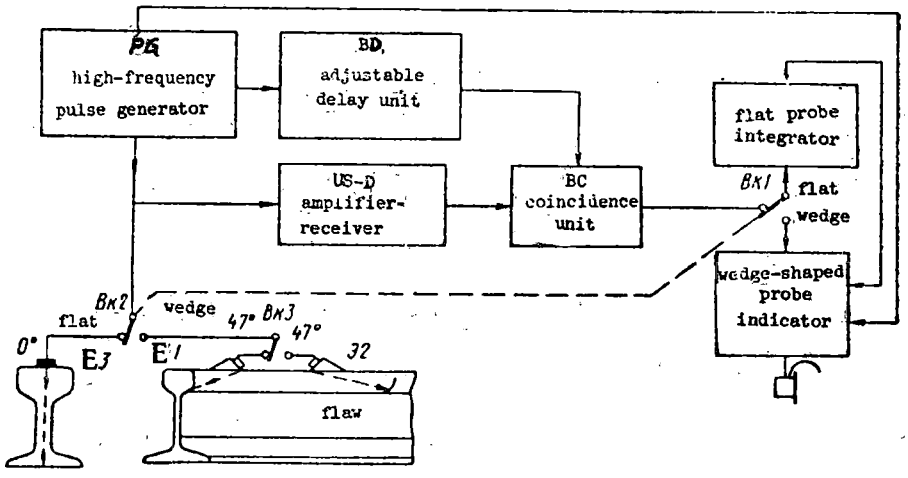

Fig. 198 Block diagram of the URD-63 flaw detector.

A triggering pulse is fed into the delay unit BD from the PG unit simultaneous with the generation of USO pulses. This unit produces a gating pulse of about 20 microsec. in duration which is delayed relative to the triggering pulse by 30-140 microsec. Adjustment of the time delay is accomplished using a variable resistor, the knob of which is situated on the front panel and designated "Rail Type."

The receiver amplifier US-D is connected to the pulse generator PG in parallel with the piezoelectric element. This component serves for amplifying the electrical pulses arising in the piezoelectric element when USO pulses reflected from the base of the rail or from flaws are received.

Besides being amplified, the electrical signals are transformed in shape in the receiver-amplifier. They are rectified, and, after further amplification, are fed to the coincidence unit BC. In unit BC, an operation takes place which separates from all entering pulses those which coincide with the artificially delayed gating pulse entering from unit BD. As a result, the only signals at the output of unit BC are those corresponding to the bottom pulses or echo signals from flaws.

Signals from unit BC are fed either to the integrator or to the amplifier-indicator. The headset is connected to the output of the amplifier-indicator through switch BK2.

Switch BK2 serves to switch in either the normal (flat) or the angle probe, as well as switching in the indicator unit.

If the level of the bottom signals decreases, an integrator, which switches the audio frequency current and feeds it to the headsets, is switched on during the operation of the normal probe. Either the "front" or the "back" probe, E1 or E2, may be used for connecting the angle probe. They are switched using the BK3 switch. The flaw detector power supply unit B is a battery consisting of six dry "Saturn" elements. The normal voltage is 9-10 v. The entire flaw detector, including the pulse generator PG, which requires a current of not more than 20 mamp, takes its power from this source.

2. Electrical Schematic of the Flaw Detector.

The electrical circuit of the URD-63 flaw detector is shown in Fig. 199. The high-frequency pulse generator which excites the USO in the piezoelectric

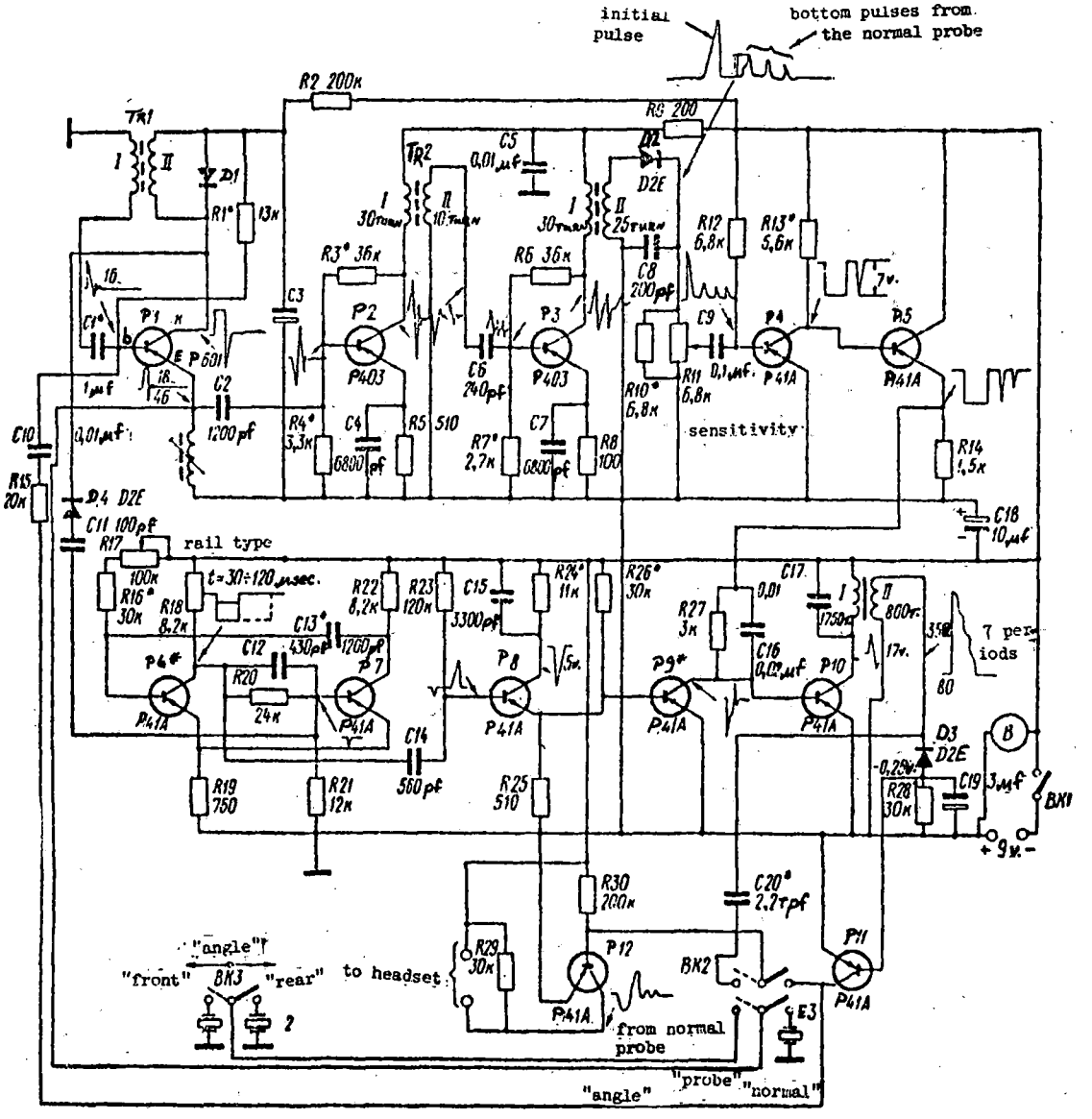

NOTE--Labels P6* and P9* supplied by translator.

Fig. 199 Primary electrical schematic of the URD-63 flaw detector.

element is designed around P-601 transistor P1 in accordance with a blocking oscillator circuit. The natural frequency of the blocking oscillator is determined primarily by capacitance C1 and resistance R1. However, the transistor parameters have an effect on the pulse generation frequency. The blocking oscillator's oscillation frequency has a range of 300-1000 Hz associated with the broad spread of P-601 transistor characteristics.

The high-frequency pulse generator power supply is obtained through a decoupling circuit R2 C3. Diode D1, connected in parallel with the winding of transformer TR1, prevents an extra-current surge when the current through the transistor ceases abruptly.

Excitation of the high-frequency pulse in the piezoelectric element circuit and in inductance coil L1 takes place when there is a sharp drop in the current on the collector-emitter circuit of P1. Connecting the inductance coil L1 to the transistor emitter circuit permits a simple commutation to be realized when the various probes are replaced. The high-frequency oscillations in the circuit inductance L1-probe piezoelectric element arises due to energy stored in coil L1. The amplitude of the pulses exciting the piezoelectric element is 25v. The triggering pulse for unit BD (transistors P6 and P7) should have negative polarity. This pulse is taken from the collector of P1 and fed into the pulse delay unit through diode D4 and capacitor C11, forcing the delayed multivibrator, which is connected to transistors P6 and P7, to activate.

In the normal state (no triggering pulse), the delay unit multivibrator is stable, transistor P6 is open, and P7 is closed by the voltage taken from the load in the emitter circuit of P6. The parameters are selected so that when there is a negative pulse, transistor P7 opens with a current pulse in the transistor base circuit. When P7 opens, the voltage drop from

the collector is transferred to the base of P6, forcing it to close. The time during which transistor P6 is closed is determined primarily by the parameters of the circuits R16 + R17·C13. The circuit consisting of resistances R20 and R21 is necessary for thermal stabilization of the circuit. The instability of the circuit's time characteristics is about 1.5% when the power supply voltage varies within ± 20% and temperatures vary within the range -20 — +50° C.

As the specified time period ends (the delay time), transistor P6 opens and the circuit again becomes stable until the next triggering pulse. A negative square pulse is fed from the collector of P6 to the differentiating circuit (RC) C14R23. The time constant of this circuit is chosen so that only abrupt changes in current, i.e. the leading and trailing fronts of the square pulse, are permitted to pass.

The differentiated pulse is fed to the base of transistor P8. Transistor P8 is closed. The negative pulse obtained from differentiation of the square pulse does not cause a substantial increase in current through transistor P8. It is not detected in the emitter circuit. The positive pulse cuts off the current through transistor P8. A small positive current surge which is then used for controlling the switching circuit of the coincidence unit BC (transistors P9 and P10) arises in the emitter circuit.

Thus, by varying the duration of the square pulse, the time at which the positive pulse appears in the emitter circuit of transistor P8 can be changed so as to obtain a strong pulse which is delayed for the necessary time period relative to the start pulse. The time period is equal to either the time the USO takes to pass through the rail from the running surface to the base and back or, when using the pulse-echo method, to the time during which the USO passes from the wedge-shaped probe to the flaw and back.

The switching circuit for the coincidence unit consists of two interconnected transistors P9 and P10. (In the delay block, the switching circuits, and the pulse amplifiers, only two types of transistor are used--MP-41 and MP-39.) The circuit operates in the following manner. All of the signals from the receiver-amplifier output enter the collector of P9 and the base of P10. These signals have a negative polarity. The "collector-emitter" circuit of transistor P9 is connected in parallel to the base (the input) of transistor P10. If transistor P9 is open, i.e. the resistance of the collector-emitter is small, then all signals entering from the receiver-amplifier will be shunted. These signals are not fed to the output of transistor P10, but if transistor P9 is cut off along the base circuit, the resistance in the emitter-collector section increases sharply. As a result, signals from the receiver will be fed into the amplifier. At the moment that a positive pulse arises at the base of P9 from the delay unit, a sharp increase in the resistance of the collector-emitter section of P9 takes place. The shunting action of P9 ceases and signals pass to the base of transistor P10 from the receiver.

A "resonance circuit" consisting of transformer TR4 and capacitor C17 are connected in the collector circuit of this transistor. The pulse from the receiver amplifier, arriving at the base of P10, cuts off the current sharply in the collector-emitter circuit. The frequency of the oscillations arising in the transformer-capacitor C17 circuit is about 100 kHz. The duration of the free oscillations of this electrical circuit is about 10 cycles, which permits a single pulse-echo passing from the receiver into the rail after each USO pulsing to be substantially lengthened. After rectification by diode D3, the pulse length which was increased by the "resonance circuit" permits the constant component of the leakage current through the circuits

of the base of transistor P11 and the circuit of resistance R28 to be received on capacitor C19.

Using a rectifier with a reservoir capacitor C19 permits the electrical pulses corresponding to the bottom pulses to be integrated during testing of the rails. A negative potential, which is used subsequently for controlling the indicator switching circuit (transistors P11 and P12), appears at capacitor C19 when there is a systematic pulsing through diode D3 from the resonance circuit.

This circuit permits the audio frequency current from the base of the blocking oscillator to be shunted using the resistance in the emitter-collector P11 circuit. The audio frequency current is therefore prevented from entering into the terminal amplifier P12 and the headsets when there is a bottom pulse.

Resistance R28 and capacitor C19 are matched so that a break of two anticipated bottom pulses in an uninterrupted series of signals creates a sharp decrease in the shunting action of transistor P11 and causes the audio signal to appear in the headsets.

The terminal amplifier is based on transistor P12 in accordance with the usual circuit. The headsets are connected in the collector circuit. Switch BK2 permits signals to be fed to the terminal amplifier directly after the resonance circuit signals, by-passing the switching circuit. Such a system is used with the pulse-echo monitoring method, when angle probes are employed.

The duration of the gate pulse delayed by the delay unit is 20 microsec., and it is determined by the parameters of the differentiating circuit (C14·R23). An increase in capacitance C14 leads to an increase in the duration of the gate pulse.

Using the gate pulse when working with wedge-shaped probes and the pulse-echo method permits the location of a flaw in the rail head to be determined more accurately than is possible with the "zig-zag" probes. This is because the wedge-shaped "zig-zag" probes, when passing a sound wave through the head, do not give a clear representation of the distance at which the flaw reflecting the USO is situated from the probe (it is possible to receive the reflected signal on the first, second, and third reflection from the flaw).

The flaw detector's receiver-amplifier is built in accordance with a direct amplification circuit. Transistors P2 and P3 (P-403s) amplify the high frequency oscillations. There is a transformer coupling between the stages. Resistances R5 and R8 in the circuits of the emitters for transistors P2 and P3 are necessary for thermal stabilization.

The work regime of the transistors (the collector current) is selected using resistors R3* and R6.

The coupling transformers TR2 and TR3 are built on torroidial ferrite cores with a permeability μ equal to 600. The inductance of the commutator windings should be 180 microhenry $\pm$ 10%. The amplification coefficient of the two stages is not less than 500 when a modulated sinusoidal signal with a voltage of up to 0.01 v. at a frequency of 2 MHz and 100% modulation is fed to the receiver input with the connected probe.

After rectification, the pulse no longer contains a high-frequency component and may be amplified in a videoamplifier.

Adjustment of the receiver amplification is accomplished after rectification. This is preferred since putting the attenuator on the amplifier input strongly changes the operating regime of the first transistor at the expense of transitional processes arising when a transmitted pulse with a large

*Tr. note--Text reads ". . . resistors B3 and R6."

amplitude is fed to the input. After the videoamplifier, negatively polarized pulses are fed to the emitter repeater P5 for matching the low input resistance of the coincidence stage P9 and the relatively high output resistance of the videoamplifier P4.

Resistance R9 serves as a current limiter in the receiver in case the polarity of the power supply battery is erroneously switched. The electrolytic capacitor permits the likelihood of circuit self-excitation to be reduced, particularly when the internal resistance of the power supply source is increased (battery aging).

The current requirements are as follows: the flaw detector, from 13-15 milliamp; voltmeter, 3-5 milliamp; the total current required from the batteries is about 20 milliamp.

In the later models of the URD-63 flaw detector, the high-frequency oscillation was modified somewhat with the aim of increasing the power of the transmitted pulse. Using a KN-102I diode thyristor in the high-frequency oscillator generator circuit permitted the amplitude of the transmitted pulse to be increased by more than three times. The schematic of a high-frequency oscillator assembled on a diode thyristor is shown in Fig. 200. There is a blocking oscillator assembled in accordance with an ordinary circuit on an MP-26 transistor used for providing the high-frequency oscillation generator with high voltage (about 250 v.). A step-up transformer, on the third winding of which a voltage of 250-300 v. arises at the instant the blocking oscillator operates, is connected in the commutator circuit of the transistor. The shape of this voltage is shown in Fig. 200.

The frequency of the blocking oscillator determines the frequency of USO pulsing since the high-voltage pulses are fed through resistance R1 + R2 to the reservoir capacitor C1 and the diode thyristor. When the voltage

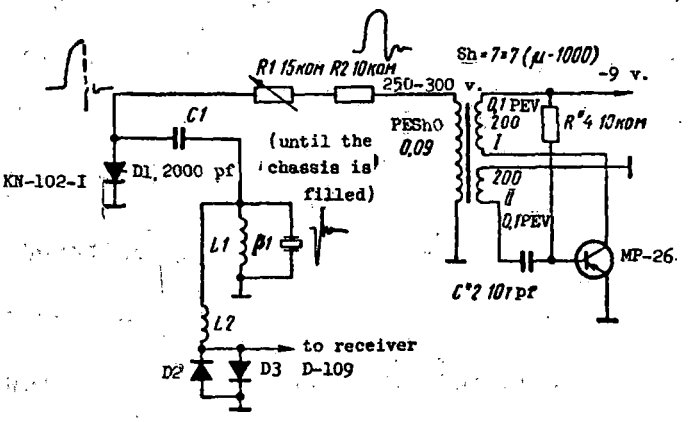

Fig. 200 Circuit of the high-frequency pulse generator for the URD-63 flaw detector using a KN-102-I diode thyristor.

at capacitor C1 increases, a "break-down" of the diode thyristor D1 takes place. The internal resistance decreases sharply (from 500 kohm to 5 ohm), which permits a high power to be obtained briefly and allows it to be directed to the excitation of oscillations in the piezoelectric element.

The diode thyristor plays the part of the thyratron in the high-frequency pulse generator of the URD-58 flaw detector. An electrical circuit consisting of inductance L1 and the capacitance of the piezoelectric element is connected in series with the diode thyristor. Attenuating oscillations with a frequency determined by the parameters of the electrical circuit arise during brief periods of impact excitation. The amplitude of the transmitted current is about 75 v., at a current of up to 10 amp. Capacitance C1 is not a part of the oscillatory circuit since the diode thyristor has unilateral conductivity.

Two D-109 diodes, connected in opposition, are connected to the receiver input in order to protect the receiver transistors from the high voltage of the transmitted pulse. These diodes permit all signals with

an amplitude of more than 0.5 v. to be limited. An inductance L2 (50-100 microhenry) is connected between the diode limiter and the piezoelectric element for excitation of the piezoelectric element. This inductance is a large resistance for a pulse with a steep front, and it insignificantly lowers the amplitude of weakly reflected signals arising on the piezoelectric element facings.

The current requirement from the batteries for the blocking oscillator and the transmitted pulse oscillator is not more than 2.5 mamp on the diode thyristor.

Using this type of circuit for the transmitted pulse generator permits the use of the URD-63 flaw detector to be broadened significantly, especially when used in the harsh northern regions at temperatures of down to -30° C., when the receiver amplification and the characteristics of the probes become markedly worse.

3. Construction of the URD-63 Flaw Detector.

The flaw detector is built in the shape of a hollow tube with a handle and the probe assembly at either end. The length of the flaw detector is chosen for ease of operation out on the line when testing rails. The operator can place the probe on the running surface of the rail without bending over and test the doubtful section of track. This is particularly important when rail testing takes place over a significant distance, e.g. on bridges, in tunnels, and on the track in front of stations. Using the tank which is built into the flaw detector for the moistening liquid permits one operator to monitor the rails.

The probe shoe centering device is a bracket made of steel wire. When it is worn out, the bracket is easily replaced in the repair shop.

The probe shoe makes a hinged connection with a flat U-shaped bracket connected to the flaw detector body, and it may turn in two mutually perpendicular planes at an angle of 10-15°. This type of fastening permits the shoe to seat itself on the running surface of the rail.

In the probe shoe (Fig. 201), three probes (one normal and two angle probes with a wedge angle of 47°) are mounted on the plexiglass protector. The wedge-shaped probes are mounted at a 34° angle relative to the longitudinal axis. All three probes have identical piezoelectric elements (TsTS-19, 12 mm in diameter and 0.72-0.75 mm thick). The probes are filled with a damping mass and form an integral block. The damping mass is a mixture of ED-5 epoxy resin with carbon black or red lead in the following proportions: ED-5, 100 pt/weight, red lead or carbon black, 12 pt/weight, solidifier/hardening agent, 10 pt/weight.

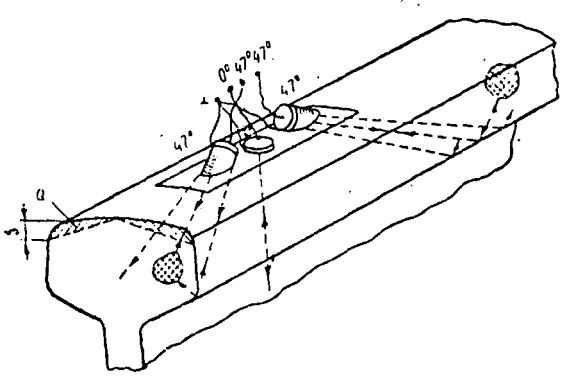

Fig. 201 Probe shoe of the URD-63 flaw detector.

Before filling, the piezoelectric elements and the plexiglass wedges are coated with "88" glue.

Upon polymerization of the epoxy resin, bubbles of gas which effectively damp the USO are fixed throughout its volume. In addition to USO

damping, this composition has high mechanical strength and is completely impervious to moisture.

Among the disadvantages of integral probe construction, a certain difficulty in repairing the worn plexiglass protectors exists. However, this drawback is compensated for by the more stable characteristics of the integral probes in comparison with those which may be dismantled.

The USO angle of transmission into the rail and the angle of rotation for the probes relative to the longitudinal axis of the rail are chosen experimentally when a large number of rails with 21.2 flaws is encountered. The probe of this construction permits transverse fatigue flaws to be detected in the early developmental stages. Unfortunately, the high interference level when monitoring old rails does not permit the sensitivity of probes of similar construction to be fully realized. Only flaws with a reflecting surface with a normal orientation to the USO beam may be detected with a high degree of reliability.

The large number of transverse flaws having significant development reflect USO with only the upper and lower edges, the reflection being intensified if there are so-called flaw growth rings present.

In certain rare instances, large (developed) flaws are missed because the USO beam, having reflected from a surface, does not return to the probe. As a rule, there is no "growth ring" for such a flaw, and its dimensions are such that they occupy 25-30% of the area of the rail head. These flaws should be detected by changing the probe turn angle from 2-5^{o} during multiple testing of a suspicious section of rail.

4. Preparation for Work on the Line and Evaluation of Readings.

Preparing the flaw detector for operation consists of testing the serviceability of the power supply batteries and filling the tank with a

supply of the moistening liquid. The flaw detector is switched on with switch BK1, situated under a cover on the handle. When the flaw detector is switched on, the voltmeter shows the battery voltage and simultaneously indicates that the device is on.

Two operating conditions have been foreseen for the flaw detector: 1) working with the normal probe using the mirror-shadow method, and 2) working with an angle probe using the pulse-echo method. In this case, it is possible for two angle probes with different rotation angles mounted in a common shell (the shoe) to be used. Switching from one angle probe to another is done using switch BK3 situated down near the probe shoe. The position of this switch for changing the angle probes is designated by the inscriptions "front" and "rear."

Rails are tested using a normal probe when it is necessary to monitor a zone in the web and base within the thickness of the web. In order to operate using the mirror-shadow method, it is necessary to achieve a coincidence of the gating pulse and the bottom pulse (the first bottom reflection) by setting the "Rail type" knob (Fig. 202) and to establish a receiver amplification exceeding the indicator activation threshold by two divisions on the "Sensitivity" knob scale.

Switching is done in the flaw detector circuit using switch BK2 (normal-angle) when working using angle probes. One of the angle probes is connected simultaneously instead of the flat (normal) probe.

When working with the angle probe, it is first of all necessary to test the gate pulse setting. To do this, the flaw detector probe is set at a distance of about 30 mm from the end of the rail (from the edge of the probe jacket). The sensitivity knob is set in the maximum amplification position by turning it clockwise until it stops. The "Rail type"

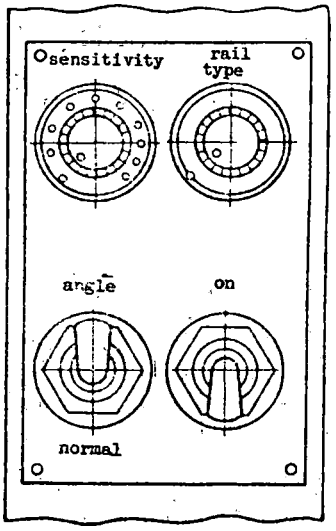

Fig. 202 Control panel of the URD-63 flaw detector.

knob should be set in the position at which the audio signal appears in the headsets.

It is necessary to turn the knob slowly counter-clockwise almost to the stop. In this position, there will be a minimum delay time for the gate pulse. For great accuracy of the gate pulse setting, it is necessary to lower the amplification to the limit at which there will still be an audio signal using the "Sensitivity" knob. The probe position is set more accurately moving it towards and away from the end of the rail ± 10 mm.

As is known, 21.2 type flaws are usually situated at a distance of 5-10 mm from the running surface of the rail head. Consequently, when setting the delay according to the end of the rail, there will be a time reserve corresponding to the width of the gate pulse, which is entirely adequate for flaws at any depth in the rail head.

Use of gating permits only the direct reflection of USO from flaws situated in the rail head to be received. This permits the location of a

flaw in the rail head to be noted more accurately. In certain instances, it is possible to detect a flaw, having set the gate pulse so that the sound wave is passed through the rail twice, i.e. it is possible to detect a flaw located near the fillet side.

Optimal flaw detector sensitivity is set according to a test sample before going out onto the line. A rough sensitivity test may be made on any rail end when working on the line. The test sample (the standard) for setting the necessary sensitivity is a section of R50 rail 750 mm long, which has been in use (Fig. 203).

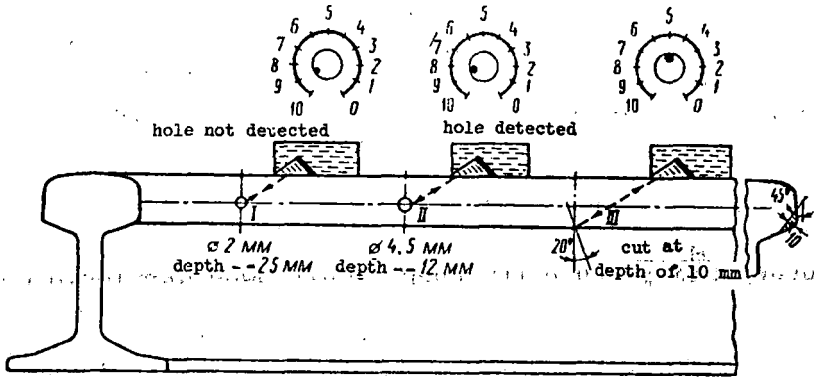

Fig. 203 Test sample for setting the sensitivity of the URD-63 flaw detector.

A hole I, 2 mm in diameter and 25 mm deep, is bored into the center of the side of the rail head at a distance of 200 mm from the end. A second hole II, 4.5 mm in diameter and 10-12 mm deep, is bored 150 mm from the first. Beyond that by 150 mm, a cut (III) is made in the lower side of the head to a depth of 10 mm with an angle of 20° relative to the cross-section using a cutter.

The choice of flaw detector sensitivity based on the test specimen permits the upper and lower boundaries to be established. If the upper

sensitivity boundary for the flaw detector is not limited, it is possible to remove rails with 11.1-2 flaws and with large structural nonhomogeneities, especially in the lower work-hardened layer. It is necessary to tune the flaw detector so that hole I (cf. Fig. 203) is not detected and hole II is indicated clearly by the "front" and "rear" probes. As flaw III is detected, there should be reserve amplification available, i.e. the "Sensitivity" knob may be turned counter-clockwise two or three divisions. The audio signal should still be heard in the headset.

In those cases when flaw I is clearly detected, it is necessary to turn down the "Sensitivity" knob until the audio signal from that hole disappears. The position of the knob should be remembered, and amplification should not be increased beyond this limit when working on the line. Hole II should be detected clearly. When working on the line, it is necessary to have a clear understanding of which rail must be monitored using the "front" probe and which must be monitored using the "rear" probe. As a rule, transverse fatigue flaws in the rail head are inclined in the direction of movement on double-track sections. On single-track sections, the inclination is to the side of greater freight traffic. If this circumstance is not considered, it is possible to miss a dangerous flaw only because the USO bundle will fall on the flaw surface at an angle sharply different from the perpendicular.

It is recommended that testing of doubtful sections of rails take place using two wedge-shaped probes, one after the other. A lack of alignment of the probe (with the rail axis) should be conscientiously created in order to vary the wedge turn angle by plus or minus two to three degrees.

5. Repair and Adjustment of the URD-63 Flaw Detectors.

When repairing and adjusting URD-63 flaw detectors (Table 12), as a minimum, it is necessary to have an electron oscillograph with a slave sweep, a tester, and an instrument for testing transistors. Use of transistors in all of the flaw detector units creates certain peculiar repair problems. For example, the small dimensions of the parts and transistors requires that they be handled with care and that a soldering iron of no more than 30 wt be used. Soldering should be done using a special non-acidic paste and POS-70 solder. When there is no soldering paste, a solution of rosin and alcohol may be substituted.

Before beginning repair of the flaw detector, the power supply should be switched off and the measuring devices disconnected. Not observing this rule may lead to breakdown of transistors when some part is being soldered.

As preventive maintenance, the URD-63 should be dismantled no less than once a month and the battery compartment, as well as all parts of the battery, should be wiped down with a rag. The separate dry cells, showing a voltage less than 1.4 v. when tested by a tester without a load, should be replaced with new ones. Small defects should be corrected upon external examination of the flaw detector.

It is necessary to begin flaw detector repair by identifying the trouble and determining which element is out of order (Table 12). For this, the flaw detector cover is removed and the probe shoe is taken out of the fastening strap-frame. The length of the connecting cable for the probe permits the probe to be placed on a piece of rail not more than 250 mm long on a table, with the flaw detector lying alongisde. It is convenient to prepare special wire supports which permit the flaw detector to be placed in a position convenient for working on it. The flaw detector power supply is taken from its battery.

Table 12

Possible Difficulties in the URD-63 Flaw Detector and Means for Correcting Them

#	Difficulty	Possible Cause	Procedure for Correction
1	Flaw detector operates operates only with the normal probe	a) The wedge-shaped probes are defective (broken wire)	a) Test the current-conducting wires and solder them to the socket (in the case of an internal break, replace the KMM-3 wire)
		b) Inadequate receiver amplification	b) Shunt R9 (200 ohm), replace transistors P2 and P3 one after another with P-416 transistors known to be good
		c) The input circuit is maladjusted. (coil L1)	c) Test the presence of the ferrite core and tune coil L1 to the maximum of the signal reflected from the butt-end of the rail
		d) Worn probe protector	d) File the protector or restore it by gluing on a new one and working it down to an overall thickness of 2.5-3.0 mm
		e) Capacitor C3 (10 microfarad, 15 v.) is defective	e) Replace capacitor C3
2	Extraneous noise (hum) audible in headset	Switching circuit of the coincidence stage is passing extraneous signals through	Decrease resistance R24 to 5.6 kohm, replace transistors P8 and P9
3	A delayed gating pulse is observed on the detector load. The flaw detector does not work.	There is feedback through diode D4	Replace diode D4
4	When the normal probe is in operation there is no audio signal in the headsets	The piezoelectric element has come unglued, there is no damping. The transmitted pulse has a duration of more than 40 microsec.	Replace the probe

Table 12 (Continued)

#	Difficulty	Possible Cause	Procedure for Correction
5	The flaw detector does not operate at temperatures below -10° C.	a) The pulse generator is not excited b) The pulse generator works but the wedge-shaped probe does not	a) Decrease resistance R1 to 10 kohm, replace transistor P1 (p-601) b) There is inadequate receiver amplification. Replace transistors P2 and P3 for P-416 transistors. Shunt resistance R9 (200 ohm)
6	Clicks are heard in the headset as the probe is moved along the rail	The time at which the gate pulse appears from the delay block is changing spontaneously	Replace resistance R17 (100 Kohm), replace diode D4 (start circuit)
7	There is no audio signal in the headset when the probe is removed from the rail	There is a large trailing off of the transmitted pulse in the receiver. Replacing the probe does not help	Impregnate transformers TR1, TR2, TR3 with BF-2 (two to three drops) and let dry for 24 hours.

When searching for trouble, if it is not clearly distinguishable, an electron oscillograph (SI-1, S1-20, or S1-13) is used. With this oscillograph, the amplitude of the signal and the time characteristics of the pulses may be measured. It is necessary to begin testing from the radio pulse generator. There should be damping oscillations with an amplitude of not less than +25 v. and -15 v. on the emitter of transistor P1 (P-601) when power is supplied (cf. Fig. 199). These oscillations are observed on the oscillograph screen.

The frequency of the oscillations which make up the pulse should be about 2 MHz. If the oscillation frequency is significantly higher and the amplitude is lower than the indicated value, this indicates that there is a break in the piezoelectric element circuit. It is necessary to connect another piezoelectric element, e.g. the normal or one of the angle probes,

using switch BK2. If the picture on the electron oscillograph does not change, this indicates that it is necessary to test the circuit from the circuit coil L1 to switch BK2 and to the probes. In the same manner, a break in the probe circuits (the most likely spot for damage being the flexible cable) is determined.

If the oscillator is functioning normally, i.e. the pulsing frequency is from 300-1000 Hz, and the amplitude of the first positive pulse is about 25 v., the receiver must be tested.

S1-8 and S1-13 oscillographs, which have high amplification and broad band pass frequencies, permit the bottom pulse taken directly from the piezoelectric element to be seen on the screen. If the angle probe receives a bottom pulse from a normal probe and the reflected signal from the butt-end of the rail when a sound wave is passed through R50 rail, this indicates sound operation of the radio pulse generator.

Testing the flaw detector receiver is done stage-by-stage. At first, the oscillograph is connected to the detector (resistance R11 or capacitor C8). When the receiver is working well, the first bottom pulse should be no less than 5 v. and should have positive polarity.

The signal reflected from the butt-end of the rail when the wedge-shaped probe is connected should not be less than 2.5 v. If these values are not maintained when a new probe which is known to be in good repair is connected, transistors P2 and P3 must be replaced, one after the other, using a P-416 transistor which has been tested beforehand on an L-2-1 (testing device).

Only those transistors which have a current amplification coefficient of not less than 40 are installed in the flaw detector.

Receiver self-excitation may be eliminated by switching the ends of the secondary winding of transformer TR2 or TR3. When changing transistors, it is necessary to test the collector current, which should not be more than 1 mamp. Selecting the operating conditions for transistor P2 is done by trimming the size of resistance R3. Increasing capacitances C4 and C7 to 0.05 microfarad may raise the total amplification of the receiver by 20%.

When the necessary amplification cannot be achieved by replacing the transistors, transformers TR2 and TR3 must be replaced. These transformers are tested at the manufacturing plant by measuring the inductance. The inductance of the primary winding of TR2 measured on a "Q-meter" should be 180 microhenry ± 10%. The large spread in the ferrite core parameters (nominal value $\mu = 600$) does not permit the strictly required number of turns to be wound (30 and 10 turns). Thus, fifty turns of PEShO-0.12 wire are wound onto the cores on hand and then the inductance is measured. The value of 180 microhenry is obtained by unwinding turns, then the secondary winding is wound on with the aid of a shuttle (Fig. 204).

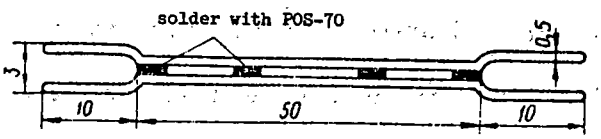

Fig. 204 Shuttle for winding torroidial transformers.

The inductance of the winding on transformer TR3 should be 220 microhenry ± 10%. Tuning transformers TR2 and TR3 to different resonance frequencies permits a broader bandpass width to be obtained. In several instances, selection of capacitor C6 permits the amplification of the receiver to be increased.

If the amplitude of the bottom pulses on the detector load is 5 v., further testing must be conducted in the videoamplifier. Transistor P4 (P-41) permits the rectified pulses to be amplified and their polarity changed. In this stage, a certain limiting of the powerful bottom pulses takes place. However, weak signals from flaws are effectively amplified when working with angle probes. The amplitude of the negative signals on the collector of P4 should be about 7 v. when a full voltage is taken from the detector load. The emitter repeator (transistor P5) is set to match the low input resistance of the coincidence stage's switching circuit to the relatively high output resistance of the videoamplifier. The transmission coefficient for this stage is about 0.9.

Testing the operation of the delay unit is done by connecting the oscillograph to the collector of transistor P8. A negative pulse having a duration near the base of 20-30 microsec. may be observed at this point. This pulse is not used in the circuit, but it is easily observed because of the great amplitude. The positive pulse arising in the emitter circuit of transistor P8 is used in the circuit. It is observable only at high amplification since the base-emitter section of transistor P9 is connected in parallel with resistance R25.

By turning the knob of the variable resistor marked "Rail Type," the limits within which the pulse delay unit may be regulated can be tested. This test must be made preliminarily. External synchronization should be supplied to the oscillograph from the emitter of transistor P1, inasmuch as if there is internal synchronization, the delayed signal may "lock-on" to the synchronization.

The limits of the gate pulse delay is 30-120 microsec. The lower limit is set by the selection of resistance R16. The upper limit is most

easily obtained by changing capacitance C13. The width of the gate pulse is increased as capacitance C14 is increased.

A poor quality resistor at R17 leads to spontaneous displacement of the gate pulse on the oscillograph screen. In this case, this resistor must be replaced with a new one.

Testing the operation of the coincidence stage is done when the oscillograph is connected to the connector of transistor P10. Positive pulses caused by the onset of bottom pulses, and the coincidence of the gate pulse with the time at which the bottom pulse arrives, are observed on the collector of P10 when the switching circuit is operating properly.

The instant of precise coincidence of the delayed gate pulse with the bottom pulse may be followed on the oscillograph screen if it is connected to the rectifier load and the signal from the collector of transistor P8 is fed to the same point through a resistance of not less than 50 kohm.

When the "resonance circuit" of transistor P10 is operating properly, a negative voltage with a magnitude of not less than 1 v. appears on the integrator capacitor C19. This voltage may be measured using a tester. If the voltage does not appear when the probe is placed on the rail and the gate pulse is set, it may be due to the poor quality of diode D3 (D2E).

Operation of the output stage is tested by connecting the headsets. If in the "angle probe" mode, the strong background hum of the blocking oscillator is heard, resistance R26 (51 kohm) must be replaced. This opens the base circuit of transistor P9 a little and creates a shunt on the input of transistor P10.

In addition, more precise operation in the switching circuit P9·P10 is achieved by increasing the gate pulse amplitude, which, in turn, is achieved by decreasing resistance R24 in the collector circuit of transistor P8 by 3-5 kohm.

In the first model of the flaw detector (with separate tanks for the liquid), receiver amplification was inadequate for working with wedge-shaped probes.

The following modifications are required for these flaw detectors, as well as those which, for one reason or another, do not provide a reflected signal voltage of 2 v. or more, to the detector load:

a) Disconnect resistance R9 (200 ohm) after shorting its leads with a jumper; this permits the power supply voltage to be increased to the high-frequency transistors P2 and P3

b) Remove resistance R10; the variable resistance R11 (6.8 kohm alone will be the detector load)

c) Decrease the resistance in the emitter circuit of transistor P2 to 200 ohm, having shunted it using a 0.05 microf capacitor.

All of this permits the receiver amplification to be raised by approximately 30%.

Unfortunately, a wide-spread device such as the L-2-1 for testing transistors does not permit the P-601 (P-602I) to be tested. This is a powerful high-frequency transistor with a generation frequency limit of about 2 MHz. This transistor is tested by comparing the amplitude of the pulse reflected from the butt-end of the rail on the detector load when a "standard" transistor and the one being tested (P-601) are used in the circuit. To do this, it is necessary to make leads from the emitter, base and collector in the flaw detector using short wires with alligator clips.

Testing the probe shoes is done according to the amplitude of the bottom pulse from the first probe and the reflection from the butt-end of the rail when working with angle probes.

Additionally, the quality of the normal as well as the angle probe is tested according to the magnitude of the trailing zone of the transmitted pulse. The width of the transmitted pulse for the normal probe should be not more than 30-40 microsec when it is observed on the detector load. In this case, the probe should lie on its side and not touch extraneous objects. The quality of the bonding between the piezoelectric element and the plexiglass bottom-protector is determined according to the width of the transmitted pulse. The transmitted pulse, expanding to 50-60 microsec, shows the poor quality of the bonding.

Probes of this type are rejected. A trailing zone of the pulse of up to 20 microsec is permitted for an angle probe.

Repair and restoration of the probe protectors. As the probe protector wears out, which usually takes place unevenly over the area of the protector, the protector is filed until an even surface is obtained. The decrease in protector thickness from 3 mm to 1.5 mm results in an increase in the sensitivity since the plexiglass layer, which conducts USO poorly, is reduced. The probe should be used until the thickness of the protector is down to 1 mm. After this, it is necessary to glue on a new protector, which is kept as a spare. The operation to restore the protector consists of filing the worn protector until a flat surface is obtained and gluing the spare protector to the worn one (Fig. 205).

The gluing process is conducted in the following manner using pure dichloroethane. The filed probe surface is quickly moistened with dichloroethane using a clean brush. Then the new protector is laid on top of the moistened surface and pressed down with the finger. It is necessary to press the two surfaces being glued together for 1-2 minutes. Then the probe is placed protector-down on a flat surface and a 1-2 kg weight is placed on

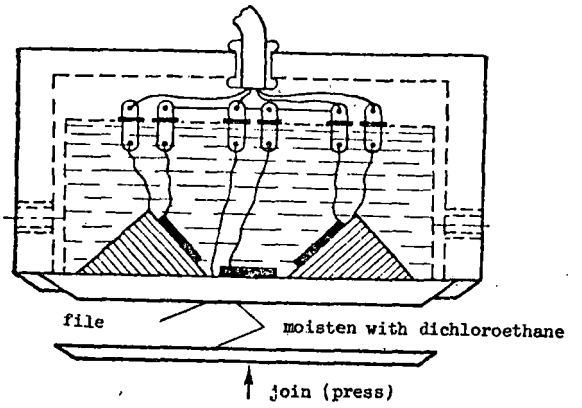

Fig. 205 Restoration of worn probes.

top of it for 12 hours. The quality of the connection is determined visually. If there are no air bubbles and the two plexiglass plates have fused together, the gluing has been done well. An assembly which is merely satisfactory is obtained due to inexperience or, more importantly, due to a lower level of dichloroethane purity or cleanliness of the brush. After gluing, it is convenient to file the new protector to an overall thickness of 2.5 mm.

As practice has shown, restored probes work as well as new ones.

With this, work repairing integral probes stops. There is no sense in restoring a probe from which the piezoelectric element has come unglued from the inside inasmuch as disassembling the probe (removing the damping mass) will certainly result in fracture of the piezoelectric plates and a break in the current-carrying wires.

IX. The DUK-11IM and DUK-13IM Ultrasonic flaw Detectors.

1. Intended use and working principles.

The DUK-11IM and DUK-13IM, as well as UZD-59 flaw detectors are designed in accordance with the unified functional circuit of UZD-NIIM-5 type devices. In the pulse mode, these instruments operate using the pulse-echo and mirror shadow methods, and are distinct from each other only in their electrical circuitry and construction.

The instruments are designed for detecting internal flaws and determining the coordinates of their position without special mechanical processing in both welded joints and metal items with a rolled surface not containing flaking rust and pitting.

They are used in the railroad industry for monitoring the quality of welded joints when the rails are welded at rail-welding plants or out on the line, as well as for monitoring bolt joints, and for secondary monitoring of individual sectors which are in use.

The flaw detectors permit detection of 26.3, 56.3, and 66.3 type flaws; flaws which have originated when the rails were welded on the line and which are situated in various zones of the welded joint, as well as 30G.1; 30V.1; 53.1; 52.1; 55.1; and 50.1 type flaws in the bolt joints. These devices operate at frequencies of 1.8 or 2.5 MHz. The maximum sensitivity of the flaw detectors when monitoring items made of steel at depths of up to 100 mm is about 2 mm^2. The dead zone of instruments with 30- and 40-degree probes is not more than 8 mm, and with 50-probes, not more than 3 mm.

There is an electronic depth meter which permits the coordinates of detected flaws to be calculated immediately when monitoring items made of steel, and when monitoring items made of other materials (having a different wave velocity), to determine the propagation time for the ultrasonic oscillations to the re-

flecting surface. The instruments permit monitoring to be carried out at a given depth, beginning at the surface, from which flaw detection is conducted ("monitoring from the surface") or at a given depth ("layer-by-layer monitoring"). The technical characteristics of the DUK-11IM and DUK-13IM are presented in Table 13.

Table 13

General Characteristics of UZD-NIIM-5 Flaw Detectors

Feature	DUK-11IM	DUK-13IM
maximum depth to which a sound wave is passed into the rail	750 mm in the "layer-by-layer" mode	600 mm in the "layer-by layer" mode
indication of detected flaw	on a cathode-ray tube screen and by auxiliary indicators (light, sound)	on a cathode-ray tube tube screen and by an auxiliary sound indicator
working temperatures	+5 — +40 deg. C.	0 — +40 deg. C.
flaw detector power supply	a.c. current circuit, 220 v. + 5%/-10%, frequency 50 Hz	a.c. current circuit, 220 v. + 10%/-20% or 36 v., frequency 50 Hz; d.c. circuit; or 12 v. storage battery
Power consumption	not more than 100 w.	not more than 65 w. when working from the a.c. circuit through a special regulator, and not more than 20 w. from a 12 v. d.c. source
Dimensions	197 x 278 x 330 mm	110 x 233 x 274 mm
Weight	9.8 kg	4.0 kg

The functional diagram of the UZD-NIIM-5 instruments is shown in Fig. 206. The distinctive feature of this circuit is the use of separate units to carry out a series of functions, permitting portable flaw detectors to be designed based on this circuit. The primary units of the functional circuit for UZD-NIIM-5

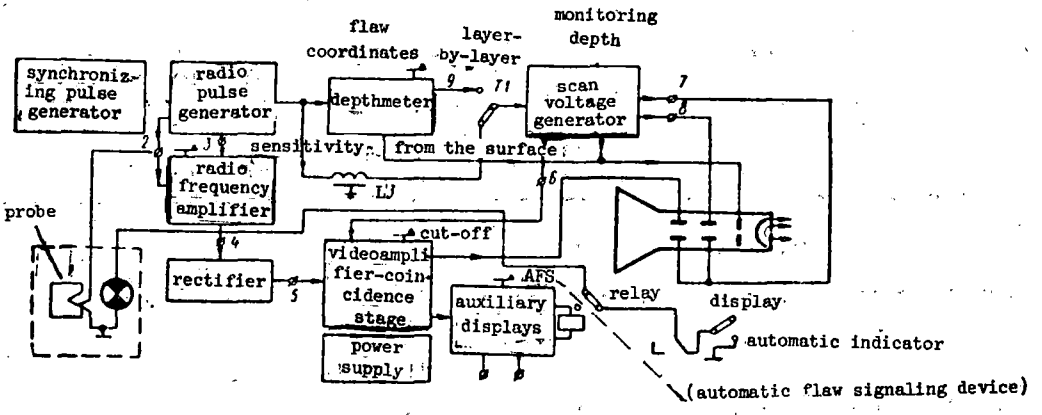

Fig. 206 Functional circuit of UZD-NIIM-5 type flaw detectors (DUK-11IM, DUK-13IM, UZD-59).

devices are: a synchronizing pulse generator; a radio pulse generator; a probe, a radio frequency amplifier; a rectifier, a video amplifier-coincidence stage, a scan voltage generator; a depthmeter; a cathode-ray display; auxiliary displays, and a power supply unit.

Time diagrams for the operation of the units within the device in the "monitoring from the surface" mode are shown in Fig. 207.

The synchronizing pulse generator is intended to control the operation (synchronization) of the units in the device's functional circuit. Pulses produced by this generator are shown in diagram 1, Fig. 207.

When the flaw detector is in operation, ultrasonic pulses with a frequency F equal to $1/T_s$ are transmitted into the item being monitored. The synchronizing pulse generator is designed in accordance with one of the oscillator circuits operating in the self-excitation mode, i.e. one of those

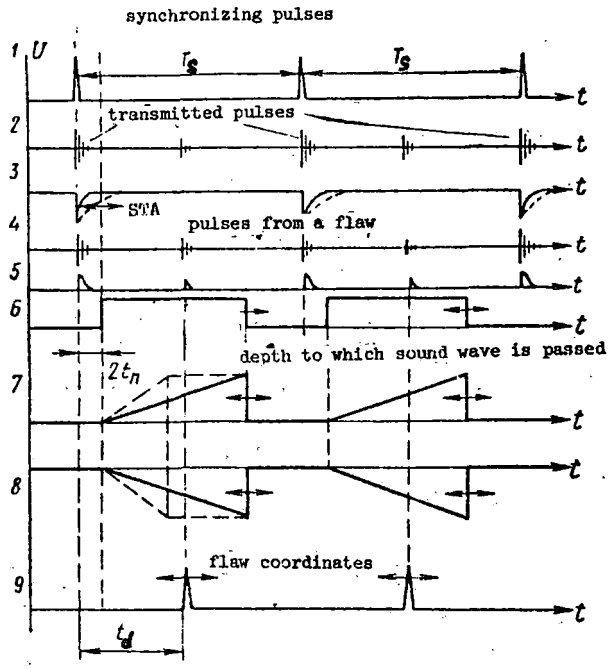

(STA -- sensitivity time adjustment)

Fig. 207 Voltage forms at various points in the functional circuit of the UZD-NIIM-5 type flaw detectors when working in the "monitoring from the surface" mode.

devices which produce electrical pulses when they are connected to a direct current source.

The radio pulse generator is intended to produce high-frequency electrical pulses which are used to excite the piezoelectric converter in the probe, i.e. to excite the transmitted pulses. These pulses are damped electrical oscillations, the frequency of which is determined by the size of the inductance and the capacitance of an oscillatory circuit; this frequency is selected to be approximately equal to the natural frequency of the piezoelectric converter which is used. The pulses from this generator are conventionally represented in diagram 2, Fig. 207. The shape of these oscillations is shown in Fig. 165.

Radio pulse generators in the UZD-NIIM-5 flaw detectors are assembled based on circuits of generators with an impact excitation circuit.

Normal and angle probes are used with UZD-NIIM-5 flaw detectors. The construction of these probes is described in Chapter V. The electrical oscillations produced by the radio pulse generator are transformed into ultrasonic oscillations by the piezoelectric plate of the probe. When there is an acoustical contact between the probe and the surface of the item being monitored, pulses of these oscillations penetrate into the metal and disperse within it. Having come to the boundary of any kind of non-homogeneous medium (a flaw or the opposite surface of the metal), the pulses are reflected. A portion of the energy from the reflected ultrasonic pulses falls on the piezoelectric plates of the probe, transforming them into electrical oscillation pulses (pulse-echos). Pulse echos are fed to the radio frequency amplifier input. The size of the pulse echos should be noted to be approximately 1/1,000,000 the size of the transmitted pulses.

The radio frequency amplifier (RF amplifier) is intended for amplification of the high-frequency electrical pulses corresponding to the reflections of the ultrasonic oscillations. As may be seen from the functional circuit, UZD-NIIM-5 flaw detectors envisage operation with one probe, which is used both in the sending and receiving modes. When the transmitted pulse is fed to the RF amplifier input, the amplifier is overloaded and the sensitivity of the flaw detector decreases for a certain time. This leads to an increase in the flaw detector's dead zone M. Since the radio pulse generator and the RF amplifier may not be separated electrically when working with a single probe, and, consequently, the transmitted pulse may not be prevented entirely from falling on the amplifier input, it is necessary to strive to obtain maximum reduction in the time the flaw detector sensitivity is decreased due to the overloading of the receiver by the transmitted pulse. Accomplishing this would decrease the size of dead zone. In the UZD-NIIM-5

flaw detectors, this is attained by feeding a cut-off voltage, which is produced in the radio pulse generator circuit, to the RF amplifier input at the moment the transmitted pulse is emitted. The shape of this voltage pulse is shown in diagram 3, Fig. 207. The amplitude and the duration of this cut-off voltage may be regulated using the STA (sensitivity time adjustment) knob on the front panel of the instrument. This adjustment is absolutely necessary when the probes are replaced. Thus, the introduction of a system for sensitivity time adjustment provides a decrease in the dead zone, and, consequently, better detection of flaws situated at shallow depths.

The pulses on the flaw detector's RF amplifier output are shown in diagram 4, Fig. 207. Here it is assumed that the size of the voltage used for the sensitivity time adjustment is set so that there is a small transmitted pulse on the RF amplifier output.

High-frequency pulse echoes pass from the RF amplifier output to the rectifier, which converts them to video pulses. These are more convenient for viewing on a cathode ray screen. The intended use of the rectifier and the essence of rectification were examined in Chapter VI when the URD-52 flaw detector was studied. Rectified pulses are shown on time diagram 5. The intended use of the video amplifier, also carrying out the functions of the coincidence stage, consists of amplifying the pulse echoes taken from the rectifier to a magnitude which permits their observation on the cathode ray screen and which is adequate to activate the auxiliary displays. This stage simultaneously executes the time selection of the pulses fed to its input. Time selection of pulse echoes consists of isolating from among all of the amplified and rectified pulses only those which correspond to the reflections from flaws in the rail being monitored. Pulse echo time selection

is also necessary so that the transmitted pulse does not penetrate to the auxiliary displays of the flaw detector. The working principle of time selection is that the video amplifier-coincidence stage opens only for the time during which pulse echoes from possible flaws situated within the layer being monitored are anticipated. Control of the operating mode for the video amplifier-coincidence stage is provided by a special rectangular pulse which is called a strobe or gate pulse.

There is no special gate pulse oscillator in the UZD-NIIM-5 flaw detectors. Instead, rectangular pulses produced by the scan voltage generator (cf. Fig. 207, diagram 6) are used. The thickness of the layer being monitored H is determined by the duration of the gate pulse t. Knowing the necessary value of H, the corresponding value for the duration of the strobe pulse t may be calculated:

$$t = \frac{2H}{\cos \alpha} \cdot \frac{1}{C_{t_2}}$$

The symbols are defined in Chapter V.

It may be seen from Fig. 207 that only the pulse echo from a flaw coincides with the gate pulse, and therefore, only this pulse will be amplified by the video amplifier-coincidence stage.

The scan voltage generator is intended for shaping the voltage into saw-tooth form. The voltage is then used to provide the bottom line on the cathode ray screen (cf. Fig. 207, diagrams 7 and 8). The principle of obtaining a bottom line on a cathode ray screen by supplying a saw-tooth voltage is explained in Chapter VI. The saw-tooth voltage is fed to both horizontal deflecting plates, in opposition in the UZD-NIIM-5 flaw detectors.

The duration of the saw-tooth voltage pulse determines the size of the layer which is being monitored, and it may be adjusted using the "Inspection

depth" knob which is on the instrument's front panel. The electrical circuits of the DUK-11IM and DUK-13IM flaw detectors are designed so that when the duration of the saw-tooth voltage is changed, its amplitude does not change, and, consequently, the length of the bottom line is kept constant on the cathode ray screen.

The voltage scan generator produces a rectangular pulse of the same duration and simultaneous with the saw-tooth voltage pulse. This pulse is used as a gating pulse, and it is fed to one of the video amplifier-coincidence stage inputs (cf. Fig. 207, diagram 6). This pulse is also fed to the cathode ray tube as the brightening illumination for increasing the intensity of the image during the straight-line period of the beam.

The start-up of the scan voltage generator in the "monitoring from the surface" mode is made by the synchronizing pulse, which is passed through the delay line (LD in Fig. 206). The delay line is necessary so that the transmitted pulse does not pass to the displays when monitoring using angle probes. The delay time ($2t_p$) is primarily determined by the construction of the probe, and it is about 8 microsec.

The depthmeter is intended for measuring the coordinates of the reflecting surface (of the flaw), and for measuring the thickness of the layer being inspected, which is set using the "Inspection depth" knob. It is additionally used for setting the layer to be inspected at a specified depth when inspecting layer-by-layer. As is known, the principle for measuring the coordinates when using the pulse-echo method of ultrasonic flaw detection consists of measuring the time between the instant the pulse is transmitted and when the reflection is received.

Knowing the time, the propagation speed of ultrasonic waves, and the wave transmission angle, it is possible to determine the appropriate

coordinates using known formulae (cf. Chapter V). In order to facilitate coordinate determination during flaw detection, the depth meter scales in the UZD-NIIM-5 flaw detectors are also graduated directly in millimeters for the depth H at which a reflecting surface (a flaw) lies below the surface for a normal probe. The coordinates H and L are also shown for the position of the reflecting surface for angle probes with a wedge angle β equal to 30, 40, and 50 degrees in the DUK-11IMs (Fig. 208) and β equal 40 and 50 degrees in the DUK-13IMs.

For convenience in calculating the coordinates, this scale is glued onto a cylindrical drum in the flaw detectors.

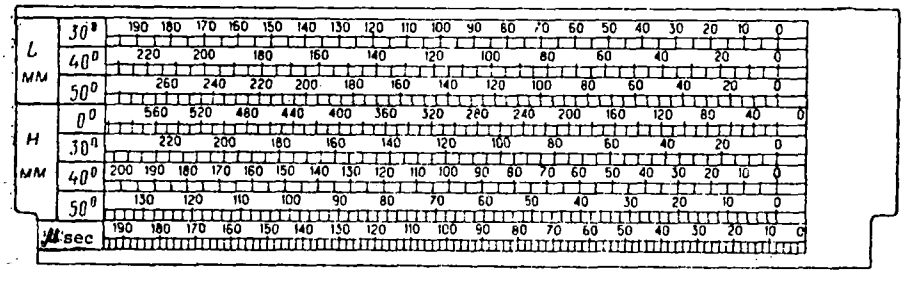

Fig. 208 Scale of the DUK-11IM flaw detector's depthmeter.

To determine the coordinates H and L, the known time values t are marked on the lower scale, and, having drawn a vertical line to this point, the unknown coordinates are read off where this line intersects the line corresponding to the probe which is being used. The time measurement in the UZD-NIIM-5 flaw detectors is made by comparing the unknown time interval t on the cathode ray screen with the delay time of the synchronizing pulse which is fed to the cathode ray tube as a marker in the depthmeter circuit. The depthmeter contains an adjustable delay circuit, the magnitude of which is determined by the angle of rotation of one of the variable resistors in the circuit. This magnitude has been recorded earlier on the "microsec"

time scale for this purpose. Rotating the shaft of this variable resistor is done with the "Flaw coordinates" knob on the front panel of the instrument. Thus, if the marker is alligned with the pulse echo from the flaw on the cathode ray screen (as is shown in Fig. 207, diagram 9), it is possible to determine the propagation time of an ultrasonic pulse to the flaw and back t_d, and, consequently, its coordinates as well.

A picture of the propagation of the ultrasonic oscillations in the item being monitored is reproduced, as it were, on the cathode ray display. Measurement of flaw coordinates takes place on the display screen.

The auxiliary indicators (light and sound) signal the detection of flaws. Using the auxiliary indicators frees the operator from the necessity of having to watch simultaneously for the displacement of the probe and for pips on the cathode ray screen.

As has previously been indicated, UZD-NIIM-5 flaw detectors permit the inspection of specimens and welded joints "layer-by-layer." In the "layer-by-layer" mode, the flaw detector displays register only pulse echoes from flaws situated in a given layer within the specimen. When inspecting "layer-by-layer," as well as when the flaw detector is operating in the "from-the-surface" mode, the thickness of the layer being inspected H is determined by the duration of the gate pulse. The depth of the boundary layer being inspected which is closest to the surface h depends on the instant at which the scan voltage generator begins to produce the gate pulse, i.e. on the time interval t_z between the instant the transmitted pulse is emitted and the instant at which the strobe pulse begins. The size of this interval may be determined by the formula

$$t_z = \frac{2h}{\cos \alpha} \cdot \frac{1}{C_{t_2}} + 2t_p$$

Normally the size of h, and therefore of t_z are varied when inspecting various items and welded joints, e.g. when monitoring various parts of the cross-section of a welded rail. In the UZD-NIIM-5 flaw detectors, this adjustment is carried out by triggering the scan voltage with the depth meter pulse. Switching over to the "layer-by-layer" mode is done with switch T1 as shown in the functional circuit. This switch changes the mode of the scan voltage trigger. In this manner, it is possible to vary the size of the layer being inspected using the "Inspection depth" knob, and the depth of this layer, using the "Flaw coordinates" knob. In order to explain the principle of layer-by-layer inspection more clearly, the item being inspected is shown turned 90° (Fig. 209). As is the case when inspecting from the surface, it is possible to measure the size of the layer being inspected if the depthmeter marker is brought up to the right end of the base line using the "Flaw coordinates" knob, and the figure for the probe being used is read off from scale H. Switch T1 must be set in the "from the surface position" when measuring the layer size. When inspecting layer-by-layer, the depthmeter marker coincides with the left end of the base line. Therefore, it is necessary to bring the echo signal to the beginning of the base line using the "Flaw coordinates" knob in order to determine the flaw coordinates.

2. The electrical schematic of the DUK-11IM

The electrical circuit of the DUK-11IM flaw detector is designed in accordance with the functional circuit of UZD-NIIM-5 instruments (cf. Fig. 206), and is represented in Fig. 210. The operation of the separate units of the instrument's circuits may be examined as follows.

The synchronizing pulse generator is designed around the right half of tube Tu3 (6N1P) in accordance with the circuit of a blocking

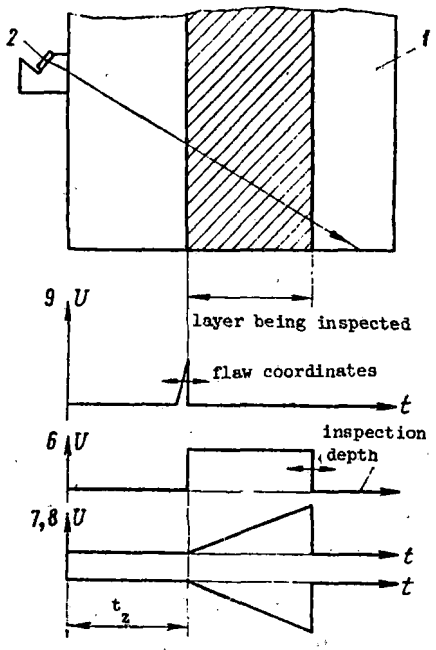

Fig. 209 Explanation of the "layer-by-layer" inspection principle
1. item being inspected 2. probe 6, 7, 8, and 9 voltage forms at corresponding points in the functional circuit of the instrument (cf. Fig. 207).

oscillator working in the self-excitation mode.* The blocking oscillator produces pulses about 1 microsec. in duration, with a pulse repetition frequency F of about 100 Hz and an amplitude of 200 v. A positive pulse is fed from the auxiliary winding (point 6) of the pulse transformer TR2 (cf. Fig. 210) to the control grid of tube Tul (the radio pulse generator) through capacitor C4. A negative pulse is fed to a capacitor C5 to trigger

*The blocking oscillator is a generator of short, rectangular pulses, and may be seen as an amplifier with transformer feedback.

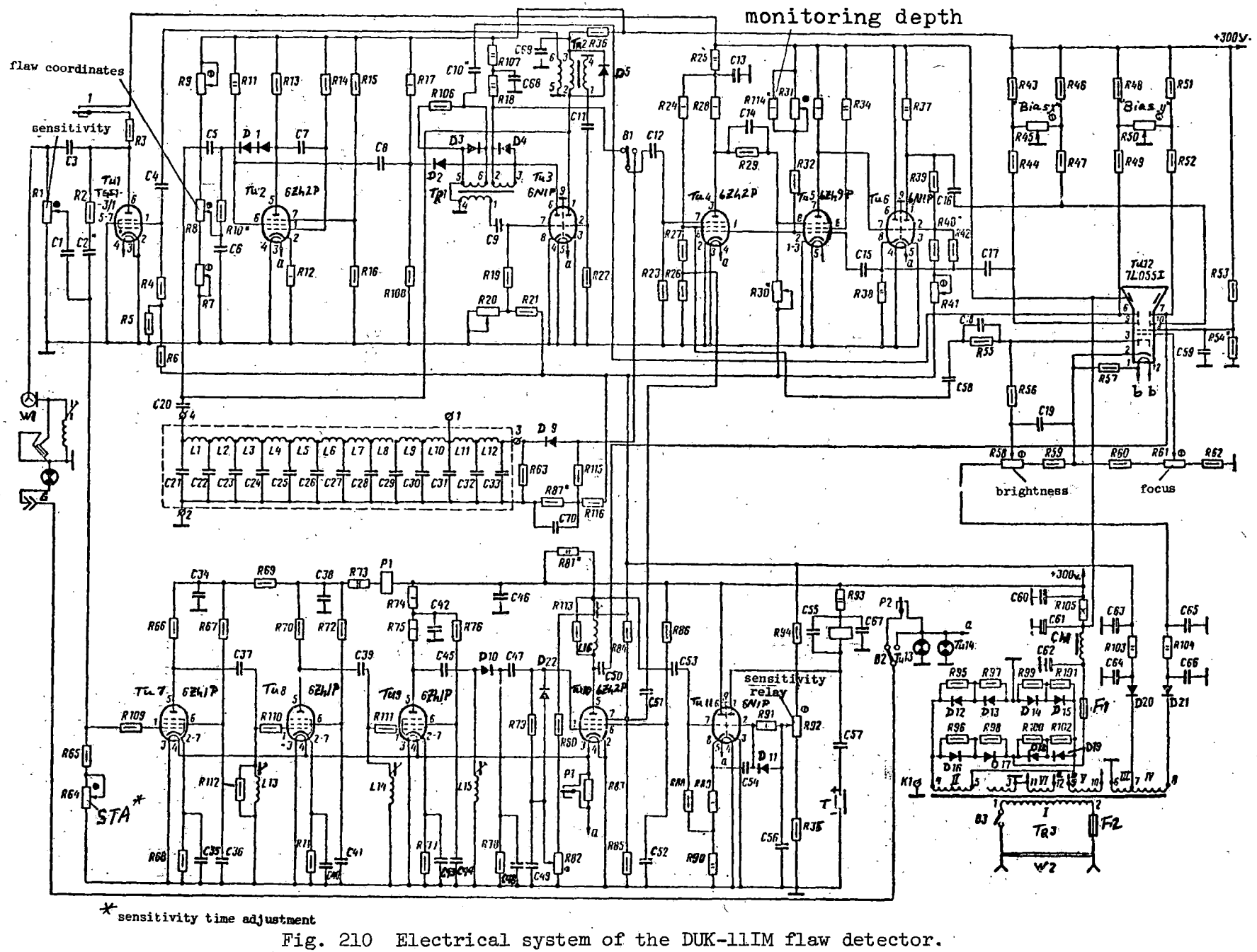

Fig. 210 Electrical system of the DUK-11IM flaw detector.

the depthmeter, and through capacitance C20 from the plate of the blocking oscillator tube to the delay line to trigger the scan voltage generator.

The radio pulse generator is designed around a TGI1-3/1 thyratron (tube Tu1). A negative cut-off voltage is fed to the control grid of this tube from the divider R5-R6 through resistor R4. The positive pulses of the synchronizer are fed to the control grid of tube Tu1 through capacitor C4 to fire the thyratron. As a result of this, as is the case in the URD-52 flaw detector, a high-frequency damped electrical oscillation pulse appears on the piezoelectric plate of the probe. Mechanical oscillations therefore occur in this piezoelectric plate. In order to obtain ultrasonic oscillations of the greatest amplitudes, an oscillatory circuit consisting of the piezoelectric plate capacitance and an inductance, located either in the probe body or in a special adapter, is tuned to resonance at the natural frequency of the piezoelectric plate.

The plate voltage is fed to the thyratron through resistor R3 with a delay of 40-60 sec. to prevent premature malfunctioning.

The plate voltage is connected using the contacts of relay P1, which closes them only after tubes Tu7 and Tu8 of the RF amplifier have heated up. A potentiometer R1 ("Sensitivity") is connected in parallel with the oscillatory circuit of the generator. This varies the size of the pulse echos fed into the input of the radio frequency amplifier and, hence, changes the sensitivity.

The radio frequency amplifier of the DUK-11IM flaw detector is designed around three 6Zh1P tubes, Tu7, Tu8, and Tu9, in accordance with a resonance circuit with a resonance frequency of 2.5 MHz and a band width $2\Delta f$ of about 0.5 MHz. The total amplification coefficient of the RF amplifier is not less than 30,000. The total capacitance of the wiring, the output capacitance

of the amplifier tube, and the input capacitance of the following stage are used as the capacitance of the oscillatory circuits in the amplifier stages.

Other conditions being equal, the amplification coefficient of the RF amplifier depends on the magnitude of the voltage on the control grid of the amplifier's first tube. A negative voltage pulse is fed from the thyratron plate to the control grid of this tube at the moment the transmitted pulse is emitted in order to provide a time adjustment for the sensitivity. This leads to a sharp decrease in the amplification coefficient of this stage, and, consequently, of the entire receiver. As the charge on capacitance C2 increases, the voltage on the control grid returns to the initial value relative to the cathode. This is accompanied by an increase in the amplification coefficient of the receiver. The nature of the voltage variance on the control grid in time, and, consequently, the nature of the variance in the amplification coefficient of the receiver in time is varied by changing the magnitude of the variable resistor R64. The shaft of this variable resistor is on the front panel of the flaw detector and is labeled "RF Amp."

A D2E diode, D10, serves as the rectifier in the flaw detector. This diode has as a load resistance R78 and capacitance C48.

The video amplifier-coincidence stage is assembled around tube Tu10 (6Zh2P) in accordance with a rheostat circuit. In the initial stage, the tube's control and suppressor grids are closed by a negative voltage taken from dividers R82-R80 and R85-R84. Positive pulses are fed from the rectifier to the control grid of tube Tu10 through capacitance C47; a positive gate pulse taken from divider R26-R27 in the screen grid circuit of tube Tu4 (the scan voltage generator) is fed to the suppressor grid through capacitor C51. Diode D22 is intended for restoration of the positive component, and potentiometer R82 for varying the limiting threshold of this stage.

Pulses appear on the plate of the video amplifier only when those pulses fed to the first and third grids correspond in time.

Negative amplified pulses are fed to the relay triggering stage from the video amplifier plate through capacitor C53, and, through capacitor C50, to one of the vertical deflecting plates of the cathode ray tube.

The depthmeter consists of a phantastron,* designed around tube Tu2 (6Zh2P), and the driven blocking oscillator on the left half of triode Tu3 (6N1P).

In the initial stage, grid potentials of tube Tu2 are set so that there is no plate current from the tube. Capacitor C7 is charged to a voltage which is determined by the voltage on the tube plate, i.e. by the position of the slide for potentiometer R8.

Negative pulses from the synchronizer anode, which are fed through capacitor C5, diode D1 and capacitor C7 to the controlling grid of the 6Zh2P, open the tube to the anode current. At this instant the linear discharge of capacitor C7 begins, continuing until the voltage on the plate reaches a specific, constant value for the circuit. Upon reaching this value, the circuit returns to the initial state.

In the process of capacitor discharge, a linearly decreasing voltage forms on the phantastron plate, a negative rectangular pulse on the cathode, and a positive rectangular pulse on the screening grid.

The larger the size of the initial voltage of the capacitor charge, i.e. the initial voltage on the tube plate, the greater will be the discharge time for the capacitor. Thus, the duration of pulses produced by the phantastron depends linearly on the size of the voltage on the tube plate,

---

*The phantastron is an electronic generator producing voltage which varies linearly, i.e. a voltage which is characterized by a constant rate of change.

and may be varied by adjusting this voltage. In the given circuit, this adjustment is accomplished using potentiometer R8, the shaft of which is on the front panel of the flaw detector with the label "Flaw coordinates."

Potentiometer R8 permits the duration of the phantastron pulse to be varied within a range of 5-190 microsec. R7 and R9 are intended for tuning the depthmeter. A positive rectangular pulse from the screen grid of the phantastron is rectified by circuit R17·C8, and its moveable trailing edge (negatively polarized) is used to trigger the driven blocking oscillator.

The positive pulse of the blocking oscillator is fed through capacitor C10 to the vertically deflecting plate of the cathode ray tube as the amplitude mark of the depthmeter. Therefore, the position of the amplitude mark on the cathode ray screen depends on the angle to which the shaft of potentiometer R8 is rotated. When working in the "layer-by-layer" inspecting mode, the negative pulse produced by the blocking oscillator is fed from resistor R18 through switch B1 to trigger the scan voltage generator, the depthmeter marker not being visible on the screen.

The scan voltage generator is designed around tubes Tu4 (6Zh2P), Tu5 (6Zh9P) and Tu6 (6N1P). It is a three-tube circuit for a saw-tooth voltage generator which is called a "sanatron." This circuit contains an amplifier stage at tube Tu4 for improving the linearity of the voltage, in addition to the basic discharge tube (Tu5) (as in the phantastron). A cathode repeater (the left triode of Tu6) is connected to the feedback circuit of Tu5. A phase inversion stage is assembled around the right triode in the circuit of tube Tu6.

An auxiliary amplifier stage, together with the primary, forms a closed feedback circuit. The control grids of both tubes are interconnected. In the initial state, tube Tu4 is open, a sufficiently large plate current

passes through it, and the voltage on the plate of the tube is sufficiently small. Tube Tu5 is closed to the plate current by a large negative bias fed through resistor R30. A negative triggering pulse, cutting off this tube to the plate current, is fed to the third grid of tube Tu4 to trigger the "sanatron." Here a positive gradient exceeding the voltage on the third grid of tube Tu5 is created on the plate, unblocking this tube. The negative gradient of the plate voltage which occurs on the plate of Tu5 is transmitted almost entirely to the control grids of both tubes through the cathode repeater and capacitor C15. The operating mode of tube Tu4 is selected so that this drop is adequate to maintain it in a closed state during the entire operating cycle. Due to this, the voltage on the plate of this tube and on its third grid remains unchanged throughout the operating cycle. After the "sanatron" is triggered, capacitor C15 discharges. When the plate voltage of tube Tu5 is decreased to a certain constant value for the given circuit, the voltage on the first grid of tube Tu5 begins to grow. As a result, tube Tu4 unblocks and tube Tu5 cuts off rapidly due to the negative voltage gradient fed from the plate of Tu4 to the third grid of Tu5. The circuit returns to the initial state. During the discharge process for capacitor C15, a pulse of linearly decaying voltage is formed on the cathode resistance of tube Tu6, whereas on the screen grid of tube Tu4, a positive rectangular pulse is formed. The duration of these pulses is the same, and may be regulated within a range of 16-190 microsec. by varying the potential on the control grids of the tubes using resistor R31. The shaft of this resistor is on the front panel of the instrument with the label "Inspection depth." A positive rectangular pulse is fed through C51 from the screen grid of tube Tu4 to the third grid of tube Tu10 (the video amplifier-coincidence stage), and, through C58, to the control electrode

of the cathode ray tube. A saw-tooth voltage pulse is fed from the cathode resistance R38, through C17, to the left horizontally deflecting plate in the circuit, and, through R42, to the control grid of the phase inverter. A saw-tooth voltage pulse is fed from the phase inverter plate to the second horizontally deflecting plate.

A 7L055I oscillograph tube with electrostatic beam deflection and electrostatic control is used as the cathode ray display in the flaw detector. The principle by which an image is obtained on the screen in this type of tube was examined in detail in Chapter VI when the URD-52 was studied. Unlike the URD-52, the saw-tooth scan voltage is fed to both horizontally deflecting plates in order to improve the quality and increase the length of the base line on the screen. The power supply for the tube is not pulsed, but direct (-1000 v.). The requisite voltages are fed to the electrodes of the tubes from the divider at resistors R58-R62. Image brightness is adjusted by changing the voltage between the cathode and the modulator (the control grid) using variable resistor R58. The beam is focused by adjusting the voltage on the first plate of the tube (using R61).

The image on the cathode ray screen is displaced by varying the voltage between the appropriate pairs of deflecting plates. Horizontal displacement is achieved through regulator R45 and vertical displacement is accomplished with R50. The cathode of the tube is under a constant, high voltage relative to the instrument's chassis. Therefore, in order to avoid a breakdown between the cathode and the filament, the filament voltage (approximately 6.3 v.) is fed from a separate winding of the power transformer (b-b) which is insulated from the chassis. Electrical pulses which correspond to pulse echoes from flaws are fed to the vertically deflecting plate in the right-hand side of the circuit through capacitor C50. A pulse

is fed to the left-hand plate in the circuit from the blocking oscillator through capacitor C10. A positive rectangular pulse is fed to the tube's modulator from the scan voltage generator through capacitor C58 to improve the brilliance of the image.

The auxiliary displays. The auxiliary display unit is designed around tube Tul1 (6N1P). The cathode repeater is a buffer stage, and it protects the circuit from stray currents from the display stage which might fall on the amplifier. It is assembled around the left-hand triode in the circuit. The right half of tube Tul1 is the display stage. Initially, this stage is closed by a negative voltage which is fed to the control grid from the center tap of potentiometer R92. Pulses which correspond to reflections from flaws and which are taken from the cathode repeater charge capacitor C54 so that there is a positive voltage on the right-hand plate. At this point, the tube opens, current flows through relay R2, which is connected to its plate circuit, and the relay contact closes the circuit of indicator tube Tul5, which is mounted in a special socket on the probe. An audible signal, the frequency of which corresponds to the pulse repetition frequency of the synchronizer, appears in the headset T, located on the instrument chassis. The sensitivity of the display stage may be adjusted using potentiometer R92. Tube Tul5 may be switched to a stage of continuous glow using switch B2 ("Light-relay"). Tubes Tul3 and Tul4 are instrument lights for the depthmeter scale.

A transistorized circuit for supplimentary amplification was suggested by workers of the October Rail Line to increase the volume of the audio indicator. The circuit for such an amplifier is presented in Fig. 211.

The power supply unit is designed for operation from a 220- or 36-volt alternating current. To obtain the voltages necessary for supplying power to

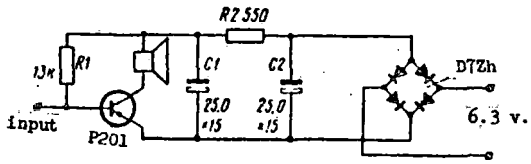

Fig. 211 Circuit of an auxiliary amplifier for increasing the volume of the audio indicator in the DUK-11IM flaw detector.

the individual circuits within the instrument, a power transformer TR3 and a system of rectifiers are used. The high voltage for providing power to the plate circuits of the tubes is obtained by rectifying a voltage taken from winding II of transformer TR3 using the rectifier at diodes D12-D19 (type D226), which is designed in accordance with a bridge circuit. Resistors R95-R102, which are connected in parallel with the rectifying diodes, serve to equalize the values of the voltages on these diodes. A fuse F1 protects the plate winding from short-circuiting. Choke coil Ch1, resistor R105, and capacitors C60, C61, and C62 form a filter.

A voltage of +330 v. is taken from the rectifier for supplying power to tubes Tu1, Tu4-Tu6, and the third plate of the cathode ray tube, whereas +300 v. is taken for supplying power to the plate circuits of the remaining tubes. The half-wave rectifier at diode D20 (D226 type), with a filter C64, R103, C63, is used for supplying the bias circuits with power. The high voltage for powering the circuits of the cathode ray tube is obtained using a half-wave rectifier on the selenium stack of D21 (TBS-7-19M) (the filter is C66, R104, C65). There are two windings in the transformer for obtaining filament voltage: winding VI, one lead of which is grounded, for supplying power to the filament circuits of the tubes, and winding V (ungrounded), for supplying power to the filament circuits of the cathode ray tube.

3. Construction of the DUK-11IM and preparation for work.

The DUK-11IM flaw detector (Fig. 212) is a portable instrument, which is supplied with a handle for carrying. When the flaw detector is being transported or is in storage, the face panel is covered with a removable lid. The main controls, which are situated on the front panel of the flaw detector, are:

1) The "Monitoring depth" knob, for selecting the thickness of the section being inspected

2) The switch for selecting the inspection mode; "inspecting from the surface"-"layer-by-layer inspection"

3) The "light-relay" switch, for selecting the mode into which the display tube is connected

4) The "Flaw coordinate" knob, for measuring the coordinates of the reflecting surface

5) The "Sensitivity" knob, for adjusting the minimum size of the flaw to be indicated by the instrument

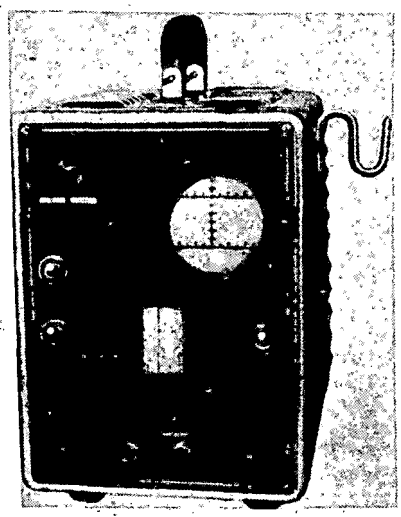

Fig. 212 The DUK-11IM flaw detector.

6) The connector for hooking up the probe

7) The "Sensitivity time adjustment" knob, for regulating the depth to which the flaw detector is sensitive

8) The switch for turning the device off and on.

In addition, the cathode ray tube screen and the depthmeter scale, with a viewing line on the window for reading the flaw coordinates, are situated on the front panel. Auxiliary flaw detector controls situated on the back under a cover are the focus and brilliance knobs, "X" and "Y", used for adjusting the image on the cathode ray tube screen; the "Relay sensitivity" knob, with which the activation threshold of the auxiliary indicators may be varied as well as a connector for hooking up the power supply line and the grounding terminal.

The instrument is wired on three chassis:

a) The power transformer, the choke switch, capacitors, filters for power supply sources, the radio pulse generator stage, and the relay triggering sources, the radio pulse generator stage, and the relay triggering stage are mounted on the lower chassis. A jack for connecting the instrument to the (outside power supply) network, fuse holders, and the grounding post are also set on the lower chassis

b) The electronic circuits for the depthmeter and the scan generator are mounted on a chassis situated in the upper left-hand corner of the instrument. The inductance-capacitance delay line is also mounted there

c) The high-frequency amplifier, the rectifier, and the video amplifier-coincidence stage are mounted on the chassis set to the right of the cathode ray tube.

The DUK-11IM flaw detector is supplied with 30, 40, and 50-degree angle probes and with normal probes. A feature of these probes is that the

inductance coil is situated directly in the probe body (Fig. 213a). In order to use the probes without a built-in inductance with the instrument, the flaw detector comes with an adaptor containing an inductance coil (Fig. 213b).

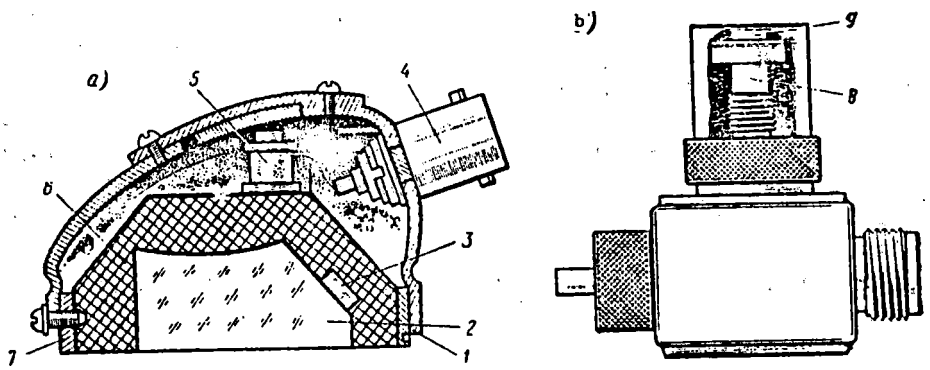

Fig. 213 Designs: a) of the angle probe with built-in inductance coil; b) of the adapter for connecting probes without a built-in inductance. 1. body; 2. wedge; 3. piezoelectric element; 4. connector; 5. coil; 6. damper 7. ring; 8. coil; 9. core.

The flaw detector also includes: a #1 calibration device, plates for preparing the #2 calibration device, a set of cables for connecting the instrument to the (outside power supply) network, for connecting the probes and for grounding the flaw detector. A device intended to limit the displacement of the probes is also furnished.

Before the device is plugged in, the flaw detector must be reliably grounded. Then the probe cable and the power supply cable must be connected.

The power cord must be plugged into a 220 v., 50 Hz. a.c. circuit and switch 8 (cf. Fig. 212) moved to the "on" position.

Forty to sixty seconds after the transmitted pulse appears at the left end of the bottom line, the image is adjusted on the cathode ray tube screen, using the knobs "X," "Y," "Brightness," and "Focus." The narrowest bottom line (1-2 mm) is obtained and positioned in the lower half of the screen (5-10 mm below the axis).

After adjusting the image, the auxiliary displays are set using the "Relay sensitivity" knob so that the indicators activate from pulse echoes which are 5 mm or greater on the screen.

The flaw detector is tuned to inspect items at a given depth, starting at the surface. This is done in the following sequence (cf. Fig. 212): a) using the "Flaw coordinates" knob, set the number on the depthmeter scale which corresponds to the given depth for the probe which is to be used; b) using the "Sounding depth" knob, shift the depthmeter mark to the right end of the bottom line.

The probe must be set in a position so that the amplitude of the echo signal on the cathode ray tube screen is the greatest. Using the "Flaw coordinates" knob, the depthmeter mark must be moved to the beginning of the reflected pulse for measuring the flaw coordinates in this mode. The numbers on the H and L scales opposite the line on the window show the flaw coordinates for the selected probe.

The flaw detector is tuned to inspect a given layer in the following sequence: a) when the flaw detector is operating in the "from the surface" mode set the given size of the layer to be inspected; b) move the switch "Inspection from the surface-layer-by-layer inspection" into the "layer-by-layer" position, and, moving the "Sounding depth" knob, set on scale H of

the depthmeter the number for the selected probe corresponding to the depth at which the upper edge of the layer to be inspected is situated. This number should be set opposite the line on the window using the "Flaw coordinates" knob.

To measure the flaw coordinates in this mode, it is necessary to move the pulse echo to the beginning of the scan using the "Flaw coordinates" knob. The numbers in the window opposite the line on scales H and L for the selected probe type show the flaw coordinates. After the flaw coordinates have been calculated, it is absolutely necessary to return the "Flaw coordinates" knob to the initial position in order to preserve the given values of the monitoring parameters.

4. The electrical schematic of the DUK-13IM

The electrical system of the DUK-13IM flaw detectors is designed in accordance with the functional circuit of UZD-NIIM-5 devices. Unlike the DUK-11IM, the DUK-13IM is mainly transistorized. Only a few small-sized vacuum tubes are used. Several design peculiarities in the circuits are caused by the selection of elements. There is no synchronizing pulse generator in the flaw detector. A radio pulse generator operating in a self-excitation mode carries out its functions. A constant voltage of 12 v. is fed to the instrument, both when operating from an alternating current circuit and when working from batteries. There is a special converter in the flaw detector for obtaining the necessary power supply voltages. The construction of the separate units of the device's circuitry can be seen in Fig. 214.

The radio pulse generator is assembled around a special diode thyristor D-228 (KN-102I).

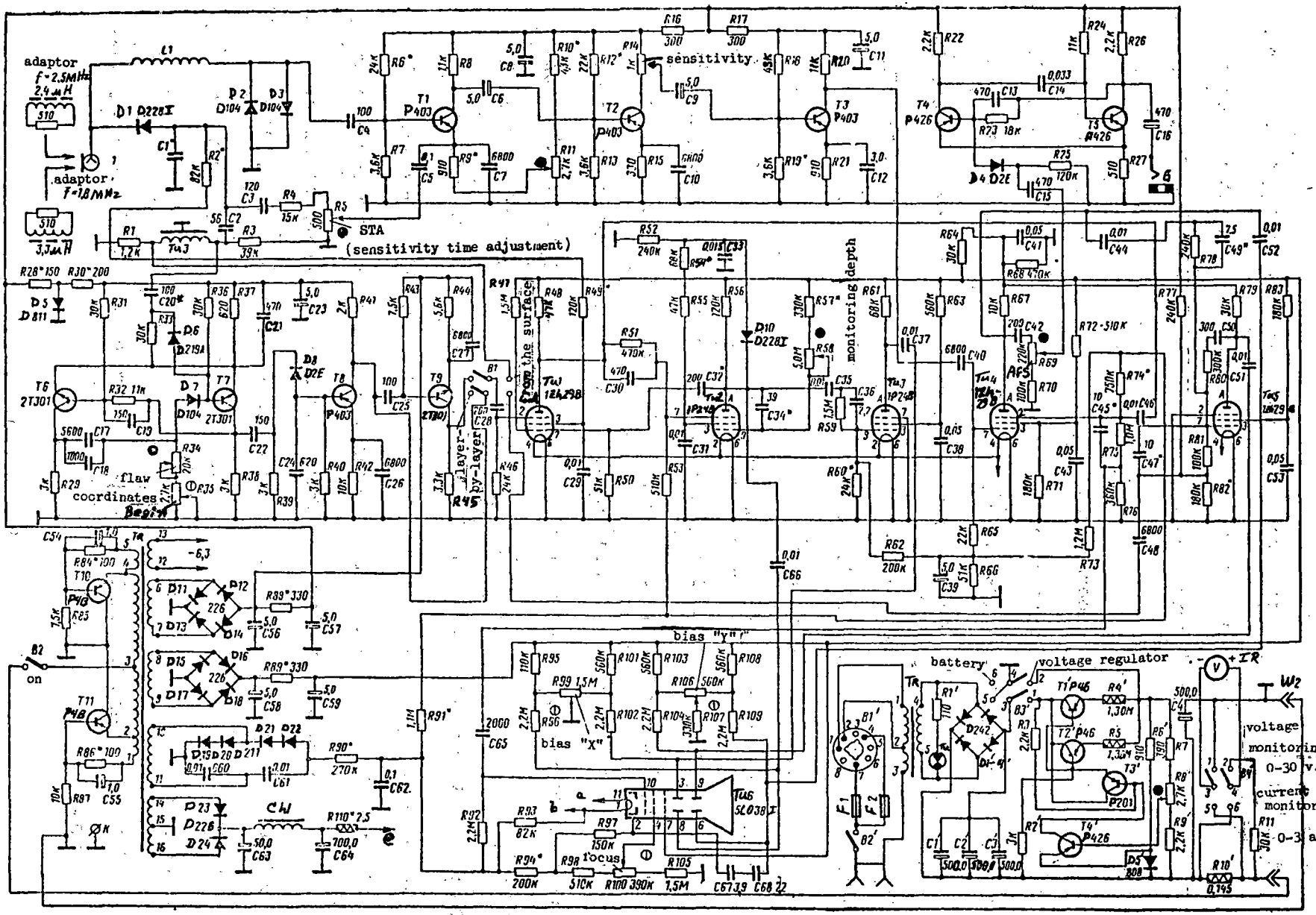

Fig. 214 Electrical circuit of the DUK-13IM flaw detector.

This diode (D1) serves as a switch in an oscillator assembled in a circuit having an impact excitation. The operating principle of such an oscillator using a semiconductor diode is in no way different from the oscillator using a thyratron which is employed in the URD-52 flaw detector (cf. Chapter VI). The oscillator operates in a self-excitation mode. The pulse repetition frequency F depends on the size of capacitance C1, resistance R2, the size of the power supply voltage, and the diode switching voltage. The smaller the product of R2·C1 and the smaller the diode switching voltage, the higher the frequency will be.

The inductance coil which is situated in the adapter (Fig. 213b) is used as the oscillatory circuit inductance. Depending on the natural frequency of the probes which are employed, an adapter with an inductance L = 2.4 microhenry (f = 2.5 MHz) or L = 3.3 microhenry (f = 1.8 MHz) is used. A more accurate tuning of the circuit to the natural plate frequency may be made using the core. The same type of probes are used in the DUK-13IM as are used in the DUK-11IM. Pulse echoes from the probe are fed to the input of the radio frequency amplifier.

The radio frequency amplifier (RF Amp) is constructed around transistors T1-T3 (type P403). The amplifier design uses resistances with a capacitance connection between the stages. The RF amp has a broad bandpass width which permits probes to be used at a frequency of 1.8 or 2.5 MHz without retuning the amplifier. The total amplification coefficient of the RF amp is not less than 20,000.

As in the DUK-11IM flaw detector, a sensitivity time adjustment was installed in the DUK-13IM. The voltage gradient from the radio pulse generator is used for this adjustment. This pulse is also fed to the emitter of the amplifier's input transistor through the circuit C3, R4, R5, and C5, and it is adjusted using variable resistance R5 (STA).

The sensitivity of the RF amplifier is adjusted using potentiometer R14, which is a load on the second stage of the RF amplifier. An adjustable negative voltage is fed from the variable resistor R11 to the emitter of the amplifier's first transistor for cutting off noises.

The temperature dependence of the properties of semiconductor triodes is one of their well-known features. This is caused by a change in the current through the emitter junction due to temperature. Additionally, the back current of the collector junction varies sharply with changes in temperature. This current, passing through resistances connected in the base circuit, creates an auxiliary voltage which influences the size of the collector current.

A negative direct current feedback, which is created by connecting resistance stages (R9, R15, R21) in the emitter circuit is used to stabilize the working conditions of the RF amp for a broad range of temperatures. Improvement in the stability is also obtained by a selection of the voltage dividers which are used for feeding the positive potential to the base of the transistors (R6, R7; R12, R13; R18, R19).

There is a limiting circuit made up of inductance L1 and diodes D2 and D3 (type D104) on the RF amplifier input to protect the first transistor from breaking down when transmitted pulses, which may reach 150 v., are fed to its base. These diodes are non-linear elements, their resistance strongly depending on the size of the signal which is applied. For large signals, the resistance of these diodes is small, whereas for small signals, corresponding to the reflections from flaws, it is high. Therefore, the transmitted signals will be strongly shunted by these diodes, while pulses corresponding to echo signals will pass through almost without distortion. There is no special stage for signal rectification in the DUK-13IM.

Rectification is accomplished in the third stage of the RF amplifier due to the appropriate selection of the mode of operation.

There is an auxiliary stage at tube Tu5 (1Zh29B) in the DUK-13IM, along with the video amplifier-coincidence stage (at tube Tu4, a 1Zh29B). These stages are required in order to obtain signal amplitude adequate for display on the cathode ray tube screen.

The working principle of the video amplifier-coincidence stage in the DUK-13IM corresponds fully to the operation of the same stage in the DUK-11IM flaw detector (cf. Fig. 214). Positive rectified pulses from the output of the RF amplifier are fed to the control grid of this tube through capacitor C40, and positive pulses from the scan voltage generator are fed to the third (grid) through capacitor C46. Negative pulses from the plate of tube Tu4 are fed to one of the vertically deflecting plates of the tube (lead-out 6, through C52), as well as to the control grid of tube Tu5. This is done through capacitor C44 and the compensating circuit R78-C49, which is intended for compensation of the video pulse fronts. Tube Tu5 is an amplifier and phase inverter. Positive video pulses corresponding to the reflections from flaws are fed from the plate of tube Tu5 to the second vertically deflecting plate of the cathode ray tube (lead-out 9), which permits the amplitude of these pulses to be increased when they are displayed on the cathode ray screen. Tube Tu5 also serves to amplify the depthmeter marker pulse in the "inspection from the surface" mode. A positive marking pulse is fed to the control grid of tube Tu5 from switch B1, while a negative pulse, which is also fed to the vertically deflecting plate of the cathode ray tube, is taken from the plate (circuit R80-C50 is a compensating circuit).

The depthmeter, strictly speaking, consists of an apparatus for measuring the propagation time of the ultrasonic oscillations, a differentiating circuit, and two amplifiers.

A driven multivibrator designed around transistors T6 and T7 (2TZ01 silicon transistors) is used as the time-measuring circuit. The multivibrator is a two-stage, resistor-coupled amplifier in which the output of each stage is connected to the input of the other. The task of the multivibrators is to generate rectangular pulses. In the given circuit, the multivibrator using transistors T6 and T7 operates in an external synchronization mode. Transistor T6 is closed and transistor T7 is open when there is no triggering pulse.

The multivibrator circuit in question permits a constant state of equilibrium to be obtained without a special auxiliary bias voltage source. The voltage which keeps triode T6 closed is developed at resistance R37 due to the current of the open transistor. The depthmeter is triggered by negative pulses from the radio pulse generator which cause the multivibrator to change suddenly to a new mode when transistor T6 is open and T7 is closed due to interstage coupling. In this event, a positive pulse is produced on the collector of T7 and is then fed to the differentiating circuit C22·R39. A brief negative pulse corresponding to the trailing edge of the multivibrator pulse is fed from the output of this circuit, through diode D8 to the base of transistor T8, and, after amplification, from the collector of T9, through switch B1 to the control grid of tube Tu5.

The depthmeter pulse is used in the "layer-by-layer" mode for triggering the scan voltage generator. To this end, the pulse passes to the scan voltage generator through switch B1 after amplification at transistor T9.

The selected multivibrator circuit provides a high linearity of change in the pulse duration, depending on the value of resistor R34. This permits a linear scale to be obtained for gaging the location of flaw coordinates, using a PPZ-12 linear potentiometer as a resistor. For short pulse durations from the multivibrator, the linearity is obtained by varying resistor R35.

To provide the required accuracy for gaging the flaw coordinates when varying the power supply voltage, the depthmeter stages take their power from the stabilized voltage obtained at the stabilitron D5 (D811).

The scan voltage generator is designed around tubes Tul (1Zh29B), Tu2 (1P24B), Tu3 (1P24B) and diode D10. A sanitron oscillator based on tubes Tul and Tu2 is included, as well as a phase inversion stage at tube Tu3. The oscillator is triggered by negative pulses from a differentiating circuit C28-R46 (when inspecting from the surface) or from resistor R45 (in the "layer-by-layer" mode). These pulses are fed to the third grid of tube Tul.

The operating principle of the sanitron oscillator in the DUK-13IM flaw detector corresponds completely to the operating principle of the scan voltage generator in the DUK-11IM flaw detector (cf. Section 2 of this chapter). A positive intensifier pulse, which is fed to the control electrode of the cathode ray tube (lead-out 10), is taken from the plate of tube Tul (cf. Fig. 214), through capacitor C46 from the divider R75, R76. A linearly decreasing scan voltage, which is fed to one of the horizontally deflecting plates of the tube (lead-out 8) and to the phase inverter through capacitor C66, is taken from the plate of tube Tu2. A linearly increasing saw-tooth voltage (positively polarized) is taken from the plate of the phase inverter tube Tu3 and fed through capacitor C37 to the second vertically deflecting plate of the cathode ray tube (lead-out 3).

The scan duration is varied between 14 and 100 microsec. using variable resistor R58. The shaft of this resistor is on the front panel of the flaw detector, labeled "Monitoring depth."

A 5L038I cathode ray tube is used as the cathode ray display in the flaw detector. This tube is an electronic device with electrostatic beam deflection and electrostatic beam control. This is the same as the cathode ray tubes used in the ultrasonic track flaw detectors. The circuit diagram for this tube is analogous with the circuit diagram of the oscillograph display in the DUK-11IM. The required voltages are taken from divider R94, R98, R100, R105, to which a constant voltage of -750 v. is fed from the power supply voltage converter. Resistors R99 and R106 provide the necessary image shift on the screen. A filament voltage (6.3 v., 1000 Hz) is fed to the tube from the winding of the power supply voltage converter transformer, which is insulated from the chassis (leads a-b in Fig. 214).

In the DUK-13IM, headphones, to which the signal is fed from a special stage consisting of a driven multivibrator designed around transistors T4-T5 (P42B's) when a flaw is detected, serves as the auxiliary indicator. This multivibrator is triggered by a negative pulse from the anode of tube Tu4. The amplitude of the multivibrator pulses, and, consequently, the volume of the sound in the headset, do not depend on the size of the signal at the stage input. The activation level of the multivibrator is set according to the amplitude of the pulse echo on the cathode ray tube screen, and it may be adjusted using the variable resistor R69, the AFS (automatic flaw signaling device).

A constant voltage converter (input voltage of 12 v.), together with a system of rectifiers and filters, is used to obtain the necessary values for the power supply voltages in the flaw detector. This voltage is transformed

initially into alternating voltage by a transistorized oscillator. The voltage is then transformed (stepped up or down) and, where necessary, it is also rectified and smoothed.

The converter is designed in accordance with the circuit of a push-pull generator with a common collector built around transistors T10 and T11 (P4B's) operating in the self-excitation mode. The operating principle of this type of converter was examined in detail in Chapter III, when the MRD flaw detectors were studied. The pulse repetition frequency for the converter is approximately 1000 Hz.

The rectifier for obtaining the power supply voltage for the transistor collector circuits (-15 v.) is designed around diodes D11-D14 in a bridge circuit. Elements C56, R88 and C57 form a filter.

The power supply voltage for the tube plate circuits (+250 v.) is obtained by rectifying an alternating voltage from winding 8-9 of the converter transformer. The rectifier is assembled in a bridge circuit around diodes D15-D18, with C58, R89, or C59 as the filter.

The high voltage for supplying power to the cathode ray tube circuits is obtained using the rectifier built around diodes D19-D22 (D211's), which is assembled according to a voltage multiplication circuit (the filter is R90, C62).

A constant 2.4 v. voltage is used for heating the tubes. In order to obtain this voltage, there is a rectifier which uses diodes D23-D24 (D226's) with the filter C63, Ch1, C64, and an absorbing resistor R10 in the device.

When working with the flaw detector from an a.c. circuit, a special unit, consisting of a rectifier and a regulator, is used. The primary winding of the rectifier transformer is fitted with leads to provide a power supply from 36- and 220-volt alternating voltage sources. Voltage rectification

is accomplished by the rectifier designed around the D242 diodes in a bridge circuit. The stability of the power supply voltage fed to the instrument is obtained using a semiconductor voltage regulator consisting of a regulating element (two P4B transistors connected in parallel), connected in series with a load, an equalizing and amplification element (an amplifier using a P42B transistor with an emitter repeater using a P201 transistor), and a reference element (diode D5', a D808). Diodes of this type are analogues of the gas-filled voltage regulators (stabilitrons) which are widely used when designing circuits using vacuum tubes. Semiconductor voltage regulators are junction-type silicon diodes operating in the saturation region. In this region the volt-ampere characteristic of diodes is such that when the current through the diode varies within a broad range, the voltage gradient across it changes insignificantly.

When the regulator output voltage is changed, the potential of the base of the P42B regulating transistor changes, while the potential of the emitter remains unchanged due to diode D5'. Here a misalignment voltage, which is fed through the emitter repeater to the regulating transistors, appears on the collector of the P42B. As a result, the voltage drop in these transistors changes so that the output voltage is maintained constant within the given range. The initial value of the voltage (12 v.) is set using the variable resistor R8'.

The shaft of this potentiometer is on the front panel of the power supply unit, labeled "12 v. adjustment." Within the unit, there is a meter which is used to measure the output voltage or the load current. The shunt and the instrument multiplier are connected by a special switch.

The power supply unit may also be used for charging the storage batteries. The input of the unit is connected directly to the rectifier using switch B3'. The procedure for charging the storage batteries is given in Chapter XIII.

5. Construction of the DUK-13IM

The DUK-13IM consists of three separate units: the electronics unit (Fig. 215), the unit for taking power from the power network (Fig. 216), and the storage battery.

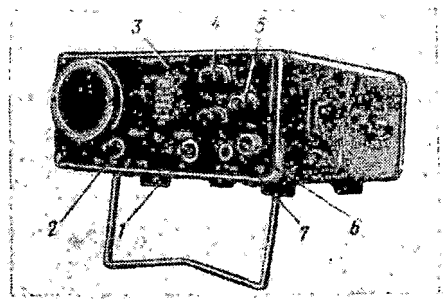

Fig. 215 The DUK-13IM flaw detector.

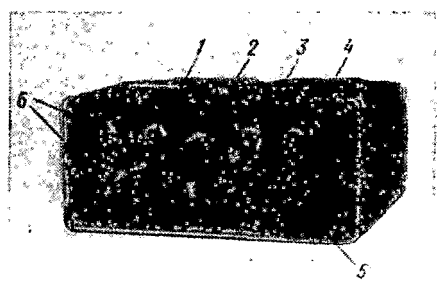

Fig. 216 The unit for powering the DUK-13IM from the external power supply network.

The basic controls of the flaw detector are located on the front panel of the electronics unit (cf. Fig. 215).

The intended use of these controls is the same as in the DUK-11IM flaw detector. Two potentiometers are brought out into a groove on the right side panel: "Suppression" to regulate the level of the noise cut-off, and "AFS" (automatic flaw signaling device) to vary the activation level of the audio indicator.

The connector for hooking up the power supply cable and the terminal for grounding the flaw detector are on the back. On the front panel of the power supply unit are (cf. Fig. 216):

1) A switch "network-off" for switching the unit on

2) A meter for measuring the input voltage (scale 0-30 v.), or the load current (scale 0-3 amp)

3) A switch "Current-Voltage" used for changing the mode of operation for the meter

4) A switch "Bat-Reg" for changing the rectifier work mode: supplying power to the instrument or charging the batteries

5) A knob "12 v.-Reg." designated for setting the power supply voltage

6) A 2-amp fuse (used when working from a network with 36 v.) and a 0.5 amp fuse (used when working from a network with 220 v.).

The flaw detector is connected to the power supply unit (or to the storage battery) using two types of flexible cable (0.5 and 20 m. in length). The electronics unit of the flaw detector may be fastened onto the chest of the operator using special straps.

A removable magnifying glass may be used to increase the size of the image on the cathode ray tube screen. The instrument is also fitted with a detachable, telescoping viewing hood with "kallimator" for observing the image in bright light.

The electronics part of the instrument is mounted on folding plates which are fastened to hinges with screws and may be easily removed. The scan voltage generator, the video amplifiers and the depthmeter are mounted on one plate. The radio pulse generator, the RF amplifier, and the auxiliary indicator circuit are situated on the second. The cathode ray tube electrode power supply circuit is mounted on a separate plate. A power supply voltage converter, consisting of a transformer, transistors, as well as rectifiers, and voltage source filters, is designated as a separate, removable component.

The instrument is supplied with NKN-2.25 and NKN-10 storage batteries having a working voltage of 12 v. Each of the batteries is stored in a special carrying case with a handle. The box also contains an on-off toggle switch, a measuring device, and a connector for hooking up the connecting cable.

6. Preparation for work and working with the DUK-13IM in the field; evaluation of readings.

The DUK-13IM flaw detector is used to monitor welded and bolted joints and for secondary monitoring of individual sections of the base metal of rails which are in use. As a rule, the flaw detector and its storage batteries are mounted on a carriage from other types of flaw detectors (e.g. the carriage of the URD-52 flaw detector, which has been re-designed for use on the Pribaltijsky line). However, on sectors where there is heavy traffic, using the instrument without a carriage is more effective.

Inspection of welded joints, which requires a large number of operations, may be conducted successfully at air temperatures no less than +5° C.

In practice, bolt joints may be inspected an any temperature at which there is a bottom pulse visible on the flaw detector screen. However, at below zero temperatures, the flaw detector's converter triggering breaks down.

Therefore, in individual cases, when it is necessary to inspect bolted joints in the wintertime, it is preferred to turn the flaw detector on in a room where the temperature is not below 0° C. and not to turn it off during the work shift.

Inspecting bolted joints from the running surface is done using a normal probe. A normal probe with a metallic wear face is supplied with the flaw detector. However, as working experience has shown, a more reliable acoustical contact is achieved if the face of the probe is made of plexiglass. A normal probe with a plexiglass face (Fig. 217) may be prepared from a worn-out angle probe. Both the pulse echo and the mirror shadow methods are used for monitoring the bolted joint using normal probes (Fig. 218).

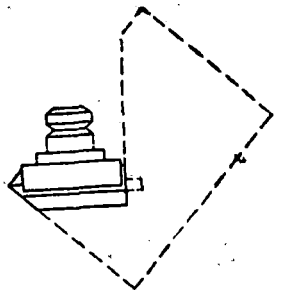

Fig. 217 Preparing a normal probe from an angle probe (the dotted line shows the section of the wedge which is removed when preparing the normal probe).

The running surface of the rail head is covered with a layer of mineral oil before inspecting the bolted joint. The number corresponding to twice the height of the rail is set on the depthmeter scale for the normal probe, and the marker is displaced to the right end of the base line using the

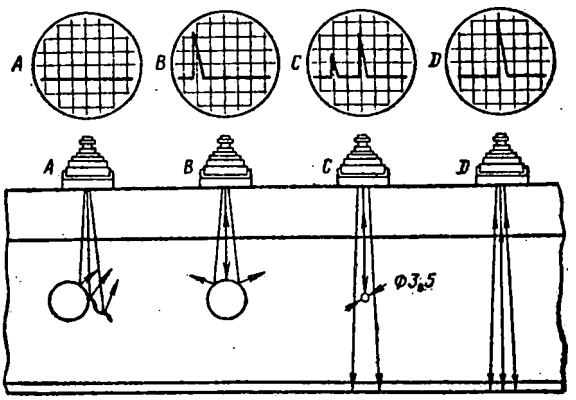

Fig. 218 A schematic for inspecting the bolted joint of a rail.

"Monitoring depth" knob. When the probe is placed on the running surface of the head above the web, a bottom pulse appears at the center of the base line on the flaw detector screen. Then it is necessary to set the "Sensitivity" and "STA" knobs in the position where there would be no transmitted pulse (the probe is in position D), whereas the bottom pulse would be clearly examined on the screen and sound would be audible in the headsets.

When the flaw detector is tuned to the indicated settings, it is necessary to follow changes in amplitude for the bottom pulse and the appearance of reflected pulses to the left of the bottom pulse while moving the probe along the running surface above the rail web.

When inspecting bolted joints, the disappearance of the bottom pulse or the appearance of a reflected pulse when the probe is not above a bolt hole (probe in position A), is a signal that a flaw has been detected.

Before going out onto the line, the flaw detector's working capability with the normal probe is tested on a rail specimen containing an artificial reflector. A hole 3-4 mm in diameter and bored through the center part of the rail web may be used as a reflector of this type.

The operation of a flaw detector with a normal probe is considered satisfactory if the bottom pulse and the pulse echo from the hole (probe in position C) are sharply distinctive on the screen when there is no transmitted pulse and when the probe is placed on the running surface of the rail head.

Inspecting welded joints and individual sections of the parent metal of rails which are in use is accomplished using angle probes in accordance with the recommendations set forth in Chapter XI.

7. Testing and adjusting the flaw detector.

The DUK-11IM and DUK-13IM flaw detectors are tested and adjusted at least once a month by a set-up specialist, either where the instrument is being used or, when necessary, in section repair shops or traveling repair shops.

The following operations should be carried out:

1) The probe emission center and the beam transmission angle into steel are determined for all probes, according to Calibration Standards No. 2 and 3.

At the rated wedge angles and with the air temperature between 15 and 25 degrees C., the measured beam transmission angles should lie within the range:

$50^{\circ} \pm 2^{\circ}$ for a probe with a wedge angle of 40°, and

$65^{\circ} \pm 2^{\circ}$ for a probe with a wedge angle of 50°.

Should the measured value of the beam transmission angle exceed the indicated limits, the wedge must be replaced. In exceptional instances, reworking the working surface of the wedge so that it is perpendicular to the front and lateral edges of the probe (Fig. 219) is permitted.

The wedge should be at least 32 mm high after repair. Probes from the "Elektrotochpribor" plant in metal casings are not repairable.

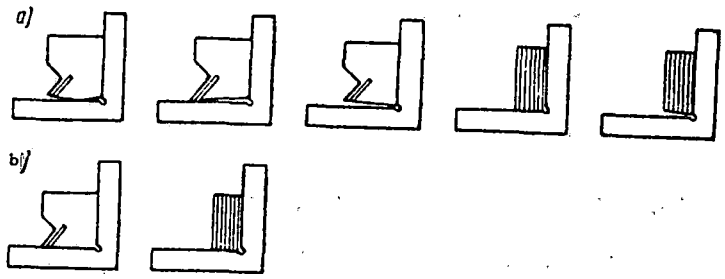

Fig. 219 Probe wedges: a--after wear b--after repair

Defective probes and wedges which are not repairable should be removed from the set.

2) The sensitivity and the dead zone are determined for all probes, according to Calibration Standards No. 1 and 2.

The sensitivity of the DUK-11IM and DUK-13IM flaw detectors is considered satisfactory if holes in Standard No. 1 from 15-40 mm in diameter (when probes with a wedge angle of 50° are used), or from 15-45 mm in diameter (when probes with a wedge of 40° are used) may be made to register on all of the flaw detector displays using the "STA" and "Sensitivity" knobs.

The dead zone of the flaw detector with its probes is tested at the same sensitivity by detecting a hole in Standard No. 2.

A flaw detector and its probes is operating satisfactorily if it provides detection of a hole 2 mm in diameter in Standard No. 2 located at the following depths under the surface on which the probe is placed:

8 mm using a probe with a 40-degree wedge angle, and

3 mm using a probe with a 50-degree wedge angle.

Should the magnitudes of the sensitivity and the dead zone not correspond to the indicated values, it is necessary to make supplimentary adjustments using the switch supplied with the flaw detector. Probes in a metal casing are not adjustable.

3) The accuracy with which the depthmeter operates is tested by measuring time intervals between the pulse echoes reflected from the cuts in Standard No. 1. To do this, a normal probe is placed over a cut and the depthmeter mark is moved over each of the bottom signals in sequence using the "Flaw coordinates" knob. The number on the "microsec." scale opposite the line on the window shows the propagation time for ultrasonic oscillations to the cut and back. Measurements are taken with the flaw detector at maximum sensitivity. To do this, the "STA" and "Sensitivity" knobs are turned clockwise with the normal probe connected. Then, turning the "STA" knob counter-clockwise, it is set in the left-most position at which pulses caused by reflections in the probe are not yet visible on the cathode-ray tube screen.

The accuracy of the depthmeter operation in the DUK-11IM flaw detector is considered satisfactory if the readings on the instrument scale are 20 $\pm$ 2 microsec. for the first reflection, and 60 $\pm$ 2 microsec. for the third.

The accuracy of the depthmeter operation in the DUK-13IM flaw detector is tested based on the first reflection. Readings from the depthmeter scale for the first reflection should be within a range of 20 $\pm$ 2 microsec. If the readings from the depthmeter scale do not correspond to the given values, further fine adjustments are required.

The DUK-11IM's depthmeter is fine-tuned using the two potentiometers "End" and "Start" in the following sequence:

a. Having set the number 20 opposite the line in the window of the depthmeter's "microsec." scale, a probe is placed above a cut in Standard No. 1, and the depthmeter marker is moved to the leading edge of the first reflected pulse by turning the "Start" potentiometer shaft

b. Then, the number 60 is set on the depthmeter's "microsec." scale, and the depthmeter marker is moved to the leading edge of the third bottom reflection by turning the "End" potentiometer shaft

c. Executing steps "a" and "b" in sequence, a coincidence is obtained between the depthmeter pulse and the first and third bottom reflections without readjusting the "End" and "Start" potentiometers.

The DUK-13IM's depthmeter is fine-tuned according to the leading edge of the first reflected pulse using the "Start" potentiometer.

4) Measurements of the resistance of the power supply cable's insulation are taken using a megohmmeter. The value of the insulation resistance should not be less than 100 megaohm. Cables with an insulation resistance of less than 100 megaohm should be removed from service.

5) A test of the serviceability of the flaw detector's chassis ground and the rectifier ground is conducted by measuring the resistance between the probe cable connector and the ground terminal on the instrument's chassis.

The resistance, which is measured using an ohmmeter, should not exceed 5 ohm. If it does, the flaw detector's ground circuit must be examined, the cause for the resistance increase should be established, and it should be eliminated.

8. Trouble-shooting the DUK-11IM and DUK-13IM

The DUK-11IM and DUK-13IM are rather complex radio devices for which extensive knowledge of the interactions of the individual units of the instrument and their electrical circuits is often required for determining faults. Due to the variety of reasons for which the flaw detector may become inoperative, as a whole or within any one of the individual units, it is impossible to indicate beforehand all possible faults to be found.

If the instrument refuses to work, the fuses and the power supply connecting cables are checked first with an ohmmeter. Then, when necessary, faults are identified and eliminated in the instruments. Certain characteristic faults of the flaw detectors and means for eliminating them are presented in Tables 14 and 15 for convenience.

It is necessary to note that the most vulnerable units of the DUK-11IM and the DUK-13IM flaw detectors are the probes.

When repairing the probes, it is necessary to pay particular attention to providing the acoustical contact between the piezoelectric plate and the wedge. To do this, the wedge is washed with alcohol or acetone, and the piezoelectric plate is wiped on both sides of a sheet of writing paper before assembly. Then the jacket is put on the wedge, a drop of pure mineral oil is inserted, and the foil padding on which the piezoelectric plate seats is inserted. Asbestos paper 45 mm thick is recommended as the plate damper. The wire for connecting the upper face of the plate into the circuit is inserted through this damper.

The plate damping is adjusted using a special wrench which is included with the instrument. Observing the instrument's screen, the damping* is regulated so that the amplitude of noise pulses is minimal.

Oil drying up under the foil padding may be a primary reason for a decrease in the probe sensitivity.

After eliminating detected faults, the correspondence of the instrument's basic characteristics with technical requirements must be tested.

---

*Tr. note--lit. "pressure of the damper (medium)".

Table 14

Possible Faults in the DUK-11IM Flaw Detector

#	Fault Indication	Possible Cause	Correction
1	There is no depthmeter mark in the "Inspecting from the surface" mode, and there is no base line in the "Layer-by-layer" mode	The depthmeter is inoperative; variable resistor R20 is misadjusted; tube Tu2 or Tu3 is out of order	Adjust the bias on the depthmeter's blocking oscillator grid using resistance R20; replace tubes Tu2, Tu3 with ones known to be good
2	There is no transmitted pulse on the base line at any position of the "Sensitivity" and "STA" knobs	The radio pulse generator or the receiver amplifier channel is inoperative	Test the operating modes of the tubes, replace the tubes with ones known to be good
3	There is no base line in the "Inspecting from the surface" mode	The scan voltage generator is defective; the rectifier at diode D21 is out of order; the cathode-ray tube is out of order	Test the operating modes of the tubes; replace the tubes with ones known to be good. If there is a base line in the "layer-by-layer" mode, test the soundness of the delay line
4	There is no base line only in the "layer-by-layer" mode	The depthmeter is inoperative; switch B1 is out of order	Test the operating modes of the depthmeter tubes; when necessary, replace them with ones known to be good; replace the switch
5	The base line occupies half the screen on the cathode-ray tube	The stage around tube Tu6 is out of order	Replace tube Tu6 (6N1P)
6	The depthmeter mark does not move along the base line	There is an opening in the "Flaw coordinates" potentiometer	Replace the potentiometer (PPZ-12-20 kohm)
7	The auxiliary displays do not activate when there is a transmitted or a reflected pulse on CRT screen	The auxiliary indicator stage is inoperative (around tube Tu11)	Adjust the potential on the control grid of the right triode of tube Tu11 using R92 ("Relay sensitivity"); replace tube Tu11 (6N1P)

Table 15

Possible Faults in the DUK-13IM Flaw Detector

#	Fault Indication	Possible Cause	Correction
1	The voltage converter does not operate when the flaw detector is turned on.	a. No voltage to the power supply unit	a. Using a needle indicator, test the voltage on the power supply unit when the output cable is disconnected. If there is no voltage, test the input voltage, the fuse, the input cable, the voltage regulator, diodes and transistors; when there is power supply from the storage batteries, test the quality of the connections, the regulator, and the voltage on the bank. Should the voltage drop sharply on several banks when the flaw detector is turned on it is necessary to replace them.
		b. A cable from the power supply unit to the electronics unit is defective	b. Replace or repair the cable
		c. The voltage converter is defective	c. The converter may not operate due to the appearance of a short circuit in the load circuit, due to transistors or capacitors C54, C55 malfunctioning, or due to a transformer fault. In order to test the circuits, it is necessary to disconnect the load of each secondary winding in sequence and turn on the flaw detector. If the

Table 15 (continued)

#	Fault Indication	Possible Cause	Correction
			converter begins to work, it means that it is necessary to test for a load which has previously come unsoldered: diodes, capacitors, resistors, and the entire circuit. If the converter does not operate with all of the loads unsoldered, it is necessary to test capacitors C54, C55, the transistors, and the transformer.
2	The voltage converter operates, but there is no base line.	a. There is no contact of the coil in the adapter. b. The radio pulse generator does not operate, i.e. there is no triggering pulse	a. Test for good contact or replace adapter and coil b. Using an oscillograph, test the operation of diode D1. There should be exponential shaped pulses on the screen with an amplitude of about 100-200 v. with a repetition frequency of about 2000 Hz. If there are no such pulses, it is necessary to test all of the generator circuits carefully and replace diode D1. After that, set the pulse repetition frequency at 800-1000 Hz by matching resistor R2 and capacitor C1.
		b. The voltage on the voltage converter output is below normal.	c. Test the voltage at capacitor C57, C59, C62, C64; they should be equal to 12, 240-250 (600-700) and 2.45 volts, respectively.

Table 15 (continued)

#	Fault Indication	Possible Cause	Correction
			Fine tuning using resistors R88, R89, R90 and R110 is permitted if there are small voltage discrepancies with the indicated values. When there are large deviations, it is necessary to test the load circuits of the corresponding sources and the voltage converter according to Point 1.c. of this Table.
		d. The stages designed around tubes Tu1 and Tu2 do not operate.	d. Test the voltages and resistances on the tube outputs and the shapes of the signals, eliminate deviations, replace tubes Tu1 and Tu2. Fine tuning is permitted after the tubes have been replaced.
		e. No contact in the CRT panel	e. Set the CRT to the stop.
3	The base line occupies half the screen on the CRT	Tube Tu3 is defective	Cf. Point 2d. of this Table.
4	There is no transmitted pulse in any position of the "STA," "Sensitivity," or "Cut-off" knobs	a. The high-frequency cable is defective	a. Test and repair or replace the cable
		b. The probe is defective	b. Replace the probe
		c. A transistor or the electrolytic capacitors of the RF Amp are out of order.	c. Test the modes of the stages and eliminate defective transistors and capacitors. When a transistor has been replaced, the flaw detector sensitivity is set using resistors R6, R12, R18 and R19 when necessary.

Table 15 (Continued)

#	Fault Indication	Possible Cause	Correction
		d. The video amplifier tubes do not operate	d. Test the modes of the video amplifier stages, eliminate noted faults or replace tubes Tu4 and Tu5
5	There is no depthmeter mark in the "Inspecting from the surface" mode, and no base line in the "Layer-by-layer" mode	Transistors PP6, PP7, PP8, and PP9 are defective	a. Test the loads of the transistor stages and eliminate the discrepancy. Test the transistors and replace the defective ones. Fine-tune the pulse duration for small durations using potentiometer R35 and, for large ones, by matching capacitor C18. If the multivibrator ceases to function at small pulse durations, it is necessary to increase the capacitance of C20. b. Test the power supply voltage and diode D3. Test capacitor C23.
6	The audio indicator does not activate when there is a flaw pulse on the screen	a. The headset cord is defective. b. Transistors PP4 and PP5 are defective.	a. Test the headset cord and eliminate the defect. b. Test the stages according to Point 5a. of this Table.
7	Low probe sensitivity	a. Piezoelectric element depolarization b. Probe poorly assembled	a. Feed a constant voltage of 1-1.5 kv. for 30-50 min. to the piezoelectric element b. Dissemble the probe and reassemble it.

Testing the basic characteristics of the DUK-11IM. The power required by the flaw detector should be less than 110 v. The power is measured using the voltmeter-ammeter method by measuring the voltage of the power supply network and the current used by the instrument. AVO-5M, Ts-51 or other equivalent instruments may be used for the measurements.

The resistance of the insulation between the windings of the instrument's power transformer and between each winding and the transformer housing should be more than 100 Mohm. It is necessary to take the measurements using an M1101 megaohmmeter at a test voltage of 500 v., a temperature of 20 $\pm$ 2° C., and relative humidity of 65 $\pm$ 15%.

At minimum intensity, adjustment of the beam focus on the CRT screen should enable the thickness of the base line to be set no greater than 1.5 mm. The length of the base line on the CRT screen should not depend on the position of the "Inspection depth" knob, and it should be between 50-60 mm. To test this, the length of the base line should be measured with a ruler when the "Inspection depth" knob is set in the extreme left and right positions. The measurements should be made from the lighted point at the beginning of the base line to the end of the line.

When the flaw detector is operating in the "Layer-by-layer" mode, the delay of the scan generator trigger relative to the instant at which the transmitted pulse is emitted should be adjustable within the range of 5 $\pm$ 1 to 190 $\pm$ 10 microsec. using the "Flaw coordinates" knob. This parameter is tested when the flaw detector is operating in the "Layer-by-layer" mode by measuring the delay time using an S1-8 or similar oscillograph. The oscillograph is connected to capacitor C17 and synchronized using the transmitted pulse (the pulse at the thyratron anode may be used for synchronization, having connected the appropriate oscillograph input to capacitor C3),

and the delay time is measured when the "Flaw coordinates" knob is in the extreme left and extreme right positions. In the "Inspection from the surface" mode, the delay of the scan voltage generator trigger is 7-9 microsec. The test is performed in the same way.

The scan duration is measured using a cathode-ray oscillograph. The oscillograph is set in the external synchronization mode, and the measurement is taken at capacitor C17 when the flaw detector is operating in the "Inspection from the surface" mode and the two extreme positions of the "Inspection depth" knob. The flaw detector sensitivity under laboratory conditions must be tested on a Calibration Standard No. 1, and the dead zone on a Standard No. 2. The instrument conforms to technical standards if two reference reflectors, corresponding to the given type of probe, a "near" and a "far," are simultaneously detected with the "STA" and "Sensitivity" knobs set in the optimal position. The location of these reflectors is indicated in Table 16. When each of these reflectors is detected, the pulse on the CRT screen should be not less than 10 mm high, and there should be no noise pulses on the screen.

The sensitivity and the dead zone must be tested not only at normal voltage, but also when the power supply network voltage is reduced by 10%.

The amplitude of the negative half-wave produced by the radio pulse generator should be not less than 40 v. This magnitude is measured using an oscillograph hooked up to the high-frequency connector on the front panel, with the probe connected to the instrument.

The accuracy of the depthmeter operation is tested using Standard Sample No. 1 as described in Section 7 of this chapter. The delay time for switching on the plate voltage fed to the thyratron should not be less than 40 sec. This time must be measured, using a second meter, from the instant

Table 16 Sensitivity of the DUK-11IM and DUK-13IM flaw detectors.

ultrasound frequency, MHz	wedge angle, degrees	depth at which the far reflector is situated in Standard No. 1, mm	depth at which the near reflector is situated in Standard No. 2, mm
DUK-11IM			
2,5	30	50	8
	40	45	8
	50	40	3
DUK-13IM			
1,8	30	50	8
	40	50	8
	50	40	3
2,5	30	45	8
	40	45	8
	50	35	3

the instrument is switched on until the appearance of the transmitted pulse on the CRT screen and at a voltage from the power supply network which is diminished by 10% relative to the rated value. Here the flaw detector should operate in the "Inspection from the surface" mode. The "Sensitivity" potentiometer should be in the extreme right position, and the "STA" in the extreme left position.

The resonance frequency of the RF amplifier in a tuned flaw detector should be within the range 2.5 MHz ± 5%, the amplification coefficient of the RF amp should not be less than 30,000, the band pass width at the 0.7

level should not be less than 500 kHz. These parameters are tested with tubes Tul (the radio pulse generator) and Tu3 (the synchronizer) removed. A 100 microv. voltage with a frequency close to resonance is fed from the G41A generator to the input of the RF amp (the high-frequency connector on the front panel of the instrument). A VK7-3 device, set to measure constant voltages, is connected in parallel with resistance R78. A 0.01 microfarad capacitor should be connected with the rectifier load.

The amplifier's resonance frequency may be determined by measuring the frequency of the input signal, keeping its size constant, from the maximum reading of the VK7-3. Knowing the voltage on the input and the output of the RF amp, it is possible to determine the amplification coefficient using the formula

$$K = \frac{U_{out}}{U_{in}}$$

While varying the signal frequency at the RF amplifier input (with the level kept constant), it is possible to determine the band pass width at the 0.7 level from the readings from the VK7-3. The frequency characteristic of the RF amp for the DUK-11IM flaw detector is presented in Fig. 220.

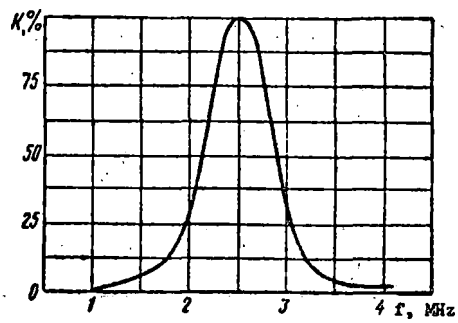

Fig. 220 Frequency characteristic of the RF amplifier for the DUK-11IM flaw detector.

The radio pulse repetition frequency should be in the range 900-1100 Hz. This magnitude is determined by measuring the time τ (in microsec.) between two consecutive pulses. The measurement is made using an S1-8 oscillograph, or one similar to it, connected to the first pin of tube Tu3. The pulse repetition frequency is calculated in Hz by the ratio

$$F_r = \frac{10^6}{\tau}.$$

The flaw detector's auxiliary indicators should activate from pulse echoes 5 mm and greater in height on the flaw detector screen.

Testing the basic characteristics of the DUK-13IM. The power required by the flaw detector is determined by measuring the voltage and current on the input using an AVO-5M or its equivalent. The pertinent values when the instrument is receiving power from an alternating current power supply network or from storage batteries are presented in Table 13.

The base line should be 38-44 mm long on the CRT screen, and it should be completely visible for any scan duration. The length of the base line is measured using graph paper, and with the "Monitoring depth" knob in the extreme right and extreme left positions.

The beam focus adjustment should provide a base line on the CRT screen not more than 1 mm thick, and the line should be situated from 4-6 mm below the central horizontal axis on the screen. The amplitude of the depthmeter mark on the screen should be 2-5 mm. These values are measured directly on the screen using graph paper.

For any scan duration, with the depthmeter mark at any position on the base line, no jitter or distortion of the mark should be observed. In addition, when the depthmeter mark is shifted beyond the right boundary of the base line, its image should not be observed upon the base line's return.

These requirements are tested visually by observing the depthmeter mark when it is positioned at the beginning and the end of the base line, and when the "Monitoring depth" knob is set in the extreme left and right positions.

The scan duration should be adjusted using the "Monitoring depth" knob so that the maximum scan duration is at least 100 microsec., and the minimum is 14 microsec. or less. The scan duration should not change when the oscillator trigger is in the different modes ("from the surface" and "layer-by-layer"). It is possible to measure the characteristics of this oscillator using an oscillograph connected to capacitor C30. In this case, a rectangular pulse will be visible on the oscillograph screen. It is necessary to use a pulse from the radio pulse generator for synchronization. To do this, the appropriate oscillograph input should be connected to capacitor C1.

When the flaw detector is operating in the "Inspection from the surface" mode, the delay in triggering the scan voltage generator is 7-9 microsec., while the "layer-by-layer" mode, the minimum delay should be more than 12 microsec., and the maximum, less than 100 microsec.

The delay time in the "Inspection from the surface" mode is measured by connecting the oscillograph to capacitor C28, while in the "layer-by-layer" mode, it is connected to capacitor C30.

The ultrasonic oscillation pulsing frequency of a correctly tuned flaw detector should be within the range 700-1400 Hz; the frequency is determined by an estimate based on measurements of the pulse repetition period. The peak-to-peak amplitude (separation) of a radio pulse on the piezoelectric plate of any probe used with the instrument should not be less than 145 v. The sum of the positive and negative half-waves of the transmitted pulse are measured using an oscillograph.

The audio signal device for the flaw detector should activate from pulse echoes, whose magnitude is 5 mm and more on the CRT screen. A pulse echo from any reflector may be used to test this characteristic.

The instrument's sensitivity when working with angle probes should provide simultaneous detection of the reference reflectors in Standards No. 1 and 2. The position of the reflectors is presented in Table 16. Here the amplitude of the pulse echoes from any of the reflectors should not be less than 7 mm, and when the probe is lifted, there should be no noise pulses on the base line.

When operating with a normal probe, detection of the third bottom reflection from the cuts in Standard No. 1 at a frequency of 2.5 MHz, and of the fourth at a frequency of 1.8 MHz, should be guaranteed. The amplitude of the bottom reflections on the CRT screen should also be no less than 7 mm.

The amplitication should be smoothly adjustable. In order to test this, it is necessary to be assured of the ability to tune the flaw detector so that detection only of holes 15, 15-25, and 15-30 mm is provided in Standard No. 1. The amplitude of the pulse echoes from the following hole should not be more than 4 mm on the screen.

The accuracy of the depthmeter is tested according to the test specimen No. 1 in accordance with the requirements stated in Section 7 of this chapter.

The duration of the pulse echo signals on the CRT screen with the pulse echoes at maximum amplitude at the level of the base line should not be more than 4 microsec. These measurements are taken using a depthmeter. The power supply unit should provide an output to the flaw detector input of 12 $\pm$ 0.5 v. direct voltage from the storage batteries and from the power supply network, when the power supply voltage of a 50 Hz alternating current source varies within a range of 176 - 250 v. or from 34.5 to 37.5 v.

Chapter X -- The UZD-NIIM-6M Ultrasonic Rail Flaw Detector Cart

1. Intended use and working principles.

The UZD-NIIM-6M (Fig. 221), the first model of a multi-purpose rail flaw detector, permits inspection of the parent metal, and of the bolted joints in both rails simultaneously. Welded joints may also be inspected. A number of new principles are employed in the flaw detector for the first time, including the following: the mirror-shadow method using the second bottom signal; an "ultrasonic gauge" for monitoring rail bolted joints; a meter for direct read-out of flaw coordinates; and a flaw simulator for tuning the flaw detector sensitivity without the use of calibration standards.

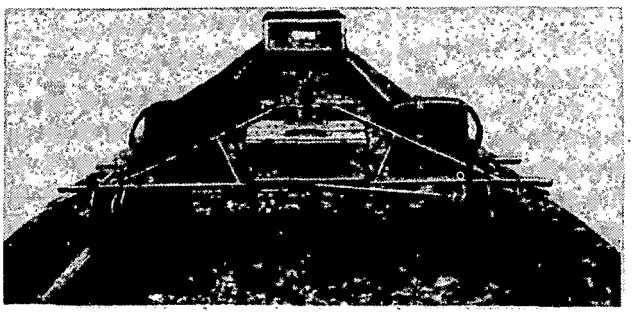

Fig. 221 Over-all view of the UZD-NIIM-6M flaw detector

The following flaw types are detected in the rail joint by the flaw detector:

a) Cracks in the upper fillet (flaw type 52.1) and horizontal cracks in the web (flaw type 55.1) not less than 7.5 mm deep and 10 mm long, provided the projection of these cracks to the running surface does not coincide with the projections of the bolt holes

b) Inclined cracks developing from bolt holes (flaw type 53.1) provided the length of the projection extends beyond the edge of the bolt hole by at least 10 mm

c) Vertical longitudinal cracks in the head more than 5 mm deep which are situated over the web (flaw type 30V.1), provided the projection extends beyond the bolt hole projection more than 10 mm

d) Horizontal longitudinal cracks in the head situated over the web and extending at least 7.5 mm (flaw type 30G.1), provided the projection extends beyond the projection of the bolt holes more than 10 mm

e) Transverse cracks in the shape of light and dark spots situated in the rail head over the web and to the gage side (flaw types 20.1, 21.1) which are more than 12 mm in diameter.

A flaw situated above the bolt holes may be detected when inspected by hand, using a probe with an incidence angle of 38°. Those flaws detected in the parent metal of the rails include the following:

a) Longitudinal vertical separations of the metal more than 5 mm deep and 10 mm or more long in the head over the web (flaw type 30V.2)

b) Horizontal separations in the rail head more than 10 mm in length which extend into the web at least 7.5 mm (flaw type 30G.2)

c) Horizontal separations or cracks in the web more than 10 mm in length which extend at least 7.5 mm into the web (flaw type 52.2 or 55.2)

d) Cracks in the rail base from hair-line cracks which are 3 mm or more deep and more than 10 mm in length, and which are situated beneath the rail web (flaw type 60.2)

e) Inclined and vertical cracks situated at any height in the rail within the bounds of a rectangle limited by the thickness of the web (flaw types 50.2 or 55.2)

f) Transverse (inclined) vertical cracks in the form of dark or light spots situated in the rail head over the web and to the gage side (flaw types 20.2 or 21.2) which are not less than 12 mm in diameter.

Flaws with an area of 25 mm^2 and more may be detected in rail joints (flaw types 26.3, 56.3, and 66.3).

The flaw detector is designed for operation in the field with the relative humidity of the air up to 95%, and at temperatures of from -30 to +50°C for the normal probe channel; and -20 to +50°C for the hand-held angle probes.

The ultrasonic oscillation frequency is 2.5 MHz, and the pulsing frequency is 750-1100 Hz.

An audible sound appears in the headset to indicate the detection of a flaw. Any storage battery with a voltage of 13 - 16v. may serve as the power supply for the flaw detector. The flaw detector is supplied with KNGK-10 and KN-10 batteries with a capacity of 10 amp. hr. The current drawn from the storage batteries by the flaw detector is not more than 0.4 amp.

The weight of the instrument, including the probes, cable, and headset (without the carriage and storage batteries) is 13 kg.

The total weight of the flaw detector, including 20 liters of water, is not more than 80 kg.

The flaw detector is set on the carriage, and, while working, it is moved along the track being inspected. Two compound probes, each of which consists of two normal and one angle element which emit ultrasonic pulses into the rail, slide along the rails. Water is fed beneath the probe to provide the accoustical contact between the probe and the rail; the rail in front of the probe is first moistened by cleaning devices situated on the carriage. (At below zero temperatures, a solution of technical-grade alcohol is used instead of water) The rail is inspected over its entire length in a zone including the web and the head to the gage side, and including the rail head in a weld zone. The inspection of welded joints and the secondary inspection of individual sectors throughout the entire

cross-section are done by hand. When inspecting by hand, the flaw detector permits the coordinates of detected flaws to be determined with an accuracy of not less than $\pm(5\%H+4)$ mm.

Inspection of the web and its extensions into the head and the base is accomplished using the mirror-shadow method and the normal element in the compound probe. As was shown in Chapter V, inspection using the second bottom signal permits the flaw detector's sensitivity to internal flaws to be increased in a number of cases. It also reduces the effect of the quality of the acoustical contact upon the results. Therefore, the possibility of operating with both the first bottom pulse as well as the second was anticipated in the UZD-NIIM-6M flaw detector.

The search for flaws in the shape of cracks developing from the bolt holes is also conducted while the instrument is moving. When approaching a joint, an auxiliary element set in the same compound probe, and forming, together with the primary element, the "ultrasonic gauge", is connected to the primary element by pushing a button. This is done to provide more reliable detection of cracks.

The rail head is monitored along its entire length using the pulse-echo method, employing the angle element which is also mounted in the compound probe.* The wedge angle and the angle it is rotated relative to the axis of the rail is the same as in the URD-63 flaw detector.

When monitoring the welded joint of a rail, a compound probe with incident angles of 38° and 50° is used. The indication that a flaw has

*Presently, an experimental UZD-NIIM-6M flaw detector with two angle elements emitting oscillations in opposite directions is in use on the October ("Oktyabr'skaya") Line. This permits the reliability with which flaws from the second group are detected to be increased.

been detected comes from the sound which arises in the headset and from the readings of the meter by means of which the flaw's coordinates are also determined. In the same manner, secondary monitoring of the head, base, and web of the rail may be conducted.

Headsets are used as the indicator for detected flaws during continuous monitoring. A signal arises in the headset when the bottom pulses diminish a given number of times. For the first time, a flaw simulator is employed in a flaw detector for tuning the monitoring sensitivity when using the mirror-shadow method. Activation of the audio indicator when even one bottom pulse diminishes the given number of times, and an increased pulsing frequency for transmitted pulses (on the order of 1000 Hz) is one of the features of the UZD-NIIM-6M flaw detector. This increases the reliability with which vertical transverse cracks are detected at higher speeds.

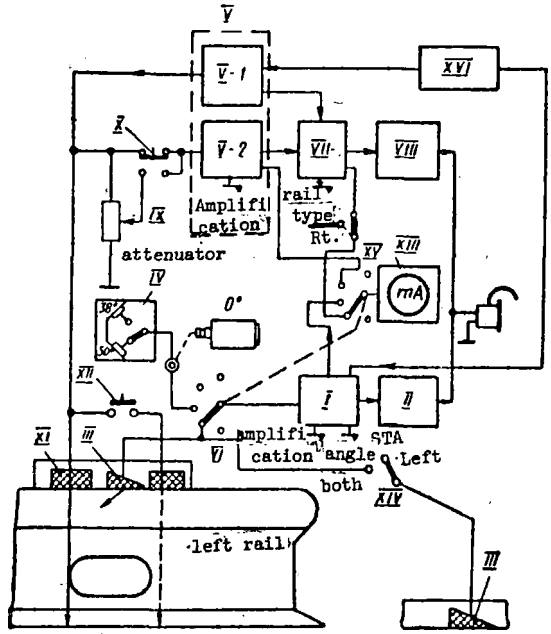

Fig. 222 Functional circuit of the UZD-NIIM-6M flaw detector (on one rail)

The numbers of the units in the functional circuit are designated by Roman numerals.

It may be seen from what has been stated that the UZD-NIIM-6M flaw detector permits simultaneous detection of all of the flaws in a rail which

may be detected by the URD-52, URD-58, URD-63, and UZD-NIIM-5 flaw detectors.

The operating principle of the flaw detector is explained by the functional circuit shown in Fig. 222 (the normal probe monitoring channel for only one rail is shown in the circuit.)

The flaw detector consists of the following components:

a) A receiver-transmitter channel I operating with time and amplitude selection of the pulse echoes received by the angle probes monitoring the heads of the right and left rails

b) A driven audio frequency voltage generator II which activates from the pulse echoes reflected from flaws in the rail detected by the angle probe

c) Angle probes III intended for detection of flaws in the rail head during constant monitoring

d) A compound angle probe IV which is connected to the receiver-transmitter channel I during hand inspection

e) A receiver-transmitter channel V for normal probes, consisting of an ultrasonic oscillation generator V-1 and an amplifier V-2

f) A normal probe XI, which is intended for the continuous monitoring of the rail web and its extension into the head and base

g) Circuits VII, consisting of a gate pulse generator and an anti-coincidence stage connected to the output of the receiver-transmitter channel, for isolating the bottom pulse; the circuit is designed so that when even one bottom pulse echo from the rail base diminishes a definite, predetermined number of times, a pulse will arise at its output

h) A driven audio frequency voltage generator VIII, which activates with the appearance of even one bottom pulse on the output of circuit VII.

For an indication that generators II and VIII have activated when using only one headset, they are tuned to different frequencies of the audible spectrum

which are easily distinguished by ear; the time for which they operate after being triggered by a solitary pulse is worked out to be adequate for reliable aural discrimination

i) An inspection attenuator IX

j) An inspection switch X for turning on the attenuator

k) An auxiliary normal probe VI used when inspecting rails in the bolted joint zone

l) A button XII for connecting probe VI

m) A needle display XIII

n) A toggle switch XIV for disconnecting the angle probe inspecting the head of the right rail

o) A switch XV for changing the operating mode of the flaw detector and the meter

p) A voltage converter XVI

The inspection attenuator IX and switch X are designed for tuning the sensitivity of the normal probe channel and for testing it while in operation.

When flaws are detected in the right or left rail by the normal probe channels, a high-tone signal appears in the right or left ear piece of the headset, respectively.

If a flaw is detected in the right or left rail by the angle probes, a low tone appears only in the left earpiece. To clarify in which rail the flaw was detected by the angle probes, secondary inspection is performed with the right probe switched off using switch XIV (switch XIV is in the "Left" position).

The meter XIII is used for the following purposes, depending on the operating mode of the flaw detector, as determined by the position of switch XV:

a) to measure the feed voltage, b) to set the single or doubled height of the left and right rails (inspection using the first or second bottom signal when the mirror-shadow method is employed), c) to determine the coordinates of the flaws detected by the angle probe during hand inspection using the pulse-echo method, d) to evaluate the amplitude of the bottom signal from the left and right rails when inspecting using the mirror-shadow method.

The voltage converter XVI is used for converting a constant voltage into the pulsed voltage necessary for synchronization and for the power supply for the ultrasonic oscillation generators.

A complete block diagram of a two-rail device showing the contruction principles for the separate functional units is shown in Fig. 223.

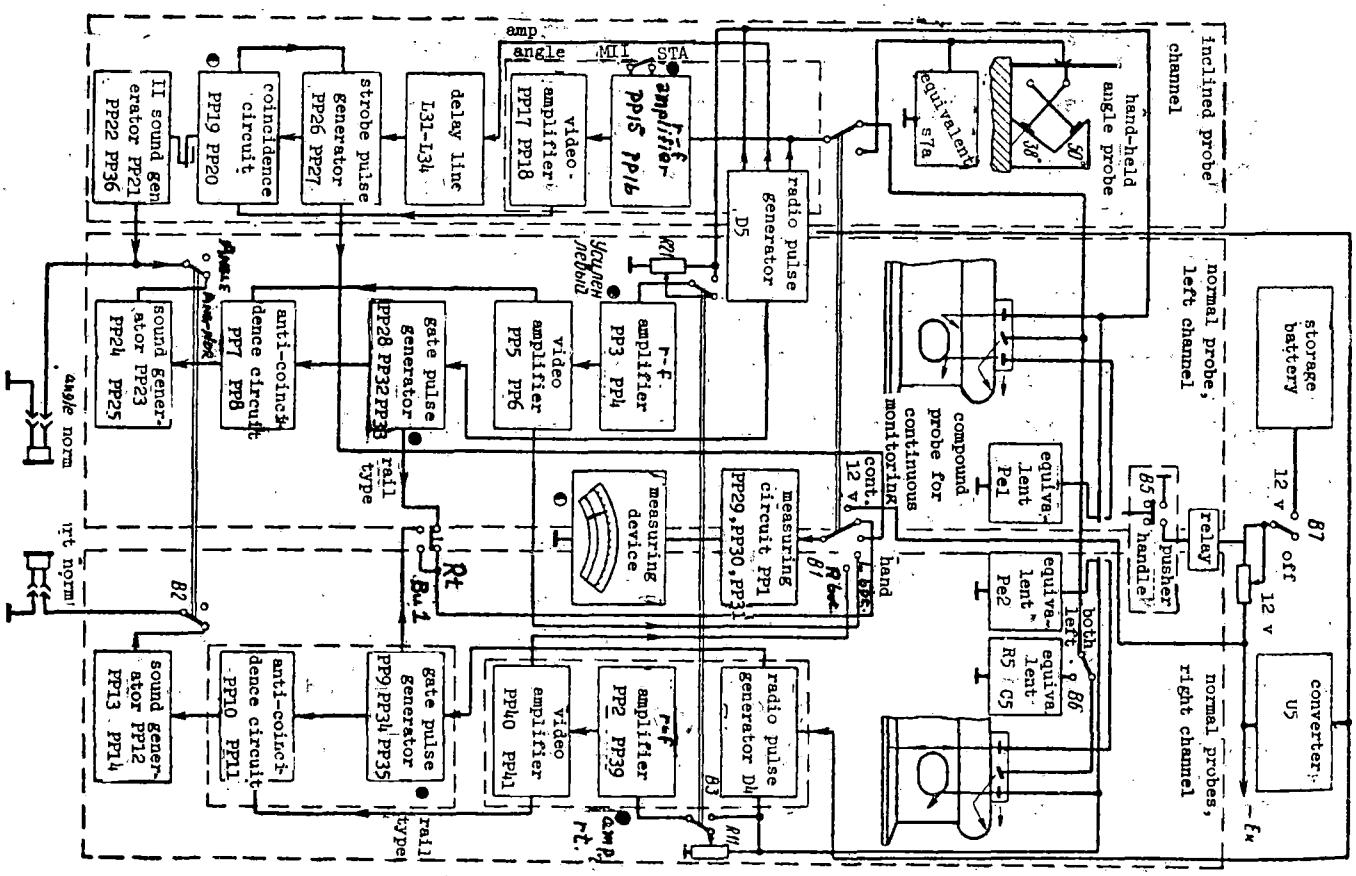

Fig. 223 Block diagram of the UZD-NIIM-6M flaw detector

As may be seeen from the schematic, the receiver-transmitter train of the angle probe channel consists of a radio pulse generator (common for the angle probe channel and the left channel for the normal probes), a high-frequency amplifier, a video amplifier, a delay line, a gate pulse generator, and a coincidence circuit.

The gate pulse generator is triggered by a pulse from the radio pulse generator which passes through the delay line. The purpose of this is to delay the instant at which the gate pulse generator is triggered so as to prevent the transmitted pulse from falling on the displays. The maximum duration of the gate pulse is 170 microsec.

The angle probe channel is used both during continuous as well as during hand-held inspection. During hand-held inspection, the size of the triggering delay is 12 microsec, and during continuous inspection, it is 20 microsec. In the hand inspection mode, the gate pulse generator is used for measuring the coordinates of the detected flaws. As has already been indicated, in the UZD-NIIM-6M flaw detectors, as distinct from the UZD-NIIM-5 devices, measurement of the coordinates of detected flaws is made by direct read-out from a meter.

The principle for measuring the coordinates in the UZD-NIIM-6M is to measure the size of the linearly varying voltage at the instant the pulse echo arrives. In order to measure the coordinates from the output of the coincidence circuit, the pulse corresponding to the one reflected from the flaw is fed to the gate pulse generator and stops it. The duration of the pulse from this generator is measured using a special circuit containing a saw-tooth voltage generator; the meter-type measuring device is connected to the output of this circuit.

The normal probe channels (left and right) are identical and each consists of a radio pulse generator, an RF amplifier, a video amplifier, a

gate pulse generator, an anti-coincidence circuit and an audio generator..

The gate pulse generator produces a short pulse whose position in time may be varied using the "Rail type" knob.

The radio pulse generators operate in series and are synchronized by pulses from the converter.

2. The electrical schematic of the flaw detector cart

The electrical schematic of the flaw detector cart is presented in Fig. 224. The radio pulse oscillators are assembled around switching silicon diode thyristors (diodes) D4 and D5 (D2281 type).* Up to a set value for the voltage applied to the diodes (the switching voltage), the current in the diodes is very small (on the order of several microamperes), and, after the switching voltage has been exceeded, the diodes' resistance drops sharply and the current abruptly increases.

The operation of the two oscillators is identical. Considering the oscillator around diode D5, when the instrument is switched on, capacitor C10 discharges through a circuit consisting of capacitor C10, diode D5 and inductances L3 and L4. At the same time, impulsive oscillations, which continue after the discharge of capacitor C10, when the initial (closed) state of diode D5 is being restored, arise in the circuits of inductances L3 and L4 and the capacitances of the probes' piezoelectric plates. The process is repeated at equal time intervals, the duration of which depends on the repetition frequency of the converter and on the time constant of the RC circuit R19 C10. The peak-to-peak value of the impulsive oscillations from the piezoelectric converters is from 30 to 60 v.

---

*While this book was in preparation for publication certain changes were introduced into the instrument's circuits. In the UZD-NIIM-6M flaw detectors which are currently being produced, the radio pulse oscillators are built separately around D235G thyristors.

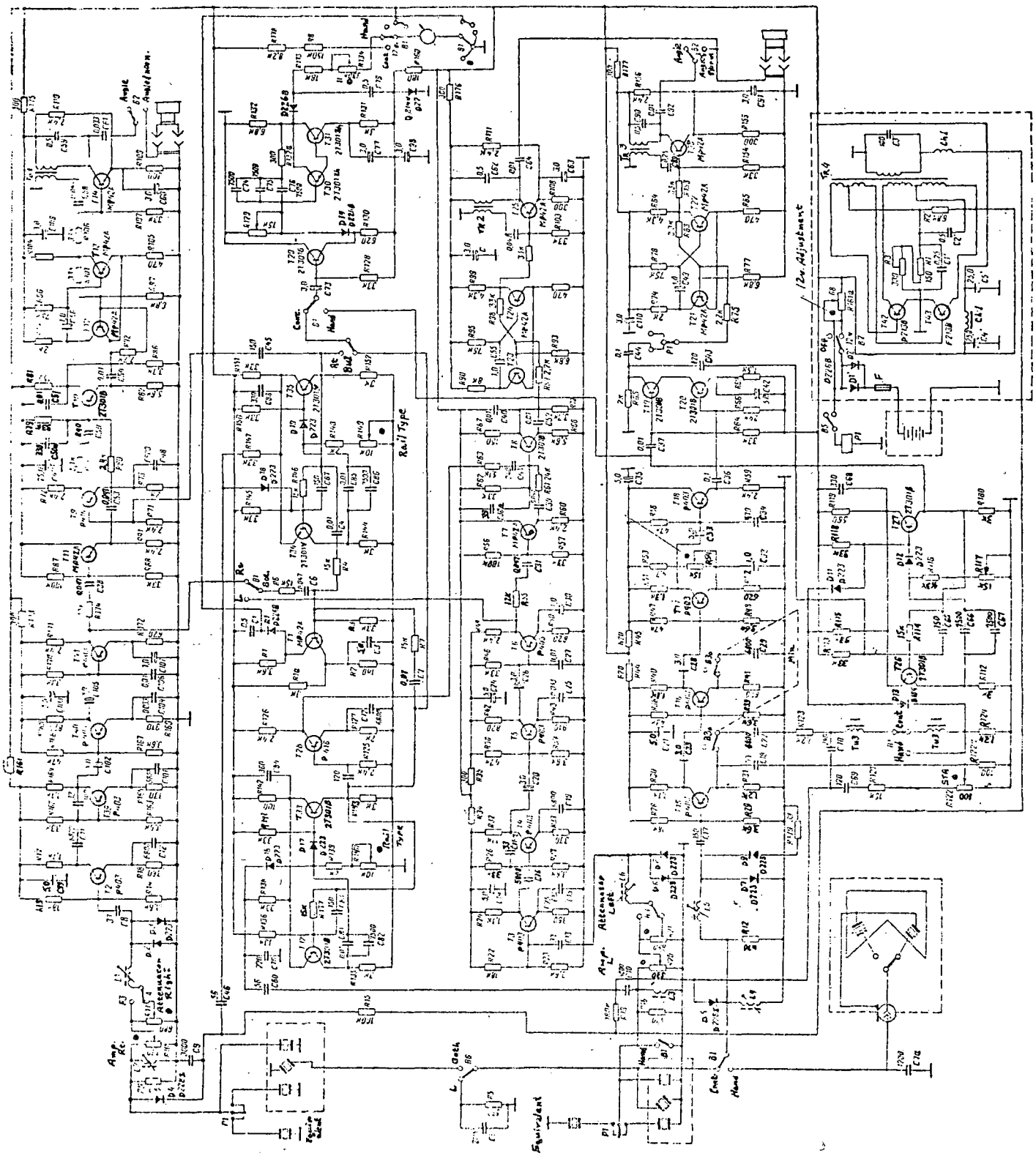

Fig. 224 Electrical schematic of the DUK-NIIM-6M flaw detector.

The angle probes intended for inspecting the two rails are connected to inductance L4, and the normal probes, for inspecting the left rail, are connected to inductance L3. The normal probes for inspecting the right rail are included in an oscillator consisting of diode D4, capacitor C9, resistor R15 and coil L2.

The RF amplifier and video amplifier stages are assembled around transistors T3-T6 (the left channel for the normal probes), T15-T18 (the channel for the angle probes) and T2, T39-T41 (the right channel for the normal probes). All transistors are P403's. The amplifiers are assembled according to a wide-band circuit. This simplifies preparation and tuning of the amplifiers and reduces the variation of their parameters when transistors are replaced.

In order to avoid a break-down of the first transistor as a result of the oscillator's transmitted pulses, signals at the amplifier input are fed through a circuit consisting of an inductance, a capacitance, and diodes (for the angle probe channel, these are C17, D7, D9). The role of this circuit is to limit the amplitude of high-amplitude entering signals. In this case low-amplitude signals pass through almost undiminished.

In the amplifier for the angle probe channel, a sensitivity time adjustment (STA) is used in the circuit of the first stage emitter; the adjustment is accomplished using resistor R122. An exponential voltage taken from capacitor C10 and differentiated by the RC circuit C69 R121 R122 is fed to the first stage emitter resistance through capacitance C18, providing bias of the transistor's working point and a change in the stage's amplification coefficient.

The amplifier sensitivity and noise cut-off are adjusted with resistance R54 by feeding a cut-off voltage to the third stage emitter. By-passes along the power supply circuit are used to exclude amplifier self-excitation.

For sudden changes in the sensitivity of the angle probe channel, there is a switch in the amplifier, through which capacitances may be connected into the feedback circuit. The emitter repeater is the output stage of this channel.

Stabilization of the transistors' working point in the given temperature interval is provided by bias circuits as well as feed-back resistances in the emitter circuits. The resistances in the emitter circuits are shunted with capacitors so that they do not decrease the amplification of the stages.

The amplifiers in the normal probe channel are analogeous with the amplifier in the angle probe channel, but they contain four stages and have no amplification time adjustment. Amplification adjustment for the stages is provided using potentiometers R10 and R20.

Attenuators in the forms of regulators R11 and R21 provide for tuning the flaw detector to a specific sensitivity for the normal probes channel.

There are three gate pulse generators in the flaw detector. The gate pulse generator for the normal probe's left channel is assembled around transistors T32 and T33. Transistors T32 and T33 (2T301 type) form a driven multivibrator, the pulse duration of which may be adjusted using the variable resistor R140 (Rail type). Temperature stabilization for the multivibrator is provided through the use of silicon triodes, diode D17, and resistor R142.

The moveable trailing edge of the multivibrator's rectangular pulse is differentiated by the RC circuit R125 C17 (120PF), is amplified by the stage around T28, and is fed as a gate pulse (of positive polarity) to the anti-coincidence circuit for separation of the appropriate bottom pulse. The principle of measuring the gate pulse delay relative to the instant the transmitted pulse is emitted is the same as for measuring the coordinates of flaws detected by the angle probe channel.

The emitter repeater around transistor T29 (2T301 type), which is common for all channels, is used for matching the high impedance output of the multivibrator with the low input impedance of the saw-tooth voltage stage.

The gate pulse generators for the right channel and the angle probe channel are assembled around transistors T34, T35 and T26, T27 respectively, and are analogeous to the one which was described. The differentiating RC circuit C45 R71 and the stage around transistor T9 are the right channel gate pulse shaper.

The coincidence stage for the angle probe channel consists of two transistors T19 and T20 (2T301 type) connected in series and sharing a common load. Both transistors are closed since they have a bias voltage E_b equal to zero at the base. When positive pulses are fed to the input of one of the transistors, it opens, but the other remains closed, and there is no signal on the load. When positive pulses are fed simultaneously to the bases of both transistors, they open, and a signal appears on the load and is then fed to the headsets at the frequency of the pulsing rate for the transmitted pulses. The pulse from the gate pulse oscillator is fed to the base of transistor T19, and the pulse from the repeater output to T20. The temperature stabilization for the coincidence stage is provided by resistance R69 in the emitter circuit of transistor T20.

The anti-coincidence stages for both normal probe channels are identical, and they are assembled from transistors T7, T8, T10 and T11. Transistors T8 and T10 are normally closed since the voltage of the emitter base E_{be} is equal to zero.

The stages assembled around transistors (semiconductor triodes) T7 and T11 are emitter repeaters. A negative pulse corresponding to the bottom reflection is fed from the emitter resistance R60 (R91)* to the base of triode

* The designations for elements in the second channel are indicated in parenthesis.

T8 (T10); since this is a cut-off pulse, there is no signal on the load resistance R68 (R82).

A positive gate pulse opens triode T8 (T10) and a negative pulse triggering the sound generator multivibrator forms in its collector circuit. If the signal from the emitter repeater coincides in time with the gate pulse, their amplitudes are combined at the input resistance of the amplifier stage. In this case, should the amplitudes of these pulses be equal, there would be no signal at the amplifier output. If the amplitude of the gate pulse is greater than the amplitude of the pulse from the emitter repeater, the amplifier produces a signal which triggers the sound generator.

The saw-tooth voltage generator, which is assembled according to a circuit with capacitance feedback around a compound triode consisting of transistors T30 and T31 (2T301 type), is the basic unit of the measuring circuit. In the initial stage, capacitors C74-C76 are charged to the magnitude of the voltage on the collector. A rectangular pulse from the gate pulse generators is fed to diode D14. Here the triode opens and capacitors C74-C76 discharge through the triode and resistor R129. The discharge current is held constant due to the capacitance feedback between the collector and the base. The discharge time for these capacitors is equal to the duration of the input pulse. During the discharge process, capacitor C79 charges up to a voltage which is proportional to the amplitude of the saw-tooth voltage through diode D15, and discharges through a circuit consisting of R133, R134 and the resistance of the meter winding. The average discharge current is proportional to the voltage to which C79 is charged.

The sound generator for the right channel of the normal probes consists of the driven multivibrator around transistors T12 and T13 and an LC free oscillation generator designed around transistor T14.

The driven multivibrator is triggered by the negative pulse which passes from the anti-coincidence stage and produces rectangular pulses with a duration on the order of 30 microsec.

A negative pulse is fed to the LC oscillator. In the normal state, the LC oscillator is closed by the voltage which is fed from the divider R110, R109 to the transistor's emitter. A negative pulse from the multivibrator opens the transformer, and the LC oscillator begins to oscillate at a frequency of 1-5kHz, which is determined by the circuit consisting of the inductance of the coil in the MIT-4 transformer TR1 and capacitance C59.

A voltage of this frequency is fed to the headsets. The two other sound generators are analogeous, and are assembled around transistors T23, T24, T25 (the left channel for the normal probes), and T21, T22, T36 (the angle probe channel).

The LC oscillator frequency for the angle probe channel is 100-350 Hz.

The voltage converter is designed in the form of a push-pull blocking oscillator assembled around transistors T42 and T43. A high voltage in the form of bi-polar pulses, which are fed to the radio pulse generators, providing synchronization of their operation through the cycle, is received at the converter output.

A filter, consisting of a choke coil Ch1 and capacitor C3', is intended for reducing the stray currents which appear as a result of the high voltage, and a filter consisting of choke coil Ch2 and capacitor C4' and C5' decreases the stray currents which appear as a result of the power supply voltage.

Diodes D1' and D2' serve to protect the transistors from break-down should the polarity of the power supply voltage be incorrect.

3. Construction of the UZD-NIIM-6M

The flaw detector is mounted on a carriage (Fig. 225).

There is a handle for moving the carriage, upon which the button for

connecting auxiliary probes when inspecting bolted joints is situated.

The electronics unit is fastened to the carriage so that it is easy to place it in the position which is most convenient for operation. After the desired position has been selected for the electronics unit, a nut and some screws must be tightened. A voltage converter and the storage battery unit are contained in the power supply unit. The power supply unit is fastened to the carriage using adapter locks. All external electrical connections are made using cable with the appropriate connectors.

A water tank is situated in the center of the frame. It is connected to a tap and to control devices which permit the regulation of the liquid flow rate under the probe systems and into the preliminary rail moistening device.

To the right and the left of the carriage are centering mechanisms with the probe systems. They are affixed onto the carriage using nuts.

The electronics unit consists of three mounting plates: the front panel, upon which the controls and the meter are brought out; the rear panel, to which a high-frequency connector is affixed for hooking up the hand-held probe; and a plug-type connector which connects the instrument with the voltage converter, the compound probes, and the handle.

The upper and lower mounting plates are hinged, and can open for convenience when tuning or repairing the instrument; the front panel is fastened with four screws and may be removed.

The instrument is kept in a case. There is a rubber strip around the front panel to reduce the clearance. The meter is also installed with a rubber seal. A lid with a viewing window made of plexiglass, which fits over the front panel, was installed to protect the instrument from dust. In the upper part of the case there is a hole which is covered by a special screw-type plug. The opening is provided so that potentiometer R129 may be

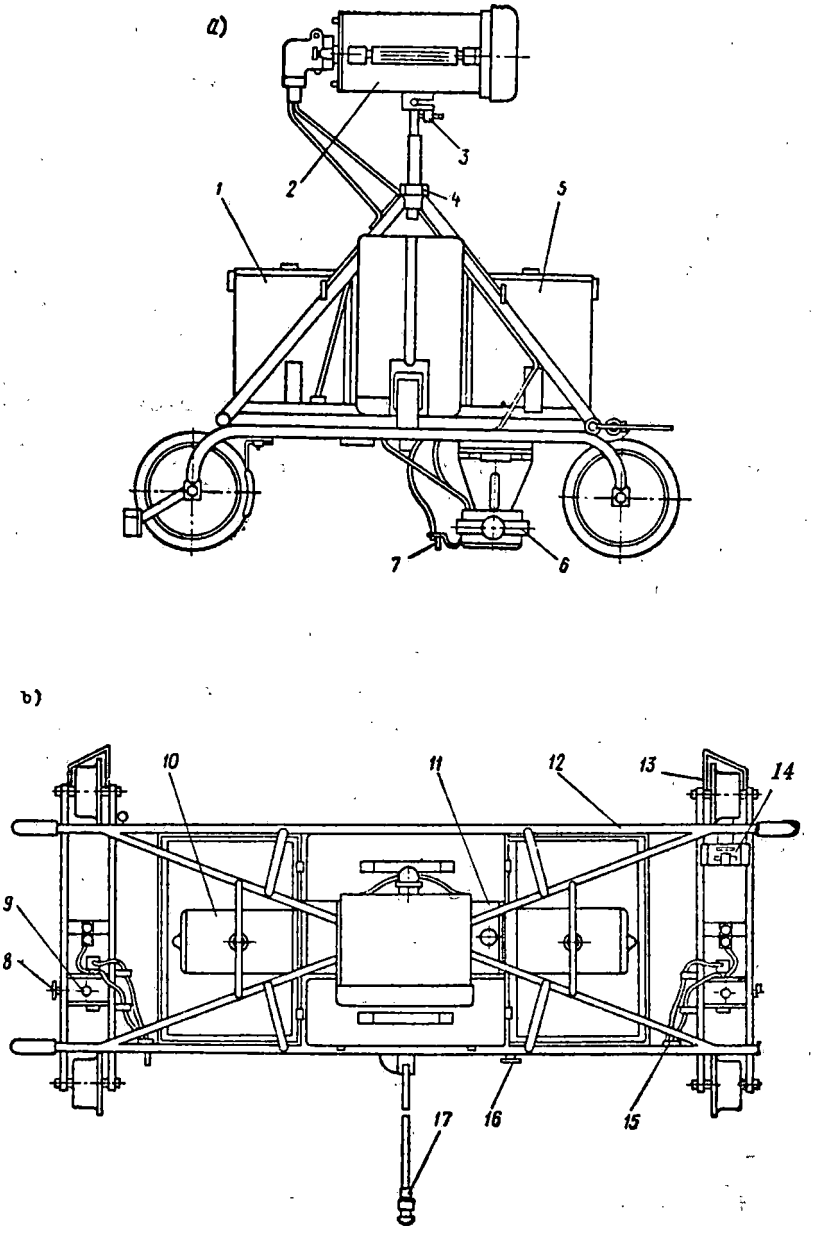

Fig. 225 Constuction of the UZD-NIIM-6M flaw detector; a. side view, b. top view

1. power supply unit with storage battery; 2. electronics unit; 3. screws for securing the electronics unit; 4. lock nut for securing the electronics unit; 5. box for the device; 6. centering mechanism with probes; 7. preliminary rail moistening apparatus; 8. screw for centering the probes; 9. nut for tightening the centering mechanisms; 10. canister for the contacting fluid; 11. water tank; 12. carriage; 13. cleaning device; 14. break; 15. control device; 16. liquid feed tap; 17. handle for moving carriage

adjusted with a screwdriver when fine-tuning the depthmeter.

All of the primary controls for the instrument are situated on the front panel (Fig. 226) and on the handle for moving the carriage.

The flaw detector's mode of operation switch 8 and the meter have five positions. When switch 8 is set in the "12 v." position, the meter shows the magnitude of the power supply voltage fed into the instrument on the lower scale. In the second switch position "Cont" (continuous inspection of the parent metal and of rail bolted joint zones), the meter indicates on scale H_o the height or the doubled height of the rail being monitored on the left line, depending on whether the first or the second bottom signal is used for inspection. When button 16 ("Rt") is pressed, the meter shows the same magnitude for the right rail. The third switch position is "Hand" (inspection by hand); when switch 8 is set in this position, the meter shows the depth of the section being monitored (for the selected probe) on scales H50 and H38, whereas its length is shown on scales L50 and H38. Coordinates of detected flaws are determined on these same scales.

If the switch is set in the fourth or fifth position ("Left bottom" "Right bottom"), the meter will show the intensity of the bottom signal which is being received.

A button for connecting auxiliary direct elements and for disconnecting the angle elements when inspecting bolted joints is located on the carriage handle.

The voltage converter is designed as a separate unit which is fastened in the box by four screws. The converter's transistors, resistors and capacitors are deployed on a mounting plate. The transformers and choke coils are designed with a formless winding. A Sh-12 F1000 ferrite core is used as the magnetic circuit. There is a plug-type connector for hooking up the converter to the instrument. A potentiometer is brought out into a

groove, and serves for varying the pulse repetition rate. There is a button on the carriage handle, with which the auxiliary normal elements of the compound probes are connected and the angle elements are disconnected when passing over the bolted joint zones

The hand-held probe (Fig. 227) consists of a wedge, piezoelectric elements, a microswitch, and a connector. The plexiglass wedge with the piezoelectric elements glued to it is kept in a steel jacket which is filled with a damping compound. A radio pulse is fed to only one of the piezoelectric elements in order to avoid acoustically induced currents. Switching is automatically accomplished using a microswitch and stem when the probe is set on the surface being inspected. The probe is connected to the cable via a connector. The wedge angles and the exit points are indicated on the probe jacket.

The compound probe (Fig. 228) consists of a base, the elements, a top, and the connector. Two normal elements and one wedge-type are set in the probe base. The distance between the piezoelectric plates of the normal elements may be varied, making it possible to inspect bolt holes of varying diameters. The contacting liquid is fed through an opening in the front part of the base. The probes are closed at the top by a rubber strip. The probes are connected to the instrument via a connector. The words "Left" or "Right" and a line marking the exit point of the normal element (which is always connected) are found on the top of the probe.

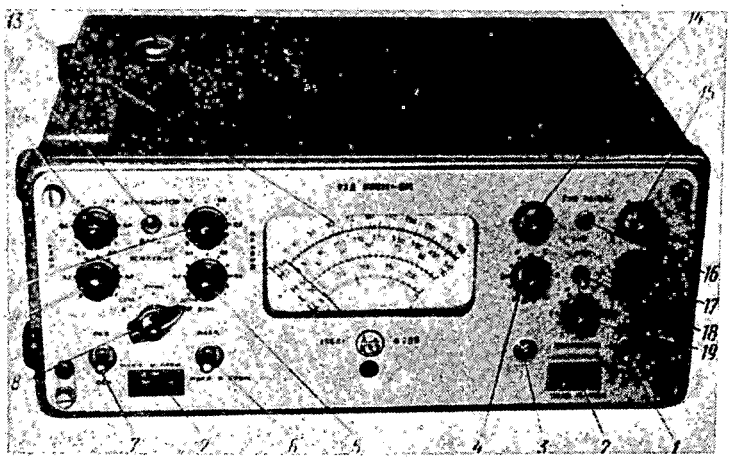

Fig. 226 Front panel of the UZD-NIIM-6M flaw detector

1. off-on switch; 2. jack for connecting headsets; 3. depthmeter adjustment potentiometer; 4. sensitivity time delay knob (STA); 5,9. knobs for adjusting the sensitivity of the normal probe channels; 6. switch for turning off the audio indicators of the normal probe channels; 7. cut-off switch for the inclined elements of the right compound probe; 8. operating mode switch for the flaw detector and the needle display; 10,11. knobs for the attenuators to set the necessary sensitivity for the mirror-shadow method; 12. attenuator cut-on switch; 13. meter; 14,15. knobs for tuning the instrument for monitoring rails of a given type; 16. button to connect the needle display when the flaw detector is tuned to monitor the right rail; 17. adjustment for setting the magnitude of the power supply voltage; 18. switch for sudden decrease in the sensitivity in the angle probe channel; 19. knob for adjusting the sensitivity of the angle probe channel

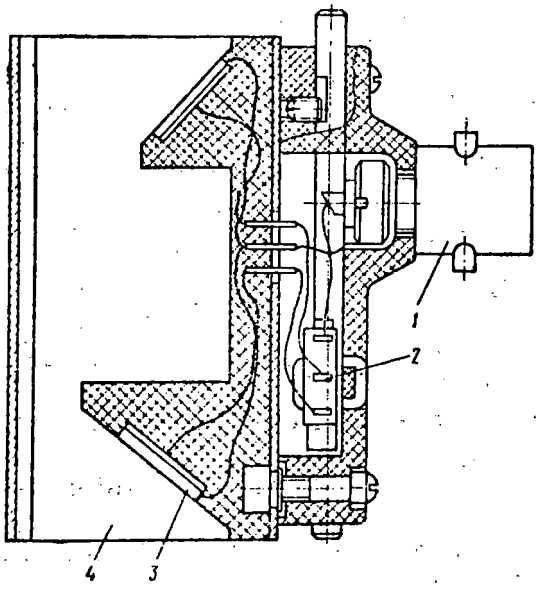

Fig. 227 The probe for monitoring rails by hand
1. connector; 2. microswitch; 3. piezoelectric elements; 4. wedge.

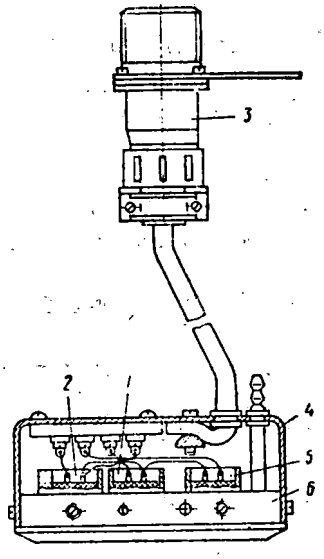

Fig. 228 Compound probe for continuous rail monitoring
1. angle element; 2, 5. normal elements; 3. connector; 4. top; 6. base.

4. Preparation for operation and working with the flaw detector.

External examination of the electronics unit, centering systems, the carriage wheels, the probes, the connecting cables, and the storage battery is made before beginning work with the flaw detector, and noted defects are corrected; the centering system bearings are cleaned and lubricated with machine oil; the probes are set in the centering systems, the probe with the notation "Right" being set on the right hand side when looking at the flaw detector from the side with the handle. The tank, the compound probes, and the cleaning devices are connected with hoses and, having closed all of the taps, the necessary quantitity of the moistening liquid (either water or a solution of alcohol and water) is poured into the tank. The cables and the headset are connected to the instrument. The cable marked "Right" must be connected to the right probe, and the proper polarity must be maintained when connecting the storage battery.

The flaw detector is then set on the rails of a reference siding beyond the zone in which the artificial flaws are situated, and, having set switch 8 (cf. Fig. 226) in the "12 v." position, the flaw detector is turned on with the "12 v." switch, and a voltage of 12 v. is set according to the meter. After the instrument has been turned on, a test for the accuracy of the power supply voltage converter operation is begun. To do this, it is necessary to set switch 8 in the "Cont" position, set the needle of the meter in the sector corresponding to the first bottom signal using knob 14, and be sure that the meter needle does not change its position when the voltage is varied within a range 11.5-12.5 v. Should the readings of the meter change suddenly at one of the positions of knob 17, a fine tuning adjustment is required using the variable resistance on the converter, and the test must be repeated.

Having assured oneself of the converter's consistent operation, the flaw detector's working capability may be tested. To do this, an acoustical contact is established between the probes and the rail with the taps open, and while moving the carriage. Knob 9 is set in the "0.4" position, knob 14 in the position in which the needle of the measuring meter is located within the bounds of the sector corresponding to the selected bottom signal (the first or the second) on the H_o scale, and at which there is no sound in the headsets; then, switch 8 is moved to the "L. bot." position.

After this, the left centering system is set on the axis of the rail by turning the adjusting screw on it. Then, turning the screw little by little, maximum deflection of the meter needle is obtained. The right probe is centered in a similar manner.

The following steps are required in order to test the flaw detector's working capability when inspecting the parent rail metal using normal probes:

a) Set the "Attenuator" and "Amplification" knobs of the normal probe channels in the extreme right positions; set the "Angle-Angle and norm." switch in the "Angle and norm. position

b) Turning the "Rail type" regulator 14, set the meter needle within the bounds of the sector corresponding to the first bottom signal of the left rail; when tuning the right normal channel, it is necessary to press the "Rt" button, set the needle within the bounds of the given sector on scale H_o using knob 15 then release the button. Both channels are then more accurately tuned according to the audio indicator, the amplification of the normal probes being gradually decreased as the minimum angle to which the "Rail type" knob may be turned, within the range of which the audio signal disappears in the headsets, is achieved

c) Switch on the attenuators, having set switch 12 in the "Attenuator" position; set the "Attenuator" knob at the 0.25 position; rotating the "

"Amplification" knobs one after the other, set them in the extreme right position in which the audio signal is still heard in the headset; turn off the attenuators

d) While rolling the carriage along the rails, be sure that the sound signal appears when the probes pass over bolt holes or artificial flaws situated in the web and in the web extension zone into the base.

To test the flaw detector's working capability when inspecting bolted joints, it is necessary to do the following:

a) Set the carriage in the position in which detection of bolt holes without artificial flaws is assured. In this position, the audio signal will be heard in both sides of the headset

b) Without moving the carriage, press the button on the handle and be sure that the signal in the headsets disappears.

To test the flaw detector's working capability during continuous inspection of the rail head using the angle probes, the following steps are required:

a) Switch off the sound indicators for the normal channels, having set switch 6 ("Angle-Norm") in the "Angle" position

b) Set the maximum possible sensitivity at which, when the carriage is in motion at a distance from the joint and from the defective sections of the rail head, no signals or cracking are heard in the headsets using the "Amplification" and "STA" knobs for the angle probe channel; set switch 18 in the "Min" position when necessary for improving the smoothness of adjustment

c) Having switched the "Both-Left" switch to the "Left" position and while moving the flaw detector, be sure that the artificial flaws in the left rail head are detected

d) Having changed the "Both-Left" switch to the "Both" position, having raised the left probe assembly slightly and while moving the flaw detector, make sure that the artificial flaws in the right rail head are being detected

e) Set the flaw detector in the position in which a pulse echo from the butt-end of the rail is registered, then make sure that the angle probes turn off when the button on the flaw detector handle is pressed by noting the disappearance of the signal in the left earpiece.

Should the angle elements of the compound probes be replaced, be sure that the flaw detector provides detection of a hole at a depth of 30 mm in Standard No. 1.

The test of the flaw detector's working capability when inspecting by hand reduces to the following procedure:

a) The cable with the hand-held probe is hooked up to the connector on the back of the device

b) The operation mode switch 8 is set in the "Hand" position

c) The "Amplification" and "STA" knobs are set in the position for the maximum possible sensitivity at which signals and static are not heard in the headset while the hand-held angle probe is moved along the running surface of the rail

d) Make sure that the flaw detector provides for detection of the "15-45" and "15-40" holes in Standard No. 1 with the thirty-eight degree and fifty-degree probes, respectively, and for the artificial flaws in the head and web of the rail when the hand-held probe is placed on the running surface of the rail. The detection is indicated with a registration on the sound and meter indicators

e) Make sure that the meter shows the known coordinates of an artificial flaw with an accuracy of not less than $\pm(5\%H+4)$ mm. in the temperature range -2 to +40°C. At other temperatures, an error in the depthmeter readings

twice this size is permissible. The depthmeter must be fine tuned if the readings do not correspond to the indicated accuracy. The end of the scale is tuned using resistance H (on the front panel). Readings at the beginning of the scale are tuned with the resistance whose shaft is located under the sealing plug, on the top of the instrument. When necessary, fine tuning should be repeated. Fine tuning is done when measuring the dimensions of a rectangular sample 150x80x240 mm made of steel using the normal probe.

Having completed the test, the taps must be closed and the flaw detector turned off. Then raise the probes to the transport position, and wipe the running surface of the rails in the reference siding dry.

Before beginning to inspect the rails, the rail type and the degree to which they are worn or dirty must be determined. These factors govern the optimum sensitivity value for the flaw detector and its operating mode.

Optimum sensitivity must be understood to be that sensitivity which provides the greatest probability of detecting inadmissible flaws and the least probability of false rejection. At a sensitivity significantly less than the optimum, dangerous flaws will be missed. If, however, the sensitivity greatly exceeds the optimum, the number of false signals may grow sharply, which make inspection impossible. Thus, the smaller the degree to which the rails are worn or dirty, the higher will be the value of the optimum sensitivity.

The optimum sensitivity of the inspection channel using normal probes is assigned by the reduction value of the first or second bottom signal at which the audio signals activate. Tuning the flaw detector sensitivity and measuring the sensitivity at which the flaw detector operates is done using an attenuator, which weakens the bottom signal any number of times necessary. The degree to which the bottom signal is weakened is determined according to the attenuator scale.

Nominal values for tuning the flaw detector sensitivity are given in Table 17.

Table 17

Nominal sensitivity of the normal element channels

amount of wear and dirt on rail	tuning using the bottom pulse	sensitivity according to attenuator
little wear:		
small amount of dirt	second	0.25-0.3
large amount of dirt	"	0.25 and less
large amount of wear:		
small amount of dirt	first	0.3-0.4
large amount of dirt	"	0.1-0.2

After selecting the sensitivity, it is necessary to turn on the flaw detector, adjust the power supply voltage, feed some of the contacting liquid under the probes, and orient the probes as was described. Then, having set the work mode swith in the "Cont." position, it is necessary to tune the instrument to the optimum selected sensitivity. If it is necessary to inspect using the second bottom pulse, it is important to set the needle in the section corresponding to the doubled height for the rail being inspected according to the H_o scale using the "Rail type" knobs. In other respects, the tuning is no different from tuning using the first bottom pulse. In the process of tuning the angle probe channel, the maximum possible sensitivity at which there is no crackling in the headsets when the flaw detector is in motion must be set using the "STA" and "Amplification" knobs.

After tuning the channels, the "Both-Left" switch must be in the "Both" position, and the "Angle -- Angle-norm" switch must be in the "Angle-norm" position. The rails may be inspected on the line after this.

During continuous inspection, it is necessary to test the magnitude of the instrument's power supply voltage periodically, as well as the sensitivity of the normal probe channels, with the aid of the attenuators. Sensitivity of the angle probe channel is tested by how well the rail ends are registered. If the high pitched audio signal, which usually registers the detection of a flaw by the normal probe channel, appears in the headsets continuously or with small interruptions when the flaw detector is in motion, the cause of this phenomenon must be clarified. A decrease in the bottom pulse echo, which is recorded as a flaw, may take place due to poor probe centering, inaccurate setting of the "Rail type" knob, uneven rail wear, or a very dirty running surface. When the sound appears in the headsets, the probe centering must be tested very carefully, and the sound eliminated using the "Rail type" knob. If the sound cannot be eliminated, it is necessary to decrease the instrument's sensitivity somewhat by turning knobs 9 or 5 clockwise, trying to achieve the state in which there are no audio signals in the headset when the flaw detector is in uniform motion, and then to measure the sensitivity.

In order to measure the sensitivity, it is necessary to turn on the attenuator using the toggle switch, and to turn the attenuator to the left to that position at which the sound in the headset is on the verge of fading out, and then to take the reading on the attenuator scale opposite the mark on the handle. The measured value should be recorded in the monitoring logbook.

The audio signal may also arise when sand and dirt get beneath the shoe face, but, as a rule, during a repeated pass over the same site, the signal is not heard. If the high-pitched tone appears in the headset again during the repeat pass, the given section of the line must be studied

carefully. Here it is necessary to take into consideration that the constant appearance of a radio signal when a probe is moved over a specific site may be caused not only by the presence of an internal flaw, but also by the following:

a) Very dirty running surface (to eliminate this cause, clean the running surface carefully using either a rag or emory cloth)

b) The presence of a welded joint, which may be established by visual examination, but sometimes only after the rail has been cleaned

c) The presence of a hole in the rail

d) The presence of small depressions in the base of the rail under the web (these may be detected using a mirror).

If none of the enumerated possible causes for the appearance of false signals is detected upon examination, the given section of rail must be considered to be defective.

In the case when a low pitched sound is heard in the left earpiece, this, as a rule, attests to the detection of a flaw in one of the rail lines by the angle probe.

If the sound appears again in the headset when the toggle switch is set in the "Left" position, and upon repeated passes over the "defective" sector, this attests that the flaw is situated in the left rail. One must note that the angle probe may register dents under the head which appeared when the spikes were driven.

Several passes are made with lowered sensitivity in the normal probe channel to evaluate the nature of the flaw.* If the distance at which the flaw is picked up decreases and the sound becomes intermittent, this most often signifies the presence of a flaw in the form of a longitudinal crack.

---

* It is necessary to turn knobs 9 and 5 "Amplification" clockwise (cf. Fig. 226) to decrease the sensitivity of the normal probe channel.

Transverse flaws in the web are detected by the normal probe channel only on a very short section of the rail. When these flaws are situated in the head, they are, as a rule, detected by the angle probes (the appearance of a low-pitched tone in the left earpiece). If the transverse flaw in the head emerges in the web zone, it may be recorded by both the normal and the angle probe channels. It is necessary to test the places where there are indications made by the angle probes very carefully, making obligatory secondary passes with the hand-held probe with a fifty-degree wedge angle. To do this, the work mode switch 8 is placed in the "Hand" position and switch 6 in the "Angle" position, and the rail is inspected using the hand-held compound probe as is indicated below.

On several sections of the line, flaws in the form of transverse cracks in the rail head may develop from the field side. To increase the reliability for detecting such flaws, these sections must be inspected with the right probe placed on the left rail line and the left on the right line.

The results of the inspection are recorded in the log.

As has already been noted, an "ultrasonic gage," which consists of two normal elements, and which provides for passing over bolt holes without flaws without a sound appearing in the headset, has been used in the flaw detector for inspecting the rail bolt joints. The appearance of a high-pitched sound in the headset attests to the presence of a flaw. However, this very sound signal may arise when acoustical contact is broken or as a result of non-conformity of the position and diameter of the bolt holes with the ultrasonic gage.

To make the inspection results more accurate, it is necessary to repeat the pass, having cleaned the running surface of dirt beforehand. During the second pass, which, as a rule, is made at a slow speed, a careful examination

is required of the places in the rail where sound appears in the headset. Then the places in which flaws are registered are compared with the position of the bolt holes.

To monitor the joint parts of the rails for the absence of longitudinal cracks situated beyond the bolt holes, as well as for transverse cracks in the head, a repeat pass is required, without pressing the button on the flaw detector handle. One must note that, as a rule, when the probe is moved from one rail to the other, and, occasionally, when the probe approaches the end, the high-pitched audio signal arises in the headset even when the button is pressed.

It is possible to inspect bolted joints by hand using a normal probe with the UZD-NIIM-6M flaw detector.

To do this, the cable with the connector for hooking up the normal probe is attached to the connector situated on the back of the instrument. The work mode switch should be placed in the "Hand" position; inspection is conducted based solely on the meter. The running surface must be covered with a layer of mineral oil before inspecting the joint. Having placed the probe on the running surface along the axis of the rail head and beyond the joint, and while turning the "Angle amplification" knob clockwise from the extreme left position, the position where the meter consistently indicates the rail height when the probe is moved along the axis of the rail according to the H_o scale must be determined. Set the "STA" knob in the extreme right position.

Then the probe is moved along the running surface within the joint zone, trying not to move it from the axis. When a flaw is present, or when the probe is placed on the running surface above the bolt hole zone, the meter needle will deflect to the left or right from the initial position.

Testing and adjustment of flaw detectors is done at least once a month at section repair shops or in railroad repair shops.

The following work should be done:

1) Determine the exit point and the beam transmission angle in steel for all probes which are in use for hand monitoring. Measurements are made according to Standards No. 2 and No. 3 when the probes are connected to a DUK-111M or DUK-131M flaw detector. The measured transmission angles should be within the range:

$45^{\circ}\pm2^{\circ}$ for a probe with a wedge angle of 38°, and

$65^{\circ}\pm2^{\circ}$ for a probe with a wedge angle of 50°.

Probes not corresponding with these requirements should be removed from service.

2) Dissembly, cleaning, and reassembling of compound probes

3) Testing the serviceability of the cable terminations in the connectors and elimination of noted defects

4) Cleaning the water filter and washing the water-feed system

5) Cleaning the centering systems and lubrication of the bearings

6) Testing the condition of the storage batteries, addition of electrolyte, and performing an aging charge and discharge cycle.

7) Testing the insulation between the wheels and the frame. The test is conducted using an M-1011 megohmmeter. The insulation resistance should be no less than 2 Megaohm.

8) Testing and fine-tuning the depthmeter

9) Testing the working capability of the flaw detector when monitoring parent metal and bolted and welded rail joints on a reference siding.

5. Trouble shooting

Determining the defects in the UZD-NIIM-6M and eliminating them, as is the case with other rail flaw detectors, requires an understanding of

the interactions between the individual units of the instrument, as well as knowledge of the operating principles of the individual stages. Naturally, it is impossible to point out all possible defects and the means for eliminating them. The characteristic defects of the flaw detector are presented in Table 18. If any of the flaw detector units fail, it is necessary to test the voltage and the resistance on the transistor electrodes, to test the connecting cable, and the printed boards, paying attention to the possibility that the "tracks" on them may have come unsoldered.

Elements (transistors, diodes, etc.) should be replaced only after the power supply voltage has been switched off.

After detected defects have been eliminated, it is necessary to test the conformity of the basic characteristics of the instrument to technical requirements.

The current consumed by the flaw detector from the power supply source should not exceed 0.4 amp. The measurements should be taken using an AVO-5M instrument, or one analogeous with it, at a voltage of 12 v. according to the flaw detector's meter.

The flaw detector's sensitivity when working with normal elements of the compound probes should provide detection of flaws corresponding to a weakening of the first or second bottom signal from 1.0 to 0.25 on the amplifier input by the attenuator.

Table 18

Possible defects in the UZD-NIIM-6M flaw detector

#	Fault indication	Possible cause of fault	Correction
1	When the instrument is turned on, the indicator does not show a voltage	a. faulty cable b. blown fuse c. break in power supply cable	a. repair the common cable b. replace the fuse c. test the cable from the batteries to the instrument and eliminate the short or break

Table 18 (continued)

#	Fault indication	Possible cause of fault	Correction
		d. the "12 v." regulator has burned out	d. test the "12 v." regulator and replace it
2	The indicator shows a voltage but does not operate when the "Monitor" switch is in the "Cont" position	a. faulty cable	a. repair the cable
		b. no voltage to the ultrasonic oscillation generator	b. measure the voltage; eliminate the defect in the converter, the cable, and the oscillator circuits; test and replace triodes T42, T43
		c. diodes D4 and D5 (D2281 type) are out of order	c. replace diodes D4 and D5
3	The indicator does not function only in the "Cont" position of switch 8 when "Rt" button is in one or in both positions	the gate delay multivibrators, or one of them, does not function	test and replace triodes T32-T35 or diodes D16-D19
4	The indicator does not function only when switch 8 is in the "Man" position. The indicator does not operate when switch 8 is in either the "Cont" or "Man." position	a. the gate multivibrator for the angle probe channel does not work	a. test and replace triodes T26-T27 and diodes D11-D12
		b. the emitter repeater does not operate	b. test and replace triode T29
		c. the saw-tooth voltage generator does not operate	c. test and replace triodes T30, T32 and diodes D14-D15
5	The audio signaling devices do not work when there is no contact between the rail and the head	a. poor contact in the jacks	a. eliminate the broken contact
		b. sound generators for the normal heads do not work	b. test and replace triodes T12-T14; T23-T25
		c. gate pulse shaper does not operate	c. test and replace triodes T28 and T29
		d. the anti-coincidence stage does not operate	d. test and replace triodes T7, T8, T10, T11
6	The audio signal for the normal channel does not stop when there is an acoustical contact	a. the "Rail type" potentiometers are defective	a. test and eliminate the defect or replace the potentiometers
		b. the "Rf amp" train for the normal probe channels does not operate	b. test and replace triodes T2-T7 and T11; T39-T41

Table 18 (continued)

#	Fault indication	Possible cause of fault	Correction
7	When switch 8 is in the "Man." position, the coordinates are measured but there is no sound signal	the sound generator does not work	test and replace triodes T21-T22 and T36
8	There is no sound signal in the angle probe channel and the needle shows a large value but does not measure coordinates in the "Man." mode	a. the angle probe channel train does not work b. the probe is defective	a. test and replace triodes T15-T20 b. replace the probe

To test the sensitivity, the probe in the centering system is placed on the surface of the traveled rail and the instrument is tuned using the "Rail type" and "Amplification" knobs to inspect using either the first or second bottom reflection. Then the attenuator is switched on and set in position 1 (cf. Fig. 226), and the "Amplification" knob is turned until the signal appears in the headsets. The channel sensitivity is considered to be satisfactory if the signal appears when the "Amplification" knob is set in a position other than "zero".

The test is similarly conducted at an attenuation of 0.25. Here the signal in the headset should appear when the "Amplification" knob is set in the 0.8 position or less.

The power supply converter for the flaw detector should produce rectangular pulses with an amplitude of not less than 250 v. at a frequency of 750-1100 Hz; potentiometer R3' in the converter should be set at normal temperature conditions with a power supply voltage of 14.5 v. according to the meter. There should be no cessation of the oscillations. Measurement of half of the common peak-to-peak value for the pulse and the rectangular period is taken at resistance R15.

The peak-to-peak value of the rapid pulses at the piezoelectric plates of the normal elements of the combined probes should not be less than 30 v., and at the plates for the angle elements, not less than 60 v. Consistent operation of the radio pulse oscillators is guaranteed by the proper selection of the circuit's time constants (R19, C10; R15, C9), which determine the instant at which the radio pulse generators activate. Oscillograms of the converter voltages when the time constants of the above mentioned circuits are matched correctly and incorrectly are shown in Fig. 229. If the generator is properly tuned, the secondary triggering will not take place when the voltage is increased to 12.5 v.; when the power supply voltage is decreased to 11.5 v., there should be no cessation of the oscillations.

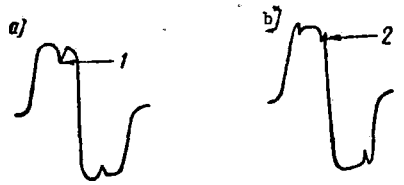

Fig. 229 Oscillograms of the voltage at the flaw detectors radio pulse oscillators

a. generators properly tuned; b. generators improperly tuned
1. instant at which the generator pulse diode is switched on
2. secondary triggering of the generator

The duration of the angle probe channel's gate pulse should be smoothly regulated. The minimum duration of this pulse should be no more than 60

microsec, and the maximum, no less than 170 microsec. An oscillograph should be connected to resistance R120 to measure these values.

For the normal probe channels, the minimum delay duration of the gate pulses should be not more than 35 microsec, and the maximum, not less than 135 microsec. The measurements are taken using an oscillograph connected to resistances R143 and R152 when the "Rail type" regulators are set in the extreme positions and the work mode switch 8 is set in the "12 v." position.

The sensitivity of the instrument with angle probes should provide simultaneous detection of holes at a depth of 15-45 mm for the probe with a wedge angle of 38° and a hole 2 mm in diameter at a depth of 8 mm in a steel No. 2 Calibration Standard at normal temperature; holes at a depth of from 15-30 mm should be detected in Standard No. 1 by a probe with a wedge angle of 47°, and in Standard No. 2, a hole 2 mm in diameter should be detected at a depth of 15 mm. When using a probe with a wedge angle of 50°, it is necessary to record a hole at a depth of from 15-40 mm in Standard No. 1, and a hole 2 mm in diameter at a depth of 8 mm in a Standard No. 2 made of steel.

In all cases, the amplitude of the pulse echo signals from the indicated reflectors should be adequate to trigger the sound generators. The sensitivity should be smoothly adjusted using the "Angle amplification" knob. This may be tested, having made sure that when the "Min." switch is turned off the adjustment of the sensitivity for an instrument with a 38-degree probe within the range of 15-25 and 15-45 is made by turning the "Amplification" knob within a range of not less than half the adjustment band width (e.g. 0-5; 2-7, etc.)

The resistance of the insulation between the probe systems and the wheels with regard to the instrument chassis should not be less than 1 Moh. The measurements should be taken between the bodies of the compound probes as well as between the wheels using an M-1101 megohmmeter.

1. Welding Defects

Welding is the primary means for preparing lengthy sections of rail and for restoring old rails. As a rule, Electro-contact (Flash-butt) welding is employed using the method of continuous flashing with intermittent preheating. Welding is done on fully automated electrical contact welders at the rail welding plants (RWP), as well as out on the line with the aid of mobile rail welders (MRW).

The ends of the rail are cleaned of rust and dirt, and are clamped in the jaws of the rail welder before welding. An electrical voltage is fed through the jaws to the rails, the butt ends of which are situated some distance from each other. During the welding process, the rail ends are periodically moved closer to each other. A current of approximately 800 amp, which causes the formation of heat in the ends being welded, passes through the butt-ends of the rails when the rails are touching. Due to thermal conductivity, heat is transfered into the depths of the rails and along the surface. This results in the pieces of the rail which are being welded being heated through to a relatively great depth.

Upon reaching a specific temperature, the flashing-off process automatically switches to the next phase in the welding process, upset forging. The liquid metal is forced from the flashed surfaces as a result of the force which was applied, and the butt-ends of the rails, which are in a plastic state, are welded together. The pressure is then released automatically, and the welded rails are freed from the machine's clamps. The metal which was squeezed out during the welding process is knocked off and the joint is polished flush with the parent metal. The metal joint is normalized in the area of the base: it is heated to a temperature of 800-850°C

and subsequently cooled in the open, being protected from precipitation.

The width of the contact weld is primarily determined by the heat effect zone; the longer the heat-up and the higher the heat-up temperature, the greater the width of the weld.

According to the technical specifications in (publication) TU 32/ TsP-28-67, "Old Rails Repaired Using Contact Welding," when there are no internal welding flaws, the quality of the joint is considered satisfactory if, during static testing of the control samples, the deflection is not less than 30 mm and the breaking load is not less than 180 tons for R75 type rails; 150 tons for R65; 100 tons for R50; and 75 tons for R43.

Local surface irregularities at the weld joints after polishing should not exceed 0.5 mm for old rails from groups I and II, and 1.0 mm for rails from group III.

The presence of internal flaws in the joint, or unsatisfactory mechanical processing of the metal extruded during welding lead to the development of transverse, diagonal, or longitudinal cracks in various zones of the welded joint under usage conditions.

All flaws and fractures which have appeared in the joint, as well as within 100 mm to either side of the joint, are related to three groups according to the "Classification of Flaws and Damage to rails" (PTM 32/ TsP-1-66): 26.3; 56.3; and 66.3.

The characteristic contact welding flaws are usually caused by mechanical separation of the purer solid and contaminated liquid phases. Even with the completely automated welding process, flaws are formed in connection with irregularities in the welding process. The most frequent welding flaws are: the porosity, the incomplete weld (a flat fracture), the fissure, poor fusion, crater shrinkage, and silicate build-up (light and gray).

It is necessary to distinguish oxidized and unoxidized porosities. Oxidized porosity, known in practice as "burn-out," has the structure shown in Fig. 230 b at the place of fracture. The fracture may be dark, or there may be temper colors. As distinct from "burn-out," the non-oxidized porosity has a light-mat, grainy fracture and is encountered much less frequently. Porosity forms both near the surface as well as within the rail, occasionally reaching such dimensions that the joint collapses in the welding machine.

Metal impurities, protracted welding when the welding current is too low, unequal warm-up across the cross section due to an improper preparation of the rail ends, and asymmetrical positioning of the joint in the machine jaws may be causes for the formation of porosities.

The incomplete weld (Fig. 230a) seldom arises independently. Its appearance is usually accompanied by fissures and crater shrinkage. This flaw type arises during inadequate warm-up and cool-down of the ends after they have been separated. In the fracture, this flaw appears as a very flat gray spot; signs of the preliminary butt-end processing are sometimes noticeable on the gray surface and sometimes there are spots of blackish scale. The plane of the spot is perpendicular to the rail axis.

Fissures and (areas of) poor fusion (Fig. 230c) arise as a rule when the welding current is too great, during preliminary up-setting of a joint which is not uniformly preheated, as well as, on occasion, when the up-setting pressure in inadequate.

The surface of these types of flaws is usually smooth and shiny. If the flaws emerge onto the surface, they take on a dark coloration as a result of oxidation.

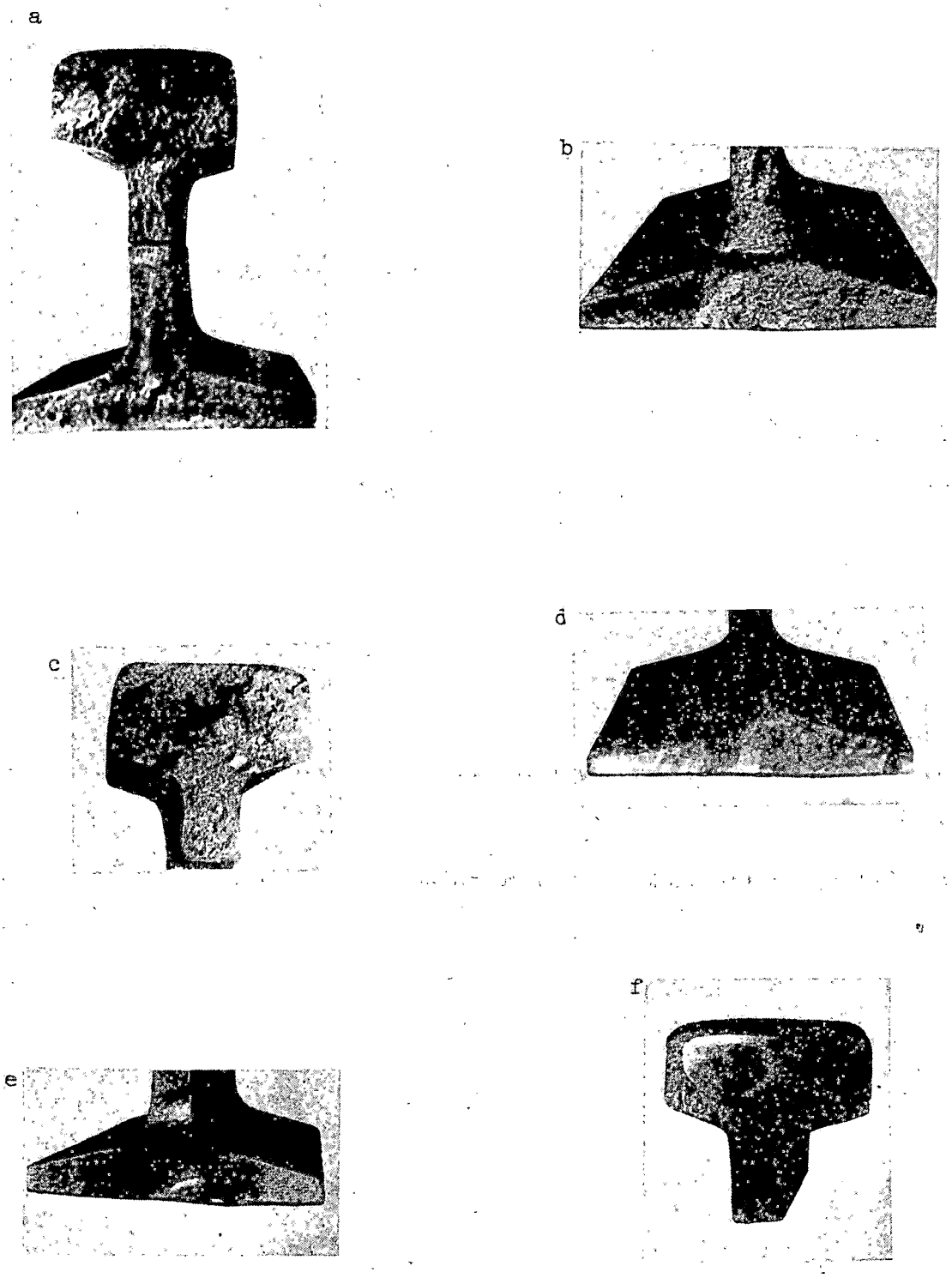

Fig. 230 Flaws in welded rail joints detected during ultrasonic inspection

a. incomplete weld b. burning c. poor fusion d. crater shrinkage e. (air) hole f. transverse crack in the head which propogated from a welding flaw

Fissures and (areas of) poor fusion are often surrounded by crater shrinkage, represented as a smooth light-silver spot with tempering colors or a black (oxidized) spot which is occasionally grayish, or has a gray border (Fig. 230 d). Crater shrinkage may be of any size, and most frequently originates in the center of the base. The causes for formation are the same as in the case of fissures and (areas of) poor fusion.

The (air) hole (Fig. 230 e) is a variety of fissure. This flaw is similar in nature and external characteristics to the fissure, but it always emerges onto the surface, and therefore, the flawed place most often has a dark coloration due to oxidation.

(Areas of) silicate build-up (gray and light) are the result of silicate inclusions contained in the steel. The gray silicate build-up is a flat, as a rule small, mat-gray spot in any part of the cross-section. The number of these spots increases when up-setting is poor, and the clarity of the borders is less pronounced. A light silicate build-up occurs when there is a very high up-setting pressure, and it has a long, narrow form. The shining, silverish spot, which consists of the very fine longitudinal bands of the silicate inclusions is always directed across the cross-section (vertically in the base, horizontally in the web.)

All of the enumerated flaws, with the exception of the gray silicate build-up with an area of less than 15 mm^2, or areas where not more than three build-up areas, with a total area of no more than 25 mm^2, are inadmissible.

It is necessary to note that internal welding flaws exert no influence on the static strength of the joint in a number of instances. Therefore, joint fracture very often takes place at a point beyond the defective sector. For example, a flaw has been detected in one of the welded joints in a length of R65 rail. The joint was cut out and destroyed on a hydraulic press

so that the base was subjected to elongation. Here the rail fracture began in the base along the welded joint, but in the head area, it passed along the heat effect zone, and not along the flawed cross-section (Fig. 231 a). Subsequent metallographic examination confirmed that there was burnout in the head with an area of approximately 40% of the cross-section of the head (Fig. 231 b).

Fig. 231 Welded joints

a - fracture diagram

b - location of flaw (from metallographic analysis data)

When there are flaws in the base zone, fracture often takes place under loads and deflections which are equal to or significantly exceed those required by technical specifications.

At the same time, tests of welded rail joints under a fluctuating load have shown that welding flaws reduce the fatigue strength of the welds substantially. In this case, it was established that flaws situated in the head and web effect the weld's life less than flaws in the rail base. However, under usage conditions, welding flaws may be the cause of the development of flaws which are of a fatigue nature (Fig. 230 f) and cause the destruction of the rail at the welded joint.

Timely detection of the internal flaws in welded joints may be assured only by employing non-destructive testing methods. Presently, the most reliable method is that of ultrasonic flaw detection.

2. Methodology for ultrasonic inspection of welded rail joints

The thickness of the contact weld is a small quantity in comparison with the dimensions of a rail. Flaws have their greatest development in the welded joint plane. Therefore, it would be necessary to pass a sound wave through a weld using a normal probe in a direction which is perpendicular, or close to it (Fig. 232 a).

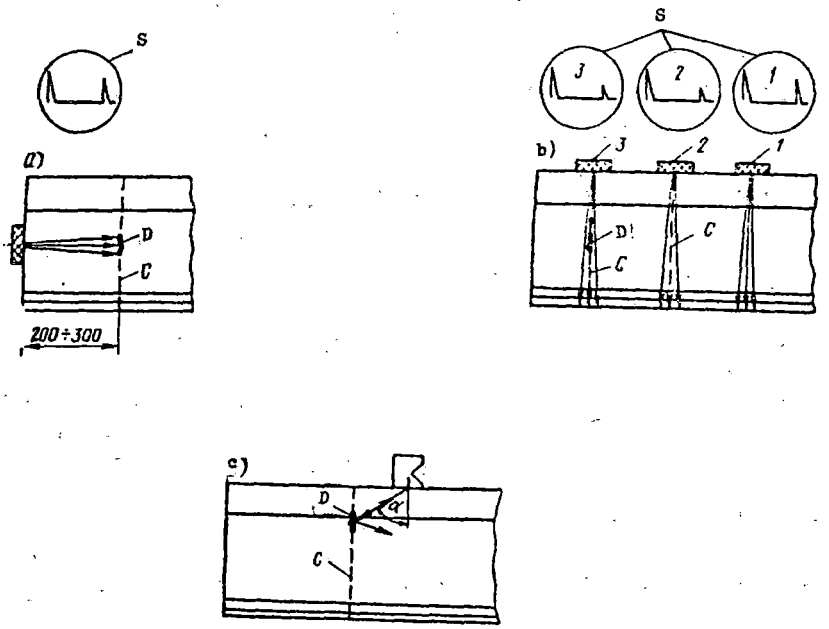

Fig. 232 Diagram for passing sound waves through the welded joint C using probes a, b -- normal; c - angle

1 - probe on the parent metal; 2 - probe on a flawless welded joint with large, grainy structure; 3 - probe on a defective joint with a fine-grained structure; S - flaw detector screen with the scan images

However, employing the diagrams according to Fig. 232 a is not possible if the weld joint is removed from the surface on which the probe is placed by more than 200-300 mm, or is closer than the probe's dead zone. When passing a sound wave through the weld from the running surface of the rail head using a normal probe (Fig. 232 b), the ultrasonic wave, passing a distance of 150 mm or more alongside the weld, decays significantly. This is related to

the dispersion of oscillations at the grain boundaries in the weld zone. It is exactly this which explains the appearance of the audio signal in the URD-58, URD-63 and UZD-NIIM-6M in most cases, as well as the decrease in the bottom pulse amplitude on the screens of the URD-52, DUK-11IM and DUK-13IM flaw detectors, when the probe is situated above the joint. Therefore, flaw detectors which operate on the mirror-shadow principle using normal probes may not be used to inspect welded joints. At the same time, the elastic oscillations of an ultrasonic frequency do not disperse, for practical purposes, when they intersect the welded joint at an angle to its plane.

In connection with this, the inspection of the quality of welded rail joints is accomplished using the pulse-echo method and angle probes. Ultrasonic oscillations are transmitted into the weld through the parent metal (Fig. 232 c). Since diffuse scattering of the elastic wave which strikes the flaw is observed, a pulse echo from the flaw being sought will be received by the probe. However, along with the useful pulse echoes, the appearance of false ultrasonic oscillations from irregularities on the rail surface is also possible. Therefore, inspection should take place after the removal of metal which was extruded during welding. The probe is shifted along the rail perimeter within the welded joint zone.

When passing a sound wave through the rail, the operator must follow the position of the probe constantly, and make sure that acoustical contact is being maintained between the probe and the rail surface. Naturally, a sound or light flaw indication signal should be built into the flaw detector to free the operator from having to observe the cathode ray tube screen or meter and the probe, which is being moved around, simultaneously. In addition, as was indicated in Chapter V, the flaw detector should have a depth meter to measure the coordinates of the reflecting surface.

The specialized UZD-NIIM-5 (UZD-59 DUK-11IM, and DUK-13IM) and the UZD-NIIM-6M most fully satisfy the indicated requirements.

The basic condition for quality control of a welded joint is to provide the most reliable detection of internal flaws using the least number of operations. Therefore, a series of investigations concerning the selection of the basic monitoring parameters and the schemes for passing sound waves through the rail preceded the development of the methodology of ultrasonic welded joint inspection.

During the investigations, ultrasonic monitoring data were compared with data from the examination of fractures and from metallographic analysis. As a result, the desirability of employing ultrasonic oscillations at a frequency of 2.5 MHz and the necessity of passing sound waves through each welded joint using two probes, with wedge angles of 40° and 50° in the following sequence, was established:

a) Pass a sound wave through the base from above (Fig. 233 a) using a probe with a wedge angle of 50° with a direct and a multiply reflected beam

b) Using a probe with a wedge angle of 50°, pass a sound wave through the lower fillet zone using a direct beam, and the outer part of the base from the bottom (Fig. 233 b) using a direct and a multiply reflected beam

c) Pass a sound wave through the web from the side (Fig. 233 c) using a direct and a multiply reflected beam and a probe with a wedge angle of 50°

d) Pass a sound wave through the head from above (Fig. 233 d) using a direct beam and a probe with a wedge angle of 50°

e) Pass a sound wave through the head from above and from the sides (Fig. 233 e) using a direct beam and a probe with a wedge angle of 40°

f) Pass a sound wave through the head, web, and the section of the base under the web (Fig. 233 f) from the running surface of the rail using a direct beam and a probe with a wedge angle of 40°.

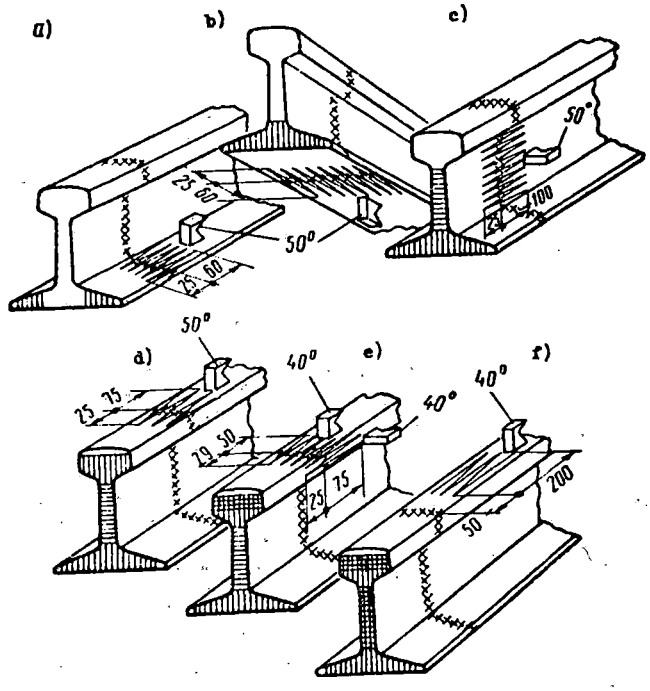

Fig. 233 Diagram for passing a sound wave through a welded rail joint

When monitoring rails installed on the line, the operation of passing a sound wave through the base from below is excluded.

When passing sound waves through the rail, the probe should be placed perpendicular to the weld and, systematically rotating it 10-20°, moved in a zigzag along the welded joint. The displacement across the rail should not exceed 2-3 mm at one time.

The probe displacement limits are selected in order to make the operation of passing sound waves through the rail the most thorough. These displacement boundaries are:

a) 200 mm when inspecting a welded joint in the web and its extension into the head and base from the running surface using a probe with a 40° wedge angle

b) 100 mm when inspecting a welded joint in the rail head from the side using a probe with a wedge angle of 40°, and when inspecting the head from above with a 50° probe

c) 85 mm when inspecting the rail base from below or above using a probe with a wedge angle of 50°

d) 125 mm when inspecting the web from the side with a 50°- probe.

In this case, sound waves are passed through the welded joint in the base and the web by a multiply reflected beam, which provides the detection of flaws situated near the surface along which the probe is being moved (Fig. 234 a). Flaws situated near the lateral surfaces in the head are detected when the probe is moved along the opposite surface (Fig. 234 b). When sound waves are passed through the head from the running surface, flaws situated in the layer corresponding in size to the dead zone of the probe will naturally not be detected.

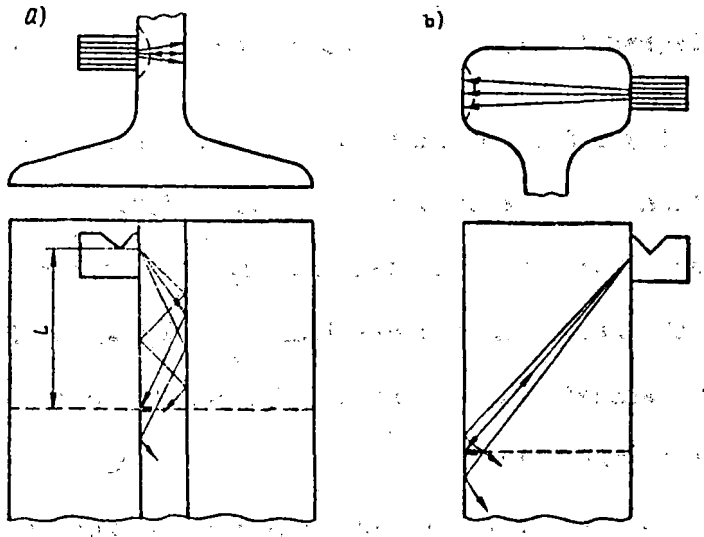

Fig. 234 Flaw detection diagram when sound waves are passed through the rail

a. web b. head

Experience shows that flaws in the welded joint very frequently form around the edges of the base. For more reliable detection of these flaws, sound waves should be additionally passed through the edges of the base from above using a probe with a wedge angle of 50° when the probe is moved within a radius of 0-30° of the edge of the base (Fig. 235).

Before inspecting the welded joint, the sector along the perimeter of the rail within which the probe is to be moved is cleaned of residual oil, dust, and mud and covered with a layer of the contacting medium. Poor processing and cleaning of the sectors of the rail surface within which the probe is to be moved reduces the inspection reliability.

It is necessary to note that during inspection, false pulse echoes may be received in addition to the pulse echoes from flaws.

The most probable cause of the origination of false pulses are:

a) (when monitoring the base) a reflection from an irregularity on the edge of the base or in the lower fillet

b) (when monitoring the web) a reflection from the alphanumeric signs on the lateral surface of the web

c) (when monitoring the head) a reflection from irregularities on the lower surfaces on the rail head.

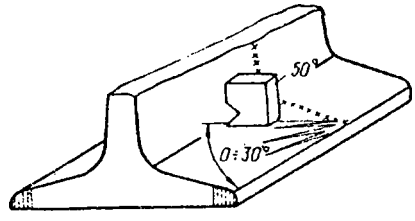

Fig. 235 Diagram for passing sound waves through the edges of the base

In order to distinguish false pulses from pulses caused by the presence of flaws, it is necessary, first of all, to determine the coordinates at which the reflecting surface lies using the flaw detector's depth meter. It is necessary to note that when inspecting the base and web, only the distance L from the point of beam transmission to the reflection surface is measured. (cf. Fig. 234).

If the results of the measurements and an examination of the sector being inspected confirm the possibility that pulse reflections may arise, the surface must be recleaned.

The methodology which has been presented is common for inspecting welded rail joints using the UZD-59, DUK-11IM, DUK-13IM, and the UZD-NIIM-6M flaw detectors and is the basis for the current instructions on ultrasonic flaw detection of rail joints.

3. Inspection of welded rail joints using the DUK-11IM, DUK-13IM, and UZD-NIIM-6M flaw detectors

The reliability of the results from ultrasonic welded joint inspection using any of the indicated instruments is, to a great degree, determined by the correspondence of the primary inspection parameters to the parameters given in the instructions. The following are included in the basic parameters for welded joint inspection: rated sensitivity of the flaw detector with probe, the beam transmission angle, the dead zone, and the accuracy of the depth meter.

Calibration Standards No. 1, 2, and 3 are used to tune the flaw detectors and test their basic parameters.

According to Standard No. 1,, the rated sensitivity should be 35 mm when inspecting using a probe with a wedge angle of 50°, and 40 mm when monitoring using a probe with a wedge angle of 40°. A decrease in the sensitivity may be the cause for missing a flaw, and an increase may lead to an inordinate number of welded joints being rejected. Therefore, flaw detector sensitivity should be tested systematically during operation. The beam transmission angle is determined according to Standard No. 2 using flaw detectors with a cathode ray tube (DUK-11IM and DUK-13IM). A change in the beam transmission angle and the position of the emission center are primarily associated with wear of the probe wedge. Therefore, the given parameters must necessarily be checked after monitoring 30-40 joints, i.e. every day before work.

The size of the dead zone depends, to a significant degree, on the setting of the "Sensitivity" and "STA" knobs, and it, therefore, should be checked systematically after the instrument has been tuned to the given rated sensitivity. The accuracy of the depth meter should be tested before beginning to work.

The beam transmission angle, the size of the dead zone, and the accuracy of the depthmeter for the DUK-11IM, DUK-13IM and UZD-NIIM-6M flaw detectors should correspond to the data presented in Chapters IX and X.

The flaw detector should be tuned to the appropriate working mode before monitoring, depending on the welding joint zone which is to have the sound waves passed through it.

When inspecting welded rail joints using the DUK-11IM and DUK-13IM flaw detectors, the following must be done:

a) Connect the cable and probe to the instrument via an intermediate connector at a frequency of 2.5 MHz, connect the headsets to the DUK-13IM or the signal light to the DUK-11IM, and turn on the instrument according to the instructions given in Chapter IX

b) Set the "Inspection from the surface /Layer-by-layer" switch in the "From the surface" position and the "Monitoring depth" knob in the extreme right position

c) Set the "Sensitivity" knob in the extreme right position and the "STA" knob in the leftmost position at which the transmitted pulse is not present on the cathode ray tube screen. In case the transmitted pulse is of lengthy duration, and the amplitude decreases unevenly when the "STA" knob position is changed, it is necessary to set the "Cut-off" potentiometer in that position at which pulses caused by noises in the probe wedge would no longer be present

d) Test for the possibility of tuning the flaw detector with the complex

of probes intended for operation to the given rated sensitivity and dead zone. Be sure that the "AFS"* knob is in the position at which the audio indicators activate when the pulse echo has an amplitude of 5-7 mm on the cathode ray tube screen.

To pass a sound wave through the base, web, and head of the rail from above using a probe with a wedge angle of 50°, it is necessary to do the following:

a) Switch on the probe with the 50° wedge angle

b) Set the "Flaw coordinates" knob in the position at which the number 100 will be opposite the line on the window on the "H" scale for a 40° probe

c) Set the "Monitoring depth" knob in the position at which the marker will be at the right end of the base line

d) Using the "Sensitivity" and "STA" knobs, set the flaw detector sensitivity to 35 mm according to Standard No. 1. The "STA" knob should be in the leftmost position at which there is no transmitted pulse on the flaw detector screen. A flaw detector with a 50° probe is considered to be tuned to the given pre-assigned sensitivity if holes in a No. 1 Standard at depths of from 15-35 mm, inclusively, are detected by all of the indicators, and the amplitude of the pulse echo from a hole at 40 mm is less than the amplitude of the pulse corresponding to the "AFS" activation threshold.

To pass a sound wave through the head from the side and from the running surface of the rail using a probe with a wedge angle of 40°, it is necessary to do the following:

a) Replace the probe with a 50° wedge angle with one with a 40° wedge angle

b) Tune the flaw detector with probe to a pre-assigned sensitivity equal to 40 mm in Standard No. 1 by turning the "Sensitivity" and "STA" knobs.

---

*"AFS" -- automatic flaw signaling device. Tr.

To pass a sound wave through the head, web, and the section of the base under the web from the running surface using a 40° probe, set the scan time which corresponds to the height of the rail being inspected using the "Monitoring depth" knob and the depth meter scale.

Inasmuch as the DUK-13IM flaw detector does not permit rails to be inspected through their entire height in the "Inspection from the surface" mode, to inspect the aforementioned zone, it is necessary to do the following:

a) Be sure that the marker pip is at the right end of the base line and the number 100 is set on the "H" scale for a 40° probe

b) Switch the flaw detector work mode switch to the "Layer-by-layer Inspection" position

c) Set the "Flaw coordinates" disc in a position so that the digit opposite the line on the window on the "H" scale which corresponds to the 40° probe would indicate a magnitude of 82 mm for R65, 52 mm for R50, and 40 mm for R43.

When monitoring welded rail joints using the UZD-NIIM-6M flaw detector, it is necessary to do the following:

a) Connect the cable with the compound angle probe

b) Switch the instrument on and adjust the power supply voltage according to the directions given in Chapter X

c) Set the switch in the "Hand monitoring" position and the "Normal-angle" toggle switch in the "Angle" position

d) Set the 50° wedge angle side of the probe on Standard No. 1 and tune the flaw detector with the specified probe to a pre-assigned sensitivity of 35 mm. The flaw detector with probe is considered tuned to the given pre-assigned sensitivity if a signal occurs in the headset and the meter needle deflects when holes at depths of from 15-35 mm are detected. In this case, sonic irradiation of a hole at a depth of 40 mm should not be accompanied by the appearance of an audio signal or a deflection of the meter needle.

Inspection of the base, web, and head from the running surface of the rail is accomplished using a probe with a 50° wedge angle. To pass a sound wave through the head from the lateral surface, as well as the web and the part of the base under the web from the running surface, it is necessary to set the compound probe on the rail head with the side corresponding to the 38° wedge angle. Here the pre-assigned sensitivity, based on Standard No. 1 should be 40 mm. Measurement of the coordinates of the reflecting surface (of the flaw) is carried out by the DUK-11IM, DUK-13IM, and UZD-NIIM-6M flaw detectors according to the directions given in Chapters IX and X.

When even one flaw is detected in the RWP, the welded joint is rejected and the rail is returned to the welder for rewelding. When a flaw is detected on the line, the rail with the defective joint is replaced with a new one, or else the welded joint is cut out and the rail is again welded using a portable rail welder.

In order to determine the frequency with which flaws are detected, depending on their nature and location, as well as to establish causes for the increase or decrease in the number of detected defective joints, systematic accumulation of the results from ultrasonic inspection of welded rail joints and their analysis are kept at each RWP. For this purpose, special charts are compiled for each defective joint (Fig. 236). The results of ultrasonic inspection (USFD) and inspection of the welded joint fracture (Fracture) are represented in the chart.

The rail profile is conditionally divided into ten zones outlined on the chart in thick lines, which simplifies the process of compiling the results of USFD and fracture inspection. The scale grid which has been drawn in facilitates compilation of the chart when monitoring different types of rails.

When USFD results are recorded on the rail profile depicted in the chart to the left, the zone corresponding to the section of the welded joint in which the flaw was detected is shaded in. Here the nominal extent of the defective sector and the distance between the defective sector and the rail contour are indicated. The position of the probe at which the given flaw was detected is indicated by an arrow. Above the line at the end of the arrow, the minimum pre-assigned sensitivity at which the flaw may still be detected by all of the flaw detector indicators is given, and below the line, the wedge angle of the appropriate probe.

Rail type, temperature, and the inspection date, as well as the pre-assigned sensitivity at which inspection is carried out are recorded on the appropriate graphs of the inspection chart table. On this very same table, the load and defelction at which the welded joint fractures on a hydraulic press are recorded.

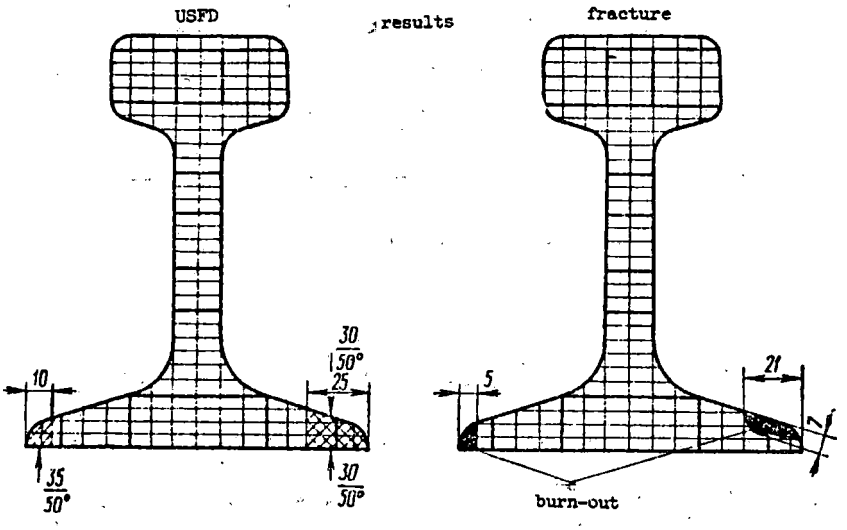

Fig. 236 Chart of a defective joint detected at RWP-23

The flaw which is visible in the fracture is entered to scale on the rail profile represented on the chart to the right, strictly observing its outline and location. The actual flaw dimensions, its length and height,

and horizontal and vertical distances from the rail surface are measured using a ruler, and are recorded on the rail profile. The nature of each flaw visible on the fracture is recorded on the chart near the appropriate flaw representation.

When there is a large quantity of such data on hand, it is possible to evaluate the detectability of flaws as a function of their dimensions, nature, and position (in the rail), and to evaluate the stability of the technological welding process at the RWP.

4. Flaw detectability and use of inspection data to improve welding technology

Flaw detectability, i.e. the capability of flaws to reflect an ultrasonic wave incident on them in the direction of a probe, other conditions being equal, as has been shown in Chapter V, is determined to a great extent by their nature, dimensions, and position.

It is possible to evaluate the detectability of welding flaws during ultrasonic inspection only by careful generalization and analysis of the results from the practical application of ultrasonic flaw detection. Therefore, the NII mostov LIIZhTa* has conducted a systematic accumulation of inspection data for a number of years using special data information sheets and the inspection charts shown in Section 3. These charts are obtained from the rail welding plants. An analysis of the charts for more than 3000 welded rail joints which were rejected at various rail welding plants shows that employing the indicated devices when the monitoring methodology is strictly observed permits internal flaws in various zones of the welded joint to be detected with adequate reliability. It has been established that porosity (44%), poor fusion (28.4%), cracks (7.4%), silicate build-up (12.8%), and gas fissures (4.8%) occur and are most frequently detected in welded rail joints. In most cases (77%), flaws originate in the base

*Scientific Research Institute for Bridges, Leningrad Institute for Engineers for Railroad Transportation -- Tr.

which is the most dangerous from the point of view of usage, and most time consuming from the point of view of inspection; they occur significantly less frequently (8%) in the rail head (Fig. 237). The dependence of the flaw detection frequency on their dimensions is shown in Fig. 238. The area S of the flaw is plotted along the abscissa of the chart in mm^2, and the number of flaws N, the area of which is equal to or less than the given value of S, is plotted along the ordinate.

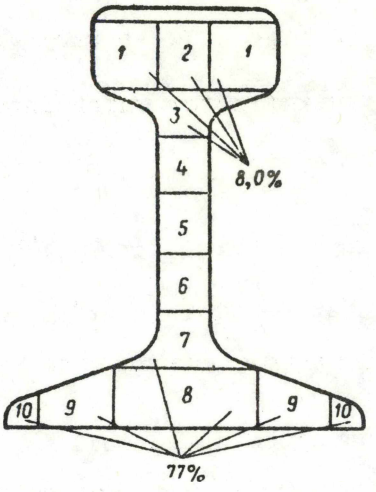

Fig. 237 Distribution of flaws through the cross-section of a welded rail joint

The detectability of flaws in the same joint zone (the head, the web, the base) depends to a significant degree on the distance between the flaw and the surface, other conditions being equal. When the flaw is situated near the surface, and when the flaw and the surface create an angular reflector for the ultrasonic wave incident on it, the detectability of that flaw is from 5-10 times greater than the detectability of the same flaw situated at a greater distance from the surface. It is necessary to note that the detectability of flaws is in most instances greater when monitoring using a probe with a wedge angle of 40° than when using a probe with an angle of 50°.

The detectability of flaws located in the center part of the web depends to a significant degree on the method used to pass the sound wave through the joint from the surface of the web. Passing the sound waves

(through the web) using a reflected beam permits flaws to be detected more reliably than when passing sound waves (through the web) using a direct beam. When flaws are sonically irradiated by a beam reflected a single time the detectability of a flaw displaced toward the surface on which the probe is located is approximately twice as great as is the case when the flaw is situated in the center of the web. This is associated with the fact that, for an ultrasonic beam having a relatively high divergence angle for the primary lobe in the directivity diagram, the flaw and the surface of the rail web, which are in close proximity, form a reflector which is close to being an angular corner reflector.

When flaws situated in the rail web and in the upper and lower fillet zones are sonically irradiated, flaws situated in the approximate center of the rail have the worst detectability from the running surface (Fig. 239). When the flaw is situated near the base of the rail, its detectability increases sharply as a result of the formation of a corner reflector. The fact that flaws situated in the rail base near the surface opposite that from which the sound waves are passed through (the rail) have the best detectability is also explained by the formation of the corner reflector.

Flaws which are located in the web and which are reliably detected from the lateral surfaces may not be detected from the running surface. In connection with this, exclusion of any of the operations described by the inspection techniques may result in welding flaws being overlooked.

Welded joints in which flaws were detected upon inspection are repaired. They are, therefore, related to intra-factory waste, and not to finished output waste.

An analysis of inspection data showed that the average yearly percentage of intra-plant waste at various rail welding plants, for any time interval is, as a rule an approximately constant quantity.

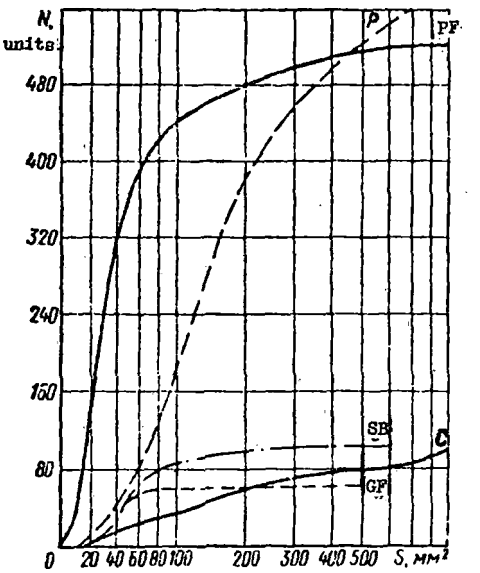

Fig. 238 Toward the detectability of flaws depending on their dimensions

P- porosity; PF- poor fusion; SB- silicate build up
C- crack; GF- gas fissure

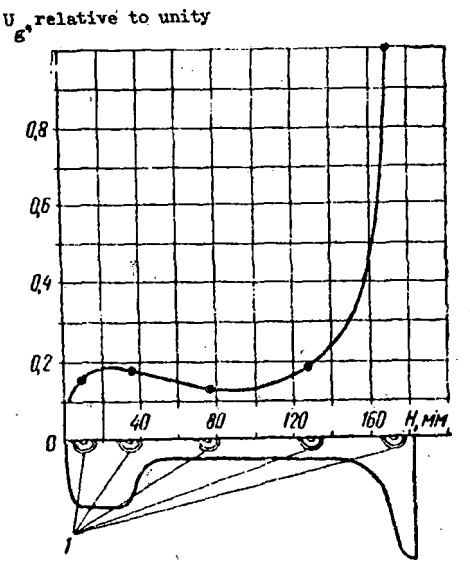

Fig. 239 Dependence of the amplitude U_g of a pulse echo on the depth H at which simulated flaws are situated in a rail: 1 - simulated flaws, manufactured by milling

Therefore, experimental data from ultrasonic rail welded joint inspection may be used to evaluate the stability and the improvement of the technological welding process.

The average yearly intra-plant waste P may be determined by the relationship

$$P = \frac{\Sigma m_i}{\Sigma n_i},$$

where Σm_i is the sum of the welded joints projected for a twelve month period, and

Σn_i is the sum of the welded joints inspected during the same time interval.

In this case, the average value of the waste for a month is

$$p = \frac{m_i}{n_i},$$

where m_i, n_i are the number of welded joints which are rejected and which were inspected during the month, respectively.

Deviations of the intra-plant waste p from the annual yearly value P to one side or the other are equally probable, and constitute a random variable which changes within definite limits. This is conditioned by features in the established technological process which is distinctive for a given plant.

Significant deviations may apparently originate due to irregularities in both the technological welding process and in the ultrasonic inspection process. In this case, the irregularities in welding technology may only result in an increase in waste $(p>P)$ whereas, irregularities in monitoring technology, only to a decrease in the waste which is detected $(p<P)$, inasmuch as false rejection is exluded for practical purposes.

The possibility exists that a situation could occur in which a substantial break-down in welding technology, causing an increase in the number of defective joints, would be accompanied by a break-down in the inspection

organization, during which it is possible that flaws may be overlooked. This is not taken into consideration since the possibility of this occuring is highly insignificant, and is associated with an over-all disorganization of the operation of the plant.

Thus, a significant increase in the amount of waste detected during a month, as compared to the yearly average ($p \gg P$) may be the signal for testing the industrial welding process (preparation of the rails, operation of the welding machine, etc.), whereas a sharp decrease in the waste detected for the month ($p \ll P$) may signal the need for testing how well the inspection methodology is being observed, testing the working capabilities of the flaw detector, and a verification of its parameters.

The fact that a decrease in the waste detected for a month may be the results of improvement in the organization of the manufacturing process as a whole is not excluded.

5. Organization of inspection at the rail welding plant

Rails which have come to a rail welding plant (RWP) for repair are tested over their entire length by external examination and by MRD-52 and URD-63 flaw detectors. Defective sections which are detected are cut out, after which, the individual rail sections, which have been assembled into a single rail, are welded together.

At the beginning and during the course of a shift, reference samples are welded and tested to evaluate the metal structure in the welded joint. After cooling, the reference samples are tested on the hydraulic press according to the diagram shown in Section 1 of this chapter. If the deflection and load at which fracture occured corresponds to the technical specifications, and at the same time, there are no internal flaws, this welded joint is considered to have passed the test. All rail links of the same type are prepared according to a welding routine which is tested in this manner.

After the metal which was extruded during welding has been polished off and the welded joint has been cooled to a temperature of not less than 60° C., each joint is subjected to external examination and ultrasonic inspection. When necessary a welded joint having a temperature of no more than 250° C. may be artificially cooled by feeding an air-water mixture over the welded joint in ac accordance with the instructions approved by the Main Administration of the Line, Ministry of Railroads.

As a rule, ultrasonic monitoring at the rail welding plant is done using a DUK-11IM flaw detector, based on the methodology set forth in Section 2.

Any mineral oil without "mechanical inclusions", or water flowing in a uniform layer over the surface along which the probe is moved may be used as the contacting liquid.

Joints in which flaws are indicated by the ultrasonic inspection data are rejected, and they are marked with paint on the running surface of the rail in the joint zone. The (flaw detector) operator informs the head of the shop or the shift foreman concerning the detection of a flaw in a welded joint. The monitoring results are recorded in a log and on inspection charts, the form of which has been approved by the Main Administration of the Line, Ministry of Railroads.

Ultrasonic flaw detection at the RWP is permitted only at a specially equipped work site at a temperature no lower than +10° C. At the operator's work site there are standards for determining and testing the basic ultrasonic monitoring parameters; rail samples with actual flaws in the head, web, and base; a scraper and brush for removing scale and rust from the rail surface in the monitoring zone, a millimeter scale for measuring the nominal dimensions of the flaws, etc.

The flaw detector is mounted away from the joint being monitored at a distance which permits the operator to use the instrument's controls freely

while simultaneously moving the probe. A panel for supplying a 220 v. voltage from the regulator, 36 v. for the portable lamp, and wires from the grounding circuit should be mounted close to the instrument.

The condition of the flaw detector apparatus is tested at least once a month by a representative from the track maintenance flaw detector laboratory of the appropriate rail line and the head of the welding shop. If, while the flaw detector is in use, it is discovered that the quality of its work is declining, the flaw detector is examined ahead of schedule. Results of the examination, together with an indication of the work done to eliminate the detected defects, are entered in a special log book.

Other conditions being equal, the reliability of ultrasonic flaw detection depends in many ways on the qualifications of the operator. Therefore, only persons who have passed special theoretical training and practical study in accordance with the program approved by the Ministry of Railroads, and who have received a diploma conferring the right to work in such a position, are permitted to work at ultrasonic flaw detection of welded rail joints.

Operators who have received their diploma conferring the right to work as inspectors and who work regularly at ultrasonic inspection of welded rail joints are subsequently examined by a qualifications commission at least once a year. When the operator successfully passes the examinations, the certification to conduct inspection is extended. In case an operator has not taken the examinations, or has received an unsatisfactory grade on the exams, he is deprived of the right to conduct inspection until such time as he passes the examination.

Operators having a break of more than six months in their work with ultrasonic flaw detection are denied the right to conduct inspections until they have passed the examinations.

The organization of the qualifications commission and supervision of their work is entrusted to the head of the RWP.

The following are members of the qualifications commission:

a) the chief engineer of the RWP

b) the chief or the senior foreman of the welding shop

c) a flaw detection engineer from track maintenance or the head of the railroad flaw detection laboratory.

The accuracy of the operator's work is tested by comparing the data from ultrasonic inspection of samples specially welded by improper welding techniques with data from the examination of the fracture and, when neccessary, from metallographic analysis.

The indicated requirements for qualifying are presented to all operators carrying out ultrasonic inspection of welded joints both during welding at the RWP as well as during secondary inspection of welded joints under usage conditions.

6. Organization of inspection when rails are welded in the field

Welded joints are inspected on the line both when the rails are welded, using mobile rail welders, as well as when the welded rail has been in use on the line.

Rails which are welded in the field are inspected before welding, using various flaw detection equipment, along their whole length, whereas, after welding, only the welded joint zone is inspected, using an ultrasonic flaw detector. In this case, as practice has shown, the DUK-13IM with power supply from storage batteries is most expediently used.

Before the sound waves are passed through the welded joint, the rail surface is cleaned of rust, scale, sand and residual oil (on rails which are in use), and are covered with mineral oil around the perimeter within 100-120 mm to either side of the joint, excluding the bottom of the base.

After the basic monitoring parameters have been checked and the flaw detector with the appropriate probe has been tuned to the given work mode, the welded joint has sound waves passed through it according to the methodology set forth in Section 2 of this chapter.

Welded joints are monitored in the field by a maintenance engineer and his assistant, both of whom have received special theoretical and practical training. Based on the experiences of the Belorussian line, it is expedient to entrust the job of cleaning the welded joint surfaces to a worker with lower qualifications.

The ultrasonic inspection of welded joints may be conducted when the temperature of the surrounding air is not lower than +5°C. At lower temperatures, it is possible to overlook flaws due to deterioration of the working conditions. Rails which have been welded in the field may have sound waves passed through them only after the metal in the welded zone has cooled to the temperature indicated in Section 5 of this chapter.

The welded joints which are rejected because of ultrasonic inspection are cut out and the rails are again welded. USFD* and fracture examination data are recorded in documents similar to the documents which are filled out at the RWP**.

All rails in use, in whose welded joints flaws are detected, are considered to be highly defective and are immediately replaced. The results of the ultrasonic inspection are recorded in a service log.

The markings for such rails and the order for permitting trains to pass over them are determined in accordance with instructions set forth in the technical reference materials (RTM) 32/TsP-3-66 "Characteristics of Defective and Highly Defective Rails," and with instructions for providing safety of train movement when track repair is in progress.

---

* Ultrasonic flaw detection -- Tr.
** Rail welding plant -- Tr.

Chapter XII -- Organization of Co-ordinated Use of Rail Flaw Detectors

1. Planning and organization of the work of flaw detectors

At the present time, the propagation speed and danger of various flaw types in rails are still unknown. Because of this, the timely detection of defective rails, with the cracks still in the earliest developmental stages, and their removal from the line, is the basic goal of the rail flaw detection system. For this purpose, the track facilities of the railroad lines are equipped with a large number of rail flaw detectors of various types. With the aid of one or another type of flaw detector, it is not possible to detect all types of flaws in rails. It is possible, however to detect a specific group or variety of these flaws.

More complete and reliable detection of all flaws in rails which are dangerous for train movement may be assured with the co-ordinated use of all types of rail flaw detectors. The comprehensive use of flaw detectors in outlying districts and track divisions, and, as a whole, along the line, lies in rationally planning the operation of various flaw detectors along the same sector of track. The initial data for rational planning of flaw detector operation should originate from an analysis of the failure of defective rails in outlying districts, track divisions, and main lines in the winter, spring, summer, and fall periods.

While analyzing the rail failures, special attention is directed toward determining the frequency of repeated rail failure from each flaw type on the sector of track being set out for inspection. Depending on which flaw types originate in the rails in a given sector, the preferential use of one or another type of flaw detector is determined. If, for example, on a sector of track, an overwhelming number of rail fractures occurred due to the presence of transverse fatigue cracks (flaw types 20.1-2 or 21.1-2) it is obvious that it is most often necessary to test this sector using

UZD-NIIM-6M and MRD flaw detectors and flaw detector cars. These rails may be tested less frequently using the other types of flaw detectors (in case other flaw types might appear in them.)

On track sectors where the rails break down primarily due to cracks around the bolt holes, horizontal and vertical separations in the head, longitudinal cracks near the upper and lower fillet, etc., ultrasonic flaw detectors and flaw detectors using a variable magnetic field are used. These rails are tested less frequently using flaw detectors of different types (in the event that internal transverse fatigue cracks might appear in them).

When planning flaw detector operations, it is necessary to take into consideration the possible productivity of each type of flaw detector when testing one or another section of track.

The productivity of magnetic flaw detectors depends on the state of the rails on the section of track being tested. All types of non-hazardous damage to the running surface of the rail head, e.g. metal flow, engine burns, dents, burrs, etc., make the operation of flaw detectors significantly more difficult. Magnetic flaw detectors frequently activate at these types of damage as they would over dangerous flaws. This results in the operator spending much time examining a large number of sites noted by the flaw detector. On rails without these types of damage, the flaw detectors primarily react only to flaws and the operator wastes less time examining the rails.

The productivity of ultrasonic flaw detectors also depends on the cleanliness of the running surface of the rail. The presence of residual oils, sand, and other contaminants which are capable of breaking the acoustical contact on the running surface make operation of ultrasonic flaw detectors more difficult. In this case, the operator wastes considerable time cleaning the rails and making secondary passes over one and the same spot in the rail being inspected. Therefore, the daily norm for the flaw detector's working

distance may be different, depending on the state of the rails on the sector being tested. It is set by the operator set-up specialist and the track division supervisor.

Compilation of a flaw detector work chart is a responsible part of organizing rail flaw detection on track divisions. When the chart is being compiled, the state of the rails, the nature of the damage and the possible productivity of flaw detectors on the track sector being tested are considered first of all. A correctly compiled schedule determines the periodicity with which rails should be tested using the various types of flaw detectors. With this schedule, each dangerous defective rail will be detected on time and removed from the line.

Not only the number of kilometers which are to be tested, but also the high quality flaw detection for each rail on the sector being inspected are the basic indicators by which the schedule is drawn up. Inasmuch as removable rail flaw detectors are assigned to track divisions, their work schedule is compiled monthly by an engineer of the track division and approved by the head of the division.

Depending on the conditions under which approaching trains are visible, sections of the line on which protection of the flaw detector by signalmen is required are anticipated by the schedule. Places where the flaw detector is to be stored and where the operating personnel will rest upon termination of the work are also forseen in the schedule.

The flaw detector car's work schedule is compiled by a senior track maintenance engineer (flaw detection), and approved by the head of track maintenance. First of all, track sectors with a high freight traffic density where work with removable flaw detectors is made more difficult due to the large number of passing trains, are included in the flaw detector car's work schedule. Time for interpreting the film, examination of the rails noted on

the line, locomotive crew changes, "windows" in the train traffic schedule and other operations following from the conditions of use on the track sector to be monitored are foreseen by the work schedule.

The productivity of the flaw detector car operation is determined by the working speed of the car, taking into consideration all of the conditions enumerated above.

2. Flaw detector work sequence between stations

Inspection quality for rails on the line depends to a significant extent on the qualifications of the flaw detector operator-engineer. The operator should not only know the equipment and the flaw detector work sequence well, but he should also know the condition of the track for the sector of the line which is being tested. The evaluation of the flaw detector readings and formulation of conclusions concerning the danger of a detected rail flaw is facilitated substantially if the flaw detector operator has the necessary information about the rails: the rail type, the manufacturing plant, the time the rails were laid, a kilometer-by-kilometer record of rail failure, types of flaws most frequently encountered on the given sector; the melt numbers for defective rails which have failed previously; and the causes for the development of these flaws. The operator obtains this information at the track division office and goes over it with the railroad foreman in each district.

Working with the flaw detector between stations is done away from repair and recharging bases and, frequently, under inclement weather conditions. Therefore, the question of preparing the flaw detector for operation on the line is very important. It is necessary, first of all, to test the power supply sources carefully. Should the power supply sources be in an unsatisfactory state, it will show up on the flaw detector work mode, which may result in defective rails being missed. A careful examination of all

current-carrying wires and cables, the probe assembly plugs, fasteners, etc. is no less important

All noted defects must be eliminated before going out onto the line between stations. After this, it is necessary to test the flaw detector sensitivity on rail samples which have flaws. Having made certain that the flaw detector is in good working order and that its sensitivity to flaws is satisfactory, the operator then goes out onto the line.

The flaw detector operator should have with him a traffic schedule and, before setting out onto the line from the station, he should receive information from the assistant station master concerning actual train movement. In addition, the operator should have hand flags, pennants, and an air-operated horn for giving a danger signal or, if necessary, for stopping a train.

The operator works with the removable flaw detectors. The operator's assistant watches for the approach of trains, helps when the flaw detector cart is removed from the track, and during examination of the rails. In addition to the operator and his assistant, the railroad foreman or the work gang foreman within the bounds of his own district, accompanies the flaw detector.

The conventional symbols are marked on the web of any detected defective rail in light-colored oil paint. Then the rail marks stamped into the rail are examined and the rail type, plant mark, year the rail was rolled and the melt number are recorded in the work log. In addition, a detailed description of the detected flaw is given. The railroad foreman or work gang foreman acknowledges that he has been informed of the detection of a flaw by signing the work log, and takes measures to replace the defective rail.

When a highly defective rail which threatens the safety of train movement is detected, it is necessary to protect this site immediately according to the signaling plan for an unexpectedly occuring obstruction. This is done according to the instructions for signaling on railroad lines on the USSR. A call is made for the track crew to replace the rail.

At the end of the working day, the flaw detector operator conveys the information about detected defective rails, for each kilometer of the line, to the track division dispatcher either by telephone or in person.

The railroad foreman informs the track division office and the flaw detector operator of the date at which defective rails were replaced. The flaw detector operator makes a note to this effect in his work log, as given below.

In the winter, work is done after the snow plow has passed. During snowfalls or rain, work on the line with the flaw detector ceases.

There are operator-set-up-specialists, each of whom service the flaw detectors for three or four track divisions, for periodic testing of the flaw detector's working properties and their technical state. The operator-set-up specialists are at the disposal of the track maintenance (section) and they go out to the track divisions assigned to them according to an established schedule. In the case of a damaged flaw detector, the operator-set-up specialist goes out to this track division immediately upon call or on the instructions of the senior track maintenance engineer.

The operator-set-up specialist repairs and adjusts the flaw detector together with the flaw detector operator directly out on the line between stations or in the track division repair shops. If it is impossible make repairs in the division shops, the flaw detector is sent to the railroad flaw detection laboratories.

number	date, month, year	span	kilometer	hundred meter mark	link	track number	right or left rail	rail type	plant mark	year rolled	nature of flaw from internal inspection with indication of flaw number	signature of track foreman signifying notification	date rail replaced
1	2	3	4	5	6	7	8	9	10	11	12	13	14

Working log of the.....flaw detector track division
(filled in by the flaw detector operator)

3. Joint operation of the flaw detector car and removable carts

It is necessary to search out flaws which are dangerous to train movement in rails from among the numerous non-hazardous types of damage to the metal on the running surface of the rail. These non-hazardous types of damage occur in the form of dents, pitting, flaking, scabs, etc. In addition, metal on the running surface may have a localized structural non-homogeniety caused by work hardening or by the heat effect from slippage of the wheels of rolling stock. The enumerated types of non-hazardous rail damage create a specific interference level which complicates operations, particularly with magnetic flaw detector cars.

In the flaw detector cars, interpretation of the emf pulse recordings induced in the probes when passing over flaws is based on the fact that pulses from dangerous flaws are distinguished by a small number of characteristic forms, whereas pulses from non-hazardous flaws have a relatively large diversity of forms corresponding to the large number of non-hazardous damage

types found on the running surface of the rail head.

The shape, phase and amplitude of the electromotive force pulses induced in the probe above a flaw are usually taken into consideration when interpreting the film from the flaw detector car. Based on these characteristics, the worker who is interpreting the recording film separates the pulses caused by dangerous flaws from among the many pulses on the film which relate to non-hazardous damage to the rail metal. However, on rails where the running surface is damaged by pitted places, engine burns, scabs, and separations, the shape and amplitude of the electromotive force pulses above dangerous flaws may be distorted. These are labeled doubtful pulses.

Cases are frequent where the shape, phase and amplitude of the pulse above a non-hazardous point of damage, e.g. above a transverse shatter crack in metal flow which has separated off, are similar in shape, phase and amplitude to a pulse above a dangerous flaw, e.g. above a transverse fatigue crack in the rail head.

It is difficult, and sometimes impossible, to distinguish the readings taken above a dangerous flaw from those taken above points of non-hazardous metal damage on the running surface of the rail head.

When interpreting such a complex recording, it is possible to overlook dangerous flaws or to remove rails with non-hazardous flaws from the line. At the same time, given the proper joint organization of a flaw detector car with removable flaw detectors, instances in which dangerous rail flaws are overlooked or when rails containing no dangerous flaws are removed from the line may be eliminated for practical purposes. For this, after the flaw detector car has passed over a specific sector on the line, the recording film is interpreted in the normal sequence established by the instructions. The interpretations are recorded in two lists. Those dangerous rail flaws from which the emf pulses leave no doubt are entered in the first list.

The first list is handed over to a representative of the track division office. Defective rails which are entered on this list are subject to immediate replacement.

Defective rails from which emf pulses cause some doubt ("dubious pulses") are entered in the second list. The second list is also furnished to the representative of the track division office, who then gives a copy of this list of dubiously defective rails noted by the flaw detector car to each operator of a removable flaw detector for the track sector serviced by that operator. Each operator working with a removable flaw detector, in addition to his usual work doing routine tests of the rails on the track sector assigned to him, makes secondary inspection of all sites of dubiously defective rails noted by the flaw detector car and draws a final conclusion concerning their nature and the danger of the flaws in these rails. Secondary inspection for detecting transverse fatigue cracks in dubiously defective rails is carried out using the MRD-52 or MRD-66 flaw detectors with the fillet probes. The DUK-13IM or URD-63 flaw detectors are used to detect horizontal and vertical separations in the dubiously defective rails.

The results of the secondary inspection of dubiously defective rails noted by the flaw detector car are submitted to the track division office and to the flaw detector car workers. Secondary inspection of dubiously defective rails permits fatigue cracks to be detected in an early stage of development and excludes the possibility of overlooking those which have already developed.

When the use of flaw detector cars and removable flaw detectors are thus coordinated, the reliability and the quality of rail inspection to detect flaws in rails which are dangerous to the passage of trains, as well as the productivity of the flaw detector car operations, is increased.

Chapter XIII -- Organization of Flaw Detector Repair

1. Railroad laboratories and section flaw detector repair shops

Contemporary magnetic and ultrasonic flaw detectors contain complex radiotechnical equipment requiring systematic technical inspection and preventive testing and maintenance. To accomplish this, there are permanent and portable flaw detector laboratories for each rail line. There are shops for routine flaw detector repair for each track division.

The permanent railroad laboratories are equipped with inspection and measuring equipment, are outfitted with machine tools, and have a permanent staff of workers. Major repair of all types of flaw detectors used in the track, locomotive, and car facilities is done in the railroad laboratories.

The portable flaw detector laboratories (laboratory cars) are basically equipped with inspection and measuring equipment, have a permanent working staff, and are intended for periodical testing of the technical condition of the rail line flaw detectors immediately at the track division (facilities).

Workers in the flaw detection laboratory car instruct flaw detector operators on the line, generalize and introduce advanced operating methods, and test and study new types and designs for flaw detection under usage conditions. When necessary, the laboratory cars carry out the repair, set-up and adjustment of flaw detectors immediately at the track division (facilities). The section repair shops are not as completely equipped with measuring devices and machine tool equipment. They have no permanent work staff. In these repair shops, the flaw detector operators and operator-set-up specialists carry out routine flaw repair through their own efforts.

The railroad laboratory premises usually consist of three rooms. The machine tool equipment (a small drill press, a milling machine, a lathe, and a coiling machine), a work bench with a vice, and a table for dissembling and installing the apparatus is set up in one of them. Rail samples containing

artificial and natural flaws are also located here. In this room, the mechanical equipment for the flaw detector is repaired, the parts necessary for repair are stocked, and the electrical wiring is done. The flaw detector is also tested here after repair. The testing bench (Fig. 240) with the inspecting and measuring devices is located in another room.

A panel with measuring instruments and sockets, to which voltages from power supply sources are fed, are mounted on the test bench.

The generator amplifier devices for all types of flaw detectors are tuned and adjusted at this bench. This type of organization of the work site makes it possible to work with the equipment open, which provides access to all of the parts.

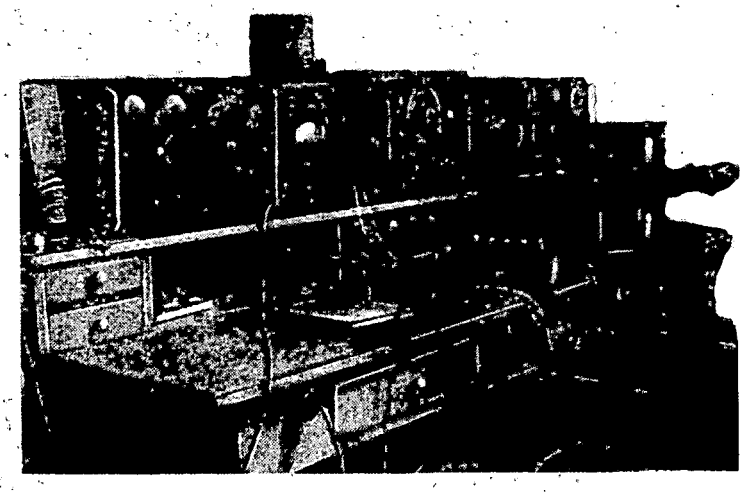

Fig. 240 The test bench in the railroad flaw detection laboratory

The power supply sources (storage and dry cells) and a rectifier device for charging the storage batteries are in the third room. Most often a VSA-5 rectifier is used to these ends.

A technical data sheet for each flaw detector is kept in the railroad laboratory. All of the basic technical data are entered on this work sheet.

When repair is terminated on a flaw detector, the entire list of repairs which were made is recorded on the data sheet. If certain parts (resistors, capacitors, inductances, etc.) were replaced, these changes are also entered on the data sheet. Keeping this type of data sheet up to date facilitates the work of the repairman and the operator-set-up man when searching for one type of damage or another. It permits the nature of the most frequently encountered types of damage to the given flaw detector to be discerned, as well as regulating control over the flaw detector upkeep.

Fig. 241 A flaw detector laboratory car

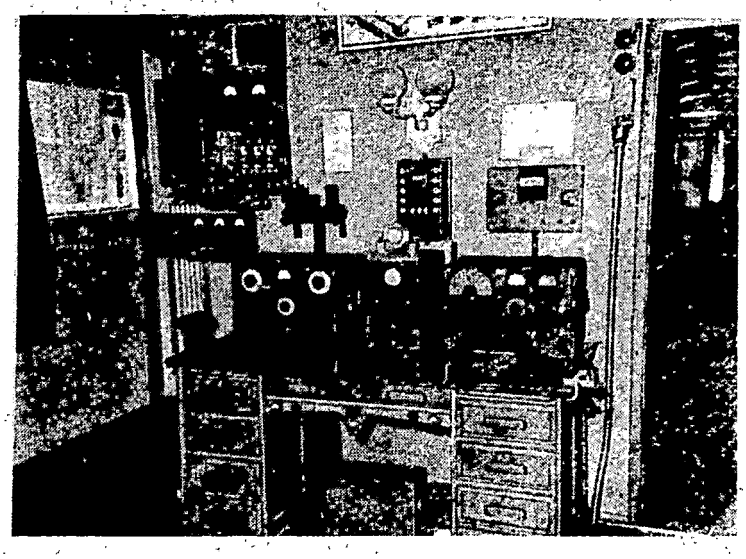

Fig. 242 The laboratory car equipment room

Section repair shops are set up in one or two rooms. In these repair shops, there are a work bench with vice, means for carrying out electrical wiring operations, an AVO-5 meter or a TT-1 tester, a VSA-5 rectifier, and an instrument for carrying out routine and preventive maintenance on the flaw detectors, as well as samples of rail with flaws. Flaw detectors are kept in the repair shops.

The portable laboratories are set up in standard passenger cars (Fig. 241).

The laboratory cars are equipped with approximately the same inspection and measuring equipment as are the railroad laboratories. The primary power supply sources in the laboratory car are the car's dynamo and a 400 amp-hour storage battery. There are rotating converters to supply variable current. In addition, there is a transformer for power supply to the laboratory equipment from the variable current network when standing at the station. There is an equipment room in the car (Fig. 242) where the inspection and measuring equipment and the switching gear (switchboards, measuring devices, etc.) are situated. The remaining part of the car is intended as a resting place for the laboratory workers and conductors.

The laboratory cars are registered to one of the track division offices. The track maintenance supervisor sets the crew, depending on the number of flaw detectors working on the line.

The laboratory car operation is carried out according to a plan approved by the track maintenace foreman.

2. Test sidings

Test sidings are intended for the tuning and adjustment of flaw detectors after they have been repaired, and for testing the sensitivity and over-all working order before they go out on to the line. There are test sidings at all railroad laboratories and track division repair shops.

Sections of rails with various types of flaws are laid in the test sidings for a length of 10-15 m. Rail samples for the test sidings are selected from among the defective rails removed from the line. The length of the rail laid in the siding is approximately 3 m. Each segment contains a definite flaw type.

Samples of rails containing the following flaw types are laid in the test siding for tuning and testing the RDP-56 flaw detectors: transverse cracks in the rail head which emerge on the lateral surface of the head (flaw type 21.2), transverse cracks in the base which emerge in the web up to 2/3 of its height (flaw type 65.2), vertical (flaw type 30V.2) and horizontal (flaw type30G.2) separations which emerge on the surface of the rail head, and through transverse cracks in the upper fillet (flaw type 52.2) not less than 200 mm long.

Rail samples with transverse fatigue cracks in the rail head (flaw types 20.1-2 or 21.1-2) are laid in the siding for testing and tuning MRD type flaw detectors. Before the rail samples are laid in the siding, the flaws in them are calibrated according to the methodology presented in Chapter III.

Rail samples with cracks about the bolt holes in the joint area of the rail (flaw type 53.1), with internal vertical and horizontal separations in the rail head and web (flaw types 50.1-2; 52.1-2; 20.1-2; 21.1-2; 30V.1-2 and 30G.1-2), and with hairline cracks (flaw type 60.2) in the base at a depth of not less than 3 mm and which are situated within the projection of the thickness of the web are laid for tuning and testing the ultrasonic URD-58, URD-63 and UZD-NIIM-6M flaw detectors. Besides this, artificial reference flaws are made in the rail samples laid in the test siding for tuning the ultrasonic flaw detectors.

The methodology for preparing artificial reference flaws is set forth in Chapters VII and X.

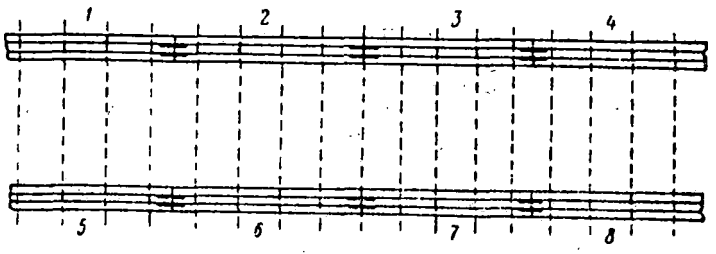

Fig. 243 Rough diagram of a test siding

Rail samples of those heavy rail types which are used on a given line or track division are laid in the test siding.

The rail samples are joined using normal cover plates with the normal number of bolts. A rough diagram of a test siding is given in Fig. 243.

The test sidings are laid on normal crossties with base plates and spikes. The distance between flaws should be not less than 0.5 m so that signals from neighboring flaws do not interfere with each other.

Three-track test sidings (Fig. 244) are employed on some railroad lines. This siding consists of three rails, the center rail of which has a transverse fatigue crack in the rail head which is situated nearer to one side of the head (flaw type 21.2). The three-track test siding permits all four probes of the MRD flaw detectors to be tested individually. This is impossible on a two-track siding. The testing order and the direction which the flaw detector travels when passing over the siding are shown in Fig. 244. Here probes 1 and 2 on the left side are inspected on the first and second passes, and on the third and fourth passes, probes 3 and 4 on the right side are inspected.

A data sheet with the detailed description of all types of flaws in the test rail samples, as well as a diagram showing where the rail samples were laid and the exact location of each flaw is compiled at each test siding.

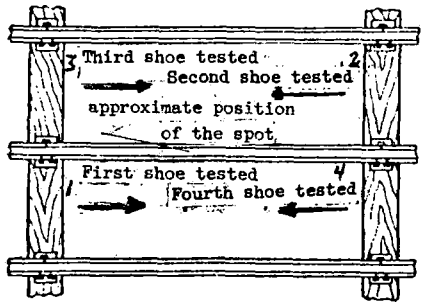

Fig. 244 A three-track test siding

A data sheet with the detailed description of all types of flaws in the test rail samples, as well as a diagram showing where the rail samples were laid and the exact location of each flaw is compiled at each test siding.

The test rail samples laid in the test siding should be protected from blows from hard objects, rusting, and other types of damage, particularly the surface of the rail head. The indicated types of damage to the metal of the rail head surface increase the interference level, which makes the working conditions for tuning the flaw detectors more complex.

3. Recharging points

Both the railroad and track division repair shops are equipped with recharging devices to recharge the flaw detector storage batteries.

The basic element of the recharging device is the VSA-5 selenium rectifier (Fig. 245).

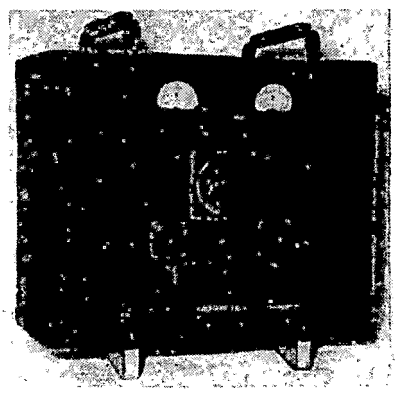

Fig. 245 The VSA-5 selenium rectifier

Conversion of the network alternating current into direct current is accomplished by the selenium rectifying elements. These are iron discs covered on one side with a thin layer of selenium. For practical purposes, this type of element passes current in one direction, from the iron disc to the selenium layer (the cathode layer). The current passing in the opposite direction (the reverse current) is insignificant, but it begins to increase sharply when the voltage on the elements increases beyond 18 v. To obtain a higher rectified voltage, the rectifying elements are connected in series. The size of the rectifying current is determined by the area of the elements and the cooling conditions. Elements 100 mm in diameter, which are used in the VSA-5 rectifiers, permit a load of up to 4 amp. To obtain a higher value of the rectifier current, the rectifier elements are connected in parallel.

The selenium rectifier elements are assembled into the so-called "stack" on an insulated rod with contact discs being placed between the elements, and with the spacing washers which create the clearances necessary for proper cooling.

The VSA-5 rectifier (Fig. 246) consists of a step-down transformer Ts, two selenium stacks C1 and C2 connected according to a bridge circuit, an adjusting autotransformer Tr, a knife switch P, a switch S, a 150-volt voltmeter, a 20-amp ammeter, and two 20-amp melt-type safety fuses.

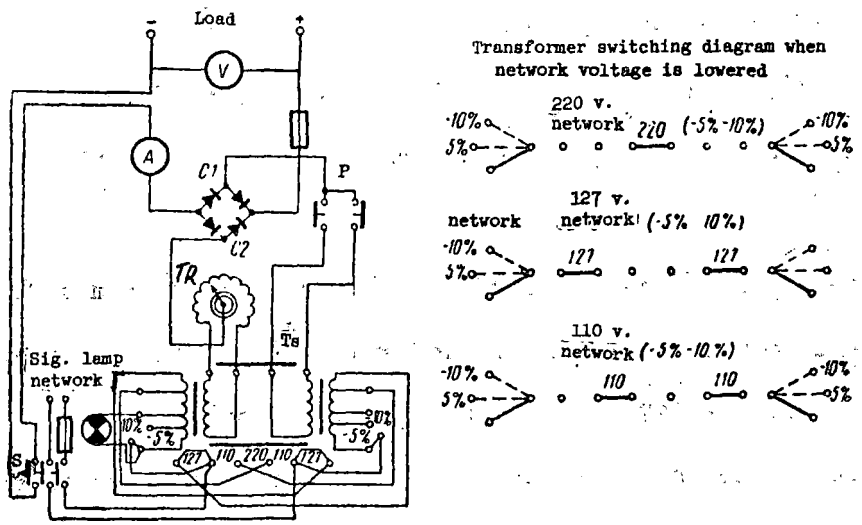

Fig. 246. Circuit of the VSA-5 rectifier.

The secondary winding of the step-down transformer Ts is divided into two parts. Voltage from one part of the transformer's secondary winding is fed to the selenium stacks through the adjusting auto transformer Tr and the knife switch (the "first degree" position on the instrument panel). In this case, the rectifier provides a rectified voltage of from 0-27 v. When the knife switch P is set in the "second degree" position, both sides of the secondary winding of transformer Ts are connected in series, and the rectifier provides a rectified voltage of from 25-27 to 64 v. with smooth adjustment.

The maximum permissible load should not exceed 12 v. Overloading the selenium stacks leads to the elements overheating and being damaged. Heating the elements above 75°C. is not permitted.

When the rectifier is switched on after long breaks in operation, crackling and isolated sparking may be observed on the surface of the selenium elements. This is not a sign of a flaw in the rectifier. It is explained by the breakdown of the selenium elements. In this case, it is necessary to reform the selenium elements by switching on the rectifier with no load, with a gradual increase in the rectified voltage from 0-64 v. before switching on the rectifier under load. The voltage is increased in four steps and is held at each step for from 5-10 minutes.

If the rectifier is set in operation in a warm room after a lengthy period in freezing weather, it is necessary to dry it off well before switching it on.

The VSA-5 rectifier is set at the factory for working from a 220-volt alternating current network. When it is necessary to connect the rectifier into a network with 110 or 127 v. current, the upper cover of the rectifier is removed and the connecting links on the transformer panel are set in the position corresponding to this voltage (cf. the switching diagram in Fig. 246).

"-5%" and "-10%" terminals were installed in the step-down transformer Ts in case the line voltage should decrease. The connecting links are switched on the right and left sides simultaneously and in pairs.

After a break in operation or a lengthy storage period, the rectifier is reformed before it is switched on, then the adjustment limits are tested. For this, the knife switch P is set in the "first degree" position, and the adjustment limits of the rectifier voltage are tested by turning the knob. Further, having placed the knife switch in the "second degree" position, the adjustment limits for the rectified voltage at the second degree are tested. After the indicated rectifier tests, it is turned on under load.

4. Storage battery service and care

General information on alkaline batteries. Alkaline storage batteries of two types are used as the power supply source in removable rail flaw detectors: nickle-cadmium batteries, designated by the letters KN and nickle-iron batteries, designated by the letters ZhN. Alkaline batteries with a capacity below 10 amp. hour are intended for supplying power to the plate circuits of the amplifier tubes. Therefore, the letter A is added before their designation, e.g. AZhN or AKN. Storage batteries rated at 10 amp. hour or more are intended for supplying power to the filament* circuits and, therefore, have the letter N in front, e.g. NZhN or NKN. The number following the letter designation indicates the capacity of the battery, e.g. NKN-45 (a nickle-cadmium filament battery rated at 45 amp. hr). The primary data concerning alkaline storage batteries are presented in Table 19.

The nickle-cadmium and nickle-iron batteries have the same electrical specifications and dimensions; they are distinguished only by their weight.

*Tr. note -- Russian "nakal' nye tsepi"

ZhN-22	22	5.5	2.75	32	105	125	200	213	0.27	1.41	1.73
ZhN-45	45	11.25	5.60	53	104	125	200	213	0.45	2.31	2.85
ZhN-60	60	15	7.50	45	128	148	330	349	0.75	3.88	4.78
ZhN-100	100	25	12.50	70	128	148	330	349	1.2	5.4	6.8

Table 19

Battery type	Rated capacity, amp·hr	Rated charging current for 7-hr. charge, amp	Rated discharge current for 8-hr. discharge, amp	Dimensions, mm					Electrolyte capacity, l.	Weight, kg	
				Thickness	Width		Height			Without electrolyte	With electrolyte
					Without pins	With pins	Without caps	With caps			
Nickel-cadmium storage batteries											
ANK-2.25	2.25	0.56	0.28	20	45	65	120	132	0.042	0.28	0.33
NKN-10	10	2.5	1.25	31	80	100	110	132	0.12	0.60	0.74
NKN-22	22	5.5	2.75	32	105	125	200	213	0.270	1.35	1.67
NKN-45	45	11.25	5.65	53	105	125	200	213	0.45	2.18	2.72
NKN-60	60	15	7.50	45	128	148	330	349	0.75	3.7	4.6
NKN-100	100	25	12.50	70	128	148	330	349	1.2	5.1	6.5
Nickel-iron storage batteries											

Potassium hydroxide with a density of 1.19-1.21 (23-25° Beaumé) with an addition of 20 g/l of lithium monohydrate serves as the electrolyte for the alkaline batteries. In the absence of potassium hydroxide, a solution of caustic soda with a density of 1.17-1.19 (21-23 °Be), with an addition of 10 g/l of lithium monohydrate may serve as the electrolyte. Distilled water is used in preparing the electrolyte. It is possible to operate using this electrolyte at temperatures of from -15 to +35° C. At temperatures below -15°C., the storage battery should operate on a potassium hydroxide solution having an increased density of 1.26-1.28 (30-32 °Be).

When replacing the normal density electrolyte with an electrolyte of higher density, the following must be kept in mind:

1) Sto age batteries which were operating on a solution made of potassium hydroxide with the normal density before changing over to the increased density caustic potash electrolyte are filled with the increased density caustic potash solution without any type of preparations

2) Storage batteries which were operating on caustic soda before converting to the increased density electrolyte are first filled (for 2-3 charge-discharge cycles) with a potassium hydroxide solution with a density of 1.19, after which the electrolyte is changed for the increased density caustic potash solution

3) The electrolyte which is poured out of the storage batteries should be kept in a hermetically sealed container; when necessary it may be re-used.

The old electrolyte is replaced with a new solution every one hundred cycles, but no less than once a year. However, if the rating of the storage battery declines noticeably, the electrolyte must be changed before the indicated period expires.

Before the electrolyte is replaced, the battery is discharged using a standard 8-hour discharge current (cf. Table 19) down to one volt/element.

The old electrolyte is pured out, shaking the bottle vigorously to remove dirt from the jar. After the electrolyte has been removed, the storage batteries are flushed out using distilled water. The flushed batteries are filled immediately with electrolyte. Storage batteries flushed with distilled water must not be left without electrolyte since, otherwise, corrosion is unavoidable.

Putting new batteries or batteries which have been without electrolyte in operation. The dust and salts are removed from the surface of the battery containers and battery storage boxes using a clean rag, the correctness of the connection between the elements in the battery is tested, and the inter-element connection nuts are tightened snugly. Then the storage batteries are filled with electrolyte. Two hours after filling, the voltage is checked on each storage battery. Should there be no voltage on any battery, it is left for another ten hours, after which it is again tested. If no voltage appears on the battery terminals after standing for twelve hours, the battery is considered unservicable and removed from the (battery) bank.

Electrolyte is poured into the batteries through a clean glass, ebonite, or porcelain funnel since metallic funnels may cause short-circuiting inside the battery. The electrolyte should not be poured onto the tops of the battery or the battery box since this increases the self-discharge of the battery.

The electrolyte level, which should be no less than 5 and no more than 12 mm above the battery plates, is checked before charging. The electrolyte level should be carefully observed to prevent the electrolyte from bubbling out of the battery during charging. The electrolyte level is measured using a glass tube 5-6 mm in diameter with markings at 5 and 12 mm. The glass tube is inserted into the battery to the plates, then, with the finger firmly covering the upper end, it is removed. The height of the electrolyte in the

tube will show the electrolyte level above the plates.

A rubber bulb is used to reduce or increase the electrolyte level in the battery.

After the normal electrolyte level has been established, the storage batteries are connected for charging. For this, the positive pole of the battery is connected to the positive pole of the current source, and the negative to negative. For connecting storage batteries of the same type for charging, they are hooked up in series.

The number of batteries which may be connected in series is determined by the voltage of the current source, calculating 1.8-1.9 v. per element, or, when charging in cold weather, calculating 2.0-2.1 v. per element.

The batteries are charged using a normal charging current for 12 hours and discharged, using a normal discharge current, for 4 hours. Two or three cycles (charging-discharging) are conducted following the indicated sequence. After this, the storage batteries may be set into operation. Occasionally, the storage batteries have a temporary decrease in their capacity, due to a lengthy period of inactivity. This requires an auxiliary aging charge before the battery is put into use. In these cases, the battery is given a normal charge and then discharged using a normal current for eight hours, paying no attention to the batteries' voltage. Initially, discharge is carried out without an external current on the rheostat, until such time as it is possible to maintain a constant force for the discharge current. The normal discharge current strength is maintained using an external current source for deeper discharge. For this, the storage battery is connected to the rectifier positive-to-negative and negative-to-positive. The current strength is adjusted by the rectifier rheostat. After this type of deep discharge, a charge is given using a normal current for sixteen hours, after which the battery is placed in service.

Subsequent charges are given for seven hours using a normal charging current.

Liquid parafin is pured into each storage battery to protect the electrolyte from absorbing carbonic acid from the air. Eight cc. of liquid parafin are poured into one NKN-45 or ZhN-45 element. The same quantity of kerosene may be used when there is no liquid parafin on hand.

Storage batteries which have been stored for up to one year with the electrolyte are put into service without changing the electrolyte. The electrolyte is changed if the storage period is longer. The electrolyte is also changed when the storage batteries have a reduced capacity when in use.

Charging storage batteries while in use. Batteries and storage batteries are charged using the normal charging sequence current. The charge lasts seven hours. It is necessary to keep in mind that regular, incomplete charging ruins the batteries.

In the case of extreme necessity, an accelerated charge is permitted according to the following schedule: 2.5 hr. at a current twice that of the normal current, and 2 hr. at normal current.

Every ten to twelve cycles or once a month during periods of irregular use, an intensified charge is given for six hours using the normal current and six hours at a current equal to half the normal current. The storage batteries are charged with the battery box lid open and with the valve plugs unscrewed. Charging storage batteries with the plugs screwed in may lead to significant bulging of the battery walls.

When batteries are charged with the plugs unscrewed, the electrolyte level is tested after each charge, and, if necessary, electrolyte is added to the full mark. The electrolyte which is bubbled out during charging is gathered using a rubber bulb, and the battery tops are wiped off using a dry rag.

During the battery charging period, it is absolutely forbidden to approach them with fire since the gases which are given off during the charging process may ignite and cause a dangerous explosion.

Appendix A

Afanas'ev, Yu. V. Ferroprobes. Leningrad: "Energiya," 1969. (Russian)

Gerasimov, S.M., I.N. Migulin, V.N. Yakovlev. Semiconductor Amplifier and Oscillator Design. Kiev: Ukrtekhizdat, 1963. (Russian)

Grejl', E.A. "Evaluation of Electro-contact (Flash-butt) Rail Welding Quality Based on the Results of an Examination of Fracture Surfaces." Works TsNII MPS (Central Scientific Research Institute, Ministry of Railroads), No. 430, Moscow: Transzheldorizdat, 1958. (Russian)

Kozlov, V.B. and I.M. Lysenko. Experiment in Using Rail Flaw Detectors. Moscow: Transzheldorizdat, 1962. (Russian)

Sokolov, V.S. Flaw Detection in Materials. Moscow-Leningrad: Gosenergoizdat, 1961. (Russian)

Uspensky E.I. Automation of Rail Inspection Using Magnetic Flaw Detector Cars. Moscow: "Transport," 1970. (Russian)

GOST (State Standard Specification) 14782-69. "Welded Connections. Ultrasonic Flaw Detection Methods." Moscow: Izd-vo standartov (Standards Publishing House), 1969. (Russian)

"Investigations into the Operation of Rails on the Line." Works TsNII MPS (Central Scientific Research Institute, Ministry of Railroads). No. 292, Moscow: "Transport," 1965.

"Classification of Flaws and Damage to Rails," RTM 32/TsP-1-66. Moscow: "Transport," 1967. (Russian)

"The MRD-66 Magnetic Rail Flaw Detector. Instructions for Use and Servicing." Moscow: "Transport," 1968. (Russian)

"An Experiment in Using the DUK-13IM and UZD-NIIM-6M Ultrasonic Flaw Detectors," Series "The Track and Track Facilities," No. 51, Moscow: Izd. TsNIITEI MPS (Central Scientific Research Institute of the TEI, Ministry of Railroads), 1969. (Russian)

"The RDP-56 TsNII Removable, Variable Field Flaw Detector. Information Letter No. 379." Moscow: Transzheldorizdat, 1956. (Russian)

"The URD-63 Ultrasonic Rail Flaw Detector. Instructions for Use." Moscow: "Transport," 1968. (Russian)

"The URD-58 Ultrasonic Rail Flaw Detector. Instructions for Use." Moscow: "Transport," 1970. (Russian)

The UZD-NIIM-6M Ultrasonic Flaw Detector. Instructions for Use and Service." Moscow: "Transport," 1971. (Russian

Shur, E.A. Damage to Rails. Moscow: "Transport," 1971. (Russian)

*U.S. GOVERNMENT PRINTING OFFICE: 1978 0-622-508/531

Flow Detection in Rails, 1978
US DOT, FRA